IMAGING THE NEOCORTEX IN EPILEPSY WITH ADVANCED MRI TECHNIQUES

Fergus James Rugg-Gunn MB BS MRCP

Department of Clinical and Experimental Epilepsy

Institute of Neurology

University College London

Queen Square

Thesis submitted to the University of London

for the Degree of Doctor of Philosophy

2004

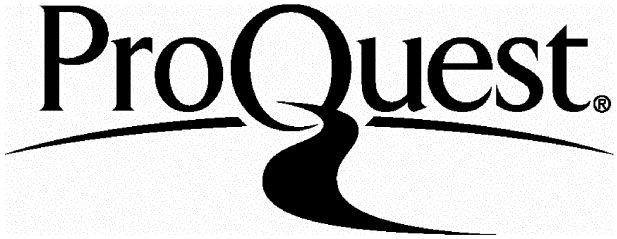

Abstract

Current optimal MRI reveals an identifiable abnormality in up to 80% of patients with refractory focal epilepsy. The remaining 20% are classified as "MRI-negative" and surgical treatment of such patients is often associated with a poor outcome. The identification of a cerebral lesion is, therefore, an important goal in the management of these patients. The aim of this thesis was to implement four novel advanced MRI techniques - diffusion tensor imaging (DTI), magnetisation transfer imaging (MTI), T2-mapping (T2M) and double inversion recovery (DIR), to provide insights into the structural basis of seizure disorders that are currently cryptogenic. For each technique, normative data from 30 healthy control subjects were obtained. These were compared on a statistical voxel-by-voxel basis to imaging data derived from patients with refractory epilepsy and non-progressive acquired cerebral lesions, malformations of cortical development (MCD), or normal conventional MR imaging ("MRI-negative patients").

In patients with acquired lesions (infarcts, cerebral trauma, intracranial infections), and MCD (gyral abnormalities, heterotopias and focal cortical dysplasia) the advanced MRI techniques were sensitive in identifying abnormalities which had previously been visualised on conventional MRI. More importantly, however, there were areas that appeared normal on conventional imaging but which were identified as abnormal with the advanced MRI techniques, indicating additional sensitivity from the new methods. Individual analyses of the MRI-negative patients identified abnormalities which concurred with the presumed seizure foci in approximately 33% (DTI - 23%, MTI - 36%, T2M - 44% and DIR 30%). The areas of abnormality in the MRI-negative patients are most likely caused by disruption in the microstructural environment due to aetiological factors such as, occult dysgenesis or acquired damage, or as a result of repeated seizures, for example, atrophy, gliosis, and neuronal loss.

In an MRI-negative patient with refractory focal epilepsy, histopathological examination of surgically excised tissue which displayed abnormal diffusion revealed extensive white matter gliosis. Further histopathological correlative data is required to validate these advanced MRI techniques more definitively. It is likely that that our positive findings in individual patients represent the most structurally abnormal of all the MRI-negative patients. With improvements in these techniques, further occult epileptogenic regions may be identified, which may guide invasive diagnostic procedures and possible epilepsy surgery.

Table of Contents

Acknowledgments

The completion of 3 years of research and the creation of this Thesis would not have been possible without the help and support of a significant number of colleagues, friends and family.

Firstly, I am indebted to my principal supervisor, Professor John Duncan, who has been, and continues to be, an inspiration to me in both academic and clinical epilepsy. He has been unwaveringly supportive and enthusiastic, approaching even the most challenging times with encouragement and good humour. A better mentor and supervisor, I am sure, does not exist. Professor Gareth Barker has also been an important influence, and I am grateful for his enthusiastic discussions on all aspects of MR physics and image analysis. I would like to thank the physicists, Phil Boulby and Mark Symms, who have been pivotal in the completion of this research. Mark, in particular, spent many hours patiently, and often repeatedly, explaining the fundamentals of MRI and quantitative analysis. He always did so with enthusiasm, kindness and good humour, and I am indebted to him for this.

MRI-based research relies on dedicated and highly skilled MR radiographers. I was, therefore, very fortunate to be working with Philippa Bartlett, Jane Burdett, Elaine Williams and Penny Hitchings who were always kind, understanding and accommodating, even when requests for scans arrived in the middle of a busy schedule.

I am grateful to the consultants, Ley Sander, Sanjay Sisodiya, Matthias Koepp, and Mark Richardson, for referring patients and, moreover, taking an interest in the results of these novel techniques. This work would not have been possible without all the healthy control subjects and patients who willingly gave their time to participate in these studies, and I thank them for their enthusiastic altruism.

I would like to thank my research fellow colleagues at Chalfont, in particular, Sofia Eriksson, Rebecca Liu, Tejal Mitchell, Rob Simister and Afraim Salek-Haddadi, for our stimulating discussions on all aspects of medicine and life and, more importantly, their friendship and support. Sofia Eriksson's contribution to the work on diffusion tensor imaging is acknowledged in the Statement of Originality, however, our struggles and successes with the finer aspects of DTI and SPM early on in the research had a greater impact on the rest of the work than this suggests.

I wish to thank my parents for their love and encouragement; and especially my father for his valuable advice at all stages of this research.

I am grateful to my wonderful children, Charlotte, Sophie and James for reminding me of what is important in life; and for enduring my physical and mental absence with quiet understanding. Finally, but most importantly, I would like to thank my wife, Philippa, for her unconditional love and support. None of this work would have been possible without her. She undoubtedly gave the most, yet received the least and I, therefore, dedicate this work to her, with love.

Original Articles & Awards

PEER-REVIEWED PAPERS

Rugg-Gunn FJ, Eriksson SH, Boulby PA, Symms MR, Barker GJ, Duncan JS.
Magnetization transfer imaging in focal epilepsy.
Neurology. 2003 May 27; 60 (10):1638-1645. (Thesis chapter 4)

Eriksson SH, Symms MR, Rugg-Gunn FJ, Boulby PA, Wheeler-Kingshott CA, Barker GJ, Duncan JS, Parker GJ.
Exploring white matter tracts in band heterotopia using diffusion tractography.
Ann Neurol. 2002 Sep; 52 (3):327-34.

Rugg-Gunn FJ, Eriksson SH, Symms MR, Barker GJ, Thom M, Harkness W, Duncan JS.
Diffusion tensor imaging in refractory epilepsy.
Lancet. 2002 May 18; 359 (9319):1748-51. (Thesis chapter 3.2)

Rugg-Gunn FJ, Symms MR, Barker GJ, Greenwood R, Duncan JS.
Diffusion imaging shows abnormalities after blunt head trauma when conventional magnetic resonance imaging is normal.
J Neurol Neurosurg Psychiatry. 2001 Apr; 70 (4):530-3. (Thesis chapter 3.3)

Rugg-Gunn FJ, Eriksson SH, Symms MR, Barker GJ, Duncan JS.
Diffusion tensor imaging of cryptogenic and acquired partial epilepsies.
Brain. 2001 Mar; 124 (Pt 3):627-36. (Thesis chapter 3.1)

Eriksson SH, Rugg-Gunn FJ, Symms MR, Barker GJ, Duncan JS.
Diffusion tensor imaging in patients with epilepsy and malformations of cortical development.
Brain. 2001 Mar; 124 (Pt 3):617-26. (Thesis chapter 3.1)

ARTICLES UNDER REVIEW BY PEER-REVIEWED JOURNALS

Rugg-Gunn FJ, Boulby PA, Symms MR, Barker GJ, Duncan JS
Whole brain T2-mapping demonstrates occult abnormalities in focal epilepsy.
Submitted to Brain 9/03. (Thesis chapter 5)

Rugg-Gunn FJ, Boulby PA, Symms MR, Barker GJ, Duncan JS
Imaging the neocortex in epilepsy: initial experience with double inversion recovery imaging
Submitted to Ann Neurol. 12/03. (Thesis chapter 6)

REVIEWS

Rugg-Gunn FJ
Clinical applications of diffusion tensor imaging in epilepsy
Epilepsia. 2002 Jan; vol 43, suppl 1, 69-77.

Taber KH, Pierpaoli C, Rose SE, Rugg-Gunn FJ, Chalk JB, Jones DK, Hurley RA.
The future for diffusion tensor imaging in neuropsychiatry.
J Neuropsychiatry Clin Neurosci. 2002 Winter; 14 (1):1-5.

INVITED BOOK CHAPTERS

Boulby PA, Rugg-Gunn FJ. T2: the transverse relaxation time. In: Tofts, PJ, editor. Quantitative MRI of the Brain - Measuring Changes Caused by Disease. John Wiley and Sons. New York 2003:141-186.

Rugg-Gunn FJ, Duncan JS. Three-dimensional analysis of MRI. In: Rosenow, F and Luders, HO, volume Eds. Pre-surgical assessment of the epilepsies with clinical neurophysiology and functional imaging. In: Daube J and Maguiere F, series Eds. Clinical Neurophysiology Handbook. Elsevier. New York, April 2004.

Rugg-Gunn FJ, Symms M. Novel MR contrasts to reveal more about the brain. In: Duncan JS, editor. Neuroimaging clinics of North America – Epilepsy. Elsevier, Philadelphia, 2004 (in preparation).

ABSTRACTS

Rugg-Gunn FJ, Boulby PA, Symms MR, Barker GJ, Duncan JS. T2-mapping of the neocortex in localisation-related epilepsy. Epilepsia 2002; vol 43, suppl 7, pg 304.

Rugg-Gunn FJ, Boulby PA, Symms MR, Barker GJ, Duncan JS. T2-mapping of the neocortex in epilepsy. Association of British Neurologists, Oxford, Spring 2002.

Rugg-Gunn FJ, Eriksson SH, Symms MR, Barker GJ, Duncan JS. Diffusion tensor imaging of cryptogenic and acquired partial epilepsies. Epilepsia 2002; vol 43, suppl 1.

Rugg-Gunn FJ, Eriksson SH, Boulby PA, Symms MR, Barker GJ, Duncan JS. Magnetisation transfer imaging in patients with cerebral dysgenesis, cryptogenic and acquired partial epilepsies. Journal of Neurological Sciences 2001; vol 187, suppl 1, pg 295.

Diaz-Daza O, Morales D, Hlatky R, Funke M, Barkley J, Rugg-Gunn FJ, Taber KH, Hayman LA. An update on traumatic brain injury. Radiological society of North America 87th Scientific Assembly, Chicago, Nov 2001.

Rugg-Gunn FJ, Guye M, Eriksson SH, Parker G, Barker GJ, Wheeler-Kingshott C, Duncan JS. Exploring the connectivity of band heterotopia using diffusion tensor imaging. Association of British Neurologists, Durham, Autumn 2001.

Rugg-Gunn FJ, Eriksson SH, Boulby PA, Symms MR, Barker GJ, Duncan JS. Magnetisation transfer imaging in localization-related epilepsy. International Society for Magnetic Resonance in Medicine Annual Meeting, Glasgow, 2001.

Rugg-Gunn FJ, Eriksson SH, Symms MR, Barker GJ, Duncan JS. Diffusion tensor imaging of cryptogenic and acquired partial epilepsies. The Third International Magnetic Resonance and Epilepsy Symposium, Birmingham, Alabama, 2001.

Eriksson SH, Rugg-Gunn FJ, Symms MR, Barker GJ, Duncan JS. Diffusion tensor imaging in patients with epilepsy and malformations of cortical development. The Third International Magnetic Resonance and Epilepsy Symposium, Birmingham, Alabama, 2001.

Rugg-Gunn FJ. Application of interictal diffusion tensor imaging. The Third International Magnetic Resonance and Epilepsy Symposium, Birmingham, Alabama, 2001.

Rugg-Gunn FJ, Eriksson SH, Symms MR, Barker GJ, Duncan JS Diffusion tensor imaging of cryptogenic and acquired partial epilepsies. International Society for Magnetic Resonance in Medicine Annual Meeting, Denver, 2000.

Rugg-Gunn FJ, Boulby PA, Symms MR, Barker GJ, Duncan JS. New windows on the brain. International League Against Epilepsy, British Branch, Scientific Meeting, Edinburgh, 2000.

Eriksson SH, Symms MR, Wieshmann UC, Barker GJ, Woermann FG, Rugg-Gunn FJ, Duncan JS. Diffusion tensor imaging of anisotropy in malformations of cortical development. Epilepsia 1999; vol 40, suppl 7, pg 178.

Rugg-Gunn FJ, Eriksson SH, Symms MR, Barker GJ, Duncan JS. Diffusion tensor imaging in "MRI-negative" partial epilepsy demonstrates focal abnormalities. Epilepsia 1999; vol 40, suppl 7, pg 181.

Eriksson SH, Symms MR, Rugg-Gunn FJ, Barker GJ, Wieshmann UC, Woermann FG, Duncan JS. Diffusion tensor imaging shows reduced anisotropy in malformations of cortical development. J Neurol Neurosurg Psychiatry 2000; vol 68, suppl 1, 257.

AWARDS

American Epilepsy Society - Young Investigator Award: Rugg-Gunn FJ, Eriksson SH, Boulby PA, Symms MR, Barker GJ, Duncan JS. Magnetisation Transfer Imaging in Patients with Localisation-Related Epilepsy. Epilepsia. 2002 Jan; vol 42, suppl 7.

Radiological Society of North America Investigator Award: Diaz-Daza O, Morales D, Hlatky R, Funke M, Barkley J, Rugg-Gunn FJ, Taber KH, Hayman LA. An update on traumatic brain injury. RSNA, Chicago, 2001.

Abbreviations

2D	two-dimensional
3D	three-dimensional
ADC	apparent diffusion coefficient
AT2	amygdala T2 value
BHT	band heterotopia
CPMG	Carr-Purcell-Meiboom-Gill sequence
CSF	cerebrospinal fluid
CSI	chemical shift imaging
CT	computed tomography
DIR	double inversion recovery
DNET	dysembryoplastic neuroepithelial tumour
DSI	double inversion recovery signal intensity
DTI	diffusion tensor imaging
DWI	diffusion weighted imaging
EEG	electroencephalography
EPI	echo-planar imaging
FA	fractional anisotropy
FACT	fibre assignment by continuous tracking
FCD	focal cortical dysplasia
FLAIR	fluid attenuated inversion recovery prepared imaging
FLE	frontal lobe epilepsy
fMRI	functional magnetic resonance imaging
FSE	fast spin echo
FWHM	full width at half maximum
GABA	γ-aminobutyric acid
GLX	glutamate + glutamine
GM	grey matter
HCT2	hippocampal T2 value
HCV	hippocampal volume
HS	hippocampal sclerosis
HSE	herpes simplex encephalitis
IEA	interictal epileptiform activity
IGE	idiopathic generalised epilepsy
MCD	malformation of cortical development
MD	mean diffusivity
MRA	magnetisation resonance angiography
MRI	magnetic resonance imaging

MRS	magnetic resonance spectroscopy
MS	multiple sclerosis
MTC	magnetisation transfer contrast
MTI	magnetisation transfer imaging
MTR	magnetisation transfer ratio
NAA	N-acetyl-aspartate
NAWM	normal appearing white matter
OLE	occipital lobe epilepsy
PET	positron-emission tomography
PVE	partial volume effect
RF	radiofrequency
ROI	region-of-interest
SAR	specific absorption rate
SCH	subcortical heterotopia
SEH	subependymal heterotopia
SNR	signal to noise ratio
SPM	statistical parametric mapping
T2M	T2-mapping
TLE	temporal lobe epilepsy
WM	white matter

Tables

Figures

Statement of Originality

The work described in this Thesis, including image processing, recording and analysis of data, interpretation and presentation of the results, was undertaken solely by the author, other than diffusion tensor imaging in malformations of cortical development (chapter 3.1.4.3) which was a collaborative project between the author and Dr Sofia Eriksson.

The Thesis was written entirely and solely by the author.

CHAPTER ONE

Introduction & Background

1.1. EPILEPSY

1.1.1 Introduction

Epilepsy can be defined as the occurrence of recurrent and unprovoked transient paroxysms of excessive or uncontrolled discharges of cerebral neurons, resulting in a variety of clinical manifestations. Depending on the site of epileptic activity and subsequent spread, these may include an alteration in consciousness, sensory, motor, autonomic or psychic events. Despite most patients having only a small number of seizures, each lasting no longer than a few minutes, the physical, psychological and social impact on an individual may be considerable.

Epilepsy is the commonest serious neurological disease, affecting over 300,000 people in the United Kingdom. The overall incidence of epilepsy (excluding febrile convulsions and single seizures) is approximately 70 cases per 100,000 persons per year (Hauser 1997). The lifetime prevalence of seizures (the risk of having a non-febrile epileptic seizure at some point in the average lifetime) is between 2 and 5% (Sander and Shorvon 1996; Hauser *et al.* 1993). For most patients, the condition remits and subsequent relapse is uncommon. In approximately 30% of patients with focal epilepsy, however, seizures are refractory to medication (Kwan and Brodie 2000). In these patients, surgery is a potentially curative therapeutic option should an epileptic focus be localised accurately.

1.1.2 Classification of Seizures and Epilepsy Syndromes

The classification of epileptic seizures and syndromes has investigative, therapeutic and prognostic implications (Mosewich and So 1996; Watanabe 1997). Classification systems are also used in clinical pharmacology trials, epidemiological studies and to facilitate communication between the clinical and research settings through the development of common terminology used to identify seizure disorders (So 1995; Engel, Jr. 1998). It is therefore important to establish a practical and reproducible, yet flexible classification system, which can be applied both in the field for large epidemiological studies and in specialist epilepsy centres where greater emphasis is placed on readily available investigations, such as neuroimaging and EEG.

1.1.2.1 Seizure Classification

Early epilepsy classification systems did not differentiate between seizures and syndromes, employing terms such as grand mal, petit mal and psychomotor epilepsy. This terminology was non-discriminatory; for example, grand mal was frequently used to describe any tonic-clonic seizure and petit mal referred to any "small attack" including both absences and complex partial seizures. The classification of epileptic seizures was revised in 1981 and divided seizures on clinical and electrophysiological grounds into partial (focal onset), generalised and unclassified

(Commission on Classification and Terminology of the International League Against Epilepsy 1981) (Table 1.1). The partial seizures were further subdivided into "complex" and "simple" partial seizures depending on the level of consciousness during the ictal event.

Although its simplicity promoted universal acceptance, a number of limitations of the revised ICES classification system were recognized (Luders *et al.* 1993). Firstly, the classification disregarded presumed pathophysiological and anatomical information and utilised electroclinical data only, assuming that clinical seizure semiology and electrophysiological data were anatomically concordant. This premise is frequently incorrect (Manford *et al.* 1996). Furthermore, the reliance on EEG data biases epidemiological studies towards specialist centres with unrestricted EEG availability and patients with more severe epilepsy. Secondly, it is not always possible to determine whether consciousness is preserved or lost and without prolonged videotelemetry, distinguishing between simple and complex partial seizures is often difficult. This problem was highlighted in a study by Manford et al of patients with epilepsy diagnosed in the primary care setting, where 23.3% of the patients were unclassifiable (Manford *et al.* 1992). This was despite an aetiological basis for the epilepsy being suggested from the history in a proportion of these cases. Finally, the use of unwieldy terminology and omission of lateralising or somatotopic information has also been criticised (Benbadis and Luders 1995). In view of these limitations, alternative classification systems for seizures have been proposed. Luders et al recommended a classification scheme based solely on seizure semiology, dividing ictal events into auras, autonomic, "dialeptic", motor and special seizure categories (Luders *et al.* 1998). Other proposed classifications include those based on presumed pathophysiological and anatomical information established from all available clinical and investigative evidence (Engel, Jr.1998), or re-stratifying seizure types with diminished emphasis on the dichotomy of partial versus generalised seizures whilst utilising current electroclinical knowledge (Herranz 1998).

Table 1.1 International Classification of Epileptic Seizures (ICES); simplified version.

1. **Partial (focal, partial) seizures**
    1.1. Simple (consciousness not impaired)
        1.1.1. With motor symptoms
        1.1.2. With somatosensory or special sensory symptoms
        1.1.3. With autonomic symptoms
        1.1.4. With psychic symptoms
    1.2. Complex (with impairment of consciousness)
        1.2.1. Simple partial seizure onset followed by impairment of consciousness
        1.2.2. Impairment of consciousness at onset
            a) Impairment of consciousness only
            b) With automatism
    1.3. Partial seizures evolving to secondarily generalised seizures (tonic-clonic, tonic or clonic)
        1.3.1. Simple partial seizures evolving to generalised seizures
        1.3.2. Complex partial seizures evolving to generalised seizures
        1.3.3. Simple partial seizures evolving to complex partial, evolving to generalised seizures
2. **Generalised seizures (convulsive or non-convulsive)**
    2.1. Absence seizures
        2.1.1. Typical
        2.1.2. Atypical
    2.2. Myoclonic seizures
    2.3. Clonic seizures
    2.4. Tonic seizures
    2.5. Tonic-clonic seizures
    2.6. Atonic seizures
3. **Unclassified epileptic seizures (inadequate or incomplete data)**

1.1.2.2 Syndromic classification

Epileptic seizures represent the clinical manifestation of an abnormal cerebral discharge, and only infrequently yield important aetiological or prognostic information. In contrast, the determination of an epilepsy syndrome may have therapeutic or prognostic implications. Furthermore, terminology used in the clinical and research settings often involves descriptions of syndromes rather than seizures. To fulfil the requirement for a syndrome-based classification system, Gastaut (Gastaut 1969), and then shortly afterwards, the International Commission for Classification of the Epilepsies (ICCE) proposed schemes based on electroclinical data (Merlis 1970). To date, three classifications have been proposed by the ICCE.

International Classification of the Epilepsies (ICE, 1970)

The epilepsies were classified into three major divisions: generalised, partial and unclassifiable. Generalised epilepsies were subdivided into primary, secondary, and undetermined. This led to confusing terminology with similar terms assigned to very different epilepsies; for example, secondarily generalised (i.e. partial onset) epilepsy and secondary generalised (i.e. West syndrome) epilepsy.

International Classification of the Epilepsies and Epileptic Syndromes (ICEES, 1985)

The ICEES classification system attempted to address the limitations of the 1970 system by adopting a more pluralistic, "inclusive" approach whilst endeavouring to maintain practicality. A number of epileptic syndromes were included, each defined as an epileptic disorder characterized by a cluster of signs and symptoms customarily occurring together. These included seizure type, aetiology, neurological signs, precipitating factors, age of onset, severity, chronicity, diurnal and circadian rhythm. However, an individual syndrome may have a large number of aetiologies. This results in a wide range of associated prognoses thereby limiting the clinical usefulness of such a classification system. Moreover, patients may evolve from one syndrome to another during the course of their epileptic condition; for example, a child with West syndrome may later fulfil the criteria for the Lennox-Gastaut syndrome (Watanabe 1989).

The customary division between generalised and focal epilepsy formed the basis for the 1985 classification. Each branch was subsequently subdivided into idiopathic (primary, unknown aetiology), and symptomatic (secondary, known aetiology). The focal epilepsies were also subdivided according to their proposed anatomical localisation (e.g. frontal, temporal). Furthermore, in contrast to the earlier classification, the 1985 ICEES expanded the generalised epilepsy group to recognize the increased number of clinical subtypes of idiopathic generalised epilepsy (IGE) and the complex taxonomy of the static and progressive encephalopathies. Two new major divisions were also introduced: epilepsies and syndromes undetermined whether focal or generalised, and the special syndromes. The first category was created to acknowledge the occasionally unclear boundary between generalised and focal epilepsy (as seen in those patients with only nocturnal seizures, unhelpful EEG, or lack of localising / lateralising signs during a seizure) and also to enable those patients with both partial *and* generalised seizures to be appropriately classified. The category of special syndromes included those patients with febrile, isolated, or provoked seizures.

International Classification of the Epilepsies and Epileptic Syndromes (ICEES, 1989b)

The ICEES was revised in 1989 and differed from its predecessor by the inclusion of a new category of cryptogenic epilepsy. This referred to those cases presumed to be symptomatic but without confirmatory evidence. A potential drawback of this terminology is the erroneous assumption that every patient is investigated to the same degree. Following the 1989 revision, the term "idiopathic" was only used to describe epilepsies with a suspected genetic aetiology (Table 1.2).

1.1.2.3 Additional Classification Systems and Future Directions

The ICEES was developed in specialist epilepsy centres which are unrepresentative of epilepsy at a population level. This has led to a lack of uniformity in case ascertainment, electroclinical data interpretation, use of additional ancillary investigations and application of the classification system between population-based studies (Eadie 1996; Everitt and Sander 1999). Comparison of these studies is important in identifying variations in aetiology in different countries or populations and establishing the requirements for health care services. However, methodological inconsistencies between studies adversely affects the validity of such comparisons. To address this limitation, the ILAE published guidelines for epidemiological studies in which a simplified classification system was based on clinical risk factors rather than electrophysiological evidence (ILAE 1993).

The 10th International Classification of Diseases (ICD-10) was based on a combination of both ICEES and the 1981 ICES systems and continued to employ confusing terminology such as petit mal and grand mal (WHO 1992). An attempt to be all-encompassing precludes its use in either clinical or epidemiological settings.

Recent advances in neuroimaging, particularly MRI, have permitted the identification of epileptogenic abnormalities in a significant proportion of patients with epilepsy (Li *et al.* 1995; Duncan 1997). Current classification systems however do not exploit this information and rely on electroclinical data only. This may be due, at least in part, to the limited availability of high quality MRI, and the possibility of classification difficulties due to discordant MRI and EEG findings.

The ICEES is currently being reappraised by the ILAE in light of recent advances in neuroradiology, genetics and pathophysiology. The resulting classification is likely to apply the established dichotomy of generalised versus localised, in addition to dividing epilepsies by age. Furthermore, the increasing numbers of genetic abnormalities identified in patients with epilepsy (Phillips *et al.* 1995; Berkovic *et al.* 1996; Scheffer *et al.* 1995; Steinlein *et al.* 1995) necessitates the creation of additional divisions; for example, into those in which epilepsy occurs in isolation, or into those diseases with epilepsy as an associated feature (Engel, Jr.1998; Engel, Jr. 2001b; Engel, Jr. 2001a).

Alternative proposals for classification systems include those based on aetiological factors rather than the localisation of epileptogenic foci (Everitt and Sander 1999; Bauer 1994), a multi-modal approach incorporating seizure semiology, aetiology, anatomical localisation and pathophysiological data (Blume *et al.* 1997), and a system based on a fundamental division into developmental and mature aetiologies (Spencer 1998).

An ideal classification system should be able to be used by both specialists and non-specialists, in hospital and in community-based studies, yet remain flexible enough to integrate advances in complimentary investigations such as imaging and neurogenetics as they become more widely available (Mosewich and So 1996; Everitt and Sander 1999; So 1995).

Table 1.2 The 1989 International Classification of the Epilepsies (ICEES)

1. **Localization-related epilepsies and syndromes**

   1.1. Idiopathic (with age-related onset)
   - Benign childhood epilepsy with centrotemporal spike
   - Childhood epilepsy with occipital paroxysms
   - Primary reading epilepsy

   1.2. Symptomatic
   - Chronic progressive epilepsia partialis continua of childhood
   - Syndromes characterized by seizures with specific modes of precipitation.
   - Temporal, frontal, parietal and occipital lobe epilepsies

   1.3 Cryptogenic
   - Temporal, frontal, parietal and occipital lobe epilepsies

2. **Generalized epilepsies and syndromes**

   2.1. Idiopathic (with age-related onset)
   - Benign neonatal familial convulsions
   - Benign neonatal convulsions
   - Benign myoclonic epilepsy in infancy
   - Childhood absence epilepsy (pyknolepsy) / Juvenile absence epilepsy
   - Juvenile myoclonic epilepsy
   - Epilepsy with GTCS seizures on awakening
   - Other generalized idiopathic epilepsies not defined above
   - Epilepsies with seizures precipitated by specific modes of activation.

   2.2. Cryptogenic or symptomatic
   - West syndrome (infantile spasms, Blitz-Nick-Salaam Krampfe)
   - Lennox-Gastaut syndrome
   - Epilepsy with myoclonic-astatic seizures
   - Epilepsy with myoclonic absences

   2.3. Symptomatic

   2.3.1. Non-specific aetiology
   - Early myoclonic encephalopathy
   - Early infantile epileptic encephalopathy with suppression burst
   - Other symptomatic generalized epilepsies not defined above

   2.3.2. Epilepsies due to specific neurological diseases

3 **Epilepsies and syndromes undetermined whether focal or generalized**

   3.1 With both generalized and focal seizures
   - Neonatal seizures
   - Severe myoclonic epilepsy in infancy
   - Epilepsy with continuous spike-waves during slow wave sleep
   - Acquired epileptic aphasia (Landau-Kleffner-syndrome)
   - Other undetermined epilepsies not defined above

   3.2 Without unequivocal generalized or focal features.

4 **Special syndromes**

   4.1 Situation-related seizures
   - Febrile convulsions
   - Isolated seizures or isolated status epilepticus
   - Seizures occurring only when there is an acute metabolic or toxic event

1.1.3 Aetiology of epilepsy

1.1.3.1 Introduction

Epileptic seizures can be broadly classified into those arising from a focal cortical region (focal or partial epilepsy) and those characterised by an immediate, synchronous electrical discharge of both hemispheres (generalised epilepsy). The incidence of generalised and focal epilepsies are approximately equal and, of patients with focal epilepsy, most have seizures arising from the temporal lobe (Juul-Jensen and Foldspang 1983).

Table 1.3 Risk factors for epilepsy in adults. (Adapted from Hesdorffer and Verity, 1997)

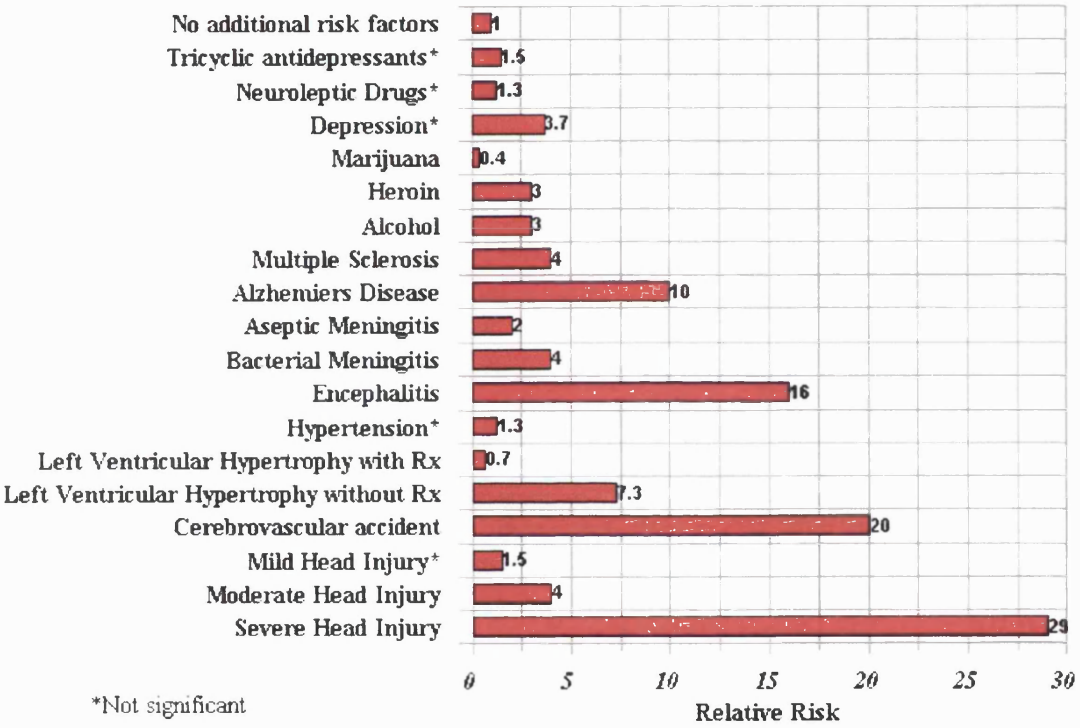

*Not significant

Any cortical lesion may give rise to epileptic seizures, hence the aetiology of focal epilepsy is heterogeneous (Table 1.3). The range of aetiologies is dependent on a number of factors including age and geographical location (Sander and Shorvon 1996; Hauser, Annegers, and Kurland 1993). In previous epidemiological studies, a presumed aetiology was identified in only a third of patients with epilepsy (Sander *et al.* 1990; Hauser, Annegers, and Kurland 1993; Placencia *et al.* 1992). More recently, a prospective community based study utilising high-resolution MRI identified an aetiological basis in approximately 70% of patients with focal epilepsy (Everitt *et al.* 1998).

By definition, patients with generalised epilepsy have normal qualitative MRI. However, with advanced post-processing techniques and quantitative assessment, imaging abnormalities have been identified (Woermann *et*

al. 1998b; Savic *et al.* 1998b), consistent with the pathological finding of microdysgenesis in such patients (Meencke and Janz 1984). More recently however, it has been suggested that the frequency of microdysgenesis in normal subjects is the same as in patients with idiopathic generalised epilepsy suggesting that alternative microscopic structural abnormalities are responsible (Opeskin 2000).

The pathophysiology of seizure generation, spread and cessation is currently poorly understood. It has been suggested that some lesions possess intrinsic epileptogenicity, for example focal cortical dysplasia (Ferrer *et al.* 1992; Spreafico *et al.* 1998), whilst others may be irritative to surrounding tissue, such as tumours (Fish 1999). Combined experimental and theoretical work suggests that potentiation of excitatory synapses and depression of inhibitory synapses are critical events in epileptogenesis (March 1998; Traub and Jefferys 1998; Jefferys 1990). This concurs with an immunocytochemical investigation of resected cortical tissue from patients with refractory focal epilepsy due to MCD which revealed an increase in excitatory pyramidal neurons combined with a decrease in GABAergic inhibitory interneurons (Spreafico *et al.* 1998).

The rhythmic, bilateral and synchronous EEG activity underlying spike-wave discharges in generalised epilepsy has been correlated with oscillatory patterns involving interconnected cortical and thalamic neurons (Avanzini *et al.* 2000). The pacemaker structure responsible has been identified as the reticular thalamic nucleus, a GABAergic structure projecting exclusively to the other thalamic nuclei. Experimental work suggests that in generalised epilepsy there is a genetically determined enhancement of the pacemaker properties of the thalamic nucleus, which propagates pathological synchronization and spike-wave discharges (Danober *et al.* 1998).

1.1.3.2 Hippocampus

1.1.3.2.1 Hippocampal Epilepsy

Approximately 60-70% of focal seizures originate in the temporal lobes, the majority arising from the hippocampus. In hospital-based MRI studies, hippocampal sclerosis (HS) was identified in approximately 25-30% of patients with focal epilepsy (Everitt *et al.* 1998; Wieshmann 2003; Li *et al.* 1995). Although HS is the commonest pathologically confirmed lesion in chronic temporal lobe epilepsy (Babb and Brown 1987), other pathologies exist, for example, dysembryoplastic neuroepithelial tumours, vascular abnormalities, MCD and gliosis.

1.1.3.2.2 Anatomy

The hippocampus is a curved structure lying on the medial surface of the temporal lobe, approximately 3-4cm in length with a volume of 2-6cm^3 in normal subjects. It is a rhinencephalic (olfactory) derivative and with the dentate gyrus comprises the trilaminar cerebral archecortex. During embryological development, with the growth of the cerebral hemispheres and corpus callosum, the hippocampus is displaced inferiorly and rolled medially to occupy a position adjacent to the floor of the lateral ventricle in the medial temporal lobe (Gray's Anatomy 1989a).

1.1.3.2.3 Hippocampal Sclerosis

In 1825, Bouchet and Cazauvielh first described the macroscopic appearance of a hard, shrunken hippocampus in an autopsy specimen of a patient with epilepsy (Bouchet and Cazauvielh 1825). Early microscopic descriptions of hippocampal sclerosis, by Sommer in 1880 (Sommer 1880) and then Bratz in 1899 (Bratz 1899), detailed loss of

pyramidal neurons in Ammon's horn and supplementary damage involving the granule cells and dentate. More recently, the cell loss has been quantified and showed severe pyramidal neuron loss and gliosis throughout the hippocampus proper, particularly in Sommer's sector (CA1), and the end folium (including the CA4 pyramids and hilar neurones). The subiculum and the granule cells of the dentate gyrus are only partially destroyed and a number of pyramidal neurones in sector CA3 and particularly in CA2 appear comparatively resistant to injury (Mouritzen-Dam 1980; Babb *et al.* 1984a; Babb *et al.* 1984b; Mathern *et al.* 1996). Histopathological studies have shown that in temporal lobe epilepsy pathological changes are often bilateral, but nearly always asymmetrical (Babb *et al.* 1984a; Meldrum and Bruton 1992), and within a single hippocampus, changes may be focal or diffuse. Furthermore, the adjacent amygdala or fornix and, in rare instances, the whole temporal lobe ipsilateral to the HS, may be smaller (Watson *et al.* 1992).

Hippocampal sclerosis (HS) is the most common pathology underlying focal seizure disorders that is amenable to surgery. It is found in approximately 60% of temporal lobes removed for the treatment of epilepsy, and is associated with 60-70% chance of the patient becoming seizure free following resection (Cascino *et al.* 1992; Berkovic *et al.* 1995; Babb and Brown 1987; Bruton CJ 1988). An initial precipitating injury, such as acute hippocampal damage caused by complex febrile convulsions (Davies *et al.* 1996; Lewis 1999; Sagar and Oxbury 1987; Cendes *et al.* 1993a) appears to be an important step in the development of HS. Hippocampal susceptibility to these acute insults may be determined by a pre-existing lesion (e.g. familial subtle hippocampal malformation) (Fernandez *et al.* 1998), genetic factors (e.g. interleukin-1b gene polymorphism) (Kanemoto *et al.* 2000) or associated developmental lesion (e.g. malformations of cortical development) (Raymond *et al.* 1994).

The principal MRI features of HS are hippocampal atrophy, demonstrated with coronal T1-weighted anatomical images, and increased signal intensity within the hippocampus on T2-weighted images (Jackson *et al.* 1990; Berkovic *et al.* 1991). Additional features, seen inconsistently, include decreased T1-weighted signal intensity, disruption of the laminar structure of the hippocampus (Jackson *et al.* 1993a) and atrophy of the ipsilateral fornix (Baldwin *et al.* 1994), mamillary body and amygdala (Kuzniecky *et al.* 1996). Atrophy of the temporal lobe, dilatation of the temporal horn and a blurring of the grey-white matter junction in the temporal neocortex have also been reported (Meiners *et al.* 1994; Mitchell *et al.* 1999).

The extent of hippocampal atrophy and increased T2 signal vary along the length of the hippocampus in HS. Classical HS is commonly unilateral and diffuse (Quigg *et al.* 1997), but may be bilateral or focal, with the head affected most frequently (Van Paesschen *et al.* 1997a; Woermann *et al.* 1998a), although this is not universally accepted (Kuzniecky *et al.* 1996; Bronen *et al.* 1995a). HS may be associated with severe pathological change, as seen in chronic HS, or with only minor abnormalities, for example, in "end-folium sclerosis" where hippocampal damage is centred on the hilus and dentate gyrus (Van Paesschen *et al.* 1997b). Abnormal signal change in the hippocampus is not specific for HS and may also be due to cysts, tumours or dysgenetic tissue as well as a partial volume effect from CSF, particularly when slice thickness is increased to improve the signal to noise ratio and/or resolution. Similarly, isolated hippocampal atrophy is not specific for HS and may be a secondary phenomenon related to previous head injury, dementia (Price *et al.* 2001) or temporal lobe surgery (Cook and Sisodiya 1996). However, the *combination* of volume loss and abnormal signal intensity is highly specific for HS. (See chapter 1.3.1 Quantitative analysis of mesial temporal lobe structures).

A number of studies have found that ipsilateral hippocampal atrophy on preoperative MRI predicts good seizure control following anterior temporal lobe resection (Berkovic *et al.* 1991; Garcia *et al.* 1994).

1.1.3.3 Neocortex

1.1.3.3.1 Neocortical Epilepsy

Neocortical epilepsy describes seizures arising from cortex outside the mesial temporal lobe. Approximately 60-70% of focal seizures originate in the temporal lobe. About 40% of these arise from the neocortex (Pacia *et al.* 1996). Approximately 20-30% of focal seizures derive from the frontal lobes, 8% from the occipital lobes and 1.4% from the parietal lobes. Neocortical epilepsy is commonly due to an identifiable lesion; however, in about 50% of patients with focal epilepsy no aetiological basis can be determined. This decreases to approximately 20% in patients with *refractory* focal epilepsy (Duncan 1997). Almost any cortical lesion may give rise to seizures, therefore, a wide range of aetiologies exists: idiopathic (presumed genetic abnormality), structural, including both congenital and acquired causes, and cryptogenic. Acquired causes include head injury, stroke, tumours, intracranial infections, inflammation and toxins.

1.1.3.3.2 Normal development

The external cerebral surface is a grey mantle (pallium) of approximately 14 billion neurons and accompanying neuroglia. Cortical thickness varies from 4mm in the precentral gyrus to 1.5mm in the primary visual area and is thicker over the exposed convexities of the gyri than in the sulci. Primitively, the cortex was trilaminar and primarily served olfaction. In human brain these rhinencephalic derivatives comprise the archecortex (hippocampus and dentate gyrus) and paleocortex (olfactory areas and amygdaloid complex). The neocortex, which comprises 90% of the total human cortex is six layered. These horizontal layers, from superficial to deep, are: layer I - molecular (relatively devoid of neurons); layer II - external granular; layer III - external pyramidal; layer IV - internal granular; layer V - internal pyramidal; layer VI - multiform or polymorphous. The cingulate gyrus which is part of the limbic system, is intermediate in histological and functional terms. The gyral and sulcal arrangement is approximately constant between hemispheres within the same individual, and between individuals, although minor differences in dimensions and convolutions exist (Gray's Anatomy 1989a).

Cerebral development commences with the formation of the neural plate in the early embryonic disc. This evolves into a neural tube, the rostral end of which develops into three vesicles from which the fore, mid and hindbrain are formed. By the eighth gestational week, two zones have become apparent within the prosencephalic (forebrain) vesicle, a deeper ventricular zone composed of radially orientated undifferentiated columnar neuroepithelium, and an outer, fibre-rich marginal zone. Cajal-Retzius cells are the first neurons to differentiate within the marginal zone (Meyer and Goffinet 1998). These are transient cells which secrete reelin, a protein involved in the final stages of cortical migration and organisation (Meyer *et al.* 1999). Towards the end of the eighth gestational week, neuroblasts forming the cortical plate accumulate in the marginal zone, progressively separating layers I and VII. These cells migrate into this layer along radially disposed processes of glial cells in an "inside-out" fashion, with cells destined for deeper layers preceding those destined for more superficial layers. Migration occurs predominantly between the 7^{th} and 16^{th} gestational weeks although is not fully complete until the 5^{th} postnatal month (Sidman and Rakic 1973; Sarnat 1991). Previously it has been suggested that neuroblasts originating from a single proliferative stem cell migrate along the same radial glial cell resulting in a single column of mature neurons in the cortex. Thus, the periventricular germinal matrix is a protomap of the future cortical plate

(Rakic 1978; Rakic 1988b). More recently, this "radial unit hypothesis" has been challenged with the description of additional tangential migration of neuroblasts in animal models (Walsh and Cepko 1993; Walsh and Cepko 1992; Tan and Breen 1993). It has been estimated that normal mitotic proliferation results in a 25-50% overproduction of neuroblasts, which later undergo programmed cell death (Finlay and Slattery 1983).

Layer VII, the subplate zone, is an active interface between incoming afferents (predominantly thalamocortical) and the developing cortical plate cells (Kostovic and Rakic 1990). Transfer of the afferent terminals to the cortical plate results in degeneration of the subplate zone, although some neurons survive and settle in the mature subcortical white matter. Selective, regional ablation of cells in the subplate leads to failure of the thalamic afferents to pass eventually into the overlying cortical plate even though their predestined targets are in the correct position. This suggests a precocious role for early interneuronal connectivity in the formation of later definitive connectivity (Ghosh *et al.* 1990).

Cortical maturation, including neurite formation and growth, development of membrane polarity and excitability, synaptogenesis, synthesis of secretory products and myelination (Sarnat 1991), commences before the completion of migration and continues into the post-natal period (Rakic 1978).

Cerebral white matter comprises a compact mass of association, commissural and projection fibres with associated neuroglia. A small number of neurons exist in white matter, however, their role remains unclear. It is likely that they represent the remnants of subplate neurons or misplaced cortical neurons. Microdysgenesis describes a number of subtle architectural abnormalities, most frequently an excess of white matter neurons, and has been identified in a number of conditions including normal subjects (Kaufmann and Galaburda 1989), dyslexia, autism, and epilepsy. The significance of microdysgenesis in epilepsy continues to be debated, but may have some prognostic value (Thom *et al.* 2001).

1.1.3.3.3 Malformations of cortical development

With the introduction and subsequent advances in MRI, malformations of cortical development (MCD) are being increasingly diagnosed in patients with epilepsy in vivo (Brodtkorb *et al.* 1992; Chan *et al.* 1998; Kuzniecky *et al.* 1991; Palmini *et al.* 1991b; Kuzniecky 1994; Raymond *et al.* 1995). Previously these abnormalities were not detectable with CT scanning and the seizure disorders were regarded as being "cryptogenic". More recently, in community-based prevalence studies using optimal, high resolution MRI, MCD were detected in approximately 3% of patients (Everitt *et al.* 1998; Wieshmann 2003). In patients with refractory epilepsy, MCD may be seen in 8-12% of cases (Li *et al.* 1995; Semah *et al.* 1998; Lehericy *et al.* 1997), and in up to 14% in children with MCD and learning disability (Brodtkorb *et al.* 1992; Steffenburg *et al.* 1998; Steffenburg *et al.* 1996). Despite recent advances in MRI however, in some patients, MCD may only be identified post-operatively on histopathological examination (Spreafico *et al.* 1998; Ying *et al.* 1998). It is likely therefore that a proportion of those patients with refractory epilepsy and normal MRI also harbour MCD.

MCD have previously been classified and described on the basis of macro- or microscopic appearances (Barth 1987), imaging (Palmini *et al.* 1991c), electrophysiological or clinical features (Barkovich *et al.* 1996). More recently, a classification system based on embryological, anatomical, and genetic information has been proposed (Kuzniecky and Barkovich 1996) (Table 1.4). This classification system will need revision as the genetic

bases of MCD are elucidated further.

A disturbance at any stage of neuronal proliferation, migration or organisation, caused by genetic or external factors, involving either neurons or glial cells, may result in abnormal cortical development. A particular defect during corticogenesis may result in more than one type of MCD, and a particular MCD may have more than one aetiology (Rakic 1988a).The type of insult, time of occurrence and severity influences the extent, location and type of MCD, and thus determines the degree of clinical disability.

In addition to genetic factors, a number of extraneous agents and insults have been proposed as causes of MCD, including: intrauterine infections (e.g. toxoplasmosis, cytomegalovirus), toxins (e.g. alcohol, isoretinoic acid, methylmercury, carbon monoxide), local ischaemia or haemorrhage, and ionizing radiation which may interfere with both nucleic acid and cell membrane or radial glial fibre integrity (Barth 1987; Jensen and Killackey 1984; Sarnat 1987; Ferrer *et al.* 1993).

The common pathological features are loss of tissue organisation and abnormalities of neuronal structure. Epileptogenicity may result from neuronal hyperexcitability and abnormal neuronal connectivity (Jacobs *et al.* 1996; Jacobs *et al.* 1999; Barth 1987).

Table 1.4 Classification of malformations of cortical development

A: Malformations due to abnormal neuronal and glial proliferation

I. Generalised:

1. Decreased proliferation - (microlissencephaly)
   a. thin cortex
   b. normal cortex
2. Increased proliferation - none known
3. Abnormal proliferation - none known

II. Focal or multifocal:

1. Decreased proliferation - none known
2. Increased and abnormal proliferation - (megalencephaly and hemimegalencephaly)
2. Abnormal proliferation
   a. Non-neoplastic - (tuberous sclerosis, focal cortical dysplasia, focal transmantle dysplasia)
   b. Neoplastic (ass. with disordered cortex) - (DNET, ganglioglioma, gangliocytoma)

B. Malformations due to abnormal neuronal migration

I. Generalized:

1. Classical (Type 1) Lissencephaly and subcortical band heterotopia
2. Cobblestone (Type 2) Lissencephaly
3. Lissencephaly - not otherwise classified
4. Heterotopia

II. Focal or multifocal malformations of neuronal migration

1. Focal agyria / pachgyria (partial lissencephaly)
2. Focal or multifocal heteroptopia
3. Focal or multifocal heterotopia with organisational abnormality of the cortex
4. Excessive single ectopic white matter neurons.

C. Malformations due to abnormal cortical organization

I. Generalized:

1. Polymicrogyria

II. Focal or multifocal:

1. Bilateral and symmetric polymicrogyria
2. Asymmetrical polymicrogyria and schizencephaly
3. Focal or multifocal cortical dysplasia without balloon cells
4. Microdysgenesis

D: Malformations. of cortical development, not otherwise classified

Lissencephaly describes a brain in which gyration is absent. The migratory defect is thought to occur between 12 and 16 weeks of gestation and may be due to a genetic abnormality or extraneous factor, such as an ischaemic event (Stewart *et al.* 1975), irradiation (Ferrer, Alcantara, and Marti 1993) or CMV infection (Hayward *et al.* 1991). There are two distinct histopathologies (Dambska *et al.* 1983). In type I there are both agyric and pachygyric regions and the affected cortex is four-layered. Patients may present with variable phenotypes, including the Miller-Dieker syndrome (resulting from a defect on chromosome 17 (LIS1)) (Dobyns *et al.* 1993; Reiner *et al.* 1993), the Norman-Roberts syndrome (Dobyns *et al.* 1984), or with isolated lissencephaly (Dobyns *et al.* 1992). Recent studies have established that lissencephaly and X-linked subcortical band heterotopia (XLIS/DCH) are genetically related, with band heterotopia (BHT) seen in heterozygous females and lissencephaly in homozygous males (des Portes *et al.* 1997). The LIS1 gene product is a regulatory subunit of platelet activating factor acetylhydrolase, but has also been found to co-regulate microtubule function (Sapir *et al.* 2000). Most recently, a new form of lissencephaly with cerebellar hypoplasia has been described and linked to a gene coding for reelin on chromosome 7 (Ross *et al.* 2001). Other malformations associated with lissencephaly include callosal agenesis, enlarged ventricles, and heterotopia (Harding 1992). Clinically, most patients have microcephaly, severe hypotonia, and infantile spasms. MRI reveals a thickened cortex, diminished white matter, and vertical sylvian fissures, giving the typical eight-shaped brain appearance on axial images (Raymond *et al.* 1995; Barkovich *et al.* 1988). Type II lissencephaly is characterized by a smooth cerebral surface and a thickened cortex in which there is little discernible layering of any sort with neurons being grouped in clusters and columns. Associations include congenital muscular dystrophy in genetic syndromes such as Walker-Warburg syndrome (Dobyns *et al.* 1985) and Fukuyama syndrome (Dambska *et al.* 1982). MRI reveals a thick cortex, hydrocephalus, and hypomyelination (Barkovich, Chuang, and Norman 1988).

Polymicrogyria describes a large number of narrowed, thinned gyri. Histologically, there are layered and unlayered types (Harding 1992). The former is characterised by post-migrational destruction of cells, mainly in lamina V, which is probably due to transient vascular insufficiency between 18 and 24 weeks gestation (Richman *et al.* 1974). Unlayered polymicrogyria is macroscopically indistinguishable, but a cell-sparse layer suggestive of lamina destruction is not present. Other than ischaemia, infections and metabolic disorders have been implicated including cytomegalovirus, toxoplasmosis (Friede and Mikolasek 1978), Zellweger's syndrome (Volpe and Adams 1972; Evrard *et al.* 1978), neonatal adrenoleukodystrophy (Powers 1985), and Pelizaeus-Merzbacher disease (Norman *et al.* 1966). Clinical presentation is dependent on location and extent of the abnormality. Diffuse polymicrogyria may present with severe developmental delay, microcephaly and hypotonia. MRI findings demonstrate a thickened cortex with shallow sulci, and underlying white matter signal abnormality (Barkovich, Chuang and Norman 1988). Polymicrogyria may present as the congenital bilateral perisylvian syndrome, consisting of pseudobulbar paresis, learning disability, epilepsy and perisylvian lesions on MRI (Kuzniecky and Andermann 1994; Kuzniecky *et al.* 1994). Most recently, an increased number of reelin-expressing Cajal-Retzius-like cells have been identified in polymicrogyric tissue, suggesting an association between reelin overexpression and polymicrogyria (Eriksson *et al.* 2001a).

Schizencephaly describes the presence of clefts extending across the wall of the hemisphere, from the pia to the ependyma. The walls of the cleft are lined by grey matter, which may be polymicrogyric (Barth 1987). The walls may be apposed (Type I) or separated (Type II). Patients may present with a contralateral hemiparesis, moderate to severe developmental deficit, infantile spasms and focal motor seizures. The MRI characteristics of schizencephaly are unilateral or bilateral grey matter lined clefts extending from the calvarium to the ventricle (Barkovich and Kjos 1992b). Associated features include subependymal heterotopia (Harding 1992), abnormal cortical gyration and absence of the septum pellucidum (Brodtkorb *et al.* 1992). There is some evidence from experimental studies that mutations of the EMX-2 gene, which is normally expressed in proliferating neuroblasts and Cajal-Retzius cells may be implicated in abnormalities of cortical subdivision, such as schizencephaly (Cecchi and Boncinelli 2000).

Heterotopia is defined as abnormally located clusters of neurons. They are late disorders of neuronal migration (>20 weeks gestation) and are described according to their morphology, location and distribution.

Subependymal heterotopias (SEH) are solitary or multiple, discrete or confluent nodules of grey matter in the subependymal region lining the ventricular wall. The occipital horns and trigones are the most commonly involved sites. Patients usually have normal intellectual and motor function or mild learning disability. Epilepsy develops in approximately 75% of patients, usually in the second decade (Raymond *et al.* 1994). SEH is associated with trisomy 13-15 and 18, and 4p- syndrome. More recently, mutations in the X-linked FLN gene, resulting in a defective protein, Filamin 1, have been described in female patients with bilateral confluent SEH (Huttenlocher *et al.* 1994; Fox *et al.* 1998; Eksioglu *et al.* 1996). Filamin 1 encodes an actin-cross-linking phosphoprotein that transduces ligand-receptor binding into actin reorganization, and which is required for locomotion of many cell types (Fox *et al.* 1998). The mutations cause loss of cytoskeleton function in neurons in the ventricular zone resulting in migration failure of the neuronal population that expresses the defect gene. FLN mutations are associated with pre- or perinatal lethality in hemizygous males. MRI reveals multiple smooth ovoid nodules, isodense with cortical grey matter, lining the lateral ventricles (Barkovich and Kjos 1992a). Approximately 75% of patients have bilateral lesions and 30% also have focal subcortical heterotopia. Callosal and cerebellar malformations may be present in 25% of cases (Kuzniecky and Jackson 1997).

Subcortical heterotopias (SCH) are nodules or bands of neurons in white matter. Patients with *band* heterotopia (double cortex, BHT) present with mild epilepsy, pyramidal signs, dysarthria and a variable degree of developmental delay and cognitive impairment. MRI reveals a circumferential band of subcortical grey matter underlying the cortical mantle and separated from it by a thin rim of white matter (Livingston and Aicardi 1990). The overlying cortex may be normal or macrogyric. Mutations in the *doublecortin* gene (DCX) result in microtubular dysfunction and impaired neuronal migration, and are thought to be responsible for almost all familial cases, approximately 80% of sporadic female cases, and 25% of sporadic male cases of BHT (des Portes *et al.* 1997; Sicca *et al.* 2003) (see ***lissencephaly***). The MRI features of *focal subcortical* heterotopia include clusters of heterotopic nodules with irregular margins surrounded by normal appearing white matter (Barkovich and Kjos 1992a). Patients present with epilepsy in the second decade and contralateral pyramidal signs if the heterotopic nodules are extensive. Associated malformations include abnormalities of the corpus callosum, polymicrogyria and megalencephaly (Friede 1989).

Focal cortical dysplasia is characterized by a spectrum of histological features ranging from mild cortical

disruption without giant neurons to the most severe forms in which cortical dyslamination and large bizarre "balloon" cells, which include neuronal and glial elements, are present (Taylor *et al.* 1971; Barth 1987). The pathogenesis is currently unknown with histopathological features consistent with disruption occurring both early and late in cerebral development (Mischel *et al.* 1995). The typical MRI features include focal cortical thickening with blurring of the grey/white matter interface and shallow sulci (Chan *et al.* 1998). Subcortical white matter changes are present to a variable extent. Patients present with refractory partial seizures, although, surgical resection is possible in carefully selected patients and is associated with seizure freedom in about 40% of cases (Sisodiya 2000).

Microdysgenesis describes the presence of microscopic architectural disturbances of grey matter and has been classified into a number of distinct subgroups. These include, a diffuse or focal increase in neurons (mainly Cajal-Retzius horizontal cells) within the molecular layer, protrusions of lamina II neurons into the molecular layer, subpial neurons bulging into the subarachnoid space, and heterotopic neurons in the white matter. A standard definition and classification does not exist and debate continues into the epileptogenic significance of this type of MCD (Lyon and Gastaut 1985; Meencke and Janz 1984; Hardiman *et al.* 1988; Thom *et al.* 2001). Microdysgenesis has been identified in normal subjects (Kaufmann and Galaburda 1989) and in those with non-epilepsy neurological disorders (Humphreys *et al.* 1990; Inagaki *et al.* 1987; Bloom 1993) It has previously been thought to be more common in patients with primary generalized (Meencke and Janz 1984) or focal epilepsy (Nordborg *et al.* 1999; Eriksson *et al.* 1999), although this has recently been challenged (Opeskin 2000). Postulated pathogeneses include defective programmed cell death, failure of single radial glial fibres, neuronal overmigration or abnormal persistence of Cajal-Retzius cells (Mischel, Nguyen, and Vinters 1995). Although microdysgenesis cannot be appreciated on conventional MRI (Raymond *et al.* 1995), in some patients, imaging may reveal an associated abnormality such as hippocampal sclerosis, focal cortical dysplasia or dysembryoplastic neuroepithelial tumour (Raymond *et al.* 1995).

1.1.3.3.3 Other aetiologies, including genetic & cryptogenic

Head injury

Head injury results in altered vasoregulation, disruption to the blood brain barrier, increased intracranial pressure, ischaemia, haemorrhage, inflammation, necrosis and disruption of fibre tracts (Willmore 1990). Overall, post-traumatic epilepsy (PTE) occurs in approximately 7% of patients with head trauma (Annegers *et al.* 1980). The risk is dependent on the severity of injury (Jennet 1995). In patients with mild head injury, as defined by unconsciousness or post-traumatic amnesia of less then 30 minutes duration, the risk of seizures was increased 1.5 times above the risk for those without head injury. Moderate head injury, as defined as skull fracture or 30 minutes to 24 hours of unconsciousness or post-traumatic amnesia, is associated with a four-fold increased risk. A 29-fold increased risk is seen with severe head injury, as defined as more than 24 hours of unconsciousness or post-traumatic amnesia, brain contusion, or intracerebral haematoma (Annegers *et al.* 1980). Guidice et al used the duration of amnesia and unconsciousness as measures of the severity of head injury and reported that in those with amnesia and loss of consciousness lasting longer than one hour, the risk of developing PTE was approximately 25%. In those comatose for over three weeks, the risk increased to 35% (Guidice and Berchou 1987). Specific risk

factors for PTE include dural penetration, central-parietal location of injury, occurrence of early seizures (<1 week from injury), a focal abnormality on EEG one month after head injury, MRI apparent cortical hamosiderin, and depressed skull fracture (da Silva *et al.* 1992; Feeney and Walker 1979; Jennet 1995; Angeleri *et al.* 1999; Asikainen *et al.* 1999).

Prophylactic use of anti-epileptic agents (AEDs) has been advocated in patients with severe head injury following experimental evidence that phenytoin may have a neuroprotective effect mediated by sodium channel blockade (Tasker *et al.* 1992; Vartanian *et al.* 1996). In addition, a number of uncontrolled, retrospective studies have reported a significant reduction of PTE with administration of AEDs after head trauma (Servit and Musil 1981; Wohns and Wyler 1979). Recent systematic reviews of randomised controlled trials reported a beneficial effect of AEDs in reducing early seizures but, no evidence that treatment reduces the occurrence of late seizures (Temkin 2001), or has any effect on death or disability (Schierhout and Roberts 1998). Brain injury is associated with deposition of haem-containing compounds in brain parenchyma (Adams 1975), free radical generation and peroxidation reactions (Willmore *et al.* 1983). In addition to intrinsic enzymatic mechanisms for control of free radical reactions (Fridovich 1974), steroids and tocopherol also terminate peroxidative reactions (Witting 1980) and selenium is effective in preventing tissue injury initiated by haem compounds (Saunders *et al.* 1987). Antioxidants and chelators may also be neuroprotective. Furthermore, it has been suggested that gamma-aminobutyric acid (GABA) agonists, NMDA receptor antagonists and barbiturates may offer neuroprotection following injury (Willmore 1990; Faden *et al.* 2001; Gaviria *et al.* 2000).

Cerebral tumours

Epilepsy is a common presenting symptom of primary brain tumours with seizures occurring in approximately 35-50% of adults (LeBlanc and Rasmussen 1997; Rasmussen 1975; Cascino 1990). The proportion of newly diagnosed epilepsy due to brain tumours presenting at the primary care level is approximately 6% (Sander *et al.* 1990). Epileptogenesis in tumours arises from a combination of disinhibition, excitatory coupling and "burst" generation mediated by altered concentrations of GABA (Houser *et al.* 1986; Chagnac-Amitai and Connors 1989), glutamate and NMDA (Strowbridge *et al.* 1992; Dingledine *et al.* 1986). Specific mechanisms involve the presence of epileptogenic haemosiderin (Spencer *et al.* 1987; Kraemer and Awad 1994), altered glial function and blood flow abnormalities (Bakay and Harris 1981).

The propensity for a tumour to cause seizures is dependant on a number of factors. Seizures occur much more frequently in supratentorial (22-68%) rather than infratentorial or pituitary lesions (6%) (Smith *et al.* 1991; Chan and Thompson 1984). Furthermore, seizures are more common in patients with temporal rather than frontal or parietal tumours (Shorvon 1992). Tumours developing near the cortex are more likely to induce seizures than those arising from the deep white matter (e.g. lymphoma), or the grey/white matter junction (e.g. cerebral metastases) (Delattre *et al.* 1988). The histology of a tumour is also important in determining the probability of producing seizures. Slowly growing tumours, such as low grade gliomas are highly epileptogenic with seizures present in approximately 90% of patients (Vertosick *et al.* 1991). Seizure incidence is lower for high grade gliomas, (approximately 30-50%) (Scott and Gibberd 1980; Rasmussen 1975) although this may represent a selection effect, with less time available for seizures to become clinically evident. Seizures occur in 30-60% of patients with meningiomas (Chozick *et al.* 1996; Al-Mefty and Origitano 1994) and 10-20% of patients with primary cerebral lymphoma (Freilich and DeAngelis 1995).

Dysembryoplastic neuroepithelial tumours (DNET) are indolent cerebral lesions consisting of cystic, dysplastic and glioneuronal elements (Daumas-Duport *et al.* 1988; Prayson and Estes 1992). The MRI features are of a focal, circumscribed, predominantly cortical mass with low signal on T1 and high signal on T2 (Raymond *et al.* 1995). Often the calvarium overlying the lesion is expanded. They are most commonly found in the temporal lobes and often present with partial seizures before the age of 20 years (Daumas-Duport *et al.* 1988). Although potential for malignancy is low, they are highly epileptogenic. Surgical resection is frequently associated with excellent seizure control post-operatively (Kirkpatrick *et al.* 1993; Raymond *et al.* 1995).

Gangliogliomas are benign tumours composed of dysplastic neurones resembling pleomorphic ganglion cells, and glial elements which may be astrocytic and/or oligodendroglial in appearance (Smith *et al.* 1992). It has been suggested that gangliogliomas may arise from glioneuronal hamartias through neoplastic transformation of the astrocytic component (Wolf *et al.* 1994) although their origin has previously been attributed to ectopic sympathetic tissue (Rubinstein and Herman 1972), a form of tuberous sclerosis or neurofibromatosis (Wahl and Dillard 1972), or from a pluripotential progenitor cell which may give rise to both gangliogliomas and DNETs (Hirose and Scheithauer 1998; Shimbo *et al.* 1997). In common with DNETs, gangliogliomas are most commonly found in the temporal lobes in young patients (Zentner *et al.* 1994; Celli *et al.* 1993; Rosemberg and Vieira 1998; Isla *et al.* 1991). Surgical treatment is often associated with a good outcome, which is dependant on the complete removal of the lesion and surrounding epileptogenic tissue, a normal EEG post-operatively, younger age at operation, shorter duration of epilepsy, and a low-grade astrocytic component on histopathological examination (Morris *et al.* 1998; Smith *et al.* 1992; Otsubo *et al.* 1990).

Tuberous sclerosis (TS) is an autosomal dominant disorder characterized by learning disability and hamartomas affecting several organs including the skin, CNS, retinae, lungs and kidneys. Epilepsy occurs in approximately 80% of patients (Evans and Curtis 2000; Webb *et al.* 1991). Seizure severity correlates with the number of intracranial tubers although extensive histopathological changes have been identified throughout the entire cerebral cortex despite normal appearance on MRI (Mitchell *et al.* 2000).

Cerebrovascular pathology

Seizures occur in approximately 7 - 11% of patients following acute stroke (Lancman *et al.* 1993; So *et al.* 1996; Burn *et al.* 1997). It is one of the commonest causes of epilepsy in those over the age of 60 years (Sung and Chu 1990). Compared to cerebral infarction, the risk of developing seizures is approximately 10 times greater in patients who survive either intracerebral or subarachnoid haemorrhage (Lancman *et al.* 1993; Burn *et al.* 1997; Paolucci *et al.* 1997). Additional risk factors for the development of epilepsy following stroke include: larger infarcted region, particularly if the cortex was involved (Awada *et al.* 1999), the presence of islands of apparently preserved tissue within the infarcted area (Awada, Omojola, and Obeid 1999; Ryglewicz *et al.* 1990), and the involvement of specific cerebral regions, for example the middle or superior temporal gyri, supramarginal gyrus and/or the post-central gyrus (Heuts-van Raak *et al.* 1996). Focal epilepsy is the most common seizure type following stroke although primary generalised seizures have also been reported, possibly as a result of global neurotransmitter dysfunction or altered cerebral autoregulation (Holmes 1980; Hornig *et al.* 1990; Kotila and Waltimo 1992). Alternatively, the seizures may have been misclassified due to incomplete electroclinical data. Following the finding that the prevalence of epilepsy is greater than expected even before the occurrence of a first clinical stroke (Shinton *et al.* 1987), it has been postulated that vascular risk factors may increase the risk of

developing epilepsy, possibly due to occult cerebrovascular disease. Whereas this elevated risk is small in patients with hypertension (Shapiro *et al.* 1990), the presence of untreated left ventricular hypertrophy increases the risk of seizures (prior to a stroke) by eleven-fold (Hesdorffer *et al.* 1996).

Cavernous haemangiomas are small, non-shunting vascular lesions commonly associated with epilepsy. Typically they are single and located either in or adjacent to the cortex. They have a characteristic MRI appearance due to the range of blood products present, including a typical "halo" of low signal on T2-weighted images due to haemosiderin deposition from occult haemorrhage (Requena *et al.* 1991). Surgical treatment is usually associated with seizure remission in approximately 70% of patients, provided the surrounding epileptogenic haemosiderin-containing tissue is also resected.

Arteriovenous malformations (AVMs) commonly present with acute intracerebral haemorrhage, seizures, neurological deficit or headache (Hofmeister *et al.* 2000; Kupersmith *et al.* 1996; Rosenfeld *et al.* 1991). AVMs smaller than 3cm in diameter often present with haemorrhage, whereas AVMs greater than 3cm frequently present with seizures (Piepgras *et al.* 1993). Familial predisposition to the development of AVMs has been reported (Herzig *et al.* 2000). Mechanisms for epileptogenicity include haemorrhage and haemosiderin deposition (Wong *et al.* 2000), mass effect (Miyasaka *et al.* 1997; Bronen *et al.* 1995b) and vascular "steal" phenomenon (Costantino and Vinters 1986). Factors predictive of the occurrence of seizures include a cortical location, feeding vessels from the middle cerebral artery, varices in the draining venules, and the absence of aneurysms (Turjman *et al.* 1995). Treatment with conventional surgery (Zimmerman *et al.* 2000; Yeh *et al.* 1993), radiosurgery (Kurita *et al.* 1998; Heikkinen *et al.* 1989) (including gamma knife (Gerszten *et al.* 1996; Herzig *et al.* 2000)) and endovascular embolisation (Pasqualin *et al.* 1991; Fournier *et al.* 1991) are often associated with a good clinical outcome.

Alcohol

The risk of experiencing a first seizure in patients with chronic alcohol abuse is approximately 5 times the risk observed in the general population (Leone *et al.* 1997). Furthermore the risk of seizures is proportional to daily total alcohol intake (Lechtenberg and Worner 1992). Possible mechanisms for the increased risk of seizures in patients with chronic alcohol abuse include acute alcohol withdrawal, head injury, acute metabolic derangements such as hypoglycaemia, hyponatraemia and hypocalcaemia (Kayath *et al.* 1999), neoplasms, cerebrovascular accidents, and infections such as meningitis (Mattson 1990). It has been suggested that seizures occurring during acute alcohol withdrawal are due to alcohol-related GABA receptor desensitisation and subsequent NMDA receptor activation (Hoffman *et al.* 1992). Furthermore, there is evidence that repeated detoxification results in a kindling effect with subsequent alcohol withdrawal carrying an increased risk of seizures (Lechtenberg and Worner 1992; Moak and Anton 1996; Booth and Blow 1993; Brailowsky and Garcia 1999).

Infection

Infections are one of the commonest causes of seizures worldwide, for example, 50% of adult-onset epilepsy in developing countries has been attributed to neurocysticercosis (NCC) (Medina *et al.* 1990). Seizures may be the only presenting symptom, for example in NCC, or may be part of a global CNS abnormality, for example subacute sclerosing panencephalitis or rabies.

Herpes simplex encephalitis (HSE) occurs in all age groups and is the most common form of sporadic fatal encephalitis with an annual incidence of one in 250,000 to 500,000 (Whitley 1991; Whitley 1990). It results

from either primary infection (one third of cases) or reactivation (two thirds of cases) of the herpes simplex virus (HSV) (Whitley and Lakeman 1995). Pathologically, HSE is characterised by intense meningitis and parenchymal inflammation with necrosis and haemorrhage, most commonly involving the frontal and temporal lobes. Focal or generalised seizures frequently occur during the acute stages of the encephalitis and continue following recovery in approximately 5-10% of patients. Overall the mortality rate of HSE is 15% at 3 months with only 40% of patients surviving with minimal or no neurological sequelae (Whitley *et al.* 1986). Other viruses that cause encephalitis and seizures include cytomegalovirus, particularly in the immunocompromised (Bale 1984), Epstein-Barr virus (Russell *et al.* 1985; Bale 1993; Cinbis and Aysun 1992), arboviruses such as Eastern equine encephalitis virus (Przelomski *et al.* 1988), flaviviruses such as Japanese encephalitis virus (Bale 1993), rabies (seizures occur in approximately 10% of patients) (Dupont and Earle 1965) and Human Immunodeficiency Virus (HIV). Seizures occur in 4 to 11% of patients with HIV infection (Van Paesschen *et al.* 1995a; Wong *et al.* 1990). This can be secondary to opportunistic cerebral infection, AIDS-dementia complex, CNS lymphoma, metabolic disturbances, such as hyponatraemia, hypomagnesaemia and hypocalcaemia, and anti-viral treatment (Holtzman *et al.* 1989; Wong, Suite, and Labar 1990; Van Paesschen, Bodian, and Maker 1995a; Fan-Harvard *et al.* 1994; Lor and Liu 1994; Rachlis and Fanning 1993).

Parasitic infections that cause seizures include NCC, malaria and toxoplasmosis. NCC occurs when humans inadvertently become the intermediate host for the pork tapeworm, *Taenia solium*. It accounts for approximately 10% of all neurological patients in developing countries (Garcia *et al.* 1995a). Epilepsy is the most frequent manifestation of NCC, occurring in two-thirds of affected patients (Del Brutto *et al.* 1992). Most patients with epilepsy due to NCC have partial seizures (Medina *et al.* 1990) and a normal neurological examination (Del Brutto *et al.* 1992). Calcified nodules representing cysts previously destroyed by the host's immune system are readily apparent on CT scanning (Del Brutto *et al.* 1993). Studies of long-term prognosis in epilepsy due to NCC suggest that seizures can be well controlled on anti-epileptic medication (Del Brutto *et al.* 1992). Relapse is common however on cessation of treatment (Del Brutto 1994). Malaria is the most common fatal parasitic disease. Two percent of patients have cerebral involvement which is fatal in 20-50% of cases. Seizures occur in the majority of patients with cerebral malaria, with impaired consciousness and a high degree of parasitaemia carrying the highest risk of seizures during the acute illness (Akpede *et al.* 1993). *Toxoplasma gondii* is a ubiquitous obligate intracellular protozoan that causes cerebral toxoplasmosis in foetuses infected in utero, and cerebral abscesses in immunocompromised hosts. In addition to headache, confusion and focal neurological signs, seizures occur in approximately a third of patients with AIDS and cerebral toxoplasmosis (Ragnaud *et al.* 1993).

Bacterial meningitis causes inflammation and bacterial toxin accumulation in the subpial space resulting in generalised seizures and a depressed level of consciousness. As the infection progresses, focal seizures and neurological deficits develop due to thrombosis of meningeal veins (Adams and Victor 1985). Meningitis may be caused by a number of different bacteria depending on the age of the patient and time of the year (Tureen and Sande 1989). Seizures are most frequently associated with *Haemophilus Influenzae* infection, however, *Neisseria meningitides* and *Streptococcus pneumoniae* are more common pathogens outside the neonatal period. Tuberculous meningitis accounts for approximately 5% of the extrapulmonary cases of tuberculosis infection, and occurs most commonly in children. Ten percent of patients with tuberculous meningitis present with seizures (Kennedy and Fallon 1979). The prognosis is often poor, with a 50% mortality rate in patients over the age of 50 years, and neurological sequelae, such as cranial nerve palsies, epilepsy, deafness and blindness present in a large proportion

of the survivors (Tureen and Sande 1989).

Brain abscesses occur as a result of local spread from a contiguous focus of infection in the middle ear, sinuses or mastoid air cells, or as a result of haematogenous spread, for example from infective endocarditis. Seizures occur in approximately a third of patients. Additional presenting features include: headache, fever, vomiting, confusion and visual disturbance (Chun *et al.* 1986). The mortality rate is approximately 20%, and 30-50% of the survivors have neurological sequelae.

Inflammation

Rasmussen's encephalitis is an uncommon progressive disorder comprising unilateral cerebral atrophy and dysfunction, intractable focal seizures and inflammatory histopathology (Rasmussen *et al.* 1958). Following the discovery that rabbits immunised with glutamate receptor protein (GluR) developed seizures and histopathological changes similar to Rasmussen's encephalitis, and the finding of anti-GluR3 antibodies in the serum of some patients, it has been suggested that an autoimmune basis may underlie this condition (Rogers *et al.* 1994). Confirmatory evidence for this hypothesis is lacking however.

Autoantibodies directed against brain endothelial cells have also been detected in Landau-Kleffner syndrome (Connolly *et al.* 1999), and anecdotal evidence reports successful treatment with intravenous immunoglobulin (IVIg) (Mikati and Saab 2000; Lagae *et al.* 1998). Similarly, there are reports of West's syndrome and Lennox-Gastaut (L-G) syndrome responding well to IVIg (Duse *et al.* 1996; van Engelen *et al.* 1994b). Evidence of a functionally impaired immune system (van Engelen *et al.* 1995), increased serum imunoglobulins (Haraldsson *et al.* 1992), and a HLA DR5 association with L-G syndrome further supports immunological involvement in these conditions (van Engelen *et al.* 1994a).

Seizures are recognised in a number of autoimmune diseases such as systemic lupus erythematosus (approximately 5-10% of patients (Herranz *et al.* 1994; Liou *et al.* 1996)), stiff man syndrome (12% (Solimena *et al.* 1990)) and Hashimoto's encephalopathy (10% (Henchey *et al.* 1995)). Furthermore, autoantibodies, which recognise brain antigens, have been detected in groups of patients with isolated epilepsy (Plioplys *et al.* 1989). These include antiphospholipid (Inzelberg and Korczyn 1989), antinuclear (Verrot *et al.* 1997), antiganglioside (Bartolomei *et al.* 1996), antiglutamate receptor (Dambinova *et al.* 1997), and antiglutamic acid decarboxylase antibodies (Giometto *et al.* 1998; Palace and Lang 2000). However, it is not clear if the autoantibodies are a cause or consequence of seizures, as epilepsy itself and anti-epileptic drugs are known to alter immune responses (De Ponti *et al.* 1993; Jain 1991; Aarli 1993).

In the peripheral nervous system, it is recognised that genetic mutations and autoantibodies targeted to the muscle acetylcholine receptor cause similar clinical features. The recent discovery of mutations in genes encoding for K^+ ion channels in benign familial neonatal epilepsy (Biervert *et al.* 1998; Singh *et al.* 1998), or Na^+ ion channels in generalised epilepsy with febrile convulsions (Scheffer and Berkovic 1997), suggests that an autoimmune attack directed at these ion channels may underlie some epileptic disorders (Lang *et al.* 2003).

It is well established that the relative risk of developing epilepsy in patients with multiple sclerosis is between 3 and 5 times greater than in the general population (Spatt *et al.* 2001; Ghezzi *et al.* 1990; Moreau *et al.* 1998; Kinnunen and Wikstrom 1986). The type of epilepsy is almost invariably focal, and seizures are believed to arise from cortex adjacent to plaques of demyelination at the grey/white matter interface (Koopmans *et al.* 1989). Seizures occurring during an acute demyelinating episode often respond more effectively to corticosteroid therapy

than conventional anti-epileptic medication (Spatt *et al.* 1995). In over 50% of patients with MS and a history of seizures, however, epilepsy remains active and long term treatment with anti-epileptic drugs is required (Kinnunen and Wikstrom 1986).

Genetic

There have been significant recent advances in the elucidation of the genetic basis of inherited epilepsies. It is now recognised that genetic factors may contribute to aetiology in up to 40% of patients with epilepsy (Gardiner 1999).

There are in excess of 180 inherited Mendelian (single gene locus) traits which include epilepsy as part of the usually more complex condition; however, these account for only 1% of patients with epilepsy (McKusick 1994).

Epilepsy associated Mendelian diseases may be inherited as autosomal dominant or recessive, X-linked, or mitochondrial inheritance patterns (table 1.5).

Table 1.5 Epilepsy associated Mendelian disorders

Chromosomal disorders :	trisomy 13, 18, 21, fragile X
Metabolic disorders :	porphyria, homocystinuria, glycogen storage disorders, mitochondrial disorders
Neurocutaneous disorders :	tuberous sclerosis and Sturge-Weber syndrome
Malformations of cortical development :	lissencephaly, band heterotopia and agenesis of the corpus callosum
Neurodegenerative disorders :	progressive myoclonic epilepsies (Unverricht-Lundborg disease, Lafora disease, and the neuronal ceroid lipofuscinoses), neuroacanthocytosis, and Hallervorden-Spatz disease
Non-specific genetic disorders :	xeroderma pigmentosum and acrocallosal syndrome.

In contrast, a number of Mendelian inherited epilepsies are not associated with a detectable structural or metabolic abnormality of the brain. It has been suggested that these idiopathic epilepsies are characterised by mutations in the genes encoding for ion channels (Gardiner and Lehesjoki 2000).

Ion channels have an important role in the control of neuronal excitability, therefore, diseases which are characterised by abnormal excitability, such as epilepsy, might be expected to be caused by ion channel dysfunction. To date, there are nine ion channel sub-unit genes implicated in ten syndromes of idiopathic epilepsy (Mulley *et al.* 2003). Benign familial neonatal convulsions (BFNC) is an autosomal dominant idiopathic generalised epilepsy of the newborn. Genetic mutations have been demonstrated on chromosomes 20 and 8 in

regions coding for voltage-gated K^+ channels (Biervert *et al.* 1998; Singh *et al.* 1998). Mutations in genes coding for Na^+ channels on chromosomes 2 and 19 (Wallace *et al.* 2001b; Scheffer and Berkovic 1997) and the gamma2-subunit of the GABA (A) receptor (Wallace *et al.* 2001a; Baulac *et al.* 2001) have been identified in families with generalised epilepsy and febrile seizures plus ($GEFS^+$). This is an autosomal dominant condition characterised by febrile and afebrile generalised seizures continuing beyond the age of 6 years. The genetic mutations in autosomal dominant nocturnal frontal lobe epilepsy (ADNFLE) have been mapped to regions coding for the α4 (Steinlein *et al.* 1995) and β2 (Phillips *et al.* 2001) subunits of the neuronal acetylcholine receptor on chromosome 20. It has been suggested that mutations in the genes encoding for subunits of the nicotinic acetylcholine receptor on chromosome 15 are associated with juvenile myoclonic epilepsy (Elmslie *et al.* 1997), and rolandic epilepsy with centrotemporal spikes (Neubauer *et al.* 1998). The rare syndrome of autosomal dominant juvenile myoclonic epilepsy was recently shown to be associated with a GABA receptor α1 subunit mutation (Cossette *et al.* 2002). Most recently, there has been a suggestion through association studies that the α1A subunit of the voltage-gated calcium channel gene (CACNA1A), the opioid receptor mu subunit gene (OPRM1) and the chloride-channel gene CLCN2 are implicated in idiopathic generalized epilepsy, however specific molecular changes to substantiate these associations have not yet been reported (Chioza *et al.* 2001; Wilkie *et al.* 2002; Haug *et al.* 2003). The majority of idiopathic familial epilepsies are inherited in a complex, non-Mendelian pattern and are yet to be genetically characterized; however, ion channelopathies represent the most biologically plausible class of candidate gene. Non-ion channel genes have also been reported in specific epilepsy syndromes, for example, mutations of LGI1, thought to be important in signal processing and neuronal placement, have been described in autosomal dominant lateral temporal lobe epilepsy with auditory features (Kalachikov *et al.* 2002). Identification of rare mendelian epilepsies will continue and the pathophysiology of seizure generation in these diseases will be elucidated. It is likely that with advances in genomics and in high-throughput genetic analysis methods, the genetic description of some of the complex epilepsies will be resolved within the next decade.

Cryptogenic

Twenty percent of patients with refractory focal epilepsy have an undetermined aetiological basis for their epilepsy despite extensive investigation, including optimal MRI (Duncan 1997). Surgical treatment of this group is associated with a less favourable post-operative outcome (Cascino *et al.* 1992; Yoon *et al.* 2003). This may be due to incomplete resection of a discrete, isolated lesion or, more likely, the presence of unrecognized, widespread pathological change or multifocal abnormalities. Previous histopathological studies of surgically resected epileptic regions that have appeared normal on conventional MRI have shown features of cortical dysplasia and dyslamination, and in the white matter, microdysgenesis, astroglial proliferation, and heterotopia (Zentner *et al.* 1995; Siegel *et al.* 2001; Rugg-Gunn *et al.* 2002b). Most commonly however, the histological appearances were normal, suggesting that either the focal lesion was undetected during surgery or pathological assessment, or seizures arose through an alternative mechanism, such as a channelopathy or biochemical abnormality (Mulley *et al.* 2003). Undoubtedly, even with improvements in imaging techniques, a proportion of these patients will remain "MRI-negative". It is likely, however, that some of the discrete macroscopic focal lesions that are currently occult, will be identified by techniques interrogating different microstructural characteristics. These patients may be offered potentially curative surgical treatment. Whether the post-operative outcome similarly improves, in accordance with other MRI apparent focal lesions, remains undetermined at present.

1.2 MAGNETIC RESONANCE IMAGING IN EPILEPSY

1.2.1 Conventional Magnetic Resonance Imaging

Magnetic resonance imaging (MRI) has become the imaging modality of choice in the clinical evaluation of the brain in normal and pathological states. MRI allows the anatomical differentiation of grey and white matter tissues and thus permits the topographic and volumetric characterisation of specific regions of the cerebral cortex and subcortical structures in vivo.

Neuroimaging procedures prior to the introduction of X-ray computed tomography (CT) in the 1970s, and MRI in 1984 (Sostman *et al.* 1984; Oldendorf 1991), were limited to plain radiographs of the skull, pneumoencephalography, and conventional radioisotope imaging. All techniques were associated with a low diagnostic yield and most carried some risk of serious morbidity. CT scanning proved sensitive for macroscopic pathology associated with focal epilepsy, for example, large tumours or infarcts (Gastaut and Gastaut 1976; Kuzniecky *et al.* 1993b), but was frequently normal in those with chronic epilepsy and more discrete lesions, such as hippocampal sclerosis or cavernous haemiangiomas (Kuzniecky *et al.* 1993b; Bergen *et al.* 1989). Additional limitations of CT scanning include radiation exposure, bony artefact in the middle temporal fossa which adversely affects temporal lobe imaging, and the inability to perform multiplanar imaging.

The development of MRI has been the most important advance in the evaluation of patients with epilepsy in the last 20 years. MRI has consistently demonstrated superior sensitivity and specificity, in terms of identifying an epileptogenic cerebral lesion in children and adults, than CT scanning (McLachlan *et al.* 1985; Latack *et al.* 1986; Lesser *et al.* 1986; Kuzniecky *et al.* 1987; Heinz *et al.* 1990; Heinz *et al.* 1989). It is a non-invasive technique that acquires multiplanar anatomical and functional data without ionising radiation, thereby allowing comprehensive longitudinal studies to be performed and healthy control subjects to be scanned for comparison studies (Liu *et al.* 2001). X-ray CT may be preferable to MRI where patient access is an essential requirement such as if a patient is acutely unwell or agitated or where contraindications to MR scanning exist, for example, in patients with cardiac pacemakers, aneurysm clips or cochlear implants. It is also valuable in the investigation of possible acute intracranial haemorrhage or skull fracture, and in the investigation of suspected intracranial calcification which is not easily identified on MRI (Kuzniecky *et al.* 1993b).

The key clinical applications of MRI in epilepsy are to elucidate the aetiological basis of a patient's epilepsy including possible syndromic classification, and the identification of patients who are suitable for surgical treatment. The most common abnormalities identified on MRI in patients with focal epilepsy are hippocampal sclerosis (HS), malformations of cortical development (MCD), vascular malformations, tumours and acquired cerebral damage (Everitt *et al.* 1998; Li *et al.* 1995).

The optimum imaging protocol has not been universally established, however, should include whole brain T_1- and T_2-weighted sequences, with the minimum slice thickness technically possible. The acquisition of a volume dataset with slice thickness of 1.5 mm, and approximately cubic voxels, allows reformatting in any orientation and three-dimensional reconstruction to be undertaken. The use of gadolinium contrast enhancement may improve the conspicuity of certain specific abnormalities but is not routinely indicated (Cascino *et al.* 1989; Elster and Mirza 1991).

Ideally, MRI should be obtained in all patients with epilepsy, with the exception of those children with a

definite diagnosis of idiopathic generalized epilepsy. MRI is particularly indicated in patients with one or more of the following: (i) the onset of partial seizures at any age; (ii) the onset of generalized or unclassified seizures at less than 1 year old or in adulthood; (iii) evidence of a fixed neurological or neuropsychological deficit; (iv) difficulty obtaining seizure control with first line antiepileptic drugs; (v) loss of seizure control, or a change in the pattern of seizures (Commission on Neuroimaging of the International League Against Epilepsy 1997; 1998).

In those who are considered for epilepsy surgery, a more detailed imaging assessment is warranted. This should include a high resolution, volumetric, whole brain, T1-weighted acquisition in the oblique coronal plane, orthogonal to the long axis of the hippocampus. This provides optimal grey/white matter contrast and allows measurement of hippocampal volumes, three-dimensional reconstruction and surface rendering of the brain to be performed (see sections 1.3.1 Quantitative analysis of mesial temporal lobe structures, and 1.3.2 Neocortical post-processing techniques). Furthermore, the volumetric structural data may be co-registered with functional imaging information. In addition, oblique coronal proton density and heavily T2-weighted acquisitions should be taken, again orthogonal to the long axis of the hippocampus. The use of a dual or multiecho T2-weighted sequence allows hippocampal T2 relaxation times (HCT2) to be measured. Nulling of the signal from cerebrospinal fluid, using a fluid attenuated inversion recovery (FLAIR) imaging sequence may increase lesion conspicuity, particularly when adjacent to CSF (see section 1.2.2, FLAIR imaging)

The complete removal of a discrete epileptogenic lesion characterised on preoperative MRI is associated with a good seizure outcome postoperatively (Cascino *et al.* 1992; Jack, Jr. *et al.* 1992; Kuzniecky *et al.* 1993a; Williamson *et al.* 1992). Failure of preoperative MRI to define a cerebral lesion is associated with a poorer surgical outcome (Boon *et al.* 1991; Lorenzo *et al.* 1995). It is important to note, however, that following the identification of a structural abnormality, clinical and neurophysiological data are required to determine whether the lesion is the likely cause of the epilepsy.

Additional uses of preoperative MRI include the stereotactic placement of intracerebral recording electrodes, and as a basis for surgical guidance systems (Pillay *et al.* 1992). Routine postoperative imaging is also important, particularly in those patients with a poor post-operative outcome. The recognition of a surgical complication, or subtotal resection, may influence prognosis or long-term management strategies (Awad *et al.* 1991; Kitchen *et al.* 1993; Kitchen *et al.* 1994).

In summary, MRI has revolutionised the investigation and treatment of patients with epilepsy. As the spatial resolution of conventional MRI continues to improve, advanced sequences are developed and the sophistication of quantitative and post-processing techniques increases, the number of patients who have an undetermined basis for their epilepsy will diminish further. It is likely, however, that a proportion of patients will remain "MRI-negative" despite advances in imaging methods because either the lesion, such as a MCD or gliosis is too subtle, small or diffuse, or because the aetiological basis of the epilepsy is a biochemical / receptor abnormality or channelopathy (Scheffer *et al.* 1995; Mulley *et al.* 2003).

1.2.2 Fluid Attenuated Inversion Recovery prepared (FLAIR) imaging

Fluid Attenuated Inversion Recovery prepared (FLAIR) imaging was introduced in 1992 to overcome problems of the partial volume effect due to CSF encountered during heavily T2-weighted imaging (De Coene *et al.* 1992; Hajnal *et al.* 1992a; Hajnal *et al.* 1992b). The FLAIR sequence produces images which are T2-weighted but have the signal from CSF nulled. This is achieved by coupling an inversion pulse, followed by a long inversion time (TI), to a long echo time (TE). Nulling of the CSF results in a tissue abnormality becoming the brightest object in the images, thereby enhancing its conspicuity. In addition, in standard T2-weighted sequences, the length of the echo time is limited by increasing artefact and partial volume effects of CSF (De Coene *et al.* 1993). FLAIR imaging remains unaffected, which allows longer TEs to be used thereby increasing the T2-weighting of the images.

Early FLAIR sequences were limited by lengthy acquisition times due to long inversion and repetition times (TRs) required to both null CSF and allow adequate recovery of the signal from non-CSF tissues. Recent developments have focused on reducing the acquisition time to allow a more clinically applicable examination. This has been achieved by using the rapid acquisition with relaxation enhancement (RARE) readout in fast FLAIR (Rydberg *et al.* 1994), with interleaved inversion pulses in OIL FLAIR (Listerud *et al.* 1996), and with echo-planar imaging (Falconer and Narayana 1997; Tomura *et al.* 2002). Furthermore a 3D version of FLAIR which provides thin slices without an interslice gap has been developed (Barker 1998). This improves image resolution and allows the images to be reformatted in any plane for further analysis.

FLAIR sequences have been utilised in a number of conditions, both qualitatively and quantitatively (Bendersky *et al.* 2003). In multiple sclerosis, an increase in lesion volume was seen with the FLAIR sequence compared to conventional T2-weighted images. This was particularly pronounced in periventricular (Tubridy *et al.* 1998) and subcortical regions (Bastianello *et al.* 1997). In addition, it has been reported that the presence of hypointense lesions on FLAIR images is a strong predictor of disease severity (Rovaris *et al.* 1999).

This technique has also been shown to be useful in other multifocal cerebral diseases; for example, systemic lupus erythematosus (Jr *et al.* 2003), multiple metastases and lacunar infarcts. More accurate delineation of infiltrative white matter lesions (e.g. gliomatosis cerebri and lymphomas), an increase in both number and conspicuity of inflammatory or traumatic lesions, improved differentiation of cystic from necrotic cavities and precise characterisation of cortical damage in cerebral infarcts, have also been reported (De Coene *et al.* 1992; Arakia *et al.* 1999; Essig *et al.* 1998).

Patients with epilepsy have also been investigated with FLAIR imaging. Compared to conventional T2-weighted images, FLAIR imaging has been shown to increase the conspicuity of cerebral lesions, particularly in the hippocampus, amygdala, cortex and periventricular regions (Bergin *et al.* 1995; Jack, Jr. *et al.* 1996; Meiners *et al.* 1999a; Morioka *et al.* 1998; Taillibert *et al.* 1999; Takanashi *et al.* 1995; Van Paesschen *et al.* 1996; Wieshmann *et al.* 1998a). FLAIR does not however improve the identification of heterotopias and variable suppression of CSF in mesial temporal lobe structures may erroneously suggest the presence of hippocampal sclerosis in normal subjects (Wieshmann *et al.* 1996).

Hippocampal relaxometry using conventional T2-weighted sequences is prone to partial volume effects from surrounding CSF, particularly in the presence of hippocampal atrophy. Elevated T2 times in a quantitative assessment of hippocampal sclerosis may therefore be due to CSF contamination rather than parenchymal changes.

To address this issue, FLAIR imaging was combined with dual-echo T2 relaxometry in a quantitative assessment of patients with hippocampal sclerosis. Both conventional spin echo and FLAIR imaging identified abnormal relaxometry in the same patients suggesting that the cause of signal change in hippocampal sclerosis imaged with T2-weighted sequences is unlikely to be due to CSF contamination (Woermann *et al.* 2001).

1.2.3 Magnetic Resonance Spectroscopy

In vivo magnetic resonance spectroscopy (MRS) permits the evaluation of brain biochemistry non-invasively. The resonance frequency of a nucleus provides chemical information which may be displayed as a spectrum of signal intensity against frequency, in which the area under the trace indicates amplitude of the signal at that frequency. Only nuclei with an odd number of protons resonate. Both ^{1}H and ^{31}P are present in sufficient concentration to be detectable in the brain in vivo. Dynamic investigations using ^{13}C allow measurement of glucose transport, oxidation, glutamate turnover and glutamine synthesis in vivo (van Zijl and Rothman 1995; Gruetter *et al.* 1992). Carbon 13 is much less abundant so compounds labelled with ^{13}C must be administered to subjects for studies to be performed.

^{31}P MR spectroscopy provides information about the energetic status of the brain by measuring the intracerebral concentration of phosphocreatine (PCr), adenosine triphosphate (ATP), phosphomonoesters (PME), phosphodiesters (PDE) and inorganic phosphate (Pi). In addition, intracellular pH can be directly determined on the basis of the value of the chemical shift of the Pi signal. However, despite the potential wealth of information available, ^{31}P MRS lacks sensitivity, resulting in limited spatial resolution (minimum voxel size 60cm^3) and/or poor temporal resolution with a large number of scans required to achieve adequate signal-to-noise ratio. The MRI sensitivity of the ^{1}H nucleus is about 14 times that of ^{31}P. As a consequence, metabolic profiles can be obtained from regions of the brain as small as 1ml in volume. ^{1}H MR spectroscopy examines the energetic metabolism of a tissue by quantifying the creatine/phosphocreatine signal (tCr), measures the neuronal status with N-acetyl aspartate (NAA) signal, assesses membrane integrity and turnover based on choline-containing compounds, and detects the presence of anaerobic glycolysis with markers such as lactate (Lac). Depending on the parameters used in the acquisition of spectra, for example, short echo time or editing methods, it is also possible to assess the glial cell integrity by quantifying the inositol signal (INS), to monitor the concentration of neurotransmitters, such as glutamate/glutamine (Glx) and γ-aminobutyric acid (GABA), and to observe inflammatory and degenerative processes through the variations in the concentration in macromolecules and mobile lipids.

There are two methods for acquiring metabolic spectra. The first is using a single voxel technique in which the data are acquired from a single volume of interest (minimum volume of 1ml for proton spectroscopy and approximately 60ml for ^{31}P spectroscopy). Constraints of acquisition time limit the metabolic spatial coverage of the brain. This is important in focal pathologies where accurate a priori data on the location of the cerebral lesion, such as an epileptogenic focus, are therefore required. The second method, which circumvents this limitation, is spectroscopic imaging or chemical shift imaging (CSI). This technique allows the acquisition of several contiguous voxels by phase-encoding a large region of interest in one, two, or three spatial dimensions, as is done for the water signal in conventional MRI. The spatial distribution of a selected metabolite can be displayed as a metabolic image, which can be superimposed onto the anatomical MR image. The signal-to-noise ratio of metabolite maps is

low relative to conventional MR images, but sufficient to detect regions exhibiting abnormal metabolism. Limitations of this method include distortions resulting from a non-static field and radiofrequency inhomogeneities across the large volume, and contamination from neighbouring voxels.

The earliest MRS studies in epilepsy focused on changes during status epilepticus (SE). An increase in lactate was seen in the brains of rabbits following bicuculline-induced SE (Petroff *et al.* 1984) and in humans, Matthews et al. reported reduced NAA in two patients with Rasmussen's encephalitis and focally reduced lactate in a patient with epilepsia partialis continua (Matthews *et al.* 1990). Similarly, increased glutamate and/or glutamine have been reported in a patient with partial SE (Fazekas *et al.* 1995). Most of the MRS studies in epilepsy undertaken during the last 10 years have focused on temporal lobe epilepsy (TLE). The main objective of these studies has been to determine lateralisation of a seizure focus prior to surgical resection. In patients with TLE, interictal ^{31}P MRS has disclosed increased inorganic phosphate and pH, reduced phosphomonesters (PME) and unchanged ATP in the affected lobe (Hugg *et al.* 1993; Kuzniecky *et al.* 1992; Younkin *et al.* 1986). It has been suggested that a decrease in PME may reflect altered metabolism associated with neuronal loss and glial proliferation (Hugg *et al.* 1993), and an increase in pH may be the consequence of buffering in response to repeated acidotic episodes associated with seizures (Hugg *et al.* 1993). Proton MRS has shown abnormalities of NAA signal in 99% of cases of TLE, concordant with quantitative amygdala-hippocampal volumetry and EEG (Cendes *et al.* 1997). Similarly, reduced NAA and increased choline-containing compounds and CR were seen in the epileptogenic temporal lobe in 22 out of 25 patients with well-defined TLE (Connelly *et al.* 1994), and most recently, reduced myo-inositol has also been identified (Mueller *et al.* 2003). Reduced NAA is thought to reflect neuronal damage or loss, or altered mitochondrial metabolism (Urenjak *et al.* 1992; Petroff *et al.* 1995a), while the increase in choline and total creatine concentrations have been related to gliosis (Urenjak *et al.* 1993). An in-vitro study of the metabolic composition of resected hippocampi recently revealed no significant associations between hippocampal neuron loss and the cellular content of NAA, glutamate, GABA, glutamine, or aspartate. A significant association between hippocampal NAA and glutamate content was seen however, suggesting that increased intracellular glutamate content or increased glutamatergic neurons may contribute to the epileptogenic nature of hippocampal sclerosis (Petroff *et al.* 2002).

Metabolic abnormalities have also been detected with proton MRS in MRI-negative TLE patients, thereby conferring additional sensitivity over conventional MR techniques. In particular, the NAA/ (choline+CR) ratio was found to be abnormal in five out of seven MRI-negative patients (Connelly *et al.* 1998), and in a study conducted with quantitative short echo time single voxel proton spectroscopy, 27% of patients had reduced NAA ispilateral to clinical and electrophysiological lateralisation of the TLE (Woermann *et al.* 1999c). In a CSI study of 10 patients with TLE, one patient with a reduced NAA/CR ratio had normal hippocampal appearance on conventional MRI, yet had mild mesial temporal sclerosis on histopathological examination of the surgically resected region (Cendes *et al.* 1994). In a study of 48 children who had temporal lobe resections, abnormal ^{1}H-MRS on the unoperated side was not identified as a prognostic indicator for the occurrence of seizures postoperatively. However, patients with right temporal lobe resections who also had abnormal MRS in the left temporal lobe had verbal memory deficits postoperatively suggesting that MRS data may be a useful indicator of functional integrity (Incisa della Rocchetta *et al.* 1995). The metabolic profiles of patients with hippocampal sclerosis (HS) and MRI-negative TLE patients differ significantly. MRI-negative patients are characterised by an increase in glutamate/glutamine signal and less marked reduction in NAA than patients with HS (Woermann *et al.* 1999c). Additionally, the extent of HS

correlates with increased inositol concentrations observed on short echo time proton MR spectra (Woermann *et al.* 1999c; Tossetti *et al.* 1998). Recently, Simister et al used short-echo-time MRS to evaluate the variation of metabolite concentration throughout the temporal lobes of patients with HS or normal conventional MRI. Low NAA, Cr, and Cho were found in the anterior sclerotic hippocampus and low NAA, although less frequently than in the patients with HS, was observed in the MRI-negative group in the middle mesial temporal lobe region. Furthermore, glutamate / glutamine was elevated in the anterior voxel, contralateral to seizure onset in the MRI-negative group (Simister *et al.* 2002).

The increasing use of MRS in extratemporal epilepsy has arisen as a direct result of methodological improvements in CSI. This is because the absence of prior knowledge regarding the precise location of the seizure focus necessitates examining a larger volume of tissue. Using ^{1}H CSI in patients with MRI-negative extratemporal epilepsy, it has been shown that the relative NAA resonance intensities (NAA/phosphocreatine plus creatine (CR), NAA/choline-containing metabolites (choline) and NAA/CR + choline), were all significantly reduced compared to control subjects. Furthermore, reduction of the NAA ratios were greater in the epileptogenic region as compared with the non-epileptogenic regions, as defined by EEG recordings (Stanley *et al.* 1998). Similar results were reported in eight patients with frontal lobe epilepsy, in whom the NAA/CR ratio was lower by 27% in the epileptogenic frontal lobe compared to the normal contralateral lobe (Garcia *et al.* 1995c). Simister et al recently reported elevated GLX (glutamine + glutamate) and normal NAA and GABA in the occipital lobes of patients with cryptogenic occipital lobe epilepsy, consistent with earlier reports that elevated GLX is present in regions of seizure onset (Woermann *et al.* 1999c). Extratemporal regions have also been evaluated in patients with mesial TLE. Reduced NAA in ipsi- and contralateral frontal grey and non-frontal white matter was demonstrated suggesting more widespread structural or functional abnormalities than suggested by conventional MRI (Mueller *et al.* 2002). Local extension of metabolic abnormalities was reported by Guye et al in a study of patients with various subtypes of TLE. NAA/choline+creatine ratio was significantly lower in all regions associated with epileptiform EEG activity compared to controls, irrespective of the boundaries of any structural lesion. No differences between the metabolic profiles of epileptogenic and irritative zones were found (Guye *et al.* 2002). A reduction of thalamic NAA/Cr has been demonstrated in patients with idiopathic generalized epilepsy (IGE), with a significant negative correlation between thalamic NAA/Cr and duration of epilepsy, irrespective of the amount of spike-wave activity (Bernasconi *et al.* 2003a). Using short echo time MRS, GABA and glutamate were quantified in the occipital lobes of patients with photosensitive IGE. Both GABA and glutamate were elevated, however, increased grey matter concentration in the IGE group may account for a significant proportion of this change (Simister *et al.* 2003).

Investigating patients with extratemporal lobe epilepsy using ^{31}P CSI has shown interictal alkalosis and decreased phosphomonoesters in the epileptogenic region in the majority of patients (Garcia *et al.* 1995b).

Correlative studies using MRS and PET have shown a relationship between decreased NAA/ (Choline+CR) ratio and decreased interictal glucose metabolism in patients with TLE (Lu *et al.* 1997), indicating that MRS abnormalities are associated with concomitant quantitative abnormalities of local glucose utilisation. In addition, an increase in GLX has been observed in the epileptogenic focus located by ^{11}C flumazenil and ^{18}FDG PET (Savic *et al.* 1996; Savic *et al.* 1998a). In a comparative study of MRS, FDG-PET, hippocampal volumetry and T2 relaxometry in patients with temporal lobe epilepsy and normal conventional MRI, FDG-PET was found to be the most sensitive imaging modality, with 87% concordance with EEG data. NAA/ (Choline + CR) and NAA

concurred with EEG data in 61% and 57% of the patients respectively. Only unilateral hippocampal atrophy, assessed quantitatively, was predictive of seizure freedom post-operatively (Knowlton *et al.* 1997).

GABA is the major inhibitory neurotransmitter in human cortex and changes in its metabolism may play an important role in the origin, spread and cessation of seizure activity. The detection of GABA by MRS is demanding however, due to its low concentration and the overlapping of its resonance with those of CR and NAA. However, like lactate, glutamate and glutamine, GABA displays J-modulation which may be exploited by spectral editing, thereby allowing the signal from GABA to be quantified accurately (Rothman 1999). There have been many studies measuring levels of GABA and homocarnosine 2-pyrrolidinone (a lactam resulting from the cyclisation of GABA) using MRS (Rothman *et al.* 1997; Rothman *et al.* 1993; Hetherington *et al.* 1998; Petroff *et al.* 1996c), in particular observing increased brain GABA induced by a number of anti-epileptic drugs, such as topiramate (Kuzniecky *et al.* 1998; Petroff *et al.* 1999b), vigabatrin (Verhoeff *et al.* 1999; Petroff *et al.* 1995b; Petroff *et al.* 1996b; Petroff *et al.* 1999a; Novotny Jr. *et al.* 1999; Weber *et al.* 1999; Petroff *et al.* 1998) and gabapentin (Petroff *et al.* 1996a). It is possible that in the future, ^{1}H-MRS investigations of neurotransmitters might assist in the initial selection and monitoring of the effect of anti-epileptic therapy, and aid localisation of a seizure focus prior to more invasive investigations and possibly epilepsy surgery.

Monitoring of anti-epileptic therapy is also possible using ^{31}P CSI. A small but significant improvement in energy metabolism, assessed using ratios of PCr/(g-ATP) and PCr/Pi, was seen in seven patients with intractable epilepsy on a ketogenic diet (Pan *et al.* 1999).

Proton CSI has been combined with diffusion tensor imaging (DTI) and EEG-triggered functional MRI (fMRI) in the study of a patient with a large subcortical heterotopic nodule. The area with the lowest concentration of NAA also had the highest mean diffusivity but was distinct from the area of fMRI activation. This suggests that although DTI and MRS are sensitive in identifying abnormal cerebral structure in patients with epilepsy, the actual epileptogenic focus may be located elsewhere (Krakow *et al.* 1999a). This is further confounded by the knowledge that the origin of interictal epileptiform activity (the irritative zone), as identified by EEG-triggered fMRI, may itself be distant to the seizure onset zone. Ictal intracranial EEG recordings may provide a means to resolve this issue.

In summary, MRS investigations currently provide clinically useful information in the investigation of temporal and extratemporal lobe epilepsy. It is likely that further work will contribute to a better understanding of the clinical significance and reliability of MRS abnormalities when lateralising data from other investigations, such as imaging, electrophysiological and psychological testing, are discordant. In addition, the prognostic implications of MRS abnormalities need to be clarified further. Future studies, particularly focusing on the evaluation of neurotransmitters, and improvements in both imaging hardware and post-acquisition processing, are likely to have significant consequences for both the investigation and treatment of patients with epilepsy.

1.2.4 Functional MRI

Early studies of functional MRI (fMRI) applied to epilepsy used phase mapping techniques (Fish *et al.* 1988) and dynamic contrast enhancement with gadolinium (Warach *et al.* 1994) to demonstrate abnormal blood flow in epilepsia partialis continua. Technical advances in MRI acquisition and post-processing have enabled cerebral activity, causing changes in regional blood flow and volume, to be monitored indirectly through the effects of changing deoxyhaemoglobin concentration (Ogawa *et al.* 1993). This is termed the blood oxygen level-dependent (BOLD) effect, and is analogous to the results obtained with blood flow tracers and PET, but with improved temporal resolution.

Localisation of ictal blood flow changes using this technique was first described in 1994 in a 4 year old child with frequent right-sided motor seizures (Jackson *et al.* 1994b). Each clinical seizure was accompanied by increased MR signal intensity in the left hemisphere. In addition, abnormal signal was observed in-between clinically apparent seizures suggesting that the method was sensitive to detect subclinical electrical activity. Subsequently, an fMRI study of a similar patient by Detre et al. produced identical results (Detre *et al.* 1995). Neither of these studies, however, used concurrent EEG monitoring to determine seizure activity. It has been shown that the EEG can be recorded inside an MR scanner with sufficient quality to detect high amplitude discharges and to trigger fMRI acquisitions after these events (Ives *et al.* 1993; Warach *et al.* 1996), however, safety issues (Lemieux *et al.* 1997) and imaging artefacts on the EEG initially precluded its wider application (Huang-Hellinger *et al.* 1995). Recent advances, particularly on-line subtraction of pulse (Allen *et al.* 1998) and scanner artefact (Allen *et al.* 2000) have allowed continuous fMRI data acquisition without obscuration of the EEG, thereby allowing accurate temporal correlation of epileptiform abnormality with imaging data (Allen, Josephs, and Turner 2000).

In a study of 10 patients with well-defined focal epilepsy, investigated with EEG-triggered fMRI, six showed reproducible focal changes of the BOLD signal which concurred with localising electroclinical data (Krakow *et al.* 1999b). Case reports using this technique have also detected electroclinically concordant fMRI activations associated with interictal epileptiform discharges (Seeck *et al.* 1998; Symms *et al.* 1998). Limitations of these studies include the restricted application to only those patients with relatively frequent interictal epileptiform discharges (approximately one event per minute), the assumption that there is close anatomical correlation between the area of cortex that generates interictal spikes and the ictal onset zone which initiates seizures (Ebersole and Wade 1991; Luders *et al.* 1996), and the difficulty in distinction between cortical regions that generate discharges and regions which are sequentially activated within fractions of a second. Pathological validation and studies of surgical outcome in patients with focal fMRI activations and correlation with ictal onset zones shown with intracranial EEGs are required. Most recently, a patient with idiopathic generalized epilepsy and frequent absences was studied with EEG-fMRI. Runs of generalized spike-wave discharge were associated with bilateral thalamic activation and widespread cortical deactivation demonstrating the reciprocal participation of focal thalamic and widespread cortical networks during human absence seizures (Salek-Haddadi *et al.* 2003).

A further important application of fMRI in epilepsy is in the delineation of areas of the brain responsible for specific functions, such as the primary motor and sensory cortex, and possibly language and memory loci. In particular, to identify their anatomical relation with respect to an area of planned neurosurgical resection, thereby allowing a more targeted resection while minimizing postoperative morbidity (Hammeke *et al.* 1994; Morris, III *et*

al. 1994; Jack Jr. *et al.* 1994; Puce *et al.* 1995; Morioka *et al.* 1995; Macdonell *et al.* 1999; Holloway *et al.* 1999; Schwartz *et al.* 1998; Rao *et al.* 1995). Bookheimer et al reported the postoperative outcomes of six patients with cortical lesions who had preoperative fMRI mapping of motor and visual areas. In three patients, the neurosurgical procedure was modified based on the fMRI results and, in each case, there was no postoperative deficit. In one patient, there was no overlap between the proposed resection and functional activation zone. In two patients, "functional" tissue was resected with the lesions and, as predicted, postoperative deficits were seen in both (Bookheimer *et al.* 1995). Recently, activations within regions of cerebral dysgenetic tissue have been observed during simple and complex fMRI paradigms. In particular, disturbances of cortical organisation, such as polymicrogyria and schizencephaly, showed greater activation than in MCDs caused by disturbances of early cortical development, such as heterotopia and Taylor-type FCD. This permits a greater understanding of the functional connectivity of MCD and, in particular, their relationship to eloquent cortex (Janszky *et al.* 2003).

The intracarotid amytal examination, also known as the Wada test (Wada and Rasmussen 1960) is used to determine lateralisation of speech and adequacy of contralateral memory functions in patients undergoing presurgical evaluation. However, the invasive nature of this examination carries a small risk of morbidity and, in addition, may be hampered by technical limitations, such as incomplete amytal perfusion of the posterior portion of the hippocampus resulting in an inadequate evaluation (Rausch and Risinger 1990). Several studies have used fMRI in normal volunteers to demonstrate lateralised language activation with a variety of paradigms (Cuenod *et al.* 1995; McCarthy *et al.* 1993; Rueckert *et al.* 1994; Binder *et al.* 1995). In patients with epilepsy, a number of studies have compared fMRI with Wada testing and found it to be equally discriminating in determining hemispheric dominance (Desmond *et al.* 1995; Binder *et al.* 1996; Bahn *et al.* 1997; Bazin *et al.* 2000; Hertz-Pannier *et al.* 1997; Woermann *et al.* 2003; Adcock *et al.* 2003). Moreover, preoperative fMRI was as effective as Wada testing in predicting significant language decline post-operatively (Sabsevitz *et al.* 2003)

A more difficult challenge for fMRI is to replace the Wada test in determining memory lateralisation. Complex neuroanatomical circuits involving a specific system of related neocortical (frontal and temporal) and medial temporal brain regions mediate memory function (Scoville and Milner 2000; Kapur *et al.* 1992; Tulving *et al.* 1994; Buckner *et al.* 1996) and hence the development of a paradigm to specifically activate these regions is complicated. In particular, the principle of a resting state with which to compare against an active state is difficult to conceptualise.

Despite these concerns there have been a number of fMRI studies that have demonstrated medial temporal lobe activation in control subjects using paradigms testing encoding and retrieval of information (Stern *et al.* 1996; Bookheimer *et al.* 1996a; Bookheimer *et al.* 1996b; Schacter and Wagner 1999). It is of note, however, that Bookheimer et al were unable to demonstrate activations when comparing active against control/resting state but only when correlating signal intensity with memory load (Bookheimer *et al.* 1996a; Bookheimer *et al.* 1996b). This is a similar finding to a PET study by Grasby et al which found increasing cerebral blood flow in the hippocampus according to the number of items memorised and recalled (Grasby *et al.* 1993). A recent fMRI study of seven patients with left temporal lobe epilepsy comparing resting against an active state of memory demonstrated bilateral parahippocampal activation (right greater than left) in both control subjects and patients. Furthermore, the patient group also exhibited consistent and extensive left prefrontal activation in all memory tasks. This was possibly as a result of a reallocation of cognitive function or recruitment of additional cortical areas in response to the demands of the task not met by dysfunctional temporal lobe regions. It was suggested that this

may be interpreted as a dysfunctional response to the epilepsy and left hippocampal sclerosis (Dupont *et al.* 2000).

It is important to note when comparing fMRI to the Wada test that each test obtains information differently. The Wada test uses inactivation, and therefore provides information only on the functional reserve of the remaining cerebral tissue. Functional MRI identifies regions in a neural network involved in a successful task performance. There is a potential risk therefore, of attributing function to areas that are active in, but not necessarily critical to a particular task performance. Furthermore, there is no evidence that areas that are not activated in fMRI studies are not involved in the performance of the task.

In summary, studies of EEG-correlated functional MRI have reported meaningful and potentially clinically useful information regarding the localisation of seizure foci in selected groups of patients with epilepsy. However, unequivocal validation of the technique is lacking because of a deficiency of either histopathological data or studies of surgical outcome in these patients. Using fMRI to investigate "eloquent" cortex in patients prior to resective surgery to enable a more targeted surgical approach and thereby attempt to reduce postoperative morbidity has shown promising results in individual case reports and small series studies. Larger studies are required, however, to substantiate this evidence and allow fMRI to become more widely utilised in this domain. Investigating hemispheric dominance of language with fMRI has demonstrated consistent agreement with Wada testing in a large number of studies suggesting that the lateralisation of language component of Wada tests could be replaced by fMRI. The investigation of memory using fMRI is currently in its infancy and further work is required, particularly in the development of robust, reproducible and targeted paradigms which will allow clinically useful information to be obtained.

1.2.5 Diffusion Imaging

1.2.5.1 Theory

Diffusion, also known as Brownian Motion, is a random process which results from the thermal translational motion of molecules. In a homogeneous fluid without boundaries, the distance a molecule diffuses can be modelled as a "random walk" with a Gaussian distribution. The average distance l that molecules travel in time t in a given medium is described by the Einstein equation where motion in three dimensions is considered (Einstein A 1905).

$$l^2 = 6Dt$$

D is a proportionality constant known as the *diffusion coefficient*. It is essentially a measure of mobility at the molecular level and varies with both viscosity and temperature of the substance. For pure water at 37°, $D = 3.4 \times 10^{-3}$ mm^2/s. In biological systems however, the diffusing medium is not of infinite extent, and molecular diffusion is restricted by intra- and extracellular boundaries. On very short time scales, the molecules diffuse as if they were in a homogeneous medium, however, over progressively longer times the chance of a molecule encountering a boundary and therefore being hindered increases. The diffusion coefficient therefore is no longer simply a property of the diffusing medium and an alternative term is used, the *apparent diffusion coefficient (*ADC) which is

dependant on the time interval over which the diffusion is measured (T_d). The nature of the restricting boundaries in terms of spacing, permeability and orientation govern the relationship between ADC and T_d, however, in general, ADC is smaller than the unrestricted value of D and decreases from a value close to D for values of T_d near zero to a small limited value as T_d approaches infinity. Variation in the pulse direction and timing in the diffusion sensitive imaging sequence can therefore be used to selectively reveal highly restricted diffusion in one direction within a tissue whilst retaining less restricted diffusion within other directions. This is the basic contrast mechanism of diffusion imaging.

Values for ADC in human tissue range from ~0.2 x 10^{-3} to 2.9 x 10^{-3} mm^2/sec. and are dependant on the type and, in white matter, the orientation of the cerebral tissue (Pierpaoli *et al.* 1996; Hajnal *et al.* 1991). The diffusion displacement distances are comparable to cellular dimensions. Water molecules, if unrestricted, will typically diffuse in any given direction through a distance of 20 micrometres in 100 msecs, or through 60 micrometres in 1 second, raising the possibility that the measurement of water diffusion might provide a means of probing cellular integrity and pathology. In particular, if cellular components impede the diffusion of water molecules then any disruption to these structures might influence the degree of restriction and hence typical diffusion distances.

1.2.5.2 Development of diffusion imaging

In routine MRI, diffusion effects contribute relatively little to overall signal intensity, causing signal attenuation of no more than 2%. However, images that are sensitive to the diffusional properties of water can be obtained by incorporating pulsed magnetic field gradients into a standard spin echo sequence. As the diffusing protons traverse intrinsic and extrinsic magnetic field gradients, they experience unrecoverable phase shifts resulting in a loss of T2 signal. This signal attenuation depends on the pulse sequence applied but in general has the form of an exponential decay

$$(\exp(-k\,D\,G^2\,TE^3))$$

where $\boldsymbol{k}$ is a constant, $\boldsymbol{G}$ is the amplitude of the gradient pulses and $\boldsymbol{TE}$ is the echo time. The natural logarithm of the attenuated signal is compared with the degree of diffusion weighting (gradient b factor) on a pixel-by-pixel basis to calculate a diffusion map. This represents the spatial distribution of diffusion coefficients for the imaged object, where bright areas represent increased diffusion (i.e. maximal signal attenuation) and dark areas represent regions of decreased diffusion. These maps are independent of T1- and T2-relaxation.

1.2.5.2.1 Diffusion-weighted imaging

Early measurements of diffusion employed a Hahn spin echo collected in the presence of an applied constant gradient (Hahn 1950). This method however, undesirably linked the contrasts due to restricted diffusion and T2 relaxation. In 1965, Stejskal and Tanner introduced a pulsed gradient spin echo (PGSE) technique, in which sensitivity to diffusion was produced by gradient pulses placed on either side of the 180° refocusing pulse (Stejskal

and Tanner 1965). This sequence offered a number of advantages. In particular, the contrasts of diffusion and T2 were uncoupled, the diffusion weighting could be manipulated without affecting other sequence properties such as slice thickness and voxel size, and an estimation of the diffusion time and hence apparent diffusion coefficients could be made more accurately. The suggestion that it was theoretically possible to combine diffusion pulsed gradient experiments and Fourier NMR imaging was raised by Mansfield in 1982 (Mansfield and Morris 1982a), and studies of the effect of diffusion on conventional MR images was investigated by Wesbey in 1984 (Wesbey *et al.* 1984). The earliest diffusion-weighted images were obtained in 1985 by applying diffusion sensitising gradients to spin echo (Taylor and Bushell 1985) and later to stimulated echo imaging sequences (Merboldt *et al.* 1991).

Diffusion-weighted imaging using the pulsed gradient spin echo technique (PGSE) has been extensively utilised in the investigation of both normal and pathological states (Hajnal *et al.* 1991; Doran *et al.* 1990). Less commonly used methods of diffusion imaging include stimulated echo, gradient echo and B1 field gradients (LeBihan and Basser 1995). Early diffusion studies of white matter in normal subjects reported ADC values which were particularly dependant on the orientation of the sensitising diffusion gradients to the tracts examined, so that ADC values of ~0.5 x $10^{-3}mm^2/s$ or ~1.0 x $10^{-3}mm^2/s$ were obtained with the gradients transverse or parallel to the white matter fibres respectively (Turner and LeBihan 1990; Larsson *et al.* 1990; Hajnal *et al.* 1991). This finding introduced the concept of directionality to diffusing molecules, also known as *anisotropy*. This property is encountered if the restriction to diffusion within a biological system is asymmetrical, so that the molecular mobility is impeded in certain directions but free in others (Basser 1995).

Classically, diffusion-weighted imaging used the ratios of ADCs obtained by diffusion sensitising gradients being applied in two or three mutually perpendicular directions to evaluate the anisotropic property of a tissue. This resulted in *rotationally variant* indices where the calculated ADC was dependant on the orientation of the subject to the gradients (Basser *et al.* 1994b). Fibre tracts that lie parallel to an applied gradient exhibit the greatest ADC whereas those lying oblique or transverse to a gradient possess a reduced ADC. In biological systems, for example the brain, tracts often follow tortuous paths resulting in a single tract during its course at times lying parallel and at times oblique to the gradient. This results in an erroneous variation of the anisotropic value in an individual tract during its course or underestimation of anisotropy in a whole tissue if it lies oblique to the diffusion sensitising gradients (Pierpaoli and Basser 1996). In addition, the method is sensitive to subject repositioning within the scanner so that minor alterations of head orientation with respect to the gradients result in inconsistent values of ADC.

Different scalar indices derived from diffusion-weighted images have been used to characterise diffusion within tissues. A quantity that is independent of fibre or tract orientation is the average ADC (ADC_{av}) as defined by:

$$\mathbf{ADC_{av}} = \frac{(\mathbf{ADC_x} + \mathbf{ADC_y} + \mathbf{ADC_z})}{3}$$

where x, y, z are the orthogonal directions of the diffusion measurements.

An estimation of diffusion anisotropy using diffusion weighted imaging has previously been made in a number of ways, for example, using the ratio of the differences and sums of diffusion weighted images, using the ratio of two ADCs with diffusion sensitising gradients applied to two perpendicular directions, or by using the standard deviation of the three mutually perpendicular directions, divided by their mean value (Douek *et al.* 1991; van Gelderen *et al.* 1994; Matsuzawa *et al.* 1995). In each case however, the anisotropy measures are not quantitative. The diffusion weighted image contrast does not correspond to a single meaningful variable but rather a complicated combination of a number of parameters including both diffusion and T2 "shine-through" effects.

1.2.5.2.2 Diffusion Tensor Imaging

To overcome the problems of characterising diffusion in anisotropic, heterogeneously orientated tissues, diffusion tensor imaging (DTI) was developed (Basser *et al.* 1994a; Basser, Mattiello, and LeBihan 1994a). In contrast to earlier estimations of anisotropy using diffusion sensitising gradients applied in two or three mutually perpendicular directions, diffusion weighting in DTI is applied in at least six directions. This allows *rotationally invariant* parameters to be calculated and thus corrects for any orientation bias.

If a small drop of dye is placed in a large quantity of a homogeneous fluid, over time by a process of diffusion the molecules spread out equally in all directions to create an expanding sphere. In biological systems, for example the brain, this shape or *ellipsoid* is dependant on restricting boundaries. In axonal pathways, diffusion is less restricted parallel to, rather than perpendicular to, the main fibre axis (Neil 1997). This yields an eccentric or elongated, cigar-shaped ellipsoid with the long axis parallel to the fibre tract. The more eccentric or elongated the shape, the greater the anisotropy. This ellipsoid can be described mathematically as a diffusion tensor ($\underline{\mathbf{D}}$) and to be fully determined requires diffusion weighting to be applied in at least six directions (xx, xy, xz, yy, yz, zz) (Basser 1995; Conturo *et al.* 1996). A seventh image is also acquired with no diffusion weighting which is used to eliminate T2-weighted effects from the final diffusion image.

$$\underline{\mathbf{D}} = \begin{pmatrix} D_{xx} & D_{xy} & D_{xz} \\ D_{yx} & D_{yy} & D_{yz} \\ D_{zx} & D_{zy} & D_{zz} \end{pmatrix}$$

Although the diffusion tensor for each voxel ($\underline{\mathbf{D}}$) is described by nine individual diffusion constants, water diffusion is equal in exactly opposite directions, that is, the tensor is symmetrical ($D_{xy} = D_{yx}$). There are, therefore, only six independent terms (D_{xx}, D_{xy}, D_{xz}, D_{yy}, D_{yz}, D_{zz}). These are determined from the amount of signal attenuation during the application of the diffusion gradients in each of the six directions. When the diffusion tensor is diagonalised, the *eigenvectors* and *eigenvalues* are obtained. The eigenvectors represent the three mutually perpendicular directions along which the molecular displacements appear uncorrelated (ε_1, ε_2, ε_3), while the eigenvalues represent the magnitude of the diffusivities along these directions. These values can be sorted in order of decreasing magnitude ($\lambda_1 > \lambda_2 > \lambda_3$). In anisotropic tissues organised into parallel bundles, the largest eigenvalue, λ_1, represents the diffusion coefficient in the direction parallel to the fibres in each voxel, while λ_2 and

λ_3 are the transverse diffusion coefficients.

The distinct shape of diffusion ellipsoid is governed by the local architecture of fibre tracts and bundles. Several possibilities exist in cerebral tissue:

$\lambda_1 = \lambda_2 = \lambda_3$ - this is the typical distribution of the eigenvalues expected in a medium in which diffusion is isotropic at a microscopic level; for example, free water or cerebrospinal fluid. However, it is also possible that anisotropy exists at a molecular level but is randomly orientated and therefore appears isotropic at the voxel level, for example, when white matter fibres cross in a symmetrically spherical pattern.

$\lambda_1 >> \lambda_2 = \lambda_3$ - this configuration corresponds to a cigar-shaped diffusion ellipsoid that is cylindrically symmetrical. This is consistent with the arrangement of white matter fibres in parallel bundles with their longitudinal axis aligned with ε_1, the eigenvector associated with λ_1.

$\lambda_1 > \lambda_2 > \lambda_3$ - this corresponds to an asymmetric diffusion ellipsoid whose major axes are all unequal. In general, this suggests the presence of fibres that run in multiple directions within the voxel but that maintain on average a preferential direction. This is the most likely arrangement in cerebral tissue.

A set of quantitative rotationally invariant parameters can be calculated from the product of the diffusion tensor which characterise diffusion isotropy and anisotropy, and fibre-tract organisation. These parameters include: *mean diffusivity* which is used to measure the orientationally averaged diffusivity (figure 1.1), and *fractional and relative anisotropy, volume ratio and lattice anisotropy index* which measure the degree of directionality of the diffusion (Pierpaoli and Basser 1996; Basser and Pierpaoli 1996) (figure 1.2).

Mean diffusivity is independent of the position and orientation of the patient within the magnetic field.

$$\text{mean diffusivity} = \frac{\text{Trace}(\underline{D})}{3} = \frac{\lambda_1 + \lambda_2 + \lambda_3}{3}$$

Intrinsically, mean diffusivity has a lower background noise level than an individual ADC and is highly uniform throughout normal brain parenchyma within the same subject, as well as between age-matched subjects (Pierpaoli *et al.* 1996). These factors make mean diffusivity a desirable diagnostic parameter since small deviations from the normal value are statistically significant. Consequently it may be possible to detect more subtle changes in mean diffusivity in patients.

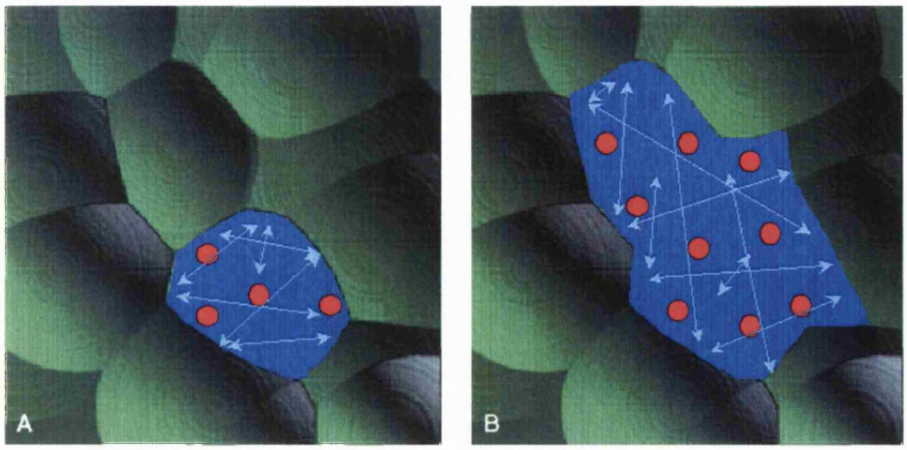

Figure 1.1: A diagram illustrating the principle of mean diffusivity in a biological system. Image A represents normal extracellular space with relatively restricted diffusion of water molecules (red circles). Image B shows expansion of the extracellular space. The water molecules are able to diffuse further during the same time period, and will be subject to greater signal loss during a diffusion weighted scan.

A number of indices may be calculated to determine anisotropy within cerebral tissue (figure 1.2). The simplest of these is an anisotropy ratio, for example, λ_1 / λ_3, which measures the relative magnitudes of the diffusivities parallel and transverse to the fibre tract. However these require the eigenvalues to be sorted in order of magnitude and this introduces a systematic sorting bias which artificially overestimates the anisotropy. To overcome this bias, indices insensitive to eigenvalue sorting such as *relative* and *fractional anisotropy* were developed (Basser and Pierpaoli 1996).

Relative anisotropy (RA) is a measure of the anisotropic component of the tensor divided by the magnitude of the isotropic part; it is therefore quantitative and dimensionless. For an isotropic medium, RA = 0 and increases as the anisotropic component of the tensor becomes greater. Alternatively *fractional anisotropy* (FA) may be used which measures the fraction of the magnitude of the tensor that we can ascribe to anisotropic diffusion. Like RA, it is quantitative and dimensionless. For an isotropic medium, FA = 0 and for a cylindrically symmetrical medium ($\lambda_1 >> \lambda_2 = \lambda_3$), FA = 1.

Other anisotropic indices include volume ratio and lattice index (Pierpaoli and Basser 1996). The volume ratio represents the volume of an ellipsoid whose semi-major axes are the 3 eigenvalues of $\underline{\mathbf{D}}$ divided by the volume of a sphere whose radius is the mean diffusivity, Trace ($\underline{\mathbf{D}}$) / 3. Since the volume of the ellipsoid approaches 0 as anisotropy increases, the values of volume ratio range between 0 and 1 where 0 represents the highest anisotropy and 1 represents complete isotropy.

The lattice anisotropy index is an intervoxel measure of diffusion anisotropy that exploits information about the orientational coherence of the eigenvectors of $\underline{\mathbf{D}}$ in adjacent voxels to improve the estimate of diffusion anisotropy within a region of interest. This index is especially immune to background noise in the images; however, as with other diffusion indices, it has no effect on systematic errors such as motion artefact, ghosting, misregistration, distortion of DWIs by eddy currents, miscalibration of the gradients, or errors in the computation of the b-matrix. In addition, quantitative measures from the lattice index are dependent on the size of the voxels and the anatomical structures being studied. It therefore serves a limited function in the brain where tissue is

heterogeneous and all the fibres within a region of interest are unlikely to be similarly orientated.

A study comparing *relative* and *fractional* anisotropy and volume ratio showed that FA maps provided the most detailed and extensive estimation of anisotropy with the greatest signal to noise ratio (SNR) (Papadakis *et al.* 1999). Volume ratio provided the most contrast between areas of high and low anisotropy at the expense of increased noise contamination and reduced resolution in some areas. Relative anisotropy occupied an intermediate position between FA and VR.

In conclusion, using information derived from diffusion imaging, quantitative maps of a number of parameters, such as mean diffusivity, fractional anisotropy and volume ratio, can be constructed and used to compare between individuals or populations. Alternatively, anisotropy information can be used to deduce the pathways of major nerve fibre tracts using the technique of tractography (see chapter 1.2.5.5 Tractography).

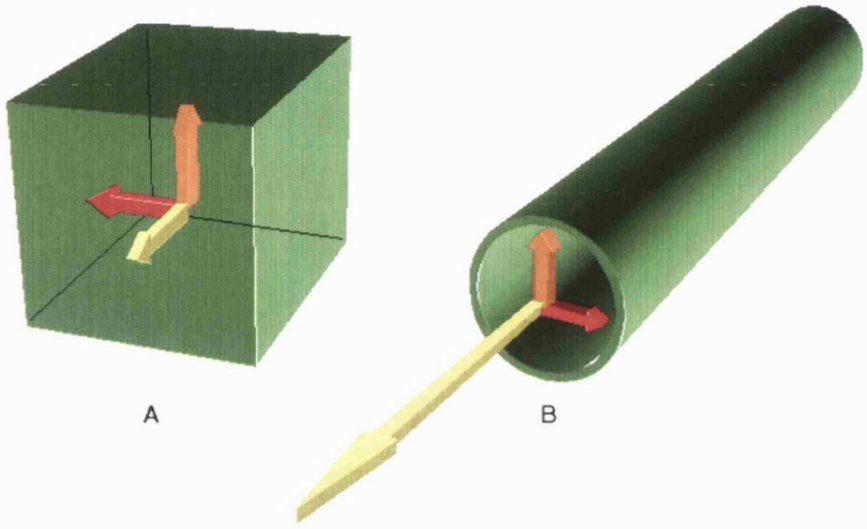

Figure 1.2: A diagram illustrating the principle of anisotropy. Image A represents isotropic diffusion, with no restriction on the movement of water molecules in, for example, CSF or where the restriction is equal in all directions in, for example, adult grey matter. Image B represents anisotropic diffusion, where movement of water molecules is asymmetrically restricted, for example, a myelinated axon.

1.2.5.3 Limitations of in vivo diffusion imaging

Diffusion imaging studies the movement of water molecules over very short distances, typically less than 100 micrometres. The sequence is therefore susceptible to motion artefact. This may arise through head motion in uncooperative or uncomfortable patients, or pulsatile brain motion due to the inflow of blood during cardiac ventricular systole. Brain motion is greatest during the first 300 milliseconds of the cardiac cycle (Poncelet *et al.* 1992). In MR sequences where k-space (the array of numbers obtained by measuring the MR signal received from the patient over time, and which can be converted to a MR image by applying a Fourier transform mathematical algorithm) is filled over several cycles, uncorrected MR images are degraded through ghosting. This affects conventional spin echo, fast spin echo and multishot echoplanar imaging (EPI). In single-shot EPI, k-space is filled

in about 100 ms, therefore images acquired during the first 300 ms of the cardiac cycle are affected by movement. In diffusion-weighted imaging, this causes an overestimation of the apparent diffusion coefficient when the brain motion is parallel to the diffusion gradient. A variety of measures can be undertaken to reduce motion artefact. These include the use of head restraints, cardiac gating (Wieshmann *et al.* 1997a), applying sequences with short acquisition times such as single-shot EPI (Turner *et al.* 1990; Stehling *et al.* 1991), oversampling and rejecting outliers (Wieshmann *et al.* 1998c), or using a navigator echo with multi-shot EPI (Anderson and Gore 1994; de Crespigny *et al.* 1995).

Other problems with diffusion imaging include the estimation of the contribution of flow and perfusion to the diffusion measurements, calculation of the contribution of the imaging gradients to the b-value (degree of diffusion weighting), optimal b-value, number of b-value steps, and signal to noise ratio (Xing *et al.* 1997). In addition, there are fluctuations in the strength of the scanner gradients which can affect quantitative analysis of DTI in individual subjects. These fluctuations can be followed by regular diffusion measurements in a standard water phantom.

Echo-planar imaging, which has become the sequence of choice in diffusion imaging studies due to its short acquisition time and minimal motion artefact distortion, has itself a number of specific problems. In particular, susceptibility artefacts in the orbito-frontal and temporal regions, image distortions due to eddy currents and a reduced signal to noise ratio (Symms *et al.* 1997).

In summary, clinical diffusion imaging is often a compromise between acquisition time, signal to noise ratio and hardware limitations.

1.2.5.4 Clinical applications of diffusion imaging

1.2.5.4.1 Normal tissue

The description of diffusion in biological systems is complex as it represents the result of a number of variable, independent factors. These include the presence of impermeable or semi-permeable membranes resulting in either restricted or hindered diffusion (Hansen 1971), the concentration and placement of macromolecules which further hinder diffusing molecules, and intra- and extracellular microcirculatory effects (Le Bihan *et al.* 1999; LeBihan and Turner 1992). The diffusion properties of water in simple biological systems such as frog muscle and human erythrocytes have been described (Tanner 1979; Tanner 1983; Latour *et al.* 1994). In addition, more complex structures such as the human brain have been studied resulting in the appreciation of the anisotropic property of white matter and offering insights into the anatomical connectivity of cerebral regions (Moseley *et al.* 1990a; Doran *et al.* 1990; Hajnal *et al.* 1991; Moseley *et al.* 1991; Behrens *et al.* 2003; Catani *et al.* 2003).

Anisotropy in cerebral tissue is highly heterogeneous. Major white matter tracts such as the corpus callosum and optic tract demonstrate higher levels of anisotropy (fractional anisotropy values of 0.81 and 0.87 respectively) than, for example, subcortical white matter or parietal cortex (0.46 and 0.31 respectively) (Pierpaoli and Basser 1996) (figures 1.2 & 1.3). Many studies have not shown significant anisotropic diffusion in human adult grey matter, with values close to the noise level (Shimony *et al.* 1999; Pierpaoli *et al.* 1996; Neil *et al.* 1998). Grey matter anisotropy has however been demonstrated in neonatal piglet and mature rat brain, albeit at low values

(Thornton *et al.* 1997; Hoehn-Berlage *et al.* 1995). It is possible that this reflects a degree of structural organisation and microscopic geometrical order within cortical tissue. More recently anisotropy has been demonstrated in the grey matter of premature human neonates (Neil *et al.* 2000). This is consistent with changes in cortical histology. Between 24 and 32 weeks gestational age, cortical cytoarchitecture is dominated by the apical dendrites of pyramidal cells. These long dendrites have few branches and are arranged radially giving rise to unidirectional fibre orientation and hence diffusion anisotropy. As development progresses, pyramidal cells form highly branched basal dendrites which tend to be arranged parallel to the cortical surface. In addition, thalamocortical afferent fibres are added and are orientated parallel to the cortical surface. With these changes, cortical architecture is no longer dominated by pyramidal apical dendrites and anisotropic diffusion is reduced, approaching zero by the gestational age of 32 weeks (Marin-Padilla 1992).

Mean diffusivity in the human brain varies considerably less than fractional anisotropy throughout the different parts of the brain (Pierpaoli and Basser 1996) (figure 1.3). For example, the mean diffusivities in the corpus callosum and posterior internal capsule (747 $x10^{-6}mm^2/s$ and 702 $x10^{-6}mm^2/s$ respectively), are comparable to subcortical white matter and parietal cortex (670 x $10^{-6}mm^2/s$ and 686 $x10^{-6}mm^2/s$ respectively). This most likely reflects the relatively uniform density of neurons and glial cells within all regions of the brain, and is independent of the orientation of fibre tracts. The mean diffusivity in cerebrospinal fluid is approximately 3191 $x10^{-6}mm^2/s$.

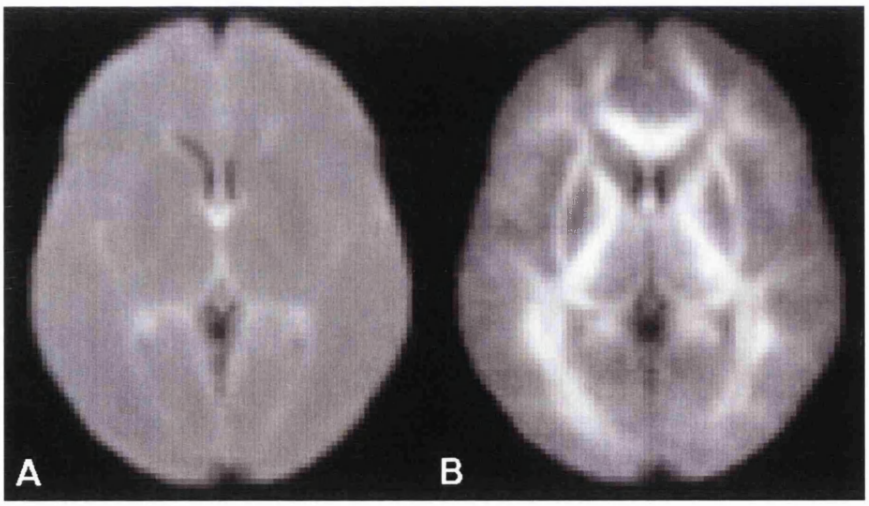

Figure 1.3: Axial mean diffusivity (A) and fractional anisotropy (B) maps. (Average of 30 control subjects).

Anisotropy is considered to be determined by cellular and extracellular components such as concentration of macromolecules and intracellular organelles, regional differences in fibre packing density, degree of myelination, fibre diameter and density of neuroglial cells (Pierpaoli *et al.* 1996). It has been observed that anisotropy within the cerebral hemispheres changes little from the age of six months through to adulthood. However, in a recent study of the effects of normal ageing on diffusion parameters, it was reported that both mean ADC and maximum FA correlated significantly with increasing adult age, suggesting the presence of subtle microstructural age-related changes (Rovaris *et al.* 2003b). Values of anisotropy are lower in infants below the age of six months (Nomura *et al.* 1994). This is thought to reflect the lack of myelin and hence lack of restriction to diffusion perpendicular to the

white matter tracts. The permeability to water of myelin lipid bilayers is 10 to 50 times smaller than the permeability of axoplasmic membranes; therefore, it has been suggested that the addition of a myelin sheath would significantly impair perpendicular movement of water (Rutherford *et al.* 1991). In-vitro experimental work on excised myelinated and unmyelinated nerves observed similar degrees of anisotropy for both nerve types, suggesting that myelin, although possibly contributory, is not a necessary determinant of anisotropy (Beaulieu and Allen 1994). Furthermore, the anisotropic property of the nerves was preserved following the destruction of microtubules and inhibition of fast axonal transport. Subsequent work by the same group also eliminated the possibility of neurofilaments playing a significant role, suggesting therefore that axonal membranes are the major determinant of the anisotropic property of a tissue (Beaulieu and Allen 1994). Histological examination of neonatal rat cerebral tissue following diffusion weighted imaging suggests that maturation of axonal membranes, a state of "premyelination", is the important factor in the development of anisotropy in the maturing brain (Wimberger *et al.* 1995). This is associated with alterations in membrane thickness, permeability, and transmembrane ionic changes.

In summary, diffusion of water within a tissue is governed by its molecular, microstructural and architectural properties. Experimental work suggests that the main determinants of anisotropy in the more densely packed unmyelinated fibres are the many axonal membranes, and in less dense myelinated tracts, the multiple myelin lamina. A disruption to this microstructural environment such as ischaemic injury, gliosis, or cerebral dysgenesis will lead to a less ordered arrangement of nerve fibres and subsequent reduction in anisotropy. Similarly, these cerebral abnormalities may lead to reduced cell density and/or expansion of the extracellular space resulting in increased mean diffusivity (figure 1.1).

Recently, it has been suggested that with DTI using degrees of diffusion weighting (b-values) of less than 1000 s/mm^2, the extracellular compartment is the predominant determinant of diffusion image contrast. With b-values of greater than 1000 s/mm^2, the intracellular compartment contributes to a greater extent. This supposition is based on the apparent non-linear relationship between the measured ADC and degree of diffusion weighting applied. Describing this relationship bi-exponentially to explain the two compartment model has been challenged as too simplistic and poorly supported by the available data. In particular, the volume fractions of each compartment, the contribution of water exchange between compartments and the presence of local susceptibility gradients have been neglected. Alternative suggestions include a multi-exponential relationship involving many parameters, most notably the complex underlying cerebral structure. Further work, in particular studying a variety of experimental models with multiple b-values under different imaging conditions, is required to clarify this issue (Le Bihan *et al.* 2001; Clark and LeBihan 2000).

1.2.5.4.2 Cerebral ischaemia

The advantages of diffusion-weighted imaging in the detection of early cerebral ischaemia were first suggested by Moseley in 1990 (Moseley *et al.* 1990c; Moseley *et al.* 1990b). Additional studies have confirmed that a reduction in ADC can be seen within minutes of cerebral ischaemia. This compares with a time frame of several hours for definitive changes to be observed with conventional MRI (Benveniste *et al.* 1992; Minematsu *et al.* 1992; Dardzinski *et al.* 1993; Brant-Zawadzki *et al.* 1986; Yuh *et al.* 1991; Davis *et al.* 1994; Yoneda *et al.* 1999).

Possible mechanisms include cytotoxic oedema, where the reduction in ADC occurs because of a shift of water from the relatively unrestricted diffusion environment of the extracellular compartment to the more restricted, viscous intracellular space. This hypothesis is supported by reports that the extracellular space can be reduced by up to 50% during severe cerebral ischaemia (Williams *et al.* 1991). A study of experimental cerebral ischaemia noted that diffusion changes occurred only when cerebral perfusion reduced to below the critical threshold for maintenance of tissue high-energy metabolites and ion homeostasis. This resulted in an increase in intracellular sodium and water which produced a change in cell volume (Busza *et al.* 1992). Changes in ADC have been observed in excised optic nerve under conditions of cellular swelling and shrinkage without ischaemia suggesting that the common mechanism leading to changes in diffusion in pathological conditions associated with ion membrane dysfunction is compartmental redistribution of water (Anderson *et al.* 1996). This hypothesis is challenged however by a number of considerations. Firstly, measurements of the ADCs within the extra- and intracellular spaces have been shown to be very similar. Secondly, during ischaemia, the ADCs within each compartment are both seen to decrease (Duong *et al.* 1998). Movement of water into the intracellular compartment may explain the reduced diffusion in the extracellular space, where cells are now more tightly opposed and paths between more tortuous and hindering to diffusion molecules (Sykova *et al.* 1994; van der Toorn *et al.* 1996b). Alternative mechanisms to explain the reduced ADC in the intracellular compartment must be proposed however. These include loss of cytoplasmic motion (cytosolic streaming and cytoskeletal motility) (Duong *et al.* 1998), increase in viscosity of intracellular components (Zhong *et al.* 1993; van der Toorn *et al.* 1996a; Wick *et al.* 1995; Neil *et al.* 1996), and reduction in transmembrane water movement (Helpern *et al.* 1992). It is likely that a combination of two or more of these processes are involved in the observed ADC decrease in ischaemia and further work is required to elucidate the cause more precisely.

Following the results of the experimental studies, patients with acute stroke have been investigated with diffusion-weighted MRI (Lutsep *et al.* 1997; Gonzalez *et al.* 1999; Marks *et al.* 1996; Sorensen *et al.* 1996; Kang *et al.* 2003). Superiority over CT scanning (Saur *et al.* 2003) and conventional MRI, in terms of earlier detection of ischaemia, has been demonstrated with abnormalities detected within 39 minutes of stroke onset (Yoneda *et al.* 1999). This has led to the possibility of using DWI to confirm clinical evidence of stroke within a time period appropriate for the administration of thrombolytic therapy, particularly when combined with perfusion imaging (Schellinger *et al.* 2003). Conventional MRI abnormalities do not appear until after this time period has elapsed (Yuh *et al.* 1991). In addition, thrombolysis has been shown to result in reversal of diffusion imaging abnormalities (Kidwell *et al.* 2000; Kidwell *et al.* 1999), with no difference in outcome observed between intravenous and intra-arterial administration in experimental studies (Niessen *et al.* 2002)

Following an untreated ischaemic event, ADC values normalise within 5-10 days (Warach *et al.* 1995). Subsequently however, ADC values increase further and are thought to represent expansion of extracellular space due to membrane disruption, cell death and tissue necrosis (Warach *et al.* 1995; Pierpaoli *et al.* 1993). DWI is therefore of benefit in patients with recurrent strokes as it allows new infarcts (bright regions on DWI) to be readily distinguished from chronic ones (dark regions). There are, however, a number of limitations of DWI in acute stroke. Recent studies have shown that the area of brain ischaemia defined by a map of decreased ADC during the first hours after a stroke includes a significant part of the ischaemic penumbra, a variable proportion of which may remain viable without thrombolytic therapy. DWI may therefore overestimate the degree of infarcted tissue and is generally considered to be a poor predictor of final infarct size (Nicoli *et al.* 2003). Conversely, DWI

may remain normal despite significant cerebral infarction, limiting its usefulness as a screening tool (Wang *et al.* 2003).

In view of the above evidence and the increasing use of thrombolysis in acute stroke, it is likely that diffusion imaging, particularly when combined with perfusion imaging, will become the early imaging investigation of choice in patients presenting with a clinical picture suggestive of cerebral ischaemia. Currently however, the use of thrombolysis in patients with DWI abnormalities is based only on circumstantial evidence as there have been no trials directly linking clinical outcome with treatment of patients with diffusion abnormalities.

1.2.5.4.3 Epilepsy

DWI has been used to investigate epilepsy in both experimental and clinical settings.

Experimental studies

The first reported study, in 1993 by Zhong et al, reported an immediate fall in ADC in bicuculline-induced status epilepticus in rats (Zhong *et al.* 1993). The maximal drop in ADC was approximately 15%, which is about half of the reduction seen in ischaemia. A further study on status epilepticus induced by the milder convulsant flurothyl showed less intense seizure activity accompanied by an 8% reduction in ADC (Zhong *et al.* 1995). This was largely reversed by the administration of phenobarbitone. To eliminate the possibility that the diffusion changes were related to a drug effect, ADC measurements were made in rat brain stimulated by cortical electroshocks. With single shock pairs which caused electrical after discharges lasting less than five seconds, ADC fell an average of 2-3% (Prichard *et al.* 1995). Longer shock trains produced larger ADC changes, on average 7-8%, which persisted for several minutes (Zhong *et al.* 1997; Prichard *et al.* 1995). These studies show that the magnitude of the reduction in ADC in experimental models of epilepsy correlate with the duration and severity of brain activation. Additional experiments on kainate-induced status epilepticus provide supporting evidence for ADC changes in epilepsy and suggest that the cause relates, as in ischaemia, to cellular swelling (Ebisu *et al.* 1996; Wang *et al.* 1996). The extracellular space has been investigated with ion-selective microelectrodes during enhanced neuronal activity. At sites of maximal activity, the extracellular space contracts by more than 30%. A shift of water into cells occurs because intracellular osmolarity increases. This is due to a net movement of potassium ions into glia and cleavage of intracellular macromolecules (Lux *et al.* 1986; Blennow *et al.* 1979; Howse *et al.* 1974).

The similarity of the behaviour of the ADC in both ischaemia and experimental epilepsy models suggest a common mechanism may be present. However the changes occur under very different circumstances. In ischaemia, the blood supply to the tissue is seriously compromised, resulting in energy failure, membrane dysfunction and cell death. Conversely, ongoing seizure activity leads to increased metabolic rate and cerebral blood flow so that cellular energy levels are upheld close to normal values (Meldrum and Nilsson 1976; Borgstrom *et al.* 1976; Plum *et al.* 1968; Chapman *et al.* 1977). These compensatory mechanisms may not be complete, as it has been demonstrated that the phosphocreatine content as a percentage of the total amount of high-energy phosphates in the brain decreases during the first 15 minutes of a seizure in a canine model of status (Young *et al.* 1985). Furthermore, the level of lactate can also increase, suggesting the presence of anaerobic metabolism. Systemic complications during status may also give rise to hypoxic ischaemia. However, changes in adenosine triphosphate

(ATP) content during seizures are minimal if the animals are well oxygenated and physiological parameters are tightly controlled (Petroff *et al.* 1984). This would suggest that tissue energy failure is not the primary cause of ADC decline in experimental status epilepticus. In the clinical setting however, status epilepticus may be associated with significant systemic changes which may cause tissue hypoxia.

In cerebral ischaemia, the disruption of energy metabolism not only retards membrane ion pump activity but also increases membrane ion channel permeability due to the release of excitatory neurotransmitters. This quickly results in the loss of cellular ion homeostasis, cellular swelling and eventually cell death. In status epilepticus, the cellular energy state may be upheld close to normal but enhanced membrane ion permeability results in measurable cellular swelling (McNamara 1994). It appears therefore, that loss of ionic homeostasis whether from ischaemia or from enhanced neuronal activity is a common factor in both conditions. It has been shown that during ischaemia, ADC reduces twice as much as during status (Zhong *et al.* 1993). This is most likely due to additional mechanisms caused by cellular energy loss, such as reduced cytosolic motility, which may not be present, at least to the same degree, in uncomplicated status epilepticus. In summary therefore, the exact mechanism for changes in ADC following cerebral ischaemia or experimental status remain undetermined but most likely represent a combination of one or more factors, including loss of ionic homeostasis, water compartmentalisation and intracellular macromolecular and cytosolic changes. Following an acute reduction in ADC at the onset of complex partial status epilepticus in a canine model, ADC gradually increases with status duration, and parallels histopathological changes in the epileptogenic mesial temporal lobe (Hasegawa *et al.* 2003). This suggests that DWI may be useful for finding the epileptic focus or for examining potential cerebral damage during status epilepticus.

Clinical studies of diffusion imaging in epilepsy

In addition to animal models, patients with status epilepticus have been studied with diffusion-weighted imaging. In a study of three patients by Lansberg et al cortical ADC was reduced by approximately 36% during partial status epilepticus (Lansberg *et al.* 1999). The diffusion abnormalities normalised following cessation of the seizures. These diffusion changes were mirrored by localised increased signal in T2-weighted images, and also by areas of reduced attenuation on computed tomographic (CT) scanning. In addition, in a 51 year old with focal status epilepticus, an area of *increased* ADC was observed in the subcortical white matter, adjacent to the region of focal cortical reduced ADC (Wieshmann *et al.* 1997b). This was thought to represent a shift of water into the cortical cells at the site of increased neuronal activity, and a shift of water into the extracellular space in the white matter in areas remote from this site; an observation previously seen in experimental models of epilepsy (Lux, Heinemann, and Dietzel 1986). Correlation of DWI abnormality with electrocorticographic changes has also been observed (Diehl *et al.* 1999). Most recently, Konermann et al reported significantly decreased ADC in hippocampi and parahippocampal gyri, ipsilateral to the seizure onset, in patients with flumazenil-induced temporal lobe seizures (Konermann *et al.* 2003). Further work by the same group identified significant diffusion changes only in patients with complex partial seizures of greater than 60 seconds duration and if the time from seizure to DWI scan was less than 15 minutes. Generalised seizures were associated with global ADC change (Hufnagel *et al.* 2003). The authors concluded that regions of ictally decreased ADC are useful in the localization of the seizure focus in some patients with TLE.

Interictal studies have also been performed on patients with epilepsy. To date these have focused on structural abnormalities, such as hippocampal sclerosis, head injury, ischaemic lesions and malformations of cortical development (MCD).

In a study of patients with hippocampal sclerosis, anisotropy was reduced and averaged ADC was increased in sclerotic hippocampi compared to control subjects suggesting structural disorganisation and an expansion of extracellular space. This was thought to reflect neuronal loss, reduction of dendritic branching and microstructural changes associated with epileptogenesis (Wieshmann *et al.* 1999a). These results concurred with a similar study of patients where a significantly increased averaged ADC was found in sclerotic hippocampi. Changes in the anisotropy index in this second study were not significant however (Hugg *et al.* 1999).

Patients with epilepsy and malformations of cortical development have been studied with DTI (Wieshmann *et al.* 1999c). In all three patients, fractional anisotropy was significantly reduced within the malformation but mean diffusivity was increased in only one. This suggests a loss of directional organisation in combination with a preserved cell density. This study adopted a region-of-interest based approach to evaluate areas of MR visible abnormality only; normal appearing cerebral tissue was not examined. It is known however, that developmentally abnormal tissue often extends beyond that seen on conventional MRI and may affect several lobes (Eriksson *et al.* 1999; Sisodiya *et al.* 1995b; Woermann *et al.* 1999a). It would be of interest, therefore, to examine cerebral tissue distant from the obvious abnormality for diffusion, particularly anisotropic, changes.

Patients with epilepsy as a result of head injury have similarly been studied and changes in both mean diffusivity and fractional anisotropy have been observed, concordant with neuronal loss, gliosis, and structural disorganisation (Wieshmann *et al.* 1999c; Wieshmann *et al.* 1999e). Other groups of patients with, for example, epilepsy and chronic cerebral infarcts, perinatal hypoxia, mitochondrial cytopathy, or tumours have also been examined and invariably reduced anisotropy and frequently increased diffusivity were observed within each lesion (Wieshmann *et al.* 1999c; Wieshmann *et al.* 1999b).

Anisotropic changes have been reported following temporal lobe resections for the treatment of epilepsy. In patients with a visual field defect after surgery, there was reduced anisotropy in the ipsilateral optic radiation, in areas distant from the site of resection, suggesting the presence of Wallerian degeneration (Wieshmann *et al.* 1999d; Beaulieu *et al.* 1996).

1.2.5.4.4 Other conditions

Diffusion weighted and diffusion tensor imaging have been applied to many other conditions in both experimental and clinical settings (Table 1.6).

Table 1.6 Other diseases / conditions studied with diffusion imaging

Disease / Condition	Diffusion imaging
multiple sclerosis (Werring *et al.* 1999; Droogan *et al.* 1999; Horsfield *et al.* 1996; Cercignani *et al.* 2000; Tievsky *et al.* 1999; Rovaris *et al.* 2002) and experimental allergic encephalomyelitis (model of multiple sclerosis) (Heide *et al.* 1993)	reduced anisotropy and increased mean diffusivity within inflammatory lesions and normal-appearing white matter. Correlates with pathological severity.
cerebral tumours (Hajnal *et al.* 1991; Tien *et al.* 1994; Wieshmann *et al.* 2000; Bastin *et al.* 1999; Lu *et al.* 2003; Beppu *et al.* 2003)	reduced ADC within solid tumours, increased ADC within necrotic or cystic tumours. Diffusion tractography demonstrates displacement of tracts around tumour. Peritumoral MD can be used to distinguish high-grade gliomas from metastatic tumors, peritumoral FA demonstrated no statistically significant difference. FA predicts histological characteristics such as cellularity, vascularity and/or fiber structure in astrocytic tumors
motor neuron disease (Ellis *et al.* 1999; Jacob *et al.* 2003)	reduced anisotropy and increased mean diffusivity in corticospinal tracts. Correlates with disease severity and subtype of motor neuron disease
CADASIL (cerebral autosomal dominant arteriopathy with subcortical infarcts and leucoencephalopathy) (Chabriat *et al.* 1999; Molko *et al.* 2002)	reduced anisotropy and increased mean diffusivity in lesions and normal-appearing white matter. Quantitative DTI can be used to monitor disease progression
HIV encephalopathy (Doran *et al.* 1990)	reduced anisotropy in clinically concordant white matter.
progressive multifocal leucoencephalopathy (Hajnal *et al.* 1991)	reduced anisotropy throughout white matter.
schizophrenia (Foong *et al.* 2000b; Minami *et al.* 2003)	reduced anisotropy and increased mean diffusivity in splenium of corpus callosum, and other white matter tracts.
cerebral trauma (Werring *et al.* 1998; Wieshmann *et al.* 1999e; Chan *et al.* 2003; Huisman *et al.* 2003)	reduced anisotropy in tracts concordant with clinical disability. DWI identifies diffuse axonal injury not visible on conventional MRI
transient global amnesia (Strupp *et al.* 1998)	reduced ADC in hippocampi
Alzheimers disease (Hanyu *et al.* 1999; Sandson *et al.* 1999; Yoshiura *et al.* 2002)	reduced anisotropy in white matter. Increased averaged diffusion in hippocampi. MD in the posterior cingulate white matter is proportional to degree of cognitive impairment..

Creutzfeldt-Jakob disease (Bahn and Parchi 1999; Demaerel *et al.* 1999; Matoba *et al.* 2001; Yee *et al.* 1999; Demaerel *et al.* 2003; Mendez *et al.* 2003)	DWI hyperintensity in basal ganglia and cortex. Changes seen earlier than on conventional MR imaging. Multifocal cortical and subcortical grey matter hyperintensities may be a more useful noninvasive diagnostic marker for CJD than CSF protein 14-3-3. Reported to be 100% sensitive and specific (12 patients)

As diffusion imaging develops further and as the realisation that it can offer unique information about the microstructural environment becomes more widely appreciated, many other disease processes will be studied.

1.2.5.5 Tractography

Knowledge of the link between functional brain regions and anatomical fibre connections is essential to fully characterise the organisation of cerebral tissue (Goldman-Rakic 1988; Mesulam 1990). With current conventional MRI techniques, the white matter of the brain appears homogeneous and the complex arrangement of fibre tracts remains undisclosed. Imaging sensitive to the diffusion of water can describe this complex structure and provide information on cerebral connectivity.

After diffusion weighted imaging established the anisotropic nature of cerebral white matter (Chenevert *et al.* 1990; Moseley *et al.* 1990a; Pierpaoli *et al.* 1996), attempts were made to display this information in a comprehensive, yet understandable format.

Preliminary proposals focused on the generation of colour-coded maps of nerve fibre orientation based on the anisotropic quality of each voxel. Different colours were assigned to orthogonally orientated fibres with the saturation of the colour proportional to the degree of anisotropy (Douek *et al.* 1991). These colour maps were compared with the subjects' anatomical images and regions of anisotropic diffusion identified. On coronal images, as expected, the corpus callosum and the vertical corona radiata fibres were appointed different colours. Overall, the orientation-coded colour maps were in good agreement with known anatomy and showed, for the first time, that individual white matter fibre tracts can be discerned. Limitations of this approach include the disadvantages of using diffusion-weighted imaging rather than diffusion tensor imaging, colour coding for a specific direction of anisotropy rather than an individual tract which may lead to the same tract possessing varying colours of differing intensities throughout its length, and the use of varying diffusion gradient strengths depending on the applied direction (a limitation of the hardware) resulting in inaccurate ADC calculation.

With the introduction of diffusion tensor imaging, alternative methods for displaying anisotropic information and hence nerve fibre tracts were proposed. Diffusion ellipsoid images are graphical representations of the diffusion tensor within each voxel and highlight the three-dimensional character of diffusion directionality (Plum, Posner, and Troy 1968; Pierpaoli and Basser 1996; Pierpaoli *et al.* 1996) (figure 1.4).

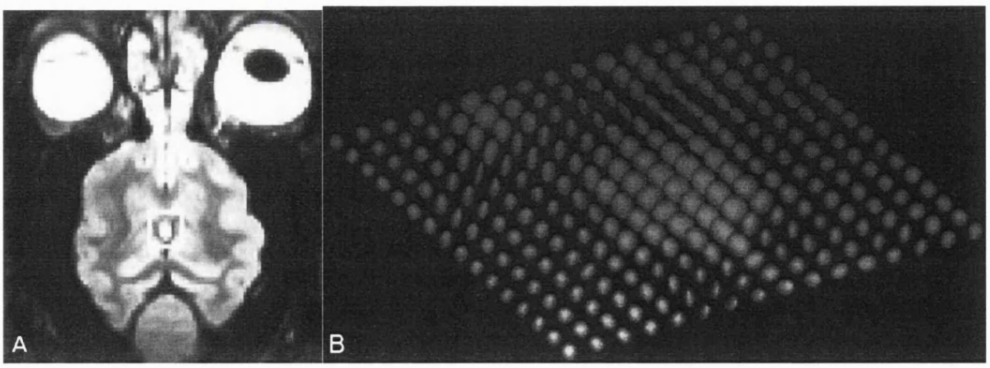

Figure 1.4: (A) Axial T2-weighted image of in vivo cat brain. (B) Diffusion ellipsoid image constructed from the effective diffusion tensor, estimated in each voxel for the ROI enclosed by the white square in (A) which contains both CSF and white matter tracts of the internal capsule. (Reproduced from Basser and Pierpaoli 1996)

Alternatively, they may be interpreted as the surfaces of constant mean-squared displacements of diffusing water molecules at a particular time after they are released at the centre of each voxel. The degree of diffusion anisotropy is characterised by the shape or eccentricity of the ellipsoid, the overall mobility of the diffusing medium is related to the size of the ellipsoid and the preferred direction of the diffusion is indicated by the orientation of the ellipsoid. An isotropic voxel is represented by a spherical ellipsoid, whereas in white matter, which possesses anisotropy, the ellipsoid is markedly eccentric and orientated parallel to the fibre tract it represents. Constraints of this technique include displaying only a single slice when tracts often traverse many slices, and the lack of quantitative information.

More recently, an alternative method of displaying anisotropy information based on colour-coding principal eigenvectors has been proposed (Makris *et al.* 1997). This approach utilises both the advantages of diffusion tensor imaging and the visual clarity of colour maps. Different colours are assigned to three principal eigenvectors in each voxel. An oblique vector is assigned a mixture of colours depending on the magnitudes of the vector components. In addition, the brightness of the colours in each voxel are proportional to the lattice anisotropy index, thereby indicating the degree of directionality. These colour maps are then compared with an atlas of human neuroanatomy and specific fibre tracts identified in normal controls. Using this method, disordered tracts within an area of damaged brain were identified in a patient with a chronic parietal infarct. Other studies have adopted similar approaches to displaying anisotropic information based on colour-coded maps and have applied them in the study of normal individuals and patients with cerebral pathology including infarcts, haemangiomas and tumours (Peled *et al.* 1998; Inoue *et al.* 1999; Nakada *et al.* 1999). It is important to note, however, that these studies were performed with anisotropic sampling voxels (for example, 1.5 x 1.5 x 6mm) which reduces the sensitivity of the technique in the slice-selecting plane. The use of isotropic voxels allows smaller tracts to be identified but at the cost of a lower SNR and longer scanning times. Recently, a DTI sequence has been developed which produces isotropic, high-resolution ($2.5mm^3$) voxels within a clinically acceptable time (Jones *et al.* 2002b). The studies which use colour-coded orientation maps display anisotropy information about the whole brain without specifically identifying the track of an individual nerve tract. To address this limitation the technique of tractography has been developed which reconstructs the neuronal projections by tracking individual vectors. Using this method, the pathway, and hence connectivity, of a specific tract can be displayed.

Initial approaches involved taking an individual voxel in a fractional anisotropy map and assigning it to a particular "class" according to its orientation (Jones *et al.* 1999). Then each of the 26 surrounding nearest neighbours (in a 3 x 3 x 3 kernel) were considered in turn for connection to the central voxel. If a neighbouring voxel satisfied the criteria of minimum fractional anisotropy and compatibility of eigenvectors, i.e. maximum of 45^0 between adjacent voxels, the voxel was assigned to the same class as the original central voxel. The algorithm thus proceeded through all the voxels in the image. A colour scheme was then applied to the map so identical colours represented the same tracts throughout the brain. Using this technique, individual tracts, such as the corpus callosum and internal capsule, were successfully tracked independent of their orientation in any given image slice. This method uses a discrete rather than a continuous vector field which tends to lead to a deviation of the tracking from the true fibre orientation. This constraint was addressed in studies of fibre tracking in the rat brain using a technique termed *fibre assignment by continuous tracking* (FACT) (Xue *et al.* 1999; Mori *et al.* 1999). This method also uses the strength of alignment between adjacent voxels to determine the orientation of the track but follows individual paths rather than assigning colour codes after indiscriminately spreading voxel-by-voxel throughout the whole brain. Discrete fibre tracts can then be identified and correlated with an atlas of rat neuroanatomy. However, this technique was unable to distinguish between afferent and efferent pathways, and was insensitive to the inadvertent switching of pathways if two tracts became close or the branching or diverging of tracts. Alternative tractographic methods applied to the study of normal human brain include following the pathway of "fastest" diffusion (direction of greatest anisotropy) (Conturo *et al.* 1999), "fast marching" algorithms to generate maps representing the likelihood of connection between seed and tracking termination points (Ciccarelli *et al.* 2003a), probabilistic (Behrens *et al.* 2003), random walk (Hagmann *et al.* 2003) and diffusion tensor deflection algorithms (Lazar *et al.* 2003). A number of principal white matter pathways have been mapped using these techniques, for example, the corpus callosum (Catani *et al.* 2002; Hagmann *et al.* 2003) (figures 1.5 and 1.6), thalamo-cortical connections (Behrens *et al.* 2003), the inferior longitudinal fasciculus (Catani *et al.* 2003) (figure 1.5), pyramidal tracts (Guye *et al.* 2003; Basser *et al.* 2000) (figure 1.6), and spinal cord tracts using a high resolution diffusion sequence (Wheeler-Kingshott *et al.* 2002). Validation remains challenging however, and relies on histopathologically established brain atlases to confirm trajectories (Parker *et al.* 2002; Hagmann *et al.* 2003).

Tractography has also been applied in pathological conditions, for example, multiple sclerosis (Wilson *et al.* 2003), cerebral tumours where the results may be used to plan resective neurosurgery to reduce the risk of injury to the major fibre tracts (Holodny and Ollenschlager 2002; Guye *et al.* 2003), stroke (Kunimatsu *et al.* 2003; Pierpaoli *et al.* 2001) and malformations of cortical development (Eriksson *et al.* 2002). In the latter study, tracts were followed through subcortical bands of heterotopic grey matter. This concurs with histopathological data which describes the existence of white matter tracts traversing these malformations (Harding 1996). Until recently, the application of tractography to human pathology has concentrated on the visual assessment of fibre trajectories and comparison with control subjects or anatomical atlases. The quantitative evaluation of tractographic or connectivity maps is an important goal however, and is more objective and possibly more sensitive and reproducible than a qualitative appraisal. A number of studies have made important advances in this regard (Ciccarelli *et al.* 2003b; Jones 2003; Guye *et al.* 2003), however, methodological constraints exist. These include inaccuracies introduced by unrestrained normalisation of either eigenvectors or the whole tensor (Jones *et al.*

2002a), wide inter-subject variation and intra-subject "uncertainty" with respect to the course and trajectory of the major white matter tracts (Ciccarelli *et al.* 2003a; Jones2003), and disturbances of anisotropy at fibre crossing points which may be variable in both position and magnitude between individuals (Pierpaoli *et al.* 2001).

In summary, tractography using diffusion tensor imaging can be used to characterise the potential anatomical connections between functional domains permitting a more detailed study of the organisation of normal and pathological cerebral tissue to be undertaken.

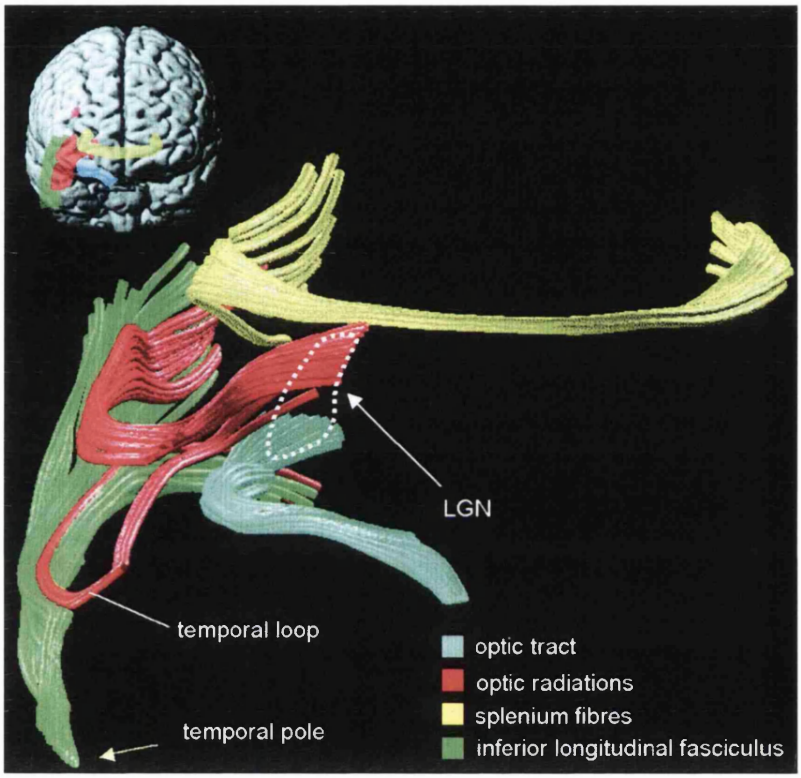

Figure 1.5: Diffusion tractographic representation of the visual pathway of the right hemisphere and splenium of the corpus callosum. (reproduced from Catani *et al.* 2003).

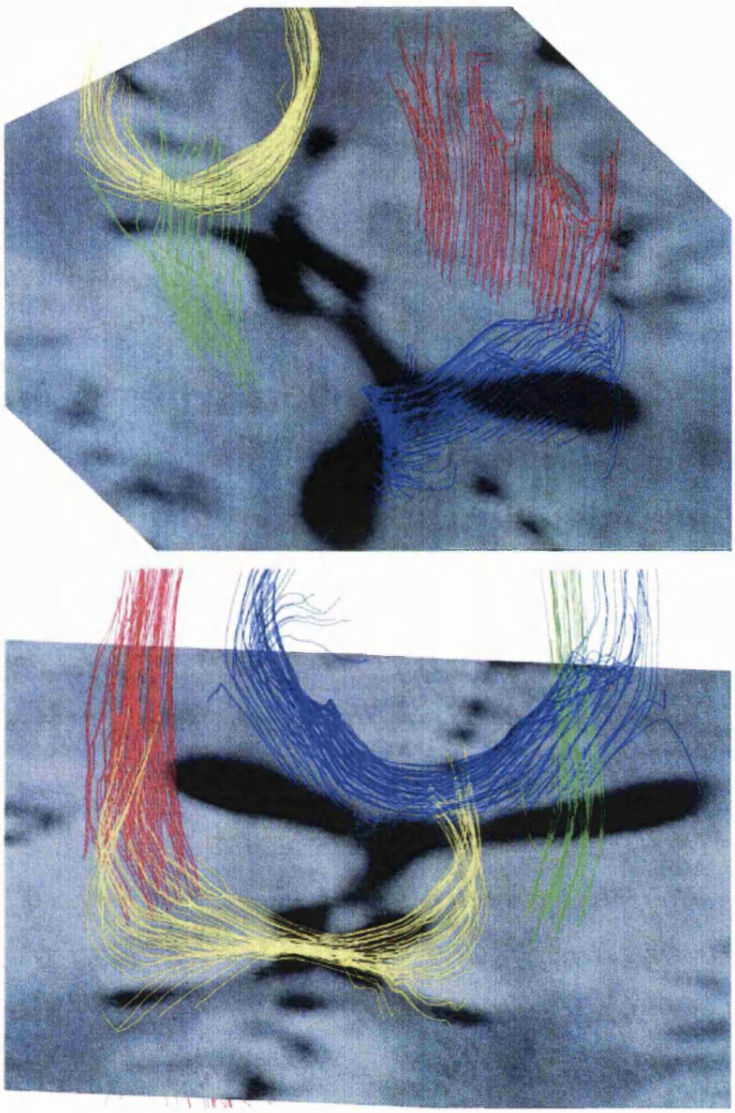

Figure 1.6: Three-dimensional tractography of a normal subject showing the anterior (yellow) and posterior (blue) part of the corpus callosum, and the left and right (green and red) cortico-spinal tract, superimposed on an axial MR image through the lateral ventricles. Top and bottom images present two different views of the same tractography result (reproduced from Westin, C.-F. et al. 2002 (Westin *et al.* 2002))

1.2.6 Magnetisation Transfer Imaging

1.2.6.1 Theory

Conventional MR imaging sequences exploit differences in the proton density, T_1 and T_2 times to provide contrast and tissue conspicuity within an object being studied. Additional contrasts may be provided by advanced MRI techniques, such as magnetisation transfer imaging (MTI).

The principle concept of MTI involves the exchange of magnetization between three separate proton pools (figure 1.7):

- free protons in bulk water
- tightly bound protons on macromolecules
- transiently bound hydration layer protons

The protons tightly bound to macromolecules, because of their immobility, have a very broad (~20kHz) MR peak and a very short T2. They are, therefore, invisible to conventional MRI. MTI, however, offers an insight into this macromolecular environment by an observable effect of the bound protons on the free water pool (Wolff and Balaban 1989; Wolff and Balaban 1994).

One of the fundamental assumptions involved in describing the magnetisation transfer (MT) process is that the state of magnetisation of a proton can be transferred to a like proton in an adjacent molecule possessing different relaxation properties. This is based upon modified Bloch equations (Bloch 1946; McConnell 1958) and magnetic resonance spectroscopy experiments evaluating chemical exchange models (Forsen and Hoffman 1963b). Chemical exchange describes a mechanism where protons are physically transferred from one molecule to another. Alternatively, a "chemical exchange equivalent" process may occur where the molecule, on which the proton resides, changes its structure or moves between chemically different compartments (for example, intra- to extracellular shift). Chemical exchange can occur even when the molecules involved have different relaxation properties, for example, free water and protons tightly bound to macromolecules, such as proteins and membrane lipids. The transference of protons between molecules is paralleled by a change in the net magnetisation in each compartment.

MT can occur in the absence of physical (chemical) exchange, due to a process termed cross-relaxation (Hoffman and Forsen 1966). This is a particular form of dipole-dipole interaction in which a proton on one molecule transfers its spin to that on another molecule without explicit chemical exchange. Cross-relaxation typically occurs when water molecules are closely associated, or transiently bound with macromolecules. The transference of spin is associated with a compartmental change in magnetisation.

Through these two atomic interaction mechanisms, chemical exchange and cross-relaxation, and through the continuous diffusional exchange of transiently bound and free water molecules, magnetisation can be transferred from one proton pool to another, despite the compartments possessing different relaxation properties. This results in the observed proton relaxation times reflecting characteristics of both the free water protons and the macromolecular environment.

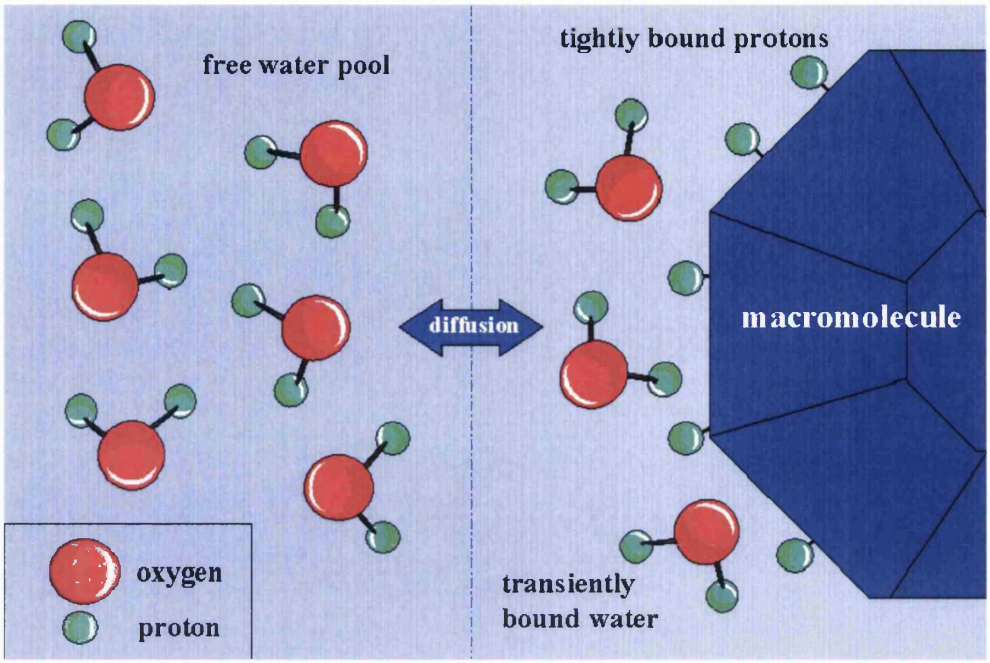

Figure 1.7: Schematic diagram of proton pools in biological tissue. The central arrow represents diffusion between the free water pool and the transiently bound surface water pool. Magnetisation transfer effects occur between macromolecular protons and transiently bound surface water molecules.

By exploiting these processes, MTI represents a window into this environment. This is achieved by selectively saturating the macromolecular pool of protons with an off-resonance pulse. This pulse typically has a bandwidth of several hundred hertz and is shifted from the water resonance by 1000 to 2500Hz. Protons in the immobile and transiently bound water pools are saturated, without affecting those in free water (figure 1.8). A standard imaging sequence is performed immediately after the saturation pulse and, because of the transfer of magnetisation between the macromolecular and free proton pools, new tissue relaxation characteristics and image contrasts are observed. The amount of saturation transfer depends on the number of protons in each pool, the rate of exchange with the free water protons, the relaxation characteristics of the tissue and properties of the saturating pulse (power, frequency and duration) (Balaban and Ceckler 1992).

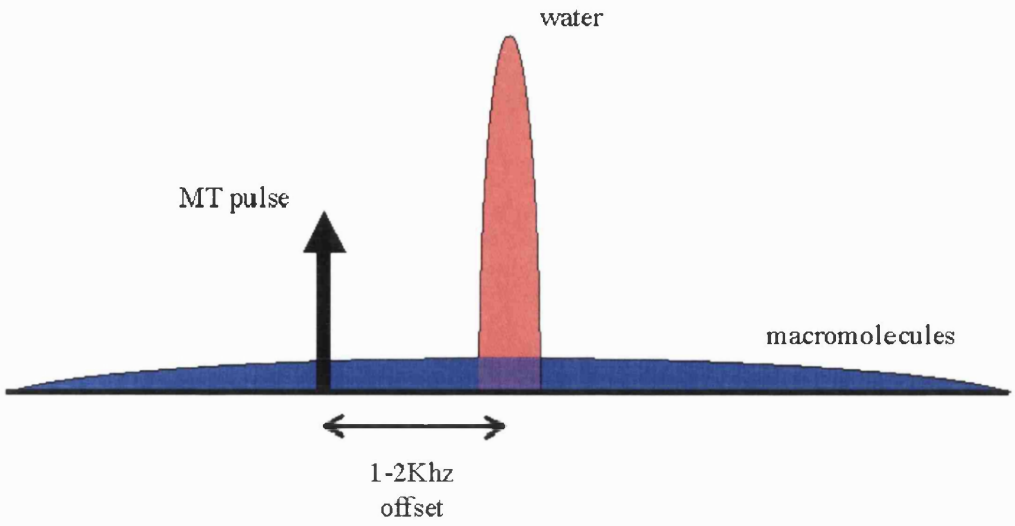

Figure 1.8: Magnetisation transfer pulse applied off water resonance saturates the broad macromolecular proton pool without directly affecting the free water pool. Indirect effects on this pool occur through transfer of magnetisation by dipolar and chemical exchange interaction.

Signal intensity on a conventional T1-weighted image is determined by the amount of longitudinal magnetisation which has been flipped into the transverse plane by a radiofrequency (RF) pulse. T1 relaxation occurs due to a transfer of energy from the nuclear spin system to the environment. This results in a regrowth of longitudinal magnetisation, and the T1 value is defined as the time taken for 63% of this magnetisation to recover. Once all the magnetisation has recovered, applying a further RF pulse will flip the longitudinal magnetisation into the transverse plane and a further signal of the same magnitude will be detected by the receiver coil. If the pulse is applied before all the longitudinal magnetisation has recovered, less magnetisation is available to be flipped into the transverse plane so less signal is "seen" by the receiver. This will result in most tissues appearing darker on the reconstructed T1-weighted image.

Following an off-resonance saturation pulse during MTI, the net longitudinal magnetisation of the macromolecular bound protons approaches zero. The free water protons possessing longitudinal magnetisation (unaffected by the off-resonance pulse) will be subject to cross-relaxation and chemical exchange with the bound macromolecular protons without longitudinal magnetisation (figure 1.9). This results in a smaller net longitudinal magnetisation component in the free water pool (the visible MRI pool) being available to be flipped into the transverse plane by the standard RF pulse. Thus, the signal intensity is reduced and tissues appear darker on the T1-weighted image (McGowan 1999). The reduction in signal intensity is greatest in regions where the transfer of magnetisation is most "efficient", and, assuming imaging parameters are kept constant, this is primarily attributable to an increased concentration of macromolecules within the voxel.

In addition to the concentration of macromolecules, characteristics that determine MT include the macromolecular surface chemistry and biophysical dynamics. Greater magnetisation transfer contrast (MTC) has been observed in tissues with a high plasma membrane content, such as kidney or brain, suggesting that one or more of the components of cell membranes are the main determinants of MT (Wolff and Balaban 1989).

Furthermore, the presence of a cross-relaxation pathway between lipid and bulk water protons, where selective irradiation of the free water pool affected the T1 values of the lipid, has also been reported (Fralix *et al.* 1991). Increasing concentrations of cholesterol in a sample of phosphatidylcholine was shown to enhance magnetisation exchange between bulk water and the macromolecular matrix, possibly by increasing the number and affinity of water interaction sites, or increasing the residency time of water per site on the lipid (Fralix *et al.* 1991). This effect of cholesterol was later confirmed by Kucharczyk et al, who also noted a similar effect with sphingomyelin. The greatest increase in MT was observed with galactocerebroside (GC) however, which was pH dependent, indicating that chemical exchange was the predominant magnetisation transfer process (Kucharczyk *et al.* 1994).

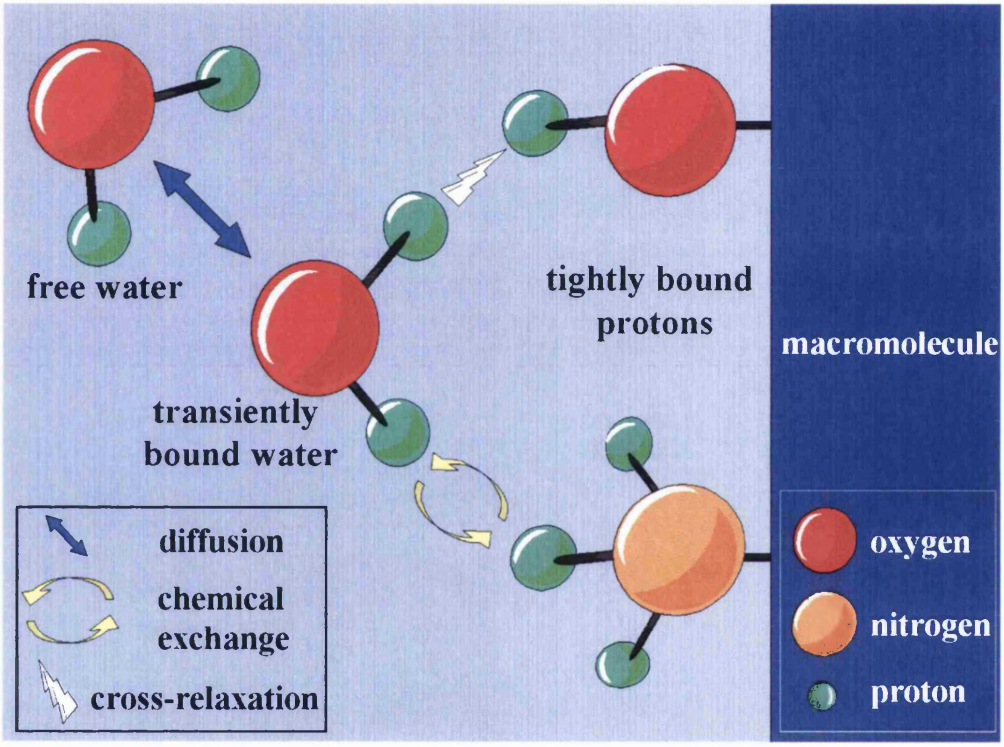

Figure 1.9: Schematic diagram of magnetisation transfer mechanisms in biological tissue, including cross-relaxation and chemical exchange interactions between macromolecular protons (hydroxyl and NH_3 groups) and transiently bound water.

Macromolecules are therefore not equally effective in modulating relaxation and MT. The presence of a hydroxyl group on the surface of a lipid membrane facilitates interaction between the molecule and surrounding water, thereby shortening the relaxation time and increasing the MT effect (Koenig 1991; Fralix *et al.* 1991; Koenig *et al.* 1990). Replacement of this hydroxyl group by, for example, a chloride, eliminates the MT effect (Koenig 1991). Cholesterol expresses a single hydroxyl group on its surface, whereas GC displays four. In addition, the hydroxyl groups in GC are orientated perpendicular to, and extend outward from the membrane surface, increasing the thickness of the interface region and further facilitating interactions with bulk water (Kucharczyk *et al.* 1994). These factors result in a greater MT effect in tissues containing predominantly GC, such as mature white matter.

Prior to myelin formation, cholesterol, phospholipids, fatty acids, and monoglycerides are abundant in white matter. With the onset of myelin synthesis, the amount of cholesterol and phospholipids increases further, and myelin-associated lipids (sphingomyelin, galactocerebrosides, and sulfatides) appear (Kinney *et al.* 1994). This results in mature white matter having a greater MTR than developing brain (van Buchem *et al.* 2001).

The concentration of sphingomyelin in mature white and grey matter is very similar and there is only one-third more cholesterol in white matter than grey (Morell *et al.* 1989). Galactocerebroside is three times more abundant in adult white than grey matter and is, therefore, the most likely explanation for the stronger MT effect in adult white than grey matter (Mehta *et al.* 1995a; Kucharczyk *et al.* 1994). In addition to the concentration of cerebroglycosides, cholesterol, sphingomyelin, and phosphatidylcholine, other possible explanations for white matter possessing a greater MT effect than grey matter include density of neurons, iron deposition, and tissue hydration and vascularity (Elster *et al.* 1994a; Silver *et al.* 1997a).

1.2.6.2 Development

In 1963, Forsen and Hoffman (Forsen and Hoffman 1963a; Forsen and Hoffman 1963b) investigated the magnetisation exchange dynamics between two chemicals with different resonant frequencies, using nuclear magnetic double resonance. Saturating RF excitation was applied sequentially at each spin resonance, whilst the magnetisation of the opposite spin resonance was measured. The first magnetisation transfer study of biological tissue was performed in 1977, by Edzes and Samulski who used the technique of "selective hydration inversion" to study collagen and muscle (Edzes and Samulski 1977). The earliest MR imaging studies employed an off-resonance RF pulse to selectively saturate the macromolecular protons, leaving the free water spins unperturbed, to improve image contrast (Muller *et al.* 1983; Wolff and Balaban 1989). Numerous methods to achieve selective saturation and hence examine the MT effect in MRI have been employed and include: continuous RF excitation via a separate channel (Wolff and Balaban 1989), off-resonance pulsed RF excitation using the same RF train as the transmit and receive signals to the coil (McGowan III *et al.* 1994), and on-resonance pulsed RF excitation after selective inversion hydration (Hu *et al.* 1992). The underlying principle of all of these MT methods is a comparison between a baseline condition and a condition in which the proton pool of interest has been indirectly disturbed in some way. The difference between these two states yields information about the imaged tissue, in particular the macromolecular environment, which is not directly obtainable from assessment of the conventional MR parameters of proton density, T1 and T2.

MT contrast can be examined by either visual qualitative assessment or by the calculation of quantitative parameters. Qualitative assessment includes the use of MT contrast (MTC) in magnetic resonance angiography (MRA) and following administration of exogenous contrast agents. The MT effect is generally more effective in tissues than fluids. In MRA therefore, the signal from tissue is suppressed whilst blood remains bright. Similarly, in studies using exogenous contrast agents, tissue signal from non-enhanced tissue is suppressed whilst contrast-enhanced tissue remains bright, thus enhancing lesion conspicuity (Elster *et al.* 1994b; Finelli *et al.* 1994; Mathews *et al.* 1995). This is because gadolinium (Gd) enhancement is caused by a water-Gd ion interaction, and not macromolecular cross-relaxation.

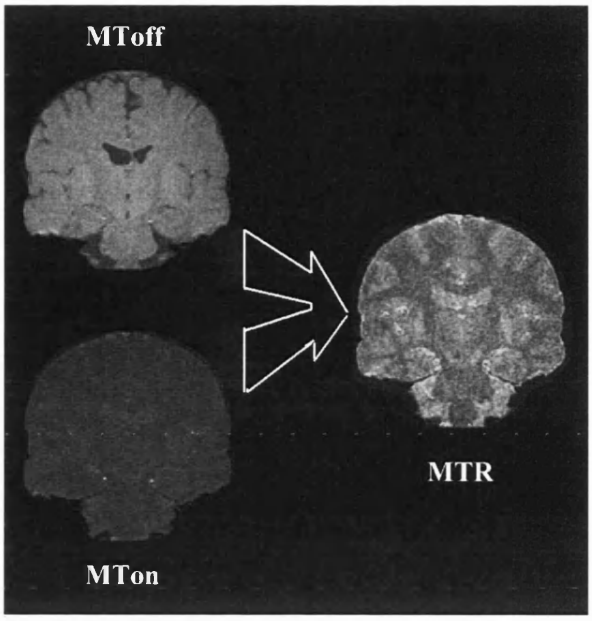

Figure 1.10: A diagram demonstrating the calculation of an MTR map from two images; one with a prior saturation pulse (MT_{on}), and the other without (MT_{off}).

Depending on the image acquisition parameters, the intensity of a region in an image obtained with MT contrast also reflects either proton density or a degree of relaxation-weighting. To obtain an index of MT effect which is relatively independent of the other tissue parameters, it is necessary to calculate a ratio of MTC derived from voxel values obtained from two sets of images, one with and one without the prior saturation pulse (Figure 1.10) The most common calculated parameter is the magnetisation transfer ratio (MTR)

$$\mathbf{MTR = (M_0 - M_s) / M_0 \times 100\%}$$

where M_s and M_0 are the magnitudes of the signals with and without the saturation pulse respectively. Each voxel therefore, contains quantitative information regarding the percentage of signal loss occurring as a result of the saturation of the immobile pool of protons, and consequently represents the efficiency of magnetisation transfer between the two pools. MTR values range from near zero in blood and CSF to greater than 50% in tissue that contains a high proportion of poorly mobile macromolecules, such as muscle (Wolff and Balaban 1989). The MTR map can be examined using region of interest analyses (Dousset *et al.* 1992), contour mapping (Kasner *et al.* 1997), or by the calculation of histograms (van Buchem *et al.* 1999).

Region of interest (ROI) analyses of MTR maps have been utilised in numerous studies of normal and pathological conditions (Silver *et al.* 1997a; Tofts *et al.* 1995; Tanabe *et al.* 1998; Foong *et al.* 2000a; Filippi *et al.* 1998c). The underlying principle of this technique is to calculate the mean MTR from a number of pixels that constitute a region drawn on an image. Although simple, reproducible and almost universally employed, ROI analyses are subject to partial volume effects from the inclusion of CSF and varying amounts of grey and white matter, and operator-induced bias, particularly regarding the sizing and positioning of the ROI. Methods of blinding the operators to the clinical data, or drawing ROI on co-registered non-MTR images have been adopted to overcome some of these limitations (Silver *et al.* 1997a). Contour mapping is an analysis technique which

demarcates tissue according to specific values of MTR, overlaying this information onto a co-registered anatomical image for accurate localisation. This display method is optimal for conditions with widespread pathological involvement, such as multiple sclerosis (MS) or progressive multifocal leucoencephalopathy (Kasner *et al.* 1997). Histogram analysis is an alternative technique for interrogating MTR data in conditions with diffuse abnormalities (van Buchem, McGowan, and Grossman 1999). Following MT imaging, the data set is segmented to remove extracerebral tissue. MTR values are then calculated for each pixel and from this, a mean MTR value and a graphical representation of the range of MTR values and pixel counts are obtained. These histograms are then normalised to account for differences in cerebral volume between individuals. A number of variables can be evaluated and compared with a control MTR histogram, processed under identical conditions. These variables include, location of the peak on the *x* axis (median MTR value) and *y* axis (number of pixels at the median MTR value), and 25^{th}, 50^{th} and 75^{th} percentiles. Differences in these parameters between controls and patients yields information about the burden of disease, or lesion load in the whole brain. MTR histogram analysis offers a number of benefits including, the assessment of normal appearing tissue in addition to conventional MRI visible pathological tissue, and the absence of operator-induced bias. However, the technique lacks localising information, is particularly sensitive to partial volume effects and tissue atrophy and, by including MTR values from every pixel in the brain, minor or subtle changes may be overlooked due to the overwhelming number of normal values. Furthermore, only a distribution of pixel MTR values, rather than absolute values is obtained (Silver *et al.* 1998). This technique has been used to study age-related changes (Tanabe *et al.* 1997) and most commonly, MS (van Buchem *et al.* 1996; van Buchem *et al.* 1997).

In addition to the calculation of MTR, alternative quantitative parameters for the evaluation of the MT effect include the measurement of T1 values with and without the saturation pulse ($T1_{sat}$ and T1 respectively). Theoretically, the variation in the T1 values under these two conditions describes the rate of magnetisation transfer more accurately than MTR which is, by comparison, more susceptible to alterations in the experimental conditions (McGowan 1999). The difficulty however, is that the measurement of T1 and $T1_{sat}$ is challenging, and relies on the creation of a perfect selective saturation condition. This is a practical impossibility which, once again, results in the estimation of MT being dependent upon the acquisition parameters. The Z-spectrum is a term used to describe the variation of MT with saturation pulse frequency. As the frequency of the offset saturation pulse is moved further and further away from water resonance, the MT effect diminishes. Applying the pulse at a frequency close to resonance will begin to affect the water spins directly. Mapping the Z-spectra for a range of saturation power levels may allow complete characterisation of a tissue with regard to its relaxation and exchange properties (Holt *et al.* 1994; Grad *et al.* 1990). This technique has most recently been applied in an MTI study of demyelination, where a number of parameters, including the bound water fraction, exchange rate, and transverse relaxation time of the bound pool were altered in cerebral tissue derived from patients with MS compared to control brain. This was achieved on a 1.5T scanner in a clinically acceptable scan time, suggesting that this technique may be extended to in vivo human studies (Ramani *et al.* 2001). A number of related techniques have been developed which yield parametric images of the fractional size of the restricted pool, magnetisation exchange rate and the relaxation times of both the restricted and free proton pools (Sled and Pike 2001).

Early MTI methods employed a continuous radiofrequency wave to provide off-resonance saturation of macromolecules (Wolff and Balaban 1989). These long pulses, delivered by an auxiliary RF amplifier, had a very narrow bandwidth to minimise direct saturation of the water resonance. Clinical application was limited, however,

by long scanning times and safety issues regarding energy deposition. Pulsed saturation techniques employ either a brief off-resonance or on-resonance RF pulse to selectively saturate the "bound" pool of protons (Hu *et al.* 1992; Yeung and Aisen 1992). Off-resonance pulse techniques exploit the different bandwidths of the proton pools in the same way as continuous wave, and similarly encounter high specific absorption rates (SAR). They are, however, more time-efficient, amenable to currently available MRI hardware, and easily incorporated into commonly used multi-slice sequences. Recent advances in off-resonance techniques, in particular the use of a double quantum filter to selectively excite the restricted proton pool, enables independent control of the effect of the macromolecule characteristics, chemical exchange, and water-related parameters on the images (Neufeld *et al.* 2003). On-resonance techniques use low flip angle saturation pulses at varying phases to obtain selective saturation (Hu *et al.* 1992). This results in reduced energy deposition in tissue and minimal direct saturation of the freely mobile pool of protons, but at the expense of greater sensitivity to motion artefacts and field inhomogeneities.

Qualitative assessment of MTC requires the acquisition of only a single image. To calculate a map of MTR, images with and without the saturation pulse must be obtained. To ensure accurate and reliable quantitative MTR results are obtained, particularly where image intensity is varying rapidly with position (for example, in small lesions), the two data sets require coregistration. Assuming that there is no significant movement over the time required to collect one complete phase encode step (typically a few seconds) interleaved MR sequences result in exact co-registration of images (Barker *et al.* 1996). These sequences, particularly MTI, are however, inherently time-inefficient as delays occur whilst the MT effect builds and diminishes between each slice. High resolution MTI with satisfactory slice-coverage in a time suitable for clinical studies is therefore not possible. An alternative approach is to acquire MT-weighted and non-MT-weighted images consecutively (Boulby *et al.* 2000). This is time-efficient, but sensitive to positional change occurring between the acquisition of the separate images (several minutes). Post-processing co-registration is possible however, permitting correction of intrasubject positional variation and serial MTI studies to be performed. Accurate translation of these images and subsequent correct calculation of the MTR map is greatly facilitated if the acquisition is 3-dimensional (Hajnal *et al.* 1997).

1.2.6.3 Limitations of in vivo MTI

MTR is not an absolute measure, but is highly dependant upon the chosen imaging parameters. These include, the bandwidth, shape, power and frequency offset of the MT pulse, inter-pulse interval, and the presence of direct saturation effects on the "free" water resonance (Silver *et al.* 1999). Further, MT pulses are not slice selective, require high RF power and deposit significant energy in the tissue, which may result in exceeding the SAR limits. MTI is also affected by patient motion which may require additional, corrective pre-processing steps (Hajnal *et al.* 1997).

The significant number of imaging variables affecting the resultant quantitative MT measures has resulted in a lack of standardisation across imaging centres. This precludes meaningful comparison of, for example, MTR maps, in patients imaged on different scanners. Furthermore, longitudinal studies require consistent imaging and processing parameters to be used over the study period; any deviation will invalidate the results. The implementation of a standardised sequence that performs identically on different scanners and provides adequate slice coverage within a clinically acceptable time is therefore an important goal. Alternatively, the use of

correction factors or histogram analysis techniques may obviate the need for a standardised imaging protocol across centres (Silver, Barker, and Miller 1999).

1.2.6.4 Clinical Applications

1.2.6.4.1 Normal tissue

Initial MT studies of biological tissue were undertaken by Edzes and Samulski in 1977, who examined excised collagen and muscle (Edzes and Samulski 1977). The first in vivo MTI studies, by Wolff and Balaban in 1989, evaluated the image contrast obtained by saturating the macromolecular proton pool, in skeletal muscle and kidney (Wolff and Balaban 1989). The qualitative finding of a greater MT effect in the renal cortex than in the renal medulla was quantified in 1991 by Eng et al, who suggested that the higher lipid bilayer content of the cortex may be responsible (Eng *et al.* 1991).

The earliest clinical application of MT imaging involved the qualitative evaluation of MTC in musculoskeletal disorders. Significant improvements in the contrast between articular cartilage and synovial fluid were observed suggesting that a more accurate assessment of arthritic conditions may be possible (Wolff *et al.* 1991a). Other normal tissues that have been studied with MTI include the heart, where improved contrast between the myocardium and vascular compartment may provide useful information in volumetric or coronary angiographic studies (Balaban *et al.* 1991); the eye, where a more detailed evaluation of the lens including the degree of hydration was possible (Ceckler *et al.* 1991); the liver, the MT of which showed considerable variation amongst normal subjects, thought possibly to relate to iron deposits or a recently ingested high fat meal (Kajander *et al.* 1996; Salo *et al.* 1997); breast tissue (Pierce *et al.* 1991); striated muscle, renal cortex, spleen (Kajander *et al.* 1996); head and neck structures (Yousem *et al.* 1994); and most extensively, the central nervous system (Wolff *et al.* 1991b; Edelman *et al.* 1992; Koenig *et al.* 1990; Silver 1997a; Mehta, Pike, and Enzmann 1995a).

In the early animal studies of MTC in cerebral tissue, significant improvement in grey-white matter contrast was observed and, furthermore, the level of contrast could be determined by the power or duration of the off-resonance RF pulse (Wolff, Eng, and Balaban 1991b). Similar improvements in contrast were seen in human brain and spinal cord (Hu *et al.* 1992). A subsequent, quantitative, experimental study on bovine optic nerve proposed that the MT characteristics of white matter related mainly to myelin, suggesting that MTI is particularly sensitive to demyelinating conditions (Stanisz *et al.* 1999).

A quantitative MTI study of normal human subjects reported a lower MTR in grey matter than white matter, with the genu of the corpus callosum possessing the greatest MT effect. There was no significant difference in MTR values between different grey matter regions, although a trend towards higher MTR values in the thalamus was observed. The higher MTR in the corpus callosum may be due to the presence of a large number of myelinated fibres (approximately 300 million), and the greater MT effect in the thalamus, compared to other grey matter tissue, is consistent with the presence of afferent and efferent myelinated fibres within this structure. This study also found no interhemispheric, sex or age-related MTR changes in either tissue compartment (Mehta, Pike, and Enzmann 1995a). More recently, Silver et al also reported that the corpus callosum possessed the highest MTR values compared to other white matter structures, and, in addition, noted interhemispheric and age-related

differences in normal subjects. Higher MTR values were found in the left hemisphere compared to the right, possibly related to cellular, morphological and functional asymmetry between the hemispheres (Wada *et al.* 1975; Shapiro *et al.* 1986). Increasing age was associated with reduced MTR in all white matter regions studied, and was attributed to neuronal and myelin loss, alterations in water content and phospholipid metabolism (Silver *et al.* 1997a). The discordant results between these two studies are probably related to differences in the imaging parameters, subject recruitment criteria, and data analysis methods, thus highlighting the importance of standardising imaging and processing techniques across centres.

Age-related MT changes have been addressed in a number of other cross-sectional studies. In particular, MTC images and MTR histograms have been examined during infant and child development (van Buchem *et al.* 2001; Engelbrecht *et al.* 1998). Engelbrecht et al qualitatively examined MTC images of normal children aged 1 week to 80 months and found increasing MTC in white matter with advancing age. This was inversely proportional to T2 relaxation times and was attributed to the formation of myelin (Engelbrecht *et al.* 1998). These findings were later quantified by van Buchem et al who used histogram analyses to examine the relationship between increasing age and MTR values in children aged 3 weeks to 16 years (van Buchem *et al.* 2001). As expected, the mean MTR increased with brain maturation, consistent with myelination and, more specifically, the increasing concentration of galactocerebrosides. However, the peak histogram height was the parameter which most closely paralleled increasing age. Although the most rapid changes in MTR parameters occurred during the first 2 years of life, the peak histogram height continued to change for a significantly longer period, in agreement with pathological data which suggests that myelination continues up to the third decade (Yakovlev and Lecours 1967).

The technique of analysing MTR histograms was also applied to the study of healthy subjects aged 65 to 85 years. In particular, areas of asymptomatic white matter signal hyperintensity, identified on T2-weighted images, were compared with normal appearing white matter. MTR values were approximately 10% lower in areas of signal hyperintensity compared to normal white matter implying loss of structural integrity, and furthermore, MTR values in all tissue compartments were inversely proportional to increasing age (Tanabe *et al.* 1997). Pathologic correlates of asymptomatic areas of white matter hyperintensity include dilated Virchow-Robin spaces, infarction, gliosis, cystic cavitation, axonal loss, and chronic extravasation of fluid. The authors hypothesised that by analysing the histograms further, in particular to see whether the histogram is constructed from a single distribution or mixture of distributions, subclassifications of abnormal tissue may be elucidated.

1.2.6.4.2 Epilepsy

The earliest MTI study in epilepsy was undertaken in 1995 by Tofts et al, who used a hippocampal region-of-interest based analysis to investigate three patients with temporal lobe epilepsy (Tofts *et al.* 1995). Reduced MTR was found in the abnormal hippocampi of all patients, as defined by MR-identified volume loss and EEG data. The contralateral hippocampus, in each case, had normal MTR values. Gliosis in the affected hippocampi was suggested as the pathological correlate for the reduced MTR. More recently, Li et al, attempted to confirm these findings in a larger cohort of patients with TLE. MTR values of amygdalae and hippocampi in 10 patients were compared with similar regions in control subjects. Three patients had significantly different MTR values compared to the control group; however, only one was concordant with electroclinical data. It was suggested that although

there was neuronal loss in the affected hippocampi, a decrease in hippocampal volume may result in the cell density, and therefore the MTR, remaining relatively preserved (Li *et al.* 2000). It is also possible that a change in the concentration and distribution of macromolecules as a result of gliosis may lead to an increase in MTR, even in the presence of neuronal loss and reduced tissue density. In addition to region-of-interest based analyses, MTR histograms have also been utilised in the investigation of patients with epilepsy. Compared with control subjects, patients with nocturnal frontal lobe epilepsy (NFLE) had lower MTR histogram peak heights, suggesting subtle widespread abnormality (Ferini-Strambi *et al.* 2000). No differences in MTR between frontal and non-frontal cerebral tissue were detected, consistent with the knowledge that NFLE is a genetically determined ion channel disorder which presumably affects all neurons. The authors proposed that the pathological substrate for the abnormal MTR in these patients was diffuse gliosis, however, the rationale behind this hypothesis is not clear and, moreover, the MTR in patients with idiopathic generalised epilepsy, who were studied concurrently, was normal. Alternative suggestions for the reduced MT effect may include: altered cell membrane structure or permeability, or reduced macromolecular concentration or cell density. MTI was also used to study patients with solitary cysticercal brain cysts and focal epilepsy (Pradhan *et al.* 2000; Gupta *et al.* 1999a). Perilesional gliosis, only visible on MTC images, was associated with refractory epilepsy and a greater chance of seizure recurrence on cessation of anti-epileptic medication. The authors concluded that in patients with neurocysticercosis, MTI provides prognostic information (Pradhan *et al.* 2000). In a region-of-interest based study of 10 patients with malformations of cortical development (MCD), abnormal MTR values were identified in the grey matter of 7 patients (Sisodiya *et al.* 1996a). These were all within the MCD identified on routine MRI. No white matter or extralesional MTR abnormalities were detected.

1.2.6.4.3 Other conditions

Initial MTI studies of CNS disorders were used to accentuate MR angiography and to increase the conspicuity of gadolinium contrast enhancement. The application of a saturation prepulse in contrast-enhanced imaging increases the contrast-to-noise ratio and improves conspicuity of normal cerebral structures and cerebral pathology (Finelli *et al.* 1994; Kurki *et al.* 1992; Elster *et al.* 1994a). Knauth et al compared MTI and a single dose of contrast agent, with non-MT imaging and a triple dose of contrast agent, in 24 patients with cerebral neoplasia and found the two methods to be equally efficacious in identifying lesions (Knauth *et al.* 1996). In demyelinating disease, however, triple-dose non-MT imaging reveals more lesions than single-dose MTI (van Waesberghe *et al.* 1997; Silver *et al.* 1997b; Bastianello *et al.* 1998).

MTR in disorders of white matter was first addressed in a study of guinea pigs with experimental auto-immune encephalomyelitis (EAE) and patients with multiple sclerosis (MS) (Dousset *et al.* 1992). The EAE induced in the animal model resulted in signal hyperintensity on T2-weighted images, only minimal demyelination on histopathological examination, and a reduction in MTR of approximately 5-8%. Intralesional MTR was reduced by approximately 26% in the patients with MS, suggesting that demyelination affects MTR more profoundly than tissue oedema. Further correlation of histopathological abnormalities with MTR was provided by a study of relapsing EAE with demyelination in non-human primates (Brochet and Dousset 1999). A close relationship between the degree of demyelination and decrease in MTR was observed. Furthermore, during pathologically

proven remyelination, MTR increased. This may have been partly due, however, to resolution of tissue oedema. A post-mortem MTI study of brains from patients with MS similarly showed a strong correlation of reduced MTR with the degree of demyelination and percentage of residual axons (van Waesberghe *et al.* 1998). Overall, it appears that demyelination and axonal loss are the principal determinants of reduced MTR in MS, although inflammation and oedema contribute, albeit to a lesser extent (Brochet and Dousset 1999).

A large number of clinical studies have been performed in MS. Region-of-interest analyses of MS lesions and normal appearing white matter (NAWM) have shown a range of abnormal MTR values within lesions suggesting the presence of a spectrum of pathological change and, in addition, reduced MTR in NAWM when compared to control subjects (Filippi *et al.* 1995a; Loevner *et al.* 1995; Filippi *et al.* 1998c; Laule *et al.* 2003). Baseline disability has been correlated to T1-lesion load (Truyen *et al.* 1996), and inversely correlated to average lesion MTR (Gass *et al.* 1994). Furthermore, the average change in brain MTR between baseline and at 1 year has shown a relatively high specificity and positive predictive value for Expanded Disability Status Scale score deterioration over a 4.5 year period in individual patients with MS (Rovaris *et al.* 2003a). MTR ROI analysis has been applied to the study of the evolution of MS lesions. Filippi et al reported that abnormal MTR in NAWM preceded the appearance of new enhancing lesions (Filippi *et al.* 1998c), a finding later corroborated by others (Goodkin *et al.* 1998; Laule *et al.* 2003; Guo *et al.* 2001). Post-mortem histological examination of NAWM in such patients revealed diffuse astrocytic hyperplasia, patchy oedema, perivascular infiltration, abnormally thin myelin, and axonal damage (Allen and McKeown 1979; Adams 1977). MTR decreases rapidly with the appearance of early enhancing lesions. This is followed either by continued decline of MTR, or complete or partial normalisation, which may represent remyelination. The lowest MTR exists in lesions which are hypointense on T1-weighted images, a lesional characteristic that is associated with severe demyelination and axonal loss (van Waesberghe, Kamphorst, and van Walderveen 1998).

A marked reduction of MTR was observed in the pons of a patient with central pontine myelinolysis, again suggesting that myelin is the principal determinant of the MT effect in biological tissue (Silver *et al.* 1996). This is further supported by evidence from a study of HIV encephalitis, a condition with significant neuronal damage but minimal demyelination. MTR was only moderately reduced within each lesion despite extensive signal change on conventional MRI and marked cognitive impairment (Dousset *et al.* 1997).

Acute cerebral infarction becomes evident on MTI after approximately 7 days (Kovacs *et al.* 1997). Subsequently, MTR progressively decreases over the next 12 months, allowing the age of an infarct to be estimated (Prager *et al.* 1994). Overall, infarction results in a less pronounced decline in MTR than demyelination, thereby providing a means to differentiate the two conditions (Mehta *et al.* 1996; Reidel *et al.* 2003).

Reduced MTR within normal-appearing white matter in patients with traumatic brain injury and persistent neurological deficit has been reported. No patients with complete recovery had an abnormal MTR within NAWM, suggesting that MTI is a sensitive method for the detection of subtle traumatic cerebral injury (Bagley *et al.* 2000).

Quantitative MTI has been applied to a number of conditions in both experimental and clinical settings (table 1.7).

Table 1.7 Other central nervous system disorders evaluated with MTI

Disease / Condition	Magnetisation transfer imaging
Schizophrenia (Foong *et al.* 2000a; Foong *et al.* 2001; Bagary *et al.* 2003; Bagary *et al.* 2002)	Reduced cortical MTR in fronto-temporal regions and in white matter incorporating the fasciculus uncinatus.
Migraine (Rocca *et al.* 2000)	Normal MTR values despite the presence of white matter abnormalities on T2-weighted images
Chronic obstructive and normal pressure hydrocephalus (Hahnel *et al.* 2000; Hahnel *et al.* 1999)	Reduced MTR in normal-appearing white matter suggesting diffuse WM injury
Cerebral infection (Mehta *et al.* 1995b; Pui 2000; Runge *et al.* 1995; Kathuria *et al.* 1998; Gupta *et al.* 1999b; Pradhan *et al.* 2000; Gupta *et al.* 1999b; Burke *et al.* 1996)	Qualitative improvement in lesion conspicuity and meningeal thickening or enhancement using MTI. MTR reduced in cystic cerebral infection although to a lesser extent than cystic infarction or tumour allowing pathological differentiation. Improved visualisation of perilesional gliosis in neurocystercicosis
Systemic auto-immune mediated disorders (Rovaris *et al.* 2000)	Abnormal MTR histogram parameters in systemic lupus erythematosus but not Bechet's disease, Wegener's granulomatosis or anti-phospholipid syndrome.
Amyotrophic lateral sclerosis (Tanabe *et al.* 1998; Kato *et al.* 1997)	Reduced MTR in corticospinal tracts, even when T2 was normal. This is not, however, universally accepted.
Cerebral tumours (Kurki *et al.* 1996; Boorstein *et al.* 1994)	Significant MT effect in high-grade gliomas and meningiomas allows differentiation from low-grade gliomas. Abnormal MTR in normal appearing tissue around metastatic tumours, even beyond inc. T2 signal.

Neurodegenerative diseases - Alzheimer's disease (Hanyu *et al.* 1999; Imon *et al.* 1998; van der Flier *et al.* 2002).	Reduced MTR in the corpus callosum despite normal conventional MRI. Peak heights of MTR histograms of patients with mild cognitive impairment and AD patients were lower than those of controls for the whole brain and, in particular, the temporal and frontal lobes.
Multiple system atrophy (Naka *et al.* 2002).	MT imaging revealed more extensive changes in pons, cerebral peduncles and putamen than conventional MRI
Parkinson's disease and progressive supranuclear palsy (Hanyu *et al.* 2001b)	No difference in MTR between patients with PD and controls, unless associated with dementia or as part of PSP when reduced MTR was seen in subcortical white matter and subcortical grey matter nuclei respectively.

1.2.7 T2 mapping

1.2.7.1 Theory

In 1946, Felix Bloch presented a set of mathematical formulations describing the phenomenon of "nuclear induction" - the stimulated absorption and emission of energy from nuclei placed within a magnetic field (Bloch 1946). Two time constants were introduced, T1 and T2 which described the re-establishment of nuclear magnetisation equilibrium following a radiofrequency pulse. T1 refers to the regrowth of longitudinal magnetisation, whereas T2 describes the decay of the transverse components, i.e. loss of phase coherence. The T2 relaxation time is the time for the transverse magnetisation to decay to e^{-1} or approximately 37% of its initial value. (Figure 1.11).

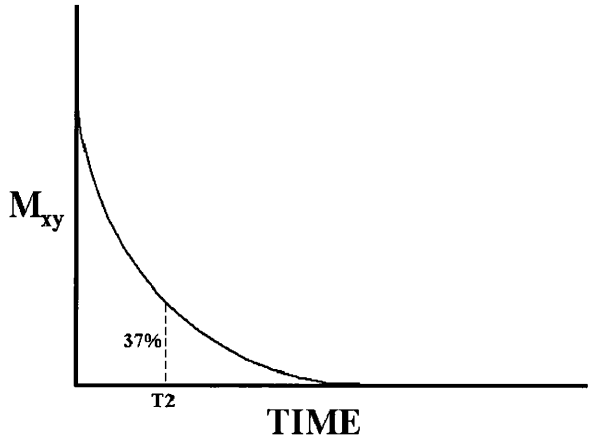

Figure 1.11 T2 decay curve. T2 is the time for the transverse magnetisation (M_{xy}) to decay to approximately 37%.

T2 relaxation, which is also called spin-spin relaxation, results from any intrinsic process that causes spins to lose their phase coherence in the transverse plane. Typically, this is due to the influence of static or slowly fluctuating variations in the local magnetic field, within the tissue itself. If a spinning proton transiently experiences a change in the local field due to a slow interaction with another spinning proton or through an alteration in the chemical environment, it temporarily precesses at a slightly different frequency and thus becomes out of phase with other spinning protons. This process is extremely efficient when protons interact with molecules, such as membrane lipids and most macromolecules, which are moving, or "tumbling", at rates significantly lower than the Lamour frequency. This results in large molecules possessing a short T2 relaxation time, often too short to be visible on standard MR sequences. Conversely, when molecular motion is rapid, for example in cerebrospinal fluid, any local field inhomogeneities experienced by a proton average to zero over a short time and an effective distortion in the local magnetic field is not seen. The T2 relaxation process is therefore inefficient and T2 values are correspondingly long (Fullerton 1992) (Table 1.8).

Table 1.8 Tissue compartments with hydrogen fractions and corresponding T2 relaxation rates.

Tissue Compartment	*Hydrogen fractions*	*T2 relaxation rate*
Macromolecules	5 - 8%	10 - 100 μsec
Partially bound / Hydration layer water	3 - 5%	5 – 10 msec
Bulk / Free water	90%	1 - 2 sec
Mobile Fatty Acids	varies with tissue	~100 msec

Theoretically, T2 relaxation results only from interactions at the atomic and molecular levels within the tissue. In practice, however, transverse magnetisation decays more rapidly than predicted, due to inhomogeneities in the main magnetic field or susceptibility-induced field distortions produced by tissue placed within the field. This results in a shorter T2 relaxation time which is designated $T2^*$ (T2-star).

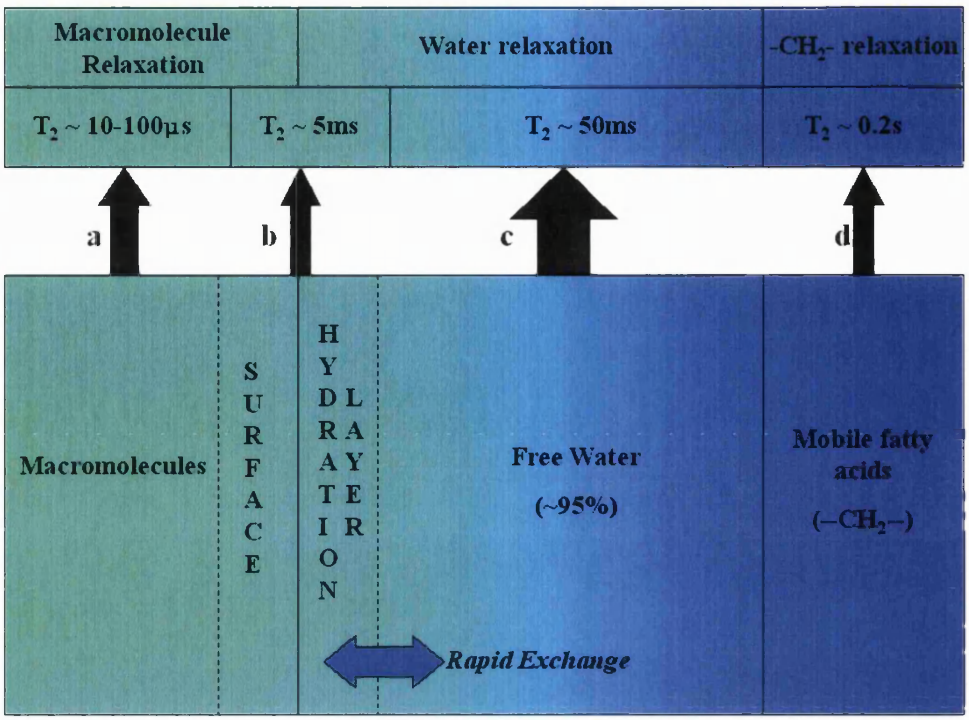

Figure 1.12: Fast exchange state model for T2 relaxation in normal tissue. Three chemically different proton pools are identified: macromolecules excluding mobile fatty acids, water protons, and mobile fatty acid protons. Rigid lattice dipole-dipole interactions (a), local field inhomogeneities at macromolecule-hydration layer interface (b), exchange diffusion (c), slower reorientation and translation (d), give rise to relaxation times indicated by the solid black arrows; the width representing the contribution to the total signal. (adapted from Bottomley *et al.* 1987).

The transverse relaxation time of a specific tissue is sensitive to the total amount of water present, its distribution, and its interaction with the microstructural environment (Figure 1.12). Pathological processes may cause a disturbance to any or all of these factors, which will in turn modify the relaxation times and, therefore, the image contrast. An increase in T2 relaxation time in pathological tissue compared to the normal state is generally considered to be due to (Mathur-De Vre 1984):

- an increase in total water content
- an increase in the ratio of free to bound water
- a change in the dynamic structure of water near macromolecules
- a change in the structure of intracellular water
- a change in the concentration of paramagnetic ions

In the presence of a single proton species in a homogeneous environment, T2 decay is monoexponential. This becomes more complicated in biological tissue, where multiple "compartments" are present, for example, the intra- and extracellular space. In addition, the molecular environment is dynamic with proton exchange and water diffusion occurring continuously. If two compartments are present but are exchanging rapidly, or if one of the compartments is small (for example, the extracellular space in normal white matter), then effectively only one

combined "compartment" can be imaged and the transverse decay will be monoexponential. If both compartments are large or exchange between them is negligible then multiexponential decay may be demonstrated. This has been reported in both normal (Whittall *et al.* 1997; Whittall *et al.* 1999; Gareau *et al.* 1999) and pathological tissue (Naruse *et al.* 1982; Kidd *et al.* 1997; Armspach *et al.* 1991; Harrison *et al.* 1995). In normal human white matter, three separate pools of protons, each with a distinct decay curve, have been described using a multi-echo spin echo sequence (Whittall, MacKay, and Li 1999; Whittall *et al.* 1997). A pool with T2 relaxation times of between 10 and 50ms was believed to be water protons compartmentalised between myelin bilayers. A larger pool of intra- and extra-cellular water possessed T2 times of approximately 70msec, and protons with T2 times greater than 1 second were believed to be CSF. Supporting evidence for the multi-compartment model is provided by experimental work by Beaulieu et al, who studied excised myelinated and non-myelinated garfish nerves. Medium and long T2 components were seen in all nerve types but the short T2 component, which was clearly demonstrated in myelinated nerves, was absent in non-myelinated fibres (Beaulieu *et al.* 1998). Using a multi-echo sequence and, for example, a least-squares algorithm to convert relaxation decays into exponential components, the total tissue water content, myelin fraction, and distribution of T2 values in each structure can be estimated. The construction, therefore, of "short T2 maps" may permit the detection of subtle demyelinating pathology before it is apparent on conventional imaging (Moore *et al.* 2000; MacKay *et al.* 1994; Vavasour *et al.* 1998).

Biexponential T2 decay has been reported in experimental oedema, with a short T2 component representing intracellular water, and a long T2 component representing oedematous intramyelinic spaces. The magnitude of the long T2 component was proportional to the degree of oedema, determined ultrastructurally (Barnes *et al.* 1986a; Barnes *et al.* 1986b). Furthermore, transverse decay curve characteristics have been shown to discriminate between vasogenic and cytotoxic oedema, reflecting the different protein contents in each state (Barnes *et al.* 1987). This distinction was not possible on visual assessment of the images. Conversely, tissue gliosis is characterised by only mildly elevated T2 relaxation times and a monoexponential decay curve, reflecting minimally increased total tissue water content and increased water shifts as a result of loss of restrictive myelin layers (Barnes *et al.* 1988).

1.2.7.2 Development

A number of different methods have been described for measuring T2. In liquids, T2 times can extend over many seconds. Over this time course, accurate measurements of T2 are hampered by inhomogeneity of the magnetic field. To overcome this, and estimate the true, "natural" T2, several techniques were proposed (see Meiboom and Gill 1958). The most widely used of these, was the spin echo method described by Hahn in 1950 (Hahn 1950). Although this compensated for field inhomogeneity, the measurement of very long T2s remained limited by molecular self-diffusion. In 1954, Carr and Purcell introduced a modification of the Hahn spin-echo experiment which reduced the error caused by diffusion (Carr and Purcell 1954). This modification used a succession of 180^0 pulses after a single 90^0 pulse, instead of the Hahn method which relied on a series of linked 90^0 and 180^0 pulses. However, small deviations in the 180^0 pulse amplitudes led to substantial cumulative error, and poor measurement reproducibility. In 1958, Meiboom and Gill published a further modification of the spin-echo experiment, in which the initial 90^0 pulse was shifted by 90^0 relative to the phase of the 180^0 pulses. This corrected the cumulative effect

of inaccurate 180^0 pulses, and therefore permitted the measurement of long T2 values without an appreciable effect from molecular diffusion, and with good reproducibility (Meiboom and Gill 1958). The Carr-Purcell-Meiboom-Gill (CPMG) sequence remains the basis for conventional qualitative and quantitative T2-weighted imaging.

In 1986, Hennig introduced a fast T2-weighted sequence, called rapid acquisition with relaxation enhancement (RARE) (Hennig *et al.* 1986). This influenced the development of fast spin echo (FSE) imaging by others in the early 1990s (Mulkern *et al.* 1990; Melki *et al.* 1991). In a standard conventional spin echo (CSE) sequence, one line of k-space (the spatial frequency domain) is completed within a single TR interval. In FSE imaging, multiple, closely spaced echoes are produced, each separately phase encoded to represent a different line in k-space. Thus k-space is filled more rapidly than with CSE, and scan times are shorter, typically by a factor of two or more. It is important to note, however, that each line in k-space has different transverse relaxation weighting (Listerud *et al.* 1992). Furthermore, image contrast between CSE and FSE imaging is often dissimilar, relaxation times can vary by 25-30% (Constable *et al.* 1992), and reproducibility of FSE is inferior to CSE (Duncan *et al.* 1996). Recently, FSE imaging has been shown to provide stable, reproducible and clinically useful T2 relaxation times in the hippocampus in patients with temporal lobe epilepsy; and considerably shorter acquisition times than is possible with CSE (Okujava *et al.* 2002). In addition to the Hahn spin-echo method for obtaining T2 relaxation times, it is possible to generate echoes using a gradient-echo technique. Instead of recovering de-phased signal using a 180^0 pulse, reversal of an applied magnetic gradient will change the direction of precession and refocus the spins. Unlike the spin-echo method, this technique does not correct for macroscopic distortions in the local magnetic field due to, for example, susceptibility effects, and the relaxation times obtained are therefore denoted T2*. This is particularly useful in, for example, functional imaging to evaluate local concentrations of deoxyhaemoglobin, and post-head injury to look for haemosiderin deposits (Parizel *et al.* 1998).

It is possible to apply an inversion pulse to standard T2-weighted sequence to suppress the signal from cerebrospinal fluid, overcome partial volume effects and increase lesion conspicuity, particularly in mesial temporal lobe structures or in the neocortex. This is the basis of fast fluid-attenuated inversion recovery (FLAIR) imaging. (See chapter 1.2.2). Although visual, qualitative evaluations of T2-weighted images are sensitive to pathological change, mostly as a result of altered tissue water, quantitative analyses yield additional abnormalities (Woermann *et al.* 1998a; Jackson *et al.* 1993b). Quantitation requires both accuracy and reproducibility, of which reproducibility is the most important. Good precision (or reproducibility) allows the comparison of individual measurements with a normal range to identify abnormalities with maximum sensitivity. It does not permit multi-centre studies however, unless identical hardware and imaging sequences are utilised (Tofts and du Boulay 1990). It has been shown that single-slice multi-echo CPMG sequences are capable of estimating T2 relaxation times accurately (Johnson *et al.* 1987; Whittall *et al.* 1997; Whittall, MacKay, and Li 1999). However, multi-echo sequences run in multi-slice mode are inaccurate due to increased artefacts and inadequate TR intervals which prevent the collection of a complete set of slices at each echo time. Current practice is to use either a single slice multi-echo sequence or a dual-echo sequence if more than one slice is required (Tofts and du Boulay1990). Multi-echo sequences, in addition to improved accuracy, also allow the magnetisation decay curve to be fully characterised, and analysed for multi-exponential components. This may prove beneficial in the future investigation of white matter diseases, such as multiple sclerosis (Moore *et al.* 2000; MacKay *et al.* 1998). Multi-

slice dual-echo experiments are more useful in, for example, temporal lobe epilepsy, where reproducible T2 measurements through the whole hippocampus are of paramount importance (Duncan, Bartlett, and Barker1996).

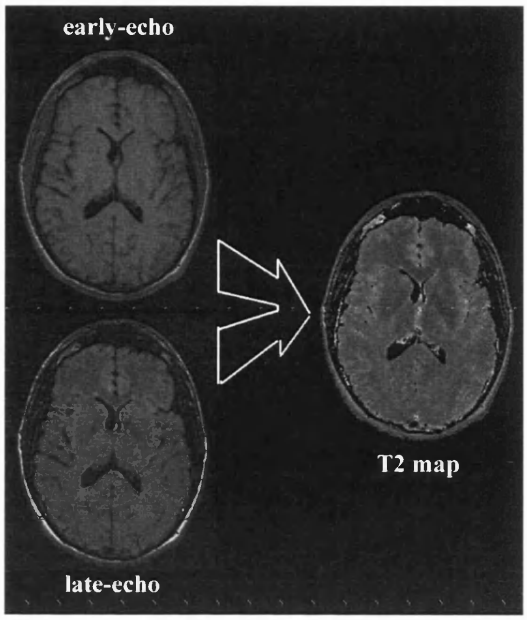

Figure 1.13: A diagram demonstrating the calculation of a T2 map from two images with different echo times.

The calculation of T2 relaxation times from dual-echo data is relatively straightforward. The T2 relaxation function of a pixel can be described as a monoexponential decay:

$$M_{xy}(1) = M_{xy}(0)\, e^{-TE(1)/T2} \qquad \text{and} \qquad M_{xy}(2) = M_{xy}(0)\, e^{-TE(2)/T2}$$

where M_{xy} is the magnetisation at times (0), (1) and (2) and TE (1) and TE (2) are two echo times where TE (2) > TE (1). T2 can then be estimated from the expression:

$$T2 = \frac{(TE(2) - TE(1))}{\ln (M_{xy}(1) / M_{xy}(2))}$$

Following the acquisition and calculation of T2 maps, quantitative evaluation can be made using a number of different methods. These include a standard region-of-interest (ROI) approach (Woermann *et al.* 1998a), histogram based analyses (Armspach *et al.* 1991; Rumbach *et al.* 1991) or semi-quantitative visual rating scales (Scheltens *et al.* 1993; O'Sullivan *et al.* 2001). More sophisticated techniques have also been employed including statistical parametric mapping (Auer *et al.* 2001), cluster analyses based on feature-space segmentation methods (Soltanian-Zadeh *et al.* 1998; Jacobs *et al.* 2001b), measures of tissue complexity using multifractal analysis (Takahashi *et al.* 2001), and texture maps (Kjaer *et al.* 1995) and colour-coded images derived from multiparametric data (Alfano *et al.* 1992).

1.2.7.3 Clinical applications

1.2.7.3.1. Normal tissue

Generally, T1 and T2 values correlate most strongly with the bulk water content of a tissue. The more water in a tissue, the longer the T1 and T2 times. Exceptions to this generalisation include tissues with a high concentration of aliphatic lipid protons. These storage fats have a short T1, but long T2. They tumble at a frequency close to the Lamour frequency and therefore cause only minimal distortion to the local magnetic field; a necessary requirement for the decay of transverse magnetisation. In cerebral tissue however, the MR signal arises almost entirely from bulk water protons and therefore changes in total water content, the degree of binding and water compartmentalization will result in alterations in T2. This was evident in studies on human preterm neonates where T2 relaxation times, analysed quantitatively, decreased with brain maturation (Ferrie *et al.* 1999; Counsell *et al.* 2001). Elevated T2 times were seen in the perinatal period, due to a high interstitial water content (Thornton *et al.* 1999). During brain maturation, tissue water decreases (from 88% by weight at birth to 82% at 6 months of age), myelin precursors, such as glycolipids, cholesterol and proteins appear, glial cells proliferate and differentiate, and a number of biochemical cell membrane changes occur (Dobbing and Sands 1973). These changes increase the proportion of bound to free water and thus shorten the T2-relaxation times, even before myelination is evident on histological examination (Van der Knapp and Valk 1995). This concurs with studies of diffusion-weighted imaging in animal models where anisotropy was apparent in this "premyelination" period of cerebral maturation (Wimberger *et al.* 1995). A number of studies have shown T2 relaxation times decrease to mature values by approximately 2 to 3 years of age (Holland *et al.* 1986; Masumura 1987; Ono *et al.* 1993), although small but definite reductions in T2 values continuing into late childhood and early adulthood have been reported (Hassink *et al.* 1992). T1 relaxation times also decrease with cerebral maturation, particularly with the onset of myelination (Holland *et al.* 1986; Johnson *et al.* 1983; Masumura 1987; Suhonen-Polvi *et al.* 1988); however, T2 times decrease more rapidly suggesting that T2-weighted imaging is more sensitive to tissue maturational changes. It has therefore been suggested that the measurement of relaxation times, particularly T2, may be useful in monitoring brain development (Ferrie *et al.* 1999; Counsell *et al.* 2001; Holland *et al.* 1986; Thornton *et al.* 1999).

Variations in T2 relaxation times exist within normal adult brain at regional, local and microscopic levels. Both qualitative and quantitative studies of T2 values in different regions of the brain have established the presence of significant heterogeneity in cortical signal intensity (Georgiades *et al.* 2001; Whittall *et al.* 1997; Zhou *et al.* 2001; Breger *et al.* 1989; Larsson *et al.* 1986). In particular, structures of the limbic system have the highest, and the primary visual and auditory cortices the lowest, T2 relaxation times (Yoshiura *et al.* 2000; Hirai *et al.* 2000; Korogi *et al.* 1997; Larsson *et al.* 1986). This has been attributed to variations in, for example, water content, cytoarchitecture, and iron concentration (Georgiades *et al.* 2001; Larsson *et al.* 1986; Whittall *et al.* 1997). The primary visual and auditory cortices are characterized by densely packed neurons, a high degree of myelination and increased iron concentrations (Yoshiura *et al.* 2000; Williams and Warwick 1975; Hock *et al.* 1975), all of which may generate shorter T2 times. Atypical cellular composition of the trilaminar cortex and increased water content and vascularity in the limbic lobe grey matter structures may be at least partly responsible for the longer T2 relaxation times in these regions (Hirai *et al.* 2000). A number of studies have shown that grey matter possesses a longer T2 relaxation time than white matter (Larsson *et al.* 1986; Drayer *et al.* 1986; Vymazal *et al.* 1999). This is thought to be due to differences in, for example, water compartmentalization, vascularity (Table 1.9) and iron

concentration (Vymazal *et al.* 1995). The total water content of grey matter is greater than white matter (0.82 and 0.72 ml/g) (Brooks *et al.* 1980). Furthermore, in white matter, approximately 13% of the total tissue water is intercalated between myelin lamellae which possesses a very short T2 relaxation time (approximately 10-50 msec) (Whittall *et al.* 1997; Whittal *et al.* 1999). Blood volume is significantly greater in grey matter than white matter (Leenders *et al.* 1990; Koshimoto *et al.* 1999). T2 times of blood water are longer than T2 times of parenchymal water and this contribution tends to increase grey matter T2 values.

Table 1.9 Cerebral tissue parameters and calculated T2 values of grey and white matter in normal human adult brain (adapted from Zhou *et al.* 2001)).

Tissue parameters	*Grey matter*	*White matter*
Cerebral water content (ml/100g)	82	72
Percentage of myelin water (%)	~0	13
Cerebral blood volume (ml/100g)	5.2	2.8
T2 relaxation times (msec)	92	87

More recently, it has been reported that this trend is reversed in the occipital lobes with grey and white matter T2 values of 79 and 87 msec respectively (Zhou *et al.* 2001). This represents both a shortening of the grey matter T2 time and a lengthening of white matter T2 relaxation time. Occipital lobe grey matter has a greater iron concentration than frontal lobe grey matter, and furthermore, occipital lobe white matter has less iron than frontal lobe white matter (Drayer *et al.* 1986). The paramagnetic property of iron produces a shortening of the proton relaxation times and reduces the signal intensity in T2-weighted images.

The prevalence of non-specific white matter hyperintense lesions on T2-weighted imaging increases with advancing age (Fazekas 1989); and may be asymptomatic (Bartzokis *et al.* 1999; Mineura *et al.* 1995; Ylikoski *et al.* 1995). The clinical significance of white matter hyperintensities is controversial however. Careful neuropsychological examination has revealed subtle disturbances of higher cortical function, particularly specific cognitive domains, such as memory and global and executive functioning which are reliant on processing speed and the presence of widely distributed neural networks (Gunning-Dixon and Raz 2000). Conversely, intelligence and fine motor performance did not correlate with the burden of white matter hyperintensities (Gunning-Dixon and Raz 2000) and lesions have been detected in both patients with dementia and normal cognition (Brun *et al.* 1990). Periventricular areas are predominantly affected, and are almost universally involved by the age of 65 years (Ylikoski *et al.* 1995; Salonen *et al.* 1997). This is most likely due to age-related fluctuations in the periventricular fluid dynamics in association with disruption of the subependymal lining (Fazekas *et al.* 1993). Additionally, subcortical or deep white matter may be involved (Ketonen 1998). Histopathological examination commonly reveals hypomyelination, neuronal loss, expansion of the extracellular space, infarction, and gliosis (Fazekas *et al.* 1998; Scarpelli *et al.* 1994; Leifer *et al.* 1990).

1.2.7.3.2 Pathology

The fundamental basis of neuroimaging is the distinction of pathological from normal tissue. It is now generally accepted that MRI is more sensitive than CT in the detection of cerebral lesions (Bydder *et al.* 1983; Bailes *et al.* 1982; McLachlan *et al.* 1985; Latack *et al.* 1986; Lesser *et al.* 1986; Kuzniecky *et al.* 1987) and, of the conventional MRI sequences, T2-weighted imaging is the most discriminating (Smith *et al.* 1985). Early studies proposed that the evaluation of a combination of NMR parameters, principally proton density and T1 and T2-relaxation times, may provide not only sensitivity, but tissue specificity, allowing the complete and accurate characterisation of pathological tissue in vivo (Damadian 1971).

Epilepsy

(See section - 1.3.1.2 T2-relaxometry)

Cerebral neoplasia

In 1971, Damadian reported significantly elevated T2 relaxation times in malignant tumours in the rat, compared to either normal tissue or benign tumours. It was suggested that this was due to an increase in the motional freedom of tissue water molecules, and may be used to discriminate between benign and malignant surgical specimens ex vivo (Damadian 1971). By 1974, however, doubts concerning the specificity and utility of NMR relaxation times for cancer diagnosis had grown, as further studies revealed overlap between normal and tumour values (Parrish *et al.* 1974; Eggleston *et al.* 1975). More recently, the principles of NMR have been translated into the field of neuroimaging and, on visual inspection of T2-weighted MRI images, tumours were reliably detected in vivo (Brant-Zawadzki *et al.* 1984; Bydder *et al.* 1983; Bailes *et al.* 1982; Schorner *et al.* 1989; Nishio *et al.* 2001; Matsumoto *et al.* 1999; Kim *et al.* 1998; Hashimoto *et al.* 1993; Schwaighofer *et al.* 1987; Smith *et al.* 1985; Elster *et al.* 1989). Tovi showed that by analysing T2-weighted images both qualitatively and quantitatively, the degree of malignancy of neoplastic tissue could be estimated. Comparison with histopathology also revealed, however, that in the majority of cases, some tumour cells were not identified on the conventional images (Tovi 1993). More recent work by Kurki and coworkers suggested that although T2 relaxation times correlated with the volume fraction of tumour cell nuclei in neoplastic tissue, visual morphometric evaluation of low and high grade gliomas was equally discriminating and quantitative analysis conveyed little benefit (Kurki *et al.* 1995). Measurements of T2 relaxation times in animal models revealed a spectrum of values throughout normal, neoplastic and oedematous brain; normal brain possessed the lowest values and regions of oedema, the highest (Hoehn-Berlage *et al.* 1992; Eis *et al.* 1995; Hoehn-Berlage and Bockhorst 1994). Differentiation between tumour types was not possible using only T2 images analysed quantitatively (Eis, Els, and Hoehn-Berlage 1995; Hoehn-Berlage and Bockhorst 1994; Wilmes *et al.* 1993; Just *et al.* 1988). The use of multiparametric or feature space analyses combining data from, for example, T1 and T2-weighted, proton density and diffusion-weighted images has been shown to improve tissue characterisation, but relies on sufficient signal to noise and good reproducibility (Eis, Els, and Hoehn-Berlage 1995; Ye *et al.* 1996; Soltanian-Zadeh *et al.* 1998).

Multiple Sclerosis

Conventional MRI is considerably more sensitive than CT imaging in delineating multiple sclerosis (MS) lesions (Bailes *et al.* 1982; Smith *et al.* 1985; Borgel *et al.* 1986). Fast Fluid Attenuated Inversion Recovery sequences are

qualitatively superior to conventional T2-weighted imaging, particularly supratentorially (Tubridy *et al.* 1998; Gawne-Cain *et al.* 1997; Stevenson *et al.* 2000), and the use of thinner slices further enhances lesion identification (Filippi *et al.* 1995c). MRI lacks pathological specificity however (van Waesberghe *et al.* 1999). Abnormalities identified on T2-weighted images reflect altered tissue water content. This may be associated with axonal loss, gliosis, demyelination and oedema; all of which can occur in MS lesions (Larsson *et al.* 1989), and all of which are associated with a variety of clinical sequelae. To attain a greater understanding of the natural history of the disorder, characterize the extent of tissue injury, and monitor the temporal evolution of both individual lesions and the overall disease activity, additional quantification or post-processing techniques need to be employed. Accurate and precise measurements of T2 relaxation times have been reported in normal subjects and in patients with MS, both in normal-appearing white matter (NAWM) and in lesional areas (Miller *et al.* 1989; Larsson *et al.* 1992). In acute MS lesions, due to inflammation and oedema, T2 relaxation times initially increase then, as the oedema resolves and before significant demyelination and axonal loss occurs, values rapidly decrease (Larsson *et al.* 1989). Chronic plaques exhibit a wide range of values resulting in considerable overlap in T2 relaxation times between acute and chronic lesions (Larsson *et al.* 1988); reflecting the substantial pathological heterogeneity (van Waesberghe *et al.* 1999). Cerebral lesions characterised by expansion of the extracellular space have previously been shown to demonstrate biexponential T2 decay (Naruse *et al.* 1982; Barnes *et al.* 1987; Rumbach, Armspach *et al.* 1991), and cellular or gliotic white matter, monoexponential decay (Rumbach *et al.* 1991; Barnes *et al.* 1988).

Quantitation of total brain lesion load on T2-weighted images has frequently been employed in exploring the natural history of MS (Filippi *et al.* 1998b; Filippi *et al.* 1998a; Filippi *et al.* 1995d) and, more recently, as an outcome measure in therapeutic trials (Molyneux *et al.* 2001). The measurement of total brain lesion load can be performed using a number of techniques including a semi-quantitative arbitrary scoring system (Ormerod *et al.* 1987), manual outlining of lesions, semi-automated lesion contouring (Wicks *et al.* 1992) (using local lesion-based thresholding), and intensity-based thresholding for the whole brain (Filippi *et al.* 1995d; Filippi *et al.* 1995b).

It has previously been proposed that, in addition to limitations of T2-weighted imaging in accurately and reproducibly characterising clinically significant MS lesions, a significant proportion of disability arises from occult white matter abnormality (Barbosa *et al.* 1994). Quantitative ROI-based studies of T2-relaxation times in normal appearing white matter (NAWM) have shown relaxation times to be prolonged by an average of approximately 5-10% compared to control subjects (Miller *et al.* 1989; Kesselring *et al.* 1989; Haughton *et al.* 1992; Armspach *et al.* 1991; Stevenson *et al.* 2000; Rumbach 1991; Barbosa *et al.* 1994), consistent with the occurrence of diffuse demyelination (Larsson *et al.* 1988), diffuse astrocytic hyperplasia (Allen *et al.* 1981), vasogenic oedema (Armspach *et al.* 1991), perivascular infiltration (Miller *et al.* 1989) or scattered products of disintegrated myelin (Ormerod *et al.* 1987). Histopathological studies have reported microscopic abnormalities in 72% of samples of macroscopically normal white matter from patients with MS (Allen and McKeown 1979). It was assumed from the numerous ROI-based imaging studies that the increased T2 relaxation times seen were due to "widespread" white matter abnormality. Barbosa et al demonstrated, however, using T2-mapping and histogram-based analyses, that scattered within the normal NAWM were discrete areas, often only 5-10mm^3, with abnormally prolonged T2 times (Barbosa *et al.* 1994). The creation of T2 histograms allows data from a defined region to be displayed and easily compared with control values. A number of parameters may be calculated including, for example, the mean value, peak position, peak height, variance and dispersion (Armspach *et al.* 1991;

Rumbach *et al.* 1991; Grenier *et al.* 2001). This can provide information on cerebral atrophy, biexponential T2 decay, and average white matter T2 relaxation times.

Neurodegenerative disorders

Quantitative analysis of T2-weighted imaging has also been utilised in neurodegenerative conditions, including for example, multi-infarct dementia, Parkinson's and Alzheimer's disease (Hauser and Olanow 1994). White matter hyperintensities are often found in patients with dementia; but have been variably correlated with severity of cognitive impairment (Bondareff *et al.* 1988; Mirsen *et al.* 1991; Barber *et al.* 1999b; Hirono *et al.* 2000; Leys *et al.* 1990). Furthermore, there is lack of consensus on the pathophysiological origin and effect of white matter changes in dementia (McDonald *et al.* 1991; Scheltens *et al.* 1995; Scheltens *et al.* 1992; Fazekas *et al.* 1996). Quantitative analysis has previously demonstrated an increased volume of white matter hyperintensities in patients with vascular dementia compared to normal subjects, but no correlation between volume of lesions and global cognitive decline (Giubilei *et al.* 1997).

Regions of extratemporal white matter signal change in Alzheimer's disease have also been assessed quantitatively on T2-weighted images using region of interest and automatic thresholding and voxel counting methods (Hirono *et al.* 2000; Parsey and Krishnan 1998). Hirono et al. reported that the volume of irregular periventricular and deep confluent hyperintensities did not correlate with dementia severity (Hirono *et al.* 2000), consistent with previous qualitative and semi-quantitative studies (Smith *et al.* 2000; Erkinjuntti *et al.* 1994; Leys *et al.* 1990).

Atrophy of temporal lobe structures, in particular the hippocampus, is a common feature of Alzheimer's disease, and can be readily identified using quantitative MRI techniques (Callen *et al.* 2001; Du *et al.* 2001; Chan *et al.* 2001). Despite a large number of studies reporting T2 relaxation times in extratemporal regions (see above), there are few reports of T2 relaxometry in mesial temporal lobe structures. In 1992, Kirsch et al demonstrated significantly elevated hippocampal T2 values in patients with Alzheimer's disease compared to patients with multi-infarct dementia and control subjects. Furthermore, the T2 values correlated with the severity of functional and cognitive impairment (Kirsch *et al.* 1992). Similar findings were reported by Laakso et al who found diffuse and symmetrical involvement of the hippocampi but not the amygdalae (Laakso *et al.* 1996). The diagnostic value was limited however, by a substantial overlap between the study groups. Most recently, using a region-of-interest based analysis, there was no statistically significant difference in hippocampal T2 relaxation times detected between control subjects and patients with Alzheimer's disease (Campeau *et al.* 1997). This finding supports earlier results of ex-vivo MR microscopy of the hippocampus in Alzheimer's disease where only a non-significant trend of increased T2 relaxation times in patients with Alzheimer's disease was apparent. The authors suggested that due to methodological limitations of performing the experiments on excised, fixed tissue and at high field strength, the sensitivity of T2 relaxometry may have been compromised (Huesgen *et al.* 1993). Additionally, reduced magnetisation transfer ratio and elevated averaged apparent diffusion co-efficient (ADC (av)) have been reported in hippocampi of patients with Alzheimer's disease suggesting the presence of loss of structural integrity and increased extracellular water (Hanyu *et al.* 2001a; Kantarci *et al.* 2001; Sandson *et al.* 1999). In the presence of these microstructural changes it is highly likely that T2 relaxation times would be elevated, and careful, more extensive in vivo quantification of T2 values is therefore required.

Cerebral ischaemia

Magnetic resonance imaging has been shown to be more sensitive than CT in the detection of acute (Barber *et al.* 1999a; Kertesz *et al.* 1987; Brown *et al.* 1988) and chronic stroke (Bailes *et al.* 1982; Kinkel *et al.* 1986; Bryan *et al.* 1991; Brant-Zawadzki *et al.* 1984). Furthermore, T2-weighted imaging is more sensitive than proton density and T1-weighted imaging (Bryan *et al.* 1983; Smith *et al.* 1985; Salgado *et al.* 1986; Yuh *et al.* 1991; Mantyla *et al.* 1999). Cytotoxic oedema develops during the first few hours of ischaemia. This phase is associated with only small changes in tissue total water content (approximately 3%), macromolecular compartmentalisation, and hydration layer binding (Schuier and Hossmann 1980) resulting in minimal alteration in T2 relaxation times. Vasogenic oedema occurs approximately 6-8 hours post-infarction. As a consequence of degeneration of the blood-brain barrier, leakage of water, proteins and other macromolecules occurs and T2 signal intensity increases quickly (Loubinoux *et al.* 1997b; Yuh *et al.* 1991).

Quantitative analysis of T2-weighted images in acute stroke has been performed in both experimental (Buonanno *et al.* 1983; Horikawa *et al.* 1986; Calamante *et al.* 1999; Messager *et al.* 2000; Lei *et al.* 1998; Loubinoux *et al.* 1997a; Knight *et al.* 1994; Hoehn-Berlage *et al.* 1995) and clinical studies (Jacobs *et al.* 2001a; Lansberg *et al.* 2001; Lutsep *et al.* 1997). T2 values became significantly elevated 4 hours post-stroke, but only in those regions which subsequently demonstrated severe neuronal damage on histopathological assessment. Regions of significantly elevated T2 values continued to grow over the next 4 hours, suggesting that very early assessment by T2-weighted images may underestimate the size of the ischaemic region, and thus may not be a suitable MRI parameter in the clinical evaluation of acute human stroke (Hoehn-Berlage *et al.* 1995).

The sensitivity and temporal resolution of diffusion weighted imaging, combined with the established histopathological correlates (Lei *et al.* 1998; Marshall *et al.* 1988; Castillo *et al.* 1996; Bose *et al.* 1988; Barone *et al.* 1991) and well-defined biophysical mechanisms (Mansfield and Morris 1982b) of altered T2 relaxation times have been shown to improve lesion characterisation. By amalgamating data from diffusion-weighted and T2-weighted imaging in a cluster plot analysis, a number of tissue "signatures" may be derived (Welch *et al.* 1995; Jacobs *et al.* 2001a; D'Olhaberriague *et al.* 1998). These can be used to predict histopathological features and, therefore, discriminate between tissue that is likely to recover and tissue that will eventually progress to necrosis. This has important implications for cytoprotective or thrombolytic therapy (D'Olhaberriague *et al.* 1998), and for predicting clinical outcome (Jacobs *et al.* 2001a). A development of this technique utilised colour-encoded overlays, in addition to the cluster plot analyses, to represent the spatial distribution of the parameter values and thus provided both simultaneous physiological and anatomical information (Bernarding *et al.* 2000). These histogram-based, cluster plot analysis methods characterise irregular, scattered or heterogeneous tissue abnormalities more precisely than region-of-interest based methods, which are more appropriate for homogeneous, discrete lesions.

The enthusiasm for imaging sequences or post-processing techniques to rapidly, accurately and completely characterise acute ischaemic lesions has been driven by the development and use of cytoprotective or thrombolytic agents. Experimental studies using quantitative T2-weighted imaging have shown either smaller volumes of infarction or less elevated T2 relaxation times in animals given thrombolysis (Jiang *et al.* 1998), or cytoprotective agents (Pan *et al.* 1995; Sauter and Rudin 1986; Loubinoux *et al.* 1997b) than those left untreated. However, T2-weighted imaging is of limited use in human, clinical studies evaluating the efficacy of pharmacological treatment of acute stroke as abnormalities are not commonly visualised on T2-weighted imaging

within the narrow therapeutic window available. T2-weighted imaging remains the imaging modality of choice in delineating subacute and chronic stroke however (Salgado *et al.* 1986; Bryan *et al.* 1983; Smith *et al.* 1985).

Cross-sectional studies evaluating patients with cerebral autosomal dominant arteriopathy with subcortical infarcts and leukoencephalopathy (CADASIL) using semi-quantitative, lesion counting methods have demonstrated extensive white matter changes in predominantly the temporal and frontal lobes (Chabriat *et al.* 1998; Yousry *et al.* 1999; Auer *et al.* 2001). A statistical parametric mapping based comparison of FLAIR images obtained from patients with CADASIL and patients with sporadic subcortical arteriosclerotic encephalopathy (Binswanger's disease) identified regions of symmetrical high signal intensity in anterior temporal white matter and superior frontal white matter in those with CADASIL. This voxel-by-voxel analysis method was more sensitive than a semiquantitative visual rating scale in identifying regions of abnormality and, because of observer-independence and absence of prior hypotheses, was potentially less biased (Auer *et al.* 2001).

Other conditions

T2-weighted MR imaging has been utilised in a number of other conditions including, for example, head injury (Yanagawa *et al.* 2000; Wardlaw and Statham 2000; Hadley *et al.* 1988; Gentry *et al.* 1988), cerebral infections (Thurnher *et al.* 1997; Bailes *et al.* 1982), migraine (Ferbert *et al.* 1991; Soges *et al.* 1988), psychiatric disorders (Buckley *et al.* 1995), and alcohol-related diseases (Sullivan and Pfefferbaum 2001; Park *et al.* 2001). The majority relied on only qualitative assessment; however, where quantitation was performed, increased sensitivity was demonstrated. In a study of central pontine T2 relaxation times in patients with alcoholic Korsakoff's syndrome (KS) and asymptomatic alcoholic patients, prolonged T2 values were detected in more patients with KS than were apparent from visual assessment. Furthermore, in asymptomatic patients, T2 values increased with advancing patient age; a trend not observed in control subjects (Sullivan and Pfefferbaum 2001). A semi-quantitative approach was used to evaluate patients with head injury. Positive correlation between clinical measures, including duration of unconsciousness and Glasgow Outcome Scale, and number of lesions identified on MRI was seen with T2*-weighted gradient-echo imaging but not with T2-weighted fast spin echo imaging, implying that following head trauma, the prevalence of small haemorrhages is more clinically significant than axonal loss and gliosis (Yanagawa, *et al.* 2000). Quantitative analysis of T2-weighted images using spatial autocorrelation statistics showed enhanced sensitivity over visual assessment in patients with Human Immunodeficiency Virus (HIV) infection and cerebral involvement by detecting abnormalities in normal appearing white matter (Corrigall *et al.* 1995). Furthermore, quantitative analysis was able to discriminate between patients with low and high CD4 lymphocyte counts (Wilkinson *et al.* 1996), and has also been employed in monitoring the response to antiretroviral treatment (Wilkinson *et al.* 1997).

1.2.8 Double Inversion Recovery

1.2.8.1 Theory

Lesion conspicuity can be enhanced by using an inversion recovery (IR) sequence such as short Tau inversion recovery (STIR) which suppresses the signal from fat (Bydder and Young 1985), or fast fluid attenuated inversion recovery imaging (FLAIR) which nulls the signal from cerebrospinal fluid (CSF) (Rydberg *et al.* 1994; De Coene *et al.* 1992; Wieshmann *et al.* 1996). Applying two carefully timed inversion pulses results in the signal from two tissues being nulled simultaneously. This is referred to as double inversion recovery (DIR) imaging, and may be beneficial if information about only one compartment is required and where an accurate evaluation, whether qualitative or quantitative, is confounded by the signal from adjacent tissues.

The underlying principles are relatively straightforward. Following the first inversion pulse, the magnetisation of grey and white matter recovers almost completely, while CSF, with its substantially longer T1 recovers to only a fraction of equilibrium magnetisation. Following the second inversion pulse, which flips any longitudinal magnetisation that had recovered after the first inversion pulse, magnetisation starts to recover again and the tissues approach the null point for the second time. As, for example, CSF and white matter pass through the null point simultaneously, image acquisition using a standard spin echo sequence commences. Grey matter, with a longer T1 remains negative and generates a signal (figure 1.14).

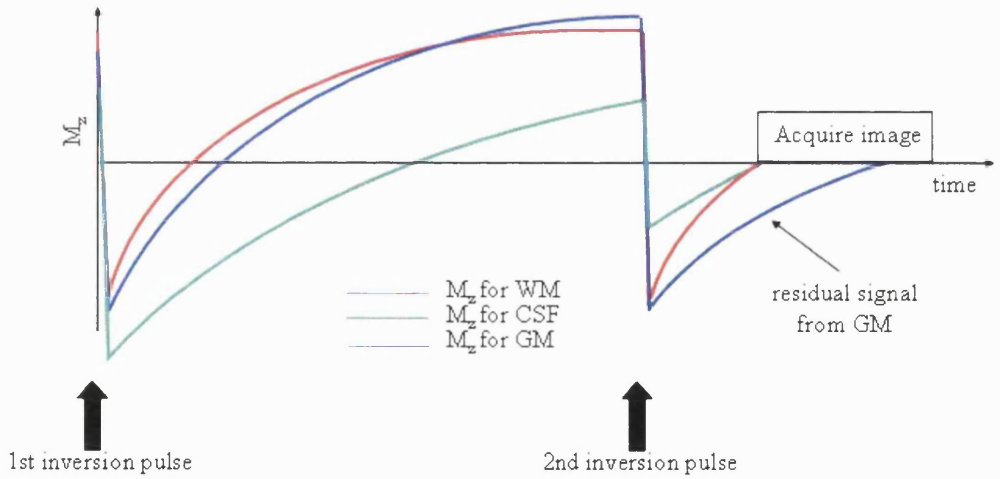

Figure 1.14: The evolution of longitudinal magnetisation (M_z) following two inversion pulses. The x-axis represents time, and also indicates the M_z null point at which the signal from each tissue is zero. Image acquisition commences following the second inversion pulse, as the null point is reached for both white matter (WM) and CSF but where residual magnetisation of the grey matter (GM) remains.

The inversion times prescribed determine whether the suppressed tissues are CSF and white matter, or CSF and grey matter. Images can thus be acquired of just grey (figure 1.15) or white matter (Redpath and Smith 1994).

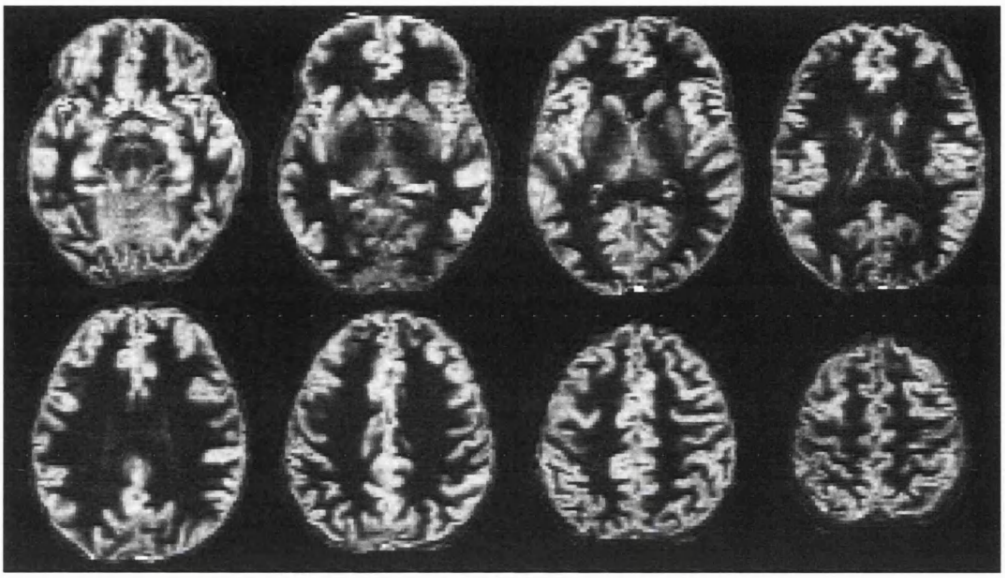

Figure 1.15: Series of normalised, axial DIR "grey matter" images from a single control subject.

For GM images, the adequate suppression of the MR signal from white matter relies on its possession of a relatively narrow range of T1 values (Redpath and Smith 1994). Deviation from this will result in insufficient suppression from the carefully timed inversion pulses, and the appearance of signal from white matter. Furthermore, depending on the echo time (TE), DIR sequences may be proton-density or T2-weighted. In addition, therefore, to altered grey matter concentration, abnormal DIR signal intensity (DSI) may be due to either abnormal proton-density, T1 or T2 relaxation times. The following principles apply:

1. increased DSI in white matter may be due to either abnormal white matter (possessing an altered T1-relaxation time), or ectopic grey matter.
2. decreased DSI in the white matter compartment is not encountered, as the MR signal derived from this compartment is completely suppressed in normal subjects and is therefore, by definition, zero.
3. increased DSI in the cortex may be due to either increased concentration of grey matter, for example thickened gyri, or increased cortical proton-density or T2 signal.
4. decreased DSI in the cortex may be due to loss of grey matter tissue, or an altered cortical T1-relaxation time.

DIR imaging therefore evaluates both white and grey matter compartments and provides information on both the quantity and microstructural environment of cerebral tissue.

T1 relaxation reflects the total water content and the dynamic structure of water, including the ratio of free to bound water, the structure and concentration of local macromolecules, and the degree of inter-compartmental exchange (Mathur-De Vre 1984). Changes in both total water content and macromolecular structure and concentration will therefore influence tissue T1 relaxation, and consequently the degree of signal suppression

during DIR imaging. White matter possesses a T1 relaxation time of approximately half that of grey matter due, most likely, to myelin and more specifically, the presence of cholesterol (Koenig *et al.* 1990). Cerebrospinal fluid has very long T1 times as there is a low concentration of macromolecules. Quantitative abnormalities of T1-weighted imaging have been reported in cerebral ischaemia (Calamante *et al.* 1999), tumours (Bastin *et al.* 2002; Hoehn-Berlage and Bockhorst 1994), and most commonly multiple sclerosis (Vaithianathar *et al.* 2002; Barkhof *et al.* 2000), where abnormal T1 times were identified both in lesions and in normal appearing white and grey matter (Griffin *et al.* 2002).

Typically, a change in the proton-density in cerebral tissue arises from altered water content. Increased proton-density is commonly seen in oedema and gliosis (Barnes *et al.* 1986b), and has been reported in Wallerian degeneration (Khurana *et al.* 1999), subtle demyelination (Oka *et al.* 2001), and as a transient post-ictal phenomenon (Aykut-Bingol *et al.* 1997). The determinants of T2 signal intensity have been described previously (see section 1.2.7.1 T2-mapping).

1.2.8.2 Development and clinical applications

The first clinical DIR sequence was developed by Redpath and Smith in 1994 (Redpath and Smith 1994). They implemented and validated a clinical sequence with inversion times of 2300 and 300ms after calculating theoretical inversion times and undertaking a "trial-and-error" scanning programme of human control subjects. Good suppression of white or grey matter was achieved; however, the repetition time (TR) was 8 seconds long which prohibited the acquisition of more than 6 slices during the 26 minute sequence. The authors also noted that the presence of magnetic field inhomogeneity, could result in variable tissue suppression and hence advocated the use of hyperbolic-secant inversion pulses.

It was not until 1998 that DIR imaging was utilised in the evaluation of pathological tissue. Bedell and co-workers implemented a fast spin echo DIR sequence to investigate patients with multiple sclerosis. This sequence exploited the principles of fast spin echo (FSE) imaging, which allowed the whole brain to be imaged in 48, 3mm thick, slices in less than 6 minutes. Suppression of the signal from white matter and CSF was satisfactory and, moreover, lesion conspicuity was good. Lesions identified on the DIR images were easily delineated from normal tissue and showed clear heterogeneity of internal structure compared to lesions demonstrated on either standard T2-weighted or FLAIR images which were less well characterised and were more homogeneous in appearance (Bedell and Narayana 1998a). Using similar FSE sequences, Turetschek et al also compared DIR with FLAIR imaging, but in patients with a variety of cerebral lesions. Both sequences proved equally efficacious in the overall identification of abnormalities, but DIR was superior in the visualisation of infratentorial lesions or those characterised by only minimally increased T2 signal. This was thought to be due to T1 contrast differences between the two sequences. Conversely, FLAIR identified more juxtacortical lesions. Overall, it was concluded that there was no evidence to support the replacement of FLAIR imaging with DIR for the majority of clinical scans (Turetschek *et al.* 1998). DIR may be important, however, in the quantitative analysis of scans of patients with, for example, dementia where the evaluation of subtle changes in grey matter volume may be confounded by partial volume effects.

In addition to evaluating the usefulness of the DIR images in identifying lesions, Bedell and Narayana studied the partial volume effect (PVE) of post-processing segmentation procedures. A comparison of tissue volumes derived from DIR images, with theoretically minimal PVE, and standard segmented tissue volumes revealed a significantly increased grey matter volume of approximately 13% and a reduced CSF volume of approximately 45% in the standard segmented images, implying the existence of a significant PVE (Bedell and Narayana 1998b). The authors suggest that the accurate determination of tissue volumes is only possible with images "segmented" at the acquisition stage, and may be useful in evaluating the course of numerous pathological processes. Previous work in diffusion imaging had demonstrated that white and grey matter possessed very similar mean diffusivity values (Pierpaoli and Basser 1996). Zacharopoulos et al suggested that this might be due to PVE and therefore developed a DIR-diffusion sequence to circumvent the potential confound of contamination from neighbouring voxels. They found that, as previously described, white and grey matter do in fact have similar mean diffusivity values (Zacharopoulos and Narayana 1998).

1.3 POST-ACQUISITION TECHNIQUES

1.3.1 Quantitative analysis of mesial temporal lobe structures

1.3.1.1 Volumetry

1.3.1.1.1 Hippocampus

The cardinal MRI features of hippocampal sclerosis are atrophy, best demonstrated on coronal T1-weighted images, and increased signal intensity on T2-weighted images (Jackson *et al.* 1990). In clinical practice, hippocampal volume asymmetry of 20% is reliably discernible to neuro-imaging specialists on qualitative visual assessment (Van Paesschen *et al.* 1995b). Lesser degrees of volume asymmetry, which may still be clinically and surgically relevant, require quantitative assessment. A number of studies have shown that measurement of hippocampal volume is superior to visual inspection, with correct lateralisation of hippocampal pathology in a larger proportion of patients (Tien *et al.* 1993; Jack Jr. 1993; Cook *et al.* 1992; Spencer *et al.* 1993). In addition, and as importantly, false lateralisations were minimal (Jack Jr. *et al.* 1990c). Several studies have demonstrated the reliability of quantitative assessment in the detection of HS (Bronen 1992; Jack Jr. 1993; Jack Jr. *et al.* 1990a), and quantitative assessment of hippocampal atrophy on MRI compares favourably with other non-invasive means of localisation (Spencer, McCarthy, and Spencer 1993; Ashtari *et al.* 1991; Baulac *et al.* 1994). The degree of hippocampal atrophy has been correlated with neuronal loss on qualitative (Cascino *et al.* 1991; Cendes *et al.* 1993a) and quantitative histopathological examination (Bronen *et al.* 1991; Lencz *et al.* 1992; Lee *et al.* 1995). Overall, these findings suggest that the pursuit of minor hippocampal volume change, smaller than can be reliably determined on visual inspection alone, is worthwhile.

The use of contiguous thin coronal slices through the hippocampus allows accurate and reliable measurements along the entire length of the structure. Thick slices result in increased partial volume effect and an unreliable estimation of hippocampal volume. Following acquisition, a manually driven cursor is used to outline the hippocampus and/or amygdala in each slice. The total hippocampal volume (HCV) is calculated by summing

the hippocampal cross-sectional areas and multiplying by the distance between two slices (Cavalieri's principle) (Cook *et al.* 1992; Gundersen and Jensen 1987). The results may be expressed as total volume, ratio or corrected volume (Jack Jr.1993). In addition, measurement of hippocampal volume may be achieved using a point counting technique (Mackay *et al.* 2000). This method uses a grid which is overlaid on coronal T1-weighted images and the number of equally spaced points contained within the boundaries of the hippocampus summed. Semi-automated methods of measuring hippocampal volumes have also been developed using signal intensity-based and global pattern matching image registration techniques, with good reproducibility and specificity (Haller *et al.* 1997; Webb *et al.* 1999).

There exists a wide normal range of hippocampal volume measurements. The use of left / right ratios, generated from the absolute values, precludes identification of bilateral HS, or lesser degrees of contralateral hippocampal damage. Correcting absolute hippocampal volume measurements for total intracranial volume allows bilateral hippocampal pathology to be recognized (Van Paesschen *et al.* 1997a; Free *et al.* 1995). In a study comparing HCV in patients with TLE against controls, it was noted that 41% of control subjects had asymmetrical positioning of the hippocampi (Van Paesschen *et al.* 1997a). This can lead to an erroneous diagnosis of hippocampal atrophy on visual inspection of the scan (Van Paesschen *et al.* 1995b), or if only the volume of the hippocampal body is measured rather than the entire structure (King *et al.* 1995; Kim *et al.* 1994). It is therefore mandatory that the whole length of the hippocampus is measured. The repeatability of hippocampal volume measurements improves with greater grey-white matter contrast, e.g. with the addition of an inversion pulse before a spoiled gradient echo sequence (IRp-SPGR). This is thought to be due to improved discrimination of hippocampal boundaries, particularly anteriorly (Wieshmann *et al.* 1998b).

In addition to quantitative assessment of hippocampal volumes being associated with the localisation of the ictal focus (Ashtari *et al.* 1991; Baulac *et al.* 1994; Cendes *et al.* 1993a), hippocampal atrophy in the resected hippocampus has been shown to correlate with a good surgical outcome (Bronen *et al.* 1991). Further, patients with atrophy of the non-resected hippocampus, and patients with bilateral, symmetrical hippocampal atrophy do less well postoperatively (Jack Jr. *et al.* 1992).

Quantitative hippocampal MRI has corroborated the pathological data associating anterior or diffuse, unilateral HS with prolonged febrile convulsions in childhood (Cendes *et al.* 1993a; Kuks *et al.* 1993; Cavanagh and Meyer 1956; Bruton CJ 1988). Bilateral hippocampal atrophy has also been reported in such patients (Theodore *et al.* 1999); however, in a study by Van Paesschen et al, none of the patients with bilateral HS had a history of febrile convulsions (Van Paesschen *et al.* 1997a). Bilateral HS was associated with a history of meningoencephalitis, as has previously been reported (Free *et al.* 1995), and also with an increased number of secondary generalised seizures, over the patient's lifetime (Van Paesschen *et al.* 1997a; Woermann *et al.* 1998a). Longitudinal studies are obligatory in establishing whether repeated seizures cause hippocampal injury. A large community-based longitudinal study of patients with newly-diagnosed seizures recently reported that over a 3.5 year period, there was no significant hippocampal atrophy in patients with newly diagnosed seizures compared to control subjects, and in those with chronic epilepsy, frequent seizures did not correlate with more rapid hippocampal volume loss (Liu *et al.* 2002b). This suggests that recurrent seizures do not inevitably cause hippocampal damage (Duncan 2002); however, this is not universally accepted (Briellmann *et al.* 2002a; Liu *et al.* 2002b). Furthermore, it is possible, that with an interval of 3.5 years, the degree of atrophic change was insufficient to be recognised as significant, over and above the coefficient of repeatability.

Hippocampal volumetry has been shown to predict the degree of verbal memory impairment in patients undergoing temporal lobe resection. The more severe the atrophy in the language-dominant hemisphere preoperatively, the less likely the patient is to develop further verbal memory impairment postoperatively (Trenerry *et al.* 1996). Most recently, it has been reported that in TLE, atrophy within the temporal lobe is often not confined to the hippocampus and extends into the adjacent entorhinal and to a lesser extent the perirhinal cortices (Jutila *et al.* 2001; Bernasconi *et al.* 2003b). This is thought to be due to cell loss, secondary to a disruption of entorhinal-hippocampal connections, and may be seen in the presence of normal hippocampal volumes (Bernasconi *et al.* 2001b).

1.3.1.1.2 Amygdala

Intracranial EEG recordings have identified focal seizures arising from the amygdala in approximately 10% of seizures in patients with intractable TLE (Quesney 1986; So *et al.* 1989; Maldonado *et al.* 1988). Isolated lesions of the amygdala, including tumours, vascular lesions, sclerosis, MCD and microdysgenesis have also been demonstrated (Bruton CJ 1988; Falconer and Cavanagh 1959; Hudson *et al.* 1993; Feindel *et al.* 1991). These abnormalities may be evident on qualitative assessment of MRI but reported detection rates have been low (Hudson *et al.* 1993; Kuzniecky *et al.* 1987; Bronen *et al.* 1995a). The amygdala has therefore become a focus for quantitative MRI techniques.

Pathological studies have shown ipsilateral amygdala sclerosis (AS) to be present in 50-76% of cases of HS (Bruton CJ 1988; Falconer *et al.* 1964; Margerison and Corsellis 1966). In studies of amygdala volumetry, Cendes *et al* detected ipsilateral atrophy in a similar percentage of patients (Cendes *et al.* 1993b). Kalviainen *et al* found amygdala atrophy in only 20% of patients with chronic TLE, and no atrophy in newly diagnosed patients (Kalviainen *et al.* 1997b). Other workers have previously found that a poor coefficient of repeatability (>20%) precludes meaningful inference from the results (Bland and Altman 1986; Van Paesschen *et al.* 1996).

More recent studies in patients with TLE, using more sophisticated image registration and display methods, report inter- and intra-observer variabilities of approximately 5% (Bernasconi *et al.* 1999), and a coefficient of repeatability of approximately 15% (van Elst *et al.* 2000). Bernasconi et al (Bernasconi *et al.* 1999) reported reduced mean amygdala volumes ipsilateral to the seizure foci in groups of patients with TLE, compared to age and gender matched control subjects. Chronic seizures resulting in neuronal loss has been suggested as the cause of the amygdala atrophy (Saukkonen *et al.* 1994; Du *et al.* 1993).

1.3.1.2 T2 relaxometry.

1.3.1.2.1 Hippocampus

Increased T2-weighted signal intensity on qualitative visual assessment has been reported in 8% to 70% of cases of HS (Bronen *et al.* 1991; Jackson *et al.* 1990; Ashtari *et al.* 1991; Kuzniecky *et al.* 1987). This variability is most likely due to subjective visual assessment of subtle signal abnormalities in images of varying quality and resolution. Quantitative measurement of hippocampal T2 relaxation time (HCT2) is an unbiased, objective way of assessing the frequency and severity of signal abnormalities in patients with temporal lobe epilepsy and has been

shown to confer additional sensitivity over qualitative assessment (Jackson *et al.* 1993b; Woermann *et al.* 1998a; Okujava *et al.* 2002; Namer *et al.* 1998; Bernasconi *et al.* 2000).

Early studies of hippocampal relaxometry measured HCT2 on only one slice using a multiecho sequence (Van Paesschen *et al.* 1997a; Jackson *et al.* 1993b; Grunewald *et al.* 1994), or on a few thick slices with interslice gaps (Pitkanen *et al.* 1996). HS may vary in severity throughout the length of the hippocampus, resulting in false negatives should the abnormality fall outside the slice selected (Kim *et al.* 1994; Van Paesschen *et al.* 1997a).The use of an interleaved, multislice sequence, in which the whole brain is imaged, improves the sensitivity of detecting lesions in patients with TLE (Woermann *et al.* 1998a). Other methodological issues regarding relaxometry include partial volume effects from surrounding cerebrospinal fluid or sulcul encystments within the hippocampus (Sasaki *et al.* 1993), and asymmetrical positioning of the head resulting in measurements being taken from different regions of the hippocampus, which may have different HCT2 values (Woermann *et al.* 1998a). The use of a multislice, contiguous sequence circumvents this latter limitation (Duncan, Bartlett, and Barker 1996; Woermann *et al.* 1998a; von Oertzen *et al.* 2002). More recently, using a CSF-nulled T2-weighted sequence, elevated HCT2 times were demonstrated in the same number of patients as a non-CSF-nulled sequence suggesting that parenchymal change, rather than CSF contamination, is the predominant determinant for prolonged HCT2 times in hippocampal sclerosis (Woermann *et al.* 2001).

An advantage of HCT2 measurements over volumetry is that the HCT2 values are absolute, so can be compared against control values without correction. The range of HCT2 values in control subjects is narrow, with values ranging from 99 to 106 msec measured on a single slice using a multiecho sequence on a Siemens 1.5T scanner (Grunewald *et al.* 1994; Jackson *et al.* 1993b). Using this sequence, in a study of 50 patients with medically refractory temporal lobe epilepsy, a HCT2 of 116 msec or higher was invariably associated with HS. Abnormal HCT2 values in the range 106 to 116 msec were detected in (i) ipsilateral hippocampi in TLE with no imaging evidence of hippocampal sclerosis; (ii) the contralateral hippocampi in 29% of patients with ipsilateral HS; (iii) the ipsilateral hippocampus in some patients with extratemporal epilepsy (Jackson *et al.* 1993b). Despite HCT2 values being significantly elevated in the vast majority of cases of HS, some patients with pathologically confirmed HS had normal HCT2 (Van Paesschen *et al.* 1995b). This may have reflected the methodological constraint of using only a single slice from which to determine HCT2 values, rather than a specific pathological or clinical entity. Minor increases in HCT2 values may be caused by hippocampal oedema secondary to prolonged seizures (Katz *et al.* 1992; Takamatsu K *et al.* 1991), lesser degrees of neuronal loss or gliosis, as has been reported in pathological studies of hippocampi contralateral to HS (Bruton CJ 1988; Margerison and Corsellis 1966), or drug effects. In rats, the administration of vigabatrin was associated with intramyelinic oedema and astrocytosis, which paralleled an increase in HCT2 values (Jackson *et al.* 1994a). Similar changes, however, have not been seen in humans on carbamazepine or vigabatrin (Van Paesschen *et al.* 1998). In a study examining the factors influencing hippocampal relaxometry, it was reported that the duration and severity of epilepsy, age of the patient, or occurrence of a single seizure immediately prior to scanning were not associated with a change in HCT2 values. Similarly, there was no significant change in HCT2 values in individual patients scanned twice with an inter-scan interval of up to 10 months, suggesting lack of progression of hippocampal pathology in patients with refractory focal epilepsy over this time (Grunewald *et al.* 1994). A large community-based longitudinal study found similar results over a longer inter-scan interval of 3.5 years (Liu *et al.* 2002a). Grunewald et al also reported that HCT2 values were significantly more abnormal in patients with a history of prolonged early childhood

seizures than in those without, reflecting the recognised association between early childhood seizures and HS (Duncan and Sagar 1987; Sagar and Oxbury 1987). Similarly, Van Paesschen and colleagues found a strong association between prolonged febrile convulsions and unilateral diffuse or focal anterior HS (Van Paesschen *et al.* 1997a). They also reported a correlation between frequency of seizures and unilateral diffuse or bilateral diffuse HS, a finding later supported by others (Woermann *et al.* 1998a). More recently, Okujava et al found a correlation between bilateral HCT2 abnormalities and an early age of seizure onset and an initial precipitating injury, but no association with seizure frequency or total number of generalised seizures (Okujava *et al.* 2002).

Previous studies have shown that hippocampal volume correlates inversely with HCT2 values allowing characterization *in vivo* of a range of severity of HS (Van Paesschen *et al.* 1995b; Van Paesschen *et al.* 1997a; Pitkanen *et al.* 1996). However, they do not have the same neuropathological basis, and elevated HCT2 times have been reported in the presence of normal hippocampal volumes (Bernasconi *et al.* 2000). In a study reporting the relationship between imaging and histopathology of the hippocampus in patients with TLE, increased HCT2 was associated with pathological changes in the hilus and cornu Ammonis (CA) 1 region of the hippocampus, whereas neuronal cell loss and concomitant gliosis in the CA1, CA2, CA3, and hilus were associated with MR-based HCV loss (Van Paesschen *et al.* 1997b). More recently, von Oertzen et al reported a strong inverse correlation between neuronal cell density and HCT2 in regions CA1 and CA3, and hippocampal volume loss was associated with a reduction in neuronal cell density in regions CA1, 3 and 4 (von Oertzen *et al.* 2002). Previously, it was proposed that increased HCT2 values reflects gliosis in the sclerosed hippocampus (Jackson *et al.* 1993a; Kuzniecky *et al.* 1987). Van Paesschen et al suggested that as HCT2 measures correlated more strongly with neuronal loss than increased glial density, gliosis per se is not the predominant factor in increased HCT2 values (Van Paesschen *et al.* 1997b). However, Briellmann et al recently demonstrated that HCT2 times was most confidently predicted by the glial cell count in the dentate gyrus. Furthermore, almost one third of the glial cells were reactive astrocytes, suggesting recent or ongoing pathological change, such as synaptic reorganisation (Briellmann *et al.* 2002b). Alternative pathological abnormalities include altered glial fibrillary acidic protein (GFAP) content (O'Callaghan 1993), density of glial cell processes (Hawrylak *et al.* 1993), size of glial cells (Krishnan *et al.* 1994), or increased extracellular space (Wieshmann *et al.* 1999a). In addition to improved sensitivity in the identification of hippocampal abnormalities, analyses of HCT2 times have been shown to be an independent predictor of neuropsychological impairment following temporal lobectomy (Wendel *et al.* 2001; Baxendale *et al.* 1998; Wood *et al.* 2000; Incisa della Rocchetta *et al.* 1995; Kalviainen *et al.* 1997a). Elevated HCT2 in the left hippocampal body in patients with left temporal lobe epilepsy (TLE) was associated with a better verbal memory outcome than high HCT2 in the left hippocampus in right TLE patients, suggesting that the measurement of HCT2 may be useful pre-operatively in predicting the risk of post-operative memory impairment (Wendel *et al.* 2001).

1.3.1.2.2 Amygdala

Detection of increased T2 signal intensity on qualitative visual assessment of the amygdala is challenging (Miller *et al.* 1994; Bronen *et al.* 1995a). T2-mapping of the amygdala (AT2) has therefore been applied in patients with epilepsy. The principle is similar to HCT2 mapping, although the image orientation may be different (Van Paesschen *et al.* 1996). In a study of patients with TLE, abnormal AT2 ipsilateral to the seizure focus was seen in 52% of patients. This represents additional sensitivity over visual assessment for the detection of amygdaloid

sclerosis (Miller *et al.* 1994; Bronen *et al.* 1995a). In a recent study by Bartlett et al, 44% of patients with HS demonstrated elevated AT2, with a satisfactory co-efficient of reliability (Bartlett *et al.* 2002). Neuropathological correlates of increased AT2, in a small number of patients who have undergone resective surgery, included gliosis and microdysgenesis (Van Paesschen *et al.* 1996). Compared with patients with HS, patients with an isolated abnormality of the amygdala developed habitual epilepsy at a significantly older age and did not have a history of febrile convulsions, in agreement with previous reports (Duncan and Sagar 1987; Bruton CJ 1988; Grunewald *et al.* 1994; Kuks *et al.* 1993; Cendes *et al.* 1993a).

1.3.2. Qualitative analysis of mesial temporal lobe structures

Hippocampal volume measurements may also be performed semi-automatically using a deformation-based segmentation algorithm (Haller *et al.* 1997). In this technique, an electronic atlas of the hippocampus is used as a deformable template that is matched to an individual MR image. The individual hippocampi can then be extracted and studied either quantitatively, for example with measures of volume and shape, or qualitatively as 3D-rendered models. In a study of five patients with mesial temporal sclerosis, Hogan and colleagues showed that this technique was more reproducible and less time-consuming and arduous than manual segmentation methods for the calculation of hippocampal volume measurements (Hogan *et al.* 2000). Furthermore, visual assessment of hippocampal morphology on 3D surface-rendered images revealed subtle structural differences between normal and sclerotic hippocampi, for example, loss of hippocampal head digitations. It has previously been proposed that such changes may exist in HS in the presence of normal volumetry (Oppenheim *et al.* 1998), suggesting that shape analysis may be useful in the evaluation of patients with cryptogenic temporal lobe epilepsy. Statistical evaluation of differences in hippocampal shape is also possible, and is a more objective method than visual interpretation. This has been applied to patients with schizophrenia and to patients with Alzheimer's dementia. Compared to control subjects, both individual analyses of volume and shape, and composite analyses using combined volumetric and morphological data were discriminatory (Csernansky *et al.* 2002; Shenton *et al.* 2002).

1.3.3 Neocortical post-processing techniques

1.3.3.1 Introduction

Conventional qualitative assessment of high resolution MRI identifies a lesion in a large proportion of patients with refractory focal epilepsy. Up to 25% of patients, however, have normal imaging (Li *et al.* 1995). Re-orientating volumetric data sets to optimise visual assessment of potentially abnormal gyri (Barkovich *et al.* 1995), improving spatial resolution by the use of surface coils (Grant *et al.* 1997), increasing scanning time or image averaging (Knowlton 2000) may improve the yield of abnormalities from visual inspection of the resultant images. Alternatively, post-processing techniques may detect additional abnormalities. These may be quantitative, such as changes in volume distribution of grey and white matter (Sisodiya *et al.* 1995b) or fractal analysis (Free *et al.* 1996b), or qualitative, such as 3-dimensional cortical surface rendering (Sisodiya *et al.* 1995a), curvilinear

reformatting (Bastos *et al.* 1995) or texture analysis (Bernasconi *et al.* 2001a).

1.3.3.2 Quantitative methods

Cerebral structural development and connectivity are determined by a relatively small number of genes suggesting that general principles and patterns of cerebral organisation exist. In dysgenetic brain, where these principles are violated, abnormalities may therefore extend beyond the margins of the visible malformation. Furthermore, acquired cerebral insults, such as head trauma, may result in focal or diffuse brain damage which is frequently distant from the principal site of injury, and which is often not visually apparent on conventional MRI. The hypothesis that cortical dysgenesis is more diffuse than can be appreciated on visual inspection of conventional MRI was tested in a quantitative study of the regional distribution of grey and subcortical matter volumes in patients with MCD (Sisodiya *et al.* 1995b). Following semiautomatic segmentation of a T1-weighted volumetric data set into cortical grey matter or subcortical matter (comprising white matter and basal nuclei, but excluding the caudate), each volume of interest was divided into 10 smaller volumes, each spanning one tenth of the total anterior-posterior extent of the hemisphere from which they were derived. A number of variables, including total hemispheric volume, and grey and subcortical matter volumes in each "block" were derived and compared to control subjects. In the majority of patients with cerebral dysgenesis, the regional distributions of grey and subcortical white matter were abnormal both within and beyond the margins of the visually apparent lesion. It was postulated that this was due to structural abnormalities that may give rise to abnormalities in interneuronal connectivity. This finding concurs with previous suggestions that cerebral dysgenesis is a more diffuse pathological entity than can be appreciated on visual inspection of either MR images or at surgery (Palmini *et al.* 1991b; Andermann 1994), and may account for the often poor surgical outcome in these patients (Bruton CJ 1988; Guerrini *et al.* 1992). This "block" method was utilised in the investigation of patients with refractory focal epilepsy and HS. A poor surgical outcome correlated strongly with widespread regional volume abnormalities on quantitative analysis of pre-operative imaging (Sisodiya *et al.* 1997b). Patients with hypothalamic hamartomata and gelastic seizures were also investigated using this technique (Sisodiya *et al.* 1997a). These patients typically have a poor seizure outcome following surgical resection of the identified lesion, although some recent success has been reported (Berkovic *et al.* 2003; Freeman *et al.* 2003). Widespread abnormalities in the volume distribution of grey and subcortical matter were again detected, suggesting the presence of extra-lesional occult structural abnormality. It was postulated therefore that in patients with cerebral dysgenesis, including hypothalamic hamartomata, and in the 30% of patients with unilateral hippocampal sclerosis who continue to have seizures post-operatively, the occult structural abnormalities possess intrinsic epileptogenicity. The authors concluded that this technique provided a useful predictor of outcome following resective surgery for refractory epilepsy (Sisodiya *et al.* 1997b).

In a study of quantitative MRI and preoperative neuropsychological function, abnormally distributed grey and white matter in patients with unilateral HS was associated with global memory impairment (Baxendale *et al.* 1999). This may explain the recognised association between preoperative cognitive dysfunction and poor surgical outcome in these patients (Helmstaedter *et al.* 1992).

This quantitative MRI method was also used to investigate patients with idiopathic generalised epilepsy

(IGE) (Woermann *et al.* 1998b). A relative increase in neocortical grey matter was detected in the IGE group when compared to a group of control subjects, and widespread structural changes were detected in a third of the patients analysed on an individual basis, possibly as a result of alterations in interneuronal connectivity. In addition, patients with juvenile myoclonic epilepsy and structural changes were more likely to have a positive family history than those without any structural change. It was therefore suggested that quantitative MRI may contribute to the determination of different IGE phenotypes, and thus aid genetic analysis.

Bekkelund et al measured cross-sectional areas of the cerebrum, cerebellum and corpus callosum in patients with generalised and focal epilepsy and found global atrophy in all patients irrespective of type and duration of seizure. Further prospectively designed studies are required to establish whether this relates to an effect of recurrent seizures, medication or underlying aetiological factors. (Bekkelund *et al.* 1996). Numerous studies have examined total cerebral and cerebral substructure volumes in conditions other than epilepsy, including: normal subjects (Filipek *et al.* 1989; Filipek *et al.* 1994; Murphy *et al.* 1992), dementia (Murphy *et al.* 1993), Rett syndrome (Reiss *et al.* 1993), schizophrenia (Lawrie and Abukmeil 1998), obsessive compulsive disorder (Jenike *et al.* 1996), hypertension (Salerno *et al.* 1992) and cerebral tumours (Filipek *et al.* 1991).

Quantitative analysis of the *surface area* of cortical grey matter in patients with MCD identified abnormalities in normal appearing hemispheres suggesting the presence of more widespread structural disruption than visually apparent and again, implicating abnormal connectivity, as a result of subtle structural abnormalities, as the likely explanation (Sisodiya and Free 1997).

Fractal geometry refers to the concept of self-similarity (Madelbrot 1983) and has been used to quantitatively assess the shape of the cerebral cortex in normal healthy subjects (Free *et al.* 1996b), and in patients with schizophrenia or bipolar disorder (Bullmore *et al.* 1994). In addition, several studies have demonstrated abnormal fractal dimensions (for example, altered complexity) of the white-grey matter interface in patients with focal epilepsy, including those with normal appearing MRI (Cook *et al.* 1995; Free *et al.* 1995a).

A further method to quantify surface complexity is the gyrification index (GI). This is derived from the surface area of the white matter compared with the surface area of the smallest smooth, enclosing, surface of the same brain region. The less convoluted the surface, the more similar the two measures will be, and the smaller the GI. In a study of patients with MCD, half of the subjects had gyrification indices outside the normal range suggesting abnormal gyral complexity (Free *et al.* 1996a).

In a quantitative MR study examining cortical thickening in patients with MCD compared with control subjects, areas of increased thickness were observed both within areas of overt dysgenesis and in normal appearing tissue, in agreement with previous studies reporting the widespread nature of abnormalities in MCD (Sisodiya *et al.* 1995b; Sisodiya and Free 1997).

1.3.3.3 Qualitative methods

Subtle gyral abnormalities cannot be fully appreciated on visual assessment of 2-dimensional MR slices. Reconstructing the data, and presenting the grey matter segment as a 3-dimensional image of the cortical surface allows meticulous examination, in vivo, of gyral width, position, relations, and complexity. This technique has been applied in presurgical planning (Jack Jr. *et al.* 1990b) and to more accurately localise and define known

cerebral lesions (Damasio and Frank 1992). More recently, visual assessment of 3D surface rendered images have identified additional gyral abnormalities both in patients with epilepsy and normal conventional MRI (Sisodiya *et al.* 1995a; Sisodiya *et al.* 1996b) and in those with cortical dysgenesis (Sisodiya *et al.* 1995a). Choi et al validated this technique in a study of patients with intractable neocortical epilepsy in which abnormalities identified only on 3D cortical images concurred with intraoperative electrocorticography and subsequent histopathological findings of cerebral dysgenesis (Choi and Kim 1999).

The conventional presentation of 2D MRI slices may artefactually suggest the presence of cortical thickening because of the obliquity of the image plane in relation to the gyrus, in addition to volume averaging of thick slices. Curvilinear reformatting is a technique which reconstructs images into thin, curved slices where the distance from the surface of the hemispheric convexities is kept constant. This results in anatomical images in which the slice plane is approximately perpendicular to the sulci thus reducing the appearance of artefactual cortical thickening. Using this technique, Bastos et al have demonstrated, and histologically verified, occult focal cortical dysplasia (FCD) in patients with epilepsy and normal conventional MRI (Bastos *et al.* 1999). Recently this technique was reported to be superior to 3D surface rendering for the visualization of extratemporal cortical lesions (Meiners *et al.* 2001), and may also be useful in accurately displaying the position of intracranial electrodes following surgical placement (Schulze-Bonhage *et al.* 2002).

A further technique employed to increase the detection rate of subtle FCD is texture analysis. This has been previously applied to normal subjects and patients with cerebral tumours to improve tissue classification (Kjaer *et al.* 1995; Schad *et al.* 1993; Lerski *et al.* 1993). Bernasconi et al investigated patients with surgically treated epilepsy and histologically proven FCD using feature maps modelled on recognised imaging features of FCD, such as cortical thickening, grey-white matter interface blurring, and signal hyperintensity. In almost all patients, including those with normal preoperative MRI, lesions were visually apparent on feature ratio maps, thus suggesting that this technique is clinically useful in patients with focal epilepsy due to occult FCD but normal conventional MRI (Bernasconi *et al.* 2001a).

In summary, more information is embodied in imaging data than is accessible from the conventional presentation of 2D imaging slices for visual assessment. The yield of lesion detection can be increased by using post-processing techniques, particularly in patients with well-defined focal epilepsy and normal MRI. However, the majority of the techniques are presently time-consuming and computationally expensive and are, therefore, limited to dedicated imaging centres.

1.3.4 Statistical parametric mapping

1.3.4.1 Methodology

Statistical parametric mapping (SPM) refers to the production of statistical images to test hypotheses about regionally specific effects or differences. In SPM, every voxel in a patient's image data set is analysed using a standard univariate statistical test. The resulting statistical parameters are assembled into a map or probability image - the statistical parametric map. Unlikely excursions of the map are interpreted as regionally specific effects or differences between groups of images, for example, patients against control subjects, or a single subject's

images acquired under a number of different experimental conditions.

Statistical parametric mapping represents the product of two earlier ideas: change distribution analysis and significance probability mapping. Change distribution analysis was a voxel-based assessment of neurophysiological changes developed for positron emission tomography (PET) (Fox and Mintun 1989). This provided a measure of the size of activation but, unlike SPM, not a measure of the statistical reliability or significance of the effect. Significance probability mapping was originally developed for the analysis of multichannel EEG data.

The analysis of an MRI image using statistical parametric mapping comprises several stages (figure 1.16):

- Spatial normalisation, including linear and non-linear transformations
- Segmentation into separate tissue compartments may be performed in some cases
- Spatial smoothing
- Voxel-wise statistical analysis (using the General Linear Model)
- Statistical inference (using the theory of Gaussian Fields)

1.3.4.1.1 Spatial Normalisation

To implement meaningful voxel-based analyses of images, data from different subjects must derive from identical regions of the brain. Spatial transformations are therefore applied that move, rotate, re-scale, shear and /or warp the images so that they all conform approximately to a standard brain. The transformation of an image into a standard anatomical space, usually that described in the atlas of Talairach and Tournoux (Talairach and Tournoux 1988), is referred to as spatial normalisation (Fox *et al.* 1985).

Spatial transformations can be broadly divided into *label-based* and *non-label-based.* Label-based techniques identify identical anatomical structures, features, or landmarks in two images and find the transformations that most closely align the labelled points (Pelizzari *et al.* 1988). However, the reliability is limited by the reproducibility of labelling. Non-label-based approaches, implemented in the image analysis software SPM96 and SPM99 (Wellcome Dept of Cognitive Neurology, Institute of Neurology, London, UK), identify a spatial transformation that minimises the difference between an object and a reference image, where both are treated as unlabelled continuous processes. The transformation may be linear (e.g. principal axes (Alpert *et al.* 1990)or image realignment (Woods *et al.* 1992; Lange 1994; Collins *et al.* 1994)) or non-linear (e.g. plastic transformation / warping (Friston *et al.* 1991b)). Without any limitations on the extent of spatial transformation, specifically when using a non-linear approach, it is possible to normalise an image so that it matches another exactly. The critical issue therefore, when using spatial normalisation, is defining the *constraints* under which the transformation occurs.

Linear (affine) normalisation uses a rigid-body transformation (translation and rotation) in addition to zoom and shear transformations to minimise the sum of the squared difference between images (Friston *et al.* 1995a). Non-linear normalisation utilises basis functions to deform and focally shape the image to correct for more subtle differences and create a more accurate fit (Ashburner and Friston 1999). These basis functions are of low spatial frequency so individual sulci are unable to be matched exactly between individuals. The use of higher spatial frequency basis functions allows this to occur but at the expense of computational time and stability of the

algorithm. To minimise excessive warping during non-linear normalisation, the Bayesian formulation is incorporated which takes account of *a priori* probability information regarding the normal variability of brain size and shape (Friston *et al.* 1995a). In the statistical parametric mapping software, SPM96 and SPM99, iterative re-sampling of the realigned images during the process of normalisation may be performed using either nearest neighbour, bilinear, or sinc interpolation. Bilinear uses eight nearest neighbours as normalisation references, whereas sinc uses several hundred; thus, it has greater resolution but is more time-consuming.

1.3.4.1.2 Segmentation

On the basis of an MR image, cerebral tissue can be broadly classified into three separate compartments: grey matter (GM), white matter (WM), and cerebrospinal fluid (CSF). This partitioning can be performed manually by selecting suitable image intensities that encompass most of the voxel intensities of a particular tissue type. The manual selection of thresholds is subjective however, and additional editing of scalp tissue is required.

An alternative, automated method involves the use of clustering algorithms (Hartigan 1975; Ashburner and Friston 1997). This assumes that each voxel in a MR image belongs to one of a small number of tissue types (clusters). Voxels are classified into one of these clusters according to their signal intensity. In addition, combining the clustering algorithm with *a priori* information about the likely spatial distribution of these compartments from averaged, normalised, multi-subject atlases, (such as that provided by the Montreal Neurological Institute (Evans *et al.* 1992)) the classification process is further improved.

This model assumes that each voxel contains tissue from only one of the underlying clusters. Those voxels which lie on the interface of neighbouring compartments may contain a mixture of tissue types and hence may be misclassified. The use of high resolution images reduces this partial volume effect but fails to eliminate it entirely.

Additional difficulties are imposed by the non-uniformity of signal intensity across the images. This artefact may also lead to aberrant tissue classification. Correcting for non-uniformity has been shown to improve the segmentation of T1-weighted images (Ashburner and Friston 2000). Incorporating additional information about each voxel in an image, such as the tissue type of the neighbouring voxels, may further improve the accuracy of the segmentation process (Van Leemput *et al.* 1999).

1.3.4.1.3 Spatial smoothing

Smoothing is a process whereby the images are convolved with a Gaussian kernel (Friston 1997; Ashburner and Friston 2000). It has several important objectives. Firstly, it generally increases the signal to noise ratio. This is because noise tends to have a high spatial frequency (as the effects of noise within each voxel may be regarded as independent), whereas the information of clinical interest is normally expressed over a larger scale. Smoothing will therefore reduce the effect of noise without affecting the signal intensity from areas of interest. Secondly, the validity of SPM is increased because the data conforms more closely to the Gaussian field model (becomes more normally distributed). This is important if one wants to use the theory of Gaussian fields to assign statistical values to the regionally specific effects. Thirdly, it further assists the normalisation process. The magnitude or spatial extent of the kernel, and thus the degree of smoothing, is numerically defined by the full-width, half-maximum (FWHM) value. For example, at a smoothing level of 8mm, the width of the kernel is 8mm at half the maximum voxel intensity. In SPM96 and 99, the smoothing is performed initially in the x, then y, then z plane (axial image).

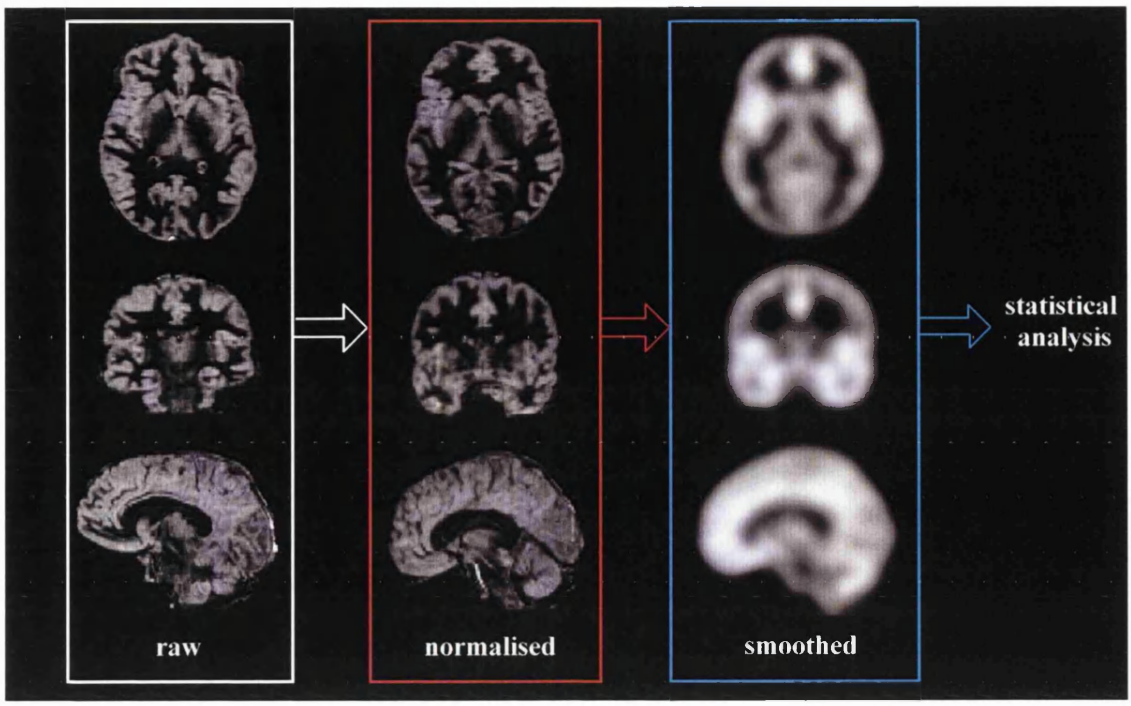

Figure 1.16: The stages of image processing in SPM (a single control subjects DIR image is shown).

1.3.4.1.4 Statistical analysis

Following stereotactic normalisation and smoothing, statistical analysis of the images is performed. The initial stage of the analysis involves creating a statistical image, reflecting evidence against a null hypothesis of no regional differences, using the general linear model. The second stage (statistical inference) assesses this statistical image, locating voxels where a difference is demonstrated, whilst controlling for false positives.

Using the general linear model, a standard univariate test is applied to each voxel in the image independently. Individual voxel values from one group of images are compared with the voxel values at the same position in another group of images. A number of covariates may be introduced to model the data. Following statistical analysis, by referring to the error variance, a *t* value for each and every voxel is calculated, creating a SPM{*t*}. Following conversion to the unit normal distribution (mean=0, sd/variance=1) a Gaussian field or SPM{Z} is obtained. This is a three-dimensional voxel-by-voxel map of Z scores (and hence p values) from which statistical inferences can be made.

1.3.4.1.5 Statistical inference

Images contain a large number of voxels; hence, during the analysis and construction of a parametric map a large number of statistical tests are performed. Correction for multiple comparisons is therefore required if inferences are to be made from the whole brain. Alternatively, if an *a priori* hypothesis regarding a specific region is employed, and all other brain regions are ignored, irrespective of the p-values in these areas, the multiple comparison correction may be less stringent (Worsley *et al.* 1995). Difficulties arise when correcting for multiple comparisons in statistical parametric maps because of the non-independence of voxel intensities due to both the initial resolution of images and to postprocessing, especially smoothing. This non-independence cannot be treated

by Bonferroni procedures, which treat voxels as if they were independent, because they are too stringent. The theory of Gaussian fields allows a corrected *P* value to be calculated whilst respecting the non-independence (Friston *et al.* 1991a; Worsley 1993). This is achieved by considering the behaviour of stochastic processes (mathematical structures used to define a phenomenon with intrinsic randomness which makes perfect prediction impossible) defined over a space of usually 3 dimensions (Cox and Miller 1990). A further statistical test, the extent statistic, can be applied to the data in SPM. This is based on the number of connected voxels in a cluster defined by a prespecified threshold (usually $p<0.05$). It describes the probability that a region (cluster of voxels) of the observed size could have occurred by chance over the entire volume analysed.

The resulting SPM{Z)} therefore provides *P* values which pertain to several levels of inference: the number of clusters / regions above some height and volume thresholds, the number of voxels comprising a particular region, and the *P* value for each voxel within that region.

1.3.4.2 Clinical applications

The technique of statistical parametric mapping was originally utilised in the analysis of PET data (Petersen *et al.* 1989). Validation of the method originated from a PET study of functional specialisation of extrastriate cortex. Regional differences in brain activity were correlated with homologous areas in the primate model which showed specific electrophysiological responses to equivalent stimuli (Lueck *et al.* 1989).

More recently, SPM has been used to process and analyze ligand and $H_2{}^{15}O$ PET data in patients with epilepsy and hippocampal sclerosis (Koepp *et al.* 1996; Van Bogaert *et al.* 2000), malformations of cortical development (Van Bogaert *et al.* 1998; Richardson *et al.* 1996), non-progressive acquired lesions (Richardson *et al.* 1998), and in those with normal conventional MRI (Koepp *et al.* 2000; Richardson *et al.* 1998; Koepp *et al.* 1997).

SPM has also been used in functional MRI experiments. Focal differences in signal intensity, due to the blood oxygen level-dependent (BOLD) contrast, between resting and active states have permitted cerebral areas involved in common tasks, such as the processing of visual and auditory stimuli to be localised (Heun *et al.* 1999; Rees *et al.* 2000; Friston and Buchel 2000). In addition, the cerebral regions associated with higher cortical functions such as memory, attention and emotion (Morris *et al.* 1996) and the functional re-organisation or recovery from a cerebral injury, have also been examined (Levy *et al.* 2001; Rosen *et al.* 2000). The processing and analysis of fMRI data differs from that used for PET data in a number of ways. Firstly, the general linear model used in the analysis of PET data assumes that each scan represents an independent observation. MR images are acquired every few seconds and thus a specific haemodynamic response, in addition to other physiological variables, may be seen over a number of scans. This is termed temporal autocorrelation and requires an extended general linear model with temporal smoothing to ensure statistical validity. Secondly, filtering is necessary to remove physiological noise. This is derived from, for example, cardiac blood flow effects, pulsatile motion, and a periodic variation in blood oxygenation and movement induced by respiration (Noll *et al.* 1993; Le and Hu 1996; Friston *et al.* 1996). A number of studies have shown good agreement between the results of functional MRI and PET experiments with identical paradigms. This suggests that, despite PET measuring blood flow variations and fMRI quantifying relative changes in the oxygenation of venous blood, the two methods are comparable (Paulesu

et al. 1995; Dettmers *et al.* 1996).

Voxel-based morphometry (VBM) is a term used to describe the application of SPM in the examination of the local concentrations of grey matter between two groups. Whereas fMRI identifies regional changes in blood oxygenation in an individual patient, in response to specific tasks, VBM examines static structural differences in grey matter between two groups of subjects. High resolution T1-weighted images are spatially normalised, then segmented and smoothed before being statistically analysed. Individual subjects may be compared to a group (usually healthy control subjects) or group analyses may be performed where one group is compared to another. VBM has been utilised in the investigation of numerous conditions, for example, patients with psychiatric disorders (Wright *et al.* 1999; Wright *et al.* 1995; Shah *et al.* 1998; Sowell *et al.* 2000; Woermann *et al.* 2000), headache (May *et al.* 1999), autism (Abell *et al.* 1999), dementia (Mummery *et al.* 2000; Frisoni *et al.* 2002), in the investigation of age-related changes (Sowell *et al.* 1999), and in epilepsy. Comparison of patients with juvenile myoclonic epilepsy with control subjects identified an increase in grey matter in the mesial frontal regions of the patients (Woermann *et al.* 1999b). In a methodologically similar study, patients with malformations of cortical development were found to have significantly abnormal grey matter within and beyond the margins of the lesion visualised on qualitative assessment of the conventional MR images (Woermann *et al.* 1999a). Processing of the images, particularly segmentation, normalisation and smoothing, preclude reliable identification of small abnormalities, such as hippocampal atrophy, in individual patients. Group analyses, however, are able to identify such lesions, but consequently are limited in terms of clinical usefulness. In patients with both left and right temporal lobe epilepsy, VBM identified local reductions of grey matter concentration (GMC) in mesial temporal lobe structures, in addition to reduced GMC in the right dorsal prefrontal cortex. It was suggested that this was due to epileptiform excitotoxic discharges from the reciprocally connected pathological hippocampus, and may be the aetiology of executive dysfunction commonly seen in such patients (Keller *et al.* 2002a). Furthermore, hippocampal grey matter concentration was unrelated to duration or age of onset of epilepsy. However, VBM demonstrated reduced GMC in bilateral thalamic, prefrontal, and cerebellar regions, which did correlate to the duration and age of onset of epilepsy (Keller *et al.* 2002b). VBM has also been applied in a small study of patients with known focal cortical dysplasia. Compared to a group of control subjects, abnormalities were detected on the patients' grey matter density maps, which concurred with previous imaging and electroclinical data. It was, therefore, postulated that VBM may be a useful screening tool for subtle dysplastic lesions (Kassubek *et al.* 2002). In individual patients however, pre-surgical evaluation of patients with focal epilepsy requires maximal specificity (to minimise false positives), frequently at the expense of sensitivity.

Recently, it has been postulated that the use of the cluster extent threshold in VBM is invalid (Ashburner and Friston 2000). Fifty normal subjects were randomly assigned to two groups. Analysis of these groups was performed to look for false-positives. With p values of 0.05, approximately 5 significant clusters would be expected by chance. Eighteen were found suggesting that the use of the cluster extent statistic should not be used in VBM. The large number of false positives found was thought to be due to the "non-stationary" nature and lack of smoothness of the underlying, variable neuroanatomy. Large size clusters occur in regions where the data are relatively stationary, i.e. smooth and uniform, and multiple, small size clusters will occur where the data are non-stationary and "rough". The distribution of cluster sizes, and hence the statistical results, will therefore be biased depending on the smoothness of the underlying data (Worsley *et al.* 1999). This finding will undoubtedly impact on future work using VBM and, importantly, questions the validity of studies previously reported. Correcting local

maxima for multiple comparisons using the Gaussian field theory to allow for the non-independence of the voxel intensities was seen to be valid, however, with only the small number of false positives allowed by chance detected (Ashburner and Friston 2000).

The underlying principle of VBM is the comparison of the local composition of brain tissue once macroscopic differences in brain shape have been discounted through normalisation. The normalisation process produces deformation fields which explicitly describe the mapping of one image onto a reference template image. It is possible to statistically analyse these deformation fields in order to interrogate brain shape and composition. This is the basis of deformation-based (DBM) and tensor-based morphometry (TBM). DBM identifies differences in the relative *positions* of brain structures following nonlinear normalisation, and TBM identifies differences in the local *shape* of brain structures. DBM can be applied on a global scale to ascertain whether there are any differences in overall brain shape between different populations, or at a voxel level, by creating a statistical parametric map. This latter approach identifies brain structures that are in relatively different positions, but does not directly localise brain regions with different shapes. This is determined by analysing statistical parametric maps of morphometric measures derived from TBM. TBM requires high dimensional warps to exactly match individual gyri, is computationally intensive and time-consuming, and is therefore currently of limited clinical usefulness. It is possible, however, to move more towards TBM by incorporating a lesser degree of tensor information from deformation fields, as a result of *imperfect* normalisation, in order to estimate changes in the volumes of cerebral compartments. Using this method, Good et al demonstrated reduced grey matter volume with increasing age and gender differences in grey and white matter volume in a cohort of 465 normal adult subjects (Good *et al.* 2001b; Good *et al.* 2001a). The use of deformation fields to modulate the data resulted in increased sensitivity over non-modulated images.

Deformation-based morphometry identified changes in volume of a number of structures in the brains of patients with schizophrenia consistent with a disturbance in the prefrontal-thalamic-cerebellar circuit (Volz *et al.* 2000). A comparison of this method with conventional MR volumetry in estimating ventricular size in patients with schizophrenia showed marked concordance between the two methods and, furthermore, by incorporating tensor information, changes in ventricular shape could be estimated. This was not possible with a standard, semi-manual tracing method. The authors concluded that DBM is therefore both valid and useful in the regional and global examination of brain morphology (Gaser *et al.* 2001). In addition, the technique is entirely automatic and, with no user bias or a priori-defined regions of interest, may prove useful in studies with large numbers of subjects.

1.4 HARDWARE DEVELOPMENTS

1.4.1 Surface Coil Imaging

The outcome following resective surgery for refractory focal epilepsy correlates strongly with the identification of a lesion on MRI (Cascino *et al.* 1992) and the extent of its subsequent removal (Palmini *et al.* 1991a). The goal therefore in the assessment of patients with conventional MR imaging is to determine accurately and characterise fully all macroscopic epileptogenic lesions. In order to achieve this objective, scanning parameters must be optimised to offer the highest spatial resolution possible. Improved signal-to-noise ratio (SNR) can be accomplished by increasing scanning time and averaging, or by the use of surface coils which reduce the distance between the patient's head and the coil elements (from approximately 5cm to 2cm) (Fitzsimmons *et al.* 1997).

MR radiofrequency coils (including surface and head coils) consist of a loop of conducting material acting as an inductive element in a magnetic field. The coil and associated circuitry are designed to maximise power transfer from the tissue MR signal to the receiver amplifier (Murphy-Boesch 1984).

Conventional MRI of the brain is performed using a standard quadrature head coil provided by the scanner manufacturer. This produces a uniform signal intensity with a large field of view and good SNR (Hayes *et al.* 1985). A surface coil provides greater signal sensitivity at the expense of field of view and field homogeneity. However, the sensitivity to the MR signal decreases rapidly with increasing distance from the coil or depth into the tissue, therefore restricting the benefit to superficial tissues. To increase the depth of improved signal sensitivity, surface coils with larger radii are required (Edelman *et al.* 1985a). To overcome the limitations of a restricted field of view imposed by a single surface coil, it is possible to use a phased-array assembly which acquires data from multiple coils simultaneously (Roemer *et al.* 1990). The signal is combined into a composite image which therefore possesses both an increased SNR and a larger field of view (Hayes *et al.* 1993). Alternatively, a close fitting "dome-shaped" birdcage coil which covers the entire brain has shown an increase in SNR of approximately 10-20%, when compared to a standard head coil design (Fitzsimmons *et al.* 1997). An increase in spatial resolution from 2 x 2mm to 1 x 1mm in-plane necessitates a 16-fold increase in scanning time to maintain the same SNR. Using a surface coil with a 4:1 SNR advantage, this level of spatial resolution can be obtained in the same imaging time as the lower resolution head-coil images. Alternatively, the increased SNR can be traded for reduced scanning time whilst maintaining the same level of resolution and SNR as obtained with the standard head-coil (Edelstein *et al.* 1983; Crooks *et al.* 1984).

Surface coils were originally used clinically in the imaging of superficial tissues, for example the orbit (Schenck *et al.* 1985), neck and chest wall (Axel 1984). This was subsequently extended into imaging deeper structures, such as the lumbar spine (Edelman *et al.* 1985b), and in the examination of abdominal viscera, a two to four-fold increase in the SNR for structures within 12cm of the coil was seen (Edelman *et al.* 1985a). An MRI study of the temporal lobes using four surface coils in a phased-array assembly showed an improved SNR throughout the region of interest. This was quantified, using a water phantom, to be approximately 1.67 times greater than the SNR of the standard quadrature head coil at the expected depth of the hippocampi (approximately 5-6 cm) and 6 times greater at cortical depth. The improved SNR allowed images with a spatial resolution of 0.3mm x 0.3mm in plane to be produced. Images with the same resolution obtained using the standard head coil were of unacceptably poor quality. In order for the surface coil to acquire satisfactory images at this improved

resolution, however, additional head restraints to prevent movement, cardiac gating and flow compensation were required (Hayes, Tsuruda, and Mathis 1993).

The question of whether these improvements in the SNR and/or spatial resolution result in improved detection or characterisation of pathological lesions has been addressed in only a small number of studies (Grant *et al.* 1997; Moore *et al.* 2002). Twenty-five patients with medically refractory neocortical focal epilepsy underwent routine (voxel size of approximately $1mm^3$) and surface-coil (voxel size of approximately $0.4mm^3$) MR imaging. The phased-array surface coil was placed over the region thought most likely to contain the epileptogenic focus as determined by the standard head-coil MR images as well as clinical and electrophysiological data. Overall, more lesions or better definition of known lesions were seen in 16 of the 25 patients. This included the detection of new lesions in three patients (heterotopia, focal cortical lesion suggestive of a neoplasm, and a small temporal lobe cyst), six scans originally classified as indeterminate were re-classified as either abnormal (focal cortical dysplasia) or normal, and two cases remained indeterminate. In addition, of the 10 cases with established diagnoses on head-coil imaging, 5 were re-classified following examination with the surface-coil. These included three patients with abnormalities thought to represent tumours which were shown to be more likely to be non-neoplastic on surface-coil imaging. Pathology was available from seven patients and in only one patient did the surface-coil add diagnostic information prior to surgery. The surface coil imaging did, however, result in surgical treatment being deferred in four patients who were originally thought to have neoplastic lesions but were re-classified as non-neoplastic (Grant *et al.* 1997).

In summary, surface-coil MR imaging can offer increased sensitivity in the identification of specific cerebral lesions. This is at the expense of additional hardware, in addition to increased scanning and reporting time. In epilepsy centres with optimised, high resolution head-coil imaging, the use of surface coils are indicated in two groups of patients; those with focal electroclinical localisation but normal conventional imaging, and those with subtle head-coil imaging abnormalities which require additional characterisation, for example focal cortical thickening. In centres with sub-optimal conventional MRI, improvements in standard head-coil imaging are more likely to produce an increase in lesion detection, rather than the introduction of surface-coil imaging.

CHAPTER TWO

Common Methodology

2.1 INTRODUCTION

The image acquisition, processing and statistical analyses were individually tailored for each of the four advanced techniques to take advantage of specific properties of each sequence, with the overall goal of enhancing lesion sensitivity and specificity. There were, however, a number of common methodological steps.

2.2 SUBJECTS

Healthy volunteers with no history of neurological disease, and patients with focal epilepsy recruited from the clinics of The National Hospital for Neurology and Neurosurgery and The National Society for Epilepsy were scanned with conventional MRI and advanced imaging techniques. The patient group comprised:

- 21 patients with clear history and imaging findings of past acute and non-progressive cerebral injury, including ischaemia, head injuries, perinatal injury, and post-encephalitis.

- 41 patients with a variety of malformations of cortical development, including gyral abnormalities, focal cortical dysplasia, heterotopia (subependymal, subcortical nodular and band), and dysembryoplastic neuroepithelial tumours.

- 100 patients with focal epilepsy and normal conventional MRI. Following video and EEG telemetry, these were diagnosed with temporal lobe epilepsy, frontal lobe epilepsy, occipital lobe epilepsy or defined as possessing less well localised, more widespread abnormalities.

Within the MRI-negative group, significant abnormalities on advanced imaging were defined as concurring with electroclinical data if they localized to the same cerebral lobe in the same hemisphere.

Written informed consent from each subject and approval by the local ethical committees of The National Hospital for Neurology and Neurosurgery and Institute of Neurology were obtained.

2.3 CONVENTIONAL MRI

All controls and patients had conventional MR imaging on a 1.5T Horizon Echospeed scanner (GE, Milwaukee, USA) which comprised a T1-weighted inversion recovery prepared - spoiled gradient recalled (IRp-SPGR) volumetric acquisition, a contiguous 5mm oblique coronal T2-weighted, a proton density and a fast FLAIR image. These were reviewed by experienced neuroradiologists who detected no abnormalities in either the control or MRI-negative subjects.

2.4 POST-ACQUISITION PROCESSING

2.4.1 Construction of quantitative maps

Following data acquisition, the images were transferred to an off-line workstation (Sun Microsystems, Palo Alto, CA) for post-processing, which was highly specific for each technique. *(See chapters 3-6 for details).*

2.4.2 Statistical parametric mapping

To allow objective voxel-by-voxel statistical comparisons to be made, all image maps were normalised to a standard template using SPM96 (DTI) or SPM99 (MTI, T2M, DIR) (Wellcome Dept of Imaging Neuroscience, Institute of Neurology, London, UK) (Friston *et al.* 1995a). Each advanced sequence necessitated the formation of a tailored template. These were created by normalising a control subject's image to standard SPM space, which approximates Talairach space, using linear (rotation, shear, translation, re-scale) and non-linear steps ("warping"). Subsequently, the images of the patients and controls were normalised to this template, which afforded a robust, reproducible normalisation.

Prior to statistical analysis, the normalised maps were smoothed with an isotropic Gaussian kernel to improve signal to noise ratio, to allow the images to conform more closely to a Gaussian field model to increase the validity of statistical inference, and to further reduce interindividual variation (Friston *et al.* 1995b). Different techniques demanded different degrees of smoothing to optimize lesion sensitivity and specificity (*See chapters 3-6 for details).*

Using SPM, a standard univariate statistical test was applied to every voxel in the image in order to create a map from which statistical inference was made. Significant increases or decreases in image voxel values were detected at an individual voxel threshold of $p<0.001$. The theory of Gaussian fields was used to calculate a corrected multiple comparison p value of 0.05 (Friston *et al.* 1994). This correction describes the probability that a region of the observed size could have occurred by chance over the entire volume analysed whilst allowing for the non-independence of voxel intensities determined by both the initial resolution of the images and the smoothing.

Each patient's map was compared to the 30 control subjects. Additionally, each control was statistically compared with the remainder of the control group with equivalent smoothing, signal intensity threshold parameters and significance levels of $p<0.001$, corrected to $p<0.05$. Group comparisons were also performed. All MRI-negative patients with distinct clinical and electroencephalographic (EEG) evidence of left or right temporal lobe, frontal lobe or occipital lobe epilepsy following video and EEG telemetry were grouped and statistically compared with the control group.

2.4.3 Region-of-interest analyses

In order to illustrate the magnitude of the statistical differences, areas highlighted by the SPM comparison as deviating significantly from normal in terms of voxel intensity and cluster extent ($p<0.05$) were then analysed using a region-of-interest (ROI) approach. These areas were automatically outlined and superimposed on the normalised maps using DispImage 4.7 (Plummer 1992). Careful visual assessment of these superimposed regions permitted accurate anatomical localization of abnormalities in both patients and controls. The mean voxel value in the ROI from each patient's map was compared to the mean value in the equivalent ROI from all 30 of the control subjects' maps and the difference expressed as a percentage of the control mean (Barker, Tofts, and Gass 1996).

2.5 METHODOLOGICAL LIMITATIONS

To enable the voxel-by-voxel analysis to compare similar brain regions between patients and control subjects, gross anatomical and positional variability between individuals needed to be corrected. An absolute metric to quantify the accuracy of normalisation does not exist. Nevertheless, on visual assessment normalisation of the maps / images to a common three-dimensional (Talairach) space worked satisfactorily in all subjects, even those with structural lesions. This was supported by only a small number of changes seen on analysis of the control subjects.

It was generally observed that central cerebral structures were most accurately matched to the other subjects after normalisation. The most peripheral cerebral structures, for example, the cortical ribbon and subcortical white matter corresponded less well, resulting in a wider range of values in these regions. Statistical comparison of these areas between controls and patients may have failed to identify subtle differences.

The parameters used for normalisation, smoothing, and signal intensity threshold were optimised to offer maximal specificity, as this is of paramount importance in pre-surgical assessment. Inevitably, this may have resulted in a lowering of sensitivity in identifying lesions in MRI-negative patients.

Specific methodological issues are discussed in Chapters 3-6 and also in Chapter 7.2.

CHAPTER THREE

Diffusion Tensor Imaging

3.1 DIFFUSION TENSOR IMAGING IN FOCAL EPILEPSY

3.1.1 Summary

Diffusion tensor imaging (DTI), analysed using Statistical Parametric Mapping (SPM96), was used to objectively examine the diffusion properties, and hence structural organisation, of cerebral tissue in 10 patients with partial seizures and acquired lesions, 22 patients with malformations of cortical development and 30 patients with partial seizures and normal MRI. Fractional anisotropy and mean diffusivity maps were calculated and using SPM, individual patients were compared to a group of 30 control subjects. Diffusion tensor imaging and objective voxel-by-voxel statistical comparison identified significant increases in diffusivity and significant reductions of anisotropy in all patients with acquired nonprogressive cerebral lesions and partial seizures. In all of these patients the areas of increased diffusivity and in nine patients the areas of decreased anisotropy concurred with abnormalities identified on visual inspection of conventional MRI. In addition there were ten areas, which were normal on conventional imaging, which exhibited abnormal anisotropy or diffusivity. Areas of reduced anisotropy were found in seventeen patients and areas of increased diffusivity in ten patients with MCD. Two patients had areas of increased anisotropy. There were no patients with reduced diffusivity. Areas of increased diffusivity were in general more extensive than areas of reduced anisotropy. Changes in tissue beyond the MCD, that appeared normal on conventional MRI, were found in six patients for anisotropy and nine patients for diffusivity. Individual analyses of the 30 patients with partial seizures and normal optimal MRI identified a significant increase in diffusivity in eight of the subjects. In six of these, the areas of increased diffusivity concurred with the localisation of epileptiform EEG abnormality. Analysis of anisotropy in the MRI-negative patients revealed significant differences in two patients, one of which concurred with electroclinical seizure localisation. Group analysis of nine patients with electroclinical seizure onset localising to the left temporal region revealed a significant increase of diffusivity and a significant reduction in anisotropy within the white matter of the left temporal lobe. DTI analysed using SPM was sensitive in patients with acquired cerebral damage and MCD. Significant differences in the diffusion indices in individual MRI negative patients and the group effect in patients with left temporal lobe epilepsy suggests minor structural disorganisation exists in occult epileptogenic cerebral lesions. These techniques are promising, non-invasive imaging methods for identifying the cause of partial seizures, and can contribute to presurgical evaluation.

3.1.2 Introduction

Diffusion is a random process resulting from the thermal translational motion of molecules. The diffusion displacement distances are comparable with cellular dimensions, raising the possibility that the measurement of water diffusion might provide a means of exploring cellular integrity and pathology. Diffusivity is a measurement of the magnitude of the diffusion and its degree of directionality can be quantified by various anisotropy indices

(Pierpaoli and Basser 1996; Pierpaoli *et al.* 1996). Tissues with more restricted diffusion in one direction than another, for example white matter, are termed anisotropic whereas those with the same diffusion in all directions are referred to as isotropic, for example cerebrospinal fluid. Pathological processes that change the microstructural environment, such as neuronal swelling or shrinkage, increased or decreased extracellular space and loss of tissue organisation, result in altered diffusivity and/or anisotropy (Anderson *et al.* 1996; Sevick *et al.* 1992).

The aim of this study was to test the hypothesis that DTI would identify areas of altered anisotropy and diffusivity in patients with epileptogenic acquired lesions and malformations of cortical development, and would identify focal abnormalities in MRI negative patients.

3.1.3 Methods

3.1.3.1 Subjects

- 30 healthy control subjects :
  - 10 men, median age 30 years, range 20-50 years

- 62 patients with focal epilepsy

  Acquired
  - 10 patients (9 men, median age 36 years, range 20-53 years)
    - 3 patients with ischaemic lesions
    - 5 patients with head injuries
    - 1 patient with a history of encephalitis
    - 1 patient with a history of perinatal injury

  Malformations of cortical development
  - 22 patients (9 men, median age 31 years, range 21-51)
    - 13 patients with gyral abnormalities
    - 11 patients with heterotopia
      - subependymal (n=5), subcortical nodules (n=1) and band heterotopia (n=5)

  Two patients had both subependymal heterotopia and gyral abnormalities (patient 12 & 21)

  MRI-negative
  - 30 patients (17 men, median age 36 years, range 18-55 years)
    - 15 were diagnosed with temporal lobe epilepsy (9 left, 6 right)
    - 6 with frontal lobe epilepsy (3 left, 2 right, 1 bilateral)
    - 2 with occipital lobe epilepsy
    - 7 had electroclinical evidence of less well-defined, more widespread abnormalities

3.1.3.2 Diffusion tensor imaging

Scans were performed on a 1.5T Horizon Echospeed scanner (G.E, Milwaukee, Wisc., USA) using single-shot CSF-suppressed diffusion weighted echoplanar imaging (EPI) (TR/TE/TI=5000/78/1788 ms, field-of-view 24cm, acquisition matrix 96x96, reconstruction matrix 128x128, slice thickness 5mm) (Barker *et al.* 1997). Pulsed unipolar diffusion gradients were used for diffusion sensitisation (δ=28ms, Δ=35ms). Two b-values (differing degrees of diffusion weighting) were applied in each of seven non-collinear directions (to allow rotationally invariant parameters to be calculated) at 13 slice positions (b_{max}=703 s/mm^2). Two interleaved series with nine repeats each were acquired, resulting in 1872 images. Repeat scans were averaged after magnitude reconstruction to increase signal to noise while retaining the low motion sensitivity of the single shot acquisition. Diffusion scanning time was 19 minutes. Total scanning time including diffusion, localiser and high-resolution EPI anatomical scan was 25 minutes. Images were transferred to an off-line workstation (Sun Microsystems, Palo Alto, CA) for post-processing.

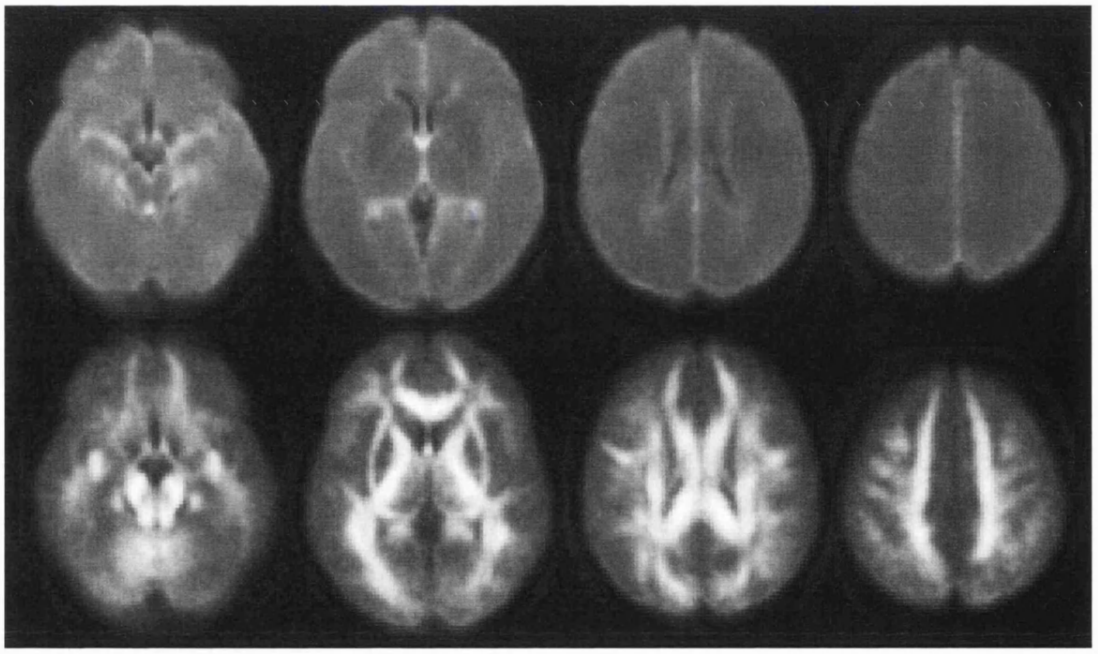

Figure 3.1: Normalised, axial mean diffusivity (top row) and fractional anisotropy (bottom row) maps. Averaged from the 30 control subjects.

3.1.3.3 Analysis

The maps of mean diffusivity and fractional anisotropy were calculated using the method proposed by Basser and Pierpaoli (Pierpaoli and Basser 1996; Pierpaoli *et al.* 1996) using in-house software. The mean diffusivity map represents the magnitude of the diffusion in each voxel measured in mm^2/s. Each voxel in the fractional anisotropy map represents a value of the anisotropy index, which is a rotationally invariant scalar index of diffusion

anisotropy with 0 representing an isotropic medium where there is no directionality to the diffusion and 1.0 representing maximum anisotropy.

To allow objective voxel-by-voxel statistical comparisons to be made, all images were normalised to a standard template using SPM 96 (Wellcome Dept. of Imaging Neurosciences, Institute of Neurology, London, UK) (Friston *et al.* 1995a; Friston *et al.* 1995b). This template was created by normalising a control subject's image with no diffusion weighting (the b=0 image) to SPM space, which approximates Talairach space using 12 linear degrees of freedom and a 4x5x4 non-linear warp. Subsequently the b=0 images of the patients and controls were normalised to this template using linear steps with 12 degrees of freedom (translation, rotation, zoom and shear). Using parameters derived from this process the mean diffusivity and fractional anisotropy maps were similarly normalized (figure 3.1).

Prior to statistical analysis, the normalised maps were smoothed with an isotropic Gaussian kernel (8mm for anisotropy maps and 10mm for diffusivity). In addition, a signal intensity threshold was set at 0.5 to reduce the level of noise from the diffusion images included within the analysis; that is, only voxels with values exceeding 50% of the whole brain mean intensity for each parameter were analysed. This procedure excluded noise that arose principally from outside the brain.

The smoothed, normalized maps were statistically analysed on a voxel-by-voxel basis, and inferences made from the resultant maps, as described in Chapter 2.3 *Common methodology: Post-acquisition processing.* Region-of-interest analyses were also performed in order to illustrate the magnitude of the differences in anisotropy and diffusivity in areas highlighted by the SPM comparison as deviating significantly from normal.

3.1.4 Results

3.1.4.1 Control group

Comparing each control subject with the remaining 29 control subjects using identical parameters and statistical thresholds as the comparison between patients and controls, two subjects had areas of significantly increased diffusivity and one subject had a significant reduction in anisotropy. At a statistical threshold of $p<0.05$ and 60 examinations (30 subjects with two contrasts each (an increase and a decrease)), up to three abnormal areas may have been anticipated by chance for each diffusion parameter.

3.1.4.2 Acquired Lesions

3.1.4.2.1 Individual SPM analyses:

In all ten patients with acquired lesions, SPM detected areas of significantly reduced anisotropy and increased diffusivity (table 3.1). In nine patients the areas of reduced anisotropy and in all patients the areas of increased diffusivity corresponded to the abnormalities identified on visual inspection of the conventional MR images (figure 3.2). In three patients areas of significantly reduced anisotropy and in a further three patients areas of significantly increased diffusivity were detected in regions previously reported as normal.

Analysis of patients 1, 2 and 3 also demonstrated significant increases in anisotropy. In patient 2, this was

within an area of visualised damage whereas, in patients 1 and 3, the areas of increased anisotropy were within normal-appearing cerebral tissue, most commonly immediately adjacent to the areas of visualised damage.

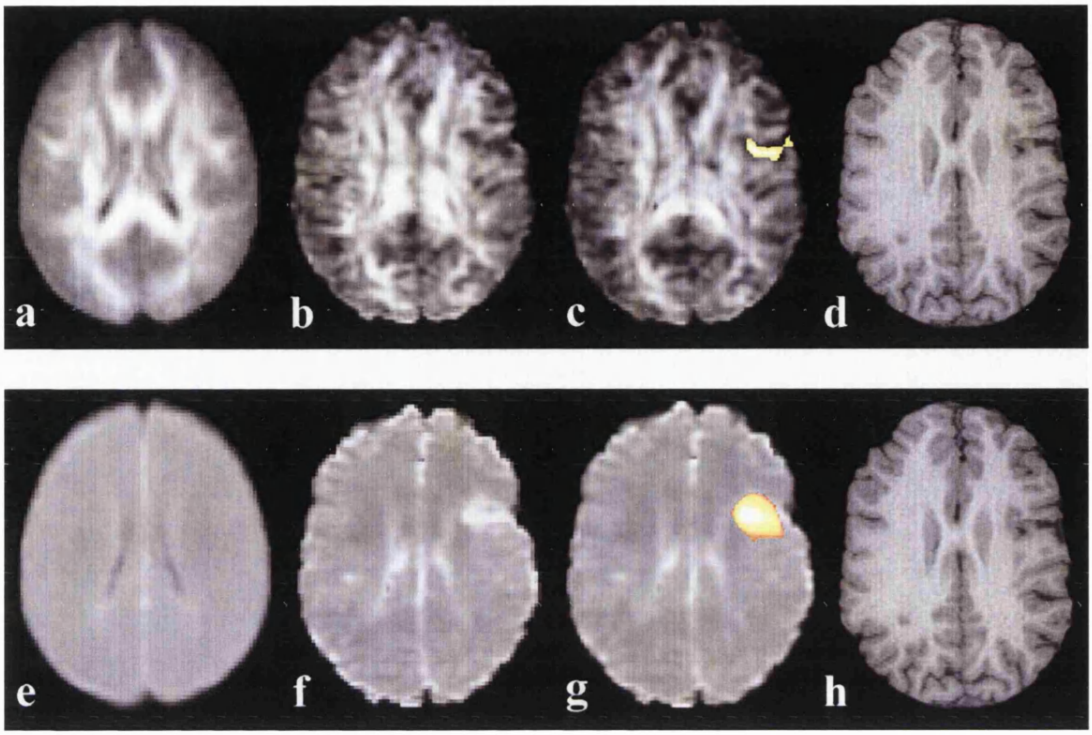

Figure 3.2: Patient 8, mature cortical infarct in right frontal lobe.

Normalised axial anisotropy maps at the same slice position for the averaged 30 control subjects (a) and the patient (b) and (c). Normalised axial diffusivity maps at the same slice position for the averaged 30 control subjects (e) and the patient (f) and (g). The difference in signal to noise between the maps is due to averaging of the 30 controls subjects. The region of significantly decreased anisotropy is superimposed on map (c) and the region of significantly increased diffusivity is superimposed on map (g). These regions coincide with the localisation of the abnormality identified on conventional MRI. (d) and (h): The equivalent slice of the patient's T1-weighted image. The regions in (c) and (g) were used for quantitative region-of-interest analyses of anisotropy and diffusivity values respectively. Note that right on the images is patient's right.

3.1.4.2.2 Region-of-interest analyses

In order to demonstrate the magnitude of the effect, quantitative ROI analyses were made in two patients whose appearances on conventional imaging were considered typical for each aetiology. In patient 1 (head injury) the average anisotropy within the identified right parietal region was 0.24. This was 41% of the mean anisotropy within the corresponding regions in the control subjects (mean anisotropy of 0.59). The average diffusivity within the identified right parietal region was 1038 $x10^{-6}mm^2/s$. This was 146% of the average diffusivity within the corresponding regions in the control subjects (average diffusivity of 710 $x10^{-6}mm^2/s$). The mean anisotropy within the region of increased anisotropy in patient 1, anterior to the identified region of cerebral damage, was 0.64, (159% of the control groups mean anisotropy of 0.40). The average diffusivity within the area of normal appearing

cerebral tissue in the right frontal region, immediately anterior to the conspicuous cerebral damage (but separate from the area of increased anisotropy) was 843mm^2/s, (117% of the control groups average of 722mm^2/s).

Two areas of reduced anisotropy were seen in patient 8 (cerebral infarction). The lateral frontal area (figure 3.2) was associated with increased T_2 signal on standard imaging, whereas the medial frontal region appeared normal. The mean anisotropy in these two frontal regions was 0.28 and 0.29 respectively. These were both 51% of the mean anisotropy within the corresponding areas in the control group (0.56 and 0.57). The average diffusivity within the lateral frontal region in patient 8 was 902mm^2/s, (128% of the control groups average of 704mm^2/s), (figure 3.2).

Table 3.1 Clinical characteristics, EEG, MRI and DTI findings in patients with non-progressive acquired lesions

Patient	Age (yr)	Gender	Aetiology of epilepsy	Duration of epilepsy (yr)	EEG features	Conventional MRI Findings	DTI findings Sig. decreases in Anisotropy (*P*-value)	DTI findings Sig. increases in Anisotropy (*P*-value)	DTI findings Sig. increases in diffusivity (*P*-value)
1	44	M	head injury	33	R. temp. i.e.a.	R. temp.par.occ. multicystic damage	R. temp. par. occ ($P<0.001$)	R. frontopar. ($P=0.003$)	R. front. temp. par ($P<0.001$) + L. par. ($P<0.001$)
2	33	M	head injury	13	bil. temp. i.e.a.	R. front.temp.par. + minor L. front damage	R. temp. ($P=0.008$)	R. front. ($P=0.018$)	R. front. temp. par ($P<0.001$) + L. front.par.($P=0.004$)
3	38	M	head injury	3	R. temp. i.e.a.	R. front.temp.par. damage	R. front. temp. par. ($P<0.001$)	L temp. ($P=0.013$) + R. front ($P=0.010$)	widespread R>L ($P<0.001$)
4	27	M	head injury	6	bil. frontotemp. i.e.a.	bifront. + R. temp. + corpus callosum damage	L. front ($P=0.046$) + bil. temp. ($P=0.003$)	nil	bifront. ($P<0.001$) + corpus callosum ($P<0.001$)
5	51	M	head injury	47	L. temporopar. i.e.a.	superficial atrophy of L. hemisphere, sparing temp.	L. mesial temp. ($P=0.007$)	nil	L. front. par. occ ($P=0.010$)
6	35	M	infarction	27	R. front + L. temp. i.e.a.	Post. L. middle cerebral artery territory damage	L. par. occ. ($P=0.013$)	nil	L. par. occ. ($P<0.001$) + R. par. ($P=0.024$)

Patient	Age (yr)	Gender	Aetiology of epilepsy	Duration of epilepsy (yr)	EEG features	Conventional MRI Findings	DTI findings Sig. decreases in Anisotropy (*P*-value)	DTI findings Sig. increases in Anisotropy (*P*-value)	DTI findings Sig. increases in diffusivity (*P*-value)
7	38	M	infarction	36	R. front.temp.par. i.e.a.	R. temp.par.occ. ischaemic damage	R. temp. par. occ. (P=0.008)	nil	R. temp. par. occ. (P<0.001)
8	20	F	infarction	12	R. frontotemp. i.e.a.	R. lat. front. cortical scar	R. med. (P=0.003) + lat. front. (P=0.036)	nil	R. lat. front. (P<0.001)
9	23	M	focal leucoencephalitis	7	R. frontotemp. i.e.a	R. front. scarring, CSF-filled cortical cavity	R. front. (P=0.003)	nil	R. frontopar. (P<0.001)
10	53	M	perinatal injury	48	R. temp. i.e.a	diffuse signal change in bil. post. WM	L. occ. WM (P=0.018)	nil	bil. occ. WM (P<0.001)

R.=Right; L.=Left; bil.=bilateral; post.=posterior; med.=medial; lat.=lateral; front.=frontal; par.=parietal; temp.=temporal; occ.=occipital; WM=white matter; i.e.a..=interictal epileptiform activity; Sig.=significant; M=male; F=female.

3.1.4.3 Malformations of Cortical Development:

3.1.4.3.1 Individual SPM analyses

Anisotropy

In seventeen of the twenty-two patients with MCD, SPM detected areas of decreased anisotropy (table 3.2). In fifteen of these patients the changes corresponded to all or part of the MCD. In six patients changes were found outside the MCD in tissue that appeared normal on conventional MRI.

Nine of the eleven patients (patients 11-21) with gyral abnormalities had areas of significantly reduced anisotropy that corresponded to all or part of the MCD. In four of the eleven, changes were found in areas beyond the margins of the evident MCD, in areas that appeared normal on T1- and T2-weighted images (figure 3.3). Reduced anisotropy was also seen in the patients with agenesis of the corpus callosum (patient 22) and subcortical heterotopia (SCH) (patients 23, 24, figure 3.4). None of the patients with band heterotopia (BHT) (patients 25-28) had any significant anisotropy changes detected by SPM in the areas of the MCD. One patient (25) however had a periventricular area of decreased anisotropy outside the evident MCD. In the patients with subependymal heterotopia (SEH), SPM detected areas of reduced anisotropy that corresponded to all or part of the SEH in three patients (29-31). In one patient (patient 31), reduced anisotropy was also shown in the frontal gyral abnormality and in normal appearing grey and white matter.

In two patients (11 and 24), SPM detected areas of increased anisotropy. Two of the areas were in white matter adjacent to MCD (figure 3.4). In one patient (patient 24) a further area of increased anisotropy was found in the left temporal lobe in grey matter that appeared normal on conventional MRI.

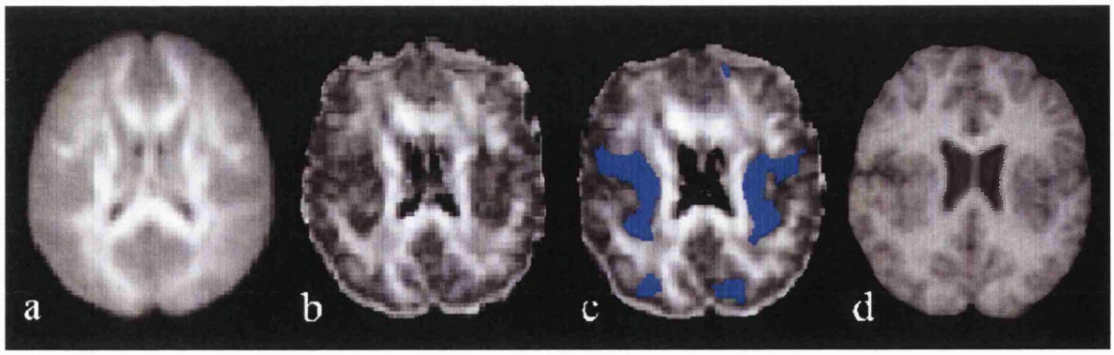

Figure 3.3: Patient 11, bilateral frontoparietal gyral abnormalities with thickened cortex.
Normalised axial anisotropy maps at the same slice localisation for the averaged 30 control subjects (a) and the patient (b) and (c). The regions of significantly decreased anisotropy are superimposed (blue) on map (c). (d): The equivalent slice of the patient's T1-weighted image. The regions of decreased anisotropy not only coincide with the localisation of the gyral abnormalities with thickened cortex but are also found in the normal appearing occipital lobes. Note that right on the images is the patient's right.

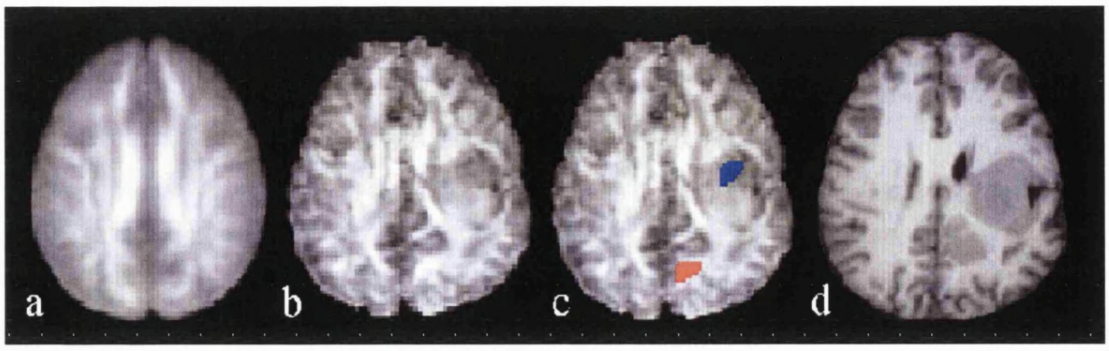

Figure 3.4: Patient 24, right fronto-parietal and occipital nodular heterotopia.
Normalised axial anisotropy maps at the same slice localisation for the averaged 30 control subjects (a) and the patient (b) and (c). The regions of significantly decreased (blue) and increased anisotropy (red) are superimposed on map (c). (d): The equivalent slice of the patient's T1-weighted image. A region of reduced anisotropy is found in the fronto-parietal heterotopia. The region of increased anisotropy is in normal appearing white matter adjacent to the occipital heterotopia. Note that right on the images is the patient's right.

Mean diffusivity

In ten of the twenty-two patients with MCD, SPM detected areas of increased diffusivity (table 3.2). In eight of these the changes corresponded to all or part of the MCD. In nine patients changes were found outside the MCD in tissue that appeared normal on conventional MRI. In seven of the ten patients the diffusivity changes were more extensive than the anisotropy changes. Seven of the eleven patients (patients 11-21) with gyral abnormalities had areas of increased diffusivity corresponding to all or part of the MCD. In six of these and in one additional patient changes were found outside the MCD in grey and/or white matter that appeared normal on conventional MRI (figure 3.5). One of the patients with nodular SCH (patient 24) had areas of increased diffusivity both within and in areas beyond the MCD. There were no diffusivity changes in the other patient with nodular SCH (patient 23), the patient with agenesis of the corpus callosum (patient 22) or the patients with BHT (patients 25-28). One (patient 29) of the patients with SEH (patients 29-32) had an area of increased diffusivity outside the MCD in normal appearing grey and white matter. There were no areas of decreased diffusivity.

3.1.4.3.2 Region-of-interest analyses

Anisotropy

Quantitative ROI analyses of decreased anisotropy were made in patient 11 and 24, whose appearance on conventional MRI were typical of gyral abnormality with thickened cortex and nodular heterotopia, respectively. In patient 11 (figure 3.3) the analyses were made in the normal-appearing left occipital white matter and right frontoparietal area with gyral abnormality. The mean anisotropy value was 0.35 in the left occipital region, which was 60% of the mean of control values of 0.58. The mean anisotropy in the right frontoparietal region was 0.30. This was 51% on the mean anisotropy in the corresponding areas in the control subjects of 0.59. In the right fronto-parietal heterotopia in patient 24 (figure 3.4) the mean anisotropy was 0.43, which was 61% of the mean

anisotropy value (0.71) in the same region in the control subjects.

ROI analyses were also made in one of the patients with areas of significantly increased anisotropy, patient 24 (figure 3.4). In this area of normal appearing occipital lobe the anisotropy value was 0.75 in the patient and 0.38 in the control subjects (197%).

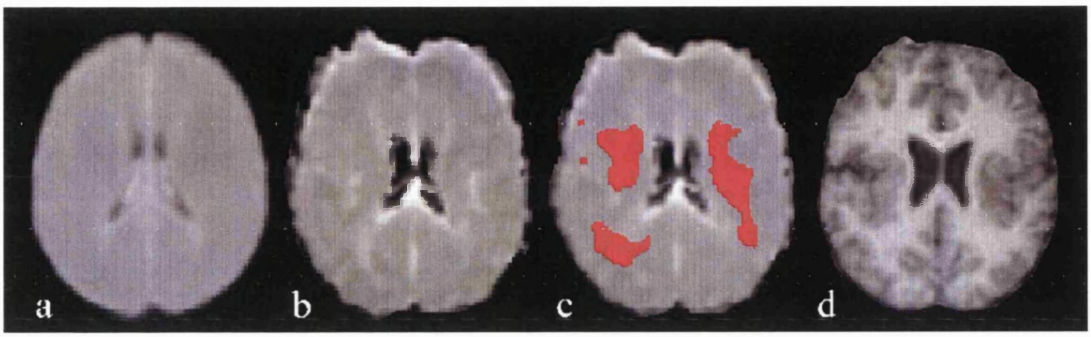

Figure 3.5: Patient 11, bilateral frontoparietal gyral abnormalities with thickened cortex.
Normalised axial diffusivity maps at the same slice localisation for the averaged 30 control subjects (a) and the patient (b) and (c). The regions of significantly increased diffusivity (red) are superimposed on map (c). (d): The equivalent slice of the patient's T1-weighted image. The regions of increased diffusivity not only coincide with the localisation of the gyral abnormalities but are also found in normal appearing white matter in parietal and frontal lobes. Note that right on the images is the patient's right.

Mean diffusivity

Quantitative ROI-analyses of increased diffusivity were made in two patients whose appearances on conventional MRI were typical of gyral abnormality with thickened cortex. In patient 1 the mean diffusivity for an area of normal appearing white matter in the left occipital lobe (figure 3.5) was 811 $x10^{-6}$ mm^2/s, compared to a mean of 712 $x10^{-6}$ $mm^2/s$for the control group in the same area (114%). In the normal appearing white matter in the left frontal lobe in patient 9 the average diffusivity was 873 $x10^{-6}$ mm^2/s. This was 119% of the average diffusivity in the corresponding area in the control group, 731 $x10^{-6}$ mm^2/s.

Table 3.2 Clinical characteristics, EEG, MRI and DTI findings in patients with malformations of cortical development

Patient	Age (yr)	Gender	Seizure types	EEG features	Conventional MRI Findings	DTI findings Sig. decreases in Anisotropy (*P*-value)	DTI findings Sig. increases in Anisotropy (*P*-value)	DTI findings Sig. increases in Mean Diffusivity (*P*-value)
11	27	F	2° gen.	Bil. abn. max L	Bil. frontopar. gyral abn. with thick cortex	Bil. frontopar. In MCD + front. bil. in NA GM + WM (p <0.0001)	L front. med. of MCD (p =0.003)	Bil. frontopar. in MCD. Bil. front. + occ. in NA G + WM + cerebellum (p <0.0001)
12	24	F	SPS, CPS, tonic	Bil. abn. max L	Bil. gen. gyral abn. with thick frontopar. cortex	Bil. frontopar. + R front. in MCD (p <0.0001)	None	Bil. frontopar. in MCD. Bil. front., temp-occ. in NA GM, WM + cerebellum (p <0.0001)
13	22	M	SPS, CPS	Bil. abn. max L	Bil. frontopar. gyral abn. with thick cortex	Bil. frontopar. in MCD (p <0.0001)	None	None
14	24	M	CPS, 2° gen.	Bil. abn. max temp.	Bil. frontopar. gyral abn. with thick cortex	Bil. frontopar. in MCD (p =0.03)	None	None
15	34	F	S+CPS, 2° gen.	No definite abn.	L frontopar. gyral abn. with thick cortex	L frontopar. in MCD (p <0.0001)	None	L NA cerebellum (p =0.001)
16	39	F	SPS, CPS	Bitemp. abn	L front. + R frontopar. schizencephaly	L front. + R frontopar. in MCD (p <0.0001)	None	None

Patient	Age (yr)	Gender	Seizure types	EEG features	Conventional MRI Findings	DTI findings Sig. decreases in Anisotropy (*P*-value)	DTI findings Sig. increases in Anisotropy (*P*-value)	DTI findings Sig. increases in Mean Diffusivity (*P*-value)
17	20	M	2° gen.	Bitemp. abn. max L	Gen. gyral abn. with thick cortex	None	None	Bil. Widespread occ. to front. in MCD and NA WM (p =0.03)
18	36	F	S+CPS, 2° gen., MJ	Bitemp. abn. max L	Gen. gyral abn. with thick cortex	Bil. in MCD (p <0.0001)	None	R parieto-occ + L occ in MCD. Bil. temp. in NA WM (p =0.001)
19	50	M	CPS, 2° gen.	R abn. max temp.	R front. + bil. par. + occ. gyral abn. with thick cortex.	Bil. in MCD. L front. in NA WM (p <0.0001)	None	R widespread temp. to front. in MCD + underlying NA WM. L front. to par. WM (p <0.0001)
20	44	M	CPS, 2° gen.	L hemisphere abn.	L front. + par. gyral abn. with thick cortex	L frontopar. in MCD. R front. in NA GM (p =0.01)	None	L frontopar. in MCD + underlying NA WM, bil cerebellum (p <0.0001)
21	25	F	SPS, MJ	R hemispere abn. max ant.	R par. and occ. gyral abn. with thick cortex.	L pericallosal in NA GM and WM (p =0.02)	None	R frontopar in MCD + underlying WM (p <0.0001)
22	31	F	2° gen.	Bil. abn.	Agenesis of corpus callosum, gen. gyral abn. and SEH	Bil. in MCD and area of corpus callosum (p <0.0001)	None	None
23	51	M	2° gen.	No definite abn.	R par. nodular heterotopia	R par. in MCD (p <0.0001)	None	None

Patient	Age (yr)	Gender	Seizure types	EEG features	Conventional MRI Findings	DTI findings Sig. decreases in Anisotropy (*P*-value)	DTI findings Sig. increases in Anisotropy (*P*-value)	DTI findings Sig. increases in Mean Diffusivity (*P*-value)
24	23	M	CPS, 2° gen.	R several foci, max post. temp. and parieto-occ.	R frontopar. + R occ. nodular heterotopia	R frontopar. in MCD (p <0.0001)	R occ. in WM adjacent to MCD and L temp. in GM (p =0.002)	R frontopar. + occ. in MCD + adj. WM. NA G + WM L occ-temp. (p <0.0001)
25	31	F	S+CPS, 2° gen.	Bil. abn.	Bil. BHT	NA L post. periventricular GM and WM (p <0.0001)	None	None
26	21	M	CPS, 2° gen.	Gen. abn. ictal bil. central	Bil. BHT	None	None	None
27	50	F	CPS, 2° gen.	No focal abn.	Bil. BHT	None	None	None
28	27	M	S+CPS, 2° gen.	Bil. abn. max L temp.	Bil. BHT	None	None	None
29	26	F	SPS, CPS	Bil. abn. max L	Bil. SEH	Bil. in MCD (p <0.0001)	None	R occ-temp. NA G + WM (p <0.0001)
30	36	F	SPS, 2° gen.	No focal abn.	Bil. SEH	L in MCD (p =0.02)	None	None
31	32	F	CPS	L temp. abn.	L post. SEH + L front. gyral abn. with thick cortex	L post. + L front. in MCD. L occ. in NA G + WM (p =0.002)	None	None
32	32	F	CPS, 2° gen.	No focal abn.	R post. SEH	None	None	None

M=Male; F=Female; S/CPS=simple/complex partial seizure; MJ=myoclonic jerks; 2° gen.=secondarily generalised tonic-clonic seizure; R=Right; L=Left; gen.=general; bil.=bilateral; ant.=anterior; post.=posterior; med.=medial; front.=frontal; par.=parietal; temp.=temporal; occ.=occipital; NA=Normal appearing: GM=grey matter; WM=white matter; MCD=malformation of cortical development; BHT=band heterotopia; SEH=subependymal heterotopia

3.1.4.3 MRI-negative patients

3.1.4.4.1 Individual SPM analyses

Anisotropy

SPM analyses of the 30 individual patients in the MRI-negative group revealed two patients with statistically significant differences in anisotropy compared to the control group (table 3.3). One (patient 45) had an area of increased anisotropy in the right temporal lobe that was concordant with both seizure semiology and interictal EEG recordings (ictal EEG data not available). The other (patient 37) demonstrated significant decreases in anisotropy in both left occipital and right occipitoparietal regions with clinical and ictal EEG recordings suggesting left temporal lobe seizure onset.

Mean Diffusivity

Eight patients had regions of significantly increased diffusivity. Six of these concurred with the location of interictal epileptiform activity, and four of these also agreed with ictal EEG recordings and clinical seizure semiology (table 3.3) (figure 3.6). Two patients therefore had areas of significantly increased diffusivity in regions distinct from EEG abnormality and clinical seizure focus. Patient 37 demonstrated increased diffusivity in the right frontal and both occipital regions. Patient 60 had areas of increased diffusivity in the right temporal lobe and bi-parietally, but ictal EEG evidence suggested a left temporoparietal seizure focus.

3.1.4.4.2 Region-of-interest analyses

Anisotropy

Quantitative ROI analyses within the right temporal lobe of patient 45 revealed a mean anisotropy of 0.50, 167% of the mean anisotropy within the corresponding regions of the control subjects of 0.30. In patient 37, the mean anisotropy within the left occipital region and right occipitoparietal region were both 0.45, 69% and 68% respectively of the mean anisotropy within the identical areas in the control group of 0.65 and 0.66.

Mean Diffusivity

Quantitative ROI analyses within the right frontal lobe of patient 49 (Figure 3.5) revealed an average diffusivity of 907 $x10^{-6}mm^2/s$, which was 117% of the average diffusivity within the corresponding regions of the control subjects of 772 $x10^{-6}mm^2/s$. In patient 53, the average diffusivity within the left frontotemporal region was 846 $x10^{-6}mm^2/s$ (118%), compared to 716 $x10^{-6}mm^2/s$ for the control group.

Table 3.3 Clinical characteristics, EEG and DTI findings in patients with normal conventional MRI.

Patient	Age (yr)	Gender	Aetiology of epilepsy	Duration of epilepsy (yr)	Seizure types	Ictal Epileptiform Abnormality	Interictal Epileptiform Abnormality	DTI findings Sig. decreases in Anisotropy (*P*-value)	DTI findings Sig. increases in Anisotropy (*P*-value)	DTI findings Sig. increases in Mean Diffusivity (*P*-value)
33	54	M	cryptogenic	34	CPS, 2° gen.	L. temp.	L. temp.	None	None	None
34	37	F	cryptogenic	21	CPS, 2° gen.	L. temp.	L. temp.	None	None	None
35	31	F	cryptogenic	30	SPS, 2° gen.	L. temp.	L. front.+ L. temp	None	None	L. frontal (P=0.005)
36	39	M	cryptogenic	11	CPS, 2° gen.	L. temp.	bil.temporal	None	None	None
37	43	M	birth injury	43	CPS, 2° gen.	L. temp.	L. > R. temp.	L. occ. (P=0.002) + R.par.occ (P=0.004)	None	bil.occ. (P<0.001) + R. frontal (P=0.041)
38	38	M	cryptogenic	35	CPS, 2° gen.	L. temp.	L. >> R. temp.	None	None	None
39	36	F	cryptogenic	32	S+CPS, 2° gen.	N/A	L. >> R. temp.	None	None	None
40	38	M	cryptogenic	13	CPS, 2° gen.	L. temp.	L. temp.	None	None	None
41	18	M	birth injury	15	CPS, 2° gen.	N/A	L. temp.	None	None	None
42	41	M	encephalitis	19	S+CPS, 2° gen.	inconclusive	R. >> L. temp.	None	None	None

Patient	Age (yr)	Gender	Aetiology of epilepsy	Duration of epilepsy (yr)	Seizure types	Ictal Epileptiform Abnormality	Interictal Epileptiform Abnormality	DTI findings Sig. decreases in Anisotropy (*P*-value)	DTI findings Sig. increases in Anisotropy (*P*-value)	DTI findings Sig. increases in Mean Diffusivity (*P*-value)
43	54	F	cryptogenic	48	CPS, 2° gen.	N/A	R. >> L. temp.	None	None	None
44	55	M	cryptogenic	2	CPS	R. temp.	L. + R. temp	None	None	L. temp. (*P*=0.025)
45	33	M	cryptogenic	18	SPS, 2° gen.	N/A	R. temp.	None	R. temp. (*P*=0.040)	None
46	42	M	meningitis	29	CPS, 2° gen.	R. temp.	bil.temporal.	None	None	None
47	36	F	cryptogenic	21	CPS, 2° gen.	inconclusive	R. >> L. temp.	None	None	None
48	22	F	cryptogenic	11	CPS, 2° gen.	L. front.	L. front.	None	None	None
49	34	F	cryptogenic	11	CPS	R. front.	R. frontotemp.	None	None	R. frontal (*P*=0.027)
50	36	M	cryptogenic	14	CPS, 2° gen.	L. front.	L.> R. frontotemp.	None	None	None
51	42	F	cryptogenic	35	CPS, 2° gen.	R. > L. front.	R. > L. front.	None	None	None
52	37	F	encephalitis	31	CPS, 2° gen.	N/A	bil. front.	None	None	None
53	18	F	cryptogenic	12	S+CPS, 2° gen.	L. frontotemp.	bil. frontotemp.	None	None	L. frontotemp. (*P*=0.045)
54	39	M	cryptogenic	4	CPS, 2° gen.	N/A	normal	None	None	None

Patient	Age (yr)	Gender	Aetiology of epilepsy	Duration of epilepsy (yr)	Seizure types	Ictal Epileptiform Abnormality	Interictal Epileptiform Abnormality	DTI findings Sig. decreases in Anisotropy (*P*-value)	DTI findings Sig. increases in Anisotropy (*P*-value)	DTI findings Sig. increases in Mean Diffusivity (*P*-value)
55	30	M	cryptogenic	22	CPS, 2° gen.	L. temp.occ	L. temp.	None	None	L. posterior temp. (P=0.011)
56	20	M	cryptogenic	15	S+CPS, 2° gen.	bil frontotemp	bil frontotemp	None	None	L. front. (P=0.001) + R frontotemp (P=0.008)
57	36	F	cryptogenic	21	S+CPS, 2° gen.	inconclusive	R. hemisphere	None	None	None
58	55	M	measles vaccination	26	SPS, 2° gen.	bil. front.	L. temp.	None	None	None
59	25	M	cryptogenic	14	CPS, 2° gen.	bil. front.	widespread	None	None	None
60	28	M	cryptogenic	24	S+CPS, 2° gen.	L. temporopar.	L. hemisphere	None	None	R. temp. (P<0.001)+ bilat. par. (P<0.001)
61	29	F	cryptogenic	19	CPS, 2° gen.	L. hemisphere	L. hemisphere	None	None	None
62	52	F	cryptogenic	14	CPS, 2° gen.	L. hemisphere	L. temp.	None	None	None

S/CPS=simple/complex partial seizure; 2° gen =generalised seizure; R.=Right; L.=Left; bil.=bilateral; front.=frontal; par.=parietal; temp.=temporal; occ.=occipital; N/A=not available; Sig.=significant; M=male; F=female.

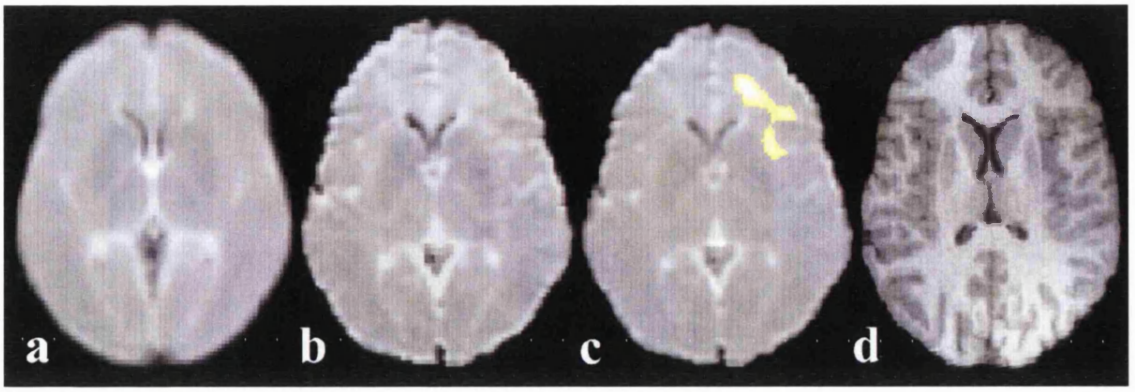

Figure 3.6: Patient 49, right frontal lobe epilepsy with normal conventional MRI.

Normalised axial diffusivity maps at the same slice position for the averaged 30 control subjects (a) and the patient (b) and (c). The region of significantly increased diffusivity is superimposed on map (c). The region of increased diffusivity is localised to the normal appearing cerebral tissue of the right frontal lobe. (d): The equivalent slice of the patient's T1-weighted image. The region in (c) was used for quantitative region-of-interest analysis of diffusivity values. Note that right on the images is patient's right.

3.1.4.4.3 Group analyses

Group analyses were performed on patients with EEG evidence of either left or right temporal lobe seizures. The left temporal lobe group consisted of nine patients (patients 33-41) and the right temporal lobe group six (patients 42-47). Compared to the 30 control subjects the left temporal lobe group had a significant decrease in anisotropy and significant increase in diffusivity within the white matter of the left temporal region (figure 3.7). The ROI analysis of this area demonstrated a mean anisotropy in the patient group of 0.40 (80%), compared with a mean of 0.50 in the control subjects. The average diffusivity in this region in the patient group was 830 mm^2/s (106%), compared to 780 mm^2/s for the control group. A similar, but non-significant trend of reduced anisotropy was found in the right temporal lobe of the right temporal lobe patients (patient mean, 0.33; control mean, 0.41; p=0.09).

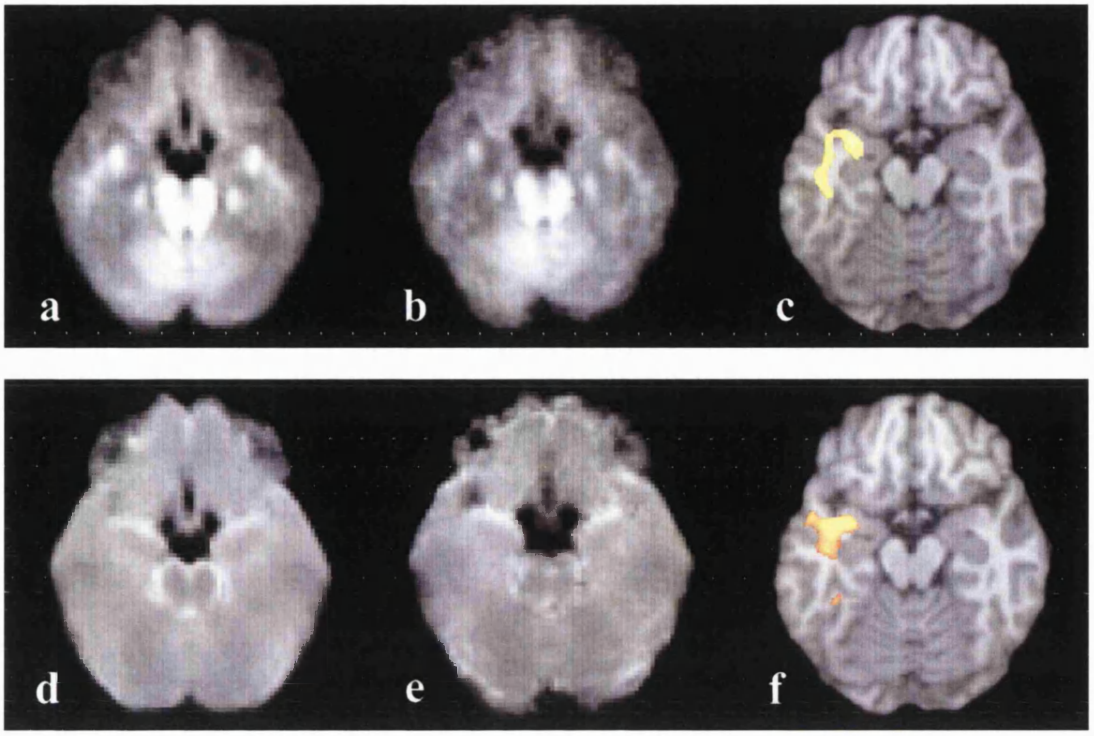

Figure 3.7: Left temporal lobe epilepsy group with normal conventional MRI.
Normalised axial anisotropy maps at the same slice position for the averaged 30 control subjects (a) and the 9 patients (b). Normalised axial diffusivity maps at the same slice position for the averaged 30 control subjects (d) and the 9 patients (e). The regions of decreased anisotropy and increased diffusivity are superimposed on normalised T1-weighted SPM templates at the same slice position ((c) and (f) respectively). These regions are localised to the left temporal lobe. The regions in (c) and (f) were used for quantitative region-of-interest analyses of anisotropy and diffusivity values. Note that right on the image is patients' right.

3.1.5 Conclusions

There were several major findings in this study. Diffusion tensor imaging and objective voxel-by-voxel statistical comparison identified significant increases in diffusivity and significant reductions of anisotropy in all patients with acquired nonprogressive cerebral lesions and partial seizures. In all of these patients the areas of increased diffusivity and in nine patients the areas of decreased anisotropy concurred with abnormalities identified on visual inspection of conventional MRI. In addition there were ten areas which were normal on conventional imaging which exhibited significantly different anisotropy or diffusivity indicating added sensitivity from the new method. Fifteen patients with MCD had areas of reduced anisotropy and eight had areas of increased diffusivity within the MCD. Reduced anisotropy was also found in tissue beyond the margins of the evident MCD in six patients, in areas that appeared normal on conventional T1- and T2-weighted images. Nine of the patients had increased diffusivity in grey and/or white matter that appeared normal on MRI. Individual analyses of 30 patients with partial seizures and normal conventional MRI identified a significant increase in diffusivity in eight of the subjects. In six of these, the areas of increased diffusivity concurred with the localisation of epileptiform EEG abnormality.

Analysis of anisotropy in the MRI-negative patients revealed significant differences in two patients, one of which concurred with electroclinical seizure localisation. Group analysis of nine patients with electroclinical seizure onset localising to the left temporal region revealed a significant increase of diffusivity and a significant reduction in anisotropy within the white matter of the left temporal lobe.

3.1.5.1 Methodological considerations and limitations

Ultra-fast echo planar imaging has enabled us to perform whole brain DTI within a reasonable time frame. The rotationally invariant diffusion parameters calculated using this technique are insensitive to variations in intersubject positioning within the scanner, allowing meaningful comparison between individuals (Pierpaoli and Basser 1996). DTI is an imaging sequence sensitive to the molecular movement of water; therefore, it is also susceptible to patient movement and pulse artefacts. These are minimised by the use of a fast MRI technique (EPI) and a final image created by the averaging of nine acquisitions at every slice position. Additionally, it is known from experimental and clinical data that cerebral diffusion changes are observed during epileptic seizures (Wieshmann, Symms, and Shorvon 1997b; Lansberg *et al.* 1999). Only one patient reported a seizure (simple partial) within the 24 hours preceding the DTI, however without simultaneous EEG recording we cannot exclude the possibility of ictal discharge occurring during the scan.

The voxel-by-voxel approach used by SPM to compare diffusivity and anisotropy in the whole brain is a more objective, statistically rigorous and unbiased method than region-of-interest analyses based on *a priori* knowledge and has previously been applied to PET and structural MRI data (Richardson *et al.* 1998; Woermann *et al.* 1999b). In addition, a ROI-based study of DTI in structural cerebral lesions failed to identify abnormalities in mean diffusivity in 30% of patients despite anisotropy abnormalities in all, and did not investigate normal appearing cerebral tissue (Wieshmann *et al.* 1999c).

3.1.5.2 Pathophysiological and clinical implications

Diffusion of water within a tissue is governed by its molecular, microstructural and architectural properties. The main determinants of anisotropy in densely packed unmyelinated fibres are axonal membranes, and in myelinated tracts, the multiple myelin laminae (Nomura *et al.* 1994; Rutherford *et al.* 1991; Beaulieu and Allen 1994; Wimberger *et al.* k1995). A disruption to this microstructural environment such as ischaemic injury, gliosis, or cerebral dysgenesis will lead to a less ordered arrangement of nerve fibres and subsequent change in anisotropy and diffusivity.

Diffusivity is reduced in seizure foci during ictal events (Lansberg *et al.* 1999; Wieshmann *et al.* 1997b) and induced status epilepticus (Zhong *et al.* 1993; Ebisu *et al.* 1996). This is thought to be the result of cellular swelling and reduction of extracellular space (Lux, Heinemann, and Dietzel 1986). Anisotropy measurements are not available from these studies, however it is likely that this would similarly be reduced. There was an acute reduction in diffusion during pilocarpine induced status epilepticus, and in rats which subsequently developed chronic seizures, a progressive increase in diffusion developed in both seizure foci and mesial temporal lobe

structures (Lynch *et al.* 1996). The hypothesis was that chronic seizures lead to cellular loss and structural disruption in both these areas. This is a possible explanation for the decreased anisotropy in the mesial temporal lobe structures of patient 5 in the acquired lesion group and also the group effect of reduced anisotropy and increased diffusivity found in the MRI-negative TLE patients.

Significant reductions of anisotropy were detected in all of the patients with acquired lesions, and in all but one patient (patient 5) these were within areas previously identified as abnormal on conventional MRI. All areas of abnormality on conventional MRI were associated with significant increases in diffusivity. These results concur with findings from previous diffusion studies on patients with acquired non-progressive cerebral lesions (Werring *et al.* 1998; Wieshmann *et al.* 1999e; Hajnal *et al.* 1991), and are consistent with pathological abnormalities, for example, structural disruption and neuronal loss, observed in such patients (Adams 1992).

In three patients with head injury (patients 1-3), increases in anisotropy were identified. In patients 1 and 3 these areas were commonly immediately anterior to the major traumatic lesion, in cerebral tissue that appeared normal on conventional MRI. This may represent displacement of white matter tracts into regions of inherently low anisotropy or the compaction of fibre bundles into denser and more structured, hence more anisotropic tracts (Beaulieu and Allen 1994). Four patients with head injuries (patients 1, 3, 4 and 5) had reduced anisotropy or increased diffusivity in regions appearing normal on conventional MRI suggesting loss of structural organisation secondary to occult cerebral damage.

In chronic ischaemic lesions, increased diffusivity and reduced anisotropy have previously been noted, concordant with gliosis, expansion of extracellular space and loss of discreet microstructural organization (Warach *et al.* 1995). In all three patients with partial seizures secondary to mature infarcts, DTI and SPM demonstrated reduced anisotropy and increased diffusivity within each lesion. In one patient (patient 8) an additional area of reduced anisotropy was demonstrated within the same vascular territory. This was in normal appearing cerebral tissue suggesting the ischaemic injury extended beyond the visible abnormality. Furthermore another patient with a mature cerebral infarct (patient 6) had an area of increased diffusivity in the contralateral hemisphere in normal appearing tissue, again suggesting the presence of occult injury. Overall six patients with head injury or ischaemic damage (patients 1, 3, 4, 5, 6 and 8) had significantly altered diffusion indices within normal appearing cerebral tissue. This finding is of importance should surgical management of similar patients be considered.

The areas of reduced anisotropy within MCD localised to regions of grey matter and/or the grey-white matter interface on high resolution MRI. The decreased anisotropy in these areas of heterotopic grey matter is likely to be due to a comparison of anisotropy in the abnormally located grey matter in the patients to anisotropy in the white matter in control subjects.

More interestingly, anisotropy and diffusivity changes were found outside the MCD in normal appearing tissue. Changes beyond the margins of the visually detected MCD were found in nine of the ten patients with increased diffusivity, and in six of the seventeen patients with decreased anisotropy, concurring with previous studies of structural MRI (Sisodiya *et al.* 1995b; Woermann *et al.* 1999a) and PET data (Richardson *et al.* 1996) in patients with epilepsy and MCD. These findings suggest that MCD is often more extensive than the visible lesion, with widespread subtle malformation.

Several histopathological epilepsy surgery and necropsy series have found microdysgenesis and an

increased number of neurons in white matter in patients with epilepsy compared to control subjects (Meencke 1983; Hardiman *et al.* 1988; Kasper *et al.* 1999; Finsterbusch and Frahm 1999; Bahn 1999). These changes may involve several lobes (Eriksson *et al.* 1999). An increased number of neuronal cell bodies in the white matter may disrupt the white matter tracts causing a reduction in anisotropy. Other studies have found a relative decrease in white matter in patients with MCD, that might be the result of an increased number of neurons projecting thinner axons (Sisodiya *et al.* 1995b), which may have altered arborisation (Mitchison 1991). Dysmyelination of white matter may also occur with MCD (Marchal *et al.* 1989), and this may also contribute to reduced anisotropy.
Areas with increased diffusivity were generally more extensive than areas with decreased anisotropy, in both MCD and normal appearing grey and white matter. The widespread increase in diffusivity suggests areas of reduced cell density and increased extracellular space due to failure of neurogenesis or later cell loss. In animal studies of status epilepticus, reduced diffusivity has been observed acutely, with spontaneous normalisation after three days (Nakasu *et al.* 1995; Hasegawa *et al.* 2003). Pyknotic neurons and vacuolated neuropil were seen on histopathological examination of these areas, suggesting neuronal damage had occurred during the prolonged seizure (Nakasu *et al.* 1995). It is likely that this would have caused increased extracellular space and increased diffusivity in the chronic phase, in agreement with studies on cerebral ischaemia (Warach *et al.* 1995). Repetitive seizures in humans may also result in neuron loss and gliosis (Vinters *et al.* 1993) and both reduced anisotropy and increased diffusivity may be caused by frequent seizures.

SPM did not detect significant changes in anisotropy or diffusivity in all MCD. Anisotropy is usually highest in the major white matter tracts and lower in the tissue close to the cortex where fibres are crossing or fanning out (Peled *et al.* 1998). MCD in areas where anisotropy is naturally low may not result in a significant reduction in anisotropy compared to control subjects. Anisotropy was however more sensitive than diffusivity in the identification of MCD. Our findings are concordant with previous ROI based analyses of a group of three patients with MCD that all had anisotropy changes but only one had altered diffusivity (Wieshmann *et al.* 1999c). Features common to all MCD include loss of tissue organisation and abnormalities of neuronal structure; which may perturb anisotropy. Despite the structural disorganisation, the cellular density is preserved in many of the MCD. The restriction of water diffusion by cell membranes and thus, the degree of diffusivity might therefore be similar to that of normal tissue. This suggests that anisotropy and diffusivity provide complementary information. These findings contrast with the results of patients with acquired lesions in which diffusivity changes were more evident than abnormalities of anisotropy. This reflects the different underlying pathological changes within each group.

Areas of significantly abnormal diffusion were detected in nine MRI-negative patients. In seven patients, these regions concurred with localisation of epileptiform EEG abnormality and in four of these, the regions also concurred with ictal EEG recordings and clinical seizure semiology. The areas of significantly increased diffusivity in the MRI-negative patients, the significant reduction of anisotropy and increase in diffusivity in the TLE group, are most likely caused by disruption in the microstructural environment due to aetiological factors, such as, occult dysgenesis or acquired damage, or as a result of repeated seizures, for example, atrophy, gliosis, and expansion of the extracellular space. One patient has undergone surgical treatment with subsequent histopathological correlation. (see chapter 3.2)

Our results suggest that diffusivity is a more sensitive diffusion index than anisotropy in identifying occult epileptogenic regions in MRI-negative patients. This implies that although expansion of extracellular space has occurred, the major white matter tracts have mostly retained their structural organisation and parallel fibre bundle arrangement.

Despite its sensitivity in patients with epilepsy and acquired lesions, the technique did not identify a clinically concordant abnormality in the majority of patients with normal conventional MRI. Histopathological studies of surgically resected epileptogenic areas which appeared normal on MRI have shown features of mild subpial or white matter gliosis, focal cortical dysplasia, clusters of neuronal aggregates in white matter, impaired cortical lamination, and subcortical laminar heterotopia (Theodore *et al.* 1990; Zentner *et al.* 1995; Palmini *et al.* 1991b; Siegel *et al.* 2001). These occult epileptogenic regions, which are most frequently encountered in the grey matter or white-grey junction are likely to be associated with only minor structural disorganisation, perhaps at a microscopic level and may not be disruptive enough to cause significant, measurable alterations in diffusion parameters. It is likely that our positive findings represent the most structurally abnormal of all the MRI-negative patients and with improvements in diffusion imaging further occult epileptogenic regions may be identified.

One MRI-negative patient (patient 45) had an electroclinically concordant significant increase in anisotropy within the right temporal lobe when compared to the control subjects. As in the case of acquired lesions, this increased anisotropy may be associated with tract displacement or compression however without pathological material, the explanation is not clear.

Two MRI-negative patients had areas of altered diffusion in non-EEG concordant regions. Patient 37 had regions of decreased anisotropy and increased diffusivity in the occipital regions bilaterally, in addition to an area of increased diffusivity in the right frontal region. This patient had suffered a perinatal hypoxic event. Patient 10 (acquired lesion group) sustained a similar injury and SPM analysis revealed comparable diffusion abnormalities, however in this patient conventional MRI revealed increased signal on T2-weighted images in occipital regions bilaterally. Patient 60 had a region of increased diffusivity distinct from the seizure focus. This patient had experienced a number of unprovoked episodes of status epilepticus. It is most likely that the regions of increased diffusivity in these patients were the consequence of the prior insults.

3.2 LOCALISATION OF SEIZURE FOCUS & HISTOPATHOLOGICAL VALIDATION

3.2.1 Subject

A 36 year-old woman (patient 49, chapter 3.1) developed focal epileptic seizures aged 23 years. There was no previous history of cerebral insult or febrile convulsions and no family history of a seizure disorder. The patient experienced only complex partial seizures. These were characterised by sudden loss of awareness without warning, followed by a variety of possible sequelae, including truncal rocking movements, inappropriate laughter, repeated crossing and uncrossing of her lower limbs, aimless wandering and repeated grabbing movements of either hand. Conventional brain MRI was normal. Routine scalp EEG recorded interictal epileptiform activity arising from the right fronto-temporal region.

Over the next 10 years, despite treatment with multiple combinations of anti-epileptic medications, including carbamazepine, sodium valproate, topiramate, phenobarbitone, lamotrigine, phenytoin, gabapentin and clobazam, the patient's seizures continued at a frequency of approximately 10-15 per month. The patient was therefore admitted to the Assessment and Treatment Centre of the National Society for Epilepsy and National Hospital for Neurology and Neurosurgery for further evaluation.

3.2.2 Methods

Conventional MRI, diffusion tensor imaging, post-acquisition processing and statistical analysis methods are described in Chapters 2 and 3.1

3.2.3 Results

3.2.3.1 SPM analysis of DTI

Compared to the control subjects, the patient had an area of increased diffusivity in the right orbitofrontal cortex (figure 3.8). No other abnormality was detected. Quantitative region-of-interest analyses within the abnormality revealed an average diffusivity of 907 x 10^{-6} mm^2/s, which was 117% of the average diffusivity within the corresponding region of the control subjects of 772 x 10^{-6} mm^2/s.

3.2.3.2 Electroencephalography

Scalp video EEG telemetry revealed interictal right fronto-temporal slow waves and ictal epileptiform activity arising from the right frontal lobe. Depth EEG electrodes were implanted through burr holes into the right orbitofrontal and laterofrontal cerebral regions to test the hypothesis that the area of increased diffusivity on DTI was the site of seizure onset. Surface electrodes were placed over the lateral cortex of the right frontal lobe extending to the pole of the temporal lobe, and over the anterior and posterior lateral left frontal cortex. During eight days of continuous videotelemetry on reduced medication, four typical complex partial seizures were recorded. On each occasion, the seizures arose from the deepest contacts of predominantly the right orbitofrontal,

but also the right laterofrontal electrode. Ten subclinical electrographic seizures were also recorded, each commencing with a run of spike/wave activity at the deepest contact of the right orbitofrontal electrode. Frequent interictal spikes and sharp waves were also recorded from the right frontolateral and orbitofrontal regions. No independent epileptiform activity was recorded from the left frontal electrodes. In conclusion, the intracranial EEG recording implicated the right inferior orbitofrontal region as the ictal onset zone.

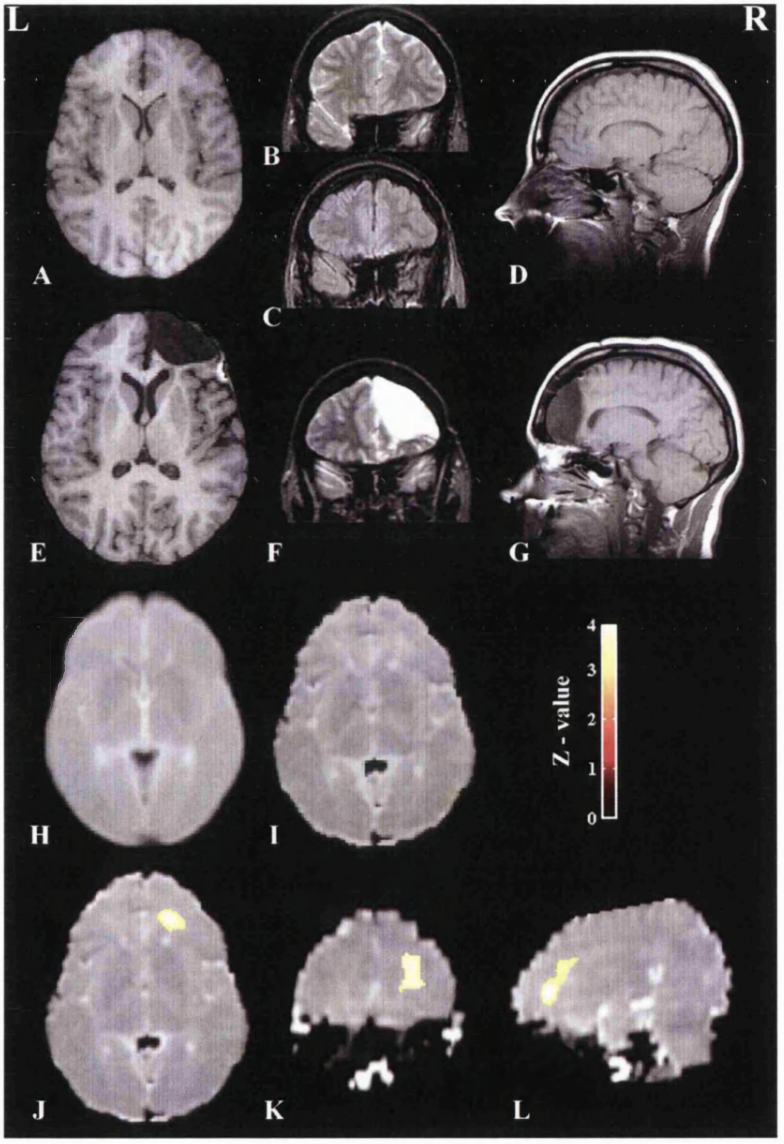

Figure 3.8: Axial T1-weighted (A), coronal T2-weighted (B), coronal fast FLAIR (C),and sagittal T1-weighted (D) preoperative images, and equivalent postoperative slices of T1- and T2-weighted images (E–G) showing extent of resection; normalized axial diffusivity maps at same slice position for averaged 30 controls (H) and patient (I); region of greatly increased diffusivity superimposed on patient's normalised axial (J), coronal (K) and sagittal (L) diffusivity maps. Region highlighted in (J) was used for quantitative region-of-interest analysis of diffusivity values. Note that right on images is patient's right. Z-value bar indicating degree of significance of highlighted regions in J–L is shown.

3.2.3.3 Surgery

The patient underwent image-guided right inferior frontal lobe resection, without complication. Conventional MRI three months postoperatively showed the site of resection in the right frontal lobe (figure 3.8). The patient had no seizures for 6 months postoperatively; in the subsequent 6 months she had occasional complex partial seizures that were much shorter and less disabling than preoperatively (Engel class IIA (Engel *et al.* 1993)). She had no psychological or neurological deficits, and 9 months postoperatively she was prescribed levetiracetam (she was already taking carbamazepine), which resulted in further improvement in her seizure control.

3.2.3.4 Histopathology

The resected brain tissue specimen measured 6x7x2 cms, was formalin-fixed, routinely processed and examined with haematoxylin and eosin, Luxol fast blue/cresyl violet and Bielchowsky silver method. Immunohistochemistry for glial fibrillary acidic protein (GFAP) (Dako, UK, dilution 1:1000), neurofilament (ICN pharmaceuticals, 1:10), and phosphorylated neurofilament (Dako, UK, 1:100) was performed using a standard avidin-biotin method. Histopathological examination showed marked gliosis, confirmed with GFAP immunostaining, predominantly and diffusely involving white matter (figure 3.9). There was superficial Chaslin's and mild intra-cortical gliosis but no evidence of cortical contusion, neoplasia, inflammatory or neurodegenerative disease process. Occasional neurones were noted in the white matter but the cyto-architecture of the cortex was normal and there was no evidence of either microdysgenesis or other malformation of cortical development.

3.2.4 Conclusions

DTI analysed on a statistical voxel-by-voxel basis identified an occult epileptogenic focus in a patient with refractory focal epilepsy and normal conventional MRI. Furthermore, seizure freedom was achieved following resection of the area of diffusion abnormality suggesting that the critical focus was accurately and completely characterised. This has important implications therefore for the investigation of similar "MRI-negative" patients; a group generally considered to have a poor postoperative prognosis in terms of seizure freedom (Cascino *et al.* 1992).

The determinants of diffusion in biological tissue have previously been attributed to structures in both intra- and extracellular compartments. More recently however, it has been postulated that, with DTI using a magnitude of diffusion weighting (b-value) of less than 1000 s/mm^2, the extracellular compartment is the predominant determinant of DTI visible water diffusion (Le Bihan *et al.* 2001). Cell membranes in unmyelinated tissue, and multiple myelin laminae in myelinated tissue, are believed to be the principal structures restricting or hindering the movement of diffusing water molecules in the extracellular space (Beaulieu and Allen 1994).

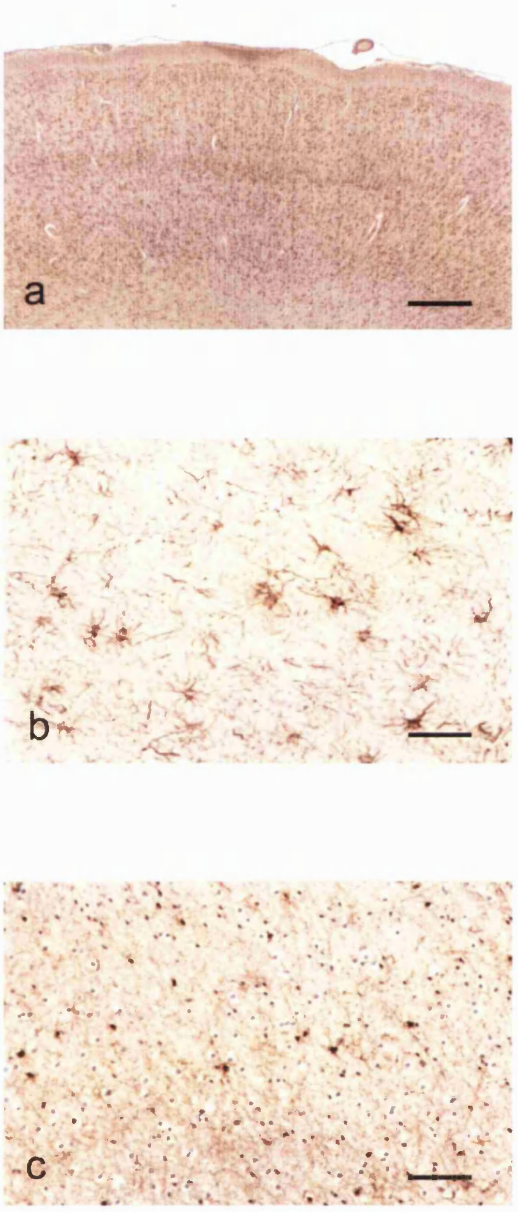

Figure 3.9: Histopathology of patient's brain (A) Normal cortical laminar cytoarchitecture, highlighted with NeuN, a neuronal marker (dilution 1 in 500, A60 Chemicon, Harrow, UK; bar=550 μm). (B) Striking gliosis with astrocytosis in tissue derived from region of increased diffusivity in white matter of right frontal lobe, shown by immunohistochemical staining for glial fibrillary acidic protein (GFAP) (dilution 1 in 400, Dako, Cambridge, UK; bar=58·5 μm). (C) GFAP staining in normal white matter from patient (bar=58·5 μm).

In our patient, marked gliosis, structural disorganisation and subsequent expansion of the extracellular space was detected by DTI as an area of increased mean diffusivity when compared to our control subjects. Abnormalities seen on diffusion imaging have only very rarely been histopathologically confirmed in humans despite a wealth of clinical and experimental animal data suggesting the association. For example, in patients with acute cerebral infarction, diffusion of water molecules initially becomes more restricted as cells swell and the extracellular space reduces. Several days later, with presumed subsequent necrosis and cell loss, water molecules are able to diffuse more freely and diffusion within the infarcted tissue increases above that seen in normal tissue (Warach *et al.* 1995; Lutsep *et al.* 1997). Similar findings have been reported in a patient with Creutzfeldt-Jakob disease. During the late stages of the disease when marked neuronal loss and gliosis are known to occur, progressively increasing water diffusion was identified by serial diffusion imaging (Matoba *et al.* 2001). In animal studies, reduced diffusivity was seen in cerebral tissue during status epilepticus due to cellular swelling. Subsequently, diffusivity increased within this tissue and histopathological examination showed pyknotic neurons and vacuolated neuropil suggesting the occurrence of neuronal damage sustained during the prolonged seizure (Nakasu *et al.* 1995). It is likely that diffusivity would have continued to increase in line with tissue necrosis and gliosis, if histopathological examination of the animals had been performed later.

Previous histopathological studies of surgically resected epileptogenic regions in patients with refractory focal epilepsy and normal MRI have shown mild gliosis, subtle MCD, disordered cortical lamination and microdysgenesis (Theodore *et al.* 1990; Zentner *et al.* 1995; Palmini *et al.* 1991b). Histopathological examination of the resected tissue from our patient found significant gliosis. In particular, there was no evidence of occult MCD, which are frequently encountered epileptogenic abnormalities in patients with refractory epilepsy (Raymond *et al.* 1995). Gliosis is a common finding in cerebral tissue from patients with chronic epilepsy and may be a consequence of seizure-related damage (Vinters *et al.* 1993). An area of gliosis and neuronal loss, however, may be epileptogenic with altered synaptic circuitry and neuronal reorganisation resulting in an excess of excitatory compared to inhibitory discharges (Marco and DeFelipe 1997), and dendritic deformation inducing denervation hypersensitivity (Gupta *et al.* 1988). Furthermore, impaired buffering of potassium by astrocytes in sclerotic cerebral tissue may lead to enhanced neuronal excitability and possibly epileptogenesis (Nishio *et al.* 2000; Schroder *et al.* 2000; Heinemann *et al.* 2000). Alternative hypotheses for the occurrence of seizures arising from apparently unremarkable tissue include the possibility that surgery has interrupted the pathways of seizure spread without removing the epileptogenic focus itself, or the presence of very subtle microscopic or electrochemical abnormalities. For example, reduced dendritic spine density and simplification of dendritic architecture has been identified in surgically resected epileptogenic neocortical tissue that appeared normal on conventional radiological and histological examinations (Multani *et al.* 1994). These changes may result in de-afferentation, loss of inhibitory input and consequent neuronal hypersensitivity (Willmore *et al.* 1980). Elevated concentrations of excitatory neurotransmitters and enzymes involved in their synthesis have been reported in human epileptogenic neocortex. Moreover, the concentrations of inhibitory neurotransmitters remained normal resulting in a relative imbalance between excitatory and inhibitory mechanisms (Sherwin *et al.* 1991).

It is likely that in some patients with refractory seizures, epileptogenic abnormalities exist at the cellular and subcellular levels that are beyond the limitations of DTI and conventional light microscopy. In some cases, therefore, DTI may detect only the sequelae of chronic seizures, such as neuronal loss and gliosis. Resection of

cerebral tissue to include the most significantly seizure-damaged area, as identified by DTI, and which could also contain the occult epileptogenic focus may still render the patient seizure free.

In conclusion, DTI was able to identify a histopathologically proven structural abnormality in a patient with refractory focal epilepsy and normal conventional MRI. This has important implications for the investigation of similar patients and, in addition, provides histopathological correlation of diffusion abnormalities in human brain.

3.3 DIFFUSION TENSOR IMAGING IN HEAD INJURY.

3.3.1 Introduction

Head injury is an important cause of physical and psychological disability. Severe blunt head trauma is associated with concussive and contusional injuries with histopathological changes of oedema, petechial and frank haemorrhage, diffuse axonal injury and ischaemia. The investigation and management of patients following head injury must include the accurate and complete identification of cerebral damage. This often includes computerised tomography acutely and MRI later to more accurately characterise chronic cerebral damage. Diffusion-weighted imaging has been shown to more accurately define the extent of cerebral damage in a closed head injury model than conventional MRI (Assaf *et al.* 1997). Diffusion-tensor imaging, a relatively novel MRI technique, detected more extensive abnormalities than conventional MRI in a patient with a severe head injury that corresponded to known neurological deficit (Wieshmann *et al.* 1999e).

Using diffusion-tensor imaging we have shown, for the first time, abnormalities of diffusion in two patients with head injury and unremarkable conventional MRI.

3.3.2 Subjects

Patient 1

A 31 year-old man sustained a severe head injury with basal skull fracture, bilateral frontal lobe contusions identified on an acute CT scan and a 12 day period of unconsciousness following a three metre fall from a balcony 18 months previously. Neurological examination revealed mild pyramidal signs and sensory loss affecting the right arm and leg. Neuropsychological examination showed mild deficits of frontal lobe function. Conventional MRI performed during the same scanning session as the diffusion tensor imaging showed no abnormality other than a few, scattered, non-specific lesions in the region of the white-grey matter interface in both hemispheres.

Patient 2

A 29 year old man sustained severe head and facial injuries and a three day period of unconsciousness following a road traffic accident 11 months previously. His acute CT scan and conventional MRI scan following recovery were normal. Neurological examination immediately following the accident revealed moderate bilateral quadraparesis,

worse on the left. Current neurological examination shows only moderately increased reflexes in the left lower limb. Neuropsychological examination revealed severe frontal lobe dysfunction and a significant change in personality was also noted. Conventional MRI performed during the same scanning session as the diffusion tensor imaging was normal.

3.3.3 Methods

Conventional MRI, diffusion tensor imaging, post-acquisition processing and statistical analysis methods are described in Chapters 2 and 3.1

3.3.4 Results

Patient 1

Comparing the patient's diffusion maps against the similarly normalised maps of 30 healthy control subjects, a significant increase in mean diffusivity was identified in the left hemisphere corona radiata, extending from the superior aspect of the internal capsule to the subcortical white matter in the frontal and parietal lobes (figure 3.10). No decreases in mean diffusivity were detected and there were no statistically significant abnormalities of anisotropy. The average mean diffusivity within the abnormal region found in the left corona radiata of the patient was 836 x 10^{-6} mm^2/s, which was 118% of the average mean diffusivity within the corresponding regions of the control subjects of 709 x 10^{-6} mm^2/s (standard deviation: 23.7 x 10^{-6} mm^2/s).

Patient 2

Comparing the patient's diffusion maps against the control subjects' maps, a significant increase in mean diffusivity was identified in the right frontal lobe (figure 3.11), adjacent to the frontal horn of the lateral ventricle and extending into the deep white matter of the right frontal lobe. No decreases in mean diffusivity were detected. The average mean diffusivity within the abnormal region found in the right frontal lobe of the patient was 862 x 10^{-6} mm^2/s, which was 115% of the average mean diffusivity within the corresponding regions of the control subjects of 747 x 10^{-6} mm^2/s (standard deviation: 22.3 x 10^{-6} mm^2/s).

In addition, a significant decrease in anisotropy was detected in the posterior limb of the right internal capsule (figure 3.12). The average anisotropy within the abnormal region found in the right internal capsule of the patient was 0.47, which was 63% of the average anisotropy within the corresponding regions of the control subjects of 0.75 (standard deviation: 0.04).

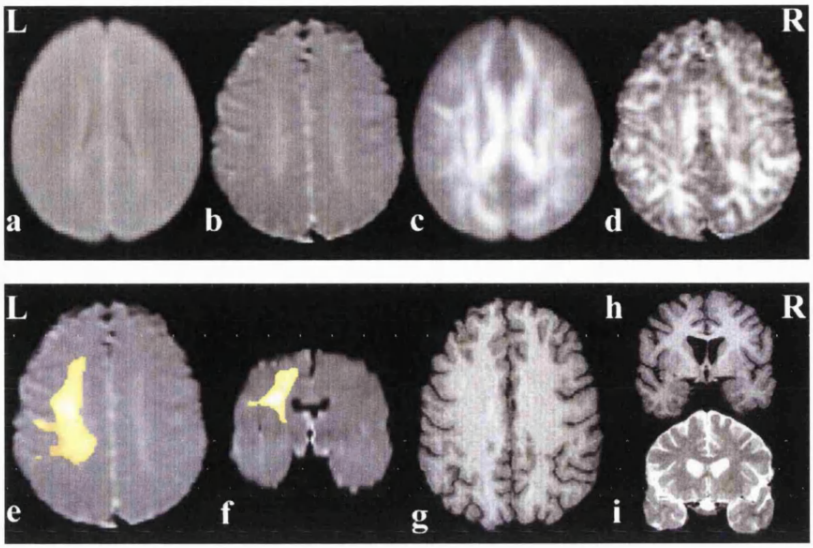

Figure 3.10: Patient 1. Normalised axial mean diffusivity maps at the same slice position for the averaged 30 control subjects (a) and the patient (b) and (e). Normalised coronal mean diffusivity map (f). Normalised axial anisotropy maps at the same slice position for the averaged 30 control subjects (c) and the patient (d). The difference in signal to noise between the maps is due to averaging of the 30 controls subjects. The region of significantly increased mean diffusivity is superimposed on maps (e) and (f). The equivalent slices of the patient's T1-weighted axial (g) and coronal (h) and T2-weighted coronal (i) images show no abnormality. The region in (e) was used for quantitative region-of-interest analyses of mean diffusivity values. Note that right on the images is patient's right.

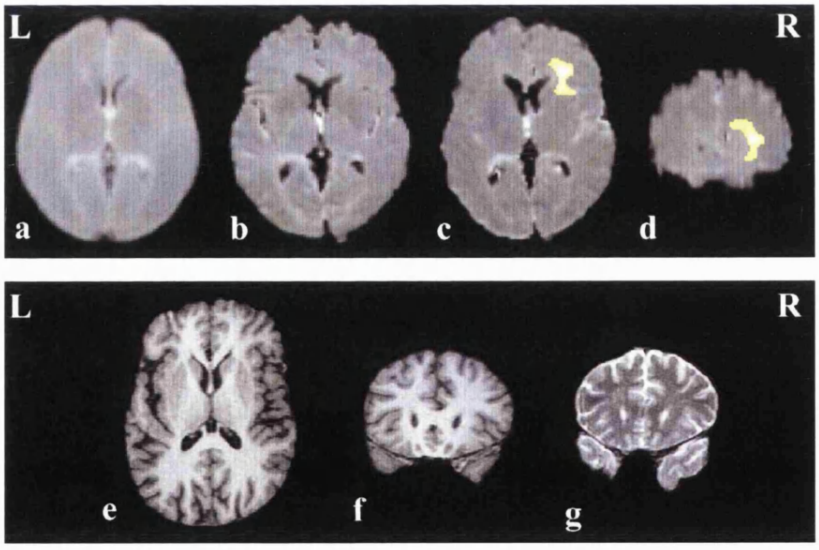

Figure 3.11 Patient 2. Normalised axial mean diffusivity maps at the same slice position for the averaged 30 control subjects (a) and the patient (b) and (c). Normalised coronal mean diffusivity map (d). The difference in signal to noise between the maps is due to averaging of the 30 controls subjects. The region of significantly increased mean diffusivity is superimposed on maps (c) and (d). The equivalent slices of the patient's T1-weighted axial (e) and coronal (f) and T2-weighted coronal (g) images show no abnormality. The region in (c) was used for quantitative region-of-interest analyses of mean diffusivity values. Note that right on the images is patient's right.

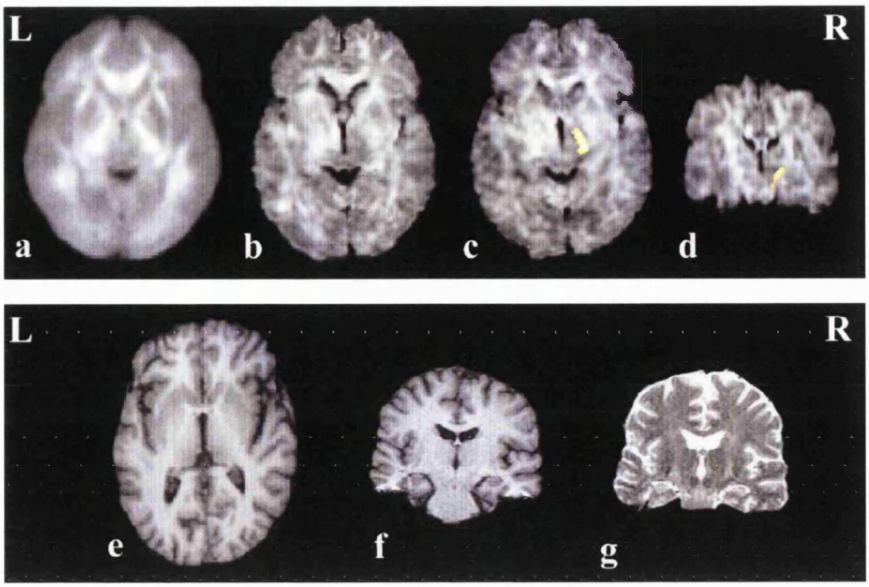

Figure 3.12 Patient 2. Normalised axial fractional anisotropy maps at the same slice position for the averaged 30 control subjects (a) and the patient (b) and (c). Normalised coronal anisotropy map (d). The difference in signal to noise between the maps is due to averaging of the 30 control subjects. The region of significantly decreased fractional anisotropy is superimposed on maps (c) and (d). The equivalent slices of the patient's T1-weighted axial (e) and coronal (f) and T2-weighted coronal (g) images show no abnormality. The region in (c) was used for quantitative region-of-interest analyses of fractional anisotropy values.

3.3.5 Conclusions

Using diffusion-tensor imaging we have shown, for the first time, abnormalities of diffusion in patients with severe head injury and unremarkable conventional MRI. This and other studies (Wieshmann *et al.* 1999e) suggest that although abnormalities in mean diffusivity are a more sensitive marker of cerebral damage, quantifying tissue anisotropy yields additional valuable clinical information. To accurately and fully examine the diffusional properties of a tissue, diffusion tensor imaging, with diffusion gradients applied in at least six directions, must be performed. Applying diffusion gradients in only three orthogonal directions leads to an underestimation of anisotropy (Pierpaoli and Basser 1996), which may result in clinically significant findings being overlooked.

In both patients it is likely that the diffusion abnormalities, which are distant from the site of impact, are caused by diffuse axonal injury. Our findings of increased mean diffusivity suggest that there was an expansion of the extracellular space, caused by neuronal or glial cell loss, which was not identified by conventional MRI despite the presence of neurological and neuropsychological symptoms and signs. In addition, a clinically concordant reduction of anisotropy in the internal capsule of patient 2 suggests that there was structural disorganisation and a loss of the parallel fibre arrangement of the major white matter tracts of the internal capsule as a result of the head injury. Again, this was without an identifiable abnormality on conventional MRI.

Our results suggest that DTI is a useful quantitative imaging method following head injury, and is more sensitive than conventional MRI.

CHAPTER FOUR

Magnetisation Transfer Imaging

4.1 MAGNETISATION TRANSFER IMAGING IN FOCAL EPILEPSY

4.1.1 Summary

Magnetisation transfer imaging (MTI) and Statistical Parametric Mapping (SPM99) was used to objectively examine the cerebral structure of 15 patients with malformations of cortical development (MCD), 10 patients with partial seizures and acquired lesions and 42 patients with partial seizures and normal MRI. Magnetisation transfer imaging maps were calculated and, using SPM, individual patients were compared to a group of 30 control subjects. Magnetisation transfer imaging and objective voxel-by-voxel statistical comparison identified significant reductions of magnetisation transfer ratio (MTR) in all 10 patients with acquired nonprogressive cerebral lesions and partial seizures. In all of these the areas of decreased MTR concurred with abnormalities identified on visual inspection of conventional MRI. In 13 out of the 15 patients with MCD, SPM detected regions of significantly reduced MTR; all of which corresponded to abnormalities identified on visual inspection of conventional MRI. In addition, in both groups, there were areas that were normal on conventional imaging, which demonstrated abnormal MTR. Voxel-by-voxel statistical analysis identified a significant reduction of MTR in fifteen of the 42 patients with cryptogenic focal epilepsy. In all of these, the areas of reduced MTR concurred with epileptiform EEG abnormality and clinical seizure semiology. Group analysis of MRI-negative patients with electroclinical seizure onset localising to the left temporal, right temporal, or left frontal regions revealed a significant reduction of MTR within the white matter of each respective lobe.

Magnetisation transfer imaging analysed using SPM was sensitive in patients with MCDs and acquired cerebral damage. Significant differences in MTR in individual and grouped MRI-negative patients suggest that minor structural disorganisation exists in occult epileptogenic cerebral lesions. This technique is a promising, non-invasive imaging method for identifying the cause of partial seizures, and can contribute to presurgical evaluation.

4.1.2 Introduction

The principal concept of MTI involves the exchange of magnetization between free protons in bulk water and tightly bound protons on macromolecules, such as myelin or membrane lipids. The macromolecular protons, because of their immobility, have a very short relaxation time rendering them invisible to conventional MRI. MTI, however, offers an insight into this macromolecular environment by its observable effect on the MR-visible free water protons (Wolff and Balaban 1989; Wolff and Balaban 1994). The exchange of magnetisation between bound protons and free water is represented by the magnetisation transfer ratio (MTR) which, therefore, provides a quantitative measure of macromolecular structural integrity.

4.1.3 Methods

4.1.3.1 Subjects

- 30 healthy control subjects :
  - 14 men, median age 33 years, range 19-56 years

- 67 patients with focal epilepsy

  Acquired

  - 10 patients (eight men, median age 34 years, range 22-51 years, median duration of epilepsy 12 years, range 6-48 years)

    3 patients with ischaemic lesions

    4 patients with head injuries

    3 patients with a history of encephalitis

  Malformations of cortical development

  - 15 patients (six men, median age 35 years, range 19-55 years, median duration of epilepsy 23 years, range 4-51 years)

    6 patients with gyral abnormalities

    9 patients with heterotopia

    subependymal (n=4), subcortical nodules (n=3) and band heterotopia (n=2)

  MRI-negative

  - 42 patients (23 men, median age 32 years, range 18-54 years, median duration of epilepsy 18 years, range 2-40 years)

    14 were diagnosed with temporal lobe epilepsy (10 left, 4 right)

    7 with frontal lobe epilepsy (3 left, 4 right)

    6 with occipital lobe epilepsy

    15 had electroclinical evidence of less well defined, more widespread abnormalities

4.1.3.2 Magnetisation transfer imaging

Magnetisation transfer (MT) weighted and non-MT weighted 3D data sets were acquired on a 1.5T Horizon Echospeed scanner (G.E, Milwaukee, Wisc., USA) using a standard quadrature head coil (TR/TE=22.6/5.4ms). Volume matrix was 256x256 (in plane) x124 over a 240x240x186mm field-of-view, giving a resolution of 0.93x0.93x1.5mm. MT-weighted images were collected following the application of a pre-pulse to saturate the broad resonance of immobile macromolecular protons. The MT rf pulse used was a 3-lobe Hamming apodised sinc pulse with a duration of 6.4ms and a B_1 of 5.1μT, applied 2Khz off-resonance (Boulby, Symms, and Barker 2000). The entire sequence was within Specific Absorption Rate limits. Total scanning time for MTI was 13 mins, 56 sec.

4.1.3.3 Analysis

Following data acquisition, the images were transferred to an off-line workstation (Sun Microsystems, Palo Alto, CA) for post-processing. Prior to calculation of the MTR map, because the two data sets were acquired consecutively and not interleaved, coregistration of the MT-weighted and non-MT-weighted images was required. To enable accurate co-registration to be performed, extracerebral tissue was initially removed from the images using the segmentation function provided by SPM99 (Ashburner and Friston 1997). White and grey matter and cerebrospinal fluid compartments were then reunited using the image calculation function of SPM99, thus discarding the majority of extracerebral tissue.

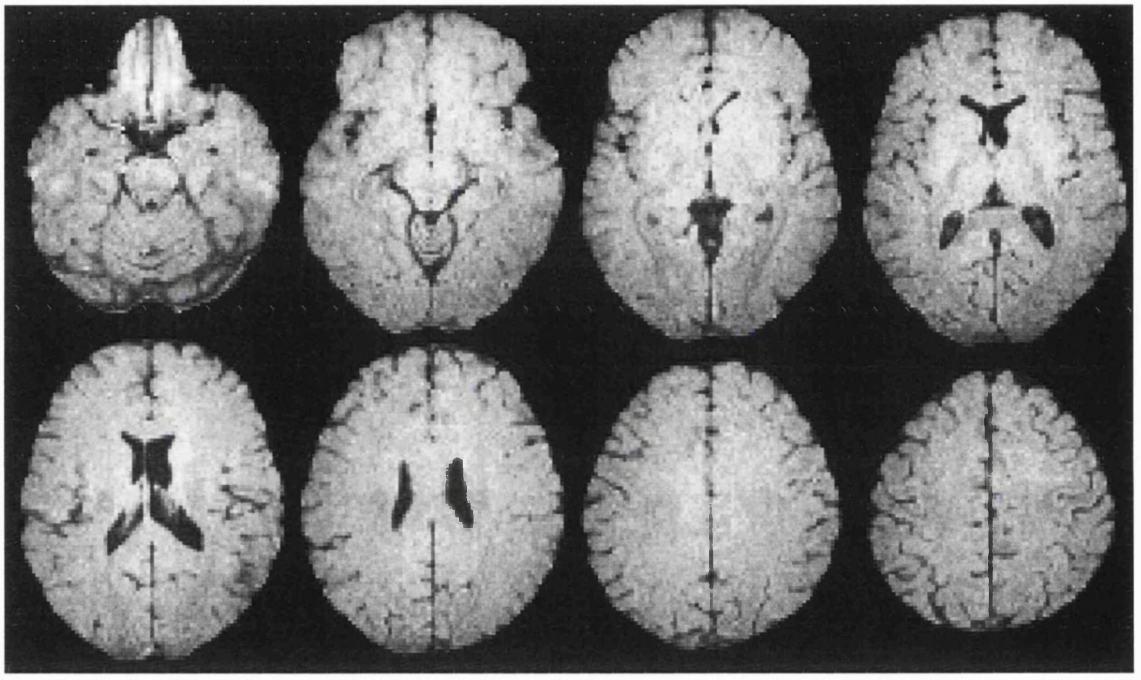

Figure 4.1: Series of normalised axial MTR maps from a single control subject.

The MT-weighted and non-MT-weighted images were co-registered using a modified version (Symms *et al.* 1996) of the Automated Image Registration software (Woods, Cherry, and Mazziotta 1992). Additional removal of extracerebral tissue was then performed on the non-MT-weighted image using a modification of publicly available brain extraction software (Exbrain (Lemieux *et al.* 1999)) and the resultant image was used to mask the MT-weighted image for identical removal of extraneous tissue. A small proportion of subjects' images required minor manual editing to remove any remaining extracerebral tissue. Using the registered skull-stripped images, MTR was calculated pixel-by-pixel according to the equation:

$$MTR = ((MT_{off} - MT_{on}) / MT_{off}) \times 100$$

where MT_{on} and MT_{off} represent the signal intensities with and without the saturation pulse respectively.

This template was created by normalising a control subject's MT image to standard SPM space using 12

linear degrees of freedom and a 7x8x7 non-linear warp (figure 4.1). Subsequently the MT images of the patients and controls were normalised to this template using linear steps with 12 degrees of freedom (translation, rotation, zoom and shear).

The normalized maps were smoothed with an 8mm isotropic Gaussian kernel. A signal intensity threshold was set at 0.5 to reduce the level of noise from the MT images included within the analysis; that is, only voxels with values exceeding 50% of the whole brain mean intensity were analysed. This procedure excluded noise that arose principally from outside the brain.

Each patient's and control's non-MT, proton density weighted (PD) image, was similarly normalised and smoothed using parameters derived from the normalisation process of the MTR maps. This resulted in "anatomical" images perfectly matched to the MTR maps of each patient and control, on which identical statistical comparisons were performed. Any differences in the PD images between patients and controls were due to morphological variation, for example, atrophy or incomplete normalisation. Significant differences in the MTR maps of patients and controls that were not associated with a similar area of abnormality in the PD images were therefore due to changes in only the magnetisation transfer properties of the tissue and not inter-subject anatomical variation.

The smoothed, normalized maps were statistically analysed on a voxel-by-voxel basis, and inferences made from the resultant maps, as described in chapter 2.3 *Common methodology: Post-acquisition processing.* Region-of-interest analyses were also performed in order to illustrate the magnitude of the differences in MTR values in areas highlighted by the SPM comparison as deviating significantly from normal. The mean MTR value (in percent units, pu) in the ROI from each patient's map was compared to the mean value in the equivalent ROI from all 30 of the control subjects' maps and the difference expressed as a percentage of the control mean (Barker, Tofts, and Gass 1996).

4.1.4 Results

4.1.4.1 Control group

Comparing each control subject with the remaining 29 control subjects using identical parameters and statistical thresholds as the comparison between patients and controls, one subject had a single area of significantly decreased MTR. At a statistical threshold of $p<0.05$ and 60 examinations (30 subjects with two contrasts each (an increase and a decrease)), up to three abnormal areas may have been anticipated by chance.

4.1.4.2 Acquired Lesions

4.1.4.2.1 Individual SPM analyses

In all ten patients with acquired lesions, SPM detected areas of significantly reduced MTR (table 4.1). In all patients the areas of reduced MTR corresponded to the abnormalities identified on visual inspection of the conventional MR images (figure 4.2). In three patients (patients 2, 3 and 8) areas of significantly reduced MTR

were detected in regions previously reported as normal. These were within the left temporal lobe in patients 2 and 3, and the right mesial temporal region in patient 8. There were no increases in MTR.

Analyses of the proton density weighted images revealed abnormalities that concurred with the conventional MR images in seven patients (patients 2, 3, 4, 5, 7, 9 and 10). The analyses of the PD images did not identify any abnormality in three patients (1, 6 and 8). In all 7 patients with areas of significantly abnormal PD, the PD changes were much less extensive than the MTR abnormalities.

4.1.4.2.2 Region-of-interest analyses

In patient 1 (head injury) the average MTR within the identified left frontal region was 46pu. This was 90% of the mean MTR within the corresponding regions in the control subjects (mean MTR of 51pu). In patient 7 (cerebral infarct), the average MTR within the identified right frontal region was 41pu. This was 80% of the average MTR within the corresponding regions in the control subjects (51pu) (figure 4.2). The mean MTR within the area of known abnormality in the right frontal lobe of patient 8 (focal leucoencephalitis) was 38pu, which was 73% of the mean MTR value (52pu) in the same region in the control subjects. Within the normal appearing right temporal region of this patient, which SPM also identified as being statistically abnormal, the mean MTR value was 44pu which was 85% of the mean of the control values of 52pu (see Table 4.4).

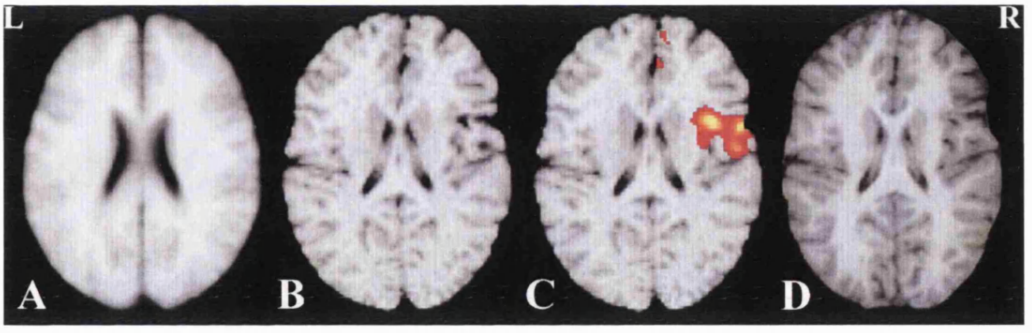

Figure 4.2: Patient 7, mature cortical infarct in right frontal lobe.
Normalised axial MTR maps at the same slice position for the averaged 30 control subjects (A) and the patient (B) and (C). The difference in signal to noise between the maps is due to averaging of the 30 controls subjects. The region of significantly decreased MTR is superimposed on map (C). This region coincides with the localisation of the abnormality identified on conventional MRI. (D): The equivalent slice of the patient's T1-weighted image. The region in (C) was used for quantitative region-of-interest analyses of MTR. Note that right on the images is patient's right.

4.1.4.3 Malformations of Cortical Development

4.1.4.3.1 Individual SPM analyses

In thirteen of the fifteen patients with MCD, SPM detected regions of reduced MTR (table 4.2). In all thirteen patients, the areas of reduced MTR corresponded to all or part of the MCD identified on visual inspection of the

conventional MR images. In addition, in eight patients changes were found outside the MCD in tissue that appeared normal on conventional MRI.

All 6 patients (patients 11-16) with gyral abnormalities had areas of significantly reduced MTR which corresponded to all or part of the MCD. In five of the six, changes were also found in areas beyond the margins of the evident MCD, in areas that appeared normal on T1- and T2-weighted images. In three patients (patients 11, 13, and 15) these regions were within the corpus callosum. In addition, patient 13 also had an area of abnormal MTR in the right posterior periventricular region. In two patients (12 and 16), reduced MTR was seen in the normal appearing left frontal lobes.

Areas of reduced MTR, which corresponded to the MCD identified on the conventional MR images, were seen in all of the patients with subcortical heterotopia (SCH) (patients 17-19), in both patients with band heterotopia (BHT) (patients 20 and 21) (figure 4.3), and in two of the four patients (patients 23 and 25) with subependymal heterotopia (SEH) (patients 22-25). All the patients with SCH (patients 17-19) also had regions of reduced MTR detected beyond the evident MCD. Patient 17 had reduced MTR within the malformation in the right temporal lobe and also in normal appearing tissue in both frontal lobes and in the right fronto-temporal region. Patient 18 had a region of heterotopia in the right occipital lobe extending anteriorly into the temporal lobe. A reduction in MTR was identified, not only in the right occipital and temporal lobes but also in the right parietal and frontal lobes. An increase in MTR was detected in this patient in the right fronto-parietal region. In addition to reduced MTR within the subcortical heterotopic nodule in the right parietal lobe, patient 19 also had an area of reduced MTR in normal appearing tissue of the left frontal lobe.

Analyses of the proton density weighted images revealed abnormalities that concurred with the conventional MR images in seven patients (patients 11, 12, 13, 15, 16, 22 and 24). The analyses of the PD images did not identify any abnormality in eight patients (14, 17, 18, 19, 20, 21, 23 and 25). In all 7 patients with areas of significantly abnormal PD, the PD abnormalities were less extensive than those identified following the analysis of the MTR maps.

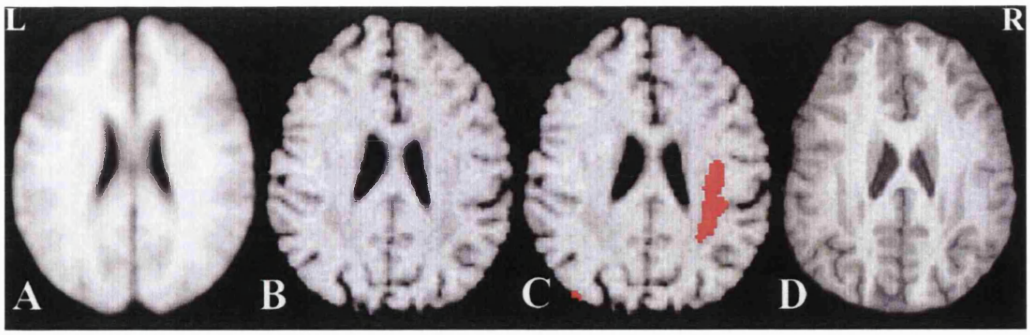

Figure 4.3: Patient 20, bilateral band heterotopia.
Normalised axial MTR maps at the same slice position for the averaged 30 control subjects (A) and the patient (B) and (C). The regions of reduced MTR are superimposed on map (C) and are predominantly localised to the heterotopic tissue in the right hemisphere. (D): the equivalent slice of the patient's T1-weighted image. Reduced MTR was also seen in band heterotopia in the left hemisphere, however this failed to reach statistical significance. Note right on images is patient's right.

4.1.4.3.2 Region-of-interest analyses

In order to demonstrate the magnitude of the effect, quantitative ROI analyses were made in two patients whose appearances on conventional imaging were considered typical for each aetiology. Patient 11 had a gyral abnormality with thickened cortex and patient 18 had subcortical heterotopia. In patient 11 the analyses were made in the SPM-identified region of reduced MTR within the normal appearing corpus callosum and in the gyral abnormality within the right frontoparietal area. The mean MTR value in the corpus callosum was 40pu which was 78% of the mean of the control values of 51pu. The mean MTR in the right frontoparietal region was 45pu. This was 86% of the mean MTR in the corresponding areas in the control subjects of 52pu. In the right occipito-temporal heterotopia in patient 18 the mean MTR was 49pu, which was 92% of the mean MTR value (53pu) in the same region in the control subjects.

A ROI analysis were also made within the area of significantly increased MTR in patient 18. The MTR value was 53pu in the patient which was 109% of the mean MTR value (48pu) in the control subjects.

4.1.4.4 MRI-negative patients

4.1.4.4.1 Individual SPM analyses

SPM analyses of the 42 individual patients in the MRI-negative group revealed 15 patients (36%) with statistically significant reductions in MTR compared to the control group (table 4.3) (figure 4.4). In 14 of these, the regions concurred with the localisation of epileptiform EEG abnormality, nine of which were ictal recordings. One patient (40) had an area of reduced MTR in the left frontal lobe which concurred with seizure semiology; the EEG data being inconclusive. Twenty-seven patients had no areas of significantly reduced MTR. There were no increases in MTR.

In two patients the MTR abnormalities could at least be partly explained by changes seen on analysis of the proton density weighted images (patients 32 and 48), however, in each case the areas of abnormal PD were much less extensive than the regions of MTR abnormality. No areas of significantly abnormal PD were seen in the remaining MRI-negative patients.

4.1.4.4.2 Region-of-interest analyses

To indicate the magnitude of the effect, quantitative ROI analyses within the right temporal lobe of patient 37 revealed a mean MTR of 40pu, 80% of the mean MTR within the corresponding regions of the control subjects (50pu). In patient 29, the mean MTR within the left frontal lobe was 46pu, 86% of the mean MTR within the identical area in the control group (53pu) (figure 4.4).

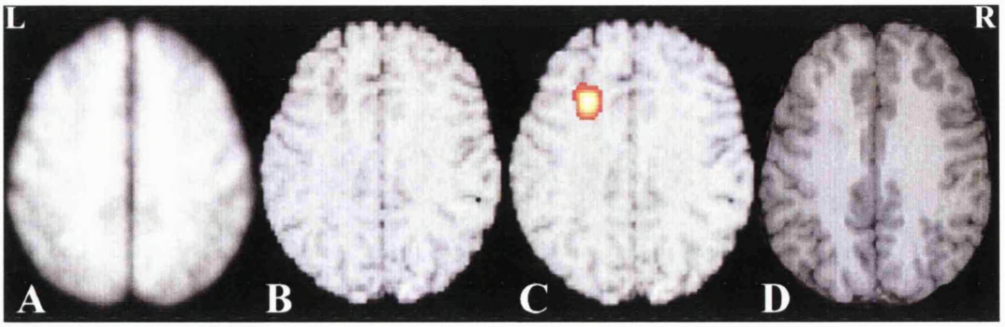

Figure 4.4: Patient 29, Patient with cryptogenic focal epilepsy and left frontal interictal epileptiform activity. Normalised axial MTR maps at the same slice position for the averaged 30 control subjects (A) and the patient (B) and (C). The region of significantly decreased MTR is superimposed on map (C). The region of decreased MTR is localised to the normal appearing cerebral tissue of the left frontal lobe. (D): The equivalent slice of the patient's T1-weighted image. The region in (D) was used for quantitative region-of-interest analysis of MTR values. Note that right on the images is patient's right.

4.1.4.4.3 Group analyses

Group analyses were performed on MRI-negative patients with EEG evidence of either left or right temporal or frontal lobe seizures. The left temporal lobe group consisted of 10 patients (patients 26-35), the right temporal lobe group four (patients 36-39), the left frontal lobe group three patients (patients 40-42) and the right frontal lobe group four (patients 43-46). Compared to the 30 control subjects the left temporal lobe group had a significant decrease in MTR within the white matter of the left temporal region. The ROI analysis of this area demonstrated a mean MTR in the patient group of 48pu, compared with a mean of 52pu in the control subjects (92%, $p<0.05$) (Figure 4.5). A similar finding of significantly reduced MTR was found in the right temporal lobe of the right temporal lobe epilepsy patients (patient mean, 47pu; control mean, 50pu, (94%, $p<0.005$)) (Figure 4.5) and in the left frontal lobe of the patients with left frontal lobe epilepsy (patient mean, 42pu; control mean, 50pu, (84%, $p<0.05$)). An area of reduced MTR in the right frontal lobe was detected in the right frontal lobe epilepsy patients however this failed to reach statistical significance. There were no abnormalities on the corresponding analyses of the PD images.

Patient	Age (yr)	Gender	Aetiology of epilepsy	Seizure Types	Duration of epilepsy (yrs)	Interictal EEG features	Conventional MRI findings	MTI findings Significant decreases in MTR (maximum *P*-value)
7	20	F	infarction	CPS, 2° gen.	12	R. frontotemp. i.e.a.	R. lat. front. cortical scar	R. lat. front. (p<0.001)
8	23	M	encephalitis	CPS, 2° gen.	7	R. frontotemp. i.e.a	R. front. scarring, CSF-filled cortical cavity	R. front. + NA R. mesial temp. (p<0.001)
9	51	M	encephalitis	CPS, 2° gen.	12	bihemispheric i.e.a	L. temp + L. occ. + minor R. temp. damage	L. temp + L. occ. + R. temp. (p<0.001)
10	45	M	encephalitis	CPS, 2° gen.	43	L. frontotemp. i.e.a.	bifrontoparietal and L. temp. damage	bifrontoparietal and L. temp. (p<0.001)

SPS=simple partial seizure; CPS=complex partial seizure; 2° gen.=secondary generalised tonic-clonic seizure; R.=Right; L.=Left; bil.=bilateral; post.=posterior; med.=medial; lat.=lateral; front.=frontal; par.=parietal; temp.=temporal; occ.=occipital; HC=hippocampus; CC=corpus callosum; i.e.a..=interictal epileptiform activity; M=male; F=female.

Table 4.2 Clinical characteristics, EEG, MRI and MTI findings in patients with malformations of cortical development

Patient	Age (yr)	Gender	Seizure Types	Duration of epilepsy (yrs)	Interictal EEG features	Conventional MRI findings	MTI findings Significant decreases in MTR (max. *P*-value)
11	36	M	SPS, CPS + tonic	36	normal	bil. frontopar. gyral abn. with thick cortex	bil. frontopar. regions in MCD + in body of NA corp.callosum ($p<0.001$)
12	52	M	CPS, 2° gen.	39	R. hemisphere i.e.a	R front. + bil. par. occ. gyral abn. with thick cortex	bil. in MCD + in NA L. front. lobe ($p<0.001$)
13	34	F	S + CPS, 2° gen.	19	normal	L. perisylvian gyral abn. with thick cortex	L. perisylvian in MCD + in NA ant./mid. body of corp. callosum + R. post. lat. periventricular region ($p<0.001$)
14	36	F	CPS, 2° gen.	28	widespread i.e.a., max. R. hemisphere	R. temporopar. gyral abn. with thick cortex	R. temporopar. in MCD ($p=0.001$)
15	24	F	SPS, CPS + tonic	22	widespread i.e.a., max. L. hemisphere	bil. frontopar. gyral abn. with thick cortex	bil. frontopar. regions in MCD + in body of NA corp.callosum ($p<0.001$)
16	51	F	CPS, 2° gen.	35	widespread i.e.a., max. R. temp.	R. hemispheric gyral abn. with thick cortex	R. hemisphere in MCD + in NA L. front. lobe ($p<0.001$)

Patient	Age (yr)	Gender	Seizure Types	Duration of epilepsy (yrs)	Interictal EEG features	Conventional MRI findings	MTI findings Significant decreases in MTR (max. *P*-value)
17	20	M	SPS, 2° gen.	18	bifrontotemp. i.e.a.	R. temp. nodular SCH	R. temp. in MCD + in NA R. frontotemp. and bil. inferior front. regions ($p<0.001$)
18	31	M	CPS	5	R. temp. i.e.a	R. occ. temp. nodular SCH	R. occ. temp. in MCD extending into NA R. par. + R. front. lobes ($p<0.001$) Also *inc.* MTR in NA R. frontopar. ($p=0.03$)
19	53	M	2° gen.	23	normal	R. par. nodular SCH	R. par. in MCD + in NA L. front. lobe ($p<0.001$)
20	28	M	S + CPS, 2° gen.	20	widespread i.e.a., max. L. temp.	bil. BHT + bil. frontopar. gyral abn. with thick cortex	R. hemisphere in BHT + bil. frontopar. in gyral abn. ($p<0.001$)
21	32	F	S + CPS, 2° gen.	27	widespread i.e.a	bil. BHT	bil. in MCD ($p<0.001$)
22	45	F	CPS	36	L. hemisphere, max L. front. i.e.a	bil. temp. + par. SEH	None
23	54	F	CPS, 2° gen.	51	R. frontotemp. i.e.a	bil. SEH	bil. in MCD ($p<0.001$)

Patient	Age (yr)	Gender	Seizure Types	Duration of epilepsy (yrs)	Interictal EEG features	Conventional MRI findings	MTI findings Significant decreases in MTR (max. *P*-value)
24	33	F	CPS, 2^{o} gen.	12	interictal -normal	R. posterior SEH	None
25	35	F	CPS	4	L. temp. i.e.a.	L. posterior SEH + L. front. gyral abn. with thick cortex	L. hemisphere in SEH and gyral abn. (p<0.001)

R.=Right; L.=Left; bil.=bilateral; ant.=anterior; post.=posterior; mid.=middle; lat.=lateral; front.=frontal; par.=parietal; temp.=temporal; occ.=occipital; NA=normal-appearing; corp.=corpus; MCD=malformation of cortical development; BHT=band heterotopia; SEH= subependymal heterotopia; SCH=subcortical heterotopia; i.e.a..=interictal epileptiform activity; abn.=abnormality; M=male; F=female; SPS=simple partial seizure; CPS=complex partial seizure; 2^{o} gen.=secondary generalised tonic-clonic seizure; inc.=increased.

Table 4.3 Clinical characteristics, EEG and MTI findings in patients with normal conventional MRI.

Patient	Age (yr)	Gender	Aetiology of epilepsy	Duration of epilepsy (yrs)	Seizure types	Ictal Epileptiform Abnormality	Interictal Epileptiform Abnormality	MTI findings Significant decreases in MTR (*P*-value)
26	19	F	head injury	13	CPS, 2° gen.	N/A	L temp	None
27	29	M	cryptogenic	14	S + CPS, 2° gen.	N/A	L temp	L. middle temporal gyrus ($p<0.001$)
28	54	M	cryptogenic	34	CPS, 2° gen.	L. temp.	L. temp.	bil. paraHC + fusiform gyri ($p<0.001$)
29	31	F	cryptogenic	30	SPS, 2° gen.	L. temp.	L. front.	L. lateral sup. frontal gyrus ($p<0.001$)
30	40	F	cryptogenic	29	CPS, 2° gen.	N/A	L temp.	None
31	38	M	cryptogenic	35	CPS, 2° gen.	L. temp.	bitemporal.	bitemporal ($p=0.001$)
32	32	M	cryptogenic	13	S + CPS, 2° gen.	L. temp.	L. temp.	L. temporal lobe ($p=0.001$)
33	31	M	cryptogenic	16	SPS, CPS	L. temp.	L. temp.	None
34	28	M	encephalitis	18	S + CPS, 2° gen.	N/A	L. temp.	None
35	32	M	cryptogenic	14	CPS, 2° gen.	L. temp.	L. temp.	None
36	40	F	feb. convulsion	36	CPS, 2° gen.	R. temp.	R.> L. temp.	None
37	28	F	cryptogenic	22	2° gen.	N/A	R. temp.	R. temp lobe + uncus ($p=0.03$)
38	33	M	cryptogenic	18	SPS, 2° gen.	N/A	R. temp.	None

Patient	Age (yr)	Gender	Aetiology of epilepsy	Duration of epilepsy (yrs)	Seizure types	Ictal Epileptiform Abnormality	Interictal Epileptiform Abnormality	MTI findings Significant decreases in MTR (*P*-value)
39	42	F	cryptogenic	10	S + CPS, 2° gen.	R. temp.	R. temp.	R. temporal lobe (p<0.001)
40	32	F	head injury	30	CPS, 2° gen.	normal	normal	L. ant. cingulate / frontal lobe (p=0.005)
41	27	M	cryptogenic	23	CPS	N/A	L. front.	None
42	44	F	head injury	38	CPS, 2° gen.	L. front.	L. front.	L frontal lobe (p<0.001)
43	39	M	cryptogenic	23	CPS	N/A	R. front.	None
44	26	F	cryptogenic	20	CPS	N/A	R. front.	None
45	53	M	cryptogenic	40	CPS, 2° gen.	N/A	R. front.	None
46	28	M	cryptogenic	12	CPS, 2° gen.	N/A	R.front.	R. frontal lobe (p<0.001)
47	19	F	cryptogenic	18	S + CPS, 2° gen.	N/A	L. occ.	None
48	29	M	cryptogenic	22	CPS, 2° gen.	L. occ	L. occ.	L. occipital lobe (p<0.001)
49	28	M	cryptogenic	4	S + CPS, 2° gen.	normal	normal	None
50	35	F	cryptogenic	28	CPS, 2° gen.	bil. occ.	bil. occ.	None
51	39	M	cryptogenic	4	CPS, 2° gen.	N/A	normal	None

Patient	Age (yr)	Gender	Aetiology of epilepsy	Duration of epilepsy (yrs)	Seizure types	Ictal Epileptiform Abnormality	Interictal Epileptiform Abnormality	MTI findings Significant decreases in MTR (*P*-value)
52	18	F	cryptogenic	6	S + CPS, 2° gen.	normal	normal	None
53	36	F	cryptogenic	21	S+CPS, 2° gen.	inconclusive	R. hemisphere	None
54	43	M	cryptogenic	31	CPS, 2° gen.	bil. front.	bil. front.	R. front. (p=0.005)
55	51	F	cryptogenic	8	CPS, 2° gen.	L hemisphere	normal	None
56	22	F	cryptogenic	5	S + CPS, 2° gen.	inconclusive	inconclusive	None
57	41	M	cryptogenic	19	2° gen.	N/A	L. frontotemporal	L. front + L. parietal (p<0.001)
58	31	M	cryptogenic	18	CPS, 2° gen.	bil. front	bil. front	bifrontal poles (p=0.004)
59	39	F	cryptogenic	8	SPS, 2° gen.	L. frontotemp.	L. frontotemp.	None
60	24	M	encephalitis	13	CPS, 2° gen.	N/A	inconclusive	None
61	30	M	measles vacc.	26	SPS, 2° gen.	bil. front.	L. temp.	bil. inf. frontal gyrus rectus (p<0.001)
62	27	M	neonatal illness	27	CPS, 2° gen.	R hemisphere	R. hemisphere	None
63	38	F	cryptogenic	31	CPS	N/A	L. frontotemporal	None

Patient	Age (yr)	Gender	Aetiology of epilepsy	Duration of epilepsy (yrs)	Seizure types	Ictal Epileptiform Abnormality	Interictal Epileptiform Abnormality	MTI findings Significant decreases in MTR (*P*-value)
64	32	M	cryptogenic	2	SPS + CPS	R. hemisphere	R. hemisphere	None
65	19	M	cryptogenic	15	S + CPS, 2° gen.	R. frontotemporal	R. > L. temp.	None
66	18	F	cryptogenic	12	S+CPS, 2° gen.	L. frontotemp.	bil. frontotemp.	None
67	46	F	meningitis	21	CPS, 2° gen.	N/A	R. hemisphere	None

S/CPS=simple/complex partial seizure; 2° gen =secondary generalised tonic-clonic seizure; R.=Right; L.=Left; bil.=bilateral; front.=frontal; par.=parietal; temp.=temporal; occ.=occipital; ant.=anterior; inf.=inferior; sup.=superior; paraHC=parahippocampal; N/A=not available; M=male; F=female; feb.=febrile; vacc.=vaccination.

Table 4.4 MTR values from the regions-of-interest defined by SPM, in patients with acquired lesions, MCD, and normal conventional MRI.

Patient	Aetiology of epilepsy	EEG features	MTR - SPM results Regions of significantly reduced MTR	Region-of interest derived MTR values (percent units) Patient		Controls mean (SD)	% difference
Acquired							
2	head injury	L. temporopar. i.e.a.	L. front. par. region + NA L. temp. lobe	L. front :	45.0	51.5 (1.9)	13% decrease
				L. temp:	44.0	52.2 (0.7)	16% decrease
3	head injury	bil. frontotemp. i.e.a.	bifrontal + R. temp. + corpus callosum	corp. call.:	44.5	50.0 (1.7)	11% decrease
			+ NA L. temp.	L. temp.:	45.6	52.7 (1.1)	13% decrease
7	infarction	R. frontotemp. i.e.a.	R. lat. frontal lobe	R. front.:	41.6	51.6 (1.0)	20% decrease
8	encephalitis	R. frontotemp. i.e.a	R. front. + NA R. mesial temp. lobe	R. front :	38.8	52.0 (0.7)	26% decrease
				R. temp.:	44.9	51.9 (1.1)	14% decrease
MCD							
11	gyral abnormality	normal	bil. frontopar. regions in MCD + in	in MCD:	45.0	52.3 (0.7)	14% decrease
			body of NA corp. callosum	corp. call :	39.9	51.4 (1.9)	23% decrease

Patient	Aetiology of epilepsy	EEG features	MTR - SPM results	Region-of interest derived MTR values (percent units)			
			Regions of significantly reduced MTR	Patient		Controls mean (SD)	% difference
18	subcortical heterotopia	R. temp. i.e.a	R. occ. temp. in MCD extending into NA R. par. + R. front. lobes. Also *inc.* MTR in NA R. frontopar.	in MCD:	49.4	53.4 (0.6)	8% decrease
				R. frontopar:	53.1	48.6 (0.8)	9% increase
20	band heterotopia + gyral abnormality	widespread i.e.a., max. L. temp	R. hemisphere in BHT + bil. frontopar. in gyral abn.	R band. :	49.7	53.6 (0.8)	8% decrease
Normal conventional MRI							
29	cryptogenic	L. front. i.e.a	L. lateral sup. frontal gyrus	45.9		53.6 (0.8)	15% decrease
37	cryptogenic	R. temp. focus	R. temp lobe + uncus	R. temp.:	40.2	50.3 (1.5)	20% decrease
42	head injury	L. front. focus	L frontal lobe	46.9		53.0 (1.9)	12% decrease
L. TLE gp.	N/A	L. temp	L. temp WM	48.9		52.2 (1.2)	7% decrease

Patient	Aetiology of epilepsy	EEG features	MTR - SPM results	Region-of interest derived MTR values (percent units)		
			Regions of significantly reduced MTR	Patient	Controls mean (SD)	% difference
R. TLE gp.	N/A	R. temp.	R. temp. WM	47.7	49.8 (1.2)	5% decrease

R.=Right; L.=Left; bil.=bilateral; post.=posterior; med.=medial; lat.=lateral; front.=frontal; par.=parietal; temp.=temporal; occ.=occipital; HC=hippocampus; i.e.a..=interictal epileptiform activity; M=male; F=female; SPS=simple partial seizure; CPS=complex partial seizure; 2^{o} gen.=secondary generalised tonic-clonic seizure; NA=normal appearing; SD=standard deviation

4.1.5 Conclusions

There were several major findings in this study. Magnetisation transfer imaging and voxel-by-voxel statistical comparison identified significant reductions of MTR in all patients with acquired nonprogressive cerebral lesions and partial seizures. In all of these patients the areas of decreased MTR concurred with abnormalities identified on visual inspection of conventional MRI. Thirteen out of fifteen patients with malformations of cortical development had areas of reduced MTR. In all of these, the areas were within areas of abnormality identified on conventional MRI. In addition, in the patients with acquired lesions there were three areas, and in the patients with MCD there were 13 areas that appeared normal on conventional imaging but which exhibited significantly reduced MTR, indicating additional sensitivity from the new method. Individual analyses of 42 patients with partial seizures and normal conventional MRI identified a significant reduction in MTR in fifteen of the subjects. In all of these patients, the areas of reduced MTR concurred with electroclinical information. Group analysis of MRI-negative patients with electroclinical seizure onset localising to the left temporal, right temporal or left frontal regions revealed a significant reduction of MTR within each respective lobe.

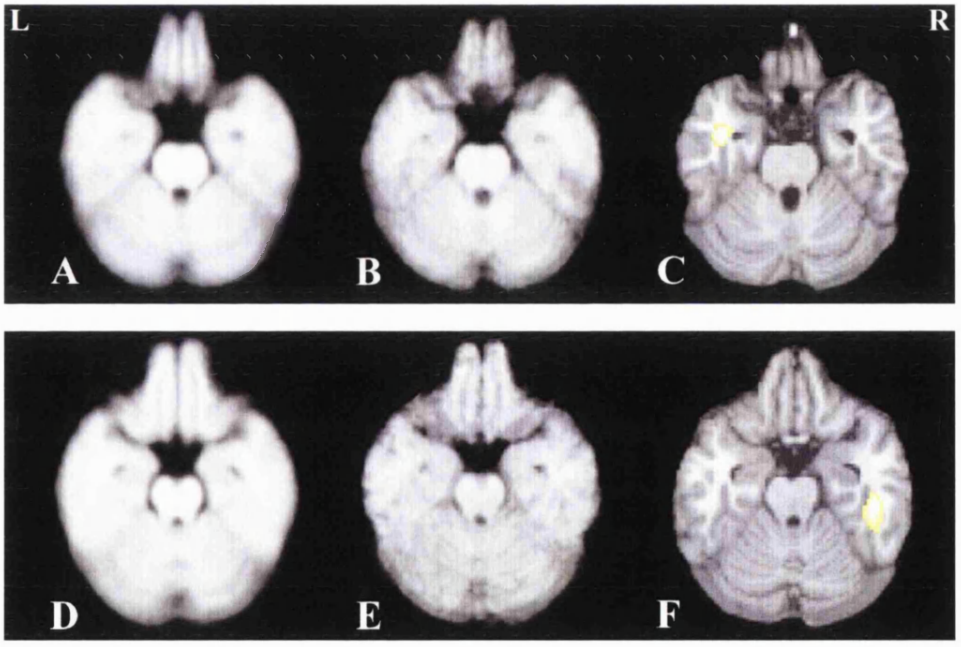

Figure 4.5: Left and right temporal lobe epilepsy (TLE) groups with normal conventional MRI.
Normalised axial MTR maps at the same slice position for the averaged 30 control subjects (A and D) and the MRI-negative patients with left TLE (B) and the MRI-negative patients with right TLE (E). The regions of decreased MTR are superimposed on normalised T1-weighted SPM templates at the same slice position ((C) and (F) respectively). These regions are localised to each respective lobe. The regions in (C) and (F) were used for quantitative region-of-interest analyses of MTR values. Note that right on the image is patients' right.

4.1.5.1 Methodological considerations and limitations

MTR is not an absolute measure, but is highly dependant upon the chosen imaging parameters. These include the bandwidth, shape, power and frequency offset of the MT pulse, inter-pulse interval, and the presence of direct saturation effects on the "free" water resonance (Silver, Barker, and Miller 1999). MTI is also affected by patient motion which may require additional, corrective pre-processing steps (Hajnal *et al.* 1997). This is to ensure accurate and reliable quantitative MTR results are obtained, particularly where image intensity is varying rapidly with position, for example, in small lesions. Assuming that there is no significant movement over the time required to collect one complete phase encode step (typically a few seconds) interleaved MR sequences result in exact coregistration of images (Barker, Tofts, and Gass 1996). These sequences, particularly MTI, are however, inherently time-inefficient as delays occur whilst the MT effect builds and diminishes between each slice. Interleaved high resolution MTI with satisfactory slice-coverage in a time suitable for clinical studies is therefore not possible. Our alternative approach was to acquire two image data sets consecutively (MT-weighted and non-MT-weighted) (Boulby, Symms, and Barker 2000). This was time efficient but sensitive to positional changes occurring between the acquisition of the separate images (several minutes). Coregistration of these data sets was therefore required, and accurate translation of these images and subsequent correct calculation of the MTR map was facilitated by the 3-dimensional data acquisition method (Hajnal *et al.* 1997).

Recently, it has been suggested that the cluster extent threshold is statistically invalid with voxel based analysis techniques, particularly voxel based morphometry (analysis of grey matter volume) because of a high false positive rate (Ashburner and Friston 2000). This is thought to be due to the non-stationary, non-Gaussian nature of the grey matter data. MTR data however, closely resembles a Gaussian distribution and furthermore, our control subject analyses confirm the validity of using both an individual voxel intensity threshold and a cluster extent threshold for a voxel based analysis of MTR maps as the number of abnormalities seen fell below that expected by chance. We believe therefore that the limitations of using the cluster extent threshold in voxel based morphometry do not compromise the analysis of MTR data.

4.1.5.2 Pathophysiological and clinical implications

The degree of magnetisation transfer (MT) within a tissue is governed principally by the local concentration of macromolecules. Loss of macromolecules, such as in demyelination or axonal degeneration results in a reduced MT effect, and consequently an area of decreased MTR. In addition, characteristics such as the biophysical dynamics or the surface chemistry of macromolecules are also important. Macromolecules are therefore not equally effective in modulating MT (Koenig 1991; Fralix *et al.* 1991; Koenig *et al.* 1990; Kucharczyk *et al.* 1994). Mature white matter possesses a greater MTR than grey matter or developing white matter due to relative concentrations of sphingomyelin, cholesterol and in particular galactocerebrosides which exhibit a considerable MT effect due to the presence of four hydroxyl groups (Kucharczyk *et al.* 1994; Morell, Quarles, and Norton 1989). Other possible explanations for a high MTR in white matter include differences in neuronal density, iron deposition, and tissue hydration and vascularity (Elster *et al.* 1994a; Silver *et al.* 1997a).

Abnormalities of MTR have been correlated with histopathological changes in both experimental and clinical

settings. Lexa et al demonstrated a relationship between MTR abnormalities and degree of histological change in a study of Wallerian degeneration in the feline visual pathway. Axonal loss, gliosis and demyelination were paralleled by a gradual reduction in MTR (Lexa *et al.* 1994). In guinea pigs with experimental auto-immune encephalomyelitis (EAE) there was oedema and minimal demyelination, and a reduction in MTR of approximately 5-8% (Dousset *et al.* 1992). Intralesional MTR was reduced by approximately 26% in patients with MS, suggesting that demyelination affects MTR more profoundly than tissue oedema (Dousset *et al.* 1992). Reduced MTR also correlated with the degree of demyelination and percentage of residual axons, even in white matter that appeared normal on conventional MRI (van Waesberghe, Kamphorst, and van Walderveen 1998; van Waesberghe, Kamphorst *et al.* 1999). MTI appears, therefore, to be sensitive to changes in the structural integrity of cerebral tissue, particularly demyelination and axonal loss may reduce MTR, although inflammation and oedema can also contribute (Brochet and Dousset 1999).

Chronic, non-progressive acquired lesions are an important cause of refractory focal epilepsy and are often associated with MR-visible structural abnormalities. In our study MTR abnormalities were identified within regions of injury in each patient. Moreover, in three patients, (patients 2, 3 and 8) abnormalities were also detected in areas of the brain that were previously reported as normal suggesting loss of structural integrity secondary to occult cerebral damage.

Severe blunt head trauma is associated with oedema, petechial and frank haemorrhage, diffuse axonal injury, ischaemia and later, gliosis (Adams 1992). MTI has been shown to be more sensitive than conventional imaging in the detection of histologically proven diffuse axonal injury (Kimura *et al.* 1996; McGowan *et al.* 1999). In a number of studies of head injury in humans, MTR abnormalities have been identified in both lesional and extra-lesional regions (Bagley *et al.* 2000; McGowan *et al.* 2000; Sinson *et al.* 2001). In the 4 patients with head injury, reduced MTR was identified in all the patients within regions of known cerebral damage. Furthermore, patients 2 and 3 had areas of reduced MTR within normal appearing tissue, and had the most significant disability as a result of the initial head injuries. This finding concurs with previous studies where the presence of MTR changes in normal appearing tissue have been associated with a worse neurological and neuropsychological outcome (Bagley *et al.* 2000; McGowan *et al.* 2000).

Reduced MTR has previously been reported in chronic ischaemic lesions (Mehta, Pike, and Enzmann 1996; Kovacs *et al.* 1997) corresponding to gliosis, neuronal loss and expansion of extracellular space (Castillo *et al.* 1996; Braffman *et al.* 1988). Furthermore, MTR values fall with increasing age of the infarct. In the present study, in all three patients with partial seizures secondary to mature infarcts (patients 5 - 7), MTR was reduced within each lesion.

Three patients with acquired lesions had conventional MR imaging and a clinical history compatible with focal encephalitis. In each patient, reductions of MTR were seen within lesional areas, consistent with known histopathological changes of tissue loss, dystrophic calcification and gliosis (Jay *et al.* 1998). MTR abnormalities have previously been reported in patients with HIV encephalitis and herpes simplex encephalitis, both within the lesions and in normal appearing tissue (Dousset *et al.* 1997; Burke *et al.* 1996). In our patients with encephalitis, patient 8 had reduced MTR in tissue that was previously reported as normal, suggesting the presence of occult injury, and supporting the hypothesis that MTI is more sensitive to pathological change than conventional MRI.

Areas of significantly reduced MTR were detected in 13 out of 15 patients with MCDs; no abnormalities were identified in two patients with subependymal heterotopia (SEH). It is well established that grey matter has a

lower MTR than white matter (Mehta, Pike, and Enzmann 1995a). Therefore, a comparison of grey matter MTR values in patients, with white matter MTR values in control subjects will be identified by SPM as a significant reduction in MTR. This is the likely explanation for the results in patients with, for example, thickened cortices or ectopic grey matter.

Of greater interest, however, was the detection of abnormal MTR in areas of the brain that were normal on visual inspection of conventional MR images. Thirteen areas of abnormal MTR, in eight patients, were identified beyond the margins of the visible MCD.

These were in patients with gyral abnormalities and heterotopia, and were seen both adjacent to and in more distant sites. This concurs with previous histopathological, imaging and electroencephalographic studies in suggesting that MCD are often more extensive than the visible lesion (Palmini *et al.* 1995; Sisodiya *et al.* 1995b; Hammers *et al.* 2001; Richardson *et al.* 1996; Eriksson *et al.* 2001b).

Gyral abnormalities are characterised on MRI by a thickened cortex with shallow sulci, and frequently, underlying white matter signal abnormality which may represent hypomyelination (Barkovich, Chuang, and Norman 1988). Correspondingly, reduced MTR was detected within the visible lesions in all patients with gyral abnormalities. Interestingly, in 5 out of 6 patients, abnormal MTR was identified beyond the margins of the visible MCD suggesting the presence of occult dysgenetic tissue, or for MTR abnormalities in the corpus callosum, aberrant tract development. Agenesis of the corpus callosum is a recognized associated feature of the most severe forms of gyral abnormality (Harding 1992). In less affected cases, a reduction in the number of normal cortical neurones projecting transcallosal fibres may result in less dense myelination and a decreased MTR in this structure (Sisodiya and Free 1997). Also, axons projected from abnormal cortical neurons may be dysplastic and hypomyelinated (Marchal *et al.* 1989). The corpus callosum contains topographically organised fibres arising from different cortical regions (Pandya and Rosene 1985). Three out of the 6 patients with gyral abnormalities had reduced MTR within the corpus callosum; in each case the MTR abnormality was topographically appropriate for the site and extent of MCD. For example, transcallosal fibres arising from the perisylvian region have been shown to cross in the anterior-mid body of the corpus callosum (Pandya and Rosene 1985). Patient 13 had thickened, dysplastic gyri in the left perisylvian region on conventional MRI, and MTR abnormalities within the MCD itself and in the anterior-mid body of the corpus callosum.

Heterotopic grey matter is indistinguishable from normal grey matter on conventional MRI, the diagnosis being made on the basis of an abnormal location. It is histologically and functionally distinct however, with aberrant cytoarchitecture, abnormal neuronal positioning, attenuated and disordered dendrites and axons, and altered cytoskeletal elements (Manz *et al.* 1979; Duong *et al.* 1994; Barth 1987). The macromolecular environment is therefore distinct from normal tissue, and has previously been shown to possess different MTR values than normal grey matter (Sisodiya *et al.* 1996a). In the present study, seven out of nine patients with heterotopic grey matter had reduced MTR within the visible MCD. In addition, three patients had areas of reduced MTR and one patient (patient 18) had an area of increased MTR in normal-appearing tissue, again suggesting the presence of occult dysgenesis. The region of increased MTR was immediately anterior to an area of subcortical heterotopia. It is possible that normal white matter had been compressed, increasing the density of myelinated fibres, or displaced into an area of inherently low MTR, which on comparison with control subjects was highlighted as an area of elevated MTR. Alternatively, an increase in neuronal cell bodies within the white matter (Nordborg *et al.* 1999; Kasper *et al.* 1999; Hardiman *et al.* 1988), or an elevated concentration of neurofilament or microtubule associated

proteins (Duong *et al.* 1994; Yamanouchi *et al.* 1996), may increase the availability of magnetisation exchange sites and increase MTR values.

Decreased MTR within normal-appearing brain in patients with MCD may result from a loss of tissue density due to either impaired neurogenesis, dysmyelination, or subsequent cell loss. It has been shown that in MCDs, there is a relative reduction in white matter, consistent with neurones projecting thinner axons (Sisodiya *et al.* 1995b), altered axonal or dendritic arborisation (Mitchison1991), or impaired myelination (Marchal *et al.* 1989). Furthermore, in grey matter, impaired neurogenesis and reduced axonal arborisation, resulting in loss of cortical density has been reported in experimental models of cortical dysplasia (Woo and Finlay 1996; Woo *et al.* 1996).

In two patients with subependymal heterotopia, no abnormality of MTR was identified. This may be due to limitations of the analysis method, in particular the position of the MCD with respect to the ventricles. Due to the variation in ventricular size amongst control subjects, it is possible that in tissue adjacent to the ventricles, due to a partial volume effect, there exists a wide range of "normal" MTR values. An area of heterotopia would therefore have to possess a particularly low MTR value for it to be identified as significantly different. Also, it is clear from recent neurogenetic studies that SEH is a heterogeneic condition, and it is therefore possible that different heterotopic nodules may display distinct cytoarchitectural and tissue characteristics resulting in a range of MTR values (Fox *et al.* 1998; Sisodiya *et al.* 1999).

Areas of significantly reduced MTR were identified in 15 of 42 MRI-negative patients. In 14 of these, the regions concurred with the localisation of epileptiform EEG abnormality, nine of which were ictal recordings. In four of the 15 patients, ictal recordings were not available and in one patient (patient 29), the area of reduced MTR concurred with the interictal abnormality, but not the scalp EEG ictal changes. In one patient (patient 40, left frontal lobe epilepsy), both ictal and interictal EEG data were unhelpful and clinical seizure semiology provided localising information that was concordant with MTR data. Overall, therefore, all areas of reduced MTR in MRI-negative patients concurred with EEG epileptiform abnormality or, if not available, clinical seizure semiology. Abnormalities, which similarly concurred with electroclinical localising information, were also seen on analysis of the proton density weighted images of two patients. These findings may be explained by the presence of occult focal atrophy, possibly as a result of chronic seizures or defective neurogenesis. MTR abnormalities in each case were more extensive than the regions of abnormal PD suggesting that the extent of microstructural abnormality extended beyond subtle volume loss.

The areas of significantly reduced MTR in the MRI-negative patients, both on an individual basis and when grouped, are most likely caused by a disruption in the macromolecular environment due to aetiological factors such as, occult dysgenesis or acquired damage, or as a result of repeated seizures, for example, atrophy, gliosis, and neuronal loss. These patients are being evaluated for surgical treatment; pathological material is not yet available. Previous histopathological studies of surgically resected epileptic foci which appeared normal on MRI have shown features of white matter gliosis, focal cortical dysplasia, microdysgenesis, impaired cortical lamination, and subcortical laminar heterotopia (Theodore *et al.* 1990; Zentner *et al.* 1995; Palmini *et al.* 1991b; Spreafico *et al.* 1998; Ying *et al.* 1998). A number of clinical and experimental studies in other neurological conditions have reported MTR abnormalities in macroscopically or radiologically normal cerebral tissue despite microscopic pathological features of diffuse axonal injury, gliosis, hypomyelination, astrocytic hyperplasia, or perivascular infiltration (van Waesberghe *et al.* 1999; McGowan *et al.* 1999; Adams 1977; Allen and McKeown

1979). This emphasizes the enhanced sensitivity to pathological change that MTI possesses over conventional MRI and supports the hypothesis that in patients with focal epilepsy and normal conventional MRI, MTI may identify similar occult structural abnormalities.

Although the significant group effects seen in the MRI-negative patients with left and right temporal lobe, and left frontal lobe epilepsy are not clinically useful for evaluating individual patients, it suggests that given greater sensitivity, an effect in additional individual patients may be demonstrated. Furthermore, it is likely that our positive findings in individual patients represent the most structurally abnormal of all the MRI-negative patients and with improvements in magnetisation transfer imaging further occult epileptogenic regions may be identified, which may guide invasive diagnostic procedures and possible epilepsy surgery.

CHAPTER FIVE

T2-Mapping

5.1 T2 MAPPING IN FOCAL EPILEPSY

5.1.1 Summary

Whole brain T2-mapping and Statistical Parametric Mapping (SPM99) was used to objectively examine the cerebral structure of 14 patients with partial seizures and acquired lesions, 20 patients with malformations of cortical development (MCD), and 45 patients with partial seizures and normal conventional MRI. T2 maps were calculated and, using SPM, individual patients were compared to a group of 30 control subjects.

T2-mapping and objective voxel-by-voxel statistical comparison identified regions of significantly increased T2 signal in all 14 patients with acquired nonprogressive cerebral lesions and partial seizures. In all of these the areas of increased T2 signal concurred with abnormalities identified on visual inspection of conventional MRI. In 18 out of the 20 patients with MCD, SPM detected regions of significantly increased T2 signal; all of which corresponded to abnormalities identified on visual inspection of conventional MRI. In addition, in both groups, there were areas that were normal on conventional imaging, which demonstrated abnormal T2 signal. Voxel-by-voxel statistical analysis identified a significantly increased T2 signal in 23 of the 45 patients with cryptogenic focal epilepsy. In 20 of these, the areas of increased T2 signal concurred with epileptiform EEG abnormality and clinical seizure semiology. Group analysis of MRI-negative patients with electroclinical seizure onset localising to the left and right temporal and left and right frontal regions revealed significantly increased T2 signal within the white matter of each respective lobe.

T2-mapping analysed using SPM was sensitive in patients with MCDs and acquired cerebral damage. Significant increases in T2 signal in individual and grouped MRI-negative patients suggest that minor structural abnormalities exist in occult epileptogenic cerebral lesions. T2-mapping is, therefore, a useful quantitative MRI technique for characterising potentially epileptic foci and may contribute to presurgical evaluation.

5.1.3 Introduction

Conventional MRI consists of a combination of proton density, T1 and T2-weighted sequences. T2-weighted imaging is sensitive for the identification of pathological change (Smith *et al.* 1985) and T2 relaxation is governed by both the total amount of water and the ratio of free to bound water, which is itself dependent on the macromolecular environment. A disturbance to this environment, such as neuronal loss or demyelination, results in an increase in free water, with a longer T2 relaxation time and greater signal intensity on a T2-weighted image. An increase in bound water, or the presence of a paramagnetic substance, for example, deoxyhaemoglobin, shortens the T2 relaxation time and reduces signal intensity on T2-weighted images (Georgiades *et al.* 2001). Quantitative evaluation of T2-weighted images is more sensitive and objective than visual assessment for the identification of subtle cerebral pathology (Jackson *et al.* 1993b; Barbosa *et al.* 1994). Region-of-interest based analyses in the neocortex are susceptible to placement bias and partial volume effects. This latter limitation is, at least partly,

overcome by using thin slices and sequences which suppress the signal from cerebrospinal fluid, such as fluid attenuated inversion recovery (FLAIR) imaging (Jackson *et al.* 1990). Further, objective voxel-based methods are able to evaluate the whole brain without bias (Melki *et al.* 1991; Mulkern *et al.* 1990). The aim of this study was to evaluate whether T2-mapping of the entire neocortex, analysed on a voxel-by-voxel basis, would identify areas of abnormal T2 signal in patients with epileptogenic malformations of cortical development, non-progressive acquired lesions, and in patients with partial seizures and normal conventional MRI.

5.1.3 Methods

5.1.3.1 Subjects

- 30 healthy control subjects :
  - 16 men, median age 33 years, range 20-51 years

- 79 patients with focal epilepsy

  Acquired

  - 14 patients (11 men median age 40 years, range 21-56 years, median duration of epilepsy 27 years, range 3-49 years)

    4 patients with ischaemic lesions

    4 patients with head injuries

    3 patients with a history of encephalitis

    3 patients with a history of perinatal injury

  Malformations of cortical development

  - 20 patients (10 men, median age 32 years, range 18-54 years, median duration of epilepsy 22 years, range 4-39 years)

    4 patients with gyral abnormalities

    5 patients with focal cortical dysplasia

    11 patients with heterotopia

    subependymal (n=3), subcortical nodules (n=3) and band heterotopia (n=5)

    1 patient with a dysembryoplastic neuroepithelial tumour

  One patient had both band heterotopia and a gyral abnormality (patient 18)

  MRI-negative

  - 45 patients (21 men, median age 36 years, range 21-58 years, median duration of epilepsy 18 years, range 2-48 years)

    23 were diagnosed with temporal lobe epilepsy (12 left, 11 right)

    12 with frontal lobe epilepsy (5 left, 7 right)

    10 had electroclinical evidence of less well defined, more widespread abnormalities

5.1.3.2 T2-mapping

Fast fluid attenuated inversion recovery (FLAIR) dual-echo data sets were acquired on a 1.5T Horizon Echospeed scanner (G.E, Milwaukee, Wisc., USA) using a standard quadrature head coil (TR/TE/TI =5000/15,120/1638ms). Twenty-eight contiguous axial slices were obtained with an acquisition matrix of 256x256 and a 24cm field-of-view, giving a resolution of 0.94 x 0.94 x 5mm. Total scanning time for T2-mapping was 11 minutes and 40 seconds.

5.1.3.3 Analysis

Following data acquisition, the images were transferred to an off-line workstation (Sun Microsystems, Palo Alto, CA) for post-processing. Using the dual-echo data sets (one set from the early echo (TE_1) and one from the late echo (TE_2)) T2 signal intensity was calculated pixel-by-pixel according to the equation:

$$T2\ signal = (TE_2 - TE_1) / \ln (S_1 / S_2)$$

where S_1 and S_2 represent the signal intensities for the early and late echoes respectively.

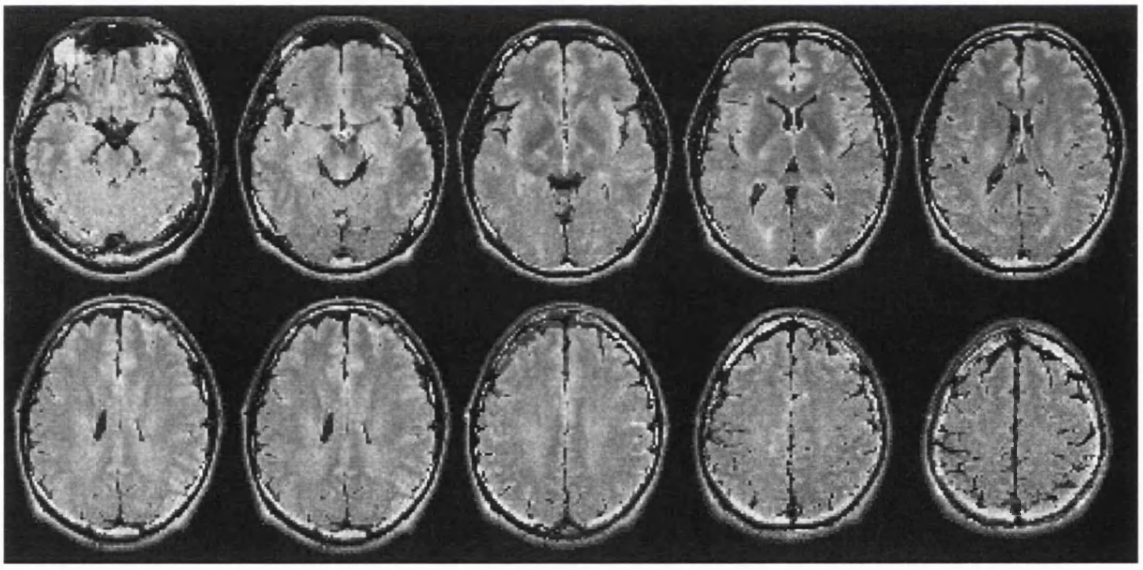

Figure 5.1: Series of normalized axial T2 maps from a single control subject

To allow objective voxel-by-voxel statistical comparisons to be made, all T2 maps were normalised to a standard template using SPM 99 (Wellcome Dept of Imaging Neuroscience, Institute of Neurology, London, UK) (Okujava *et al.* 2002). This template was created by normalising and then averaging 15 of the 30 control subjects' T2 maps to standard SPM space using 12 linear degrees of freedom and a 7x8x7 non-linear warp. Fifteen control subjects, representing the entire age range of both the control subjects and patients, were used to create the template, as the application of a template matched to the study population has been shown to improve the normalisation process (Good *et al.* 2001b). Subsequently the T2 maps of the patients and all 30 controls were normalised to this template using linear steps with 12 degrees of freedom (translation, rotation, zoom and shear) and a 7x8x7 non-linear warp (figure 5.1). The use of non-linear normalisation steps allowed global and regional anatomical differences to be minimised, thus allowing a meaningful comparison, without adversely affecting differences in signal intensity.

Prior to statistical analysis, the normalised maps were smoothed with a 4mm isotropic Gaussian kernel. In addition a signal intensity threshold was set at 0.5 to reduce the number of extraneous pixels in the T2 maps included within the analysis; that is, only voxels with values exceeding 50% of the total image mean intensity were analysed. This procedure excluded very low T2 values that arose principally from outside the brain.

The smoothed, normalized maps were statistically analysed on a voxel-by-voxel basis, and inferences made from the resultant maps, as described in Chapter 2.3 *Common methodology: Post-acquisition processing.* Region-of-interest analyses were also performed in order to illustrate the magnitude of the differences in T2 values in areas highlighted by the SPM comparison as deviating significantly from normal. This approach also ensured that areas of inadequately suppressed CSF in deep sulci were not misclassified as increased cortical T2. Furthermore, we were able to exclude regions of apparently decreased cortical T2 that arose as a result of a partial volume effect from fully suppressed CSF.

5.1.4 Results

5.1.4.1 Control group

Comparing each control subject with the remaining 29 control subjects using identical parameters and statistical thresholds as the comparison between patients and controls, three subjects had areas of significantly abnormal T2 signal. At a statistical threshold of $p<0.05$ and 60 examinations (30 subjects with two "contrasts" each (an increase and a decrease)), up to three abnormal areas were anticipated by chance alone.

5.1.4.2 Acquired Lesions

In all fourteen patients with acquired lesions, SPM detected areas of significantly increased T2 signal (table 5.1). In all patients the areas of increased T2 signal corresponded to the abnormalities identified on visual inspection of the conventional MR images (figure 5.2). In nine patients (patients 1, 2, 4, 6, 8, 9, 10, 13 and 14) areas of significantly increased T2 signal were detected in regions previously reported as normal. Quantification in regions-of-interest was performed on patients 4, 8 and 14 (see table 5.4). There were no areas of shortened T2 times.

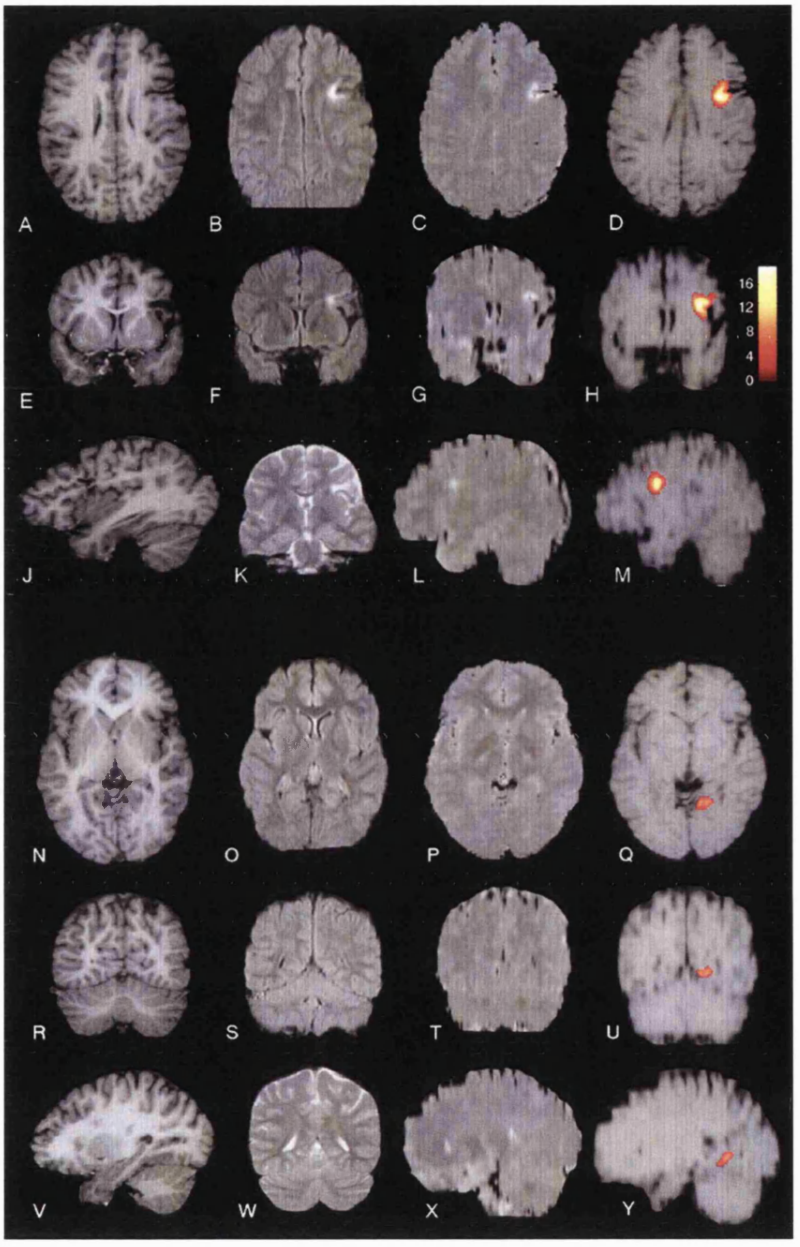

Figure 5.2: Patient 8, mature cortical infarct in right frontal lobe.

(**A**, **E**, **J** and **N**, **R**, **V**) Axial, coronal, and sagittal T1-weighted images. (**B**, **F** and **O**, **S**) Axial and coronal FLAIR images. (**K** and **W**) T2-weighted coronal images. (**C**, **G**, **L** and **P**, **T**, **X**) Axial, coronal, and sagittal T2 maps (**D**, **H**, **M** and **Q**, **U**, **Y**) Regions of significantly increased T2 superimposed on axial, coronal, and sagittal early-echo (proton-density weighted) images. These regions were used for quantitative region-of-interest analyses on the T2 maps (Table 5.4). The regions in **D**, **H**, **M** coincide with the localisation of the abnormalities identified on conventional MRI. The regions in **Q**, **U**, **Y** localized to the normal appearing cerebral tissue of the right lingual gyrus. Z-value bar indicating degree of significance of highlighted regions is shown. Note that right on the images is patient's right.

Table 5.1 Clinical characteristics, EEG, MRI and T2 mapping results in patients with non-progressive acquired lesions

Patient	Age (yr)	Sex	Aetiology of epilepsy	Seizure Types	Duration of epilepsy (yrs)	EEG features	Conventional MRI findings	T2 mapping Significantly increased T2 times (*P*-value)
1	31	M	head injury	2° gen.	11	bil. frontotemp. i.e.a.	bil. front., R. temp, posterior corpus callosal damage	bil. front. WM, R. temp. WM, post. CC + NA L. temp. WM (p<0.001)
2	51	M	head injury	CPS, 2° gen.	48	L. temp.par. + R. frontocentral i.e.a.	superficial atrophy of L. hemisphere, sparing temp.	L. front.temp.par WM + in NA R. front. WM (p<0.001)
3	40	M	head injury	CPS, 2° gen.	3	widespread bilateral i.e.a.	L. parietal lobe damage	L. par. subcortical WM (p<0.01)
4	31	F	head injury	CPS, 2° gen.	17	R. front.temp.+ minor L. front i.e.a	R. front. temp. par. damage	R. front.temp.par. W+GM + in NA L. front.temp. W+GM (p<0.001)
5	40	M	infarction	CPS, atonic.	31	bifrontal ictal foci	bil. front. par. occ damage	bil. front. par. occ WM (p<0.001)
6	56	F	infarction	CPS, 2° gen.	48	biparietal (R>L) i.e.a.	R. frontoparietal damage	R. front. par. W+GM + in NA L par. WM (p<0.001)

Patient	Age (yr)	Sex	Aetiology of epilepsy	Seizure Types	Duration of epilepsy (yrs)	EEG features	Conventional MRI findings	T2 mapping Significantly increased T2 times (*P*-value)
7	39	M	infarction	CPS, 2° gen.	36	R. front.temp.par. i.e.a.	R. temp.par.occ. ischaemic damage	R. temp. par. occ. G+WM (p<0.001)
8	21	F	infarction	CPS, 2° gen.	12	R. hemisphere i.e.a., esp front.temp. region	R. lat. front. cortical scar	R. lat. front. W+GM + in NA R. lingual gyrus (p<0.01)
9	42	M	perinatal injury	CPS, 2° gen.	42	L. hemisphere, esp. L. temp. i.e.a.	L. frontal lobe + L. hippocampal damage	L. frontotemp. W+GM + L. HC + NA R. periventricular WM (p<0.001)
10	24	M	perinatal injury	S+CPS, 2° gen.	23	bil. frontotemp. (R>L) i.e.a	L. front.temp.par ischaemic damage	L. front.temp.par W+GM + NA R. front. WM (p<0.001)
11	55	M	perinatal injury	CPS	49	R. temp. i.e.a	diffuse signal change in bil. post. WM	bil. post. WM. (p<0.001)
12	52	M	encephalitis	CPS, 2° gen.	12	bihemispheric i.e.a	L. temp + L. occ. + minor R. temp. damage	L. front. + temp. + occ. W+GM + R. frontotemp. WM (p<0.001)
13	44	M	encephalitis	CPS	35	bihemispheric, esp. R. temp. i.e.a.	L. parietal + L. HC damage	L. temp.par. WM + L. HC + NA R. temp. WM (p<0.001).

Patient	Age (yr)	Sex	Aetiology of epilepsy	Seizure Types	Duration of epilepsy (yrs)	EEG features	Conventional MRI findings	T2 mapping Significantly increased T2 times (*P*-value)
14	26	M	meningitis	CPS, 2° gen.	15	L > R frontotemp. i.e.a.	L. temporal lobe damage	L. temp W+GM + in NA R. HC + R. front. WM ($p<0.001$)

R.=Right; L.=Left; bil.=bilateral; post.=posterior; med.=medial; lat.=lateral; front.=frontal; par.=parietal; temp.=temporal; occ.=occipital; HC=hippocampus; i.e.a..=interictal epileptiform activity; M=male; F=female; SPS=simple partial seizure; CPS=complex partial seizure; 2° gen.=secondarily generalised tonic-clonic seizure; NA=normal appearing; WM=white matter; GM=grey matter

Table 5.2 Clinical characteristics, EEG, MRI and T2 mapping results in patients with malformations of cortical development

Patient	Age (yr)	Gender	Seizure Types	Duration of epilepsy (yrs)	Interictal EEG features	Conventional MRI findings	T2 mapping Significantly increased T2 times (*P*-value)
15	52	M	CPS, 2° gen.	39	R. hemisphere i.e.a	R front. + bil. par. occ. gyral abn. with thick cortex	bil. in MCD + in NA L. front. lobe GM + subcort. WM ($p<0.001$)
16	26	F	SPS, CPS + tonic	22	widespread i.e.a., max. L. hemisphere	bil. frontopar. gyral abn. with thick cortex	bil. frontopar. regions in MCD ($p<0.001$)
17	46	M	CPS, 2° gen.	38	L. hemisphere. i.e.a	L. frontopar. gyral abn. with thick cortex	L. frontopar. region in MCD ($p<0.001$) + in NA R. frontopar. GM ($p<0.05$)
18	28	M	S + CPS, 2° gen.	20	widespread i.e.a., max. L. temp.	bil. BHT + bil. temp. gyral abn. with thick cortex	bil. hemisphere in BHT + bil. temp. in gyral abn. ($p<0.001$)
19	28	F	SPS, 2° gen.	17	normal interictal	bil. band heterotopia	None
20	32	F	S + CPS, 2° gen.	27	widespread i.e.a	bil. band heterotopia	bil. hemisphere in MCD ($p<0.001$)
21	37	F	S + CPS, 2° gen.	25	bil. hemisphere i.e.a.	bil. band heterotopia	R. front. in MCD ($p<0.001$)

Patient	Age (yr)	Gender	Seizure Types	Duration of epilepsy (yrs)	Interictal EEG features	Conventional MRI findings	T2 mapping Significantly increased T2 times (*P*-value)
22	24	F	CPS, 2° gen.	15	bil. hemisphere i.e.a.	bil. band heterotopia	bil. hemisphere in MCD ($p<0.01$)
23	51	F	CPS, 2° gen.	35	normal interictal	bil. SCH	bil. hemisphere in MCD ($p=0.001$)
24	54	M	2° gen.	23	normal interictal	R. par. SCH	R. par. in MCD ($p=0.001$)
25	19	F	CPS	4	bil. frontotemp i.e.a	L. frontal + L. insula SCH	L. front. + L. temp. in SCH ($p<0.001$) + in NA R. frontotemp. WM ($p<0.001$)
26	47	F	CPS	36	L. hemisphere, max. L. front. i.e.a	bil. temp. + par. SEH	None
27	18	F	CPS, 2° gen.	9	R. frontotemp. i.e.a	bil. SEH	R. hemisphere in MCD ($p<0.001$)
28	28	M	2° gen.	4	normal	bil. SEH	L. front. temp. par. in MCD + in NA R. temp. WM ($p<0.001$)
29	30	M	SPS, CPS	24	L. frontotemp. i.e.a.	L. front. temp. FCD	L. front. temp. in FCD ($p<0.001$)
30	51	M	S + CPS, 2° gen.	45	bifrontal + R. temp. i.e.a.	R. temp. FCD	R. temp. in FCD ($p<0.001$)

Patient	Age (yr)	Gender	Seizure Types	Duration of epilepsy (yrs)	Interictal EEG features	Conventional MRI findings	T2 mapping Significantly increased T2 times (*P*-value)
31	33	M	CPS, 2° gen.	32	bil. hemisphere i.e.a.	R. frontal (superior convexity) FCD	R. front. in FCD ($p<0.05$) + in NA R. mesial temp. lobe structures ($p<0.01$)
32	44	M	CPS, 2° gen.	32	R. frontal i.e.a.	R. front. pole FCD	R. front. pole in FCD + in NA L. par. WM ($p<0.001$)
33	22	F	CPS, 2° gen.	15	R. temp. i.e.a.	R. front. temp. par FCD	R. front. temp. par in FCD ($p<0.001$)
34	39	M	SPS, 2° gen.	15	R. hemisphere i.e.a	R. front. DNET	R. front. in DNET ($p<0.001$) + in NA R. front WM [also *decreased* T2 within DNET] ($p<0.001$)

R.=Right; L.=Left; bil.=bilateral; ant.=anterior; post.=posterior; mid.=middle; lat.=lateral; front.=frontal; par.=parietal; temp.=temporal; occ.=occipital; NA=normal-appearing; corp.=corpus; MCD=malformation of cortical development; BHT=band heterotopia; SEH= subependymal heterotopia; SCH=subcortical heterotopia; i.e.a..=interictal epileptiform activity; abn.=abnormality; M=male; F=female; SPS=simple partial seizure; CPS=complex partial seizure; 2° gen.=secondary generalised tonic-clonic seizure; inc.=increased; WM=white matter; GM=grey matter

Table 5.3 Clinical characteristics, EEG and T2 mapping results in patients with normal conventional MRI.

Patient	Age (yr)	Gender	Aetiology of epilepsy	Duration of epilepsy (yrs)	Seizure types	Ictal Epileptiform Abnormality	Interictal Epileptiform Abnormality	T2 mapping Significantly increased T2 times (*P*-value)
35	40	F	feb. convulsion	36	CPS, 2° gen.	R. temp.	R.> L. temp.	R. temp. (Heschl's gyrus) ($p<0.001$)
36	36	M	cryptogenic	18	SPS, CPS	N/A	R. temp.	R. mesial temp.structures ($p<0.001$)
37	25	M	cryptogenic	6	CPS	R. temp.	bil. temp. L>R	None
38	21	F	cryptogenic	20	CPS, 2° gen.	N/A	R. temp.	R. temp. occ. GM + subcort. WM ($p<0.05$)
39	31	F	cryptogenic	23	CPS	N/A	R. temp.	bil. frontotemp. ($p<0.05$)
40	45	M	meningitis	29	CPS, 2° gen.	R. temp.	bil. temp. R>L	R. temp. WM ($p<0.01$)
41	44	F	cryptogenic	32	CPS, 2° gen.	R. temp.	bil. temp. R>L	R. mesial temp.structures ($p=0.001$)
42	42	F	cryptogenic	10	S + CPS, 2° gen.	R. temp.	R. temp.	None
43	58	M	cryptogenic	2	CPS	R. temp.	bil. temp.	None
44	30	F	cryptogenic	14	CPS	N/A	R. temp.	R. middle temp. gyrus ($p=0.01$)

Patient	Age (yr)	Gender	Aetiology of epilepsy	Duration of epilepsy (yrs)	Seizure types	Ictal Epileptiform Abnormality	Interictal Epileptiform Abnormality	T2 mapping Significantly increased T2 times (*P*-value)
45	47	F	cryptogenic	31	CPS, 2° gen.	R. temp.	R. temp.	None
46	38	F	cryptogenic	15	CPS, 2° gen.	L. temp.	L temp	None
47	56	M	cryptogenic	36	CPS, 2° gen.	L. temp.	L. temp.	None
48	51	F	cryptogenic	9	CPS, 2° gen.	L. temp.	normal	R. mesial temp.structures + corpus callosum. (p<0.05)
49	21	M	cryptogenic	15	SPS, 2° gen.	L. temp	bil. temp. L>R	L. temp. (Heschl's) + R. temp WM (p<0.01)
50	38	F	cryptogenic	35	CPS, 2° gen.	L. temp.	L. temp	None
51	32	M	cryptogenic	11	CPS, 2° gen.	N/A	L. temp.	None
52	45	F	cryptogenic	30	CPS	L. temp.	L. temp.	None
53	31	M	cryptogenic	16	SPS, CPS	L. temp.	L. temp.	R. mesial temp. (p=0.001) [L. temp. = ns]
54	29	M	encephalitis	18	S + CPS, 2° gen.	N/A	L. temp.	bil. frontotemp (p<0.001)
55	54	F	cryptogenic	14	CPS, 2° gen.	L. hemisphere	L. temp.	L. periventricular WM (p<0.001)

Patient	Age (yr)	Gender	Aetiology of epilepsy	Duration of epilepsy (yrs)	Seizure types	Ictal Epileptiform Abnormality	Interictal Epileptiform Abnormality	T2 mapping Significantly increased T2 times (*P*-value)
56	32	F	cryptogenic	18	S + CPS, 2° gen.	L. temp.	L.temp.	bil. mesial temp. structures ($p<0.01$)
57	57	F	cryptogenic	48	CPS, 2° gen.	N/A	L. temp.	None
58	27	F	cryptogenic	13	SPS, 2° gen.	N/A	clinically - R. front.	bil. inferior frontal gyri ($p=0.01$)
59	41	M	cryptogenic	23	CPS	N/A	R. front.	None
60	36	F	cryptogenic	12	CPS	N/A	clinically - R. front.	R. front. gyrus rectus ($p<0.05$)
61	28	M	cryptogenic	15	CPS, 2° gen.	bil. front. R>L	R. front.	None
62	32	M	cryptogenic	2	SPS + CPS	R. hemisphere	R. front.	R. front. WM ($p<0.001$)
63	28	M	cryptogenic	12	CPS, 2° gen.	N/A	R.front.	None
64	53	M	cryptogenic	40	CPS, 2° gen.	N/A	R. front.	bil. par. occ WM ($p<0.001$) [also *dec* T2 in L. int. capsule ($p<0.001$)]
65	41	M	cryptogenic	19	2° gen.	N/A	L. front.	None

Patient	Age (yr)	Gender	Aetiology of epilepsy	Duration of epilepsy (yrs)	Seizure types	Ictal Epileptiform Abnormality	Interictal Epileptiform Abnormality	T2 mapping Significantly increased T2 times (*P*-value)
66	37	M	cryptogenic	32	CPS	N/A	L. front.	None
67	45	F	cryptogenic	38	CPS, 2° gen.	L. front.	L. front.	None
68	27	M	cryptogenic	15	CPS	L. front.	L. front.	None (but *dec* T2 in bil. cor radiata ($p<0.01$))
69	53	M	cryptogenic	10	CPS	inconclusive	L. front.	bil. front. WM ($p<0.001$)
70	31	M	cryptogenic	18	CPS, 2° gen.	bil. front	bil. front	bil. front. pole GM ($p<0.001$)
71	27	F	cryptogenic	17	CPS, 2° gen.	N/A	bil. front.	None
72	40	F	cryptogenic	35	CPS, 2° gen.	inconclusive	bil. temp.	None
73	48	M	cryptogenic	34	S + CPS, 2° gen.	widespread	bil. front.	None
74	35	F	cryptogenic	28	CPS, 2° gen.	bil. occ.	bil. occ.	R. occ. WM ($p=0.01$)
75	22	F	cryptogenic	5	S + CPS, 2° gen.	inconclusive	bil. hemipshere	L. mesial temp. structures. + R. par. WM ($p<0.001$)
76	27	M	neonatal illness	27	CPS, 2° gen.	R hemisphere	R. hemisphere	R. insula cortex. + R. occ. WM ($p<0.001$)

Patient	Age (yr)	Gender	Aetiology of epilepsy	Duration of epilepsy (yrs)	Seizure types	Ictal Epileptiform Abnormality	Interictal Epileptiform Abnormality	T2 mapping Significantly increased T2 times (*P*-value)
77	26	F	feb. convulsion	21	CPS, 2° gen.	L. hemisphere	bil. hemisphere	L. sup. temp. gyrus. ($p<0.05$)
78	40	F	cryptogenic	33	CPS	N/A	L. frontotemporal	None
79	30	F	cryptogenic	25	CPS, 2° gen.	inconclusive	bil. frontotemp.	None

S/CPS=simple/complex partial seizure; 2° gen =generalised seizure; R.=Right; L.=Left; bil.=bilateral; front.=frontal; par.=parietal; temp.=temporal; occ.=occipital; ant.=anterior; inf.=inferior; sup.=superior; paraHC=parahippocampal; N/A=not available; M=male; F=female; feb.=febrile; vacc.=vaccination; int. capsule=internal capsule; GM=grey matter; WM=white matter; subcort. WM=subcortical white matter; ns=statistically non-significant; dec=decreased

Table 5.4 T2 values from the regions-of-interest defined by SPM, in patients with acquired lesions, MCD, and normal conventional MRI.

Patient	Aetiology of epilepsy	EEG features	T2 mapping - SPM results	Region-of interest derived T2 times (msec)			
			Regions of significantly increased T2	Patient		Controls mean (SD)	% increase
Acquired							
4	head injury	R. front.temp.+	R. front. temp. par. +	R. front	114	88 (0.97)	29%
		minor L. front i.e.a	in NA L. front. temp.	L. front	100	86 (0.99)	16%
8	infarction	R. hemisphere esp.	R. lat. front.+	R. front	120	91 (1.07)	31%
		front.temp. i.e.a.,	in NA R. lingual gyrus	R. ling.	103	89 (0.77)	16%
14	meningitis	L > R frontotemp.	L. temp +	L. temp.	106	91 (1.06)	16%
		i.e.a.	in NA R. HC + R. front. lobe	R. HC	124	107 (0.90)	16%
MCD							
18	BHT + gyral	widespread i.e.a.,	bil. hemisphere in BHT +	R. band	101	88 (1.01)	15%
	abnormality	max. L. temp.	bil. temp. in gyral abn.	R. front gyral	104	89 (1.06)	17%
31	FCD	bil. hemisphere	R. front. in FCD +	FCD	103	92 (1.13)	12%
		i.e.a.	in NA R. mesial temp. lobe structures	R. HC	122	107 (0.97)	14%
34	DNET	R. hemisphere i.e.a.	R. front. in DNET +	DNET	115	89 (1.00)	29%
			in NA R. front WM	NA R. front	102	88 (1.05)	16%

Patient	Aetiology of epilepsy	EEG features	T2 mapping - SPM results Regions of significantly increased T2	Region-of interest derived T2 times (msec) Patient	Controls mean (SD)	% increase
Normal conventional MRI						
35	feb. convulsion	R. temp. focus	R. temp. (Heschl's gyrus)	110	90 (1.25)	22%
36	cryptogenic	R. temp. i.e.a.	R. mesial temp. lobe	114	97 (1.42)	18%
56	cryptogenic	L. temp. focus	bilateral mesial temp. lobes	left HC 126 right HC 119	110 (1.25) 105 (1.19)	15% 14%
60	cryptogenic	normal - clinically R. front	R. front. pole	105	84 (1.65)	25%
Group findings						
R. TLE gp. (n=11)	N/A	R. temp.	R. temp. WM	101 (1.63)	95 (0.96)	7%
R. FLE gp. (n=7)	N/A	R. front.	R. front. WM	91 (1.47)	86 (1.03)	6%

Patient	Aetiology of epilepsy	EEG features	T2 mapping - SPM results Regions of significantly increased T2	Region-of interest derived T2 times (msec) Patient	Controls mean (SD)	% increase
L. TLE gp. (n=12)	N/A	L. temp.	L. temp. WM	93 (1.52)	88 (1.19)	6%
L. FLE gp. (n=5)	N/A	L. front.	L. front. WM	92 (1.65)	86 (1.42)	7%

R.=Right; L.=Left; bil.=bilateral; post.=posterior; med.=medial; lat.=lateral; front.=frontal; par.=parietal; temp.=temporal; occ.=occipital; HC=hippocampus; i.e.a..=interictal epileptiform activity; M=male; F=female; SPS=simple partial seizure; CPS=complex partial seizure; 2^{o} gen.=secondary generalised tonic-clonic seizure; NA=normal appearing; FCD=focal cortical dysplasia; BHT=band heterotopia; DNET=dysembryoplastic neuroepithelial tumour; WM=white matter.

5.1.4.3 Malformations of Cortical Development

In 18 of the 20 patients with MCD, SPM detected regions of increased T2 (table 5.2). In all 18 patients, the areas of increased T2 signal corresponded to all or part of the MCD identified on visual inspection of the conventional MR images. In addition, in seven patients (patients 15, 17, 25, 28, 31, 32, and 34) changes were found outside the MCD in tissue that appeared normal on conventional MRI. One patient (patient 34) also had a region of significantly decreased T2 within a DNET.

Of the 20 patients with MCD, all four with gyral abnormalities (patients 15-18) and all five with FCD (patients 29-33) had areas of significantly prolonged T2 which corresponded to all or part of the MCD. In two patients with gyral abnormalities and in two with FCD, changes were also found in areas beyond the margins of the evident MCD, in areas that appeared normal on visual assessment of conventional T1- and T2-weighted images.

Areas of increased T2, which corresponded to the MCD identified on the conventional MR images, were seen in four out of five patients with band heterotopia (BHT) (patients 18-22), in two of the three patients with subependymal heterotopia (SEH) (patients 26-28), and in the three patients with subcortical heterotopia (SCH) (patients 23-25) (figure 5.3). One of the patients with SEH (patient 28) and one of the patients with SCH (patients 25) each had a region of increased T2 detected beyond the evident MCD.

Quantification in regions-of-interest was performed on patients 18, 31, and 34 (see table 5.4).

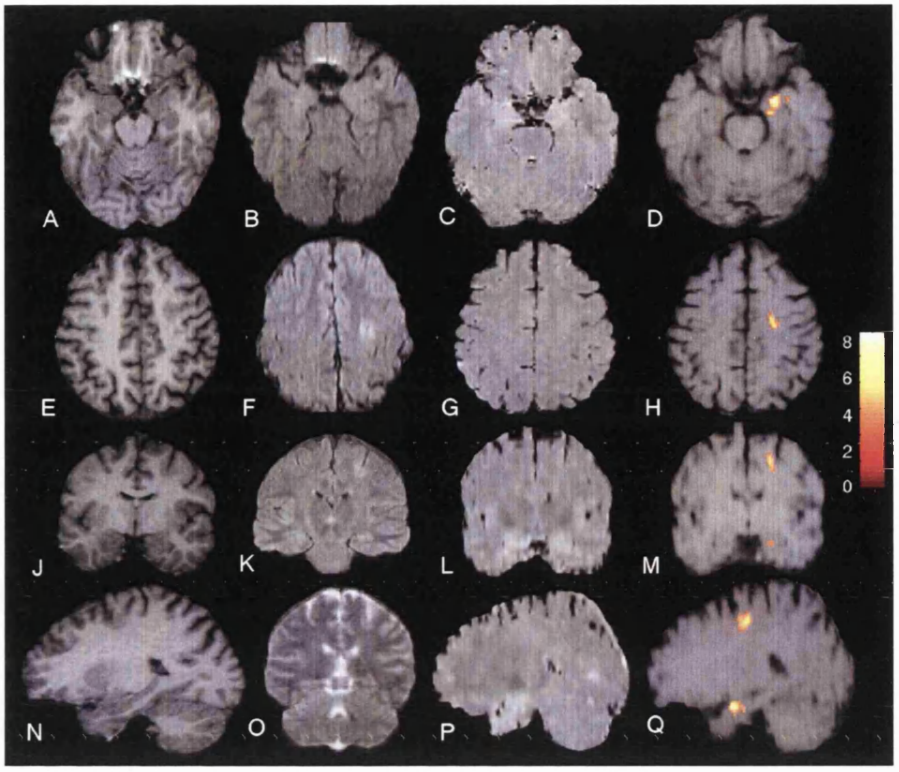

Figure 5.3: Patient 31. Right frontal (superior convexity) focal cortical dysplasia. (**A**, **E**, **J** and **N**) Inferior axial, superior axial, coronal, and sagittal T1-weighted images. (**B**, **F**, and **K**) Inferior axial, superior axial and coronal FLAIR images. (**O**) T2-weighted coronal image. (**C**, **G**, **L** and **P**) Inferior axial, superior axial, coronal, and sagittal T2 maps. (**D**, **H**, **M** and **Q**) Regions of significantly increased T2 superimposed on inferior axial, superior axial, coronal, and sagittal early-echo (proton-density weighted) images. These regions were used for quantitative region-of-interest analyses on the T2 maps (Table 5.4). The regions over the right superior frontal convexity coincide with the localization of the abnormalities identified on conventional MRI. The regions in the right mesial temporal lobe localized to normal appearing cerebral tissue. Z-value bar indicating degree of significance of highlighted regions is shown. Note that right on the images is patient's right.

5.1.4.4 MRI-negative patients

5.1.4.4.1 Individual SPM & Region-of-interest analyses

SPM analyses of the 45 individual patients in the MRI-negative group revealed 23 patients (51%) with regions of significantly increased T2 compared to the control group (table 5.3) (figure 5.4). In 20 of these, the regions concurred with the localisation of epileptic EEG abnormality, 11 of which were ictal recordings (ictal recordings were not available for the other nine patients). Three patients (patients 48, 53, 64) had significantly increased T2 in regions distant from EEG abnormality and the presumed clinical seizure focus. Patient 48 (left TLE) demonstrated increased T2 values in the right temporal lobe and corpus callosum. Patient 53 had areas of increased T2 within the left and right temporal lobes (not statistically significant on the left), but ictal EEG evidence suggested a left temporal seizure focus. Patient 64 had right frontal lobe epilepsy but increased T2 in the parieto-occipital regions

bilaterally. Two patients (patients 64 and 68) had regions of decreased T2 signal. Twenty-two patients had no areas of significantly increased T2 signal. Quantification in regions-of-interest was performed on patients 35, 36, 56 and 60 (see table 5.4).

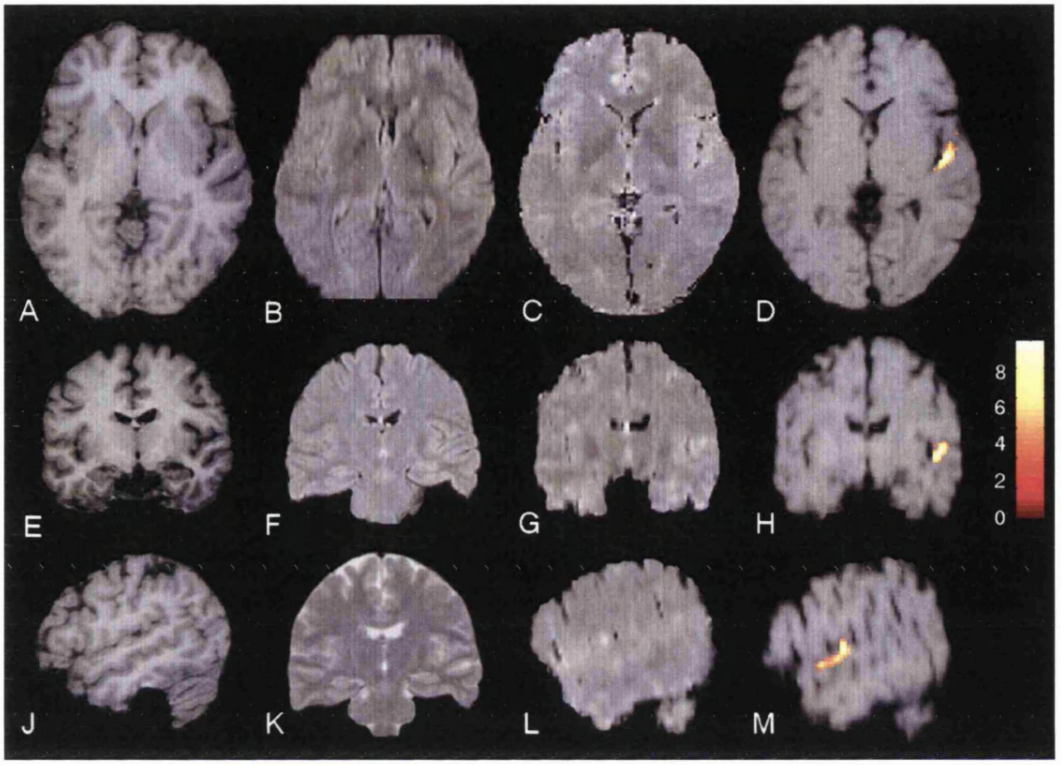

Figure 5.4: Patient 35. Patient with right temporal lobe epilepsy and normal conventional MRI. (**A**, **E**, **J**) Axial, coronal, and sagittal T1-weighted images. (**B**, **F**) Axial and coronal FLAIR images. (**K**) T2-weighted coronal image. (**C**, **G**, **L**) Axial, coronal, and sagittal T2 maps. (**D**, **H**, **M**) Regions of significantly increased T2 superimposed on axial, coronal, and sagittal early-echo (proton-density weighted) images. These regions were used for quantitative region-of-interest analyses on the T2 maps (Table 5.4). The region over the right superior temporal gyrus (Heschl's gyrus) localised to normal appearing cerebral tissue and concurred with electroclinical data regarding site of seizure onset. Z-value bar indicating degree of significance of highlighted regions is shown. Note that right on the images is patient's right.

5.1.4.4.2 Group analyses

Group analyses were performed on MRI-negative patients with EEG evidence of either left or right temporal or frontal lobe seizures. The right temporal lobe group consisted of 11 patients (patients 35-45), the left temporal lobe group 12 patients (patients 46-57), the right frontal lobe group seven patients (patients 58-64) and the left frontal lobe group five patients (patients 65-69). Compared to the 30 control subjects each group had a region of significantly increased T2 signal within the white matter of the respective cerebral lobe. In addition, there was an area of increased T2 in the anterior corpus callosum in the left temporal lobe group. Quantification in regions-of-interest was performed for each group (table 5.4).

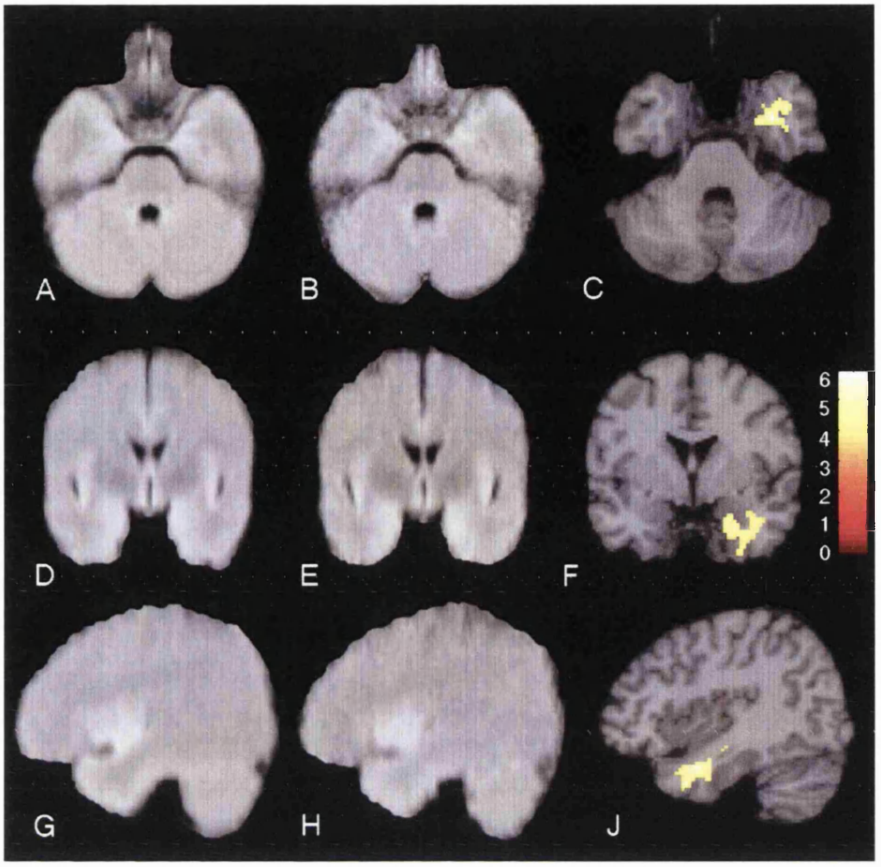

Figure 5.5 Right temporal lobe epilepsy (TLE) group with normal conventional MRI.
Normalized axial, coronal and sagittal T2 maps at the same slice position for the averaged 30 control subjects (**A**, **D** and **G**) and the MRI-negative patients with right TLE (**B**, **E** and **H**). The regions of increased T2 are superimposed on normalized T1-weighted SPM templates at the same slice position (**C**, **F** and **J**). This region localizes to the white matter of the right temporal lobe. The regions were used for quantitative region-of-interest analyses on the T2 maps (Table 5.4). Z-value bar indicating degree of significance of highlighted regions is shown. Note that right on the image is patients' right.

5.1.5 Conclusions

T2-mapping, analysed using statistical parametric mapping, identified significantly prolonged T2 in all patients with acquired nonprogressive cerebral lesions and partial seizures. In all of these patients the areas of increased T2 concurred with abnormalities identified on visual inspection of conventional MRI. Eighteen out of 20 patients with malformations of cortical development had areas of increased T2. In all of these, the regions were within areas of abnormality identified on conventional MRI. In addition, in the patients with acquired lesions there were nine areas, and in the patients with MCD there were seven areas that appeared normal on conventional imaging but which exhibited significantly prolonged T2 times, indicating additional sensitivity from the new method. Individual analyses of 45 patients with partial seizures and normal conventional MRI identified significantly increased T2 in 23 of the subjects. In 20 of these patients, the areas of increased T2 concurred with electroclinical

information. Group analyses of MRI-negative patients with electroclinical seizure onset localising to the left or right temporal or left or right frontal regions revealed significantly increased T2 within each respective lobe.

5.1.5.1 Methodological considerations and limitations

A minimum of two data points on the transverse magnetisation decay curve are required to define a monoexponential function and estimate the T2 relaxation time. Tissue within a voxel may possess multi-exponential decay, and to obtain a more accurate measure of T2, a greater number of echo times must be sampled (Whittall, MacKay, and Li 1999). However, such techniques usually allow only a single image slice to be obtained within an acceptable scan time and are therefore of limited clinical value in the localisation of occult structural lesions. A compromise is therefore required between accurate T2 measurements and brain coverage. We chose a dual-echo sequence with TE values of 15 and 120ms with the expectation that the measured T2 values lay between these time points, weighted towards the late echo image. The inclusion of a FLAIR pre-pulse minimizes the influence of CSF, the long T2 of which could otherwise make quantification inaccurate in regions susceptible to partial volume effects, such as the hippocampi and neocortex. This technique has previously been validated by comparison with multi-echo sequences and although estimations of T2 values were found to be lower than the quoted values of test objects, the dual-echo sequence was reproducible (coefficient of reliability less than 5% in repeat scans on healthy volunteers) and reliably identified abnormal tissue (Duncan, Bartlett, and Barker 1996; Jackson *et al.* 1990). Furthermore, the late echo T2 weighted image is of sufficient quality for routine qualitative radiological assessment, so can be incorporated into a standard imaging protocol without extending the total scanning time for each patient.

The non-Gaussian nature of segmented grey matter data in voxel-based morphometry has recently been shown to generate a high false positive rate when using the cluster extent statistical threshold in SPM (Ashburner and Friston 2000). The use of the cluster extent threshold to determine statistical significance in voxel-based morphometry is therefore unsound. However, on analysis of our T2 data on control subjects the number of abnormalities seen was no greater than what was expected by chance. We believe therefore that the limitations of using the cluster extent threshold in voxel-based morphometry do not compromise the analysis of T2 data.

5.1.5.2 Pathophysiological and clinical implications

The T2 relaxation time of a specific tissue is governed by the total amount of water, its distribution, and its interaction with the microstructural environment. Pathological processes may cause a disturbance to any or all of these factors, which will in turn modify the relaxation times and, therefore, the image contrast (Mathur-De Vre 1984).

Variations in T2 relaxation times exist within normal adult brain at regional, local and microscopic levels (Georgiades *et al.* 2001; Larsson *et al.* 1986). Structures of the limbic system have the highest, and the primary visual and auditory cortices the lowest, T2 relaxation times (Hirai *et al.* 2000). This has been attributed to variations in, for example, water content, cytoarchitecture, and iron concentration (Georgiades *et al.* 2001; Larsson

et al. 1986; Whittall *et al.* 1997). A number of studies have shown that grey matter possesses a longer T2 relaxation time than white matter (Larsson *et al.* 1986) probably reflecting differences in water compartmentalization, vascularity and iron concentration (Vymazal *et al.* 1995). Prolonged T2 relaxation times have been observed in a wide variety of pathological conditions including oedema, demyelination, neuronal loss, expansion of the extracellular space, infarction, and gliosis (Fazekas, Schmidt, and Scheltens 1998; Leifer, Buonanno, and Richardson Jr. 1990; Scarpelli *et al.* 1994; Autti *et al.* 1994).

A wealth of information exists regarding T2-weighted imaging in mesial temporal lobe structures, notably the hippocampus and amygdala, in patients with temporal lobe epilepsy (TLE). Furthermore, quantitative measurement of T2 relaxation time in these patients has been shown to confer additional sensitivity over qualitative assessment (Jackson *et al.* 1993b; Woermann *et al.* 1998a; Cutting *et al.* 2000; Namer *et al.* 1998; Ferrie *et al.* 1999). However, approximately 50% of patients with refractory focal epilepsy have seizures which arise from outside the mesial temporal lobe and in those patients quantitative analysis of T2-weighted imaging of the neocortex may also be profitable.

Lesion conspicuity, particularly in the hippocampus, amygdala, cortex and periventricular regions has previously been shown to be enhanced with fluid attenuated inversion recovery (FLAIR) imaging compared to conventional T2-weighted imaging (Meiners *et al.* 1999a; Wieshmann *et al.* 1998a). Furthermore, in T2-mapping, erroneous T2 values may be obtained in tissue adjacent to high signal cerebrospinal fluid due to partial volume effects. The use of FLAIR imaging allows a more accurate evaluation of T2 values in these regions and is essential in any quantitative analysis of cortical pathology.

Sensitivity of T2-weighted imaging may be further enhanced by using quantitative analysis methods, such as histogram (Barbosa *et al.* 1994), region-of-interest (Woermann *et al.* 1998a) or voxel based methods (Auer *et al.* 2001). Our method utilised a whole-brain statistical voxel-based technique and FLAIR imaging to improve both lesion identification and accuracy of T2 relaxation times.

Chronic, non-progressive acquired lesions are an important cause of refractory focal epilepsy and are frequently associated with MR-visible structural abnormalities. Abnormalities of T2 were identified within the regions of cerebral damage in all 14 patients with acquired lesions. Moreover, in nine patients, abnormalities were also detected in areas of the brain that were visually normal suggesting the presence of occult cerebral damage, due either to the original insult or as a result of recurrent seizure activity. It is of particular interest that eight of the nine extra-lesional regions concurred with the localisation of epileptiform EEG activity, suggesting that not only are occult structural abnormalities present but are relevant for seizure initiation or propagation. This is of paramount importance should surgical treatment be considered.

T2-weighted imaging is sensitive to pathological change in cerebral tissue (Smith *et al.* 1985). Irrespective of the original insult, the end result of cerebral injury is likely to be characterised histopathologically by extensive gliosis, neuronal loss and expansion of the extracellular space (Adams 1992; Castillo *et al.* 1996; Jay *et al.* 1998). This results in prolongation of T2 relaxation times due to increased total water content, an increase in the ratio of free to bound water, and a change in the dynamic structure of water near macromolecules (Mathur-De Vre1984). It has previously been demonstrated that quantitative T2 mapping is more sensitive than qualitative assessment in the detection of occult pathological change such as gliosis or demyelination (Ferrie *et al.* 1999; Allen, Glover, and Anderson 1981). It is therefore possible that the presence of extra-lesional abnormalities in our

patients with acquired cerebral damage is due to occult injury detectable only on quantitative analysis.

Eighteen out of 20 patients with MCD had regions of significantly prolonged T2 times. In all 18, these were within the areas of known abnormality identified on visual inspection of the conventional images. All of the patients with either gyral abnormalities or FCD and nine of the 11 patients with heterotopia possessed regions of prolonged T2. Two patients (patients 19 and 26) had normal T2 maps despite the presence of band and subependymal heterotopia respectively.

Grey matter possesses longer T2 relaxation times than white matter (Vymazal *et al.* 1995). A comparison of grey matter in patients with white matter in control subjects will therefore be identified as a region of significantly prolonged T2. This is the likely explanation for the results seen in patients with either gyral abnormalities and thickened cortices or, patients with grey matter heterotopia.

Furthermore, the cortex in gyral abnormalities, such as macrogyria, or in focal cortical dysplasia, is both macroscopically and microstructurally abnormal. The cortex is thickened, with poor demarcation of the grey and white matter. Cortical layers are disrupted and hypertrophic neurons are numerous (Manz *et al.* 1979). The underlying white matter is similarly abnormal with clusters of heterotopic neurons, axonal dysmyelination, gliosis and spongiolytic change (Usui *et al.* 2001; Marchal *et al.* 1989; Urbach *et al.* 2002). Heterotopic grey matter is histologically and functionally distinct to normal grey matter, with aberrant cytoarchitecture, abnormal neuronal positioning, attenuated and disordered dendrites and axons, and altered cytoskeletal elements (Manz *et al.* 1979; Barth 1987; Duong *et al.* 1994). The microscopic changes seen in both gyral abnormalities and heterotopia are invariably associated with altered water content and distribution. T2 values differ accordingly and are readily identified with both qualitative and quantitative T2-weighted imaging. Two patients had normal T2 maps despite the presence of heterotopic grey matter identified on conventional MRI. This may be due to limitations of the analysis method, for example, the abnormalities are too small or thin to be identified with this degree of smoothing. However, there is histopathological and imaging evidence to suggest that myelinated axons traverse regions of heterotopia (Harding 1992; Eriksson *et al.* 2002). The presence of myelin shortens T2 times by increasing the ratio of bound to free water, and T2 times will therefore approach those of white matter. T2 times in these regions compared with normal white matter in control subjects may not be sufficiently disparate to be identified by SPM.

More significantly, there were seven patients that possessed regions of significantly prolonged T2 beyond the margins of the visible MCD. These were in patients with gyral abnormalities, FCD and heterotopia, and were seen both adjacent to known lesions and in more distant sites. This is in agreement with previous histopathological, imaging and EEG studies suggesting that MCD are often more extensive than the visible lesion (Palmini *et al.* 1995; Sisodiya *et al.* 1995b; Richardson *et al.* 1996; Eriksson *et al.* 2001b). Prolonged T2 within normal-appearing brain in patients with MCD may result from either impaired neurogenesis, subsequent cell loss or a relative reduction in white matter, consistent with hypomyelination (Barkovich *et al.* 1988; Marchal *et al.* 1989), neurones projecting thinner axons (Sisodiya *et al.* 1995b), or altered neuropil arborisation (Mitchison1991).

The occurrence of extra-lesional T2 abnormalities is of clinical relevance, particularly regarding surgical planning and prognosis. It is also important to note that although T2 mapping is sensitive in the identification of pathological tissue, specificity is lacking, and it is possible that a proportion of the extra-lesional abnormalities are due to seizure-related damage and do not indicate the occurrence of occult dysgenesis. Further imaging,

histopathological and outcome correlative studies are required for definitive validation.

One patient with extratemporal FCD (patient 31) showed a region of prolonged T2 in the mesial temporal lobe structures in addition to the lesional T2 abnormality. This was evaluated with conventional T2 relaxometry of the hippocampus and significantly prolonged T2 times were detected (Duncan, Bartlett, and Barker 1996). This suggests the presence of occult hippocampal sclerosis and represents dual pathology in this patient. Previous studies have shown that failure to identify the occurrence of dual pathology and therefore perform incomplete surgical resection results in a poor post-operative outcome (Cendes *et al.* 1999).

Twenty-three of the 45 MRI-negative patients possessed regions of significantly prolonged T2 times. Twenty of those concurred with electroclinical data suggesting that T2-mapping analysed on a voxel-by-voxel basis is a useful technique for the detection of occult epileptic structural lesions. Regions of abnormal T2 were identified in both white and grey matter, in neocortex and archecortex.

Mesial temporal lobe structures

It is well established that quantitative assessment of hippocampal T2 times is more sensitive than visual evaluation for the identification of hippocampal sclerosis. This has previously only been possible with careful placement of regions-of-interest. Our whole-brain T2 maps, analysed using SPM, identified abnormalities in the mesial temporal lobe structures (MTL) of six MRI-negative patients (patients 36, 41, 48, 53, 56 and 75). The patients' routine images were subsequently evaluated with a standard, clinical, ROI-based T2 relaxometry technique (Duncan, Bartlett, and Barker 1996) and four possessed ipsilateral hippocampal relaxation times outside the normal range (patients 36, 48, 53 and 56). Briellmann et al recently demonstrated that hippocampal T2 times were directly related to the glial cell count in the dentate gyrus (Briellmann *et al.* 2002b). It is likely, therefore, that the regions of T2 abnormality in our patients represent occult gliosis, either solely as isolated hippocampal sclerosis or in association with a lesion outside the MTL as part of "dual pathology". EEG findings concurred with the SPM identified abnormalities in 4 of the 6 patients with abnormalities in MTL structures (patients 36, 41, 56 and 75). This suggests that these regions are important in terms of seizure generation and should be considered if surgical treatment is contemplated.

Neocortical abnormalities

Eleven patients had regions of increased T2 in the neocortex; all of which concurred with electroclinical data. For example, two patients with TLE (patients 35 and 49) had auditory auras either in isolation or immediately prior to seizure generalisation. In each patient, T2-mapping identified regions of increased T2 within the transverse / superior temporal gyri (Heschl's gyri), which contain the primary auditory area (Brodmann areas 41 and 42).

Previous histopathological studies of surgically resected epileptogenic cortical lesions that were normal on conventional MRI have shown occult focal cortical dysplasia, microgyria, cortical gliosis, and disordered lamination (Zentner *et al.* 1995; Theodore *et al.* 1990; Siegel *et al.* 2001). Compared to normal cerebral cortex, these lesions possess different microscopic and cytoarchitectural properties. They are, therefore, associated with an altered ratio of free to bound water and water compartmentalisation, and thus T2 relaxation time (Mathur-De Vre

1984). Furthermore quantitative histopathological studies have shown reduced neuropil in the neocortex of patients with TLE. This results in a smaller number of available macromolecules for efficient T2 relaxation, and hence prolonged T2 times (Bothwell *et al.* 2001). Previous studies in MS (Stevenson *et al.* 2000; Rumbach *et al.* 1991; Allen and McKeown 1979) and temporal lobe epilepsy (Namer *et al.* 1998) have reported the presence of altered T2 relaxation times in cerebral tissue that appeared normal macroscopically or on visual assessment of conventional MR images. It is likely that some occult neocortical epileptic foci also possess altered relaxation parameters which may not be of sufficient magnitude to be identified as abnormal on qualitative assessment. Using a more sensitive method of analysing imaging data, such as a voxel-by-voxel technique, a proportion of these subtle structural abnormalities may be discerned. It is feasible however, that some epileptogenic lesions in MRI-negative patients are recognised only on histopathological examination and remain beyond even the most sensitive of current imaging methods.

The identification of occult cerebral lesions is an important goal in patients with refractory focal epilepsy. The outcome following resective surgery in those with an identifiable lesion on pre-operative imaging is generally better than when imaging is normal (Cascino *et al.* 1992). Furthermore, it is likely that MRI-informed placement of intracranial EEG electrodes will identify an ictal focus more frequently than relying solely on electroclinical data; and possibly avoid the need for repeated studies (Siegel *et al.* 2001).

White matter abnormalities

Histopathological examination of white matter in patients with focal epilepsy frequently reveals subtle abnormalities, for example, gliosis, microdysgenesis, grey matter heterotopia and dysmyelination (Siegel *et al.* 2001; Zentner *et al.* 1995; Theodore *et al.* 1990; Melki *et al.* 1991). In a proportion of patients these can be seen on conventional MRI, for example, in patients with focal cortical dysplasia or band heterotopia. In a significant number, however, these abnormalities may remain occult on visual assessment despite altered relaxation parameters. Using quantitative T2-mapping, a greater number of abnormalities may be identified. Eleven MRI-negative patients possessed abnormal T2 relaxation times in white matter. In five patients, this was in combination with a cortical abnormality. Imaging abnormalities observed exclusively within the white matter compartment may occur in patients with, for example, grey matter heterotopia (Barkovich and Kjos 1992a), microdysgenesis (Nordborg *et al.* 1999), gliosis (Melki *et al.* 1991), and FCD (Palmini *et al.* 1991b). A combination of grey and white matter structural abnormalities are more commonly seen in patients with focal cortical dysplasia (Urbach *et al.* 2002), grey matter heterotopia, and as a result of acquired lesions, such as infarction, or head injury (Adams 1992). Previous studies have reported the presence of ipsilateral temporal lobe white matter signal change in approximately 60-70% of patients with HS (Mitchell *et al.* 1999; Meiners *et al.* 1999b). Histopathological evaluation revealed no increase in glial cells or ectopic neurons, but decreased myelin staining, possibly due to retrograde degeneration of axonal collaterals (Meiners *et al.* 1999b). It is possible that this phenomenon accounted for a proportion of the white matter changes seen in our individual and grouped MRI-negative patients.

Two patients (patients 64 and 68) had regions of decreased T2, both in deep white matter. This could be either artefactual, or represent pathological material such as haemosiderin (Mathur-De Vre 1984).

In summary, the abnormalities identified in MRI-negative patients could relate to either aetiological factors, such as occult dysgenesis, or acquired cerebral damage, or be the result of chronic seizures, for example, gliosis and neuronal loss. A number of these patients are undergoing pre-surgical assessment; pathological material is not yet available. Although the significant group effects seen in the MRI-negative patients with left and right temporal lobe, and left and right frontal lobe epilepsy are not clinically useful for evaluating individual patients, it suggests that given greater sensitivity, an effect in additional individual patients may be demonstrated, which may guide invasive diagnostic procedures and possible epilepsy surgery.

CHAPTER SIX

Double Inversion Recovery

6.1 DOUBLE INVERSION RECOVERY IN FOCAL EPILEPSY

6.1.1 Summary

The neocortices of 10 patients with partial seizures and acquired lesions, 14 patients with malformations of cortical development (MCD), and 33 patients with partial seizures and normal conventional MRI were quantitatively evaluated using whole brain double inversion recovery imaging (DIR) and Statistical Parametric Mapping (SPM).

Compared to a group of 30 control subjects, DIR and objective voxel-by-voxel statistical comparison identified regions of significantly abnormal DIR signal intensity (DSI) in 9 out of 10 patients with acquired nonprogressive cerebral lesions and partial seizures. In all 9 patients the areas of abnormal DSI concurred with abnormalities identified on visual inspection of conventional MRI. In all 14 patients with MCD, SPM detected regions of significantly abnormal DSI; all of which corresponded to abnormalities identified on visual inspection of conventional MRI. In addition, in both groups, there were areas that were normal on conventional imaging, which demonstrated abnormal DSI. Voxel-by-voxel statistical analysis identified significantly abnormal DSI in 15 of the 33 patients with cryptogenic focal epilepsy. In 10 of these, the areas of abnormal DSI concurred with epileptic EEG abnormality and clinical seizure semiology. Group analysis of MRI-negative patients with electroclinical seizure onset localising to the left temporal and left and right frontal regions revealed significantly abnormal DSI within the white matter of each respective lobe.

DIR analysed using SPM was sensitive in patients with MCDs and acquired cerebral damage. Significant abnormalities in DSI in individual and grouped MRI-negative patients suggest that occult epileptogenic cerebral lesions are associated with subtle structural abnormalities. DIR is, therefore, a useful quantitative MRI technique for characterising epileptic foci and may contribute to presurgical evaluation.

6.1.2 Introduction

The majority of epileptogenic cerebral lesions are located adjacent to cerebrospinal fluid (CSF) in, for example, the mesial temporal lobe or neocortex. The highly convoluted structure of the neocortex means that a proportion of image voxels contain a mixture of two, or possibly three, tissue types. This produces a partial volume effect (PVE) resulting in inaccuracy of both qualitative and quantitative assessments. Inversion recovery sequences null the signal from a particular tissue type by selecting a specific inversion time. Fluid attenuated inversion recovery imaging (FLAIR) which suppresses the MR signal from CSF on heavily T2-weighted images yields greater sensitivity and more accurately delineates cerebral lesions than conventional T2-weighted sequences (Hajnal *et al.* 1992a; Wieshmann *et al.* 1996). In addition to PVE from CSF, the identification of neocortical lesions may also be hampered by the signal arising from white matter. It is possible to suppress the signal from both CSF and normal white matter using Double Inversion Recovery imaging (DIR).

The aim of this study was to test the hypothesis that voxel-based statistical analysis of DIR images would identify regions of abnormal signal in patients with acquired lesions, malformations of cortical development and in those with focal epilepsy and normal conventional MRI.

6.1.3 Methods

6.1.3.1 Subjects

- 30 healthy control subjects :
  - 12 men, median age 33 years, range 20-52 years

- 57 patients with focal epilepsy

  Acquired
  - 10 patients (9 men, median age 42 years, range 21-55 years, median duration of epilepsy 29 years, range 3-49 years)
    - 2 patients with ischaemic lesions
    - 3 patients with head injuries
    - 2 patients with a history of encephalitis
    - 3 patients with a history of perinatal injury

  Malformations of cortical development
  - 14 patients (10 men, median age 36 years, range 19-54 years, median duration of epilepsy 24 years, range 4-39 years)
    - 3 patients with gyral abnormalities
    - 5 patients with focal cortical dysplasia
    - 6 patients with heterotopia
      - subependymal (n=1), subcortical nodules (n=2) and band heterotopia (n=3)
    - 1 patient with a dysembryoplastic neuroepithelial tumour

  One patient had both band heterotopia and a gyral abnormality (patient 13)

  MRI-negative
  - 33 patients (14 men, median age 37 years, range 21-72 years, median duration of epilepsy 20 years, range 2-40 years)
    - 13 were diagnosed with temporal lobe epilepsy (7 left, 6 right)
    - 12 with frontal lobe epilepsy (8 left, 4 right)
    - 8 had electroclinical evidence of less well defined, more widespread abnormalities

6.1.3.2 Double Inversion Recovery

DIR imaging utilises two inversion pulses to isolate the grey matter. Following the first inversion pulse, the magnetisation of grey and white matter recovers almost completely, while CSF, with its substantially longer T1 recovers to only a fraction of equilibrium magnetisation. Following the second inversion pulse, which flips the longitudinal magnetisation that had recovered after the first inversion pulse, magnetisation starts to recover again. The timing of the two inversion pulses is carefully arranged so that the magnetisation from CSF and from WM pass through the null point simultaneously. Image acquisition then commences with a standard spin echo sequence that samples the remaining magnetisation, which is predominantly from GM (Redpath and Smith 1994).

Three-dimensional DIR images were acquired using a hybrid 2D/3D fast spin-echo based sequence on a 1.5T Horizon Echospeed scanner (G.E, Milwaukee, Wisc., USA) using a standard quadrature head coil ($TR/TE/TI_{1,2}$ =6000/20/2200,360ms). Eighty interleaved axial slices were obtained with an acquisition matrix of 256x192 and a 24 x 18cm field-of-view, giving a voxel size of 1 x 1 x 2mm. Hyperbolic secant inversion pulses were used to facilitate accurate inversion. Flow compensation and a fat saturation pulse were also applied. Total scanning time for DIR was 20 minutes.

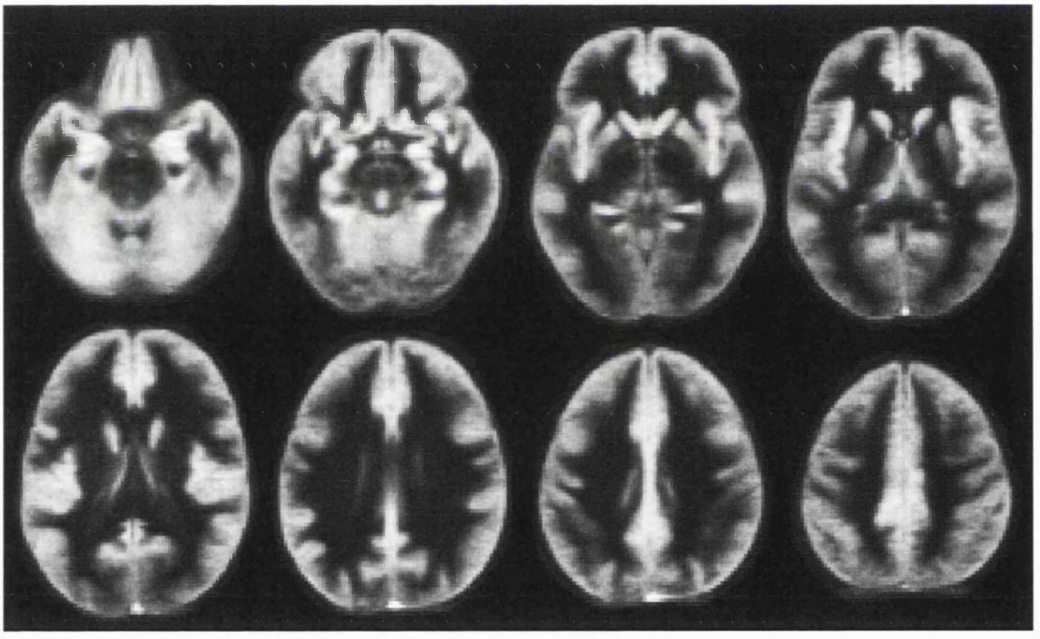

Figure 6.1: Series of normalised, axial DIR images. Average of 30 control subjects.

6.1.3.3 Analysis

Following data acquisition, the DIR images were transferred to an off-line workstation (Sun Microsystems, Palo Alto, CA) for post-processing.

Initially, remaining extracerebral tissue such as scalp and meninges, was removed using in-house software, which automatically compared patient's DIR images with a previously manually extracted GM-atlas

image. All DIR images were then normalised to a standard template which approximates the stereotaxic space defined by Talairach and Tournoux (Talairach and Tournoux1988), using SPM 99 (Wellcome Dept of Imaging Neuroscience, Institute of Neurology, London, UK) (Friston *et al.* 1995a). This template was created by normalising and then averaging 15 of the 30 control subjects' DIR images to standard SPM space using 12 linear degrees of freedom and a 7x8x7 non-linear warp. The resultant image was then smoothed with an 8mm full-width at half-maximum (FWHM) isotropic Gaussian kernel, to create the final DIR template. Subsequently, the DIR images of the patients and all 30 controls were normalised to this template using linear steps with 12 degrees of freedom (translation, rotation, zoom and shear) and a 7x8x7 non-linear warp (figure 6.1). The use of non-linear normalisation steps allowed global and regional anatomical differences to be minimised, thus allowing a meaningful comparison without adversely affecting differences in signal intensity. The non-linear normalisation was subject to a "regularisation" scheme which prevented excessive deformation of morphologically abnormal cerebral tissue, in, for example, patients with acquired lesions or major MCD (Gitelman *et al.* 2001).

Prior to statistical analysis, the normalised images were smoothed with a 14mm isotropic Gaussian kernel.

Using SPM, a standard univariate statistical test was applied to every voxel in the image in order to create a map from which statistical inference was made. The analysis included a covariate that treated global differences in DSI as a confound. The results therefore pertain to regionally specific differences in DSI rather than global measures of atrophy or global changes in signal intensity. A cluster extent threshold was not utilised as this is now considered inappropriate in voxel-wise analyses of GM maps due to an unacceptable false positive rate (Ashburner and Friston 2000). Under normal circumstances, a signal intensity threshold is set to prevent all voxels in the image, primarily those that arise from outside the brain or as a result of noise, being included in the analysis. In DIR images, due to suppression of the MR signal from other than grey matter, this also prevents the statistical evaluation of the white matter compartment which may be abnormal in, for example, band heterotopia. We, therefore, set the threshold to zero, that is, no voxels were to be excluded from the analysis. To avoid an inappropriately stringent correction for multiple comparisons an explicit mask was used to provide anatomical boundaries within which to perform the statistical analysis. This mask excluded voxels which arose from either within the ventricles or from outside the brain, but included the WM compartment.

Region-of-interest analyses were also performed in order to illustrate the magnitude of the differences in DSI in areas highlighted by the SPM comparison as deviating significantly from normal.

6.1.4 Results

6.1.4.1 Control group

Comparing each control subject with the remaining 29 control subjects using identical parameters and statistical thresholds as the comparison between patients and controls, three subjects had areas of significantly abnormal DSI. At a statistical threshold of $p<0.05$ and 60 examinations (30 subjects with two "contrasts" each (an increase and a decrease)), up to three abnormal areas were anticipated by chance alone.

6.1.4.2 Acquired Lesions

In nine out of 10 patients with acquired lesions, SPM detected areas of significantly abnormal DSI (table 6.1). In all nine patients, areas of ***increased*** DSI corresponded to abnormalities identified on visual inspection of the conventional MR images (figure 6.2). In six patients there were also regions of significantly ***decreased*** DSI, all of which corresponded to abnormalities identified on the conventional MR images (five patients) or epileptiform activity on interictal EEG (one patient). In seven patients (patients 1, 2, 4, 5, 6, 7 and 10) areas of significantly ***increased*** DSI were detected in regions previously reported as normal. There was one patient (patient 2) with significantly ***decreased*** DSI in cerebral tissue previously reported as normal. In 6 of these 7 patients the areas of abnormal DSI concurred with the localisation of epileptiform EEG activity despite normal appearances on conventional MRI. In one patient (patient 3), there was no abnormality of DSI detected and conventional MRI showed subtle left parietal lobe damage with minimal signal change in the grey and white matter.

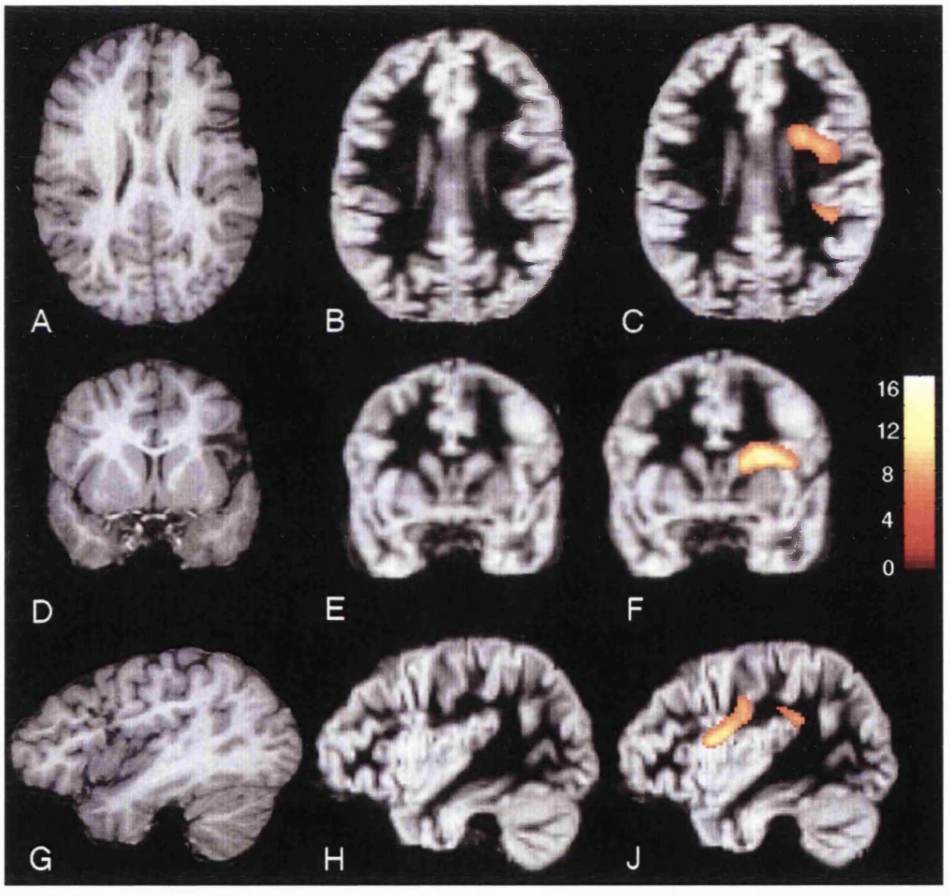

Figure 6.2: Patient 5, mature cortical infarct in right frontal lobe.
Axial (**A**), coronal (**D**), and sagittal (**G**) T1-weighted images. Normalised axial (**B** and **C**), coronal (**E** and **F**), and sagittal (**H** and **J**) DIR images, with regions of significantly increased DSI superimposed on maps **C**, **F** and **J**. The regions in **C**, **F** and **J** coincide with the localization of the abnormalities identified on conventional MRI and more posteriorly, in normal appearing tissue. Z-value bar indicating degree of significance of highlighted regions is shown. Note that right on the images is patient's right.

6.1.4.3 Malformations of Cortical Development

In all 14 patients with MCD, SPM detected regions of abnormal DSI (table 6.2). In all patients, areas of ***increased*** DSI corresponded to all or part of the MCD identified on visual inspection of the conventional MR images (figure 6.3). In addition, 5 patients had regions of ***decreased*** DSI, one of which corresponded to abnormalities seen on the conventional MR images. In eight patients (***increased*** DSI in patients 11, 12, 14, 17, 19 and 24; ***decreased*** DSI in patients 11, 13, 14, 15 and 17) changes were found outside the overt MCD, in tissue that appeared normal on conventional MRI. In 6 of these 8 patients the areas of abnormal DSI concurred with the localisation of epileptiform EEG activity despite normal appearances on conventional MRI.

Of the 14 patients with MCD, all 3 with gyral abnormalities (patients 11-13) and all five with FCD (patients 19-23) had areas of significantly ***increased*** DSI which corresponded to all or part of the MCD. Two out of three patients with gyral abnormalities (patients 11 and 13) had regions of ***decreased*** DSI. In all patients with gyral abnormalities and in one patient with FCD, changes were apparent beyond the margins of the evident MCD, in areas that appeared normal on visual assessment of conventional T1- and T2-weighted images.

Areas of ***increased*** DSI, which corresponded to the MCD identified on the conventional MR images, were seen in all patients with band heterotopia (BHT) (patients 13, 14 and 15), in both patients with subcortical heterotopia (SCH) (patients 16 and 17), and in the patient with subependymal heterotopia (SEH) (patient 18). In addition, one of the three patients with BHT (patient 14) and one of the two patients with SCH (patient 17) had regions of ***increased*** DSI in areas previously reported as normal. All of the patients with BHT and one of the patients with SCH (patient 17) had regions of ***decreased*** DSI; all of which were not within the evident MCD.

The single patient with a DNET (patient 24), had regions of ***increased*** DSI, both in concordance with conventional imaging abnormalities, and in normal appearing tissue.

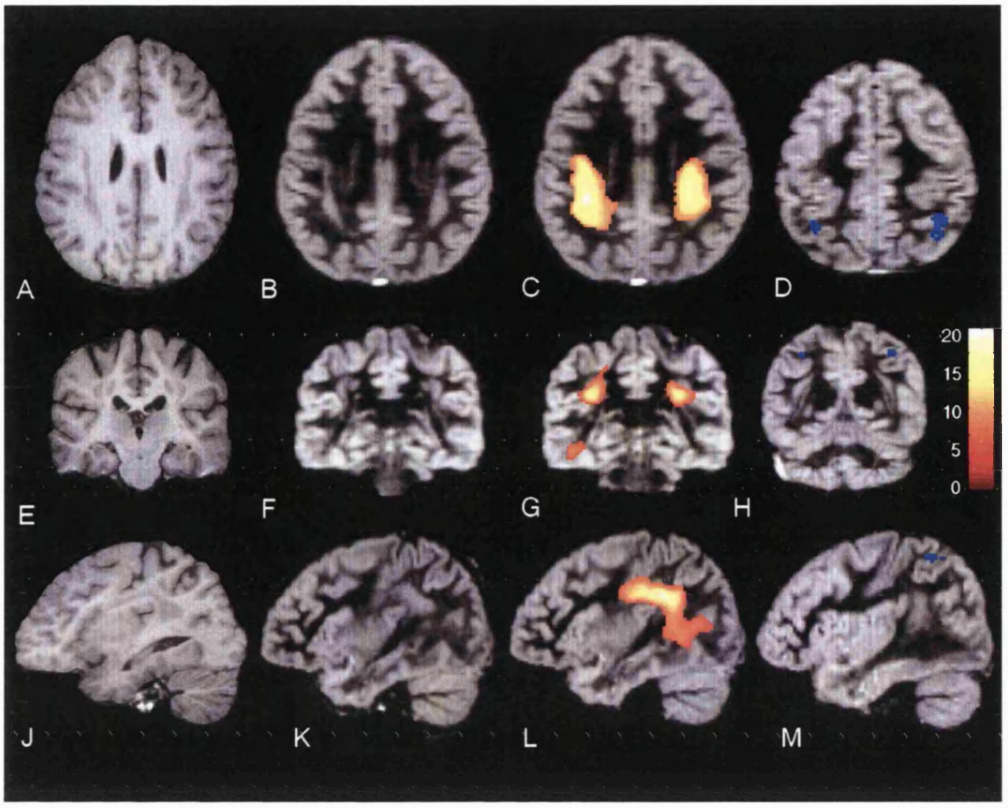

Figure 6.3: Patient 13, band heterotopia and bitemporal gyral abnormality.

Axial (**A**), coronal (**E**), and sagittal (**J**) T1-weighted images. Normalised axial (**B**, **C** and **D**), coronal (**F, G** and **H**), and sagittal (**K, L** and **M**) DIR images, with regions of significantly increased DSI (yellow-orange), and decreased DSI (blue) superimposed on maps **C, G, L** and **D, H, M** respectively. The regions in **C**, **G** and **L** coincide with the localization of the abnormalities identified on conventional MRI. The regions in **D**, **H** and **M** localise to the normal appearing parietal lobes, peripheral to the heterotopia. Z-value bar indicating degree of significance of highlighted regions of increased DSI is shown. Note that right on the images is patient's right.

6.1.4.4 MRI-negative patients

6.1.4.4.1 Individual SPM analyses

SPM analyses of the 33 individual patients in the MRI-negative group revealed 15 patients (45%) with regions of significantly abnormal DSI compared to the control group (table 6.3) (figure 6.4, 6.5). In 10 of these, the regions concurred with the localisation of epileptiform EEG abnormality (6 were ictal recordings, 3 were interictal recordings as ictal recordings were not available (or were inconclusive), and 1 was concordant with interictal but not ictal EEG data). Fourteen of the MRI-negative patients had regions of **increased** DSI, and 3 patients had regions of **decreased** DSI. Two patients therefore had both regions of **increased** and regions of **decreased** DSI. Four patients had areas of **increased** DSI, and one patient had an area of **decreased** DSI, which did not concur with electroclinical information regarding sites of seizure onset. Eighteen patients had no areas of significantly abnormal DSI.

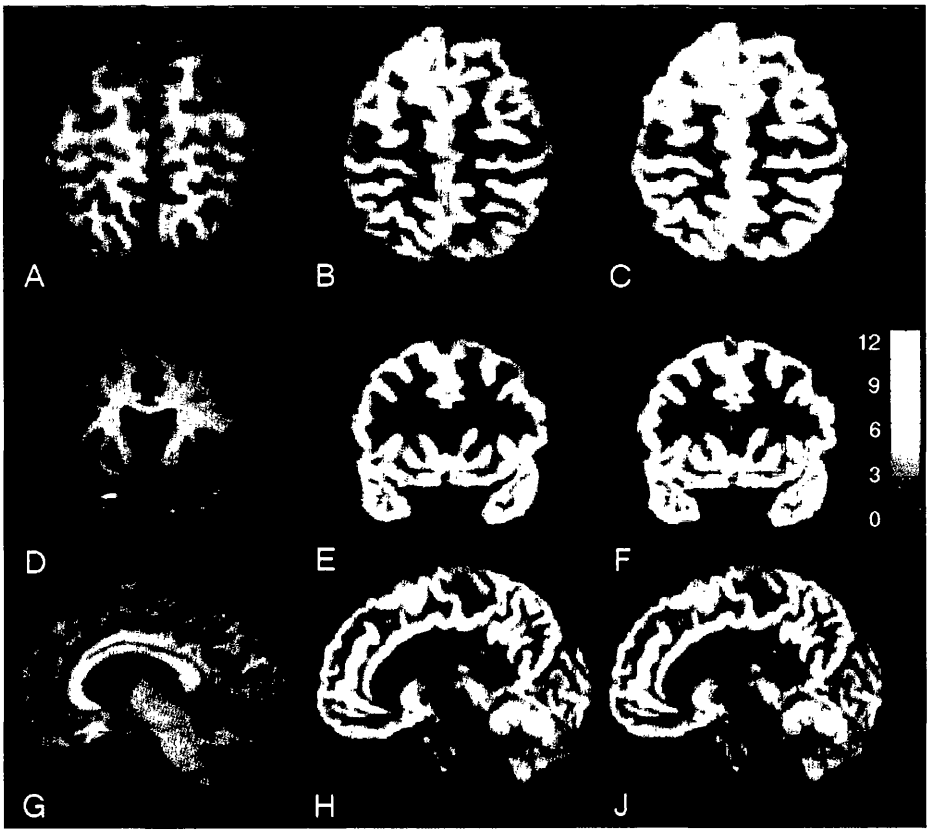

Figure 6.4: Patient 43, patient with left frontal lobe epilepsy and normal conventional MRI.
Axial (**A**), coronal (**D**), and sagittal (**G**) T1-weighted images. Normalised axial (**B** and **C**), coronal (**E** and **F**), and sagittal (**H** and **J**) DIR images, with regions of significantly increased DSI superimposed on maps **C**, **F** and **J**. The regions in **C**, **F** and **J** coincide with the electroclinical localization of seizure onset. Z-value bar indicating degree of significance of highlighted regions is shown. Note that right on the images is patient's right.

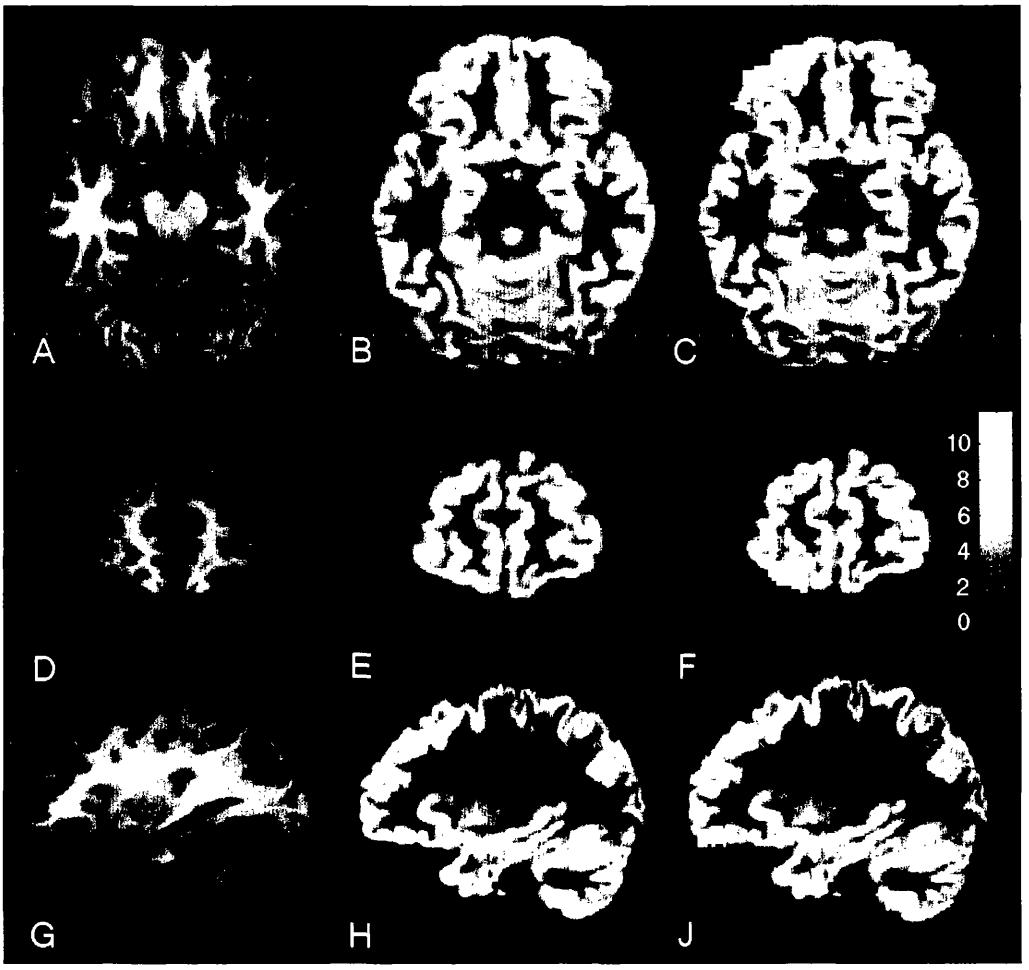

Figure 6.5: Patient 44, patient with left frontal lobe epilepsy and normal conventional MRI
Axial (**A**), coronal (**D**), and sagittal (**G**) T1-weighted images. Normalised axial (**B** and **C**), coronal (**E** and **F**), and sagittal (**H** and **J**) DIR images, with regions of significantly increased DSI superimposed on maps **C**, **F** and **J**. The regions in **C**, **F** and **J** coincide with the electroclinical localization of seizure onset. Z-value bar indicating degree of significance of highlighted regions is shown. Note that right on the images is patient's right.

6.1.4.4.2 Group analyses

Group analyses were performed on MRI-negative patients with EEG evidence of either left or right temporal or frontal lobe seizures. The right temporal lobe epilepsy (TLE) group consisted of 6 patients (patients 25-30), the left TLE group 7 patients (patients 31-37), the right frontal lobe epilepsy (FLE) group 4 patients (patients 38-41) and the left FLE group 8 patients (patients 42-49). Compared to the 30 control subjects the left TLE, the left FLE (figure 6.6) and the right FLE groups had regions of significantly increased DSI within the "white matter" compartments of each respective cerebral lobe. There were no other statistically significant regions of abnormal DSI.

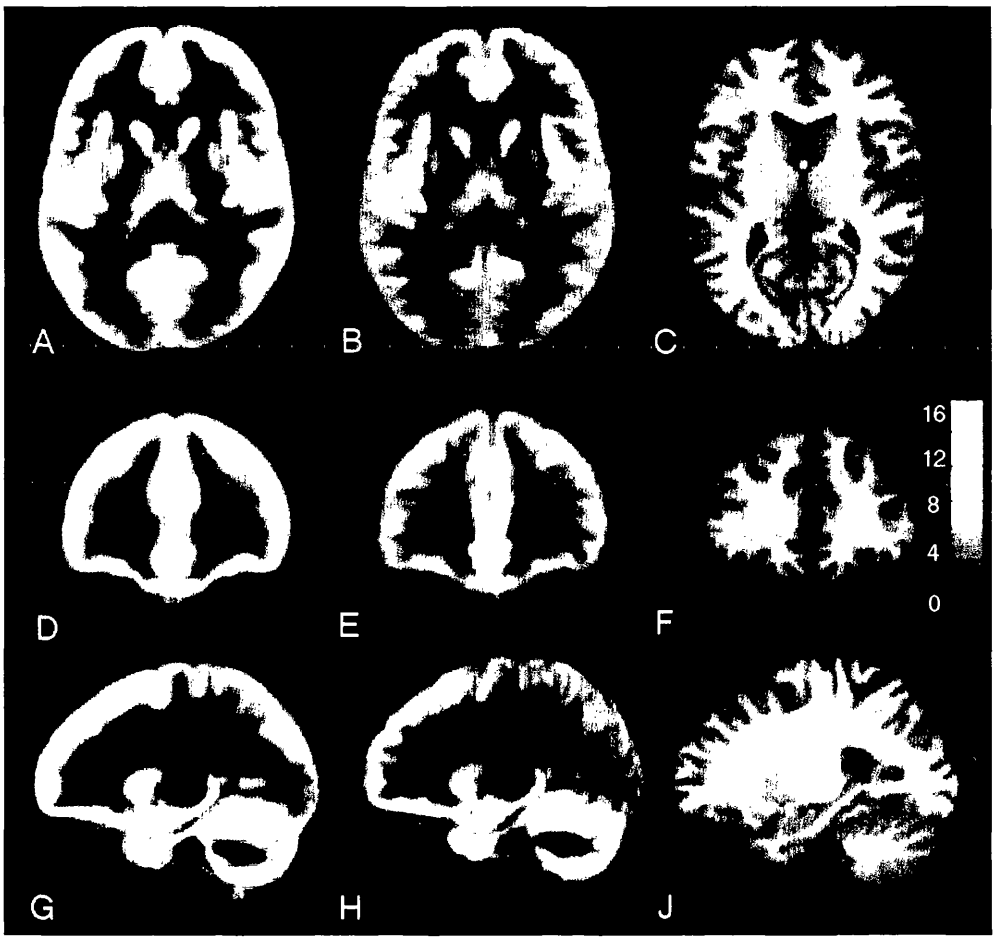

Figure 6.6: Left frontal lobe epilepsy group with normal conventional MRI.

Normalized axial, coronal and sagittal DIR images at the same slice position for the averaged 30 control subjects (**A**, **D** and **G**) and the MRI-negative patients with left FLE (**B**, **E** and **H**). The regions of increased DSI are superimposed on normalized T1-weighted SPM templates at the same slice position (**C**, **F** and **J**). This region localizes to the white matter of the left frontal lobe. Z-value bar indicating degree of significance of highlighted regions is shown. Note that right on the image is patients' right.

Table 6.1 Clinical characteristics, EEG, MRI and DIR imaging results in patients with non-progressive acquired lesions

Patient	Age (yr)	Sex	Aetiology of epilepsy	Seizure Types	Duration of epilepsy (yrs)	EEG features	Conventional MRI findings	DIR imaging Sig. increased DSI (p value)	DIR imaging Sig. decreased DSI (p value)
1	31	M	head injury	2° gen.	11	bil. frontotemp. i.e.a.	bil. front., R. temp, post. corpus callosal damage	bil. front. + R. temp., bil. post. perivent. + NA L. temp. (p<0.001)	medial bil. front. (p<0.001)
2	51	M	head injury	CPS, 2° gen.	48	L. temp.par. + R. frontocentral i.e.a.	superficial atrophy of L. hemisphere, sparing temp.	L. front. par. occ. + NA R. par. front. (p<0.001)	NA L. temp. (p<0.01)
3	40	M	head injury	CPS, 2° gen.	3	widespread bilateral i.e.a.	L. par. lobe damage	nil	nil
4	39	M	infarction	CPS, 2° gen.	36	R. front.temp.par. i.e.a.	R. temp.par.occ. ischaemic damage	R. temp. par. occ. + NA R. front. (p<0.001)	nil
5	21	F	infarction	CPS, 2° gen.	12	R. hemisphere i.e.a., esp front.temp. region	R. lat. front. cortical scar	R. lat. front. NA R. front. par. (p<0.001) [fig. 6.1]	nil

Patient	Age (yr)	Sex	Aetiology of epilepsy	Seizure Types	Duration of epilepsy (yrs)	EEG features	Conventional MRI findings	DIR imaging Sig. increased DSI (p value)	DIR imaging Sig. decreased DSI (p value)
6	43	M	perinatal injury	CPS, 2° gen.	42	L. hemisphere, esp. L. temp. i.e.a.	L. front. lobe + L. hippocampal damage	L. frontotemp. + NA R. periventricular. (p<0.001)	L front. (p<0.001)
7	24	M	perinatal injury	S+CPS, 2° gen.	23	bil. frontotemp. (R>L) i.e.a	L. front.temp.par ischaemic damage	L. front.temp.par + NA R. front. par. (p<0.001)	L front. temp. par. (p<0.001)
8	55	M	perinatal injury	CPS	49	R. temp. i.e.a	diffuse inc. T2 signal change in bil. post. WM	bil. occ. (p<0.001)	nil
9	52	M	encephalitis	CPS, 2° gen.	12	bihemispheric i.e.a	L. temp + L. occ. + minor R. temp. damage	L. front. + temp. + occ. + R. frontotemp. (p<0.001)	L. temp. + L insula (p<0.001)
10	44	M	encephalitis	CPS	35	bihemispheric, esp. R. temp. i.e.a.	L. par. + L. HC damage	L. front. par. occ. + L. temp. + NA R. insula (p<0.001).	L. par. (p<0.001)

R.=Right; L.=Left; bil.=bilateral; post.=posterior; med.=medial; lat.=lateral; front.=frontal; par.=parietal; temp.=temporal; occ.=occipital; perivent.=periventricular; HC=hippocampus; i.e.a..=interictal epileptiform activity; M=male; F=female; SPS=simple partial seizure; CPS=complex partial seizure; 2° gen.=secondary generalised tonic-clonic seizure; inc.=increased; NA=normal appearing; DSI=DIR signal intensity; GM=grey matter; WM=white matter

Table 6.2 Clinical characteristics, EEG, MRI and DIR imaging results in patients with malformations of cortical development

Patient	Age (yr)	Sex	Seizure Types	Duration of epilepsy (yrs)	EEG features	Conventional MRI findings	DIR imaging Sig. increased DSI (p value)	DIR imaging Sig. decreased DSI (p value)
11	52	M	CPS, 2° gen.	39	R. hemisphere i.e.a	R front. + bil. par. occ. gyral abn.	bil. in MCD + in NA L. front. + temp. lobes (p<0.001)	R. occ + L. occ. + NA L front. (p<0.001)
12	46	M	CPS, 2° gen.	38	L. hemisphere. i.e.a	L. frontopar. gyral abn. with thick cortex	L. frontopar. region in MCD (p<0.001) + in NA L. temp.occ. (p<0.001)	nil
13	28	M	S + CPS, 2° gen.	20	widespread i.e.a., max. L. temp.	bil. BHT + bitemporal gyral abn. with thick cortex	bil. hemisphere in BHT + bitemp. in gyral abn. (p<0.001)	NA bipar. cortex overlying BHT (p<0.001) [fig. 6.2]
14	32	F	S + CPS, 2° gen.	27	widespread i.e.a	bil. band heterotopia	bil. hemisphere in MCD + in NA L frontal pole (p<0.001)	NA bil. insula cortex overlying BHT (p<0.001)
15	24	M	CPS, 2° gen.	15	bil. hemisphere i.e.a.	bil. band heterotopia	bil. hemisphere in MCD (p<0.01)	NA bitemporopar. cortex overlying BHT (p<0.001)

Patient	Age (yr)	Sex	Seizure Types	Duration of epilepsy (yrs)	EEG features	Conventional MRI findings	DIR imaging Sig. increased DSI (p value)	DIR imaging Sig. decreased DSI (p value)
16	54	M	2° gen.	23	normal interictal	R. par. SCH	R. par. in MCD (p=0.001)	nil
17	19	F	CPS	4	bil. frontotemp i.e.a	L. frontal + L. insula SCH	L. front. in SCH (p<0.001) + in NA R. insula (p<0.001)	NA L. temp. (p<0.001)
18	47	F	CPS	36	L. hemisphere, max. L. front. i.e.a	bil. temp. + par. SEH	bil. temp. + par. in MCD (p<0.01)	nil
19	30	M	SPS, CPS	24	L. frontotemp. i.e.a.	L. front. temp. FCD	L. front. temp. in FCD + in NA R. temp. occ. (p<0.001)	nil
20	33	M	CPS, 2° gen.	32	bil. hemisphere i.e.a.	R. par. lobule FCD	R. par. lobule in FCD (p<0.05)	nil
21	44	M	CPS, 2° gen.	32	R. frontal i.e.a.	R. front. pole FCD	R. front. pole in FCD (p<0.001)	nil

Patient	Age (yr)	Sex	Seizure Types	Duration of epilepsy (yrs)	EEG features	Conventional MRI findings	DIR imaging Sig. increased DSI (p value)	DIR imaging Sig. decreased DSI (p value)
22	22	F	CPS, 2^{o} gen.	15	R. temp. i.e.a.	R. front. temp. par FCD	R. front. temp. par in FCD ($p<0.001$)	nil
23	40	M	CPS, 2^{o} gen.	20	R. occ i.e.a.	R. occ. FCD	R. occ. in FCD ($p=0.05$)	nil
24	39	M	SPS, 2^{o} gen.	15	R. hemisphere i.e.a	R. front. DNET	R. front. in DNET ($p<0.001$) + in NA R. front. ($p<0.001$)	nil

DSI=DIR signal intensity; R.=Right; L.=Left; bil.=bilateral; ant.=anterior; post.=posterior; lat.=lateral; front.=frontal; par.=parietal; temp.=temporal; occ.=occipital; NA=normal-appearing; corp.=corpus; MCD=malformation of cortical development; BHT=band heterotopia; SEH= subependymal heterotopia; SCH=subcortical heterotopia; FCD=focal cortical dysplasia; DNET=dysembryoplastic neuroepithelial tumour; i.e.a..=interictal epileptiform activity; abn.=abnormality; M=male; F=female; SPS=simple partial seizure; CPS=complex partial seizure; 2^{o} gen.=secondary generalised tonic-clonic seizure; inc.=increased.

Table 6.3 Clinical characteristics, EEG, MRI and DIR imaging results in patients with normal conventional MRI

Patient	Age (yr)	Gender	Aetiology of epilepsy	Duration of epilepsy (yrs)	Seizure types	Ictal Epileptiform Abnormality	Interictal Epileptiform Abnormality	DIR imaging Sig. increased DSI (p value)	DIR imaging Sig. decreased DSI (p value)
25	36	M	cryptogenic	18	SPS, CPS	N/A	R. temp.	nil	nil
26	21	F	cryptogenic	20	CPS, 2° gen.	N/A	R. temp.	nil	nil
27	45	M	meningitis	29	CPS, 2° gen.	R. temp.	bil. temp. R>L	R. temp. lobe ($p<0.05$)	nil
28	44	F	cryptogenic	32	CPS, 2° gen.	R. temp.	bil. temp. R>L	bil. frontopar. ($p<0.001$)	nil
29	58	M	cryptogenic	2	CPS	R. temp.	bil. temp.	R. occ + L front. lobes ($p<0.05$)	nil
30	30	F	cryptogenic	14	CPS	N/A	R. temp.	nil	nil

Patient	Age (yr)	Gender	Aetiology of epilepsy	Duration of epilepsy (yrs)	Seizure types	Ictal Epileptiform Abnormality	Interictal Epileptiform Abnormality	DIR imaging Sig. increased DSI (p value)	DIR imaging Sig. decreased DSI (p value)
31	38	F	cryptogenic	15	CPS, 2° gen.	L. temp.	L temp	L. frontotemp. + L. inf. temp. gyrus ($p<0.05$)	nil
32	56	M	cryptogenic	36	CPS, 2° gen.	L. temp.	L. temp.	nil	nil
33	51	F	cryptogenic	9	CPS, 2° gen.	L. temp.	normal	R. temp. lobe ($p<0.05$)	nil
34	38	F	cryptogenic	35	CPS, 2° gen.	L. temp.	L. temp	nil	nil
35	45	F	cryptogenic	30	CPS	L. temp.	L. temp.	nil	nil
36	54	F	cryptogenic	14	CPS, 2° gen.	L. hemisphere	L. temp.	L. periventricular frontotemp. ($p<0.01$)	nil

Patient	Age (yr)	Gender	Aetiology of epilepsy	Duration of epilepsy (yrs)	Seizure types	Ictal Epileptiform Abnormality	Interictal Epileptiform Abnormality	DIR imaging Sig. increased DSI (p value)	DIR imaging Sig. decreased DSI (p value)
37	32	F	cryptogenic	18	S + CPS, 2° gen.	L. temp.	L. temp.	nil	nil
38	27	F	cryptogenic	13	SPS, 2° gen.	N/A	R. front.	nil	nil
39	41	M	cryptogenic	23	CPS	N/A	R. front.	nil	nil
40	36	F	cryptogenic	12	CPS	N/A	R. front.	nil	nil
41	53	M	cryptogenic	40	CPS, 2° gen.	N/A	R. front.	bil. par. occ subcortical (p<0.001)	nil
42	41	M	cryptogenic	19	2° gen.	N/A	L. front.	nil	nil

Patient	Age (yr)	Gender	Aetiology of epilepsy	Duration of epilepsy (yrs)	Seizure types	Ictal Epileptiform Abnormality	Interictal Epileptiform Abnormality	DIR imaging Sig. increased DSI (p value)	DIR imaging Sig. decreased DSI (p value)
43	37	M	cryptogenic	32	CPS	N/A	L. front.	L frontal lobe - superior convexity ($p<0.001$) [fig. 6.3]	nil
44	27	M	cryptogenic	15	CPS	L. front.	L. front.	L lat. + post. orbital gyri ($p<0.001$) [fig. 6.4]	nil
45	30	F	cryptogenic	15	CPS, 2° gen.	N/A	L front.	nil	nil
46	25	F	cryptogenic	24	CPS, 2° gen.	L front	bifrontal	bifront. + L occ. lobes ($p<0.01$)	R. frontopar. ($p<0.05$)
47	18	M	cryptogenic	9	CPS, 2° gen.	L front.	L frontocentral	nil	nil
48	53	M	cryptogenic	10	CPS	inconclusive	L. front.	L. front. + L. paracentral lobule ($p<0.001$)	nil

Patient	Age (yr)	Gender	Aetiology of epilepsy	Duration of epilepsy (yrs)	Seizure types	Ictal Epileptiform Abnormality	Interictal Epileptiform Abnormality	DIR imaging Sig. increased DSI (p value)	DIR imaging Sig. decreased DSI (p value)
49	30	F	head injury	25	CPS, 2° gen.	normal	L front.	nil	R. post. temp. (p<0.001)
50	40	F	cryptogenic	35	CPS, 2° gen.	inconclusive	bil. temp.	nil	nil
51	22	F	cryptogenic	5	S + CPS, 2° gen.	inconclusive	bil. hemisphere	nil	nil
52	27	M	neonatal illness	27	CPS, 2° gen.	R hemisphere	R. hemisphere	nil	nil
53	30	F	cryptogenic	25	CPS, 2° gen.	inconclusive	bifront.	R. frontopar. cortex + bifront. (p<0.001)	nil
54	34	F	cryptogenic	23	SPS + CPS	N/A	bitemporal	nil	nil

Patient	Age (yr)	Gender	Aetiology of epilepsy	Duration of epilepsy (yrs)	Seizure types	Ictal Epileptiform Abnormality	Interictal Epileptiform Abnormality	DIR imaging Sig. increased DSI (p value)	DIR imaging Sig. decreased DSI (p value)
55	35	F	encephalitis	34	CPS, 2° gen.	L hemisphere	L hemisphere	L front. + temp. + occ. (p<0.05)	bil. mesial temp. lobe structures (p<0.05)
56	49	M	cryptogenic	4	CPS, 2° gen.	inconclusive	L > R (fronto)temp	nil	nil
57	29	M	cryptogenic	25	CPS, 2° gen.	bil frontal	bil. frontotemp.	bil. frontal superior convexity + L. frontal pole (p<0.001)	nil

R.=Right; L.=Left; bil.=bilateral; post.=posterior; med.=medial; lat.=lateral; front.=frontal; par.=parietal; temp.=temporal; occ.=occipital; perivent.=periventricular; M=male; F=female; SPS=simple partial seizure; CPS=complex partial seizure; 2° gen.=secondary generalised tonic-clonic seizure; NA=normal appearing; DSI=DIR signal intensity; GM=grey matter; WM=white matter

6.1.5 Conclusions

DIR, analysed using SPM, identified significantly abnormal DSI in 9 out of 10 patients with acquired non-progressive cerebral lesions and partial seizures. In all nine patients the areas of abnormal DSI concurred with abnormalities identified on visual inspection of conventional MRI. All 14 patients with MCD had areas of abnormal DSI within areas of abnormal tissue identified on conventional MRI. In addition, there was abnormal DSI in eight areas in 7 of the 10 patients with acquired lesions, and in 12 areas in 8 of the 14 patients with MCD that appeared normal on conventional imaging. Fifteen of 33 patients with partial seizures and normal conventional MRI had abnormal DSI. In 10 of these, the areas concurred with electroclinical data. Group analyses of MRI-negative patients with electroclinical seizure onset localising to the left temporal or left or right frontal lobes revealed significantly increased DSI within each respective lobe.

6.1.5.1 Methodological considerations and limitations

A DIR scan takes approximately 20 minutes to acquire which is clinically acceptable. It was necessary, however, to repeat the scans of a small number of patients and controls due to movement artefact. Radiofrequency "slab" overlap and inhomogeneity were minimised by optimisation of sequence parameters and the use of hyperbolic secant inversion pulses.

Our statistical analysis method is very similar to the established technique of voxel-based morphometry (VBM), which at its simplest represents a voxel-wise comparison of the estimated local concentration of grey matter, derived from segmented T1-weighted scans, between two groups of subjects (Ashburner and Friston 2000). Due to the nonlinear spatial normalisation process, certain brain regions may be expanded or contracted in volume. It is not possible therefore to infer changes in grey matter volume. The resultant statistical probability maps therefore, describe differences in grey matter concentration only. It is possible that incorporating information derived from the deformation fields created during the normalisation process may enhance sensitivity in the detection of subtle neocortical abnormalities, however this is not yet firmly established (Good *et al.* 2001b).

When comparing an individual subject to a group with VBM, a 12mm or greater smoothing kernel is recommended to avoid an unacceptable false-positive rate (Salmond *et al.* 2002). Although DIR image data is inherently different to post-acquisition segmented grey matter, a 14mm smoothing kernel was used to ensure maximal specificity, possibly at the expense of sensitivity. At this level of smoothing three control subjects with areas of abnormal DSI were identified; which is expected with 30 subjects and $p<0.05$ being taken as the level of significance.

6.1.5.1 Pathophysiological and clinical implications

A number of brain pathologies including multiple sclerosis, cerebral tumours, ischaemia, and degenerative disease have been investigated with qualitative DIR imaging, and described in case reports or small series studies. Turetschek et al reported a comparison of DIR and FLAIR imaging in patients with cerebral tumours,

inflammatory conditions, vascular lesions, lesions of unknown origin and olivopontocerebellar atrophy. Overall, lesion conspicuity on DIR and FLAIR images was comparable, although DIR imaging was possibly superior in the identification of infratentorial lesions and lesions with poor contrast on T2-weighted imaging. It was concluded that any contrast difference between the DIR and FLAIR images was due to T1 effects (Turetschek *et al.* 1998). Bedell et al similarly investigated patients with multiple sclerosis using DIR, FLAIR and conventional fast-spin echo T2-weighted imaging. MS lesions were more definitively delineated and possessed greater signal heterogeneity on DIR images than on FLAIR and conventional fast-spin echo T2-weighted imaging (Bedell and Narayana 1998a).

The principle of DIR imaging is the generation of a signal from a specific tissue whilst nulling the signal from the remaining tissue compartments, due to differences in their T1 values. Additionally, our DIR sequence has an echo time (TE) of 20ms which results in a proton-density weighted image. In addition, therefore, to altered grey matter concentration, abnormalities identified by SPM may also be due to either abnormal proton-density or T1 relaxation times. Consequently, DIR imaging interrogates both white and grey matter compartments. The adequate suppression of the MR signal from normal white matter relies on its possession of a relatively narrow range of T1 values (Redpath and Smith 1994). Deviation from this will result in insufficient suppression from the carefully timed inversion pulses, and the appearance of signal from white matter. Thus, it follows that:

1. increased DSI in white matter may be due to either abnormal white matter (possessing an altered T1-relaxation time), or ectopic grey matter.
2. decreased DSI in the white matter compartment is not encountered, as the MR signal derived from this compartment is completely suppressed in normal subjects and is therefore, by definition, zero.
3. increased DSI in the cortex may be due to either increased concentration of grey matter, for example thickened gyri, or increased cortical proton-density.
4. decreased DSI in the cortex may be due to loss of grey matter tissue, or an altered cortical T1-relaxation time.

DIR imaging therefore evaluates both white and grey matter compartments and provides information on both the quantity and microstructural environment of cerebral tissue.

Typically, a change in the proton-density in cerebral tissue arises from altered water content. Increased proton-density is commonly seen in oedema and gliosis (Barnes *et al.* 1988; Barnes *et al.* 1986b), and has been reported in Wallerian degeneration (Khurana *et al.* 1999), subtle demyelination (Oka *et al.* 2001), and as a transient post-ictal phenomenon (Aykut-Bingol *et al.* 1997).

T1 relaxation reflects the total water content and the dynamic structure of water, including the ratio of free to bound water, the structure and concentration of local macromolecules, and the degree of inter-compartmental exchange (Mathur-De Vre1984). Changes in both total water content and macromolecular structure and concentration will therefore influence tissue T1 relaxation, and consequently the degree of signal suppression during DIR imaging. White matter possesses a T1 relaxation time of approximately half that of grey matter due, most likely, to myelin and more specifically, the presence of cholesterol (Koenig *et al.* 1990). Cerebrospinal fluid has very long T1 times as there is a low concentration of macromolecules. Quantitative abnormalities of T1-weighted imaging have been reported in cerebral ischaemia (Calamante *et al.* 1999), tumours (Bastin *et al.* 2002;

Hoehn-Berlage and Bockhorst 1994) and multiple sclerosis (Vaithianathar *et al.* 2002; Barkhof, Karas, and van Walderveen 2000), where abnormal T1 times were identified both in lesions and in normal appearing white and grey matter (Griffin *et al.* 2002).

Common pathological characteristics of acquired lesions include gliosis and expansion of the extracellular space (Adams 1975; Castillo *et al.* 1996) which will give rise to a prolonged T1 relaxation time and increased proton-density. Neuronal loss will result in cortical atrophy and reduced DSI grey matter, and subsequent Wallerian degeneration in the underlying white matter will cause an increase in DSI in the white matter compartment (Khurana *et al.* 1999), as seen in the current study. It is likely that these regions are characterised microstructurally by increased free water and disruption of the macromolecular environment, producing changes in both T1 relaxation and proton-density that results in increased DIR signal. Regions of decreased DSI were almost exclusively within the cortex or sub-cortical region, and are likely to represent loss of grey matter tissue as a result of the cerebral insult. In 7 patients, abnormalities of DSI were also identified in normal appearing tissue. These were typically regions of increased DSI, and in 6 out of the 7 patients, the regions concurred with the localisation of epileptiform EEG abnormality. This suggests that not only are occult structural abnormalities present but also, that these may be relevant for seizure initiation or propagation.

Malformations of cortical development are an important cause of refractory focal epilepsy and surgical treatment is often associated with a poor post-operative outcome (Sisodiya 2000). Voxel-based morphometry relies almost exclusively on abnormalities of grey matter distribution and not subtle signal change, and has identified abnormalities of segmented grey matter both within overtly abnormal and in normal-appearing tissues (Kassubek *et al.* 2002; Woermann *et al.* 1999a). In the current study, all patients with MCD had regions of increased DSI that corresponded to all or part of the MCD identified visually on conventional MR images, such as thickened cortices in macrogyria; blurring of the grey / white matter interface in focal cortical dysplasia; or ectopic grey matter in band, subcortical or subependymal heterotopia. These abnormalities of grey matter are readily apparent on DIR images and, as such, are identified as regions of significantly increased DSI on a voxel-based comparison with control subjects. The underlying white matter may also be abnormal with clusters of heterotopic neurons, axonal dysmyelination, gliosis and spongiolytic change (Usui *et al.* 2001; Marchal *et al.* 1989; Urbach *et al.* 2002) resulting in a prolongation of T1, and consequently an increase in DSI in the white matter compartment (Steen *et al.* 2001).

Five patients also had regions of decreased DSI, predominantly in normal appearing tissue. In each of the three patients with band heterotopia, there were regions of reduced DSI in the cortices overlying the bands of heterotopic grey matter. This is consistent with the presence of thinner cortices, previously noted in band heterotopia (Barkovich *et al.* 1994).

MCDs are associated with abnormal position, quantity or morphology of grey matter on conventional imaging but in some patients the abnormalities may be imperceptible and lesions may be more extensive than the visually evident abnormalities on conventional MRI (Sisodiya *et al.* 1995b; Palmini *et al.* 1995; Richardson *et al.* 1996; Eriksson *et al.* 2001b; Rugg-Gunn *et al.* 2003). In the current study, abnormalities of DSI were identified beyond the visually apparent MCD in 8 patients, implying additional sensitivity from DSI. These were in all sub-groups of MCDs, and were seen both locally and in more distant sites. Despite similar appearances to normal grey matter on visual assessment of conventional MR imaging, dysgenetic tissue is functionally and microstructurally distinct, with aberrant cytoarchitecture, abnormal neuronal positioning and size, disordered cortical lamination,

attenuated and disordered dendrites and axons, and altered cytoskeletal elements (Duong *et al.* 1994; Barth 1987). There may also be subtle white matter abnormalities in MCD, for example, disorganised neuropil, thinner axons, or impaired myelination resulting in a relative reduction in white matter. These grey and white matter abnormalities possess a distinct macromolecular environment, appear abnormal on imaging sequences sensitive to changes at this level (Rugg-Gunn *et al.* 2003; Eriksson *et al.* 2001b), and may cause subtle alterations in relaxation parameters, identifiable only with quantitative analyses (Rugg-Gunn *et al.* 2002a). It is also possible that areas of abnormal DSI in lesional or extra-lesional sites may be due to cerebral damage secondary to chronic seizures.

Abnormalities of DSI were identified in 15 out of 33 MRI-negative patients, 10 of which concurred with the location of epileptic activity. In 14 patients there were regions of increased DSI, in both the grey and white matter compartments, and in 3 patients there were regions of decreased DSI in the grey matter compartment. Regions of abnormal DSI in MRI-negative patients may be due to aetiological factors, such as occult dysgenesis, or prior injury, or as a result of chronic seizures, such as neuronal loss or gliosis. Pathological material is not yet available, from these cases, for correlative studies. DIR signal is determined by a number of parameters, in particular proton density and T1 relaxation time. DIR imaging therefore provides sensitivity in the detection of structural lesions rather than pathological specificity. In patients with focal epilepsy and normal conventional MRI, histopathological features of surgically resected epileptic foci include cortical dysplasia and dyslamination, and in the white matter, microdysgenesis, astroglial proliferation, and heterotopia (Siegel *et al.* 2001; Rugg-Gunn *et al.* 2002b; Theodore *et al.* 1990; Zentner *et al.* 1995). Quantitative evaluation of DSI or T1 times has not previously been undertaken in epilepsy. VBM has been used to interrogate grey matter concentration (GMC) in patients with epilepsy and identified abnormal grey matter distribution both within and distant to MCD, but was unhelpful in individual MRI-negative patients (Woermann *et al.* 1999a). Group analysis of patients with hippocampal sclerosis detected increased neocortical grey matter in the ipsilateral temporal lobe, consistent with a blurring of the grey / white matter interface and misclassification of image voxels by the segmentation process (Woermann *et al.* 1999a; Meiners *et al.* 1999b; Mitchell *et al.* 1999). More recently, Keller et al reported similar findings of increased GMC in the ipsilateral temporal lobe, in addition to reduced GMC in the dorsal prefrontal cortex in patients with hippocampal atrophy. The authors suggested that epileptiform excitotoxic discharges from the pathological hippocampus may cause atrophy of reciprocally connected sites (Keller *et al.* 2002a; Keller *et al.* 2002b).

In the group analyses presented in this chapter, only increased DSI was identified within the white matter of the respective cerebral lobes. This is consistent with previous imaging and histopathological studies describing the presence of abnormal local white matter in temporal lobe epilepsy (Meiners *et al.* 1999b). The underlying pathological basis is unclear at present but may represent a disorder of myelination (Mitchell *et al.* 1999) or increased neuronal cell bodies in WM (Hammers *et al.* 2002b). Whilst group analyses are interesting and provide additional evidence for the presence of more widespread morphological abnormalities in focal epilepsy, they are of limited clinical value in individual patients. It is clear however, that additional abnormalities exist, even beyond the improved sensitivity afforded by current quantitative analyses, and with improvements in both image acquisition and post-acquisition processing techniques, further occult lesions may be identified in individual patients.

In conclusion, DIR imaging analysed on a voxel-by-voxel basis identified abnormal signal in patients with both acquired lesions and MCD. These regions concurred with abnormalities seen on visual assessment of conventional MR images and abnormalities were also demonstrated in regions previously diagnosed as normal suggesting the presence of occult injury or dysgenesis. DSI abnormalities were seen in 45% of MRI-negative

patients. In 66% of these, the regions concurred with electroclinical data, and may represent structural abnormalities associated with an occult epileptic focus. On the basis of these results, DIR imaging, analysed using voxel-based methods, may be a useful imaging tool in the pre-surgical evaluation of MRI-negative patients.

CHAPTER SEVEN

Discussion & Conclusions

7.1 CONCLUSIONS TO EXPERIMENTAL STUDIES

7.1.1 Introduction

With the advent of MRI it was hoped that in addition to improved lesion sensitivity, it would be possible to differentiate specific tissue pathology. Early studies proposed that the evaluation of a combination of NMR parameters, principally, proton density, T1 and T2-relaxation times might permit the complete and accurate characterisation of pathological tissue in vivo (Damadian1971). However, a significant overlap of relaxation values exists between normal and diseased tissue using basic imaging contrasts and these early promising reports were challenged and disproved (Parrish *et al.* 1974; Eggleston *et al.* 1975).

The aims of this thesis are to evaluate the enhanced sensitivity afforded by novel contrast mechanisms and to establish whether these new techniques afford pathological specificity. This chapter summarises the results of the four scanning techniques.

7.1.2 Results

7.1.2.1 Individual sequences (table 7.1)

7.1.2.1.1 Diffusion tensor imaging

Acquired

SPM detected areas of significantly reduced anisotropy and increased diffusivity in all patients with acquired lesions. Almost exclusively, these areas corresponded to the abnormalities identified on visual inspection of the conventional MR images. Furthermore, 30% of patients possessed areas of significantly abnormal diffusion in regions previously reported as normal. These were commonly immediately adjacent to the areas of visualised damage on conventional MRI scans.

Malformations of cortical development

In 70% of patients with MCD, SPM detected areas of decreased anisotropy. In almost 90% of these patients the changes corresponded to all or part of the MCD. Furthermore, in 35% of those patients with reduced anisotropy, changes were found outside the MCD in tissue that appeared normal on conventional MRI, 40% of which concurred with electroclinical localising information regarding site of seizure onset. Areas of increased anisotropy were detected in a small number of patients, commonly adjacent to MCDs.

SPM detected areas of increased diffusivity in 40% of patients with MCD. In addition to increased diffusivity corresponding to all or part of the MCD in the majority of these patients, changes were found outside the MCD in tissue that appeared normal on conventional MRI in 90%. In 75% of these patients, the extra-lesional regions of abnormality were in agreement with localising EEG data. In 70% of patients with abnormal diffusion,

the diffusivity changes were more extensive than the abnormalities of anisotropy.

MRI-negative

SPM analyses of patients with focal epilepsy and normal conventional imaging revealed abnormalities of anisotropy that were concordant with both seizure semiology and/or EEG data in only 7%. Eighteen percent of MRI-negative patients had regions of significantly increased diffusivity. Seventy-five percent of these concurred with electroclinical information regarding localisation of seizure onset. A small number of patients possessed abnormalities of either anisotropy (3%) or mean diffusivity (5%), which did not agree with localising data.

7.1.2.1.2 Magnetisation transfer imaging

Acquired

In all patients with acquired lesions, SPM detected areas of significantly reduced MTR. In all, the areas of reduced MTR corresponded to the abnormalities identified on visual inspection of the conventional MR images. In 35% of patients, areas of significantly reduced MTR were detected in regions previously reported as normal; 66% of which concurred with electroclinical localising information regarding site of seizure onset. There were no increases in MTR.

Malformations of cortical development

In 88% of patients with MCD, SPM detected regions of reduced MTR. In all of these, the areas of reduced MTR corresponded to all or part of the MCD identified on visual inspection of the conventional MR images. In addition, in 54% of patients, changes were found outside the MCD in tissue that appeared normal on conventional MRI, 50% of which was in agreement with the location of epileptiform EEG activity.

MRI-negative

SPM detected regions of reduced MTR in 36% of the MRI-negative patients, 80% of which concurred with the localization of epileptiform EEG abnormality. There were no increases in MTR.

7.1.2.1.3 T2 mapping

Acquired

In all patients with acquired lesions, SPM detected areas of significantly increased T2 signal. In all of these, the areas of increased T2 signal corresponded to the abnormalities identified on visual inspection of the conventional MR images. In 64% of patients, areas of significantly increased T2 signal were detected in regions previously reported as normal, 88% of which concurred with electroclinical information regarding site of seizure onset. There were no areas of significantly shortened T2 times.

Malformations of cortical development

In 90% of patients with MCD, SPM detected regions of increased T2. In all of these, the areas of increased T2 signal corresponded to all or part of the MCD identified on visual inspection of the conventional MR images. In

addition, in 35% of patients, changes were found outside the MCD in tissue that appeared normal on conventional MRI, 43% of which concurred with electroclinical information regarding site of seizure onset.

MRI-negative

SPM analyses of MRI-negative patients revealed regions of significantly increased T2 in 55%. In 76% of these, the regions concurred with the localisation of epileptiform EEG abnormality, the majority of which were ictal recordings. Four percent of patients had regions of decreased T2 signal, none of which agreed with electroclinical data regarding site of seizure onset.

7.1.2.1.4 *Double inversion recovery*

Acquired

SPM detected areas of significantly abnormal DIR signal intensity (DSI) in 90% of patients with acquired lesions. In all of these, areas of *increased* DSI corresponded to abnormalities identified on visual inspection of the conventional MR images. In 66% of those patients with abnormal DSI, there were also regions of significantly *decreased* DSI, all of which corresponded to abnormalities identified on the conventional MR images. In 70% of patients with acquired lesions, areas of significantly *increased* DSI, and in 10% of patients, areas of *decreased* DSI were detected in regions previously reported as normal. In 85% of these patients, the areas of abnormal DSI within normal appearing cerebral tissue concurred with the localisation of epileptiform EEG activity.

Malformations of cortical development

In all patients with MCD, SPM detected regions of *increased* DSI which corresponded to all or part of the MCD identified on visual inspection of the conventional MR images. In addition, 36% of patients had regions of *decreased* DSI, 20% of which corresponded to abnormalities seen on the conventional MR images. In 57% of patients, abnormalities of DSI were found outside the MCD in tissue that appeared normal on conventional MRI. In 75% of these patients, the areas of abnormal DSI concurred with the localisation of epileptiform EEG activity despite normal appearances on conventional MRI.

MRI-negative

SPM analyses revealed regions of significantly abnormal DSI in 45% of MRI-negative patients, of which 93% were regions of *increased* DSI, and 20% were regions of *decreased* DSI. Thirteen percent, therefore, had both regions of *increased* and regions of *decreased* DSI. In 66% of patients with abnormal DSI, the regions concurred with the localisation of epileptiform EEG abnormality.

sequence	*Acquired lesions*		*MCD*		*MRI-negative*					
	no. patients	*concur with conv. MRI / occult lesions*	*no. patients*	*concur with conv. MRI / occult lesions*	*no. patients*	*no. of abn. / concur with EEG*	***all abn.***		***EEG conc. abn.***	
							sens.	***spec.***	***sens.***	***spec.***
DTI- FA	10	10 / 5	24	15 / 6	72	8 / 5	**11%**	**97%**	**7%**	**91%**
DTI- MD	10	10 / 3	24	10 / 9	72	16 / 12	**22%**	**93%**	**18%**	**88%**
MTI	11	11 / 4	15	13 / 8	75	25 / 20	**33%**	**97%**	**29%**	**85%**
T2M	14	14 / 9	20	18 / 7	53	29 / 22	**55%**	**90%**	**48%**	**80%**
DIR	10	9 / 7	14	14 / 8	33	15 / 10	**45%**	**90%**	**36%**	**84%**

Table 7.1 Individual advanced MR sequences in acquired lesions, malformations of cortical development, and in MRI-negative patients. The Table describes the number of patients scanned with each sequence, the number of patients with regions that are concordant with conventional MRI and the number of patients with occult regions (acquired and MCD groups). In addition, the number of MRI-negative patients scanned, the number of patients with occult regions identified and the number that concur with EEG data, with calculated "sensitivity", "specificity". (*See Appendix 1 for definitions of statistical terms).*

7.1.2.2 Combined sequences

The scanning of patients with individual advanced MR sequences is valuable in establishing the usefulness, albeit provisionally, of a new imaging method. Scanning patients with a variety of aetiologies further enhances this evaluation. The confirmation of an area of occult abnormality with corroboratory evidence, such as histopathological data, is clearly important. Where this information is lacking, the co-localisation of an area of abnormality with additional imaging sequences is useful, and imparts greater confidence in the veracity of the findings. Table 7.2 summarises the application of the advanced MR sequences for each aetiology.

	no. of patients		
no. of sequences	*acquired*	*MCD*	*MRI-negative*
1	**8**	**23**	**31**
2	**6**	**8**	**23**
3	**3**	**6**	**25**
4	**4**	**4**	**21**
total	***21***	***41***	***100***

Table 7.2: Number of patients with focal epilepsy and acquired lesions, MCDs, or normal conventional MRI scanned with 1 or any combination of 2, 3, or all 4 of the advanced MR techniques.

7.1.2.2.1 Acquired lesions

Thirteen of the 21 patients with acquired lesions had more than one imaging sequence. In 20 patients, all of the advanced techniques used in each patient detected regions of abnormality which concurred with the lesions identifiable on visual inspection of the conventional images (figure 7.1). Of greater interest was the identification and co-localisation of occult abnormalities. Fourteen patients possessed regions of occult abnormality, 5 of which were scanned with only 1 sequence. Nine of the 13 patients who were scanned with more than one sequence possessed extra-lesional areas of abnormality. Seven of these 9 had more than one extra-lesional area. The regions from 6 of these 7 patients co-localised, five of which concurred with epileptiform EEG abnormalities. One patient had a region of abnormality in the right periventricular white matter which was identified with 3 techniques but was discordant with interictal EEG data which localised to the left temporal lobe. A further patient had 3 separate but related abnormalities on imaging using 3 advanced techniques, all of which were in agreement with EEG data.

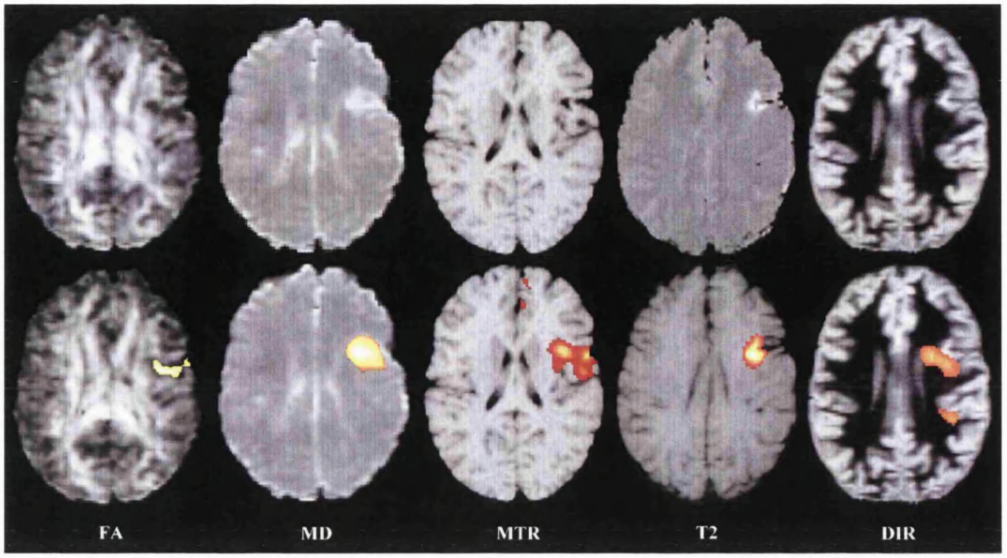

Figure 7.1: Patient with left frontal lobe infarct. (Left to right) Normalised axial fractional anisotropy (FA), mean diffusivity (MD), magnetisation transfer ratio (MTR), T2-mapping (T2), and double inversion recovery (DIR) images (top row), with superimposed regions of significant abnormality identified by SPM (bottom row).

Within the acquired lesion group, 5 of the 6 patients (83%) with cerebral infarction demonstrated occult regions of abnormality on any of the four sequences. Five of the 8 patients with head injuries (63%), 3 of the 5 patients (60%) with intra-cranial infection, and 1 of the 2 (50%) patients with a history of perinatal injury exhibited extra-lesional abnormalities (table 7.3).

7.1.2.2.2 Malformations of cortical development

Forty-one patients with focal epilepsy and malformations of cortical development were scanned with 73 sequences. Eighteen of the 41 patients had more than one imaging sequence. In 39 out of the 41 patients, the advanced techniques detected regions of abnormality which concurred with the lesions identifiable on visual inspection of the conventional images (figure 7.2). In two patients, one with band heterotopia scanned only with T2 mapping, and the other with subependymal heterotopia scanned with DTI and MTI, advanced imaging techniques failed to identify any abnormalities.

Twenty-five patients possessed regions of occult abnormality, 11 of which were scanned with only 1 sequence. Fourteen of the 18 patients who were scanned with two or more sequences possessed extra-lesional areas of abnormality. Six of these 14 had more than one extra-lesional area. The regions from 4 of these 6 patients co-localised, 2 of which concurred with epileptiform EEG abnormalities (figure 7.3)

Within the MCD group, 10 of the 14 patients (71%) with gyral abnormalities demonstrated occult regions of abnormality on any of the four sequences. Eleven of the 21 patients with heterotopia (52%), 3 of the 7 patients (43%) with focal cortical dysplasia, and the 1 patient with DNET exhibited extra-lesional abnormalities (table 7.4).

acquired lesion	*no. of patients*	*no. with occult abnormalities (% of patients)*	*no. concurred with EEG*	*no. co-localised with other sequences / no. of patients with >1 occult region*	*no. concurred with EEG*
infarction	6	5 (83%)	3	2/3	2
head injury	8	5 (63%)	2	2/2	2
infection	5	3 (60%)	2	1/1	1
perinatal injury	2	1 (50%)	1	1/1	1

Table 7.3: The concurrence of extra-lesional (occult) abnormalities with EEG and with other advanced MRI sequences in patients with acquired lesions. The table shows the total number of patients with each aetiology, the number of patients with occult abnormalities identified on any of the advanced sequences and the number of those that were in agreement with EEG data. In addition, the number of patients with more than one occult region identified, whether they co-localised, that is, different sequences identified the same cerebral region, and the number that were in agreement with EEG data.

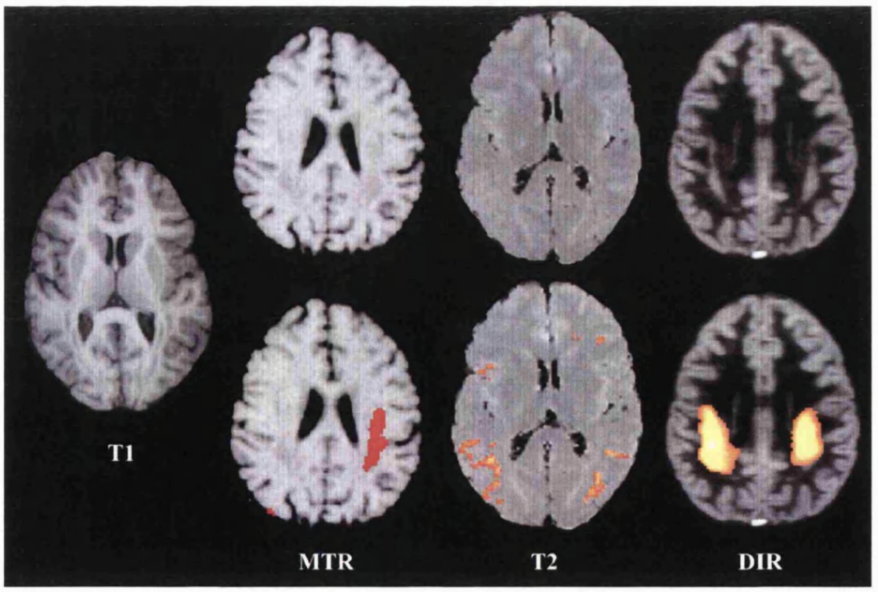

Figure 7.2: Patient with bilateral, posterior band heterotopia. (Top row, left to right): normalised axial magnetisation transfer ratio (MTR), T2-mapping (T2), and double inversion recovery (DIR) images. (Bottom row): with superimposed regions of significant abnormality identified by SPM. Axial T1-weighted image is also shown.

MCD	*no. of patients*	*no. with occult abnormalities (% of patients)*	*no. concurred with EEG*	*no. co-localised with other sequences / no of pts with >1 occult region*	*no. concurred with EEG*
gyral	14	10 (71%)	6	1/3	0
subepend het.	9	3 (33%)	1	0/0	0
subcortical het.	6	5 (83%)	4	1/1	1
band het.	6	3 (50%)	2	1/1	1
FCD	7	3 (43%)	1	0/0	1
DNET	1	1 (100%)	1	1/1	1

Table 7.4 The concurrence of extra-lesional abnormalities with EEG and with other advanced MRI sequences in patients with malformations of cortical development. (het. - heterotopia, FCD - focal cortical dysplasia, DNET - dysembryoplastic neuroepithelial tumour).

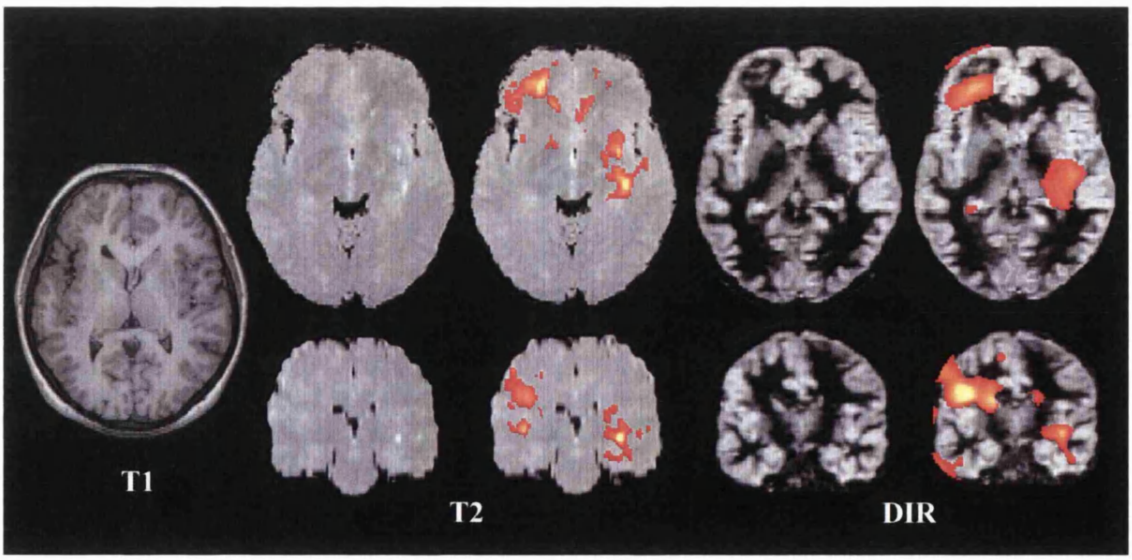

Figure 7.3: Patient with a left perisylvian gyral abnormality. Normalised axial (top) and coronal (bottom) T2-mapping (T2), and double inversion recovery (DIR) images; with superimposed regions of significant abnormality identified by SPM. The right perisylvian region / insula appeared normal on conventional MRI (T1). Note that right on the image is patient's right.

It is important to note that within each group, relatively small numbers of patients were scanned with more than one acquisition and, moreover, specific combinations of sequences were infrequent. Undoubtedly, this limits the validity of any conclusions that may be drawn from this data.

7.1.2.2.3 MRI-negative patients

One hundred patients with focal epilepsy and normal conventional MRI were scanned with 235 sequences. Thirty-eight patients had normal advanced MRI. Of these, 24 patients were scanned with 1 of the 4 sequences, 6 patients had 2 sequences, 5 patients had 3 sequences and 3 patients had all 4 sequences. Sixty-two patients had regions of abnormality identified on one or more advanced sequences. Of these, 39 patients demonstrated an abnormality with 1 technique, 17 patients demonstrated abnormalities with 2 techniques (figure 7.4 and 7.5), 6 patients demonstrated abnormalities with 3 techniques (figure 7.6), and no patients had 4 regions of abnormality (table 7.5).

MRI-negative	*no. of patients*	*no. of pts with abnormalities (%)*	*no. concurred with EEG*	*no. co-localised with other sequences / no. of patients with >1 abnormality*	*no. concurred with EEG*
TLE	44	25 (57%)	20	7/11	5
FLE	31	22 (71%)	17	6/7	5
OLE	7	2 (29%)	2	1/1	1
widespread	18	12 (67%)	10	2/4	2

Table 7.5 The concurrence of occult abnormalities with EEG and with other advanced MRI sequences in patients with cryptogenic focal epilepsy. Presumed focus defined by ictal and/or interictal EEG; TLE - temporal lobe epilepsy, FLE - frontal lobe epilepsy, OLE - occipital lobe epilepsy, widespread - EEG abnormality not localised to a single cerebral lobe.

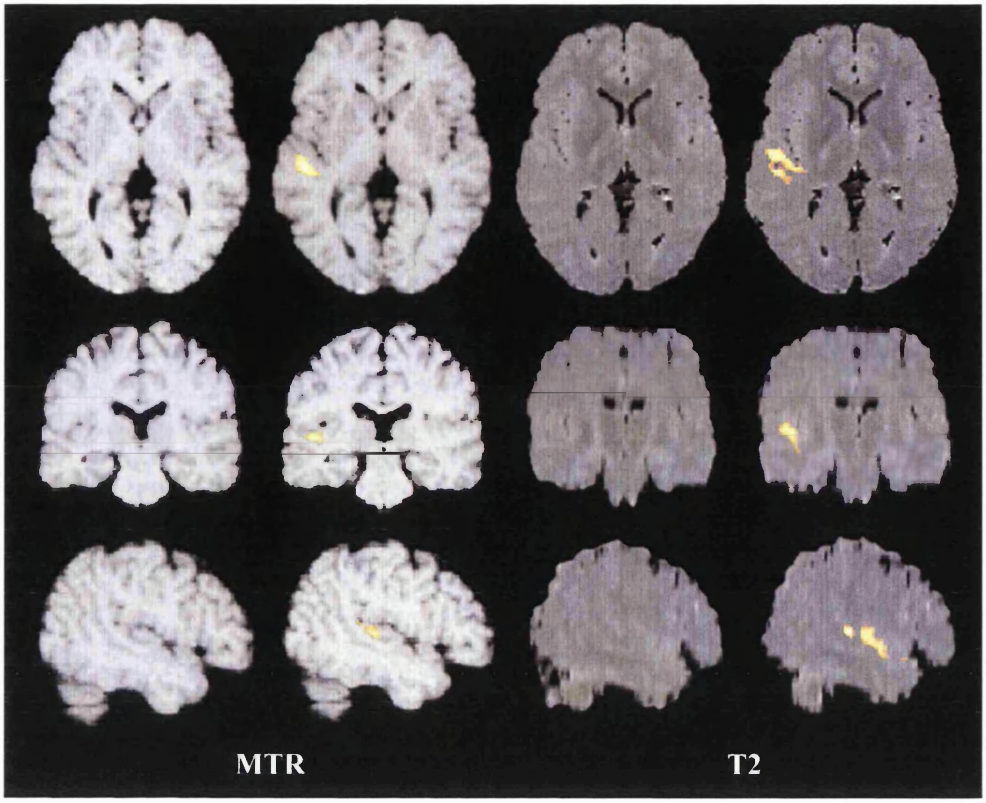

Figure 7.4: Patient with cryptogenic left temporal lobe epilepsy, associated with auditory simple partial seizures. Axial, sagittal, and coronal MTR (columns 1 and 2) and T2 maps (columns 3 and 4) are shown, with superimposed regions of abnormality identified by SPM. Note that right on the image is patient's right.

The identification of occult abnormalities in MRI-negative patients was enhanced by using a greater number of sequences. The "pick-up rate", "detection rate" or "sensitivity" was approximately 23% when only 1 imaging sequence was employed. This increased to 86% when all 4 sequences were used. This was, to some degree, dependent on which of the 4 techniques were used; Table 7.1 details the "sensitivities" of the individual sequences. With an increasing number of sequences used, the number of patients without an electroclinically concordant abnormality on advanced imaging decreased and the detection rate increased. However, as a greater number of sequences were employed, the number of control subjects with abnormalities and MRI-negative patients with discordant abnormalities on advanced imaging increased (table 7.6).

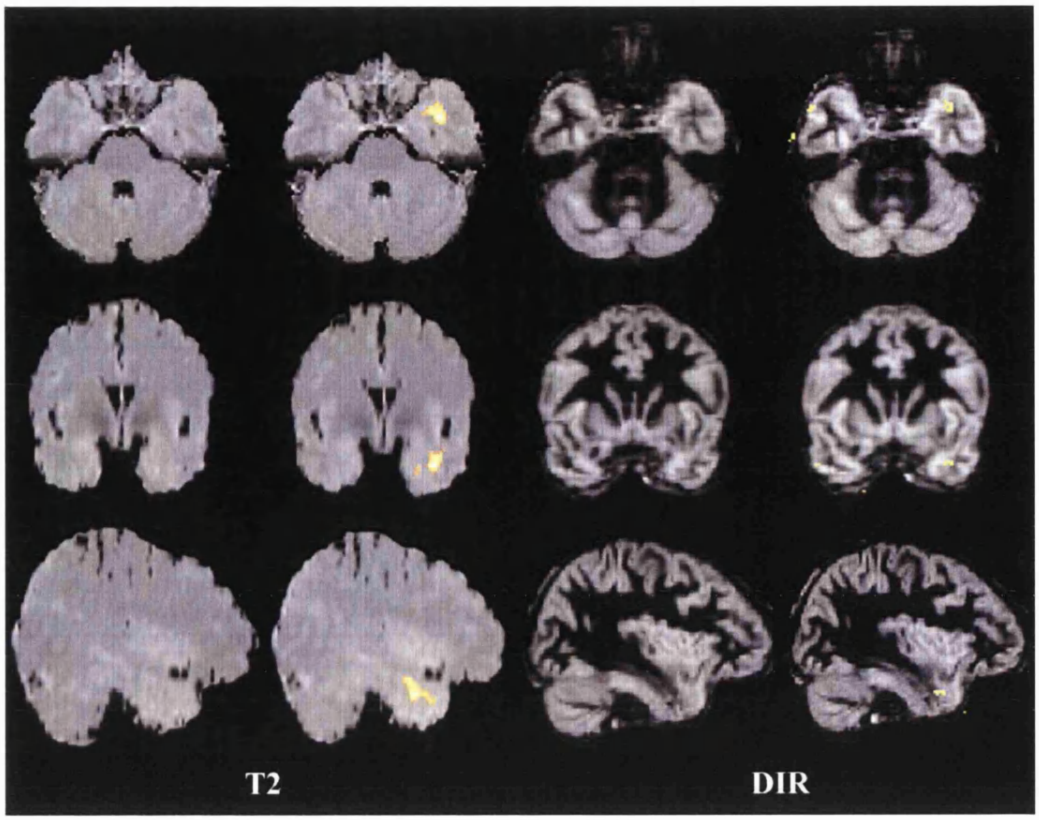

Figure 7.5: Patient with cryptogenic right temporal lobe epilepsy. Axial, sagittal, and coronal T2 maps and DIR images are shown, with superimposed regions of abnormality identified by SPM. Note that right on the image is patient's right.

It is possible that an area of abnormality in either the patient or control group reflected an underlying area of structural abnormality which was not epileptic, and as such negatively impacted on the estimated sensitivity and / or specificity despite providing accurate information. In addition, interictal epileptiform activity on EEG does not always correlate exactly with the site of seizure onset, and therefore the degree of concordance between imaging abnormalities and EEG data may be over or underestimated. The statistics should therefore be regarded as an approximation, but nevertheless, they provide a useful guide as to the potential "usefulness" of the imaging techniques.

7.1.3 Discussion

It was hypothesised that advanced MRI techniques would be capable of identifying regions of occult abnormality in patients with focal epilepsy and normal, optimal, conventional MR imaging. The techniques were initially evaluated in both normal control subjects and patients with focal epilepsy and known lesions. This allowed both the construction of a normative database and a comprehensive understanding of the imaging abnormalities, which was then applied to the results of the patients with normal conventional MRI. Overall, the advanced sequences

were sensitive in the detection of abnormalities in patients with acquired lesions or MCD. In a significant proportion of patients, extra-lesional areas were identified, most of which concurred with EEG data and other advanced sequences. A range of sensitivities was observed in the MRI-negative patients. The combination of techniques further enhanced the ability to identify occult structural abnormalities. There remain, however, a number of important questions. Firstly, why are some occult lesions identified with some of the techniques, and not with others? Does the combination of techniques afford pathological specificity, or are the results merely a sum of the individual sensitivities? Finally, if these questions remain unanswered, what are the essential steps required to resolve them in the future?

	MRI-negative					
no. of sequences	*no. of patients*	*no. of abn. / concur with EEG*	*all abnormalities*		*EEG concordant abn.*	
			sensitivity	*specificity*	*sensitivity*	*specificity*
1	31	10 / 7	23%	92%	23%	100%
2	23	23 / 13	74%	92%	68%	93%
3	25	20 / 11	80%	92%	69%	90%
4	21	18 / 13	86%	92%	81%	96%

Table 7.6: The impact, in terms of "sensitivity" and "specificity", of scanning MRI-negative patients with 1, 2, 3 or 4 advanced MR sequences. It is important to note that without a definitive "gold standard" investigation, with which to compare the results of the advanced imaging techniques, the statistics should be regarded as useful approximations only. *(See Appendix 1 for definitions of statistical terms).*

7.1.3.1 Methodological issues

It is important to note that, for the purposes of this Thesis, EEG recordings have been used as a pragmatic "gold standard" of seizure localisation. Wherever possible these were ictal intra- or extracranial recordings, however, where these data were not available, interictal recordings were used. This is an important methodological limitation and permits only an *estimate* of the degree of correlation between the localisation of presumed seizure foci and advanced imaging abnormalities. Nevertheless, the remit of advanced imaging techniques is to provide contributory localising information to be used in conjunction with EEG, clinical, neuropsychological, and PET data, and not as a replacement for adequate EEG studies.

Recent advances in genetics have demonstrated that a proportion of patients with electroclinically "focal" epilepsy possess an inherited channelopathy, for example in nocturnal frontal lobe epilepsy (Phillips *et al.* 2001). It is possible that some of the MRI-negative patients evaluated in this Thesis may have an unrecognised genetic

abnormality, and as such should be classified as *idiopathic*, rather than cryptogenic. It is, therefore, now recommended that a systematically acquired family history should be obtained from each patient prior to inclusion in a study of MRI-negative patients with focal epilepsy.

Each technique interrogated specific aspects of the microstructural environment of a tissue. In addition, despite major similarities between the methodological aspects of each technique, there were a number of important differences at the image acquisition, post-processing and statistical analysis and inference stages (table 7.7).

	acquisition		*post-processing*			*analysis*	
	sequence	*voxel size (mm)*	*normalisation*	*S.I. threshold*	*smoothing (mm)*	*voxel thresh.*	*cluster extent*
FA	DW- EPI	2.5x2.5x5	linear	0.5	8	T	T
MD					10		
MTI	3D - SE	1x1x1.5	linear	0.5	8	T	T
T2M	dual-echo	1x1x5	warp	0.5	4	T	T
DIR	2-3D FSE	1x1x2	warp	explicit mask	14	T	ς

Table 7.7 Comparison of acquisition, post-processing and statistical analysis parameters for each advanced MR technique. (DW-EPI - diffusion-weighted echo-planar imaging, SE - spin-echo, 2-3D FSE - 2D/3D hybrid fast spin-echo sequence, warp - nonlinear normalisation).

Overall, the methodology of each technique was broadly similar, in particular the use of SPM to compare individual patients with a group of control subjects. Image acquisition was optimised to offer accurate, reproducible and meaningful high-resolution data without compromising patient safety and comfort. Post-processing and statistical steps were individually tailored for each sequence to maximise the specific advantages of each technique. Therefore, important differences between the methods exist and are likely to influence the ability to identify subtle structural abnormalities.

The most sensitive of the 4 techniques in MRI-negative patients was T2 mapping which had an in-plane resolution of 1mm by 1mm, was normalised using non-linear "warping" steps, and was smoothed with a smoothing kernel of only 4mm. Double inversion recovery was of the same in-plane resolution, and was similarly normalised, but was smoothed with a 14mm kernel. This was necessary in order to maintain an acceptable false positive rate as a cluster extent threshold was not used. The sensitivity of MTI was significantly less than that of T2 mapping and DIR, despite identical in-plane voxel size. MTR maps were normalised using linear steps only and were smoothed with an 8mm kernel. This suggests that the use of nonlinear normalisation is important in maximising lesion sensitivity. This is almost certainly due to the existence of a narrow normative range. Intuitively, less smoothed images / maps should be more sensitive. Although the DIR images were smoothed with a 14mm kernel, a cluster extent threshold was not used, as this has recently been shown to be inappropriate in voxel-based morphometry

(Ashburner and Friston 2000). Repeating the analysis of the control group using a cluster extent threshold, an acceptable false positive rate was observed with a smoothing kernel of 4mm, equivalent to T2 mapping. However, as mentioned, other limitations precluded its use. MTR images were smoothed with an 8mm, and mean diffusivity maps with a 10mm, kernel. As the degree of smoothing increased, the sensitivity decreased. Fractional anisotropy maps were smoothed with an 8mm kernel, yet had the lowest sensitivity, at 7%. This is most likely due to alternative methodological limitations, specific to the analysis of FA maps, although it is possible that FA may remain relatively unperturbed by relevant occult lesions. FA maps are generally composed of two compartments, white matter with high anisotropy and grey matter and CSF with low anisotropy. This leads to significant variability in FA values in adjacent voxels at, for example, the grey / white matter interface. Inadequate normalisation, that is, incomplete matching of identical cerebral structures, in the control group will result in a wide normal range which will fail to discriminate abnormalities in the patients. FA maps were only linearly normalised. Warping was not performed with SPM96 due to the possibility of unregulated image distortion. With the development of SPM99, and significant improvements in the normalisation process, a further cohort of MRI-negative patients was scanned. The maps were normalised using linear and nonlinear steps, and consequently an improvement in sensitivity was observed (from 3% to 10%). In view of the recent developments regarding the use of cluster extent thresholds in non-stationary data, such as grey matter maps in voxel-based morphometry, it was appropriate to analyse DIR images with only a voxel / height threshold. FA maps are also highly variable due to the non-parametric distribution of anisotropic voxel values, and therefore statistical inference should not include a cluster extent statistic. By doing so, a large number of false positive abnormalities may be identified, particularly in "smooth" cerebral regions. In addition, and as importantly, small occult lesions may be overlooked, if they exist within a highly variable region and are not large enough to exceed the critical statistical threshold (Ashburner and Friston 2000). The inappropriate use of a cluster extent statistic may, therefore, adversely affect both sensitivity and specificity.

In summary, to maximise the potential to identify subtle structural abnormalities, the images / maps should be high-resolution, normalised using linear and nonlinear steps and smoothed with the smallest kernel possible. Furthermore, if the dataset is non-stationary in nature, that is, the voxel values are highly variable throughout the cerebral structure, a cluster extent statistic should not be used. An important caveat to this concerns the normality of data following smoothing. Statistical image analysis in SPM is performed using parametric tests. In order for these tests to be valid, the data must be normally distributed. Prior to smoothing, grey matter images derived from segmented T1-weighted datasets or DIR images, or FA maps are highly non-normal, with most voxels possessing a value close to the extremes. Smoothing renders the data more normally distributed. Recently, Salmond et al. reported that in group versus group VBM, no or only minimal smoothing (4mm kernel) is required to render the parametric tests valid as the "spread" of voxel values across each group produces a similar effect. In an individual versus group VBM comparison, the inherent normality of data provided by a group is absent, and at least 12mm of smoothing is required to validate the parametric tests (Salmond *et al.* 2002). Whilst this is of paramount importance in VBM, MTR, T2 and mean diffusivity maps are intrinsically more normally distributed than grey matter maps. This is because the voxel values in the grey and white matter compartments are less divergent. Fractional anisotropy maps and DIR images should be analysed like grey matter density images derived from VBM, that is, at least 12mm of smoothing, and employing the height threshold statistic only.

An important question is to what extent is it necessary to utilise complex post-processing statistics in the identification of advanced imaging abnormalities? In short, is quantitative evaluation absolutely necessary? Previous imaging studies have proposed that quantitative assessment confers additional sensitivity over visual appraisal and is objective and unbiased to clinical information (Tien *et al.* 1993; Jackson *et al.* 1993). Furthermore, the ability to accurately and confidently discern normal from abnormal tissue on visual assessment arises from extensive experience. The advanced techniques described in this Thesis produce quantitiative maps, such as fractional anisotropy or mean diffusivity images, on which it may be difficult to judge normal from abnormal, even with prior experience. DIR images or T2 or MTR maps may be more suitable for qualitiative evaluation and as such are the subject of ongoing work.

7.1.3.2 Pathophysiological and clinical implications

7.1.3.2.1. Individual sequences

Diffusion tensor imaging, magnetisation transfer imaging, T2 mapping and double inversion recovery interrogate specific molecular, microstructural and architectural properties of cerebral tissue. An important question is to what extent these techniques overlap in terms of the characterisation of pathological tissue. To some extent, this can be answered from the results of the patients with acquired lesions and MCD. In almost all patients with acquired lesions, the 4 techniques identified the visually apparent lesions. There was considerable anatomical overlap of the SPM identified regions of abnormality suggesting that either the different techniques detected the same pathological process or, less likely, there was a number of specific pathological entities co-existing within each lesion, each of which was defined by a different technique. Acquired lesions, irrespective of the underlying aetiology, have a number of pathological features in common, including axonal injury and neuronal loss, microglial proliferation, expansion of the extracellular space and demyelination (Castillo *et al.* 1996; Adams 1992; Jay *et al.* 1998). It is likely that these will be present in variable proportions depending on the nature and severity of the injury. No pathological material is available from either the acquired or MCD patient groups in this study, however, advanced imaging abnormalities have previously been correlated with histopathological changes in both experimental and clinical settings (McGowan *et al.* 1999; van Waesberghe, Kamphorst, and van Walderveen 1998; Assaf *et al.* 1997; Hoehn-Berlage *et al.* 1995).

Fractional anisotropy is sensitive to microstructural disorganization, particularly of axonal white matter tracts, and thus may not be sensitive to grey matter lesions or small, isolated lesions of the white matter unless accompanied by significant demyelination. Mean diffusivity is a marker of compartmental water content and distribution, and is therefore sensitive to alterations in the size of the intra- and extracellular spaces, irrespective of the actual total water content (Rumpel *et al.* 1997; Verheul *et al.* 1994). Increased mean diffusivity is commonly seen in acquired lesions as a result of an expansion of the extracellular space due to neuronal and glial cell loss (Nedelcu *et al.* 1999; Alsop *et al.* 1996). MTI evaluates the macromolecular environment. Loss of macromolecules, which is commonly associated with an increase in extracellular space and increased free water, is paralleled by a reduction of MTR (Lexa *et al.* 1993). Oedema and inflammation result in minor reductions of MTR, whereas the changes in

MTR observed with demyelination and axonal loss are more profound (Brochet and Dousset 1999; Dousset *et al.* 1992; van Waesberghe *et al.* 1999). T2 values are particularly sensitive to changes in total water content and more specifically, increased free water (Leifer, Buonanno, and Richardson Jr. 1990; Scarpelli *et al.* 1994; Briellmann *et al.* 2002b; Mathur-De Vre 1984). Altered water compartmentalization, as observed in cytotoxic oedema, result in minor changes in T2 as the ratio of free to bound water is modified. T2 values elevate markedly however, with increased total water content, particularly in the extracellular space, for example, in vasogenic oedema (Yuh *et al.* 1991; Hossmann and Schuier 1980; Loubinoux *et al.* 1997b). A combination of factors govern the appearance of DSI images derived from DIR. These include the proton-density, which tends to parallel the total tissue water content, and the T1 relaxation time, which is itself determined by the total water content and the dynamic structure of water, including the ratio of free to bound water, the structure and concentration of local macromolecules, and the degree of inter-compartmental exchange (Mathur-De Vre 1984). Changes in both total water content and macromolecular structure and concentration will therefore influence DSI. In this context, it appears reasonable to assume that DIR would be most sensitive as the DSI is influenced by a large number of factors. However, the dynamics are inter-related and may be antagonistic rather than synergistic and, thus, pathological change may be overlooked.

In summary therefore (and undoubtedly a gross simplification of a highly complex environment), mean diffusivity and T2 mapping are most sensitive to changes in free water, and MTI and to a lesser extent fractional anisotropy are most influenced by alterations of macromolecular concentration. DIR imaging, most likely, occupies an intermediate position.

7.1.3.2.2 Combined sequences

Acquired lesions

Mean diffusivity was marginally less sensitive than the other sequences in identifying occult lesions in patients with acquired lesions. T2 mapping and DIR imaging were the most sensitive throughout almost all of the acquired aetiologies; however, methodological limitations, particularly with respect to DTI, may be relevant. Within individual aetiologies in the acquired lesion group, occult lesions were identified most commonly in cerebral infarction and head injury. This suggests that these aetiologies are associated with more widespread subtle abnormalities. It appears (although it is important to note the small sample size) that the more sequences that are employed, the greater the chance of identifying occult abnormalities, irrespective of the original insult (table 7.2). Fourteen of the 21 patients with acquired lesions possessed regions of abnormality that extended beyond the visually apparent lesion on conventional MRI ("extra-lesional areas"). Eight of these 14 patients, possessed extra-lesional areas that were in agreement with EEG localising data. Seven of the 14 patients, after being scanned with more than one technique, had more than one extra-lesional area identified. In 6 of these 7 patients the occult regions co-localised, that is, more than one advanced imaging sequence detected an abnormality in the same anatomical location, thereby providing some corroboratory evidence. There were no combinations of sequences that were seen more frequently than others. All 6 of these regions that were identified by more than one technique were associated with epileptiform EEG abnormality, suggesting that not only were areas of occult pathology

present but they may be relevant in seizure initiation or propagation.

Malformations of cortical development

MTI and DIR were the most sensitive sequences in identifying both known and occult abnormalities in patients with MCD. DTI was the least sensitive. Within individual classes of MCDs, extra-lesional regions were more commonly encountered in patients with gyral abnormalities, or subcortical heterotopia. Occult lesions were seen infrequently in patients with subependymal and band heterotopia, and focal cortical dysplasia. Of the individual sequences, DIR was the most sensitive in detecting extra-lesional areas in patients with gyral abnormalities, and MTI was the most sensitive in SCH. This suggests that imaging sequences which interrogate the macromolecular environment, rather than solely water content are the most useful in identifying both known and occult regions of dysgenetic tissue. This contrasts with acquired lesions where T2 mapping and DIR are most sensitive, suggesting total water content is of paramount importance. Subtle pathological features of MCD include dysmyelination, cortical dyslamination, microdysgenesis, and altered neuropil arborisation (Marchal *et al.* 1989; Manz *et al.* 1979; Duong *et al.* 1994; Barth 1987; Usui *et al.* 2001). These are more likely to be associated with macromolecular irregularities than only altered water content.

Twenty-five of the 41 patients with MCD possessed extra-lesional abnormalities. Six of the 25 patients, after being scanned with more than one technique, had more than one extra-lesional abnormalities identified. In 4 of these 6 patients the occult regions co-localised - that is, more than one advanced imaging sequence detected an abnormality in the same anatomical location. There were no combinations of sequences that were seen more frequently than others. Two of these 4 regions that were identified by more than one technique were associated with epileptiform EEG abnormality. Histopathological, imaging and EEG data have previously documented the presence of widespread dysgenetic tissue in patients with MCD, beyond the margins of conventional MR techniques (Richardson 1996; Palmini *et al.* 1995; Sisodiya *et al.* 1995b). Using more sensitive methods, which probe the macromolecular environment more assiduously, a proportion of these regions may be identified. Clearly, this has implications for surgical treatment of this group, particularly those with gyral malformations or subcortical heterotopia. Conversely, patients with, for example, focal cortical dysplasia, which had a relatively low frequency of occult regions, may be more aggressively evaluated for surgical treatment (Sisodiya 2000).

MRI-negative

On the basis of the results of advanced MR imaging in patients with acquired lesions or MCDs, is it possible to predict the aetiological pathology in MRI-negative patients? Any conclusions drawn are rather speculative without extensive histopathological confirmation from surgical or post-mortem specimens. To date, only one patient has undergone surgical resection based on the results of intracranial EEG recordings and advanced imaging. Significant gliotic change within the white matter of the right frontal lobe was associated with increased mean diffusivity, suggesting greater freedom of movement of water compared to the highly disciplined environment of myelinated axons in normal tissue (Rugg-Gunn *et al.* 2002b). This concurs with previous studies evaluating diffusion parameters in pathological tissue (Nedelcu *et al.* 1999; Rumpel *et al.* 1997; Assaf *et al.* 1997). This patient was scanned and underwent surgical resection before other imaging techniques became available. Extensive gliotic change is more commonly encountered in patients with acquired lesions, rather than MCDs, although may occur as a seizure-related epi-phenomenon (Vinters *et al.* 1993). It is likely therefore, that similar

regions would be more likely to be identified on T2 imaging and possibly DIR, than MTI. Conversely, occult dysgenesis may be more readily identified with MTI.

Notwithstanding methodological considerations, T2 mapping and DIR were overall the most sensitive techniques in MRI-negative patients. MTI and DTI, particularly fractional anisotropy, were less sensitive. This may be due to the frequency of the possible underlying pathologies. Previous histopathological studies of surgically resected epileptic foci which were unremarkable on conventional MRI have frequently reported gliosis (Lorenzo *et al.* 1995; Cascino *et al.* 1992; Theodore *et al.* 1990) and microdysgenesis (Siegel *et al.* 2001). Cortical dysplasia (Pacia *et al.* 1996), disordered cortical lamination and subcortical laminar heterotopia have also been identified although much less frequently (Palmini *et al.* 1991b).

The ideal imaging sequence would therefore be sensitive to both altered water content and a disrupted macromolecular environment. Potentially, this is offered by either diffusion tensor imaging or DIR, although all imaging sequences are influenced to some degree by both pathological states. Improving the sensitivity of both these techniques, particularly DTI, is the subject of future work. It is important to note that even the most sensitive of the techniques did not identify all the abnormalities detected by the other, less sensitive methods. This emphasises the possible existence of a degree of pathological specificity with each technique, although there is undoubtedly significant overlap. It is also possible that a proportion of the regions identified by the most sensitive techniques may be "false positives". Overall sensitivity with one technique was 23%. With 4 techniques this increased to 86%. It appears therefore that each technique interrogates specific aspects of tissue microstructure and does not merely detect the most abnormal region, irrespective of the underlying pathology. Twenty-three MRI-negative patients had more than one region identified as abnormal, of which 16 co-localised, that is, more than one sequence identified the same cerebral region. Of these 16, 13 concurred with the location of epileptiform EEG abnormality. In 3 patients therefore, regions distant from the presumed epileptic focus were co-identified by more than one sequence. In two patients, these were within the white matter of the posterior parietal and occipital lobes bilaterally. One patient had a clinical history of perinatal injury, which is commonly associated with imaging abnormalities in these regions. This emphasizes an important pathophysiological limitation of these techniques. They are not specific for the epileptic focus, which may remain undetected unless accompanied by significant structural disruption. One relies on corroboratory evidence from EEG which was used as a pragmatic "gold standard", however, this is not ideal. Furthermore, without histopathological confirmation, even with congruent EEG and imaging data, it is not possible to establish whether the abnormalities represent the seizure focus or a secondary epi-phenomenon, such as subcortical gliosis. In 11 of the 13 patients, two sequences co-localised. A particular combination of techniques was not observed however. In 2 patients, 3 sequences co-localised. In each case, these were mean diffusivity, MTI and T2 mapping (figure 7.6). No patients exhibited co-localisation with all 4 techniques.

Previous imaging studies in other conditions, notably multiple sclerosis, have reported significant correlation between MTR and diffusion parameters, including anisotropy and diffusivity (Griffin *et al.* 2001; Filippi 2003; Hanyu *et al.* 1999; Ferini-Strambi *et al.* 2000). This is not universally accepted however (Guo, Jewells, and Provenzale 2001; Iannucci *et al.* 2001; Ikezaki *et al.* 1997). Experimental studies have reported that quantitative T2 values and ADC increase 3-5 times more than MTR in necrotic tissue and, in states of altered water

compartmentalisation, MTI derived parameters remained static, whilst both ADC and T2 values changed significantly (Haraldseth *et al.* 1997; Lemaire *et al.* 2000).

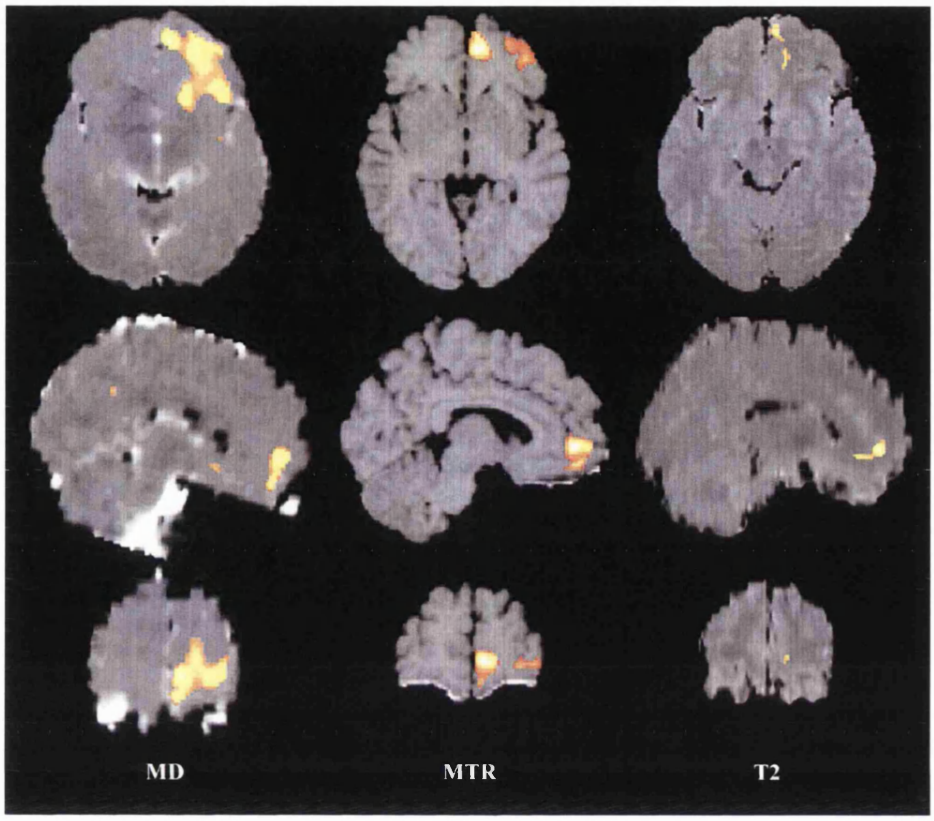

Figure 7.6: A patient with cryptogenic right frontal lobe epilepsy. Left to right: mean diffusivity (MD), magnetisation transfer imaging (MTR), and T2 mapping (T2) maps. Areas of significantly abnormality, identified by SPM, are superimposed on each image. There is clear anatomical concordance between different techniques, which is in agreement with localising EEG data.

In occult epileptic foci, the most abnormal regions, that is those just below the threshold for detection on conventional MRI, may be associated with abnormalities of all advanced MR sequences if there are significant changes to both water content and the microstructural environment. Less abnormal regions may be associated with either predominantly "water" or "macromolecular" pathology and only 2 or 3 out of the 4 sequences may detect regions of abnormality. A negative result is also of importance therefore, in elucidating the possible pathological / aetiological basis of an individual patient's seizure disorder. Nevertheless, confidence in the localisation of an abnormality in MRI-negative patients is significantly enhanced by confirmation from another source, whether this is a further experimental technique, including advanced MRI techniques, MR spectroscopy or PET, or more traditional methods such as intracranial EEG. At present, advanced MRI techniques, such as DTI, MTI, T2 mapping and DIR, provide a guide for the accurate placement of intracranial EEG electrodes. A more focussed approach, such as this, may result in less frequent negative intracranial EEG studies (Siegel *et al.* 2001), thereby reducing morbidity from repeated electrode implantation, and increasing the numbers of patients with refractory

focal epilepsy and normal conventional imaging who undergo potentially curative epilepsy surgery.

Overall, the advanced techniques were sensitive in the detection of abnormalities in patients with acquired lesions or MCD. In a significant proportion of patients, extra-lesional areas were identified, most of which concurred with EEG data and other advanced sequences. MTI and DIR were the most sensitive in patients with MCDs. T2 mapping and DIR were the most sensitive in patients with acquired lesions and in patients with normal conventional MRI. Methodological limitations, particularly with respect to DTI, may be relevant however. The results of the patients with acquired lesions and MCDs suggest that T2, mean diffusivity, and DIR are most sensitive to pathologies characterised by altered water content, and that MTI, DIR and, possibly, fractional anisotropy are more useful in identifying disruption to the macromolecular environment. The combination of techniques further enhances the ability to identify occult structural abnormalities.

In conclusion, despite a large number of MR studies evaluating a heterogeneous collection of disease entities, and MRI possessing a high degree of sensitivity in the detection of cerebral lesions, it is clear that the pursuit for pathological specificity is, as yet, unfinished. More advanced MRI acquisition and post-processing techniques, interrogating additional facets of the microstructural environment, in conjunction with correlative histopathology, may provide a means to achieve this goal.

7.2 FUTURE DIRECIONS

The work described in this thesis has concentrated on the preliminary evaluation of patients with focal epilepsy using advanced MRI techniques. There are, therefore, a number of areas that require further exploration to improve lesion sensitivity and pathological specificity, in order to better understand the structural basis of focal epilepsy.

7.2.1 Imaging

Current sequences may be improved or new sequences developed. It is of paramount importance that the images are of high resolution, produce reproducible values / maps and are acquired within a clinically acceptable time frame. This is facilitated by modern scanners with higher field strengths and enhanced imaging software and processing capability.

7.2.1.1 Current sequences

DTI - reduced voxel size will improve resolution and lesion sensitivity. However, this will negatively impact on signal to noise which may be mitigated by image averaging or increasing the field strength. Ideally, voxels should be cubic to facilitate the use of current tractography algorithms, which may be used in parallel with conventional

anisotropy and diffusivity maps. Recent sequences have utilised multi-directional diffusion gradients to improve the accuracy of anisotropic data, and multiple b-values to fully characterise the diffusional properties of tissue. Diffusion sequences are sensitive to magnetic gradient anomalies which must therefore be regularly monitored. This will enable correction factors to be utilised to maintain reproducibility. Post-ictal diffusion imaging is a promising new technique that is currently under evaluation.

MTR - images are currently acquired in a non-interleaved fashion which may permit movement artefact between non-MTR and MTR images, and thus produce inaccurate MTR values. To correct for this we co-registered the data sets following image acquisition, however, acquiring interleaved data is optimal.

T2 mapping - the current T2 sequence could be improved by developing a 3-dimensional sequence with high-resolution isotropic voxels. Furthermore, the use of a hyperbolic secant pulse during image acquisition to reduce the effects of radiofrequency inhomogeneity may produce a more accurate inversion pulse, with improved CSF suppression and accuracy of T2 values.

DIR - the duration of DIR scanning is currently 20 minutes which is just within a clinically acceptable time frame. A number of images were unacceptable however, due to movement artefact, and required repeating. The current sequence is time inefficient and may be significantly shortened without adversely affecting image quality.

7.2.1.2 New sequences

This includes perfusion imaging to assess cerebral blood flow both inter- and post-ictally, quantitative 3D T1-mapping which evaluates both the total water content and the dynamic structure of the macromolecular environment, and multi-exponential 3D T2-mapping to interrogate the microstructural compartments of cerebral tissue.

7.2.2 Post-acquisition processing

SPM uses parametric statistics to analyse image data. This assumes that the voxel values are normally distributed. The process of smoothing helps in this regard. The use of nonparametric statistical tests (SnPM) is inherently more appropriate but less well developed and understood. It is possible that SnPM will circumvent a number of problems caused by the manipulation of data into a "normal distribution", in particular, the loss of sensitivity due to smoothing, and concerns regarding the analysis of an individual subject against a group.

With improvements in normalisation, in particular the use of masking, regularisation parameters and other techniques for constraining the boundaries of nonlinear normalisation, grossly abnormal brains may be normalised without excessive, inappropriate distortion. The lack of an absolute metric for evaluating the goodness of normalisation is important to note however.

This work may be considered, to some degree, to be a natural extension of VBM. It is possible however,

that quantitative maps of, for example, T2 values or MTR should be treated very differently, in terms of normalisation, analysis, statistical thresholds and inference. Furthermore, there remains the ambiguity in the interpretation of results in the context of imprecise normalisation, inherent to standard SPM analyses. The use of tensor- or deformation-based morphometry may provide a solution (Gaser *et al.* 2001; Volz, Gaser, and Sauer 2000), but at present remains experimental and computationally expensive.

There has been recent interest in the use of anatomical templates to quantify regional volumes, and generate probabilistic atlases for more accurate representation of normal cerebral structure (Hammers *et al.* 2002a; Hammers *et al.* 2003). It is possible that these atlases, derived from a normal population and normalised into standard space, may be a useful adjunct to whole brain SPM, in particular to address specific hypotheses regarding particular cerebral regions. This is potentially more sensitive than standard SPM analyses which use the whole brain to correct for multiple comparisons. A smaller region-of-interest would permit less stringent statistical corrections to be used.

7.2.3 Pathological

Of principal importance is the histopathological correlation of imaging abnormalities. The detailed evaluation of tissue characteristics, such as microglial activation and gliosis, neuronal loss, dysplasia, and microdysgenesis in post-mortem or surgical specimens, requires careful correlation with imaging findings. This may result in the emergence of pathological specificity, and allow the prediction of histology / pathology from a "MR signature", which would have both management and prognostic implications.

References

Proposal for revised clinical and electroencephalographic classification of epileptic seizures. From the Commission on Classification and Terminology of the International League Against Epilepsy. Epilepsia 1981; 22: 489-501.

Proposal for classification of epilepsies and epileptic syndromes. Commission on Classification and Terminology of the International League Against Epilepsy. Epilepsia 1985; 26: 268-278.

Gray's Anatomy. Edinburgh: Churchill-Livingstone, 1989a.

Proposal for revised classification of epilepsies and epileptic syndromes. Commission on Classification and Terminology of the International League Against Epilepsy. Epilepsia 1989b; 30: 389-399.

World Health Organisation: ICD-10: International Statistical Classification of Diseases and Related Health Problems. Geneva: WHO, 1992.

Guidelines for epidemiologic studies on epilepsy. Commission on Epidemiology and Prognosis, International League Against Epilepsy. Epilepsia 1993; 34: 592-596.

Recommendations for neuroimaging of patients with epilepsy. Commission on Neuroimaging of the International League Against Epilepsy. Epilepsia 1997; 38: 1255-1256.

Guidelines for neuroimaging evaluation of patients with uncontrolled epilepsy considered for surgery. Commission on Neuroimaging of the International League Against Epilepsy. Epilepsia 1998; 39: 1375-1376.

Aarli JA. Immunological aspects of epilepsy. Brain Dev. 1993; 15: 41-49.

Abell F, Krams M, Ashburner J *et al.* The neuroanatomy of autism: a voxel-based whole brain analysis of structural scans. Neuroreport 1999; 10: 1647-1651.

Adams CW. Pathology of multiple sclerosis: progression of the lesion. Br.Med Bull. 1977; 33: 15-20.

Adams JH. The neuropathology of head injuries. In: Vinken PJ, Bruyn GW, editors. Handbook of neurology. Injuries of the brain and skull. New York: Elsevier, 1975: 25-65.

Adams JH. Head Injury. In: Adams JH, Duchen LW, editors. Greenfield's Neuropathology. London: Edward Arnold, 1992: 106-52.

Adams R, Victor M. Disturbances of cerebrospinal fluid circulation, including hydrocephalus and meningeal reactions. Principles of Neurology. New York: McGraw-Hill, 1985: 461-73.

Adcock JE, Wise RG, Oxbury JM, Oxbury SM, Matthews PM. Quantitative fMRI assessment of the differences in lateralization of language-related brain activation in patients with temporal lobe epilepsy. Neuroimage 2003; 18:

423-438.

Akpede GO, Sykes RM, Abiodun PO. Convulsions with malaria: febrile or indicative of cerebral involvement? J Trop.Pediatr. 1993; 39: 350-355.

Al-Mefty O, Origitano TC. Meningiomas. In: Rengachary SS, Wilkins RH, editors. Principles of Neurosurgery. London: Mosby-Wolfe, 1994: 28.1-28.12.

Alfano B, Brunetti A, Ciarmiello A, Salvatore M. Simultaneous display of multiple MR parameters with "quantitative magnetic color imaging". J Comput.Assist.Tomogr. 1992; 16: 634-640.

Allen IV, Glover G, Anderson R. Abnormalities in the macroscopically normal white matter in cases of mild or spinal multiple sclerosis (MS). Acta Neuropathol.Suppl (Berl) 1981; 7: 176-178.

Allen IV, McKeown SR. A histological, histochemical and biochemical study of the macroscopically normal white matter in multiple sclerosis. J Neurol.Sci. 1979; 41: 81-91.

Allen PJ, Josephs O, Turner R. A method for removing imaging artifact from continuous EEG recorded during functional MRI. Neuroimage 2000; 12: 230-239.

Allen PJ, Polizzi G, Krakow K, Fish DR, Lemieux L. Identification of EEG events in the MR scanner: the problem of pulse artifact and a method for its subtraction. Neuroimage 1998; 8: 229-239.

Alpert NM, Bradshaw JF, Kennedy D, Coreia JA. The principal axis transformation - A method for image registration. J Nucl.Med 1990; 31: 1717-1722.

Alsop DC, Murai H, Detre JA, McIntosh TK, Smith DH. Detection of acute pathologic changes following experimental traumatic brain injury using diffusion-weighted magnetic resonance imaging. J.Neurotrauma 1996; 13: 515-521.

Andermann F. Brain structure in epilepsy. In: Shorvon SD, Fish DR, Andermann F, Bydder GM, Stefan H, editors. Magnetic resonance scanning and epilepsy. New York: Plenum Press, 1994: 21-7.

Anderson AW, Gore JC. Analysis and correction of motion artifacts in diffusion weighted imaging. Magn Reson Med 1994; 32: 379-387.

Anderson AW, Zhong J, Petroff OA *et al.* Effects of osmotically driven cell volume changes on diffusion-weighted imaging of the rat optic nerve. Magn Reson Med 1996; 35: 162-167.

Angeleri F, Majkowski J, Cacchio G *et al.* Posttraumatic epilepsy risk factors: one-year prospective study after head injury. Epilepsia 1999; 40: 1222-1230.

Annegers JF, Grabow JD, Groover RV, Laws ER, Elveback LR, Kurland LT. Seizures after head trauma: a population study. Neurology 1980; 30: 683-689.

Arakia Y, Ashikaga R, Fujii K, Nishimura Y, Ueda J, Fujita N. MR fluid-attenuated inversion recovery imaging as routine brain T2-weighted imaging. Eur J Radiol. 1999; 32: 136-143.

Armspach JP, Gounot D, Rumbach L, Chambron J. In vivo determination of multiexponential T2 relaxation in the brain of patients with multiple sclerosis. Magn Reson Imaging 1991; 9: 107-113.

Ashburner J, Friston K. Multimodal image coregistration and partitioning--a unified framework. Neuroimage. 1997; 6: 209-217.

Ashburner J, Friston KJ. Nonlinear spatial normalization using basis functions. Hum.Brain Mapp. 1999; 7: 254-266.

Ashburner J, Friston KJ. Voxel-based morphometry--the methods. Neuroimage. 2000; 11: 805-821.

Ashtari M, Barr WB, Schaul N, Bogerts B. Three-dimensional fast low-angle shot imaging and computerized volume measurement of the hippocampus in patients with chronic epilepsy of the temporal lobe. AJNR Am.J.Neuroradiol 1991; 12: 941-947.

Asikainen I, Kaste M, Sarna S. Early and late posttraumatic seizures in traumatic brain injury rehabilitation patients: brain injury factors causing late seizures and influence of seizures on long-term outcome. Epilepsia 1999; 40: 584-589.

Assaf Y, Beit-Yannai E, Shohami E, Berman E, Cohen Y. Diffusion- and T2-weighted MRI of closed-head injury in rats: a time course study and correlation with histology. Magn Reson Imaging 1997; 15: 77-85.

Auer DP, Putz B, Gossl C, Elbel G, Gasser T, Dichgans M. Differential lesion patterns in CADASIL and sporadic subcortical arteriosclerotic encephalopathy: MR imaging study with statistical parametric group comparison. Radiology 2001; 218: 443-451.

Autti T, Raininko R, Vanhanen SL, Kallio M, Santavuori P. MRI of the normal brain from early childhood to middle age. II. Age dependence of signal intensity changes on T2-weighted images. Neuroradiology 1994; 36: 649-651.

Avanzini G, Panzica F, de Curtis M. The role of the thalamus in vigilance and epileptogenic mechanisms. Clin.Neurophysiol. 2000; 111 Suppl 2: S19-S26.

Awad IA, Rosenfeld J, Ahl J, Hahn JF, Luders H. Intractable epilepsy and structural lesions of the brain: mapping, resection strategies, and seizure outcome. Epilepsia 1991; 32: 179-186.

Awada A, Omojola MF, Obeid T. Late epileptic seizures after cerebral infarction. Acta Neurol Scand. 1999; 99: 265-268.

Axel L. Surface coil magnetic resonance imaging. J Comput.Assist.Tomogr. 1984; 8: 381-384.

Aykut-Bingol C, Tekin S, Ince D, Aktan S. Reversible MRI lesions after seizures. Seizure. 1997; 6: 237-239.

Babb TL, Brown WJ. Pathological findings in epilepsy. In: Engel J, Jr., editor. Surgical treatment of the epilepsies. New York: Raven Press, 1987: 511-40.

Babb TL, Brown WJ, Pretorius J, Davenport C, Lieb JP, Crandall PH. Temporal lobe volumetric cell densities in temporal lobe epilepsy. Epilepsia 1984a; 25: 729-740.

Babb TL, Lieb JP, Brown WJ, Pretorius J, Crandall PH. Distribution of pyramidal cell density and hyperexcitability in the epileptic human hippocampal formation. Epilepsia 1984b; 25: 721-728.

Bagary MS, Foong J, Maier M *et al.* A magnetization transfer analysis of the thalamus in schizophrenia. J Neuropsychiatry Clin.Neurosci 2002; 14: 443-448.

Bagary MS, Symms MR, Barker GJ, Mutsatsa SH, Joyce EM, Ron MA. Gray and white matter brain abnormalities in first-episode schizophrenia inferred from magnetization transfer imaging. Arch Gen.Psychiatry 2003; 60: 779-788.

Bagley LJ, McGowan JC, Grossman RI *et al.* Magnetization transfer imaging of traumatic brain injury (In Process Citation). J Magn Reson Imaging 2000; 11: 1-8.

Bahn MM. Invariant and orthonormal scalar measures derived from magnetic resonance diffusion tensor imaging (In Process Citation). J.Magn Reson 1999; 141: 68-77.

Bahn MM, Lin W, Silbergeld DL *et al.* Localization of language cortices by functional MR imaging compared with intracarotid amobarbital hemispheric sedation. AJR Am J Roentgenol. 1997; 169: 575-579.

Bahn MM, Parchi P. Abnormal diffusion-weighted magnetic resonance images in Creutzfeldt-Jakob disease. Arch.Neurol. 1999; 56: 577-583.

Bailes DR, Young IR, Thomas DJ, Straughan K, Bydder GM, Steiner RE. NMR imaging of the brain using spin-echo sequences. Clin.Radiol. 1982; 33: 395-414.

Bakay RA, Harris AB. Neurotransmitter, receptor and biochemical changes in monkey cortical epileptic foci. Brain Res 1981; 206: 387-404.

Balaban RS, Ceckler TL. Magnetization transfer contrast in magnetic resonance imaging. Magn Reson Q. 1992; 8: 116-137.

Balaban RS, Chesnick S, Hedges K, Samaha F, Heineman FW. Magnetization transfer contrast in MR imaging of the heart. Radiology 1991; 180: 671-675.

Baldwin GN, Tsuruda JS, Maravilla KR, Hamill GS, Hayes CE. The fornix in patients with seizures caused by unilateral hippocampal sclerosis: detection of unilateral volume loss on MR images. AJR Am.J Roentgenol. 1994; 162: 1185-1189.

Bale JF. Human cytomegalovirus infection and disorders of the nervous system. Arch.Neurol. 1984; 41: 310-320.

Bale JF. Viral encephalitis. Med Clin.North Am 1993; 77: 25-42.

Barber PA, Darby DG, Desmond PM *et al.* Identification of major ischemic change. Diffusion-weighted imaging versus computed tomography. Stroke 1999a; 30: 2059-2065.

Barber R, Scheltens P, Gholkar A *et al.* White matter lesions on magnetic resonance imaging in dementia with Lewy bodies, Alzheimer's disease, vascular dementia, and normal aging. J Neurol.Neurosurg.Psychiatry 1999b; 67: 66-72.

Barbosa S, Blumhardt LD, Roberts N, Lock T, Edwards RH. Magnetic resonance relaxation time mapping in multiple sclerosis: normal appearing white matter and the "invisible" lesion load. Magn Reson Imaging 1994; 12: 33-42.

Barker GJ. 3D fast FLAIR: a CSF-nulled 3D fast spin-echo pulse sequence. Magn Reson Imaging 1998; 16: 715-720.

Barker GJ, Clark CA, Franconi F, Symms MR. A CSF-suppressed, EPI-based, pulse sequence for diffusion tensor and apparent constant measurement in multiple sclerosis. Proceedings of the International Society for Magnetic Resonance in Medicine, Fifth scientific meeting, 1997; 223.

Barker GJ, Tofts PS, Gass A. An interleaved sequence for accurate and reproducible clinical measurement of magnetization transfer ratio. Magn Reson Imaging 1996; 14: 403-411.

Barkhof F, Karas GB, van Walderveen MA. T1 hypointensities and axonal loss. Neuroimaging Clin.N.Am. 2000; 10: 739-752.

Barkovich AJ, Chuang SH, Norman D. MR of neuronal migration anomalies. AJR Am J Roentgenol. 1988; 150: 179-187.

Barkovich AJ, Guerrini R, Battaglia G *et al.* Band heterotopia: correlation of outcome with magnetic resonance imaging parameters. Ann Neurol 1994; 36: 609-617.

Barkovich AJ, Kjos BO. Gray matter heterotopias: MR characteristics and correlation with developmental and neurologic manifestations. Radiology 1992a; 182: 493-499.

Barkovich AJ, Kjos BO. Schizencephaly: correlation of clinical findings with MR characteristics. AJNR Am J Neuroradiol 1992b; 13: 85-94.

Barkovich AJ, Kuzniecky RI, Dobyns WB, Jackson GD, Becker LE, Evrard P. A classification scheme for malformations of cortical development. Neuropediatrics 1996; 27: 59-63.

Barkovich AJ, Rowley HA, Andermann F. MR in partial epilepsy: value of high-resolution volumetric techniques. AJNR Am.J.Neuroradiol 1995; 16: 339-343.

Barnes D, du Boulay EG, McDonald WI, Johnson G, Tofts PS. The NMR signal decay characteristics of cerebral

oedema. Acta Radiol.Suppl 1986a; 369: 503-506.

Barnes D, McDonald WI, Johnson G, Tofts PS, Landon DN. Quantitative nuclear magnetic resonance imaging: characterisation of experimental cerebral oedema. J Neurol Neurosurg.Psychiatry 1987; 50: 125-133.

Barnes D, McDonald WI, Landon DN, Johnson G. The characterization of experimental gliosis by quantitative nuclear magnetic resonance imaging. Brain 1988; 111 (Pt 1): 83-94.

Barnes D, McDonald WI, Tofts PS, Johnson G, Landon DN. Magnetic resonance imaging of experimental cerebral oedema. J Neurol.Neurosurg.Psychiatry 1986b; 49: 1341-1347.

Barone FC, Clark RK, Feuerstein G, Lenkinski RE, Sarkar SK. Quantitative comparison of magnetic resonance imaging (MRI) and histologic analyses of focal ischemic damage in the rat. Brain Res.Bull. 1991; 26: 285-291.

Barth PG. Disorders of neuronal migration. Can.J Neurol.Sci. 1987; 14: 1-16.

Bartlett PA, Richardson MP, Duncan JS. Measurement of amygdala T2 relaxation time in temporal lobe epilepsy. J Neurol Neurosurg.Psychiatry 2002; 73: 753-755.

Bartolomei F, Boucraut J, Barrie M *et al.* Cryptogenic partial epilepsies with anti-GM1 antibodies: a new form of immune-mediated epilepsy? Epilepsia 1996; 37: 922-926.

Bartzokis G, Goldstein IB, Hance DB *et al.* The incidence of T2-weighted MR imaging signal abnormalities in the brain of cocaine-dependent patients is age-related and region-specific. AJNR Am J Neuroradiol 1999; 20: 1628-1635.

Basser PJ. Inferring microstructural features and the physiological state of tissues from diffusion-weighted images. NMR Biomed. 1995; 8: 333-344.

Basser PJ, Mattiello J, LeBihan D. Estimation of the effective self-diffusion tensor from the NMR spin echo. J.Magn Reson B 1994a; 103: 247-254.

Basser PJ, Mattiello J, LeBihan D. MR diffusion tensor spectroscopy and imaging. Biophys.J. 1994b; 66: 259-267.

Basser PJ, Pajevic S, Pierpaoli C, Duda J, Aldroubi A. In vivo fiber tractography using DT-MRI data. Magn Reson Med 2000; 44: 625-632.

Basser PJ, Pierpaoli C. Microstructural and physiological features of tissues elucidated by quantitative-diffusion-tensor MRI. J.Magn Reson B 1996; 111: 209-219.

Bastianello S, Bozzao A, Paolillo A *et al.* Fast spin-echo and fast fluid-attenuated inversion-recovery versus conventional spin-echo sequences for MR quantification of multiple sclerosis lesions. AJNR Am J Neuroradiol 1997; 18: 699-704.

Bastianello S, Gasperini C, Paolillo A *et al.* Sensitivity of enhanced MR in multiple sclerosis: effects of contrast

dose and magnetization transfer contrast. AJNR Am J Neuroradiol 1998; 19: 1863-1867.

Bastin ME, Delgado M, Whittle IR, Cannon J, Wardlaw JM. The use of diffusion tensor imaging in quantifying the effect of dexamethasone on brain tumours. Neuroreport 1999; 10: 1385-1391.

Bastin ME, Sinha S, Whittle IR, Wardlaw JM. Measurements of water diffusion and T1 values in peritumoural oedematous brain. Neuroreport 2002; %19; 13: 1335-1340.

Bastos AC, Comeau RM, Andermann F *et al.* Diagnosis of subtle focal dysplastic lesions: curvilinear reformatting from three-dimensional magnetic resonance imaging. Ann.Neurol. 1999; 46: 88-94.

Bastos AC, Korah IP, Cendes F *et al.* Curvilinear reconstruction of 3D magnetic resonance imaging in patients with partial epilepsy: a pilot study. Magn Reson.Imaging 1995; 13: 1107-1112.

Bauer G. Seizure types and epileptic syndromes in adults. Eur.Neurol. 1994; 34 Suppl 1:13-7: 13-17.

Baulac M, Saint-Hilaire JM, Adam C, Martinez M, Fontaine S, Laplane D. Correlations between magnetic resonance imaging-based hippocampal sclerosis and depth electrode investigation in epilepsy of the mesiotemporal lobe. Epilepsia 1994; 35: 1045-1053.

Baulac S, Huberfeld G, Gourfinkel-An I *et al.* First genetic evidence of GABA (A) receptor dysfunction in epilepsy: a mutation in the gamma2-subunit gene. Nat.Genet. 2001; 28: 46-48.

Baxendale SA, Sisodiya SM, Thompson PJ *et al.* Disproportion in the distribution of gray and white matter: neuropsychological correlates. Neurology 1999; 52: 248-252.

Baxendale SA, Van Paesschen W, Thompson PJ *et al.* The relationship between quantitative MRI and neuropsychological functioning in temporal lobe epilepsy. Epilepsia 1998; 39: 158-166.

Bazin B, Cohen L, Lehericy S *et al.* (Study of hemispheric lateralization of language regions by functional MRI. Validation with the Wada test). Rev.Neurol. (Paris) 2000; 156: 145-148.

Beaulieu C, Allen PS. Determinants of anisotropic water diffusion in nerves. Magn Reson Med 1994; 394-400.

Beaulieu C, Does MD, Snyder RE, Allen PS. Changes in water diffusion due to Wallerian degeneration in peripheral nerve. Magn Reson Med 1996; 36: 627-631.

Beaulieu C, Fenrich FR, Allen PS. Multicomponent water proton transverse relaxation and T2-discriminated water diffusion in myelinated and nonmyelinated nerve. Magn Reson Imaging 1998; 16: 1201-1210.

Bedell BJ, Narayana PA. Implementation and evaluation of a new pulse sequence for rapid acquisition of double inversion recovery images for simultaneous suppression of white matter and CSF. J Magn Reson Imaging 1998a; 8: 544-547.

Bedell BJ, Narayana PA. Volumetric analysis of white matter, gray matter, and CSF using fractional volume

analysis. Magn Reson Med 1998b; 39: 961-969.

Behrens TE, Johansen-Berg H, Woolrich MW *et al.* Non-invasive mapping of connections between human thalamus and cortex using diffusion imaging. Nat.Neurosci 2003; 6: 750-757.

Bekkelund SI, Pierre-Jerome C, Mellgren SI. Quantitative cerebral MRI in epileptic patients. Acta Neurol.Scand. 1996; 94: 378-382.

Benbadis S, Luders H. (Classification of epileptic seizures. Comparison of two systems). Neurophysiol.Clin. 1995; 25: 297-302.

Bendersky M, Rugilo C, Kochen S, Schuster G, Sica RE. Magnetic resonance imaging identifies cytoarchitectonic subtypes of the normal human cerebral cortex. J Neurol Sci. 2003; 211: 75-80.

Benveniste H, Hedlund LW, Johnson GA. Mechanism of detection of acute cerebral ischemia in rats by diffusion-weighted magnetic resonance microscopy. Stroke 1992; 23: 746-754.

Beppu T, Inoue T, Shibata Y *et al.* Measurement of fractional anisotropy using diffusion tensor MRI in supratentorial astrocytic tumors. J Neurooncol. 2003; 63: 109-116.

Bergen D, Bleck T, Ramsey R *et al.* Magnetic resonance imaging as a sensitive and specific predictor of neoplasms removed for intractable epilepsy. Epilepsia 1989; 30: 318-321.

Bergin PS, Fish DR, Shorvon SD, Oatridge A, deSouza NM, Bydder GM. Magnetic resonance imaging in partial epilepsy: additional abnormalities shown with the fluid attenuated inversion recovery (FLAIR) pulse sequence. J Neurol Neurosurg Psychiatry 1995; 58: 439-443.

Berkovic SF, Andermann F, Olivier A *et al.* Hippocampal sclerosis in temporal lobe epilepsy demonstrated by magnetic resonance imaging. Ann Neurol 1991; 29: 175-182.

Berkovic SF, Arzimanoglou A, Kuzniecky R, Harvey AS, Palmini A, Andermann F. Hypothalamic hamartoma and seizures: a treatable epileptic encephalopathy. Epilepsia 2003; 44: 969-973.

Berkovic SF, McIntosh A, Howell RA, Mitchell A, Sheffield LJ, Hopper JL. Familial temporal lobe epilepsy: a common disorder identified in twins. Ann.Neurol. 1996; 40: 227-235.

Berkovic SF, McIntosh AM, Kalnins RM *et al.* Preoperative MRI predicts outcome of temporal lobectomy: an actuarial analysis. Neurology 1995; 45: 1358-1363.

Bernarding J, Braun J, Hohmann J *et al.* Histogram-based characterization of healthy and ischemic brain tissues using multiparametric MR imaging including apparent diffusion coefficient maps and relaxometry. Magn Reson Med 2000; 43: 52-61.

Bernasconi A, Antel SB, Collins DL *et al.* Texture analysis and morphological processing of magnetic resonance imaging assist detection of focal cortical dysplasia in extra-temporal partial epilepsy. Ann Neurol 2001a; 49: 770-

775.

Bernasconi A, Bernasconi N, Caramanos Z *et al.* T2 relaxometry can lateralize mesial temporal lobe epilepsy in patients with normal MRI. Neuroimage. 2000; 12: 739-746.

Bernasconi A, Bernasconi N, Natsume J, Antel SB, Andermann F, Arnold DL. Magnetic resonance spectroscopy and imaging of the thalamus in idiopathic generalized epilepsy. Brain 2003a; 126 (Pt 11):2447-54.

Bernasconi N, Bernasconi A, Andermann F, Dubeau F, Feindel W, Reutens DC. Entorhinal cortex in temporal lobe epilepsy: a quantitative MRI study. Neurology 1999; 52: 1870-1876.

Bernasconi N, Bernasconi A, Caramanos Z, Antel SB, Andermann F, Arnold DL. Mesial temporal damage in temporal lobe epilepsy: a volumetric MRI study of the hippocampus, amygdala and parahippocampal region. Brain 2003b; 126: 462-469.

Bernasconi N, Bernasconi A, Caramanos Z *et al.* Entorhinal cortex atrophy in epilepsy patients exhibiting normal hippocampal volumes. Neurology 2001b; 56: 1335-1339.

Biervert C, Schroeder BC, Kubisch C *et al.* A potassium channel mutation in neonatal human epilepsy. Science 1998; 279: 403-406.

Binder JR, Rao SM, Hammeke TA *et al.* Lateralized human brain language systems demonstrated by task subtraction functional magnetic resonance imaging. Arch.Neurol. 1995; 52: 593-601.

Binder JR, Swanson SJ, Hammeke TA *et al.* Determination of language dominance using functional MRI: a comparison with the Wada test. Neurology 1996; 46: 978-984.

Bland JM, Altman DG. Statistical methods for assessing agreement between two methods of clinical measurement. Lancet 1986; 1: 307-310.

Blennow G, Folbergrova J, Nilsson B, Siesjo BK. Cerebral metabolic and circulatory changes in the rat during sustained seizures induced by DL-homocysteine. Brain Res. 1979; 179: 129-146.

Bloch F. Nuclear induction. Phys Rev 1946; 70: 460-474.

Bloom FE. Advancing a neurodevelopmental origin for schizophrenia. Arch.Gen.Psychiatry 1993; 50: 224-227.

Blume WT, Berkovic SF, Dulac O. Search for a better classification of the epilepsies. In: Engel J, Jr., Pedley TA, editors. Epilepsy: A Comprehensive Textbook. Philadelphia: Lippincott-Raven, 1997: 779-89.

Bondareff W, Raval J, Colletti PM, Hauser DL. Quantitative magnetic resonance imaging and the severity of dementia in Alzheimer's disease. Am J Psychiatry 1988; 145: 853-856.

Bookheimer SY, Cohen M, Dapretto M *et al.* Functional MRI in surgical planning. Soc.Neurosci.Abstr. 1995; 273.

Bookheimer SY, Dapretto M, Cohen M, Wang J, Small G. Functional MRI of the hippocampus during short term memory tasks: Parametric responses to task difficulty and stimulus novelty. Neuroimage 1996a; 3: 531.

Bookheimer SY, Dapretto M, Small G, Wang J, Cohen M. Hippocampal activation during memory acquisition and retrieval using functional MRI. Soc.Neurosci.Abstr. 1996b; 22.

Boon PA, Williamson PD, Fried I *et al.* Intracranial, intraaxial, space-occupying lesions in patients with intractable partial seizures: an anatomoclinical, neuropsychological, and surgical correlation. Epilepsia 1991; 32: 467-476.

Boorstein JM, Wong KT, Grossman RI, Bolinger L, McGowan JC. Metastatic lesions of the brain: imaging with magnetization transfer. Radiology 1994; 191: 799-803.

Booth BM, Blow FC. The kindling hypothesis: further evidence from a U.S. national study of alcoholic men. Alcohol Alcohol 1993; 28: 593-598.

Borgel F, Hommel M, Pollak P *et al.* (Magnetic resonance imaging in multiple sclerosis. Sensitivity and correlation with the clinical picture). Rev Neurol. (Paris) 1986; 142: 598-606.

Borgstrom L, Chapman AG, Siesjo BK. Glucose consumption in the cerebral cortex of rat during bicuculline-induced status epilipticus. J Neurochem. 1976; 27: 971-973.

Bose B, Jones SC, Lorig R, Friel HT, Weinstein M, Little JR. Evolving focal cerebral ischemia in cats: spatial correlation of nuclear magnetic resonance imaging, cerebral blood flow, tetrazolium staining, and histopathology. Stroke 1988; 19: 28-37.

Bothwell S, Meredith GE, Phillips J *et al.* Neuronal hypertrophy in the neocortex of patients with temporal lobe epilepsy. J Neurosci. 2001; 21 (13): 4789-4800.

Bottomley PA, Hardy CJ, Argersinger RE, Allen-Moore G. A review of 1H nuclear magnetic resonance relaxation in pathology: are T1 and T2 diagnostic? Med Phys. 1987; 14: 1-37.

Bouchet C, Cazauvielh Y. De l'epilpsie consideree dans ses rapports avec l'alienation mentale. Arch Gen Med Par 1825; 9: 510-542.

Boulby PA, Symms M, Barker G. A whole brain high-resolution magnetisation transfer imaging sequence. Proceedings European Society for Magnetic Resonance in Medicine and Biology 16th Meeting Seville 2000; 483.

Braffman BH, Zimmerman RA, Trojanowski JQ, Gonatas NK, Hickey WF, Schlaepfer WW. Brain MR: pathologic correlation with gross and histopathology. 1. Lacunar infarction and Virchow-Robin spaces. AJR Am J Roentgenol. 1988; 151: 551-558.

Brailowsky S, Garcia O. Ethanol, GABA and epilepsy. Arch Med Res 1999; 30: 3-9.

Brant-Zawadzki M, Norman D, Newton TH *et al.* Magnetic resonance of the brain: the optimal screening technique. Radiology 1984; 152: 71-77.

Brant-Zawadzki M, Pereira B, Weinstein P *et al.* MR imaging of acute experimental ischemia in cats. AJNR Am J Neuroradiol 1986; 7: 7-11.

Bratz E. Ammonshornbefunde bei epilptikern. Arch Psychiatr Nervenkr 1899; 32: 820-835.

Breger RK, Rimm AA, Fischer ME, Papke RA, Haughton VM. T1 and T2 measurements on a 1.5-T commercial MR imager. Radiology 1989; 171: 273-276.

Briellmann RS, Berkovic SF, Syngeniotis A, King MA, Jackson GD. Seizure-associated hippocampal volume loss: a longitudinal magnetic resonance study of temporal lobe epilepsy. Ann Neurol 2002a; 51: 641-644.

Briellmann RS, Kalnins RM, Berkovic SF, Jackson GD. Hippocampal pathology in refractory temporal lobe epilepsy: T2-weighted signal change reflects dentate gliosis. Neurology 2002b; 58: 265-271.

Brochet B, Dousset V. Pathological correlates of magnetization transfer imaging abnormalities in animal models and humans with multiple sclerosis. Neurology 1999; 53: S12-S17.

Brodtkorb E, Nilsen G, Smevik O, Rinck PA. Epilepsy and anomalies of neuronal migration: MRI and clinical aspects. Acta Neurol.Scand. 1992; 86: 24-32.

Bronen RA. Epilepsy: the role of MR imaging. AJR Am.J Roentgenol. 1992; 159: 1165-1174.

Bronen RA, Cheung G, Charles JT *et al.* Imaging findings in hippocampal sclerosis: correlation with pathology. AJNR Am.J Neuroradiol. 1991; 12: 933-940.

Bronen RA, Fulbright RK, Kim JH, Spencer SS, Spencer DD, al Rodhan NR. Regional distribution of MR findings in hippocampal sclerosis. AJNR Am.J Neuroradiol. 1995a; 16: 1193-1200.

Bronen RA, Fulbright RK, Spencer DD, Spencer SS, Kim JH, Lange RC. MR characteristics of neoplasms and vascular malformations associated with epilepsy. Magn Reson Imaging 1995b; 13: 1153-1162.

Brooks RA, Di Chiro G, Keller MR. Explanation of cerebral white--gray contrast in computed tomography. J Comput.Assist.Tomogr. 1980; 4: 489-491.

Brown JJ, Hesselink JR, Rothrock JF. MR and CT of lacunar infarcts. AJR Am J Roentgenol. 1988; 151: 367-372.

Brun A, Gustafson L, Englund E. Subcortical pathology of Alzheimer's disease. Adv.Neurol 1990; 51: 73-77.

Bruton CJ. The neuropathology of temporal lobe epilepsy. Oxford: Oxford University Press, 1988.

Bryan RN, Levy LM, Whitlow WD, Killian JM, Preziosi TJ, Rosario JA. Diagnosis of acute cerebral infarction: comparison of CT and MR imaging. AJNR Am J Neuroradiol 1991; 12: 611-620.

Bryan RN, Willcott MR, Schneiders NJ, Ford JJ, Derman HS. Nuclear magnetic resonance evaluation of stroke. A preliminary report. Radiology 1983; 149: 189-192.

Buckley P, O'Callaghan E, Mulvany F *et al.* Basal ganglia T2 relaxation times in schizophrenia: a quantitative magnetic resonance imaging study in relation to tardive dyskinesia. Psychiatry Res. 1995; 61: 95-102.

Buckner RL, Raichle ME, Miezin FM, Petersen SE. Functional anatomic studies of memory retrieval for auditory words and visual pictures. J Neurosci. 1996; 16: 6219-6235.

Bullmore E, Brammer M, Harvey I, Persaud R, Murray R, Ron M. Fractal analysis of the boundary between white matter and cerebral cortex in magnetic resonance images: a controlled study of schizophrenic and manic-depressive patients. Psychol.Med 1994; 24: 771-781.

Buonanno FS, Pykett IL, Brady TJ *et al.* Proton NMR imaging in experimental ischemic infarction. Stroke 1983; 14: 178-184.

Burke JW, Mathews VP, Elster AD, Ulmer JL, McLean FM, Davis SB. Contrast-enhanced magnetization transfer saturation imaging improves MR detection of herpes simplex encephalitis. AJNR Am J Neuroradiol 1996; 17: 773-776.

Burn J, Dennis M, Bamford J, Sandercock P, Wade D, Warlow C. Epileptic seizures after a first stroke: the Oxfordshire Community Stroke Project. BMJ 1997; 315: 1582-1587.

Busza AL, Allen KL, King MD, van Bruggen N, Williams SR, Gadian DG. Diffusion-weighted imaging studies of cerebral ischemia in gerbils. Potential relevance to energy failure. Stroke 1992; 23: 1602-1612.

Bydder GM, Steiner RE, Thomas DJ, Marshall J, Gilderdale DJ, Young IR. Nuclear magnetic resonance imaging of the posterior fossa: 50 cases. Clin.Radiol. 1983; 34: 173-188.

Bydder GM, Young IR. MR imaging: clinical use of the inversion recovery sequence. J Comput.Assist.Tomogr. 1985; 9: 659-675.

Calamante F, Lythgoe MF, Pell GS *et al.* Early changes in water diffusion, perfusion, T1, and T2 during focal cerebral ischemia in the rat studied at 8.5 T. Magn Reson Med 1999; 41: 479-485.

Callen DJ, Black SE, Gao F, Caldwell CB, Szalai JP. Beyond the hippocampus: MRI volumetry confirms widespread limbic atrophy in AD. Neurology 2001; 57: 1669-1674.

Campeau NG, Petersen RC, Felmlee JP, O'Brien PC, Jack CR, Jr. Hippocampal transverse relaxation times in patients with Alzheimer disease. Radiology 1997; 205: 197-201.

Carr HY, Purcell EM. Effect of Diffusion on Free Precession in Nuclear Magnetic Resonance Experiments. Physical Review 1954; 94: 630-638.

Cascino GD. Epilepsy and brain tumours: implications for treatment. Epilepsia 1990; 31 (Suppl): S37-44.

Cascino GD, Hirschorn KA, Jack CR, Sharbrough FW. Gadolinium-DTPA-enhanced magnetic resonance imaging in intractable partial epilepsy. Neurology 1989; 39: 1115-1118.

Cascino GD, Jack CR, Jr., Parisi JE *et al.* MRI in the presurgical evaluation of patients with frontal lobe epilepsy and children with temporal lobe epilepsy: pathologic correlation and prognostic importance. Epilepsy Res. 1992; 11: 51-59.

Cascino GD, Jack CR, Jr., Parisi JE *et al.* Magnetic resonance imaging-based volume studies in temporal lobe epilepsy: pathological correlations. Ann Neurol 1991; 30: 31-36.

Castillo M, Scatliff JH, Kwock L *et al.* Postmortem MR imaging of lobar cerebral infarction with pathologic and in vivo correlation. Radiographics 1996; 16: 241-250.

Catani M, Howard RJ, Pajevic S, Jones DK. Virtual in vivo interactive dissection of white matter fasciculi in the human brain. Neuroimage 2002; 17: 77-94.

Catani M, Jones DK, Donato R, Ffytche DH. Occipito-temporal connections in the human brain. Brain 2003; 126: 2093-2107.

Cavanagh JB, Meyer A. Aetiological aspects of Ammon's horn sclerosis associated with temporal lobe epilepsy. BMJ 1956; 1403-1407.

Cecchi C, Boncinelli E. Emx homeogenes and mouse brain development. Trends Neurosci 2000; 23: 347-352.

Ceckler TL, Karino K, Kador PF, Balaban RS. Magnetic resonance imaging of the rabbit eye. Improved anatomical detail using magnetization transfer contrast. Invest Ophthalmol.Vis.Sci. 1991; 32: 3109-3113.

Celli P, Scarpinati M, Nardacci B, Cervoni L, Cantore GP. Gangliogliomas of the cerebral hemispheres. Report of 14 cases with long-term follow-up and review of the literature. Acta Neurochir. (Wien.) 1993; 125: 52-57.

Cendes F, Andermann F, Dubeau F *et al.* Early childhood prolonged febrile convulsions, atrophy and sclerosis of mesial structures, and temporal lobe epilepsy: an MRI volumetric study. Neurology 1993a; 43: 1083-1087.

Cendes F, Andermann F, Gloor P *et al.* MRI volumetric measurement of amygdala and hippocampus in temporal lobe epilepsy. Neurology 1993b; 43: 719-725.

Cendes F, Andermann F, Preul MC, Arnold DL. Lateralization of temporal lobe epilepsy based on regional metabolic abnormalities in proton magnetic resonance spectroscopic images. Ann.Neurol. 1994; 35: 211-216.

Cendes F, Caramanos Z, Andermann F, Dubeau F, Arnold DL. Proton magnetic resonance spectroscopic imaging and magnetic resonance imaging volumetry in the lateralization of temporal lobe epilepsy: a series of 100 patients. Ann Neurol 1997; 42: 737-746.

Cendes F, Li LM, Andermann F *et al.* Dual pathology and its clinical relevance. Adv.Neurol 1999; 81:153-64.: 153-164.

Cercignani M, Iannucci G, Rocca MA, Comi G, Horsfield MA, Filippi M. Pathologic damage in MS assessed by diffusion-weighted and magnetization transfer MRI. Neurology 2000; 54: 1139-1144.

Chabriat H, Levy C, Taillia H *et al.* Patterns of MRI lesions in CADASIL. Neurology 1998; 51: 452-457.

Chabriat H, Pappata S, Poupon C *et al.* Clinical severity in CADASIL related to ultrastructural damage in white matter: in vivo study with diffusion tensor MRI. Stroke 1999; 30: 2637-2643.

Chagnac-Amitai Y, Connors BW. Horizontal spread of synchronized activity in neocortex and its control by GABA-mediated inhibition. J Neurophysiol. 1989; 61: 747-758.

Chan D, Fox NC, Scahill RI *et al.* Patterns of temporal lobe atrophy in semantic dementia and Alzheimer's disease. Ann Neurol 2001; 49: 433-442.

Chan JH, Tsui EY, Peh WC *et al.* Diffuse axonal injury: detection of changes in anisotropy of water diffusion by diffusion-weighted imaging. Neuroradiology 2003; 45: 34-38.

Chan RC, Thompson GB. Morbidity, mortality, and quality of life following surgery for intracranial meningiomas. A retrospective study in 257 cases. J Neurosurg 1984; 60: 52-60.

Chan S, Chin SS, Nordli DR, Goodman RR, DeLaPaz RL, Pedley TA. Prospective magnetic resonance imaging identification of focal cortical dysplasia, including the non-balloon cell subtype. Ann.Neurol. 1998; 44: 749-757.

Chapman AG, Meldrum BS, Siesjo BK. Cerebral metabolic changes during prolonged epileptic seizures in rats. J Neurochem. 1977; 28: 1025-1035.

Chenevert TL, Brunberg JA, Pipe JG. Anisotropic diffusion in human white matter: demonstration with MR technique in vivo. Radiology 1990; 401-405.

Chioza B, Wilkie H, Nashef L *et al.* Association between the alpha (1a) calcium channel gene CACNA1A and idiopathic generalized epilepsy. Neurology 2001; 56: 1245-1246.

Choi H-Y, Kim S-J. Tailoring of the epileptogenic zone guided by 3D-surface rendering of the MRI in patients with intractable neocortical epilepsy. Proceedings of the American Epilepsy Society Annual Conference, Orlando 1999.

Chozick BS, Reinert SE, Greenblatt SH. Incidence of seizures after surgery for supratentorial meningiomas: a modern analysis. J Neurosurg 1996; 84: 382-386.

Chun CH, Johnson JD, Hofstetter M, Raff MJ. Brain abscess. A study of 45 consecutive cases. Medicine (Baltimore) 1986; 65: 415-431.

Ciccarelli O, Parker GJ, Toosy AT *et al.* From diffusion tractography to quantitative white matter tract measures: a reproducibility study. Neuroimage 2003a; 18: 348-359.

Ciccarelli O, Toosy AT, Parker GJ *et al.* Diffusion tractography based group mapping of major white-matter pathways in the human brain. Neuroimage 2003b; 19: 1545-1555.

Cinbis M, Aysun S. Alice in Wonderland syndrome as an initial manifestation of Epstein-Barr virus infection. Br.J Ophthalmol. 1992; 76: 316.

Clark CA, LeBihan D. Water diffusion compartmentation and anisotropy at high b values in human brain. Proceedings of the International Society for Magnetic Resonance in Medicine, Eighth scientific meeting, 2000; 759.

Collins DL, Neeling P, Peters TM, Evans AC. Automatic 3D intersubject registration of MR volumetric data in standardized Tailarach space. J Comput.Assist.Tomogr. 1994; 18: 192-205.

Connelly A, Jackson GD, Duncan JS, King MD, Gadian DG. Magnetic resonance spectroscopy in temporal lobe epilepsy. Neurology 1994; 44: 1411-1417.

Connelly A, Van Paesschen W, Porter DA, Johnson CL, Duncan JS, Gadian DG. Proton magnetic resonance spectroscopy in MRI-negative temporal lobe epilepsy. Neurology 1998; 51: 61-66.

Connolly AM, Chez MG, Pestronk A, Arnold ST, Mehta S, Deuel RK. Serum autoantibodies to brain in Landau-Kleffner variant, autism, and other neurologic disorders. J Pediatr. 1999; 134: 607-613.

Constable RT, Anderson AW, Zhong J, Gore JC. Factors influencing contrast in fast spin-echo MR imaging. Magn Reson Imaging 1992; 10: 497-511.

Conturo TE, Lori NF, Cull TS *et al.* Tracking neuronal fiber pathways in the living human brain. Proc.Natl.Acad.Sci.U.S.A 1999; 96: 10422-10427.

Conturo TE, McKinstry RC, Akbudak E, Robinson BH. Encoding of anisotropic diffusion with tetrahedral gradients: a general mathematical diffusion formalism and experimental results. Magn Reson Med 1996; 35: 399-412.

Cook M, Sisodiya S. Magnetic Resonance Imaging Evaluation for Epilepsy Surgery. In: Shorvon SD, Dreifuss F, Fish DR, Thomas D, editors. The Treatment of Epilepsy. Oxford: Blackwell Science Ltd, 1996: 589-604.

Cook MJ, Fish DR, Shorvon SD, Straughan K, Stevens JM. Hippocampal volumetric and morphometric studies in frontal and temporal lobe epilepsy. Brain 1992; 115: 1001-1015.

Cook MJ, Free SL, Manford MR, Fish DR, Shorvon SD, Stevens JM. Fractal description of cerebral cortical patterns in frontal lobe epilepsy. Eur.Neurol. 1995; 35: 327-335.

Corrigall RJ, Chong WK, Paley M, Wilkinson ID, Lantos P, Everall I. Spatial data analysis in the quantitative assessment of cerebral white matter pathology on MRI in HIV infection. Neuroradiology 1995; 37: 429-433.

Cossette P, Liu L, Brisebois K *et al.* Mutation of GABRA1 in an autosomal dominant form of juvenile myoclonic epilepsy. Nat.Genet. 2002; 31: 184-189.

Costantino A, Vinters HV. A pathologic correlate of the 'steal' phenomenon in a patient with cerebral arteriovenous

malformation. Stroke 1986; 17: 103-106.

Counsell SJ, Kennea NL, Herlihy AH *et al.* T2 relaxation values in the developing preterm brain. Proceedings of the International Society of Magnetic Resonance in Medicine, 9th Annual Meeting 2001; 410.

Cox DR, Miller HD. The Theory of Stochastic Processes. London: Chapman and Hall, 1990.

Crooks LE, Hoenninger J, Arakawa M *et al.* High-resolution magnetic resonance imaging. Technical concepts and their implementation. Radiology 1984; 150: 163-171.

Csernansky JG, Wang L, Jones D *et al.* Hippocampal deformities in schizophrenia characterized by high dimensional brain mapping. Am.J Psychiatry 2002; 159: 2000-2006.

Cuenod CA, Bookheimer SY, Hertz-Pannier L, Zeffiro TA, Theodore WH, Le Bihan D. Functional MRI during word generation, using conventional equipment: a potential tool for language localization in the clinical environment. Neurology 1995; 45: 1821-1827.

Cutting LE, Koth CW, Burnette CP, Abrams MT, Kaufmann WE, Denckla MB. Relationship of cognitive functioning, whole brain volumes, and T2- weighted hyperintensities in neurofibromatosis-1. J Child Neurol. 2000; 15: 157-160.

D'Olhaberriague L, Welch KM, Nagesh V *et al.* Preliminary clinical-radiological assessment of a MR tissue signature model in human stroke. J.Neurol.Sci. 1998; 156: 158-166.

da Silva AM, Nunes B, Vaz AR, Mendonca D. Posttraumatic epilepsy in civilians: clinical and electroencephalographic studies. Acta Neurochir.Suppl (Wien.) 1992; 55: 56-63.

Damadian R. Tumor detection by nuclear magnetic resonance. Science 1971; 171: 1151-1153.

Damasio H, Frank R. Three-dimensional in vivo mapping of brain lesions in humans. Arch.Neurol. 1992; 49: 137-143.

Dambinova SA, Izykenova GA, Burov SV, Grigorenko EV, Gromov SA. The presence of autoantibodies to N-terminus domain of GluR1 subunit of AMPA receptor in the blood serum of patients with epilepsy. J Neurol.Sci. 1997; 152: 93-97.

Dambska M, Wisniewski K, Sher J, Solish G. Cerebro-oculo-muscular syndrome: a variant of Fukuyama congenital cerebromuscular dystrophy. Clin.Neuropathol. 1982; 1: 93-98.

Dambska M, Wisniewski K, Sher JH. Lissencephaly: two distinct clinico-pathological types. Brain Dev 1983; 5: 302-310.

Danober L, Deransart C, Depaulis A, Vergnes M, Marescaux C. Pathophysiological mechanisms of genetic absence epilepsy in the rat. Prog.Neurobiol. 1998; 55: 27-57.

Dardzinski BJ, Sotak CH, Fisher M, Hasegawa Y, Li L, Minematsu K. Apparent diffusion coefficient mapping of experimental focal cerebral ischemia using diffusion-weighted echo-planar imaging. Magn Reson Med 1993; 30: 318-325.

Daumas-Duport C, Scheithauer BW, Chodkiewicz JP, Laws ER, Vedrenne C. Dysembryoplastic neuroepithelial tumor: a surgically curable tumor of young patients with intractable partial seizures. Report of thirty-nine cases. Neurosurgery 1988; 23: 545-556.

Davies KG, Hermann BP, Dohan FC, Jr., Foley KT, Bush AJ, Wyler AR. Relationship of hippocampal sclerosis to duration and age of onset of epilepsy, and childhood febrile seizures in temporal lobectomy patients. Epilepsy Res. 1996; 24: 119-126.

Davis D, Ulatowski J, Eleff S *et al.* Rapid monitoring of changes in water diffusion coefficients during reversible ischemia in cat and rat brain. Magn Reson Med 1994; 31: 454-460.

De Coene B, Hajnal JV, Gatehouse P *et al.* MR of the brain using fluid-attenuated inversion recovery (FLAIR) pulse sequences. AJNR Am J Neuroradiol 1992; 13: 1555-1564.

De Coene B, Hajnal JV, Pennock JM, Bydder GM. MRI of the brain stem using fluid attenuated inversion recivery pulse sequences. Neuroradiology 1993; 35: 327-331.

de Crespigny AJ, Marks MP, Enzmann DR, Moseley ME. Navigated diffusion imaging of normal and ischemic human brain. Magn Reson Med 1995; 33: 720-728.

De Ponti F, Lecchini S, Cosentino M, Castelletti CM, Malesci A, Frigo GM. Immunological adverse effects of anticonvulsants. What is their clinical relevance? Drug Saf 1993; 8: 235-250.

Del Brutto OH. Prognostic factors for seizure recurrence after withdrawal of antiepileptic drugs in patients with neurocysticercosis. Neurology 1994; 44: 1706-1709.

Del Brutto OH, Santibanez R, Noboa CA, Aguirre R, Diaz E, Alarcon TA. Epilepsy due to neurocysticercosis: analysis of 203 patients. Neurology 1992; 42: 389-392.

Del Brutto OH, Sotelo J, Roman GC. Therapy for neurocysticercosis: a reappraisal. Clin.Infect.Dis. 1993; 17: 730-735.

Delattre JY, Krol G, Thaler HT, Posner JB. Distribution of brain metastases. Arch Neurol 1988; 45: 741-744.

Demaerel P, Heiner L, Robberecht W, Sciot R, Wilms G. Diffusion-weighted MRI in sporadic Creutzfeldt-Jakob disease. Neurology 1999; 52: 205-208.

Demaerel P, Sciot R, Robberecht W *et al.* Accuracy of diffusion-weighted MR imaging in the diagnosis of sporadic Creutzfeldt-Jakob disease. J Neurol 2003; 250: 222-225.

des Portes V, Pinard JM, Smadja D *et al.* Dominant X linked subcortical laminar heterotopia and lissencephaly

syndrome (XSCLH/LIS): evidence for the occurrence of mutation in males and mapping of a potential locus in Xq22. J Med Genet. 1997; 34: 177-183.

Desmond JE, Sum JM, Wagner AD *et al.* Functional MRI measurement of language lateralization in Wada-tested patients. Brain 1995; 118: 1411-1419.

Detre JA, Sirven JI, Alsop DC, O'Connor MJ, French JA. Localization of subclinical ictal activity by functional magnetic resonance imaging: correlation with invasive monitoring. Ann.Neurol. 1995; 38: 618-624.

Dettmers C, Connelly A, Stephan K-M *et al.* Quantitative comparison of functional magnetic resonance imaging with positron emission tomography using a force related paradigm. Neuroimage 1996; 4: 194-200.

Diehl B, Najm I, Ruggieri P *et al.* Periictal diffusion-weighted imaging in a case of lesional epilepsy. Epilepsia 1999; 40: 1667-1671.

Dingledine R, Hynes MA, King GL. Involvement of N-methyl-D-aspartate receptors in epileptiform bursting in the rat hippocampal slice. J Physiol 1986; 380: 175-189.

Dobbing J, Sands J. Quantitative growth and development of human brain. Arch.Dis.Child 1973; 48: 757-767.

Dobyns WB, Elias ER, Newlin AC, Pagon RA, Ledbetter DH. Causal heterogeneity in isolated lissencephaly. Neurology 1992; 42: 1375-1388.

Dobyns WB, Kirkpatrick JB, Hittner HM, Roberts RM, Kretzer FL. Syndromes with lissencephaly. II: Walker-Warburg and cerebro-oculo- muscular syndromes and a new syndrome with type II lissencephaly. Am J Med Genet. 1985; 22: 157-195.

Dobyns WB, Reiner O, Carrozzo R, Ledbetter DH. Lissencephaly. A human brain malformation associated with deletion of the LIS1 gene located at chromosome 17p13. JAMA 1993; 270: 2838-2842.

Dobyns WB, Stratton RF, Greenberg F. Syndromes with lissencephaly. I: Miller-Dieker and Norman-Roberts syndromes and isolated lissencephaly. Am J Med Genet. 1984; 18: 509-526.

Doran M, Hajnal JV, van Bruggen N, King MD, Young IR, Bydder GM. Normal and abnormal white matter tracts shown by MR imaging using directional diffusion weighted sequences. J.Comput.Assist.Tomogr. 1990; 14: 865-873.

Douek P, Turner R, Pekar J, Patronas N, Le Bihan D. MR color mapping of myelin fiber orientation. J Comput.Assist.Tomogr. 1991; 15: 923-929.

Dousset V, Armand JP, Lacoste D *et al.* Magnetization transfer study of HIV encephalitis and progressive multifocal leukoencephalopathy. Groupe d'Epidemiologie Clinique du SIDA en Aquitaine. AJNR Am J Neuroradiol 1997; 18: 895-901.

Dousset V, Grossman RI, Ramer KN *et al.* Experimental allergic encephalomyelitis and multiple sclerosis: lesion

characterization with magnetization transfer imaging (published erratum appears in Radiology 1992 Jun; 183 (3):878). Radiology 1992; 182: 483-491.

Drayer B, Burger P, Darwin R, Riederer S, Herfkens R, Johnson GA. MRI of brain iron. AJR Am J Roentgenol. 1986; 147: 103-110.

Droogan AG, Clark CA, Werring DJ, Barker GJ, McDonald WI, Miller DH. Comparison of multiple sclerosis clinical subgroups using navigated spin echo diffusion-weighted imaging. Magn Reson Imaging 1999; 17: 653-661.

Du AT, Schuff N, Amend D *et al.* Magnetic resonance imaging of the entorhinal cortex and hippocampus in mild cognitive impairment and Alzheimer's disease. J Neurol Neurosurg.Psychiatry 2001; 71: 441-447.

Du F, Whetsell WO, Jr., Abou-Khalil B, Blumenkopf B, Lothman EW, Schwarcz R. Preferential neuronal loss in layer III of the entorhinal cortex in patients with temporal lobe epilepsy. Epilepsy Res 1993; 16: 223-233.

Duncan JS. Imaging and epilepsy. Brain 1997; 120: 339-377.

Duncan JS. Neuroimaging methods to evaluate the etiology and consequences of epilepsy. Epilepsy Res 2002; 50: 131-140.

Duncan JS, Bartlett P, Barker GJ. Technique for measuring hippocampal T2 relaxation time. AJNR Am.J.Neuroradiol 1996; 17: 1805-1810.

Duncan JS, Sagar HJ. Seizure characteristics, pathology, and outcome after temporal lobectomy. Neurology 1987; 37: 405-409.

Duong T, De Rosa MJ, Poukens V, Vinters HV, Fisher RS. Neuronal cytoskeletal abnormalities in human cerebral cortical dysplasia. Acta Neuropathol. (Berl) 1994; 87: 493-503.

Duong TQ, Ackerman JJ, Ying HS, Neil JJ. Evaluation of extra- and intracellular apparent diffusion in normal and globally ischemic rat brain via 19F NMR. Magn Reson Med 1998; 40: 1-13.

Dupont JR, Earle KM. Human rabies encephalitis. A study of forty-nine fatal cases with a review of the literature. Neurology 1965; 15: 1023-1034.

Dupont S, Van de Moortele PF, Samson S *et al.* Episodic memory in left temporal lobe epilepsy: a functional MRI study. Brain 2000; 123: 1722-1732.

Duse M, Notarangelo LD, Tiberti S, Menegati E, Plebani A, Ugazio AG. Intravenous immune globulin in the treatment of intractable childhood epilepsy. Clin.Exp.Immunol. 1996; 104 Suppl 1: 71-76.

Eadie MJ. The I.L.A.E. classification of the epilepsies applied retrospectively to 1902 patients. Epilepsy Res. 1996; 25: 277-284.

Ebersole JS, Wade PB. Spike voltage topography identifies two types of frontotemporal epileptic foci. Neurology 1991; 41: 1425-1433.

Ebisu T, Rooney WD, Graham SH, Mancuso A, Weiner MW, Maudsley AA. MR spectroscopic imaging and diffusion-weighted MRI for early detection of kainate-induced status epilepticus in the rat. Magn Reson Med 1996; 36: 821-828.

Edelman RR, Ahn SS, Chien D *et al.* Improved time-of-flight MR angiography of the brain with magnetization transfer contrast. Radiology 1992; 184: 395-399.

Edelman RR, McFarland E, Stark DD *et al.* Surface coil MR imaging of abdominal viscera. Part I. Theory, technique, and initial results. Radiology 1985a; 157: 425-430.

Edelman RR, Shoukimas GM, Stark DD *et al.* High-resolution surface-coil imaging of lumbar disk disease. AJR Am.J Roentgenol. 1985b; 144: 1123-1129.

Edelstein WA, Bottomley PA, Hart HR, Smith LS. Signal, noise, and contrast in nuclear magnetic resonance (NMR) imaging. J Comput.Assist.Tomogr. 1983; 7: 391-401.

Edzes HT, Samulski ET. Cross relaxation and spin diffusion in the proton NMR or hydrated collagen. Nature 1977; 265: 521-523.

Eggleston JC, Saryan LA, Hollis DP. Nuclear magnetic resonance investigations of human neoplastic and abnormal nonneoplastic tissues. Cancer Res. 1975; 35: 1326-1332.

Einstein A. Ann Physik 1905; 17: 549.

Eis M, Els T, Hoehn-Berlage M. High resolution quantitative relaxation and diffusion MRI of three different experimental brain tumors in rat. Magn Reson Med 1995; 34: 835-844.

Eksioglu YZ, Scheffer IE, Cardenas P *et al.* Periventricular heterotopia: an X-linked dominant epilepsy locus causing aberrant cerebral cortical development. Neuron 1996; 16: 77-87.

Ellis CM, Simmons A, Jones DK *et al.* Diffusion tensor MRI assesses corticospinal tract damage in ALS. Neurology 1999; 53: 1051-1058.

Elmslie FV, Rees M, Williamson MP *et al.* Genetic mapping of a major susceptibility locus for juvenile myoclonic epilepsy on chromosome 15q. Hum.Mol.Genet. 1997; 6: 1329-1334.

Elster AD, Challa VR, Gilbert TH, Richardson DN, Contento JC. Meningiomas: MR and histopathologic features. Radiology 1989; 170: 857-862.

Elster AD, King JC, Mathews VP, Hamilton CA. Cranial tissues: appearance at gadolinium-enhanced and nonenhanced MR imaging with magnetization transfer contrast. Radiology 1994a; 190: 541-546.

Elster AD, Mathews VP, King JC, Hamilton CA. Improved detection of gadolinium enhancement using magnetization transfer imaging. Neuroimaging Clin.N.Am 1994b; 4: 185-192.

Elster AD, Mirza W. MR imaging in chronic partial epilepsy: role of contrast enhancement. AJNR Am J Neuroradiol 1991; 12: 165-170.

Eng J, Ceckler TL, Balaban RS. Quantitative 1H magnetization transfer imaging in vivo. Magn Reson Med 1991; 17: 304-314.

Engel J, Jr. Classifications of the International League Against Epilepsy: time for reappraisal (comment). Epilepsia 1998; 39: 1014-1017.

Engel J, Jr. A proposed diagnostic scheme for people with epileptic seizures and with epilepsy: report of the ILAE Task Force on Classification and Terminology. Epilepsia 2001a; 42: 796-803.

Engel J, Jr. Classification of epileptic disorders. Epilepsia 2001b; 42: 316.

Engel J, Jr., Van Ness PC, Rasmussen T, Ojemann LM. Outcome with respect to epileptic seizures. In: Engel Jr. J, editor. Surgical Treatment of the Epilepsies. New York: Raven Press, 1993: 609-921.

Engelbrecht V, Rassek M, Preiss S, Wald C, Modder U. Age-dependent changes in magnetization transfer contrast of white matter in the pediatric brain. AJNR Am J Neuroradiol 1998; 19: 1923-1929.

Eriksson S, Malmgren K, Rydenhag B, Jonsson L, Uvebrant P, Nordborg C. Surgical treatment of epilepsy--clinical, radiological and histopathological findings in 139 children and adults. Acta Neurol Scand. 1999; 99: 8-15.

Eriksson S, Thom M, Heffernan J, Sisodiya S. Persistent reelin-expressing Cajal-Retzius cells in polymicrogyria. Brain 2001a; 124: 1350-1361.

Eriksson SH, Rugg-Gunn FJ, Symms MR, Barker GJ, Duncan JS. Diffusion tensor imaging in patients with epilepsy and malformations of cortical development. Brain 2001b; 124: 617-626.

Eriksson SH, Symms MR, Rugg-Gunn FJ *et al.* Exploring white matter tracts in band heterotopia using diffusion tractography. Ann Neurol 2002; 52: 327-334.

Erkinjuntti T, Gao F, Lee DH, Eliasziw M, Merskey H, Hachinski VC. Lack of difference in brain hyperintensities between patients with early Alzheimer's disease and control subjects. Arch.Neurol. 1994; 51: 260-268.

Essig M, Hawighorst H, Schoenberg SO *et al.* Fast fluid-attenuated inversion-recovery (FLAIR) MRI in the assessment of intraaxial brain tumors. J Magn Reson Imaging 1998; 8: 789-798.

Evans AC, Collins DL, Milner B. An MRI-based stereotactic atlas from 250 young normal subjects. Soc.Neurosci.Abstr. 1992; 18: 408.

Evans JC, Curtis J. The radiological appearances of tuberous sclerosis. Br.J Radiol. 2000; 73: 91-98.

Everitt AD, Birnie KD, Stevens JM, Sander JW, Duncan JS, Shorvon SD. The NSE MRI Unit study: structural brain abnormalities in adult epilepsy patients and healthy controls (abstract). Epilepsia 1998; 39: 140.

Everitt AD, Sander JW. Classification of the epilepsies: time for a change? A critical review of the International Classification of the Epilepsies and Epileptic Syndromes (ICEES) and its usefulness in clinical practice and epidemiological studies of epilepsy. Eur.Neurol. 1999; 42: 1-10.

Evrard P, Caviness VS, Jr., Prats-Vinas J, Lyon G. The mechanism of arrest of neuronal migration in the Zellweger malformation: an hypothesis bases upon cytoarchitectonic analysis. Acta Neuropathol. (Berl) 1978; 41: 109-117.

Faden AI, O'Leary DM, Fan L, Bao W, Mullins PG, Movsesyan VA. Selective Blockade of the mGluR1 Receptor Reduces Traumatic Neuronal Injury in Vitro and Improves Outcome after Brain Trauma. Exp Neurol 2001; 167: 435-444.

Falconer JC, Narayana PA. Cerebrospinal fluid-suppressed high-resolution diffusion imaging of human brain. Magn Reson Med 1997; 37: 119-123.

Falconer MA, Cavanagh JB. Clinico-pathological considerations of temporal lobe epilepsy due to small focal lesions. Brain 1959; 483-503.

Falconer MA, Serafetinides EA, Corsellis JA. Etiology and pathogenesis of temporal lobe epilepsy. Arch.Neurol. 1964; 10: 233-248.

Fan-Harvard P, Sanchorawala V, Oh J, Moser EM, Smith SP. Concurrent use of foscarnet and ciprofloxacin may increase the propensity for seizures. Ann.Pharmacother. 1994; 28: 869-872.

Fazekas F. Magnetic resonance signal abnormalities in asymptomatic individuals: their incidence and functional correlates. Eur.Neurol. 1989; 29: 164-168.

Fazekas F, Kapeller P, Schmidt R, Offenbacher H, Payer F, Fazekas G. The relation of cerebral magnetic resonance signal hyperintensities to Alzheimer's disease. J Neurol.Sci. 1996; 142: 121-125.

Fazekas F, Kapeller P, Schmidt R *et al.* Magnetic resonance imaging and spectroscopy findings after focal status epilepticus. Epilepsia 1995; 36: 946-949.

Fazekas F, Kleinert R, Offenbacher H *et al.* Pathologic correlates of incidental MRI white matter signal hyperintensities. Neurology 1993; 43: 1683-1689.

Fazekas F, Schmidt R, Scheltens P. Pathophysiologic mechanisms in the development of age-related white matter changes of the brain. Dement.Geriatr.Cogn Disord. 1998; 9 Suppl 1: 2-5.

Feeney DM, Walker AE. The prediction of posttraumatic epilepsy. A mathematical approach. Arch Neurol 1979; 36: 8-12.

Feindel W, Robitaille Y, Tampieri D, Goossens L, Li M, Melancon D. Electroencephalography, magnetic resonance imaging and pathology in patients treated surgically for temporal lobe epilepsy. Can.J Neurol Sci. 1991; 18: 577-579.

Ferbert A, Busse D, Thron A. Microinfarction in classic migraine? A study with magnetic resonance imaging findings. Stroke 1991; 22: 1010-1014.

Ferini-Strambi L, Bozzali M, Cercignani M, Oldani A, Zucconi M, Filippi M. Magnetization transfer and diffusion-weighted imaging in nocturnal frontal lobe epilepsy. Neurology 2000; 54: 2331-2333.

Fernandez G, Effenberger O, Vinz B *et al.* Hippocampal malformation as a cause of familial febrile convulsions and subsequent hippocampal sclerosis. Neurology 1998; 50: 909-917.

Ferrer I, Alcantara S, Marti E. A four-layered 'lissencephalic' cortex induced by prenatal X- irradiation in the rat. Neuropathol.Appl.Neurobiol. 1993; 19: 74-81.

Ferrer I, Pineda M, Tallada M *et al.* Abnormal local-circuit neurons in epilepsia partialis continua associated with focal cortical dysplasia. Acta Neuropathol. (Berl) 1992; 83: 647-652.

Ferrie JC, Barantin L, Saliba E *et al.* MR assessment of the brain maturation during the perinatal period: quantitative T2 MR study in premature newborns. Magn Reson Imaging 1999; 17: 1275-1288.

Filipek PA, Kennedy DN, Caviness VS, Jr. Volumetric analyses of central nervous system neoplasm based on MRI. Pediatr.Neurol. 1991; 7: 347-351.

Filipek PA, Kennedy DN, Caviness VS, Jr., Rossnick SL, Spraggins TA, Starewicz PM. Magnetic resonance imaging-based brain morphometry: development and application to normal subjects. Ann.Neurol. 1989; 25: 61-67.

Filipek PA, Richelme C, Kennedy DN, Caviness VS, Jr. The young adult human brain: an MRI-based morphometric analysis. Cereb Cortex 1994; 4: 344-360.

Filippi M. MRI-clinical correlations in the primary progressive course of MS: new insights into the disease pathophysiology from the application of magnetization transfer, diffusion tensor, and functional MRI. J Neurol Sci. 2003; 206: 157-164.

Filippi M, Campi A, Dousset V *et al.* A magnetization transfer imaging study of normal-appearing white matter in multiple sclerosis. Neurology 1995a; 45: 478-482.

Filippi M, Horsfield MA, Ader HJ *et al.* Guidelines for using quantitative measures of brain magnetic resonance imaging abnormalities in monitoring the treatment of multiple sclerosis. Ann.Neurol. 1998a; 43: 499-506.

Filippi M, Horsfield MA, Bressi S *et al.* Intra- and inter-observer agreement of brain MRI lesion volume measurements in multiple sclerosis. A comparison of techniques. Brain 1995b; 118: 1593-1600.

Filippi M, Horsfield MA, Campi A, Mammi S, Pereira C, Comi G. Resolution-dependent estimates of lesion

volumes in magnetic resonance imaging studies of the brain in multiple sclerosis. Ann.Neurol. 1995c; 38: 749-754.

Filippi M, Horsfield MA, Hajnal JV *et al.* Quantitative assessment of magnetic resonance imaging lesion load in multiple sclerosis. J Neurol.Neurosurg.Psychiatry 1998b; 64 Suppl 1: S88-S93.

Filippi M, Horsfield MA, Tofts PS, Barkhof F, Thompson AJ, Miller DH. Quantitative assessment of MRI lesion load in monitoring the evolution of multiple sclerosis. Brain 1995d; 118 (Pt 6): 1601-1612.

Filippi M, Rocca MA, Martino G, Horsfield MA, Comi G. Magnetization transfer changes in the normal appearing white matter precede the appearance of enhancing lesions in patients with multiple sclerosis. Ann.Neurol. 1998c; 43: 809-814.

Finelli DA, Hurst GC, Gullapali RP, Bellon EM. Improved contrast of enhancing brain lesions on postgadolinium, T1-weighted spin-echo images with use of magnetization transfer. Radiology 1994; 190: 553-559.

Finlay BL, Slattery M. Local differences in the amount of early cell death in neocortex predict adult local specializations. Science 1983; 219: 1349-1351.

Finsterbusch J, Frahm J. Diffusion-weighted single-shot line scan imaging of the human brain. Magn Reson Med 1999; 42: 772-778.

Fish DR. How do tumours cause epilepsy? In: Kotagal P, Luders HO, editors. The Epilepsies: Etiologies and Prevention. Academic Press, 1999: 301-14.

Fish DR, Brooks DJ, Young IR, Bydder GM. Use of magnetic resonance imaging to identify changes in cerebral blood flow in epilepsia partialis continua. Magn Reson Med 1988; 8: 238-240.

Fitzsimmons JR, Scott JD, Peterson DM, Wolverton BL, Webster CS, Lang PJ. Integrated RF coil with stabilization for fMRI human cortex. Magn Reson Med 1997; 38: 15-18.

Foong J, Maier M, Barker GJ, Brocklehurst S, Miller DH, Ron MA. In vivo investigation of white matter pathology in schizophrenia with magnetisation transfer imaging. J Neurol Neurosurg Psychiatry 2000a; 68: 70-74.

Foong J, Maier M, Clark CA, Barker GJ, Miller DH, Ron MA. Neuropathological abnormalities of the corpus callosum in schizophrenia: a diffusion tensor imaging study (In Process Citation). J.Neurol.Neurosurg.Psychiatry 2000b; 68: 242-244.

Foong J, Symms MR, Barker GJ *et al.* Neuropathological abnormalities in schizophrenia: evidence from magnetization transfer imaging. Brain 2001; 124: 882-892.

Forsen S, Hoffman R. A new method for the study of moderately rapid chemical exchange rates employing nuclear magnetic double resonance. Acta Chem Scand 1963a; 17: 1787-1788.

Forsen S, Hoffman R. Study of moderately rapid chemical exchange reactions by means of nuclear magnetic double resonance. J Chem Phys 1963b; 39: 2892-2901.

Fournier D, TerBrugge KG, Willinsky R, Lasjaunias P, Montanera W. Endovascular treatment of intracerebral arteriovenous malformations: experience in 49 cases. J Neurosurg. 1991; 75: 228-233.

Fox JW, Lamperti ED, Eksioglu YZ *et al.* Mutations in filamin 1 prevent migration of cerebral cortical neurons in human periventricular heterotopia. Neuron 1998; 21: 1315-1325.

Fox PT, Mintun MA. Non-invasive functional brain mapping by change distribution analysis of averaged PET images of H15O2 tissue activity. J Nucl.Med 1989; 30: 141-149.

Fox PT, Perlmutter JS, Raichle ME. A stereotactic method of anatomical localisation for positron emission tomography. J Comput.Assist.Tomogr. 1985; 9: 141-153.

Fralix TA, Ceckler TL, Wolff SD, Simon SA, Balaban RS. Lipid bilayer and water proton magnetization transfer: effect of cholesterol. Magn Reson Med 1991; 18: 214-223.

Free SL, Bergin PS, Fish DR, Cook MJ, Shorvon SD, Stevens JM. Methods for normalization of hippocampal volumes measured with MR. AJNR Am.J.Neuroradiol 1995; 16: 637-643.

Free SL, Sisodiya S, Shorvon SD. Gyrification index from the MRI scans of patients with cortical dysgenesis. Epilepsia 1996a; 37 (suppl 4): 190.

Free SL, Sisodiya SM, Cook MJ, Fish DR, Shorvon SD. Three-dimensional fractal analysis of the white matter surface from magnetic resonance images of the human brain. Cereb.Cortex 1996b; 6: 830-836.

Freeman JL, Harvey AS, Rosenfeld JV, Wrennall JA, Bailey CA, Berkovic SF. Generalized epilepsy in hypothalamic hamartoma: evolution and postoperative resolution. Neurology 2003; 60: 762-767.

Freilich RJ, DeAngelis L. Primary central nervous system lymphoma. In: Wen P, Black P, editors. Neurologic Clinics, Vol. 13. Brain tumours in adults. Philadelphia: W.B. Saunders Company, 1995: 901-14.

Fridovich I. Superoxide dismutases. Adv.Enzymol.Relat Areas Mol.Biol. 1974; 41: 35-97.

Friede RL. Developmental Neuropathology. Berlin: Springer-Verlag, 1989.

Friede RL, Mikolasek J. Postencephalitic porencephaly, hydranencephaly or polymicrogyria. A review. Acta Neuropathol. (Berl) 1978; 43: 161-168.

Frisoni GB, Testa C, Zorzan A *et al.* Detection of grey matter loss in mild Alzheimer's disease with voxel based morphometry. J Neurol Neurosurg.Psychiatry 2002; 73: 657-664.

Friston KJ. Analysing brain images: principles and overview. In: Frackowiak RS, Friston KJ, Frith CD, Dolan RJ, Mazziotta JC, editors. Human Brain Function. San Diego: Academic Press, 1997: 25-41.

Friston KJ, Ashburner J, Frith JD, Poline JP, Heather JD, Frackowiak RSJ. Spatial registration and normalisation of images. Human Brain Mapping 1995a; 165-189.

Friston KJ, Buchel C. Attentional modulation of effective connectivity from V2 to V5/MT in humans. Proc.Natl.Acad.Sci.U.S.A 2000; %20; 97: 7591-7596.

Friston KJ, Frith CD, Liddle PF, Frackowiak RS. Comparing functional (PET) images: the assessment of significant change. J Cereb.Blood Flow Metab 1991a; 11: 690-699.

Friston KJ, Frith CD, Liddle PF, Frackowiak RS. Plastic transformation of PET images. J Comput.Assist.Tomogr. 1991b; 15: 634-639.

Friston KJ, Holmes AP, Worsley KJ, Poline JP, Frith JD, Frackowiak RSJ. Statistical parametric maps in functional imaging: a general linear approach. Human Brain Mapping 1995b; 189-210.

Friston KJ, Williams S, Howard R, Frackowiak RS, Turner R. Movement-related effects in fMRI time-series. Magn Reson Med 1996; 35: 346-355.

Friston KJ, Worsley KJ, Frackowiak RSJ, Mazziotta JC, Evans AC. Assessing the significance of focal activations using their spatial extent. Human Brain Mapping 1994; 210-220.

Fullerton GD. Physiologic basis of magnetic relaxation. In: Stark DD, Bradley Jr. WG, editors. Magnetic Resonance Imaging. St Louis: Mosby-Year Book, 1992: 88-108.

Garcia HH, Gilman RH, Tovar MA *et al.* Factors associated with Taenia solium cysticercosis: analysis of nine hundred forty-six Peruvian neurologic patients. Cysticercosis Working Group in Peru (CWG). Am J Trop.Med Hyg. 1995a; 52: 145-148.

Garcia PA, Laxer KD, Barbaro NM, Dillon WP. Prognostic value of qualitative magnetic resonance imaging hippocampal abnormalities in patients undergoing temporal lobectomy for medically refractory seizures. Epilepsia 1994; 35: 520-524.

Garcia PA, Laxer KD, van der Grond J, Hugg J, Matson GB, Weiner MW. Phosphorus magnetic resonance spectroscopic imaging in patients with frontal lobe epilepsy. Ann Neurol 1995b; 217-221.

Garcia PA, Laxer KD, van der Grond J, Hugg J, Matson GB, Weiner MW. Proton magentic resonance spectroscopic imaging in patients with frontal lobe epilepsy. Ann Neurol 1995c; 279-281.

Gardiner M, Lehesjoki AE. Genetics of the epilepsies. Curr.Opin.Neurol. 2000; 13: 157-164.

Gardiner RM. Genetic basis of the human epilepsies. Epilepsy Res. 1999; 36: 91-95.

Gareau PJ, Rutt BK, Bowen CV, Karlik SJ, Mitchell JR. In vivo measurements of multi-component T2 relaxation behaviour in guinea pig brain. Magn Reson Imaging 1999; 17: 1319-1325.

Gaser C, Nenadic I, Buchsbaum BR, Hazlett EA, Buchsbaum MS. Deformation-based morphometry and its relation to conventional volumetry of brain lateral ventricles in MRI. Neuroimage 2001; 13: 1140-1145.

Gass A, Barker GJ, Kidd D *et al.* Correlation of magnetization transfer ratio with clinical disability in multiple sclerosis. Ann Neurol 1994; 36: 62-67.

Gastaut H. Classification of the epilepsies. Proposal for an international classification. Epilepsia 1969; 10: Suppl-21.

Gastaut H, Gastaut JL. Computerized transverse axial tomography in epilepsy. Epilepsia 1976; 17: 325-336.

Gaviria M, Privat A, d'Arbigny P, Kamenka J, Haton H, Ohanna F. Neuroprotective effects of a novel NMDA antagonist, Gacyclidine, after experimental contusive spinal cord injury in adult rats. Brain Res 2000; 874: 200-209.

Gawne-Cain ML, O'Riordan JI, Thompson AJ, Moseley IF, Miller DH. Multiple sclerosis lesion detection in the brain: a comparison of fast fluid-attenuated inversion recovery and conventional T2-weighted dual spin echo. Neurology 1997; 49: 364-370.

Gentry LR, Godersky JC, Thompson B. MR imaging of head trauma: review of the distribution and radiopathologic features of traumatic lesions. AJR Am J Roentgenol. 1988; 150: 663-672.

Georgiades CS, Itoh R, Golay X, van Zijl PC, Melhem ER. MR imaging of the human brain at 1.5 T: regional variations in transverse relaxation rates in the cerebral cortex. AJNR Am J Neuroradiol 2001; 22: 1732-1737.

Gerszten PC, Adelson PD, Kondziolka D, Flickinger JC, Lunsford LD. Seizure outcome in children treated for arteriovenous malformations using gamma knife radiosurgery. Pediatr.Neurosurg. 1996; 24: 139-144.

Ghezzi A, Montanini R, Basso PF, Zaffaroni M, Massimo E, Cazzullo CL. Epilepsy in multiple sclerosis. Eur.Neurol. 1990; 30: 218-223.

Ghosh A, Antonini A, McConnell SK, Shatz CJ. Requirement for subplate neurons in the formation of thalamocortical connections. Nature 1990; 347: 179-181.

Giometto B, Nicolao P, Macucci M, Tavolato B, Foxon R, Bottazzo GF. Temporal-lobe epilepsy associated with glutamic-acid-decarboxylase autoantibodies. Lancet 1998; 352: 457.

Gitelman DR, Ashburner J, Friston KJ, Tyler LK, Price CJ. Voxel-based morphometry of herpes simplex encephalitis. Neuroimage 2001; 13: 623-631.

Giubilei F, Bastianello S, Paolillo A *et al.* Quantitative magnetic resonance analysis in vascular dementia. J Neurol. 1997; 244: 246-251.

Goldman-Rakic PS. In: Rakic P, Singer W, editors. Neurobiology of neocortex. New York: John Wiley & Sons., 1988: 177-202.

Gonzalez RG, Schaefer PW, Buonanno FS *et al.* Diffusion-weighted MR imaging: diagnostic accuracy in patients imaged within 6 hours of stroke symptom onset. Radiology 1999; 210: 155-162.

Good CD, Johnsrude I, Ashburner J, Henson RN, Friston KJ, Frackowiak RS. Cerebral asymmetry and the effects of sex and handedness on brain structure: a voxel-based morphometric analysis of 465 normal adult human brains. Neuroimage 2001a; 14: 685-700.

Good CD, Johnsrude IS, Ashburner J, Henson RN, Friston KJ, Frackowiak RS. A voxel-based morphometric study of ageing in 465 normal adult human brains. Neuroimage 2001b; 14: 21-36.

Goodkin DE, Rooney WD, Sloan R *et al.* A serial study of new MS lesions and the white matter from which they arise. Neurology 1998; 51: 1689-1697.

Grad J, Mendelson D, Hyder F, Bryant RG. Direct measurement of longitudinal relaxation and magnetization transfer in heterogeneous systems. J Magn Reson 1990; 86: 416-419.

Grant PE, Barkovich AJ, Wald LL, Dillon WP, Laxer KD, Vigneron DB. High-resolution surface-coil MR of cortical lesions in medically refractory epilepsy: a prospective study. AJNR Am.J Neuroradiol. 1997; 18: 291-301.

Grasby PM, Frith CD, Friston K, Frackowiak RS, Dolan RJ. Activation of the human hippocampal formation during auditory-verbal long-term memory function. Neurosci.Lett. 1993; 163: 185-188.

Grenier D, Pelletier D, Newitt DC, Nelson SJ, Goodkin DE, Majumdar S. In vivo T2 brain histogram in multiple sclerosis. Proceedings of the International Society of Magnetic Resonance in Medicine, 9th Annual Meeting 2001; 1424.

Griffin CM, Chard DT, Ciccarelli O *et al.* Diffusion tensor imaging in early relapsing-remitting multiple sclerosis. Mult.Scler. 2001; 7: 290-297.

Griffin CM, Chard DT, Parker GJ, Barker GJ, Thompson AJ, Miller DH. The relationship between lesion and normal appearing brain tissue abnormalities in early relapsing remitting multiple sclerosis. J Neurol 2002; 249: 193-199.

Gruetter R, Novotny EJ, Boulware SD, Rothman DL, Mason GF, Shulman GI. Direct measurements of brain glucose concentrations in humans by ^{13}C NMR spectroscopy. Proc.Natl.Acad.Sci.U.S.A 1992; 1109-1112.

Grunewald RA, Jackson GD, Connelly A, Duncan JS. MR detection of hippocampal disease in epilepsy: factors influencing T2 relaxation time. AJNR Am.J.Neuroradiol 1994; 15: 1149-1156.

Guerrini R, Dravet C, Raybaud C *et al.* Epilepsy and focal gyral anomalies detected by MRI: electroclinico-morphological correlations and follow-up. Dev.Med Child Neurol 1992; 34: 706-718.

Guidice MA, Berchou RC. Post-traumatic epilepsy following head injury. Brain Inj. 1987; 1: 61-64.

Gundersen HJG, Jensen EB. The efficiency of systematic sampling in stereology and its prediction. J Microsc 1987; 229-263.

Gunning-Dixon FM, Raz N. The cognitive correlates of white matter abnormalities in normal aging: a quantitative

review. Neuropsychology. 2000; 14: 224-232.

Guo AC, Jewells VL, Provenzale JM. Analysis of normal-appearing white matter in multiple sclerosis: comparison of diffusion tensor MR imaging and magnetization transfer imaging. AJNR Am.J Neuroradiol. 2001; 22: 1893-1900.

Gupta RK, Kathuria MK, Pradhan S. Magnetisation transfer magnetic resonance imaging demonstration of perilesional gliosis--relation with epilepsy in treated or healed neurocysticercosis (letter). Lancet 1999a; 354: 44-45.

Gupta RK, Kathuria MK, Pradhan S. Magnetization transfer MR imaging in CNS tuberculosis. AJNR Am J Neuroradiol 1999b; 20: 867-875.

Gupta, S. R., Naheedy, M. H., Elias, D., and Rubino, F. A. Postinfarction seizures: a clinical study. Stroke 19, 1477-1481. 1988.

Guye M, Le Fur Y, Confort-Gouny S *et al.* Metabolic and electrophysiological alterations in subtypes of temporal lobe epilepsy: a combined proton magnetic resonance spectroscopic imaging and depth electrodes study. Epilepsia 2002; 43: 1197-1209.

Guye M, Parker GJ, Symms M *et al.* Combined functional MRI and tractography to demonstrate the connectivity of the human primary motor cortex in vivo. Neuroimage 2003; 19: 1349-1360.

Hadley DM, Teasdale GM, Jenkins A *et al.* Magnetic resonance imaging in acute head injury. Clin.Radiol. 1988; 39: 131-139.

Hagmann P, Thiran JP, Jonasson L *et al.* DTI mapping of human brain connectivity: statistical fibre tracking and virtual dissection. Neuroimage 2003; 19: 545-554.

Hahn EL. Spin Echoes. Physical Review 1950; 80: 580-594.

Hahnel S, Freund M, Munkel K *et al.* Magnetisation transfer ratio is low in normal-appearing cerebral white matter in patients with normal pressure hydrocephalus. Neuroradiology 2000; 42: 174-179.

Hahnel S, Munkel K, Jansen O *et al.* Magnetization transfer measurements in normal-appearing cerebral white matter in patients with chronic obstructive hydrocephalus. J Comput.Assist.Tomogr. 1999; 23: 516-520.

Hajnal JV, Bryant DJ, Kasuboski L *et al.* Use of fluid attenuated inversion recovery (FLAIR) pulse sequences in MRI of the brain. J Comput.Assist.Tomogr. 1992a; 16: 841-844.

Hajnal JV, De Coene B, Lewis PD *et al.* High signal regions in normal white matter shown by heavily T2-weighted CSF nulled IR sequences. J.Comput.Assist.Tomogr. 1992b; 16: 506-513.

Hajnal JV, Doran M, Hall AS *et al.* MR imaging of anisotropically restricted diffusion of water in the nervous

system: technical, anatomic, and pathologic considerations. J.Comput.Assist.Tomogr. 1991; 15: 1-18.

Hajnal JV, Oatridge A, Saeed N, Bydder GM, Young IR. Use of image registration to increase the reliability of magnetisation transfer ratio images from single and multiple examinations. Proceedings International Society for Magnetic Resonance in Medicine 5th Meeting Vancouver 1997; 2016.

Haller JW, Banerjee A, Christensen GE *et al.* Three-dimensional hippocampal MR morphometry with high-dimensional transformation of a neuroanatomic atlas. Radiology 1997; 202: 504-510.

Hammeke TA, Yetkin FZ, Mueller WM *et al.* Functional magnetic resonance imaging of somatosensory stimulation. Neurosurgery 1994; 35: 677-681.

Hammers A, Allom R, Koepp MJ *et al.* Three-dimensional maximum probability atlas of the human brain, with particular reference to the temporal lobe. Hum.Brain Mapp. 2003; 19: 224-247.

Hammers A, Koepp MJ, Free SL *et al.* Implementation and application of a brain template for multiple volumes of interest. Hum.Brain Mapp. 2002a; 15: 165-174.

Hammers A, Koepp MJ, Hurlemann R *et al.* Abnormalities of grey and white matter (11C)flumazenil binding in temporal lobe epilepsy with normal MRI. Brain 2002b; 125: 2257-2271.

Hammers A, Koepp MJ, Richardson MP *et al.* Central benzodiazepine receptors in malformations of cortical development: A quantitative study. Brain 2001; 124: 1555-1565.

Hansen JR. Pulsed NMR study of water mobility in muscle and brain tissue. Biochim Biophys Acta 1971; 482-486.

Hanyu H, Asano T, Sakurai H *et al.* Diffusion-weighted and magnetization transfer imaging of the corpus callosum in Alzheimer's disease. J.Neurol.Sci. 1999; 167: 37-44.

Hanyu H, Asano T, Sakurai H, Takasaki M, Shindo H, Abe K. Magnetisation transfer measurements of the subcortical grey and white matter in Parkinson's disease with and without dementia and in progressive supranuclear palsy. Neuroradiology 2001a; 43: 542-546.

Hanyu H, Asano T, Sakurai H, Takasaki M, Shindo H, Abe K. Magnetization transfer measurements of the hippocampus in the early diagnosis of Alzheimer's disease. J Neurol Sci. 2001b; 188: 79-84.

Haraldseth O, Jones RA, Skottner A. A quantitative in-vivo MR imaging study of brain dehydration in diabetic rats and rats treated with peptide hormones. Magn Reson Imaging 1997; 15: 203-210.

Haraldsson A, van Engelen BG, Renier WO, Bakkeren JA, Weemaes CM. Light chain ratios and concentrations of serum immunoglobulins in children with epilepsy. Epilepsy Res. 1992; 13: 255-260.

Hardiman O, Burke T, Phillips J *et al.* Microdysgenesis in resected temporal neocortex: incidence and clinical significance in focal epilepsy. Neurology 1988; 38: 1041-1047.

Harding B. Dysplasias of cerebral cortex and epilepsy. In: Guerrini R, editor. 1996: 81-8.

Harding BN. Malformations of the nervous system. In: Adams JH, Duchen LW, editors. Greenfield's Neuropathology. London: Edward Arnold, 1992: 521-638.

Harrison R, Bronskill MJ, Henkelman RM. Magnetization transfer and T2 relaxation components in tissue. Magn Reson Med 1995; 33: 490-496.

Hartigan JA. Clustering Algorithms. New York: Wiley, 1975.

Hasegawa D, Orima H, Fujita M *et al.* Diffusion-weighted imaging in kainic acid-induced complex partial status epilepticus in dogs. Brain Res 2003; 983: 115-127.

Hashimoto M, Fujimoto K, Shinoda S, Masuzawa T. Magnetic resonance imaging of ganglion cell tumours. Neuroradiology 1993; 35: 181-184.

Hassink RI, Hiltbrunner B, Muller S, Lutschg J. Assessment of brain maturation by T2-weighted MRI. Neuropediatrics 1992; 23: 72-74.

Haug K, Warnstedt M, Alekov AK *et al.* Mutations in CLCN2 encoding a voltage-gated chloride channel are associated with idiopathic generalized epilepsies. Nat.Genet. 2003; 33: 527-532.

Haughton VM, Yetkin FZ, Rao SM *et al.* Quantitative MR in the diagnosis of multiple sclerosis. Magn Reson Med 1992; 26: 71-78.

Hauser RA, Olanow CW. Magnetic resonance imaging of neurodegenerative diseases. J Neuroimaging 1994; 4: 146-158.

Hauser WA. Incidence and prevalence. In: Engel JrJ, Pedley TA, editors. Epilepsy: A Comprehensive Textbook. Philadelphia: Lippincott-Raven, 1997: 47-57.

Hauser WA, Annegers JF, Kurland LT. Incidence of epilepsy and unprovoked seizures in Rochester, Minnesota: 1935-1984. Epilepsia 1993; 34: 453-468.

Hawrylak N, Chang FL, Greenough WT. Astrocytic and synaptic response to kindling in hippocampal subfield CA1. II. Synaptogenesis and astrocytic process increases to in vivo kindling. Brain Res. 1993; 309-316.

Hayes CE, Edelstein WA, Schenck JF, Mueller OM, Eash M. An efficient, highly homogeneous radiofrequency coil for whole-body NMR imaging at 1.5T. J Magn Reson 1985; 63: 622-628.

Hayes CE, Tsuruda JS, Mathis CM. Temporal lobes: surface MR coil phased-array imaging. Radiology 1993; 189: 918-920.

Hayward JC, Titelbaum DS, Clancy RR, Zimmerman RA. Lissencephaly-pachygyria associated with congenital cytomegalovirus infection. J Child Neurol 1991; 6: 109-114.

Heide AC, Richards TL, Alvord EC, Jr., Peterson J, Rose LM. Diffusion imaging of experimental allergic encephalomyelitis. Magn Reson Med 1993; 29: 478-484.

Heikkinen ER, Konnov B, Melnikov L *et al.* Relief of epilepsy by radiosurgery of cerebral arteriovenous malformations. Stereotact.Funct.Neurosurg. 1989; 53: 157-166.

Heinemann U, Gabriel S, Jauch R *et al.* Alterations of glial cell function in temporal lobe epilepsy. Epilepsia 2000; 41 Suppl 6: S185-S189.

Heinz ER, Crain BJ, Radtke RA *et al.* MR imaging in patients with temporal lobe seizures: correlation of results with pathologic findings. AJNR Am J Neuroradiol 1990; 11: 827-832.

Heinz ER, Heinz TR, Radtke R *et al.* Efficacy of MR vs CT in epilepsy. AJR Am.J Roentgenol. 1989; 152: 347-352.

Helmstaedter C, Hufnagel A, Elger CE. Preoperative memory profiles in patients with temporal lobe epilepsy are related to postoperative seizure outcome. J Epilepsy 1992; 5: 17-23.

Helpern JA, Ordidge RJ, Knight RA. The effect of cell membrane permeability on the apparent diffusion coefficient of water. Proceedings of the Society for Magnetic Resonance in Medicine, 11th Annual Meeting, 1992; 1201.

Henchey R, Cibula J, Helveston W, Malone J, Gilmore RL. Electroencephalographic findings in Hashimoto's encephalopathy. Neurology 1995; 45: 977-981.

Hennig J, Nauerth A, Friedburg H. RARE imaging: a fast imaging method for clinical MR. Magn Reson Med 1986; 3: 823-833.

Herranz JL. (Suggestions regarding new classification of epileptic seizures). Rev.Neurol. 1998; 26: 598-600.

Herranz MT, Rivier G, Khamashta MA, Blaser KU, Hughes GR. Association between antiphospholipid antibodies and epilepsy in patients with systemic lupus erythematosus. Arthritis Rheum. 1994; 37: 568-571.

Hertz-Pannier L, Gaillard WD, Mott SH *et al.* Noninvasive assessment of language dominance in children and adolescents with functional MRI: a preliminary study. Neurology 1997; 48: 1003-1012.

Herzig R, Burval S, Vladyka V *et al.* Familial occurrence of cerebral arteriovenous malformation in sisters: case report and review of the literature. Eur.J Neurol 2000; 7: 95-100.

Hesdorffer DC, Hauser WA, Annegers JF, Rocca WA. Severe, uncontrolled hypertension and adult-onset seizures: a case-control study in Rochester, Minnesota. Epilepsia 1996; 37: 736-741.

Hesdorffer DC, Verity CM. Risk factors. In: Engel Jr. J, Pedley TA, editors. Epilepsy: A Comprehensive Textbook. Philadelphia: Lippincott-Raven, 1997: 59-67.

Hetherington H, Newcomer BR, Pan J. Measurement of human cerebral GABA at 4.1T using numerical optimized editing pulses. Magn Reson Med 1998; 6-10.

Heun R, Klose U, Jessen F *et al.* Functional MRI of cerebral activation during encoding and retrieval of words. Hum.Brain Mapp. 1999; 8: 157-169.

Heuts-van Raak L, Lodder J, Kessels F. Late seizures following a first symptomatic brain infarct are related to large infarcts involving the posterior area around the lateral sulcus. Seizure. 1996; 5: 185-194.

Hirai T, Korogi Y, Yoshizumi K, Shigematsu Y, Sugahara T, Takahashi M. Limbic lobe of the human brain: evaluation with turbo fluid-attenuated inversion-recovery MR imaging. Radiology 2000; 215: 470-475.

Hirono N, Kitagaki H, Kazui H, Hashimoto M, Mori E. Impact of white matter changes on clinical manifestation of Alzheimer's disease: A quantitative study. Stroke 2000; 31: 2182-2188.

Hirose T, Scheithauer BW. Mixed dysembryoplastic neuroepithelial tumor and ganglioglioma. Acta Neuropathol (Berl) 1998; 95: 649-654.

Hock A, Demmel U, Schicha H, Kasperek K, Feinendegen LE. Trace element concentration in human brain. Activation analysis of cobalt, iron, rubidium, selenium, zinc, chromium, silver, cesium, antimony and scandium. Brain 1975; 98: 49-64.

Hoehn-Berlage M, Bockhorst K. Quantitative magnetic resonance imaging of rat brain tumors: in vivo NMR relaxometry for the discrimination of normal and pathological tissues. Technol.Health Care 1994; 2: 247-254.

Hoehn-Berlage M, Eis M, Back T, Kohno K, Yamashita K. Changes of relaxation times (T1, T2) and apparent diffusion coefficient after permanent middle cerebral artery occlusion in the rat: temporal evolution, regional extent, and comparison with histology. Magn Reson Med 1995; 34: 824-834.

Hoehn-Berlage M, Tolxdorff T, Bockhorst K, Okada Y, Ernestus RI. In vivo NMR T2 relaxation of experimental brain tumors in the cat: a multiparameter tissue characterization. Magn Reson Imaging 1992; 10: 935-947.

Hoffman PL, Grant KA, Snell LD, Reinlib L, Iorio K, Tabakoff B. NMDA receptors: role in ethanol withdrawal seizures. Ann.N.Y.Acad.Sci. 1992; 654:52-60.: 52-60.

Hoffman RA, Forsen S. Transient and steady-state Overhauser experiments in the investigation of relaxation processes. Analogies between chemical exchange and relaxation. J Chem Phys 1966; 45: 2049-2060.

Hofmeister C, Stapf C, Hartmann A *et al.* Demographic, morphological, and clinical characteristics of 1289 patients with brain arteriovenous malformation. Stroke 2000; 31: 1307-1310.

Hogan RE, Mark KE, Wang L, Joshi S, Miller MI, Bucholz RD. Mesial temporal sclerosis and temporal lobe epilepsy: MR imaging deformation-based segmentation of the hippocampus in five patients. Radiology 2000; 216: 291-297.

Holland BA, Haas DK, Norman D, Brant-Zawadzki M, Newton TH. MRI of normal brain maturation. AJNR Am.J Neuroradiol. 1986; 7: 201-208.

Holloway V, Chong WK, Connelly A, Harkness WH, Gadian DG. Somatomotor fMRI in the pre-surgical evaluation of a case of focal epilepsy. Clin.Radiol. 1999; 54: 301-303.

Holmes GL. The electroencephalogram as a predictor of seizures following cerebral infarction. Clin.Electroencephalogr. 1980; 11: 83-86.

Holodny AI, Ollenschlager M. Diffusion imaging in brain tumors. Neuroimaging Clin.N.Am. 2002; 12: 107-24, x.

Holt RW, Duerk JL, Hua J, Hurst GC. Estimation of Bloch model MT spin system parameters from Z-spectral data. Magn Reson Med 1994; 31: 122-130.

Holtzman DM, Kaku DA, So YT. New-onset seizures associated with human immunodeficiency virus infection: causation and clinical features in 100 cases. Am J Med 1989; 87: 173-177.

Horikawa Y, Naruse S, Tanaka C, Hirakawa K, Nishikawa H. Proton NMR relaxation times in ischemic brain edema. Stroke 1986; 17: 1149-1152.

Hornig CR, Buttner T, Hufnagel A, Schroder-Rosenstock K, Dorndorf W. Epileptic seizures following ischaemic cerebral infarction. Clinical picture, CT findings and prognosis. Eur.Arch Psychiatry Neurol Sci. 1990; 239: 379-383.

Horsfield MA, Lai M, Webb SL *et al.* Apparent diffusion coefficients in benign and secondary progressive multiple sclerosis by nuclear magnetic resonance. Magn Reson Med 1996; 36: 393-400.

Hossmann KA, Schuier FJ. Experimental brain infarcts in cats. I. Pathophysiological observations. Stroke 1980; 11: 583-592.

Houser CR, Harris AB, Vaughn JE. Time course of the reduction of GABA terminals in a model of focal epilepsy: a glutamic acid decarboxylase immunocytochemical study. Brain Res 1986; 383: 129-145.

Howse DC, Caronna JJ, Duffy TE, Plum F. Cerebral energy metabolism, pH, and blood flow during seizures in the cat. Am J Physiol 1974; 227: 1444-1451.

Hu BS, Conolly SM, Wright GA, Nishimura DG, Macovski A. Pulsed saturation transfer contrast. Magn Reson Med 1992; 26: 231-240.

Huang-Hellinger F, Breiter HC, McCormack G, Cohen MS, Kwong KK, Sutton JP. Simultaneous functional magnetic resonance imaging and electrophysiological recording. Human Brain Mapping 1995; 13-23.

Hudson LP, Munoz DG, Miller L, McLachlan RS, Girvin JP, Blume WT. Amygdaloid sclerosis in temporal lobe epilepsy. Ann.Neurol. 1993; 33: 622-631.

Huesgen CT, Burger PC, Crain BJ, Johnson GA. In vitro MR microscopy of the hippocampus in Alzheimer's disease. Neurology 1993; 43: 145-152.

Hufnagel A, Weber J, Marks S *et al.* Brain diffusion after single seizures. Epilepsia 2003; 44: 54-63.

Hugg J, Laxer KD, Matson GB, Maudsley AA, Husted CA, Weiner MW. Lateralisation of human focal epilepsy by ^{31}P magnetic resonance spectroscopic imaging. Neurology 1993; 2011-2018.

Hugg JW, Butterworth EJ, Kuzniecky RI. Diffusion mapping applied to mesial temporal lobe epilepsy. Neurology 1999; 173-176.

Huisman TA, Sorensen AG, Hergan K, Gonzalez RG, Schaefer PW. Diffusion-weighted imaging for the evaluation of diffuse axonal injury in closed head injury. J Comput.Assist.Tomogr. 2003; 27: 5-11.

Humphreys P, Kaufmann WE, Galaburda AM. Developmental dyslexia in women: neuropathological findings in three patients. Ann.Neurol. 1990; 28: 727-738.

Huttenlocher PR, Taravath S, Mojtahedi S. Periventricular heterotopia and epilepsy. Neurology 1994; 44: 51-55.

Iannucci G, Rovaris M, Giacomotti L, Comi G, Filippi M. Correlation of multiple sclerosis measures derived from T2-weighted, T1- weighted, magnetization transfer, and diffusion tensor MR imaging. AJNR Am J Neuroradiol 2001; 22: 1462-1467.

Ikezaki K, Takahashi M, Koga H *et al.* Apparent diffusion coefficient (ADC) and magnetization transfer contrast (MTC) mapping of experimental brain tumor. Acta Neurochir.Suppl (Wien.) 1997; 70:170-2: 170-172.

Imon Y, Hanyu H, Iwamoto T, Takasaki M, Abe K. (Atrophy and magnetization transfer ratio of the corpus callosum in patients with Alzheimer's disease). Rinsho Shinkeigaku 1998; 38: 1014-1018.

Inagaki M, Ando Y, Mito T *et al.* Comparison of brain imaging and neuropathology in cases of trisomy 18 and 13. Neuroradiology 1987; 29: 474-479.

Incisa della Rocchetta A, Gadian DG, Connelly A *et al.* Verbal memory impairment after right temporal lobe surgery: role of contralateral damage as revealed by 1H magnetic resonance spectroscopy and T2 relaxometry. Neurology 1995; 45: 797-802.

Inoue T, Shimizu H, Yoshimoto T. Imaging the pyramidal tract in patients with brain tumors. Clin.Neurol.Neurosurg. 1999; 101: 4-10.

Inzelberg R, Korczyn AD. Lupus anticoagulant and late onset seizures. Acta Neurol.Scand. 1989; 79: 114-118.

Isla A, Alvarez F, Gutierrez M, Paredes E, Blazquez MG. Gangliogliomas: clinical study and evolution. J Neurosurg.Sci. 1991; 35: 193-197.

Ives JR, Warach S, Schmitt F, Edelman RR, Schomer DL. Monitoring the patient's EEG during echo planar MRI.

Electroencephalogr.Clin.Neurophysiol. 1993; 87: 417-420.

Jack CR, Jr. Epilepsy: surgery and imaging. Radiology 1993; 189: 635-646.

Jack CR, Jr., Bentley MD, Twomey CK, Zinsmeister AR. MR imaging-based volume measurements of the hippocampal formation and anterior temporal lobe: validation studies. Radiology 1990a; 176: 205-209.

Jack CR, Jr., Marsh WR, Hirschorn KA *et al.* EEG scalp electrode projection onto three-dimensional surface rendered images of the brain. Radiology 1990b; 176: 413-418.

Jack CR, Jr., Rydberg CH, Krecke KN *et al.* Mesial temporal sclerosis: diagnosis with fluid-attenuated inversion-recovery versus spin-echo MR imaging. Radiology 1996; 199: 367-373.

Jack CR, Jr., Sharbrough FW, Cascino GD, Hirschorn KA, O'Brien PC, Marsh WR. Magnetic resonance image-based hippocampal volumetry: correlation with outcome after temporal lobectomy. Ann Neurol 1992; 31: 138-146.

Jack CR, Jr., Sharbrough FW, Twomey CK *et al.* Temporal lobe seizures: lateralization with MR volume measurements of the hippocampal formation. Radiology 1990c; 175: 423-429.

Jack CR, Jr., Thompson RM, Butts RK *et al.* Sensory motor cortex: correlation of presurgical mapping with functional MR imaging and invasive cortical mapping. Radiology 1994; 190: 85-92.

Jackson G, Williams SR, Weller RO *et al.* Vigabatrin-induced lesions in the rat brain demonstrated by quantitative magnetic resonance imaging. Epilepsy Res 1994a; 18: 57-66.

Jackson GD, Berkovic SF, Duncan JS, Connelly A. Optimizing the diagnosis of hippocampal sclerosis using MR imaging. AJNR Am.J Neuroradiol. 1993a; 14: 753-762.

Jackson GD, Berkovic SF, Tress BM, Kalnins RM, Fabinyi GC, Bladin PF. Hippocampal sclerosis can be reliably detected by magnetic resonance imaging. Neurology 1990; 40: 1869-1875.

Jackson GD, Connelly A, Cross JH, Gordon I, Gadian DG. Functional magnetic resonance imaging of focal seizures. Neurology 1994b; 44: 850-856.

Jackson GD, Connelly A, Duncan JS, Grunewald RA, Gadian DG. Detection of hippocampal pathology in intractable partial epilepsy: increased sensitivity with quantitative magnetic resonance T2 relaxometry. Neurology 1993b; 43: 1793-1799.

Jacob S, Finsterbusch J, Weishaupt JH, Khorram-Sefat D, Frahm J, Ehrenreich H. Diffusion tensor imaging for long-term follow-up of corticospinal tract degeneration in amyotrophic lateral sclerosis. Neuroradiology 2003; ..

Jacobs KM, Gutnick MJ, Prince DA. Hyperexcitability in a model of cortical maldevelopment. Cereb Cortex 1996; 6: 514-523.

Jacobs KM, Kharazia VN, Prince DA. Mechanisms underlying epileptogenesis in cortical malformations. Epilepsy

Res. 1999; 36: 165-188.

Jacobs MA, Mitsias P, Soltanian-Zadeh H *et al.* Multiparametric MRI tissue characterization in clinical stroke with correlation to clinical outcome: part 2. Stroke 2001a; 32: 950-957.

Jacobs MA, Zhang ZG, Knight RA *et al.* A model for multiparametric mri tissue characterization in experimental cerebral ischemia with histological validation in rat: part 1. Stroke 2001b; 32: 943-949.

Jain KK. Systemic lupus erythematosus (SLE)-like syndromes associated with carbamazepine therapy. Drug Saf 1991; 6: 350-360.

Janszky J, Ebner A, Kruse B *et al.* Functional organization of the brain with malformations of cortical development. Ann Neurol 2003; 53: 759-767.

Jay V, Hwang P, Hoffman HJ, Becker LE, Zielenska M. Intractable seizure disorder associated with chronic herpes infection. HSV1 detection in tissue by the polymerase chain reaction. Childs Nerv.Syst. 1998; 14: 15-20.

Jefferys JG. Basic mechanisms of focal epilepsies. Exp.Physiol 1990; 75: 127-162.

Jenike MA, Breiter HC, Baer L *et al.* Cerebral structural abnormalities in obsessive-compulsive disorder. A quantitative morphometric magnetic resonance imaging study. Arch.Gen.Psychiatry 1996; 53: 625-632.

Jennet WB. Epilepsy after non-missile head injuries. London: Heinemann Medical Books, 1995.

Jensen KF, Killackey HP. Subcortical projections from ectopic neocortical neurons. Proc.Natl.Acad.Sci.U.S.A 1984; 81: 964-968.

Jiang Q, Zhang RL, Zhang ZG, Ewing JR, Divine GW, Chopp M. Diffusion-, T2-, and perfusion-weighted nuclear magnetic resonance imaging of middle cerebral artery embolic stroke and recombinant tissue plasminogen activator intervention in the rat. J.Cereb.Blood Flow Metab 1998; 18: 758-767.

Johnson G, Ormerod IE, Barnes D, Tofts PS, MacManus D. Accuracy and precision in the measurement of relaxation times from nuclear magnetic resonance images. Br.J Radiol. 1987; 60: 143-153.

Johnson MA, Pennock JM, Bydder GM *et al.* Clinical NMR imaging of the brain in children: normal and neurologic disease. AJR Am J Roentgenol. 1983; 141: 1005-1018.

Jones DK. Determining and visualizing uncertainty in estimates of fiber orientation from diffusion tensor MRI. Magn Reson Med 2003; 49: 7-12.

Jones DK, Griffin LD, Alexander DC *et al.* Spatial normalization and averaging of diffusion tensor MRI data sets. Neuroimage 2002a; 17: 592-617.

Jones DK, Simmons A, Williams SC, Horsfield MA. Non-invasive assessment of axonal fiber connectivity in the human brain via diffusion tensor MRI. Magn Reson.Med. 1999; 42: 37-41.

Jones DK, Williams SC, Gasston D, Horsfield MA, Simmons A, Howard R. Isotropic resolution diffusion tensor imaging with whole brain acquisition in a clinically acceptable time. Hum.Brain Mapp. 2002b; 15: 216-230.

Jr WS, Schmidt PJ, Hart BL, Brooks WM. Fluid Attenuated Inversion Recovery (FLAIR) Imaging in Neuropsychiatric Systemic Lupus Erythematosus. J Rheumatol. 2003; 30: 1983-1989.

Just M, Higer HP, Schwarz M *et al.* Tissue characterization of benign brain tumors: use of NMR-tissue parameters. Magn Reson Imaging 1988; 6: 463-472.

Jutila L, Ylinen A, Partanen K *et al.* MR volumetry of the entorhinal, perirhinal, and temporopolar cortices in drug-refractory temporal lobe epilepsy. AJNR Am.J Neuroradiol. 2001; 22: 1490-1501.

Juul-Jensen P, Foldspang A. Natural history of epileptic seizures. Epilepsia 1983; 24: 297-312.

Kajander S, Komu M, Niemi P, Kormano M. Determination of saturation transfer parameters of human tissues in vivo. Magn Reson Imaging 1996; 14: 413-417.

Kalachikov S, Evgrafov O, Ross B *et al.* Mutations in LGI1 cause autosomal-dominant partial epilepsy with auditory features. Nat.Genet. 2002; 30: 335-341.

Kalviainen R, Partanen K, Aikia M *et al.* MRI-based hippocampal volumetry and T2 relaxometry: correlation to verbal memory performance in newly diagnosed epilepsy patients with left-sided temporal lobe focus. Neurology 1997a; 48: 286-287.

Kalviainen R, Salmenpera T, Partanen K, Vainio P, Riekkinen P, Sr., Pitkanen A. MRI volumetry and T2 relaxometry of the amygdala in newly diagnosed and chronic temporal lobe epilepsy. Epilepsy Res 1997b; 28: 39-50.

Kanemoto K, Kawasaki J, Miyamoto T, Obayashi H, Nishimura M. Interleukin (IL)1beta, IL-1alpha, and IL-1 receptor antagonist gene polymorphisms in patients with temporal lobe epilepsy. Ann Neurol 2000; 47: 571-574.

Kang DW, Latour LL, Chalela JA, Dambrosia J, Warach S. Early ischemic lesion recurrence within a week after acute ischemic stroke. Ann Neurol 2003; 54: 66-74.

Kantarci K, Jack CR, Jr., Xu YC *et al.* Mild cognitive impairment and Alzheimer disease: regional diffusivity of water. Radiology 2001; 219: 101-107.

Kapur N, Ellison D, Smith MP, McLellan DL, Burrows EH. Focal retrograde amnesia following bilateral temporal lobe pathology. A neuropsychological and magnetic resonance study. Brain 1992; 115 Pt 1:73-85: 73-85.

Kasner SE, Galetta SL, McGowan JC, Grossman RI. Magnetization transfer imaging in progressive multifocal leukoencephalopathy. Neurology 1997; 48: 534-536.

Kasper BS, Stefan H, Buchfelder M, Paulus W. Temporal lobe microdysgenesis in epilepsy versus control brains. J Neuropathol Exp Neurol 1999; 22-28.

Kassubek J, Huppertz HJ, Spreer J, Schulze-Bonhage A. Detection and localization of focal cortical dysplasia by voxel-based 3-D MRI analysis. Epilepsia 2002; 43: 596-602.

Kathuria MK, Gupta RK, Roy R, Gaur V, Husain N, Pradhan S. Measurement of magnetization transfer in different stages of neurocysticercosis. J Magn Reson Imaging 1998; 8: 473-479.

Kato Y, Matsumura K, Kinosada Y, Narita Y, Kuzuhara S, Nakagawa T. Detection of pyramidal tract lesions in amyotrophic lateral sclerosis with magnetization-transfer measurements. AJNR Am J Neuroradiol 1997; 18: 1541-1547.

Katz A, Marks D, Spencer S. Focal brain MRI findings: transient signal changes secondary to seizures. Neurology 1992; 42 (suppl 3): 206.

Kaufmann WE, Galaburda AM. Cerebrocortical microdysgenesis in neurologically normal subjects: a histopathologic study. Neurology 1989; 39: 238-244.

Kayath MJ, Argentoni M, Vieira JG. Hypocalcemia and convulsive syndrome in alcoholics--an association frequently not diagnosed. Rev.Assoc.Med Bras. 1999; 45: 24-26.

Keller SS, Mackay CE, Barrick TR, Wieshmann UC, Howard MA, Roberts N. Voxel-based morphometric comparison of hippocampal and extrahippocampal abnormalities in patients with left and right hippocampal atrophy. Neuroimage 2002a; 16: 23-31.

Keller SS, Wieshmann UC, Mackay CE, Denby CE, Webb J, Roberts N. Voxel based morphometry of grey matter abnormalities in patients with medically intractable temporal lobe epilepsy: effects of side of seizure onset and epilepsy duration. J Neurol Neurosurg.Psychiatry 2002b; 73: 648-655.

Kennedy DH, Fallon RJ. Tuberculous meningitis. JAMA 1979; %19; 241: 264-268.

Kertesz A, Black SE, Nicholson L, Carr T. The sensitivity and specificity of MRI in stroke. Neurology 1987; 37: 1580-1585.

Kesselring J, Miller DH, Macmanus DG *et al.* Quantitative magnetic resonance imaging in multiple sclerosis: the effect of high dose intravenous methylprednisolone. J Neurol.Neurosurg.Psychiatry 1989; 52: 14-17.

Ketonen LM. Neuroimaging of the aging brain. Neurol.Clin. 1998; 16: 581-598.

Khurana DS, Strawsburg RH, Robertson RL, Madsen JR, Helmers SL. MRI signal changes in the white matter after corpus callosotomy. Pediatr.Neurol 1999; 21: 691-695.

Kidd D, Barker GJ, Tofts PS *et al.* The transverse magnetisation decay characteristics of longstanding lesions and normal-appearing white matter in multiple sclerosis. J Neurol. 1997; 244: 125-130.

Kidwell CS, Alger JR, Di Salle F *et al.* Diffusion MRI in patients with transient ischemic attacks. Stroke 1999; 30: 1174-1180.

Kidwell CS, Saver JL, Mattiello J *et al.* Thrombolytic reversal of acute human cerebral ischemic injury shown by diffusion/perfusion magnetic resonance imaging. Ann Neurol 2000; 47: 462-469.

Kim DI, Yoon PH, Ryu YH, Jeon P, Hwang GJ. MRI of germinomas arising from the basal ganglia and thalamus. Neuroradiology 1998; 40: 507-511.

Kim JH, Tien RD, Felsberg GJ, Osumi AK, Lee N. MR measurements of the hippocampus for lateralization of temporal lobe epilepsy: value of measurements of the body vs the whole structure. AJR Am.J Roentgenol. 1994; 163: 1453-1457.

Kimura H, Meaney DF, McGowan JC *et al.* Magnetization transfer imaging of diffuse axonal injury following experimental brain injury in the pig: characterization by magnetization transfer ratio with histopathologic correlation. J Comput.Assist.Tomogr. 1996; 20: 540-546.

King D, Spencer SS, McCarthy G, Luby M, Spencer DD. Bilateral hippocampal atrophy in medial temporal lobe epilepsy. Epilepsia 1995; 36: 905-910.

Kinkel PR, Kinkel WR, Jacobs L. Nuclear magnetic resonance imaging in patients with stroke. Semin.Neurol. 1986; 6: 43-52.

Kinney HC, Karthigasan J, Borenshteyn NI, Flax JD, Kirschner DA. Myelination in the developing human brain: biochemical correlates. Neurochem.Res. 1994; 19: 983-996.

Kinnunen E, Wikstrom J. Prevalence and prognosis of epilepsy in patients with multiple sclerosis. Epilepsia 1986; 27: 729-733.

Kirkpatrick PJ, Honavar M, Janota I, Polkey CE. Control of temporal lobe epilepsy following en bloc resection of low-grade tumors. J Neurosurg. 1993; 78: 19-25.

Kirsch SJ, Jacobs RW, Butcher LL, Beatty J. Prolongation of magnetic resonance T2 time in hippocampus of human patients marks the presence and severity of Alzheimer's disease. Neurosci.Lett. 1992; 134: 187-190.

Kitchen ND, Cook MJ, Shorvon SD, Fish DR, Thomas DG. Image guided audit of surgery for temporal lobe epilepsy. J Neurol.Neurosurg.Psychiatry 1994; 57: 1221-1227.

Kitchen ND, Thomas DG, Shorvon SD, Fish DR, Stevens JM. Volumetric analysis of epilepsy surgery resections using high resolution magnetic imaging: technical report. Br.J Neurosurg. 1993; 7: 651-656.

Kjaer L, Ring P, Thomsen C, Henriksen O. Texture analysis in quantitative MR imaging. Tissue characterisation of normal brain and intracranial tumours at 1.5 T. Acta Radiol. 1995; 36: 127-135.

Knauth M, Forsting M, Hartmann M, Heiland S, Balzer T, Sartor K. MR enhancement of brain lesions: increased contrast dose compared with magnetization transfer. AJNR Am J Neuroradiol 1996; 17: 1853-1859.

Knight RA, Dereski MO, Helpern JA, Ordidge RJ, Chopp M. Magnetic resonance imaging assessment of evolving

focal cerebral ischemia. Comparison with histopathology in rats (published erratum appears in Stroke 1994 Sep; 25 (9):1887). Stroke 1994; 25: 1252-1261.

Knowlton R. Image Averaging. Proceedings of the Third International Magnetic Resonance & Epilepsy Symposium 2000.

Knowlton RC, Laxer KD, Ende G *et al.* Presurgical multimodality neuroimaging in electroencephalographic lateralized temporal lobe epilepsy. Ann Neurol 1997; 42: 829-837.

Koenig SH. Cholesterol of myelin is the determinant of gray-white contrast in MRI of brain. Magn Reson Med 1991; 20: 285-291.

Koenig SH, Brown RD, III, Spiller M, Lundbom N. Relaxometry of brain: why white matter appears bright in MRI. Magn Reson Med 1990; 14: 482-495.

Koepp MJ, Hammers A, Labbe C, Woermann FG, Brooks DJ, Duncan JS. 11C-flumazenil PET in patients with refractory temporal lobe epilepsy and normal MRI. Neurology 2000; 54: 332-339.

Koepp MJ, Richardson MP, Brooks DJ, Cunningham VJ, Duncan JS. Central benzodiazepine/gamma-aminobutyric acid A receptors in idiopathic generalized epilepsy: an (11C)flumazenil positron emission tomography study. Epilepsia 1997; 38: 1089-1097.

Koepp MJ, Richardson MP, Brooks DJ *et al.* Cerebral benzodiazepine receptors in hippocampal sclerosis. An objective in vivo analysis. Brain 1996; 119: 1677-1687.

Konermann S, Marks S, Ludwig T *et al.* Presurgical evaluation of epilepsy by brain diffusion: MR-detected effects of flumazenil on the epileptogenic focus. Epilepsia 2003; 44: 399-407.

Koopmans RA, Li DK, Oger JJ, Mayo J, Paty DW. The lesion of multiple sclerosis: imaging of acute and chronic stages. Neurology 1989; 39: 959-963.

Korogi Y, Hirai T, Komohara Y *et al.* T2 shortening in the visual cortex: effect of aging and cerebrovascular disease. AJNR Am J Neuroradiol 1997; 18: 711-714.

Koshimoto Y, Yamada H, Kimura H *et al.* Quantitative analysis of cerebral microvascular hemodynamics with T2-weighted dynamic MR imaging. J Magn Reson Imaging 1999; 9: 462-467.

Kostovic I, Rakic P. Developmental history of the transient subplate zone in the visual and somatosensory cortex of the macaque monkey and human brain. J Comp Neurol 1990; 297: 441-470.

Kotila M, Waltimo O. Epilepsy after stroke. Epilepsia 1992; 33: 495-498.

Kovacs Z, Ikezaki K, Takahashi M, Kawai J, Fukui M. A chronological evaluation of experimental brain infarct by diffusion-mapping and magnetization transfer contrast imaging. Acta Neurochir.Suppl (Wien.) 1997; 70:43-5: 43-45.

Kraemer DL, Awad IA. Vascular malformations and epilepsy: clinical considerations and basic mechanisms. Epilepsia 1994; 35 Suppl 6: S30-S43.

Krakow K, Wieshmann UC, Woermann FG *et al.* Multimodal MR imaging: functional, diffusion tensor, and chemical shift imaging in a patient with localization-related epilepsy. Epilepsia 1999a; 40: 1459-1462.

Krakow K, Woermann FG, Symms MR *et al.* EEG-triggered functional MRI of interictal epileptiform activity in patients with partial seizures. Brain 1999b; 122: 1679-1688.

Krishnan B, Armstrong DL, Grossman RG, et al. Glial cell nuclear hypertrophy in complex partial seizures. J Neuropathol Exp Neurol 1994; 53: 502-507.

Kucharczyk W, Macdonald PM, Stanisz GJ, Henkelman RM. Relaxivity and magnetization transfer of white matter lipids at MR imaging: importance of cerebrosides and pH. Radiology 1994; 192: 521-529.

Kuks JB, Cook MJ, Fish DR, Stevens JM, Shorvon SD. Hippocampal sclerosis in epilepsy and childhood febrile seizures. Lancet 1993; 342: 1391-1394.

Kunimatsu A, Aoki S, Masutani Y, Abe O, Mori H, Ohtomo K. Three-dimensional white matter tractography by diffusion tensor imaging in ischaemic stroke involving the corticospinal tract. Neuroradiology 2003; 45: 532-535.

Kupersmith MJ, Vargas ME, Yashar A *et al.* Occipital arteriovenous malformations: visual disturbances and presentation. Neurology 1996; 46: 953-957.

Kurita H, Kawamoto S, Suzuki I *et al.* Control of epilepsy associated with cerebral arteriovenous malformations after radiosurgery. J Neurol Neurosurg.Psychiatry 1998; 65: 648-655.

Kurki T, Lundbom N, Kalimo H, Valtonen S. MR classification of brain gliomas: value of magnetization transfer and conventional imaging. Magn Reson Imaging 1995; 13: 501-511.

Kurki T, Lundbom N, Komu M, Kormano M. Tissue characterization of intracranial tumors by magnetization transfer and spin-lattice relaxation parameters in vivo. J Magn Reson Imaging 1996; 6: 573-579.

Kurki TJ, Niemi PT, Lundbom N. Gadolinium-enhanced magnetization transfer contrast imaging of intracranial tumors. J Magn Reson Imaging 1992; 2: 401-406.

Kuzniecky R, Andermann F. The congenital bilateral perisylvian syndrome: imaging findings in a multicenter study. CBPS Study Group. AJNR Am J Neuroradiol 1994; 15: 139-144.

Kuzniecky R, Andermann F, Guerrini R. The epileptic spectrum in the congenital bilateral perisylvian syndrome. CBPS Multicenter Collaborative Study. Neurology 1994; 44: 379-385.

Kuzniecky R, Burgard S, Faught E, Morawetz R, Bartolucci A. Predictive value of magnetic resonance imaging in temporal lobe epilepsy surgery. Arch.Neurol. 1993a; 50: 65-69.

Kuzniecky R, Cascino GD, Palmini A, et al. Structural neuroimaging. In: Engel J, Jr., editor. Surgical Treatment of the Epilepsies. New York: Raven Press, 1993b: 197.

Kuzniecky R, de lS, V, Ethier R *et al.* Magnetic resonance imaging in temporal lobe epilepsy: pathological correlations. Ann.Neurol. 1987; 22: 341-347.

Kuzniecky R, Elgavish GA, Hetherington H, Evanochko WT, Pohost GM. In vivo ^{31}P nuclear magnetic resonance spectroscopy of human temporal lobe epilepsy. Neurology 1992; 1586-1590.

Kuzniecky R, Garcia JH, Faught E, Morawetz RB. Cortical dysplasia in temporal lobe epilepsy: magnetic resonance imaging correlations. Ann.Neurol. 1991; 29: 293-298.

Kuzniecky R, Hetherington H, Ho S *et al.* Topiramate increases cerebral GABA in healthy humans. Neurology 1998; 627-629.

Kuzniecky R, Jackson GD. Developmental Disorders. In: Engel.Jr. J, Pedley TA, editors. Epilepsy: A Comprehensive Textbook. Philadelphia: Lippincott-Raven, 1997: 2517-32.

Kuzniecky RI. Magnetic resonance imaging in developmental disorders of the cerebral cortex. Epilepsia 1994; 35 Suppl 6:S44-56: S44-S56.

Kuzniecky RI, Barkovich AJ. Pathogenesis and pathology of focal malformations of cortical development and epilepsy. J Clin.Neurophysiol. 1996; 13: 468-480.

Kuzniecky RI, Burgard S, Bilir E *et al.* Qualitative MRI segmentation in mesial temporal sclerosis: clinical correlations. Epilepsia 1996; 37: 433-439.

Kwan P, Brodie MJ. Early identification of refractory epilepsy. N.Engl.J.Med. 2000; 342: 314-319.

Laakso MP, Partanen K, Soininen H *et al.* MR T2 relaxometry in Alzheimer's disease and age-associated memory impairment. Neurobiol.Aging 1996; 17: 535-540.

Lagae LG, Silberstein J, Gillis PL, Casaer PJ. Successful use of intravenous immunoglobulins in Landau-Kleffner syndrome. Pediatr.Neurol. 1998; 18: 165-168.

Lancman ME, Golimstok A, Norscini J, Granillo R. Risk factors for developing seizures after a stroke. Epilepsia 1993; 34: 141-143.

Lang B, Dale RC, Vincent A. New autoantibody mediated disorders of the central nervous system. Curr.Opin.Neurol. 2003; 16: 351-357.

Lange N. Some computational and statistical tools for paired comparisons of digital images. Stat.Methods Med Res 1994; 3: 23-40.

Lansberg MG, O'Brien MW, Norbash AM, Moseley ME, Morrell M, Albers GW. MRI abnormalities associated

with partial status epilepticus. Neurology 1999; 52: 1021-1027.

Lansberg MG, Thijs VN, O'Brien MW *et al.* Evolution of apparent diffusion coefficient, diffusion-weighted, and T2-weighted signal intensity of acute stroke. AJNR Am J Neuroradiol 2001; 22: 637-644.

Larsson EM, Englund E, Gyorffy-Wagner Z, Brun A, Cronqvist S, Persson B. Regional differences in the proton magnetic resonance relaxation times T1 and T2 within the normal human brain. Acta Radiol.Diagn. (Stockh) 1986; 27: 231-234.

Larsson HB, Christiansen P, Zeeberg I, Henriksen O. In vivo evaluation of the reproducibility of T1 and T2 measured in the brain of patients with multiple sclerosis. Magn Reson Imaging 1992; 10: 579-584.

Larsson HB, Frederiksen J, Kjaer L, Henriksen O, Olesen J. In vivo determination of T1 and T2 in the brain of patients with severe but stable multiple sclerosis. Magn Reson Med 1988; 7: 43-55.

Larsson HB, Frederiksen J, Petersen J *et al.* Assessment of demyelination, edema, and gliosis by in vivo determination of T1 and T2 in the brain of patients with acute attack of multiple sclerosis. Magn Reson Med 1989; 11: 337-348.

Larsson HB, Stubgaard M, Thomsen C. In vivo measurement of diffusion in the CNS using a flow compensated spin echo sequence. Book of abstracts. Society of Magnetic Resonance in Medicine, ninth annual meeting. New York: 1990: 389.

Latack JT, Abou-Khalil BW, Siegel GJ, Sackellares JC, Gabrielsen TO, Aisen AM. Patients with partial seizures: evaluation by MR, CT, and PET imaging. Radiology 1986; 159: 159-163.

Latour LL, Svoboda K, Mitra PP, Sotak CH. Time-dependent diffusion of water in a biological model system. Proc.Natl.Acad.Sci.U.S.A 1994; 91: 1229-1233.

Laule MC, Vavasour P, I, Whittall PhD KP *et al.* Evolution of focal and diffuse magnetisation transfer abnormalities in multiple sclerosis. J Neurol 2003; 250: 924-931.

Lawrie SM, Abukmeil SS. Brain abnormality in schizophrenia. A systematic and quantitative review of volumetric magnetic resonance imaging studies. Br.J Psychiatry 1998; 172:110-20: 110-120.

Lazar M, Weinstein DM, Tsuruda JS *et al.* White matter tractography using diffusion tensor deflection. Hum.Brain Mapp. 2003; 18: 306-321.

Le Bihan D, Breton E, Lallemand D, Aubin M, Vignaud J, Laval-Jenatet M. Separation of diffusion and perfusion in intravoxel incoherent motion MR imaging. Radiology 1999; 497-505.

Le Bihan D, Mangin JF, Poupon C *et al.* Diffusion tensor imaging: Concepts and applications. J Magn Reson Imaging 2001; 13: 534-546.

Le TH, Hu X. Retrospective estimation and correction of physiological artifacts in fMRI by direct extraction of

physiological activity from MR data. Magn Reson Med 1996; 35: 290-298.

LeBihan D, Basser PJ. Molecular diffusion and nuclear magnetic resonance. In: LeBihan D, editor. Diffusion and perfusion magnetic resonance imaging. New York: Raven Press, 1995: 5-17.

LeBihan D, Turner R. The capillary network: a link between IVIM and classical perfusion. Magn Reson Med 1992; 171-178.

LeBlanc FE, Rasmussen T. Cerebral seizures and brain tumours. In: Vinken PJ, Bruyn GW, editors. Handbook of Clinical Neurology. Vol. 15. New York: Elsevier, 1997: 295-301.

Lechtenberg R, Worner TM. Total ethanol consumption as a seizure risk factor in alcoholics. Acta Neurol Scand. 1992; 85: 90-94.

Lee N, Tien RD, Lewis DV *et al.* Fast spin-echo, magnetic resonance imaging-measured hippocampal volume: correlation with neuronal density in anterior temporal lobectomy patients. Epilepsia 1995; 36: 899-904.

Leenders KL, Perani D, Lammertsma AA *et al.* Cerebral blood flow, blood volume and oxygen utilization. Normal values and effect of age. Brain 1990; 113 (Pt 1): 27-47.

Lehericy S, Semah F, Hasboun D *et al.* Temporal lobe epilepsy with varying severity: MRI study of 222 patients. Neuroradiology 1997; 39: 788-796.

Lei H, Dooley P, Peeling J, Corbett D. Temporal profile of magnetic resonance imaging changes following forebrain ischemia in the gerbil. Neurosci.Lett. 1998; 257: 105-108.

Leifer D, Buonanno FS, Richardson EP, Jr. Clinicopathologic correlations of cranial magnetic resonance imaging of periventricular white matter. Neurology 1990; 40: 911-918.

Lemaire L, Franconi F, Saint-Andre JP, Roullin VG, Jallet P, Le Jeune JJ. High-field quantitative transverse relaxation time, magnetization transfer and apparent water diffusion in experimental rat brain tumour. NMR Biomed. 2000; 13: 116-123.

Lemieux L, Allen PJ, Franconi F, Symms MR, Fish DR. Recording of EEG during fMRI experiments: patient safety. Magn Reson Med 1997; 38: 943-952.

Lemieux L, Hagemann G, Krakow K, Woermann FG. Fast, accurate, and reproducible automatic segmentation of the brain in T1-weighted volume MRI data. Magn Reson Med 1999; 42: 127-135.

Lencz T, McCarthy G, Bronen RA *et al.* Quantitative magnetic resonance imaging in temporal lobe epilepsy: relationship to neuropathology and neuropsychological function. Ann.Neurol. 1992; 31: 629-637.

Leone M, Bottacchi E, Beghi E *et al.* Alcohol use is a risk factor for a first generalized tonic-clonic seizure. The ALC.E. (Alcohol and Epilepsy) Study Group. Neurology 1997; 48: 614-620.

Lerski RA, Straughan K, Schad LR, Boyce D, Bluml S, Zuna I. MR image texture analysis--an approach to tissue characterization. Magn Reson Imaging 1993; 11: 873-887.

Lesser RP, Modic MT, Weinstein MA *et al.* Magnetic resonance imaging (1.5 tesla) in patients with intractable focal seizures. Arch.Neurol. 1986; 43: 367-371.

Levy CE, Nichols DS, Schmalbrock PM, Keller P, Chakeres DW. Functional MRI evidence of cortical reorganization in upper-limb stroke hemiplegia treated with constraint-induced movement therapy. (In Process Citation). Am.J Phys.Med Rehabil. 2001; 80: 4-12.

Lewis DV. Febrile convulsions and mesial temporal sclerosis. Curr.Opin.Neurol. 1999; 12: 197-201.

Lexa FJ, Grossman RI, Rosenquist AC. Detection of early axonal degeneration in the mammalian central nervous system by magnetization transfer techniques in magnetic resonance imaging. Ann N.Y.Acad.Sci. 1993; 679:336-40: 336-340.

Lexa FJ, Grossman RI, Rosenquist AC. Dyke Award paper. MR of wallerian degeneration in the feline visual system: characterization by magnetization transfer rate with histopathologic correlation. AJNR Am J Neuroradiol 1994; 15: 201-212.

Leys D, Soetaert G, Petit H, Fauquette A, Pruvo JP, Steinling M. Periventricular and white matter magnetic resonance imaging hyperintensities do not differ between Alzheimer's disease and normal aging. Arch Neurol 1990; 47: 524-527.

Li LM, Fish DR, Sisodiya SM, Shorvon SD, Alsanjari N, Stevens JM. High resolution magnetic resonance imaging in adults with partial or secondary generalised epilepsy attending a tertiary referral unit. J Neurol.Neurosurg.Psychiatry 1995; 59: 384-387.

Li LM, Narayanan S, Pike GB, Andermann F, Dubeau F, Arnold DL. Magnetization transfer ratio is unable to lateralize epileptic foci in patients with temporal lobe epilepsy. AJNR Am J Neuroradiol 2000; 21: 1853-1856.

Liou HH, Wang CR, Chen CJ *et al.* Elevated levels of anticardiolipin antibodies and epilepsy in lupus patients. Lupus 1996; 5: 307-312.

Listerud J, Einstein S, Outwater E, Kressel HY. First principles of fast spin echo. Magn Reson Q. 1992; 8: 199-244.

Listerud J, Mitchell J, Bagley L, Grossman R. OIL FLAIR: optimized interleaved fluid-attenuated inversion recovery in 2D fast spin echo. Magn Reson Med 1996; 36: 320-325.

Liu RS, Lemieux L, Bell GS *et al.* A longitudinal quantitative MRI study of community-based patients with chronic epilepsy and newly diagnosed seizures: methodology and preliminary findings. Neuroimage 2001; 14: 231-243.

Liu RS, Lemieux L, Bell GS *et al.* The structural consequences of newly diagnosed seizures. Ann Neurol 2002a; 52: 573-580.

Liu RS, Lemieux L, Sander JW, Sisodiya SM, Duncan JS. Seizure-associated hippocampal volume loss: a longitudinal magnetic resonance study of temporal lobe epilepsy. Ann Neurol 2002b; 52: 861.

Livingston JH, Aicardi J. Unusual MRI appearance of diffuse subcortical heterotopia or "double cortex" in two children. J Neurol Neurosurg Psychiatry 1990; 53: 617-620.

Loevner LA, Grossman RI, Cohen JA, Lexa FJ, Kessler D, Kolson DL. Microscopic disease in normal-appearing white matter on conventional MR images in patients with multiple sclerosis: assessment with magnetization-transfer measurements. Radiology 1995; 196: 511-515.

Lor E, Liu YQ. Neurologic sequelae associated with foscarnet therapy. Ann.Pharmacother. 1994; 28: 1035-1037.

Lorenzo NY, Parisi JE, Cascino GD, Jack CR, Jr., Marsh WR, Hirschorn KA. Intractable frontal lobe epilepsy: pathological and MRI features. Epilepsy Res. 1995; 20: 171-178.

Loubinoux I, Volk A, Borredon J *et al.* Spreading of vasogenic edema and cytotoxic edema assessed by quantitative diffusion and T2 magnetic resonance imaging. Stroke 1997a; 28: 419-426.

Loubinoux I, Volk A, Borredon J *et al.* The effects of a butanediol treatment on acute focal cerebral ischemia assessed by quantitative diffusion and T2 MR imaging. Magn Reson Imaging 1997b; 15: 1045-1055.

Lu D, Margouleff C, Rubin E *et al.* Temporal lobe epilepsy: correlation of proton magnetic resonance spectroscopy and 18F-fluorodeoxyglucose positron emission tomography. Magn Reson Med 1997; 37: 18-23.

Lu S, Ahn D, Johnson G, Cha S. Peritumoral diffusion tensor imaging of high-grade gliomas and metastatic brain tumors. AJNR Am.J Neuroradiol. 2003; 24: 937-941.

Luders H, Acharya J, Baumgartner C *et al.* Semiological seizure classification. Epilepsia 1998; 39: 1006-1013.

Luders H, Burgess R, Noachtar S. Expanding the International Classification of Seizures to provide localization information. Neurology 1993; 43: 1650-1655.

Luders HO, Engel J, Jr., Munari C. General principles. In: Engel, editor. Surgical treatment of the epilepsies. Philadelphia: Lippincott-Raven, 1996: 137-53.

Lueck CJ, Zeki S, Friston KJ *et al.* The colour centre in the cerebral cortex of man. Nature 1989; 340: 386-389.

Lutsep HL, Albers GW, deCrespigny A, Kamat GN, Marks MP, Moseley ME. Clinical utility of diffusion-weighted magnetic resonance imaging in the assessment of ischemic stroke. Ann.Neurol. 1997; 41: 574-580.

Lux HD, Heinemann U, Dietzel I. Ionic Changes and Alterations in the Size of the Extracellular Space During Epileptic Activity. In: Delgado-Escueta AV, Ward Jr AA, Woodbury DM, Porter RJ, editors. Advances in

Neurology. New York Raven Press, 1986: 619-39.

Lynch LA, Lythgoe D, Haga EK *et al.* Temporal evolution of CNS damage in a rat model of chronic epilepsy. Proceedings of the International Society for Magnetic Resonance in Medicine, Fourth scientific meeting, 1996; 521.

Lyon G, Gastaut H. Considerations on the significance attributed to unusual cerebral histological findings recently described in eight patients with primary generalized epilepsy. Epilepsia 1985; 26: 365-367.

Macdonell RA, Jackson GD, Curatolo JM *et al.* Motor cortex localization using functional MRI and transcranial magnetic stimulation. Neurology 1999; 53: 1462-1467.

MacKay A, Whittall K, Adler J, Li D, Paty D, Graeb D. In vivo visualization of myelin water in brain by magnetic resonance. Magn Reson Med 1994; 31: 673-677.

Mackay CE, Webb JA, Eldridge PR, Chadwick DW, Whitehouse GH, Roberts N. Quantitative magnetic resonance imaging in consecutive patients evaluated for surgical treatment of temporal lobe epilepsy. Magn Reson Imaging 2000; 18: 1187-1199.

Madelbrot BB. The Fractal Geometry of Nature. New York: Freeman, 1983.

Makris N, Worth AJ, Sorensen AG *et al.* Morphometry of in vivo human white matter association pathways with diffusion-weighted magnetic resonance imaging. Ann Neurol 1997; 42: 951-962.

Maldonado HM, Delgado-Escueta AV, Walsh GO, Swartz BE, Rand RW. Complex partial seizures of hippocampal and amygdalar origin. Epilepsia 1988; 29: 420-433.

Manford M, Fish DR, Shorvon SD. An analysis of clinical seizure patterns and their localizing value in frontal and temporal lobe epilepsies. Brain 1996; 119 (Pt 1): 17-40.

Manford M, Hart YM, Sander JW, Shorvon SD. The National General Practice Study of Epilepsy. The syndromic classification of the International League Against Epilepsy applied to epilepsy in a general population. Arch.Neurol. 1992; 49: 801-808.

Mansfield P, Morris PG. NMR imaging in biomedicine. Advances in Magnetic Resonance Imaging. 1982a.

Mansfield P, Morris PG. Water in biological systems. In: Waugh JS, editor. NMR Imaging in Biomedicine. London, England: Academic Press, 1982b: 15-31.

Mantyla R, Aronen HJ, Salonen O *et al.* The prevalence and distribution of white-matter changes on different MRI pulse sequences in a post-stroke cohort. Neuroradiology 1999; 41: 657-665.

Manz HJ, Phillips TM, Rowden G, McCullough DC. Unilateral megalencephaly, cerebral cortical dysplasia, neuronal hypertrophy, and heterotopia: cytomorphometric, fluorometric cytochemical, and biochemical analyses. Acta Neuropathol. (Berl) 1979; 45: 97-103.

March PA. Seizures: classification, etiologies, and pathophysiology. Clin.Tech.Small Anim Pract. 1998; 13: 119-131.

Marchal G, Andermann F, Tampieri D *et al.* Generalized cortical dysplasia manifested by diffusely thick cerebral cortex. Arch.Neurol. 1989; 46: 430-434.

Marco P, DeFelipe J. Altered synaptic circuitry in the human temporal neocortex removed from epileptic patients. Exp.Brain Res. 1997; 114: 1-10.

Margerison JH, Corsellis JA. Epilepsy and the temporal lobes. A clinical, electroencephalographic and neuropathological study of the brain in epilepsy, with particular reference to the temporal lobes. Brain 1966; 89: 499-530.

Marin-Padilla M. Ontogenesis of the pyramidal cell of the mammalian neocortex and developmental cytoarchitectonics: a unifying theory. J Comp Neurol. 1992; 321: 223-240.

Marks MP, de Crespigny A, Lentz D, Enzmann DR, Albers GW, Moseley ME. Acute and chronic stroke: navigated spin-echo diffusion-weighted MR imaging (published erratum appears in Radiology 1996 Jul; 200 (1):289). Radiology 1996; 199: 403-408.

Marshall VG, Bradley WG, Jr., Marshall CE, Bhoopat T, Rhodes RH. Deep white matter infarction: correlation of MR imaging and histopathologic findings. Radiology 1988; 167: 517-522.

Masumura M. Proton relaxation time of immature brain. II. In vivo measurement of proton relaxation time (T1 and T2) in pediatric brain by MRI. Childs Nerv.Syst. 1987; 3: 6-11.

Mathern GW, Babb TL, Leite JP, Pretorius K, Yeoman KM, Kuhlman PA. The pathogenic and progressive features of chronic human hippocampal epilepsy. Epilepsy Res 1996; 26: 151-161.

Mathews VP, Elster AD, King JC, Ulmer JL, Hamilton CA, Strottmann JM. Combined effects of magnetization transfer and gadolinium in cranial MR imaging and MR angiography. AJR Am J Roentgenol. 1995; 164: 169-172.

Mathur-De Vre R. Biomedical implications of the relaxation behaviour of water related to NMR imaging. Br.J Radiol. 1984; 57: 955-976.

Matoba M, Tonami H, Miyaji H, Yokota H, Yamamoto I. Creutzfeldt-Jakob disease: serial changes on diffusion-weighted MRI. J Comput.Assist.Tomogr. 2001; 25: 274-277.

Matsumoto K, Tamiya T, Ono Y, Furuta T, Asari S, Ohmoto T. Cerebral gangliogliomas: clinical characteristics, CT and MRI. Acta Neurochir. (Wien.) 1999; 141: 135-141.

Matsuzawa H, Kwee IL, Nakada T. Magnetic resonance axonography of the rat spinal cord: postmortem effects. J.Neurosurg. 1995; 83: 1023-1028.

Matthews PM, Andermann F, Arnold DL. A proton magnetic resonance spectroscopy study of focal epilepsy in

humans. Neurology 1990; 40: 985-989.

Mattson RH. Alcohol-related seizures. In: Porter RJ, Mattson RH, Cramer JA, Diamond I, editors. Alcohol and Seizures: Basic mechanisms and Clinical Concepts. Philadelphia: FA Davis, 1990: 143-7.

May A, Ashburner J, Buchel C *et al.* Correlation between structural and functional changes in brain in an idiopathic headache syndrome. Nat.Med 1999; 5: 836-838.

McCarthy G, Blamire AM, Rothman DL, Gruetter R, Shulman RG. Echo-planar magnetic resonance imaging studies of frontal cortex activation during word generation in humans. Proc.Natl.Acad.Sci.U.S.A 1993; 90: 4952-4956.

McConnell HM. Reaction rates by nuclear magnetic resonance. J Chem Phys 1958; 28: 430-431.

McDonald WM, Krishnan KR, Doraiswamy PM *et al.* Magnetic resonance findings in patients with early-onset Alzheimer's disease. Biol.Psychiatry 1991; 29: 799-810.

McGowan JC. The physical basis of magnetization transfer imaging. Neurology 1999; 53: S3-S7.

McGowan JC, McCormack TM, Grossman RI *et al.* Diffuse axonal pathology detected with magnetization transfer imaging following brain injury in the pig. Magn Reson Med 1999; 41: 727-733.

McGowan JC, III, Schnall MD, Leigh JS. Magnetization transfer imaging with pulsed off-resonance saturation: variation in contrast with saturation duty cycle. J Magn Reson Imaging 1994; 4: 79-82.

McGowan JC, Yang JH, Plotkin RC *et al.* Magnetization transfer imaging in the detection of injury associated with mild head trauma. AJNR Am J Neuroradiol 2000; 21: 875-880.

McKusick VA. Mendelian Inheritance in Man. Baltimore: Johns Hopkins University Press, 1994.

McLachlan RS, Nicholson RL, Black S, Carr T, Blume WT. Nuclear magnetic resonance imaging, a new approach to the investigation of refractory temporal lobe epilepsy. Epilepsia 1985; 26: 555-562.

McNamara JO. Cellular and molecular basis of epilepsy. J Neurosci. 1994; 14: 3413-3425.

Medina MT, Rosas E, Rubio-Donnadieu F, Sotelo J. Neurocysticercosis as the main cause of late-onset epilepsy in Mexico. Arch.Intern.Med 1990; 150: 325-327.

Meencke H-J. The density of dystopic neurons in the white matter of the gyrus frontalis inferior in epilepsies. J Neurol 1983; 171-181.

Meencke HJ, Janz D. Neuropathological findings in primary generalized epilepsy: a study of eight cases. Epilepsia 1984; 25: 8-21.

Mehta RC, Pike GB, Enzmann DR. Magnetization transfer MR of the normal adult brain. AJNR Am J Neuroradiol

1995a; 16: 2085-2091.

Mehta RC, Pike GB, Enzmann DR. Measure of magnetization transfer in multiple sclerosis demyelinating plaques, white matter ischemic lesions, and edema. AJNR Am J Neuroradiol 1996; 17: 1051-1055.

Mehta RC, Pike GB, Haros SP, Enzmann DR. Central nervous system tumor, infection, and infarction: detection with gadolinium-enhanced magnetization transfer MR imaging. Radiology 1995b; 195: 41-46.

Meiboom S, Gill D. Modified Spin-Echo Method for Measuring Nuclear Relaxation Times. The Review of Scientific Instruments 1958; 29: 688-691.

Meiners LC, Scheffers JM, de Kort GA *et al.* Curved reconstructions versus three-dimensional surface rendering in the demonstration of cortical lesions in patients with extratemporal epilepsy. Invest Radiol. 2001; 36: 225-233.

Meiners LC, van Gils A, Jansen GH *et al.* Temporal lobe epilepsy: the various MR appearances of histologically proven mesial temporal sclerosis. AJNR Am.J Neuroradiol. 1994; 15: 1547-1555.

Meiners LC, van Gils AD, De Kort G, Van Der GY, Jansen GH, Van Veelen CW. Fast fluid-attenuated inversion recovery (FLAIR) compared with T2-weighted spin-echo in the magnetic resonance diagnosis of mesial temporal sclerosis. Invest Radiol. 1999a; 34: 134-142.

Meiners LC, Witkamp TD, de Kort GA *et al.* Relevance of temporal lobe white matter changes in hippocampal sclerosis. Magnetic resonance imaging and histology. Invest Radiol. 1999b; 34: 38-45.

Meldrum BS, Bruton CJ. Epilepsy. In: Hume Adams J, Duchen LE, editors. Greenfields Neuropathology. London: Edward Arnold, 1992: 1246-83.

Meldrum BS, Nilsson B. Cerebral blood flow and metabolic rate early and late in prolonged epileptic seizures induced in rats by bicuculline. Brain 1976; 99: 523-542.

Melki PS, Mulkern RV, Panych LP, Jolesz FA. Comparing the FAISE method with conventional dual-echo sequences. J Magn Reson Imaging 1991; 1: 319-326.

Mendez OE, Shang J, Jungreis CA, Kaufer DI. Diffusion-weighted MRI in Creutzfeldt-Jakob disease: a better diagnostic marker than CSF protein 14-3-3? J Neuroimaging 2003; 13: 147-151.

Merboldt KD, Hanicke W, Frahm J. Diffusion imaging using stimulated echoes. Magn Reson Med 1991; 19: 233-239.

Merlis JK. Proposal for an international classification of the epilepsies. Epilepsia 1970; 11: 114-119.

Messager T, Franconi F, Lemaire L *et al.* MRI study of transient cerebral ischemia in the gerbil: interest of T2 mapping. Invest Radiol. 2000; 35: 180-185.

Mesulam M-M. Large-scale neurocognitive networks and distributed processing for attention, language, and

memory. Ann Neurol 1990; 597-613.

Meyer G, Goffinet AM. Prenatal development of reelin-immunoreactive neurons in the human neocortex. J Comp Neurol. 1998; 397: 29-40.

Meyer G, Goffinet AM, Fairen A. What is a Cajal-Retzius cell? A reassessment of a classical cell type based on recent observations in the developing neocortex. Cereb Cortex 1999; 9: 765-775.

Mikati MA, Saab R. Successful use of intravenous immunoglobulin as initial monotherapy in Landau-Kleffner syndrome. Epilepsia 2000; 41: 880-886.

Miller DH, Johnson G, Tofts PS, MacManus D, McDonald WI. Precise relaxation time measurements of normal-appearing white matter in inflammatory central nervous system disease. Magn Reson Med 1989; 11: 331-336.

Miller LA, McLachlan RS, Bouwer MS, Hudson LP, Munoz DG. Amygdalar sclerosis: preoperative indicators and outcome after temporal lobectomy. J Neurol Neurosurg.Psychiatry 1994; 57: 1099-1105.

Minami T, Nobuhara K, Okugawa G *et al.* Diffusion tensor magnetic resonance imaging of disruption of regional white matter in schizophrenia. Neuropsychobiology 2003; 47: 141-145.

Minematsu K, Li L, Fisher M, Sotak CH, Davis MA, Fiandaca MS. Diffusion-weighted magnetic resonance imaging: rapid and quantitative detection of focal brain ischemia. Neurology 1992; 42: 235-240.

Mineura K, Sasajima H, Kikuchi K *et al.* White matter hyperintensity in neurologically asymptomatic subjects. Acta Neurol.Scand 1995; 92: 151-156.

Mirsen TR, Lee DH, Wong CJ *et al.* Clinical correlates of white-matter changes on magnetic resonance imaging scans of the brain. Arch.Neurol. 1991; 48: 1015-1021.

Mischel PS, Nguyen LP, Vinters HV. Cerebral cortical dysplasia associated with pediatric epilepsy. Review of neuropathologic features and proposal for a grading system. J Neuropathol.Exp.Neurol 1995; 54: 137-153.

Mitchell LA, Jackson GD, Kalnins RM *et al.* Anterior temporal abnormality in temporal lobe epilepsy: a quantitative MRI and histopathologic study. Neurology 1999; 52: 327-336.

Mitchell TN, Free S, Thom M, Shorvon SD, Sisodiya SM. Quantitative MRI abnormalities with histopathological abnormalities of cerebral structure in a case of tuberous sclerosis. Proceedings of the Third International Magnetic Resonance & Epilepsy Symposium 2000.

Mitchison G. Neuronal branching patterns and the economy of cortical wiring. Proc.R.Soc.Lond B Biol.Sci. 1991; 245: 151-158.

Miyasaka Y, Kurata A, Tanaka R *et al.* Mass effect caused by clinically unruptured cerebral arteriovenous malformations. Neurosurgery 1997; 41: 1060-1063.

Moak DH, Anton RF. Alcohol-related seizures and the kindling effect of repeated detoxifications: the influence of cocaine. Alcohol Alcohol 1996; 31: 135-143.

Molko N, Pappata S, Mangin JF *et al.* Monitoring disease progression in CADASIL with diffusion magnetic resonance imaging: a study with whole brain histogram analysis. Stroke 2002; 33: 2902-2908.

Molyneux PD, Barker GJ, Barkhof F *et al.* Clinical-MRI correlations in a European trial of interferon beta-1b in secondary progressive MS. Neurology 2001; 57: 2191-2197.

Moore GR, Leung E, MacKay AL *et al.* A pathology-MRI study of the short-T2 component in formalin-fixed multiple sclerosis brain. Neurology 2000; 55: 1506-1510.

Moore KR, Funke ME, Constantino T, Katzman GL, Lewine JD. Magnetoencephalographically directed review of high-spatial-resolution surface-coil MR images improves lesion detection in patients with extratemporal epilepsy. Radiology 2002; 225: 880-887.

Moreau T, Sochurkova D, Lemesle M *et al.* Epilepsy in patients with multiple sclerosis: radiological-clinical correlations. Epilepsia 1998; 39: 893-896.

Morell P, Quarles RH, Norton WT. Formation, structure, and biochemistry of myelin. In: Siegel G, Agranoff R, Albers RW, Molinoff P, editors. Basic neurochemistry. New York: Raven Press, 1989: 121.

Mori S, Crain BJ, Chacko VP, van Zijl PC. Three-dimensional tracking of axonal projections in the brain by magnetic resonance imaging. Ann Neurol 1999; 45: 265-269.

Morioka T, Mizushima A, Yamamoto T *et al.* Functional mapping of the sensorimotor cortex: combined use of magnetoencephalography, functional MRI, and motor evoked potentials. Neuroradiology 1995; 37: 526-530.

Morioka T, Nishio S, Mihara F *et al.* (Efficacy of the fluid attenuated inversion recovery (FLAIR) sequence of MRI as a preoperative diagnosis of hippocampal sclerosis). No Shinkei Geka 1998; 26: 143-150.

Morris GL, III, Mueller WM, Yetkin FZ *et al.* Functional magnetic resonance imaging in partial epilepsy. Epilepsia 1994; 35: 1194-1198.

Morris HH, Matkovic Z, Estes ML *et al.* Ganglioglioma and intractable epilepsy: clinical and neurophysiologic features and predictors of outcome after surgery. Epilepsia 1998; 39: 307-313.

Morris JS, Frith CD, Perrett DI *et al.* A differential neural response in the human amygdala to fearful and happy facial expressions. Nature 1996; 383: 812-815.

Moseley ME, Cohen Y, Kucharczyk J *et al.* Diffusion-weighted MR imaging of anisotropic water diffusion in cat central nervous system. Radiology 1990a; 176: 439-445.

Moseley ME, Cohen Y, Mintorovitch J *et al.* Early detection of regional cerebral ischemia in cats: comparison of diffusion- and T2-weighted MRI and spectroscopy. Magn Reson Med 1990b; 14: 330-346.

Moseley ME, Kucharczyk J, Asgari HS, Norman D. Anisotropy in diffusion-weighted MRI. Magn Reson Med 1991; 19: 321-326.

Moseley ME, Kucharczyk J, Mintorovitch J *et al.* Diffusion-weighted MR imaging of acute stroke: correlation with T2-weighted and magnetic susceptibility-enhanced MR imaging in cats. AJNR Am.J.Neuroradiol. 1990c; 11: 423-429.

Mosewich RK, So EL. A clinical approach to the classification of seizures and epileptic syndromes. Mayo Clin.Proc. 1996; 71: 405-414.

Mouritzen-Dam A. Epilepsy and neuron loss in the hippocampus. Epilepsia 1980; 21: 617-629.

Mueller SG, Laxer KD, Suhy J, Lopez RC, Flenniken DL, Weiner MW. Spectroscopic metabolic abnormalities in mTLE with and without MRI evidence for mesial temporal sclerosis using hippocampal short-TE MRSI. Epilepsia 2003; 44: 977-980.

Mueller SG, Suhy J, Laxer KD *et al.* Reduced extrahippocampal NAA in mesial temporal lobe epilepsy. Epilepsia 2002; 43: 1210-1216.

Mulkern RV, Wong ST, Jakab P, Bleier AR, Sandor T, Jolesz FA. CPMG imaging sequences for high field in vivo transverse relaxation studies. Magn Reson Med 1990; 16: 67-79.

Muller RN, Marsh MJ, Bernardo ML, Lauterbur PC. True 3-D imaging of limbs by NMR zeugmatography with off-resonance irradiation. Eur.J Radiol. 1983; 3 Suppl 1: 286-290.

Mulley JC, Scheffer IE, Petrou S, Berkovic SF. Channelopathies as a genetic cause of epilepsy. Curr.Opin.Neurol. 2003; 16: 171-176.

Multani, P., Myers, R. H., Blume, H. W., Schomer, D. L., and Sotrel, A. Neocortical dendritic pathology in human partial epilepsy: a quantitative Golgi study. Epilepsia 35 (4), 728-736. 1994.
Ref Type: Journal (Full)

Mummery CJ, Patterson K, Price CJ, Ashburner J, Frackowiak RS, Hodges JR. A voxel-based morphometry study of semantic dementia: relationship between temporal lobe atrophy and semantic memory. Ann Neurol 2000; 47: 36-45.

Murphy DG, DeCarli C, Schapiro MB, Rapoport SI, Horwitz B. Age-related differences in volumes of subcortical nuclei, brain matter, and cerebrospinal fluid in healthy men as measured with magnetic resonance imaging (published erratum appears in Arch Neurol 1994 Jan; 51 (1):60). Arch.Neurol 1992; 49: 839-845.

Murphy DG, DeCarli CD, Daly E *et al.* Volumetric magnetic resonance imaging in men with dementia of the Alzheimer type: correlations with disease severity. Biol.Psychiatry 1993; 34: 612-621.

Murphy-Boesch J. Sensitivity improvement via coil and probe design. In: James TL, Margulis AR, editors.

Biomedical magnetic resonance. San Francisco: Radiology Research and Education Foundation, 1984.

Naka H, Imon Y, Ohshita T *et al.* Magnetization transfer measurements of brain structures in patients with multiple system atrophy. Neuroimage 2002; 17: 1572-1578.

Nakada T, Nakayama N, Fujii Y, Kwee IL. Clinical application of three-dimensional anisotropy contrast magnetic resonance axonography. Technical note. J.Neurosurg. 1999; 90: 791-795.

Nakasu Y, Nakasu S, Morikawa S, Uemura S, Inubushi T, Handa J. Diffusion-weighted MR in experimental sustained seizures elicited with kainic acid. AJNR Am.J.Neuroradiol. 1995; 16: 1185-1192.

Namer IJ, Waydelich R, Armspach JP, Hirsch E, Marescaux C, Grucker D. Contribution of T2 relaxation time mapping in the evaluation of cryptogenic temporal lobe epilepsy. Neuroimage. 1998; 7: 304-313.

Naruse S, Horikawa Y, Tanaka C, Hirakawa K, Nishikawa H, Yoshizaki K. Proton nuclear magnetic resonance studies on brain edema. J Neurosurg. 1982; 56: 747-752.

Nedelcu J, Klein MA, Aguzzi A, Boesiger P, Martin E. Biphasic edema after hypoxic-ischemic brain injury in neonatal rats reflects early neuronal and late glial damage. Pediatr.Res. 1999; 46: 297-304.

Neil JJ, McKinstry RC, Schlagger BL *et al.* Evaluation of Diffusion Anisotropy During Human Cortical Grey Matter Development. Proceedings of the International Society for Magnetic Resonance in Medicine, Eighth scientific meeting, 2000; 591.

Neil JJ. Measurement of water motion (apparent diffusion) in biological systems. Concepts Magn.Reson. 1997; 385-401.

Neil JJ, Duong TQ, Ackerman JJ. Evaluation of intracellular diffusion in normal and globally-ischemic rat brain via 133Cs NMR. Magn Reson Med 1996; 35: 329-335.

Neil JJ, Shiran SI, McKinstry RC *et al.* Normal brain in human newborns: apparent diffusion coefficient and diffusion anisotropy measured by using diffusion tensor MR imaging. Radiology 1998; 209: 57-66.

Neubauer BA, Fiedler B, Himmelein B *et al.* Centrotemporal spikes in families with rolandic epilepsy: linkage to chromosome 15q14. Neurology 1998; 51: 1608-1612.

Neufeld A, Eliav U, Navon G. New MRI method with contrast based on the macromolecular characteristics of tissues. Magn Reson Med 2003; 50: 229-234.

Nicoli F, Lefur Y, Denis B, Ranjeva JP, Confort-Gouny S, Cozzone PJ. Metabolic counterpart of decreased apparent diffusion coefficient during hyperacute ischemic stroke: a brain proton magnetic resonance spectroscopic imaging study. Stroke 2003; 34: e82-e87.

Niessen F, Hilger T, Hoehn M, Hossmann KA. Thrombolytic treatment of clot embolism in rat: comparison of intra-arterial and intravenous application of recombinant tissue plasminogen activator. Stroke 2002; 33: 2999-

3005.

Nishio S, Morioka T, Hisada K, Fukui M. Temporal lobe epilepsy: a clinicopathological study with special reference to temporal neocortical changes. Neurosurg.Rev. 2000; 23: 84-89.

Nishio S, Morioka T, Suzuki S, Kira R, Mihara F, Fukui M. Subependymal giant cell astrocytoma: clinical and neuroimaging features of four cases. J Clin.Neurosci. 2001; 8: 31-34.

Noll DC, Schneider W, Cohen JD. Artifacts in functional MRI using conventional scanning. Proc.Soc.Magn.Reson.Med. 1993; 3: 1407.

Nomura Y, Sakuma H, Takeda K, Tagami T, Okuda Y, Nakagawa T. Diffusional anisotropy of the human brain assessed with diffusion-weighted MR: relation with normal brain development and aging. AJNR Am.J.Neuroradiol. 1994; 15: 231-238.

Nordborg C, Eriksson S, Rydenhag B, Uvebrant P, Malmgren K. Microdysgenesis in surgical specimens from patients with epilepsy: occurrence and clinical correlations. J Neurol Neurosurg Psychiatry 1999; 67: 521-524.

Norman RM, Tingey AH, Harvey PW, Gregory AM. Pelizaeus-Merzbacher disease: a form of sudanophil leukodystrophy. J Neurol.Neurosurg.Psychiatry 1966; 29: 521-529.

Novotny EJ, Jr., Hyder F, Shevell M, Rothman DL. GABA changes with vigabatrin in the developing human brain. Epilepsia 1999; 40: 462-466.

O'Callaghan JP. Quantitative features of reactive gliosis following toxicant-induced damage of the CNS. Ann.N.Y.Acad.Sci. 1993; 195-210.

O'Sullivan M, Jarosz JM, Martin RJ, Deasy N, Powell JF, Markus HS. MRI hyperintensities of the temporal lobe and external capsule in patients with CADASIL. Neurology 2001; 56: 628-634.

Ogawa S, Menon RS, Tank DW *et al.* Functional brain mapping by blood oxygenation level-dependent contrast magnetic resonance imaging. A comparison of signal characteristics with a biophysical model. Biophys.J 1993; 64: 803-812.

Oka M, Katayama S, Imon Y, Ohshita T, Mimori Y, Nakamura S. Abnormal signals on proton density-weighted MRI of the superior cerebellar peduncle in progressive supranuclear palsy. Acta Neurol Scand. 2001; 104: 1-5.

Okujava M, Schulz R, Ebner A, Woermann FG. Measurement of temporal lobe T2 relaxation times using a routine diagnostic MR imaging protocol in epilepsy. Epilepsy Res 2002; 48: 131-142.

Oldendorf W. The continued quest for an image of brain. J Neuroimaging 1991; 1: 46-47.

Ono J, Kodaka R, Imai K *et al.* Evaluation of myelination by means of the T2 value on magnetic resonance imaging. Brain Dev. 1993; 15: 433-438.

Opeskin K. Idiopathic generalised epilepsy. Lack of significant microdysgenesis. Neurology 2000; 55: 1101-1106.

Oppenheim C, Dormont D, Biondi A *et al.* Loss of digitations of the hippocampal head on high-resolution fast spin-echo MR: a sign of mesial temporal sclerosis. AJNR Am.J Neuroradiol. 1998; 19: 457-463.

Ormerod IE, Miller DH, McDonald WI *et al.* The role of NMR imaging in the assessment of multiple sclerosis and isolated neurological lesions. A quantitative study. Brain 1987; 110: 1579-1616.

Otsubo H, Hoffman HJ, Humphreys RP *et al.* Evaluation, surgical approach and outcome of seizure patients with gangliogliomas. Pediatr.Neurosurg. 1990; 16: 208-212.

Pacia SV, Devinsky O, Perrine K *et al.* Clinical features of neocortical temporal lobe epilepsy. Ann Neurol 1996; 40: 724-730.

Palace J, Lang B. Epilepsy: an autoimmune disease? J Neurol.Neurosurg.Psychiatry 2000; 69: 711-714.

Palmini A, Andermann F, Olivier A, Tampieri D, Robitaille Y. Focal neuronal migration disorders and intractable partial epilepsy: results of surgical treatment. Ann.Neurol. 1991a; 30: 750-757.

Palmini A, Andermann F, Olivier A *et al.* Focal neuronal migration disorders and intractable partial epilepsy: a study of 30 patients. Ann.Neurol. 1991b; 30: 741-749.

Palmini A, Andermann F, Olivier A *et al.* Neuronal migration disorders: a contribution of modern neuroimaging to the etiologic diagnosis of epilepsy. Can.J Neurol Sci. 1991c; 18: 580-587.

Palmini A, Gambardella A, Andermann F *et al.* Intrinsic epileptogenicity of human dysplastic cortex as suggested by corticography and surgical results. Ann.Neurol. 1995; 37: 476-487.

Pan J, Bebin EM, Chu WJ, Hetherington H. Ketosis and epilepsy: ^{31}P spectroscopic imaging at 4.1T. Epilepsia 1999; 703-707.

Pan Y, Lo EH, Matsumoto K, Hamberg L, Jiang H. Quantitative and dynamic MRI of neuroprotection in experimental stroke. J Neurol.Sci. 1995; 131: 128-134.

Pandya DN, Rosene DL. Topography of Commissural Fibres. In: Reeves AG, editor. Epilepsy and the Corpus Callosum. New York: Plenum Press, 1985: 21-39.

Paolucci S, Silvestri G, Lubich S, Pratesi L, Traballesi M, Gigli GL. Poststroke late seizures and their role in rehabilitation of inpatients. Epilepsia 1997; 38: 266-270.

Papadakis NG, Xing D, Houston GC *et al.* A study of rotationally invariant and symmetric indices of diffusion anisotropy. Magn Reson Imaging 1999; 17: 881-892.

Parizel PM, Ozsarlak, Van Goethem JW *et al.* Imaging findings in diffuse axonal injury after closed head trauma. Eur Radiol. 1998; 8: 960-965.

Park SH, Kim M, Na DL, Jeon BS. Magnetic resonance reflects the pathological evolution of Wernicke encephalopathy. J Neuroimaging 2001; 11: 406-411.

Parker GJ, Stephan KE, Barker GJ *et al.* Initial demonstration of in vivo tracing of axonal projections in the macaque brain and comparison with the human brain using diffusion tensor imaging and fast marching tractography. Neuroimage 2002; 15: 797-809.

Parrish RG, Kurland RJ, Janese WW, Bakay L. Proton relaxation rates of water in brain and brain tumors. Science 1974; 183: 438-439.

Parsey RV, Krishnan KR. Quantitative analysis of T2 signal intensities in Alzheimer's disease. Psychiatry Res. 1998; 82: 181-185.

Pasqualin A, Scienza R, Cioffi F *et al.* Treatment of cerebral arteriovenous malformations with a combination of preoperative embolization and surgery. Neurosurgery 1991; 29: 358-368.

Paulesu E, Connelly A, Frith CD *et al.* Functional MR imaging correlations with positron emission tomography. Initial experiences using a cognitive activation paradigm on verbal working memory. Neuroim.Clin.N.Am. 1995; 5: 207-225.

Peled S, Gudbjartsson H, Westin CF, Kikinis R, Jolesz FA. Magnetic resonance imaging shows orientation and asymmetry of white matter fiber tracts. Brain Res. 1998; 780: 27-33.

Pelizzari CA, Chen GTY, Spelbring DR, Weichselbaum RR, Chen CT. Accurate three-dimensional registration of CT, PET and MR images of the brain. J Comput.Assist.Tomogr. 1988; 13: 20-26.

Petersen SE, Fox PT, Posner MI, Mintun M, Raichle ME. Positron emission tomographic studies of the processing of single words. J Cog Neurosci 1989; 1: 153-170.

Petroff OA, Errante LD, Rothman DL, Kim JH, Spencer DD. Neuronal and glial metabolite content of the epileptogenic human hippocampus. Ann Neurol 2002; 52: 635-642.

Petroff OA, Hyder F, Collins T, Mattson RH, Rothman DL. Acute effects of vigabatrin on brain GABA and homocarnosine in patients with complex partial seizures. Epilepsia 1999a; 40: 958-964.

Petroff OA, Hyder F, Mattson RH, Rothman DL. Topiramate increases brain GABA, homocarnosine, and pyrrolidinone in patients with epilepsy. Neurology 1999b; 52: 473-478.

Petroff OA, Mattson RH, Behar KL, Hyder F, Rothman DL. Vigabatrin increases human brain homocarnosine and improves seizure control. Ann Neurol 1998; 44: 948-952.

Petroff OA, Pleban LA, Spencer DD. Symbiosis between in vivo and in vitro NMR spectroscopy: the creatine, *N*-acetylaspartate, glutamate, and GABA content of the epileptic human brain. Magn Reson Imaging 1995a; 1197-1211.

Petroff OA, Prichard JW, Behar KL, Alger JR, Shulman RG. In vivo phosphorus nuclear magnetic resonance spectroscopy in status epilepticus. Ann.Neurol. 1984; 16: 169-177.

Petroff OA, Rothman DL, Behar KL, Lamoureux D, Mattson RH. The effect of gabapentin on brain gamma-aminobutyric acid in patients with epilepsy. Ann Neurol 1996a; 39: 95-99.

Petroff OA, Rothman DL, Behar KL, Mattson RH. Initial observations on effect of vigabatrin on in vivo 1H spectroscopic measurements of gamma-aminobutyric acid, glutamate, and glutamine in human brain. Epilepsia 1995b; 36: 457-464.

Petroff OA, Rothman DL, Behar KL, Mattson RH. Human brain GABA levels rise after initiation of vigabatrin therapy but fail to rise further with increasing dose. Neurology 1996b; 46: 1459-1463.

Petroff OA, Rothman DL, Behar KL, Mattson RH. Low brain GABA level is associated with poor seizure control. Ann Neurol 1996c; 908-911.

Phillips HA, Favre I, Kirkpatrick M *et al.* CHRNB2 is the second acetylcholine receptor subunit associated with autosomal dominant nocturnal frontal lobe epilepsy. Am J Hum.Genet. 2001; 68: 225-231.

Phillips HA, Scheffer IE, Berkovic SF, Hollway GE, Sutherland GR, Mulley JC. Localization of a gene for autosomal dominant nocturnal frontal lobe epilepsy to chromosome 20q 13.2. Nat.Genet. 1995; 10: 117-118.

Piepgras DG, Sundt TM, Ragoowansi AT, Stevens L. Seizure outcome in patients with surgically treated cerebral arteriovenous malformations. J Neurosurg. 1993; 78: 5-11.

Pierce WB, Harms SE, Flamig DP, Griffey RH, Evans WP, Hagans JE. Three-dimensional gadolinium-enhanced MR imaging of the breast: pulse sequence with fat suppression and magnetization transfer contrast. Work in progress. Radiology 1991; 181: 757-763.

Pierpaoli C, Barnett A, Pajevic S *et al.* Water diffusion changes in Wallerian degeneration and their dependence on white matter architecture. Neuroimage 2001; 13: 1174-1185.

Pierpaoli C, Basser PJ. Toward a quantitative assessment of diffusion anisotropy (published erratum appears in Magn Reson Med 1997 Jun; 37 (6):972). Magn Reson Med 1996; 36: 893-906.

Pierpaoli C, Jezzard P, Basser PJ, Barnett A, Di Chiro G. Diffusion tensor MR imaging of the human brain. Radiology 1996; 201: 637-648.

Pierpaoli C, Righini A, Linfante I, Tao-Cheng JH, Alger JR, Di Chiro G. Histopathologic correlates of abnormal water diffusion in cerebral ischemia: diffusion-weighted MR imaging and light and electron microscopic study. Radiology 1993; 189: 439-448.

Pillay PK, Barnett G, Awad I. MRI-guided stereotactic placement of depth electrodes in temporal lobe epilepsy. Br.J Neurosurg. 1992; 6: 47-53.

Pitkanen A, Laakso M, Kalviainen R *et al.* Severity of hippocampal atrophy correlates with the prolongation of MRI T2 relaxation time in temporal lobe epilepsy but not in Alzheimer's disease. Neurology 1996; 46: 1724-1730.

Placencia M, Shorvon SD, Paredes V *et al.* Epileptic seizures in an Andean region of Ecuador. Incidence and prevalence and regional variation. Brain 1992; 115 (Pt 3): 771-782.

Plioplys AV, Greaves A, Yoshida W. Anti-CNS antibodies in childhood neurologic diseases. Neuropediatrics 1989; 20: 93-102.

Plum F, Posner JB, Troy B. Cerebral metabolic and circulatory responses to induced convulsions in animals. Arch.Neurol. 1968; 18: 1-13.

Plummer D. A Display and Analysis Tool for Medical Images. Revista di Neuroradiologica (Italy) 1992; 489-495.

Poncelet BP, Wedeen VJ, Weisskoff RM, Cohen MS. Brain parenchyma motion: measurement with cine echo-planar MR imaging. Radiology 1992; 185: 645-651.

Powers JM. Adreno-leukodystrophy (adreno-testiculo-leukomyelo-neuropathic-complex). Clin.Neuropathol. 1985; 4: 181-199.

Pradhan S, Kathuria MK, Gupta RK. Perilesional gliosis and seizure outcome: a study based on magnetization transfer magnetic resonance imaging in patients with neurocysticercosis. Ann Neurol 2000; 48: 181-187.

Prager JM, Rosenblum JD, Huddle DC, Diamond CK, Metz CE. The magnetization transfer effect in cerebral infarction. AJNR Am J Neuroradiol 1994; 15: 1497-1500.

Prayson RA, Estes ML. Dysembryoplastic neuroepithelial tumor. Am J Clin.Pathol. 1992; 97: 398-401.

Price JL, Ko AI, Wade MJ, Tsou SK, McKeel DW, Morris JC. Neuron number in the entorhinal cortex and CA1 in preclinical Alzheimer disease. Arch.Neurol. 2001; 58: 1395-1402.

Prichard JW, Zhong J, Petroff OA, Gore JC. Diffusion-weighted NMR imaging changes caused by electrical activation of the brain. NMR Biomed. 1995; 8: 359-364.

Przelomski MM, O'Rourke E, Grady GF, Berardi VP, Markley HG. Eastern equine encephalitis in Massachusetts: a report of 16 cases, 1970-1984. Neurology 1988; 38: 736-739.

Puce A, Constable RT, Luby ML *et al.* Functional magnetic resonance imaging of sensory and motor cortex: comparison with electrophysiological localization. J Neurosurg. 1995; 83: 262-270.

Pui MH. Magnetization transfer analysis of brain tumor, infection, and infarction (In Process Citation). J Magn Reson Imaging 2000; 12: 395-399.

Quesney LF. Clinical and EEG features of complex partial seizures of temporal lobe origin. Epilepsia 1986; 27 Suppl 2:S27-45: S27-S45.

Quigg M, Bertram EH, Jackson T. Longitudinal distribution of hippocampal atrophy in mesial temporal lobe epilepsy. Epilepsy Res 1997; 27: 101-110.

Rachlis A, Fanning MM. Zidovudine toxicity. Clinical features and management. Drug Saf 1993; 8: 312-320.

Ragnaud JM, Morlat P, Dupon M, Lacoste D, Pellegrin JL, Chene G. Cerebral toxoplasmosis in AIDS. 73 cases. Clinical Epidemiology Group on AIDS in Aquitania. Presse Med 1993; 22: 903-908.

Rakic P. Neuronal migration and contact guidance in the primate telencephalon. Postgrad.Med J 1978; 54 Suppl 1: 25-40.

Rakic P. Defects of neuronal migration and the pathogenesis of cortical malformations. Prog.Brain Res 1988a; 73: 15-37.

Rakic P. Specification of cerebral cortical areas. Science 1988b; 241: 170-176.

Ramani A, Barker GJ, Tofts PS. Fast measurement of quantitative MT parameters in fixed multiple sclerosis brain. Proceedings International Society for Magnetic Resonance in Medicine.9th Annual Meeting. 2001; 259.

Rao SM, Binder JR, Hammeke TA *et al.* Somatotopic mapping of the human primary motor cortex with functional magnetic resonance imaging. Neurology 1995; 45: 919-924.

Rasmussen T. Surgery of epilepsy associated with brain tumors. Adv.Neurol 1975; 8: 227-239.

Rasmussen T, Olszewski J, Lloyd-Smith D. Focal seizures due to chronic localised encephalitis. Neurology 1958; 8: 435-445.

Rausch R, Risinger M. Intracarotid sodium amobarbitol procedure. In: Boulton AA, Baker G, Hiscock M, editors. Neuromethods, XVII, Neuropsychology. Clifton, NJ: Humana Press, 1990.

Raymond AA, Fish DR, Sisodiya SM, Alsanjari N, Stevens JM, Shorvon SD. Abnormalities of gyration, heterotopias, tuberous sclerosis, focal cortical dysplasia, microdysgenesis, dysembryoplastic neuroepithelial tumour and dysgenesis of the archicortex in epilepsy. Clinical, EEG and neuroimaging features in 100 adult patients. Brain 1995; 118: 629-660.

Raymond AA, Fish DR, Stevens JM, Sisodiya SM, Alsanjari N, Shorvon SD. Subependymal heterotopia: a distinct neuronal migration disorder associated with epilepsy. J Neurol Neurosurg Psychiatry 1994; 57: 1195-1202.

Redpath TW, Smith FW. Technical note: use of a double inversion recovery pulse sequence to image selectively grey or white brain matter. Br.J Radiol. 1994; 67: 1258-1263.

Rees G, Friston K, Koch C. A direct quantitative relationship between the functional properties of human and macaque V5. Nat.Neurosci 2000; 3: 716-723.

Reidel MA, Stippich C, Heiland S, Storch-Hagenlocher B, Jansen O, Hahnel S. Differentiation of multiple

sclerosis plaques, subacute cerebral ischaemic infarcts, focal vasogenic oedema and lesions of subcortical arteriosclerotic encephalopathy using magnetisation transfer measurements. Neuroradiology 2003; 45: 289-294.

Reiner O, Carrozzo R, Shen Y *et al.* Isolation of a Miller-Dieker lissencephaly gene containing G protein beta-subunit-like repeats. Nature 1993; 364: 717-721.

Reiss AL, Faruque F, Naidu S *et al.* Neuroanatomy of Rett syndrome: a volumetric imaging study. Ann Neurol 1993; 34: 227-234.

Requena I, Arias M, Lopez-Ibor L *et al.* Cavernomas of the central nervous system: clinical and neuroimaging manifestations in 47 patients. J Neurol.Neurosurg.Psychiatry 1991; 54: 590-594.

Richardson MP, Koepp MJ, Brooks DJ, Duncan JS. ^{11}C-flumazenil PET in neocortical epilepsy. Neurology 1998; 485-492.

Richardson MP, Koepp MJ, Brooks DJ, Fish DR, Duncan JS. Benzodiazepine receptors in focal epilepsy with cortical dysgenesis: an 11C-flumazenil PET study. Ann.Neurol. 1996; 40: 188-198.

Richman DP, Stewart RM, Caviness VS, Jr. Cerebral microgyria in a 27-week fetus: an architectonic and topographic analysis. J Neuropathol.Exp.Neurol 1974; 33: 374-384.

Rocca MA, Colombo B, Pratesi A, Comi G, Filippi M. A magnetization transfer imaging study of the brain in patients with migraine. Neurology 2000; 54: 507-509.

Roemer PB, Edelstein WA, Hayes CE, Souza SP, Mueller OM. The NMR phased array. Magn Reson Med 1990; 16: 192-225.

Rogers SW, Andrews PI, Gahring LC *et al.* Autoantibodies to glutamate receptor GluR3 in Rasmussen's encephalitis. Science 1994; 265: 648-651.

Rosemberg S, Vieira GS. Dysembryoplastic neuroepithelial tumor. An epidemiological study from a single institution. Arq Neuropsiquiatr. 1998; 56: 232-236.

Rosen HJ, Petersen SE, Linenweber MR *et al.* Neural correlates of recovery from aphasia after damage to left inferior frontal cortex. Neurology 2000; 55: 1883-1894.

Rosenfeld JV, Widaa HA, Adams CB. Cerebral arteriovenous malformation causing benign intracranial hypertension--case report. Neurol Med Chir (Tokyo) 1991; 31: 523-525.

Ross ME, Swanson K, Dobyns WB. Lissencephaly with cerebellar hypoplasia (LCH): a heterogeneous group of cortical malformations. Neuropediatrics 2001; 32: 256-263.

Rothman DL. Spectroscopic editing of gamma amino butyric acid in the human brain. Proceedings of the International Society for Magnetic Resonance in Medicine, Philadelphia, 1999; 306-311.

Rothman DL, Behar KL, Prichard JW, Petroff OA. Homocarnosine and the measurement of neuronal pH in patients with epilepsy. Magn Reson Med 1997; 38: 924-929.

Rothman DL, Petroff OA, Behar KL, Mattson RH. Localized 1H NMR measurements of gamma-aminobutyric acid in human brain in vivo. Proc.Natl.Acad.Sci.U.S.A 1993; 90: 5662-5666.

Rovaris M, Agosta F, Sormani MP *et al.* Conventional and magnetization transfer MRI predictors of clinical multiple sclerosis evolution: a medium-term follow-up study. Brain 2003a; 126: 2323-2332.

Rovaris M, Bozzali M, Iannucci G *et al.* Assessment of normal-appearing white and gray matter in patients with primary progressive multiple sclerosis: a diffusion-tensor magnetic resonance imaging study. Arch Neurol 2002; 59: 1406-1412.

Rovaris M, Comi G, Rocca MA *et al.* Relevance of hypointense lesions on fast fluid-attenuated inversion recovery MR images as a marker of disease severity in cases of multiple sclerosis. AJNR Am J Neuroradiol 1999; 20: 813-820.

Rovaris M, Iannucci G, Cercignani M *et al.* Age-related changes in conventional, magnetization transfer, and diffusion-tensor MR imaging findings: study with whole-brain tissue histogram analysis. Radiology 2003b; 227: 731-738.

Rovaris M, Viti B, Ciboddo G *et al.* Brain involvement in systemic immune mediated diseases: magnetic resonance and magnetisation transfer imaging study. J Neurol Neurosurg Psychiatry 2000; 68: 170-177.

Rubinstein LJ, Herman MM. A light- and electron-microscopic study of a temporal-lobe ganglioglioma. J Neurol Sci. 1972; 16: 27-48.

Rueckert L, Appollonio I, Grafman J *et al.* Magnetic resonance imaging functional activation of left frontal cortex during covert word production. J Neuroimaging 1994; 4: 67-70.

Rugg-Gunn FJ, Boulby PA, Symms MR, Barker GJ, Duncan JS. T2-mapping of the neocortex in localisation-related epilepsy. Epilepsia 2002a; 43 (suppl. 7): 304.

Rugg-Gunn FJ, Eriksson SH, Boulby PA, Symms MR, Barker GJ, Duncan JS. Magnetization transfer imaging in focal epilepsy. Neurology 2003; 60: 1638-1645.

Rugg-Gunn FJ, Eriksson SH, Symms MR *et al.* Diffusion tensor imaging in refractory epilepsy. Lancet 2002b; 359: 1748-1751.

Rumbach L, Armspach JP, Gounot D *et al.* Nuclear magnetic resonance T2 relaxation times in multiple sclerosis. J Neurol.Sci. 1991; 104: 176-181.

Rumpel H, Nedelcu J, Aguzzi A, Martin E. Late glial swelling after acute cerebral hypoxia-ischemia in the neonatal rat: a combined magnetic resonance and histochemical study. Pediatr.Res. 1997; 42: 54-59.

Runge VM, Wells JW, Williams NM, Lee C, Timoney JF, Young AB. Detectability of early brain meningitis with magnetic resonance imaging. Invest Radiol. 1995; 30: 484-495.

Russell J, Fisher M, Zivin JA, Sullivan J, Drachman DA. Status epilepticus and Epstein-Barr virus encephalopathy. Diagnosis by modern serologic techniques. Arch.Neurol. 1985; 42: 789-792.

Rutherford MA, Cowan FM, Manzur AY *et al.* MR imaging of anisotropically restricted diffusion in the brain of neonates and infants. J.Comput.Assist.Tomogr. 1991; 15: 188-198.

Rydberg JN, Hammond CA, Grimm RC *et al.* Initial clinical experience in MR imaging of the brain with a fast fluid-attenuated inversion-recovery pulse sequence. Radiology 1994; 193: 173-180.

Ryglewicz D, Baranska-Gieruszczak M, Niedzielska K, Kryst-Widzgowska T. EEG and CT findings in poststroke epilepsy. Acta Neurol Scand. 1990; 81: 488-490.

Sabsevitz DS, Swanson SJ, Hammeke TA *et al.* Use of preoperative functional neuroimaging to predict language deficits from epilepsy surgery. Neurology 2003; 60: 1788-1792.

Sagar HJ, Oxbury JM. Hippocampal neuron loss in temporal lobe epilepsy: correlation with early childhood convulsions. Ann.Neurol. 1987; 22: 334-340.

Salek-Haddadi A, Lemieux L, Merschhemke M, Friston KJ, Duncan JS, Fish DR. Functional magnetic resonance imaging of human absence seizures. Ann Neurol 2003; 53: 663-667.

Salerno JA, Murphy DG, Horwitz B *et al.* Brain atrophy in hypertension. A volumetric magnetic resonance imaging study. Hypertension 1992; 20: 340-348.

Salgado ED, Weinstein M, Furlan AJ *et al.* Proton magnetic resonance imaging in ischemic cerebrovascular disease. Ann.Neurol. 1986; 20: 502-507.

Salmond CH, Ashburner J, Vargha-Khadem F, Connelly A, Gadian DG, Friston KJ. Distributional assumptions in voxel-based morphometry. Neuroimage 2002; 17: 1027-1030.

Salo S, Alanen A, Komu M, Kallio T, Bondestam S. Effect of fasting and food intake on magnetization transfer of human liver tissue. Magn Reson Imaging 1997; 15: 47-50.

Salonen O, Autti T, Raininko R, Ylikoski A, Erkinjuntti T. MRI of the brain in neurologically healthy middle-aged and elderly individuals. Neuroradiology 1997; 39: 537-545.

Sander JW, Hart YM, Johnson AL, Shorvon SD. National General Practice Study of Epilepsy: newly diagnosed epileptic seizures in a general population. Lancet 1990; 336: 1267-1271.

Sander JW, Shorvon SD. Epidemiology of the epilepsies. J Neurol Neurosurg Psychiatry 1996; 61: 433-443.

Sandson TA, Felician O, Edelman RR, Warach S. Diffusion-weighted magnetic resonance imaging in Alzheimer's

disease. Dement.Geriatr.Cogn Disord. 1999; 10: 166-171.

Sapir T, Cahana A, Seger R. LIS1 is a microtubule associated phosphoprotein. Eur J Biochem 2000; 265: 181-188.

Sarnat HB. Disturbances of late neuronal migrations in the perinatal period. Am J Dis.Child 1987; 141: 969-980.

Sarnat HB. Cerebral dysplasias as expressions of altered maturational processes. Can.J Neurol.Sci. 1991; 18: 196-204.

Sasaki M, Sone M, Ehara S. Hippocampal sulcus remnant: potential cause of change in signal intensity in the hippocampus. Radiology 1993; 188: 743-746.

Saukkonen A, Kalviainen R, Partanen K, Vainio P, Riekkinen P, Pitkanen A. Do seizures cause neuronal damage? A MRI study in newly diagnosed and chronic epilepsy. Neuroreport 1994; 6: 219-223.

Saunders RD, Dugan LL, Demediuk P, Means ED, Horrocks LA, Anderson DK. Effects of methylprednisolone and the combination of alpha-tocopherol and selenium on arachidonic acid metabolism and lipid peroxidation in traumatized spinal cord tissue. J Neurochem. 1987; 49: 24-31.

Saur D, Kucinski T, Grzyska U *et al.* Sensitivity and interrater agreement of CT and diffusion-weighted MR imaging in hyperacute stroke. AJNR Am.J Neuroradiol. 2003; 24: 878-885.

Sauter A, Rudin M. Calcium antagonists reduce the extent of infarction in rat middle cerebral artery occlusion model as determined by quantitative magnetic resonance imaging. Stroke 1986; 17: 1228-1234.

Savic I, Ke Y, Thomas A, Fried I, Engel J. MRS shows increased cerebellar glutamate+glutamine (GLX) levels in partial epilepsy. Neuroimage. 1998a; S286.

Savic I, Ke Y, Thomas A, McDonald K, Curran J, Engel J. Measurements of glutamate/glutamine levels in patients with partial epilepsy using ^{1}H magnetic resonance spectroscopy. Neuroimage. 1996; S509.

Savic I, Seitz RJ, Pauli S. Brain distortions in patients with primarily generalized tonic-clonic seizures. Epilepsia 1998b; 39: 364-370.

Scarpelli M, Salvolini U, Diamanti L, Montironi R, Chiaromoni L, Maricotti M. MRI and pathological examination of post-mortem brains: the problem of white matter high signal areas. Neuroradiology 1994; 36: 393-398.

Schacter DL, Wagner AD. Medial temporal lobe activations in fMRI and PET studies of episodic encoding and retrieval. Hippocampus 1999; 9: 7-24.

Schad LR, Bluml S, Zuna I. MR tissue characterization of intracranial tumors by means of texture analysis. Magn Reson Imaging 1993; 11: 889-896.

Scheffer IE, Berkovic SF. Generalized epilepsy with febrile seizures plus. A genetic disorder with heterogeneous

clinical phenotypes. Brain 1997; 120 (Pt 3): 479-490.

Scheffer IE, Bhatia KP, Lopes-Cendes I *et al.* Autosomal dominant nocturnal frontal lobe epilepsy. A distinctive clinical disorder. Brain 1995; 118 (Pt 1): 61-73.

Schellinger PD, Fiebach JB, Hacke W. Imaging-based decision making in thrombolytic therapy for ischemic stroke: present status. Stroke 2003; 34: 575-583.

Scheltens P, Barkhof F, Leys D *et al.* A semiquantative rating scale for the assessment of signal hyperintensities on magnetic resonance imaging. J Neurol.Sci. 1993; 114: 7-12.

Scheltens P, Barkhof F, Leys D, Wolters EC, Ravid R, Kamphorst W. Histopathologic correlates of white matter changes on MRI in Alzheimer's disease and normal aging. Neurology 1995; 45: 883-888.

Scheltens P, Barkhof F, Valk J *et al.* White matter lesions on magnetic resonance imaging in clinically diagnosed Alzheimer's disease. Evidence for heterogeneity. Brain 1992; 115 (Pt 3): 735-748.

Schenck JF, Hart HR, Jr., Foster TH *et al.* Improved MR imaging of the orbit at 1.5 T with surface coils. AJR Am.J Roentgenol. 1985; 144: 1033-1036.

Schierhout G, Roberts I. Prophylactic antiepileptic agents after head injury: a systematic review. J Neurol Neurosurg Psychiatry 1998; 64: 108-112.

Schorner W, Laniado M, Kornmesser W, Felix R. Comparison of multi echo and contrast-enhanced MR scans: image contrast and delineation of intracranial tumors. Neuroradiology 1989; 31: 140-147.

Schroder W, Hinterkeuser S, Seifert G *et al.* Functional and molecular properties of human astrocytes in acute hippocampal slices obtained from patients with temporal lobe epilepsy. Epilepsia 2000; 41 Suppl 6: S181-S184.

Schuier FJ, Hossmann KA. Experimental brain infarcts in cats. II. Ischemic brain edema. Stroke 1980; 11: 593-601.

Schulze-Bonhage AH, Huppertz HJ, Comeau RM, Honegger JB, Spreer JM, Zentner JK. Visualization of subdural strip and grid electrodes using curvilinear reformatting of 3D MR imaging data sets. AJNR Am.J Neuroradiol. 2002; 23: 400-403.

Schwaighofer B, Neuhold A, Wicke L, Fruhwald F, Hamid L, Stiglbauer R. (Magnetic resonance tomography in the diagnosis of cerebral space occupying lesions). Rontgenblatter. 1987; 40: 331-337.

Schwartz TH, Resor SR, Jr., De La PR, Goodman RR. Functional magnetic resonance imaging localization of ictal onset to a dysplastic cleft with simultaneous sensorimotor mapping: intraoperative electrophysiological confirmation and postoperative follow-up: technical note. Neurosurgery 1998; 43: 639-644.

Scott GM, Gibberd FB. Epilepsy and other factors in the prognosis of gliomas. Acta Neurol Scand. 1980; 61: 227-239.

Scoville WB, Milner B. Loss of recent memory after bilateral hippocampal lesions. 1957 (classical article). J Neuropsychiatry Clin.Neurosci. 2000; 12: 103-113.

Seeck M, Lazeyras F, Michel CM *et al.* Non-invasive epileptic focus localization using EEG-triggered functional MRI and electromagnetic tomography. Electroencephalogr.Clin.Neurophysiol. 1998; 106: 508-512.

Semah F, Picot MC, Adam C *et al.* Is the underlying cause of epilepsy a major prognostic factor for recurrence? Neurology 1998; 51: 1256-1262.

Servit Z, Musil F. Prophylactic treatment of posttraumatic epilepsy: results of a long-term follow-up in Czechoslovakia. Epilepsia 1981; 22: 315-320.

Sevick RJ, Kanda F, Mintorovitch J *et al.* Cytotoxic brain edema: assessment with diffusion-weighted MR imaging. Radiology 1992; 185: 687-690.

Shah PJ, Ebmeier KP, Glabus MF, Goodwin GM. Cortical grey matter reductions associated with treatment-resistant chronic unipolar depression. Controlled magnetic resonance imaging study. Br.J Psychiatry 1998; 172:527-32: 527-532.

Shapiro IM, Neufeld MY, Korczyn AD. Seizures of unknown origin after the age of 50: vascular risk factors. Acta Neurol Scand. 1990; 82: 78-80.

Shapiro R, Galloway SJ, Shapiro MD. Minimal asymmetry of the brain: a normal variant. AJR Am J Roentgenol. 1986; 147: 753-756.

Shenton ME, Gerig G, McCarley RW, Szekely G, Kikinis R. Amygdala-hippocampal shape differences in schizophrenia: the application of 3D shape models to volumetric MR data. Psychiatry Res 2002; %20; 115: 15-35.

Sherwin AL, Vernet O, Dubeau F, Olivier A. Biochemical markers of excitability in human neocortex. Can.J Neurol.Sci. 1991; 18: 640-644.

Shimbo Y, Takahashi H, Hayano M, Kumagai T, Kameyama S. Temporal lobe lesion demonstrating features of dysembryoplastic neuroepithelial tumor and ganglioglioma: a transitional form? Clin.Neuropathol 1997; 16: 65-68.

Shimony JS, McKinstry RC, Akbudak E *et al.* Quantitative diffusion-tensor anisotropy brain MR imaging: normative human data and anatomic analysis. Radiology 1999; 212: 770-784.

Shinton RA, Zezulka AV, Gill JS, Beeves DJ. The frequency of epilepsy preceding stroke.Case-control study in 230 patients. Lancet 1987; 11-13.

Shorvon SD. Epidemiology and aetiology of epilepsy. In: Asbury AK, McKann GM, McDonald WI, editors. Diseases of the nervous system: clinical neurobiology. Philadelphia: W.B. Saunders Company, 1992: 896-905.

Sicca F, Kelemen A, Genton P *et al.* Mosaic mutations of the LIS1 gene cause subcortical band heterotopia. Neurology 2003; 61: 1042-1046.

Sidman RL, Rakic P. Neuronal migration, with special reference to developing human brain: a review. Brain Res. 1973; 62: 1-35.

Siegel AM, Jobst BC, Thadani VM *et al.* Medically intractable, localization-related epilepsy with normal MRI: presurgical evaluation and surgical outcome in 43 patients. Epilepsia 2001; 42: 883-888.

Silver NC, Barker GJ, Macmanus DG, Miller DH, Thorpe JW, Howard RS. Decreased magnetisation transfer ratio due to demyelination: a case of central pontine myelinolysis (letter). J Neurol Neurosurg Psychiatry 1996; 61: 208-209.

Silver NC, Barker GJ, Macmanus DG, Tofts PS, Miller DH. Magnetisation transfer ratio of normal brain white matter: a normative database spanning four decades of life. J Neurol Neurosurg Psychiatry 1997a; 62: 223-228.

Silver NC, Barker GJ, Miller DH. Standardization of magnetization transfer imaging for multicenter studies. Neurology 1999; 53: S33-S39.

Silver NC, Gass A, Barker GJ, Tofts PS, Miller DH. Evaluation of magnetization transfer ratio histogram analysis methods in multiple sclerosis. Proceedings International Society for Magnetic Resonance in Medicine. 1998; 1322.

Silver NC, Good CD, Barker GJ *et al.* Sensitivity of contrast enhanced MRI in multiple sclerosis. Effects of gadolinium dose, magnetization transfer contrast and delayed imaging. Brain 1997b; 120: 1149-1161.

Simister RJ, McLean MA, Barker GJ, Duncan JS. A proton magnetic resonance spectroscopy study of metabolites in the occipital lobes in epilepsy. Epilepsia 2003; 44: 550-558.

Simister RJ, Woermann FG, McLean MA, Bartlett PA, Barker GJ, Duncan JS. A short-echo-time proton magnetic resonance spectroscopic imaging study of temporal lobe epilepsy. Epilepsia 2002; 43: 1021-1031.

Singh NA, Charlier C, Stauffer D *et al.* A novel potassium channel gene, KCNQ2, is mutated in an inherited epilepsy of newborns. Nat.Genet. 1998; 18: 25-29.

Sinson G, Bagley LJ, Cecil KM *et al.* Magnetization transfer imaging and proton MR spectroscopy in the evaluation of axonal injury: correlation with clinical outcome after traumatic brain injury. AJNR Am J Neuroradiol 2001; 22: 143-151.

Sisodiya S, Barker GJ, Bartlett PA, Tofts PS, Shorvon S, Stevens J. Magnetisation transfer contrast imaging of grey matter in cerebral dysgenesis. Proceedings International Society for Magnetic Resonance in Medicine.4th Annual Meeting. 1996a; 619.

Sisodiya SM. Surgery for malformations of cortical development causing epilepsy. Brain 2000; 123 (Pt 6): 1075-1091.

Sisodiya SM, Free SL. Disproportion of cerebral surface areas and volumes in cerebral dysgenesis. MRI-based evidence for connectional abnormalities. Brain 1997; 120: 271-281.

Sisodiya SM, Free SL, Fish DR, Shorvon SD. Increasing the yield from volumetric MRI in patients with epilepsy. Magn Reson Imaging 1995a; 13: 1147-1152.

Sisodiya SM, Free SL, Stevens JM, Fish DR, Shorvon SD. Widespread cerebral structural changes in patients with cortical dysgenesis and epilepsy. Brain 1995b; 118: 1039-1050.

Sisodiya SM, Free SL, Stevens JM, Fish DR, Shorvon SD. Widespread cerebral structural changes in two patients with gelastic seizures and hypothalamic hamartomata. Epilepsia 1997a; 38: 1008-1010.

Sisodiya SM, Free SL, Thom M, Everitt AE, Fish DR, Shorvon SD. Evidence for nodular epileptogenicity and gender differences in periventricular nodular heterotopia. Neurology 1999; 52: 336-341.

Sisodiya SM, Moran N, Free SL *et al.* Correlation of widespread preoperative magnetic resonance imaging changes with unsuccessful surgery for hippocampal sclerosis. Ann.Neurol. 1997b; 41: 490-496.

Sisodiya SM, Stevens JM, Fish DR, Free SL, Shorvon SD. The demonstration of gyral abnormalities in patients with cryptogenic partial epilepsy using three-dimensional MRI. Arch.Neurol 1996b; 53: 28-34.

Sled JG, Pike GB. Quantitative imaging of magnetization transfer exchange and relaxation properties in vivo using MRI. Magn Reson Med 2001; 46: 923-931.

Smith AS, Weinstein MA, Modic MT *et al.* Magnetic resonance with marked T2-weighted images: improved demonstration of brain lesions, tumor, and edema. AJR Am J Roentgenol. 1985; 145: 949-955.

Smith CD, Snowdon DA, Wang H, Markesbery WR. White matter volumes and periventricular white matter hyperintensities in aging and dementia. Neurology 2000; 54: 838-842.

Smith DF, Hutton JL, Sandemann D *et al.* The prognosis of primary intracerebral tumours presenting with epilepsy: the outcome of medical and surgical management. J Neurol Neurosurg Psychiatry 1991; 54: 915-920.

Smith NM, Carli MM, Hanieh A, Clark B, Bourne AJ, Byard RW. Gangliogliomas in childhood. Childs Nerv.Syst. 1992; 8: 258-262.

So EL. Classifications and epidemiologic considerations of epileptic seizures and epilepsy. Neuroimaging Clin.N.Am 1995; 5: 513-526.

So EL, Annegers JF, Hauser WA, O'Brien PC, Whisnant JP. Population-based study of seizure disorders after cerebral infarction. Neurology 1996; 46: 350-355.

So N, Gloor P, Quesney LF, Jones-Gotman M, Olivier A, Andermann F. Depth electrode investigations in patients with bitemporal epileptiform abnormalities. Ann.Neurol. 1989; 25: 423-431.

Soges LJ, Cacayorin ED, Petro GR, Ramachandran TS. Migraine: evaluation by MR. AJNR Am J Neuroradiol 1988; 9: 425-429.

Solimena M, Folli F, Aparisi R, Pozza G, De Camilli P. Autoantibodies to GABA-ergic neurons and pancreatic beta cells in stiff-man syndrome. N.Engl.J Med 1990; 322: 1555-1560.

Soltanian-Zadeh H, Windham JP, Peck DJ, Mikkelsen T. Feature space analysis of MRI. Magn Reson Med 1998; 40: 443-453.

Sommer W. Erkrankung des ammonshorns als aetiologisches moment der epilepsie. Arch Psychiatr Nervenkr 1880; 10: 631-675.

Sorensen AG, Buonanno FS, Gonzalez RG *et al.* Hyperacute stroke: evaluation with combined multisection diffusion-weighted and hemodynamically weighted echo-planar MR imaging. Radiology 1996; 199: 391-401.

Sostman HD, Spencer DD, Gore JC *et al.* Preliminary observations on magnetic resonance imaging in refractory epilepsy. Magn Reson Imaging 1984; 2: 301-306.

Sowell ER, Levitt J, Thompson PM *et al.* Brain abnormalities in early-onset schizophrenia spectrum disorder observed with statistical parametric mapping of structural magnetic resonance images. Am J Psychiatry 2000; 157: 1475-1484.

Sowell ER, Thompson PM, Holmes CJ, Batth R, Jernigan TL, Toga AW. Localizing age-related changes in brain structure between childhood and adolescence using statistical parametric mapping. Neuroimage 1999; 9: 587-597.

Spatt J, Chaix R, Mamoli B. Epileptic and non-epileptic seizures in multiple sclerosis. J Neurol. 2001; 248: 2-9.

Spatt J, Goldenberg G, Mamoli B. Epilepsia partialis continua in multiple sclerosis. Lancet 1995; 345: 658-659.

Spencer SS. Substrates of localization-related epilepsies: biologic implications of localizing findings in humans. Epilepsia 1998; 39: 114-123.

Spencer SS, McCarthy G, Spencer DD. Diagnosis of medial temporal lobe seizure onset: relative specificity and sensitivity of quantitative MRI. Neurology 1993; 43: 2117-2124.

Spencer SS, Spencer DD, Kim JH, Glaser GS. Gliomas in chronic epilepsy. In: Wolf P, Dam M, Dreifuss DJ, editors. Advances in epileptology. Vol. 16. New York: Raven Press, 1987: 39-41.

Spreafico R, Battaglia G, Arcelli P *et al.* Cortical dysplasia: an immunocytochemical study of three patients. Neurology 1998; 50: 27-36.

Stanisz GJ, Kecojevic A, Bronskill MJ, Henkelman RM. Characterizing white matter with magnetization transfer and T (2). Magn Reson Med 1999; 42: 1128-1136.

Stanley JA, Cendes F, Dubeau F, Andermann F, Arnold DL. Proton magnetic resonance spectroscopic imaging in patients with extratemporal epilepsy. Epilepsia 1998; 39: 267-273.

Steen RG, Taylor JS, Langston JW *et al.* Prospective evaluation of the brain in asymptomatic children with

neurofibromatosis type 1: relationship of macrocephaly to T1 relaxation changes and structural brain abnormalities. AJNR Am.J Neuroradiol. 2001; 22: 810-817.

Steffenburg U, Hagberg G, Kyllerman M. Characteristics of seizures in a population-based series of mentally retarded children with active epilepsy. Epilepsia 1996; 37: 850-856.

Steffenburg U, Hedstrom A, Lindroth A, Wiklund LM, Hagberg G, Kyllerman M. Intractable epilepsy in a population-based series of mentally retarded children. Epilepsia 1998; 39: 767-775.

Stehling MH, Turner R, Mansfield P. Echo-planar imaging: magnetic resonance imaging ina fraction of a second. (Review). Science 1991; 43-50.

Steinlein OK, Mulley JC, Propping P *et al.* A missense mutation in the neuronal nicotinic acetylcholine receptor alpha 4 subunit is associated with autosomal dominant nocturnal frontal lobe epilepsy. Nat.Genet. 1995; 11: 201-203.

Stejskal EO, Tanner TE. Spin diffusion measurements: spin echoes in the presence of time-dependent field gradient. J Chem Phys 1965; 42: 288-292.

Stern CE, Corkin S, Gonzalez RG *et al.* The hippocampal formation participates in novel picture encoding: evidence from functional magnetic resonance imaging. Proc.Natl.Acad.Sci.U.S.A 1996; 93: 8660-8665.

Stevenson VL, Parker GJ, Barker GJ *et al.* Variations in T1 and T2 relaxation times of normal appearing white matter and lesions in multiple sclerosis. J Neurol.Sci. 2000; 178: 81-87.

Stewart RM, Richman DP, Caviness VS, Jr. Lissencephaly and Pachygyria: an architectonic and topographical analysis. Acta Neuropathol. (Berl) 1975; 31: 1-12.

Strowbridge BW, Masukawa LM, Spencer DD, Shepherd GM. Hyperexcitability associated with localizable lesions in epileptic patients. Brain Res 1992; 587: 158-163.

Strupp M, Bruning R, Wu RH, Deimling M, Reiser M, Brandt T. Diffusion-weighted MRI in transient global amnesia: elevated signal intensity in the left mesial temporal lobe in 7 of 10 patients. Ann.Neurol. 1998; 43: 164-170.

Suhonen-Polvi H, Maattanen H, Alanen A *et al.* Examination of infant brain maturation using ultra low field MRI. Acta Paediatr.Scand 1988; 77: 509-515.

Sullivan EV, Pfefferbaum A. Magnetic resonance relaxometry reveals central pontine abnormalities in clinically asymptomatic alcoholic men. Alcohol Clin.Exp.Res. 2001; 25: 1206-1212.

Sung CY, Chu NS. Epileptic seizures in elderly people: aetiology and seizure type. Age Ageing 1990; 19: 25-30.

Sykova E, Svoboda J, Polak J, Chvatal A. Extracellular volume fraction and diffusion characteristics during progressive ischemia and terminal anoxia in the spinal cord of the rat. J Cereb Blood Flow Metab 1994; 14: 301-

311.

Symms M, Wang L, Barker G, Tofts PS. Detection of serial changes in transient ischaemic attack using image registration. Proceedings International Society for Magnetic Resonance in Medicine 4th Meeting New York 1996; 558.

Symms MR, Allen PJ, Woermann FG *et al.* Reproducible localisation of interictal epileptiform discharges using EEG correlated fMRI. Proceedings of the International Society for Magnetic Resonance in Medicine, Sydney. 1998; 168.

Symms MR, Barker GJ, Franconi F, Clark CA. Correction of eddy-current distortions in diffusion-weighted echo-planar images with a two-dimensional registration technique. Proceedings of the International Society for Magnetic Resonance in Medicine, Fifth scientific meeting 1997; 1723.

Taillibert S, Oppenheim C, Baulac M *et al.* Yield of fluid-attenuated inversion recovery in drug-resistant focal epilepsy with noninformative conventional magnetic resonance imaging. Eur Neurol 1999; 41: 64-72.

Takahashi T, Murata T, Omori M *et al.* Quantitative evaluation of magnetic resonance imaging of deep white matter hyperintensity in geriatric patients by multifractal analysis. Neurosci.Lett. 2001; 314: 143-146.

Takamatsu K, Takizawa T, Sato S. Transient focal abnormalities of MRI and angiographic neuroimaging in status epilepticus: a case report. No To Shinkei 1991; 43: 289-294.

Takanashi J, Sugita K, Fujii K, Niimi H. MR evaluation of tuberous sclerosis: increased sensitivity with fluid-attenuated inversion recovery and relation to severity of seizures and mental retardation. AJNR Am J Neuroradiol 1995; 16: 1923-1928.

Talairach P, Tournoux J. A Stereotactic Coplanar Atlas of the Human Brain. Thieme,Stuttgart: 1988.

Tan SS, Breen S. Radial mosaicism and tangential cell dispersion both contribute to mouse neocortical development. Nature 1993; 362: 638-640.

Tanabe JL, Ezekiel F, Jagust WJ, Schuff N, Fein G. Volumetric method for evaluating magnetization transfer ratio of tissue categories: application to areas of white matter signal hyperintensity in the elderly. Radiology 1997; 204: 570-575.

Tanabe JL, Vermathen M, Miller R, Gelinas D, Weiner MW, Rooney WD. Reduced MTR in the corticospinal tract and normal T2 in amyotrophic lateral sclerosis. Magn Reson Imaging 1998; 16: 1163-1169.

Tanner JE. Self-diffusion of water in frog muscle. Biophys.J. 1979; 107-116.

Tanner JE. Intracellular diffusion of water. Arch Biochem Biphys 1983; 416-428.

Tasker RC, Coyle JT, Vornov JJ. The regional vulnerability to hypoglycemia-induced neurotoxicity in organotypic hippocampal culture: protection by early tetrodotoxin or delayed MK-801. J Neurosci 1992; 12: 4298-4308.

Taylor DC, Falconer MA, Bruton CJ, Corsellis JA. Focal dysplasia of the cerebral cortex in epilepsy. J Neurol Neurosurg Psychiatry 1971; 34: 369-387.

Taylor DG, Bushell MC. The spatial mapping of translational diffusion coefficients by the NMR imaging technique. Phys Med Biol 1985; 30: 345-349.

Temkin NR. Antiepileptogenesis and seizure prevention trials with antiepileptic drugs: meta-analysis of controlled trials. Epilepsia 2001; 42: 4: 515-524

Theodore WH, Bhatia S, Hatta J *et al.* Hippocampal atrophy, epilepsy duration, and febrile seizures in patients with partial seizures. Neurology 1999; 52: 132-136.

Theodore WH, Katz D, Kufta C *et al.* Pathology of temporal lobe foci: Correlation with CT, MRI, and PET. Neurology 1990; 797-803.

Thom M, Sisodiya S, Harkness W, Scaravelli F. Microdysgenesis in temporal lobe epilepsy. A quantitative and immunohistochemical study of white matter neurones. Brain 2001; 124: 2299-2309.

Thornton JS, Amess PN, Penrice J, Chong WK, Wyatt JS, Ordidge RJ. Cerebral tissue water spin-spin relaxation times in human neonates at 2.4 tesla: methodology and the effects of maturation. Magn Reson Imaging 1999; 17: 1289-1295.

Thornton JS, Ordidge RJ, Penrice J *et al.* Anisotropic water diffusion in white and gray matter of the neonatal piglet brain before and after transient hypoxia-ischaemia. Magn Reson Imaging 1997; 15: 433-440.

Thurnher MM, Thurnher SA, Fleischmann D *et al.* Comparison of T2-weighted and fluid-attenuated inversion-recovery fast spin-echo MR sequences in intracerebral AIDS-associated disease. AJNR Am J Neuroradiol 1997; 18: 1601-1609.

Tien RD, Felsberg GJ, Campi dC *et al.* Complex partial seizures and mesial temporal sclerosis: evaluation with fast spin-echo MR imaging. Radiology 1993; 189: 835-842.

Tien RD, Felsberg GJ, Friedman H, Brown M, MacFall J. MR imaging of high-grade cerebral gliomas: value of diffusion-weighted echoplanar pulse sequences. AJR Am.J.Roentgenol. 1994; 162: 671-677.

Tievsky AL, Ptak T, Farkas J. Investigation of apparent diffusion coefficient and diffusion tensor anisotrophy in acute and chronic multiple sclerosis lesions. AJNR Am.J.Neuroradiol. 1999; 20: 1491-1499.

Tofts PS, du Boulay EP. Towards quantitative measurements of relaxation times and other parameters in the brain. Neuroradiology 1990; 32: 407-415.

Tofts PS, Sisodiya S, Barker GJ *et al.* MR magnetization transfer measurements in temporal lobe epilepsy: a preliminary study. AJNR Am J Neuroradiol 1995; 16: 1862-1863.

Tomura N, Kato K, Takahashi S *et al.* Comparison of multishot echo-planar fluid-attenuated inversion-recovery

imaging with fast spin-echo fluid-attenuated inversion-recovery and T2-weighted imaging in depiction of white matter lesions. J Comput.Assist.Tomogr. 2002; 26: 810-814.

Tossetti M, Bianchi M, Guerrini R *et al.* Biochemical evaluation of temporal lobe epilepsy by single voxel ^{1}H MRS with short echo time. MAGMA. 1998; 114.

Tovi M. MR imaging in cerebral gliomas analysis of tumour tissue components. Acta Radiol.Suppl 1993; 384:1-24.: 1-24.

Traub RD, Jefferys JG. Epilepsy in vitro: electrophysiology and computer modelling. In: Engel JrJ, Pedley TA, editors. Epilepsy: A Comprehensive Textbook. Philadelphia: Lippincott-Raven, 1998: 405-18.

Trenerry MR, Jack CR, Jr., Cascino GD, Sharbrough FW, So EL. Bilateral magnetic resonance imaging-determined hippocampal atrophy and verbal memory before and after temporal lobectomy. Epilepsia 1996; 37: 526-533.

Truyen L, van Waesberghe JH, van Walderveen MA *et al.* Accumulation of hypointense lesions ("black holes") on T1 spin-echo MRI correlates with disease progression in multiple sclerosis. Neurology 1996; 47: 1469-1476.

Tubridy N, Barker GJ, Macmanus DG, Moseley IF, Miller DH. Three-dimensional fast fluid attenuated inversion recovery (3D fast FLAIR): a new MRI sequence which increases the detectable cerebral lesion load in multiple sclerosis. Br.J Radiol. 1998; 71: 840-845.

Tulving E, Kapur S, Craik FI, Moscovitch M, Houle S. Hemispheric encoding/retrieval asymmetry in episodic memory: positron emission tomography findings. Proc.Natl.Acad.Sci.U.S.A 1994; 91: 2016-2020.

Tureen J, Sande M. Acute bacterial infections of the central nervous system. In: Aminoff M, editor. Neurology and General Medicine. New York: Churchill-Livingstone, 1989: 559-76.

Turetschek K, Wunderbaldinger P, Bankier AA *et al.* Double inversion recovery imaging of the brain: initial experience and comparison with fluid attenuated inversion recovery imaging. Magn Reson Imaging 1998; 16: 127-135.

Turjman F, Massoud TF, Sayre JW, Vinuela F, Guglielmi G, Duckwiler G. Epilepsy associated with cerebral arteriovenous malformations: a multivariate analysis of angioarchitectural characteristics. AJNR Am.J Neuroradiol. 1995; 16: 345-350.

Turner R, LeBihan D. Echo-planar imaging of diffusion and perfusion. In: LeBihan D, editor. Future directions in MRI of diffusion and microcirculation. Workshop syllabus. Bethesda, Berkeley.: Society of Magnetic Resonance in Medicine., 1990: 111-22.

Turner R, LeBihan D, Maier M, Vavrek R, Hedges LK, Pekar J. Echo-planar imaging of intravoxel incoherent motion. Radiology 1990; 407-414.

Urbach H, Scheffler B, Heinrichsmeier T *et al.* Focal cortical dysplasia of Taylor's Balloon Cell type: A clinicopathological entity with characteristic neuroimaging and histopathological features, and favourable postsurgical outcome. Epilepsia 2002; 43 (1): 33-40.

Urenjak J, Williams SC, Gadian DG, Noble M. Specific expression of N-acetylaspartate in neurons, oligodendrocyte-type-2 astrocyte progenitors, and immature oligodendrocytes in vitro. J Neurochem. 1992; 55-61.

Urenjak J, Williams SC, Gadian DG, Noble M. Proton nuclear magnetic resonance spectroscopy unambiguously identifies different neuronal cell types. J Neurosci 1993; 981-989.

Usui N, Matsuda K, Mihara T *et al.* MRI of cortical dysplasia--correlation with pathological findings. Neuroradiology 2001; 43: 830-837.

Vaithianathar L, Tench CR, Morgan PS, Wilson M, Blumhardt LD. T1 relaxation time mapping of white matter tracts in multiple sclerosis defined by diffusion tensor imaging. J Neurol 2002; 249: 1272-1278.

Van Bogaert P, David P, Gillain CA *et al.* Perisylvian dysgenesis. Clinical, EEG, MRI and glucose metabolism features in 10 patients. Brain 1998; 121: 2229-2238.

Van Bogaert P, Massager N, Tugendhaft P *et al.* Statistical parametric mapping of regional glucose metabolism in mesial temporal lobe epilepsy. Neuroimage. 2000; 12: 129-138.

van Buchem MA, McGowan JC, Grossman RI. Magnetization transfer histogram methodology: its clinical and neuropsychological correlates. Neurology 1999; 53: S23-S28.

van Buchem MA, McGowan JC, Kolson DL, Polansky M, Grossman RI. Quantitative volumetric magnetization transfer analysis in multiple sclerosis: estimation of macroscopic and microscopic disease burden. Magn Reson Med 1996; 36: 632-636.

van Buchem MA, Steens SC, Vrooman HA *et al.* Global estimation of myelination in the developing brain on the basis of magnetization transfer imaging: a preliminary study. AJNR Am J Neuroradiol 2001; 22: 762-766.

van Buchem MA, Udupa JK, McGowan JC *et al.* Global volumetric estimation of disease burden in multiple sclerosis based on magnetization transfer imaging. AJNR Am J Neuroradiol 1997; 18: 1287-1290.

van der Flier WM, van den Heuvel DM, Weverling-Rijnsburger AW *et al.* Magnetization transfer imaging in normal aging, mild cognitive impairment, and Alzheimer's disease. Ann Neurol 2002; 52: 62-67.

Van der Knapp MS, Valk J. Myelin and white matter. In: Van der Knapp MS, Valk J, editors. Magnetic Resonance of Myelin, Myelination and Myelin Disorders. Berlin: Springer-Verlag, 1995: 1-17.

van der Toorn A, Dijkhuizen RM, Tulleken CA, Nicolay K. Diffusion of metabolites in normal and ischemic rat brain measured by localized 1H MRS. Magn Reson Med 1996a; 36: 914-922.

van der Toorn A, Sykova E, Dijkhuizen RM *et al.* Dynamic changes in water ADC, energy metabolism,

extracellular space volume, and tortuosity in neonatal rat brain during global ischemia. Magn Reson Med 1996b; 36: 52-60.

van Elst LT, Woermann FG, Lemieux L, Thompson PJ, Trimble MR. Affective aggression in patients with temporal lobe epilepsy: a quantitative MRI study of the amygdala. Brain 2000; 123: 234-243.

van Engelen BG, de Waal LP, Weemaes CM, Renier WO. Serologic HLA typing in cryptogenic Lennox-Gastaut syndrome. Epilepsy Res. 1994a; 17: 43-47.

van Engelen BG, Renier WO, Weemaes CM, Gabreels FJ, Meinardi H. Immunoglobulin treatment in epilepsy, a review of the literature. Epilepsy Res. 1994b; 19: 181-190.

van Engelen BG, Weemaes CM, Renier WO, Bakkeren JA, Borm GF, Strengers PF. A dysbalanced immune system in cryptogenic Lennox-Gastaut syndrome. Scand.J Immunol. 1995; 41: 209-213.

van Gelderen P, de Vleeschouwer MH, DesPres D, Pekar J, van Zijl PC, Moonen CT. Water diffusion and acute stroke. Magn Reson Med 1994; 31: 154-163.

Van Leemput K, Maes F, Vandermeulen D, Suetens P. Automated model-based tissue classification of MR images of the brain. IEEE Trans.Med Imaging 1999; 18: 897-908.

Van Paesschen W, Bodian C, Maker H. Metabolic abnormalities and new-onset seizures in human immunodeficiency virus-seropositive patients. Epilepsia 1995a; 36: 146-150.

Van Paesschen W, Connelly A, Johnson CL, Duncan JS. The amygdala and intractable temporal lobe epilepsy: a quantitative magnetic resonance imaging study (published erratum appears in Neurology 1997 Jun; 48 (6):1751). Neurology 1996; 47: 1021-1031.

Van Paesschen W, Connelly A, King MD, Jackson GD, Duncan JS. The spectrum of hippocampal sclerosis: a quantitative magnetic resonance imaging study. Ann.Neurol. 1997a; 41: 41-51.

Van Paesschen W, Duncan JS, Connelly A. A comparison of the neuropathological effects of vigabatrin and carbamazepine in patients with newly diagnosed localisation-related epilepsy using MR-based cerebral T2 relaxation time measurements. Epilepsy Res 1998; 29: 155-160.

Van Paesschen W, Revesz T, Duncan JS, King MD, Connelly A. Quantitative neuropathology and quantitative magnetic resonance imaging of the hippocampus in temporal lobe epilepsy. Ann.Neurol. 1997b; 42: 756-766.

Van Paesschen W, Sisodiya S, Connelly A *et al.* Quantitative hippocampal MRI and intractable temporal lobe epilepsy. Neurology 1995b; 45: 2233-2240.

van Waesberghe JH, Castelijns JA, Roser W *et al.* Single-dose gadolinium with magnetization transfer versus triple-dose gadolinium in the MR detection of multiple sclerosis lesions. AJNR Am J Neuroradiol 1997; 18: 1279-1285.

van Waesberghe JH, Kamphorst W, De Groot CJ *et al.* Axonal loss in multiple sclerosis lesions: magnetic resonance imaging insights into substrates of disability. Ann Neurol 1999; 46: 747-754.

van Waesberghe JH, Kamphorst W, van Walderveen M. Histopathologic correlate of MTR and hypointense signal intensity on T1 SE in multiple sclerosis lesions. A direct postmortem study. Mult.Scler. 1998; 4: 272.

van Zijl PC, Rothman DL. NMR studies of brain ^{13}C-glucose uptake and metabolism: present status. Magn Reson Imaging 1995; 1213-1221.

Vartanian MG, Cordon JJ, Kupina NC *et al.* Phenytoin pretreatment prevents hypoxic-ischemic brain damage in neonatal rats. Brain Res Dev.Brain Res 1996; 95: 169-175.

Vavasour IM, Whittall KP, MacKay AL, Li DK, Vorobeychik G, Paty DW. A comparison between magnetization transfer ratios and myelin water percentages in normals and multiple sclerosis patients. Magn Reson Med 1998; 40: 763-768.

Verheul HB, Balazs R, Berkelbach van der Sprenkel JW *et al.* Comparison of diffusion-weighted MRI with changes in cell volume in a rat model of brain injury (published erratum appears in NMR Biomed 1994 Dec; 7 (8):374). NMR Biomed. 1994; 7: 96-100.

Verhoeff NPLG, Petroff OA, Hyder F *et al.* Effects of vigabatrin on the GABAergic system as determined by ^{123}I iomazenil SPECT and GABA MRS. Epilepsia 1999; 1433-1438.

Verrot D, San Marco M, Dravet C *et al.* Prevalence and signification of antinuclear and anticardiolipin antibodies in patients with epilepsy. Am J Med 1997; 103: 33-37.

Vertosick FT, Selker RG, Arena VC. Survival of patients with well-differentiated astrocytomas diagnosed in the era of computed tomography. Neurosurgery 1991; 28: 496-501.

Vinters HV, Armstrong DD, Babb TL, Daumas-Duport C, Robitaille Y, Bruton CJ. The neuropathology of human symptomatic epilepsy. In: Engel J J, editor. Surgical Treatment of the Epilepsies. New York: Raven Press, 1993: 593-608.

Volpe JJ, Adams RD. Cerebro-hepato-renal syndrome of Zellweger: an inherited disorder of neuronal migration. Acta Neuropathol. (Berl) 1972; 20: 175-198.

Volz H, Gaser C, Sauer H. Supporting evidence for the model of cognitive dysmetria in schizophrenia--a structural magnetic resonance imaging study using deformation-based morphometry. Schizophr.Res 2000; 46: 45-56.

von Oertzen J, Urbach H, Blumcke I *et al.* Time-efficient T2 relaxometry of the entire hippocampus is feasible in temporal lobe epilepsy. Neurology 2002; 58: 257-264.

Vymazal J, Hajek M, Patronas N *et al.* The quantitative relation between T1-weighted and T2-weighted MRI of normal gray matter and iron concentration. J Magn Reson Imaging 1995; 5: 554-560.

Vymazal J, Righini A, Brooks RA *et al.* T1 and T2 in the brain of healthy subjects, patients with Parkinson disease, and patients with multiple system atrophy: relation to iron content. Radiology 1999; 211: 489-495.

Wada J, Rasmussen T. Intracarotid injection of sodium amytal for the lateralisation of cerebral speech dominance. J Neurosurg. 1960; 17: 266-282.

Wada JA, Clarke R, Hamm A. Cerebral hemispheric asymmetry in humans. Cortical speech zones in 100 adults and 100 infant brains. Arch.Neurol. 1975; 32: 239-246.

Wahl RW, Dillard SH. Multiple ganglioneuromas of the central nervous system. Arch Pathol. 1972; 94: 158-164.

Wallace RH, Marini C, Petrou S *et al.* Mutant GABA (A) receptor gamma2-subunit in childhood absence epilepsy and febrile seizures. Nat.Genet. 2001a; 28: 49-52.

Wallace RH, Scheffer IE, Barnett S *et al.* Neuronal sodium-channel alpha1-subunit mutations in generalized epilepsy with febrile seizures plus. Am J Hum.Genet. 2001b; 68: 859-865.

Walsh C, Cepko CL. Widespread dispersion of neuronal clones across functional regions of the cerebral cortex. Science 1992; 255: 434-440.

Walsh C, Cepko CL. Clonal dispersion in proliferative layers of developing cerebral cortex. Nature 1993; 362: 632-635.

Wang W, Goldstein S, Scheuer ML, Branstetter BF. Acute stroke syndrome with fixed neurological deficit and false-negative diffusion-weighted imaging. J Neuroimaging 2003; 13: 158-161.

Wang Y, Majors A, Najm I *et al.* Postictal alteration of sodium content and apparent diffusion coefficient in epileptic rat brain induced by kainic acid. Epilepsia 1996; 37: 1000-1006.

Warach S, Gaa J, Siewert B, Wielopolski P, Edelman RR. Acute human stroke studied by whole brain echo planar diffusion-weighted magnetic resonance imaging. Ann.Neurol. 1995; 37: 231-241.

Warach S, Ives JR, Schlaug G *et al.* EEG-triggered echo-planar functional MRI in epilepsy. Neurology 1996; 47: 89-93.

Warach S, Levin JM, Schomer DL, Holman BL, Edelman RR. Hyperperfusion of ictal seizure focus demonstrated by MR perfusion imaging. AJNR Am J Neuroradiol 1994; 15: 965-968.

Wardlaw JM, Statham PF. How often is haemosiderin not visible on routine MRI following traumatic intracerebral haemorrhage? Neuroradiology 2000; 42: 81-84.

Watanabe K. The localization-related epilepsies: some problems with subclassification. Jpn.J Psychiatry Neurol. 1989; 43: 471-475.

Watanabe K. Implications of the International Classification of Seizures and Syndromes in the management of

epilepsy. Nihon Shinkei Seishin Yakurigaku Zasshi 1997; 17: 39-43.

Watson C, Andermann F, Gloor P *et al.* Anatomic basis of amygdaloid and hippocampal volume measurement by magnetic resonance imaging. Neurology 1992; 42: 1743-1750.

Webb DW, Fryer AE, Osborne JP. On the incidence of fits and mental retardation in tuberous sclerosis. J Med Genet. 1991; 28: 395-397.

Webb J, Guimond A, Eldridge P *et al.* Automatic detection of hippocampal atrophy on magnetic resonance images. Magn Reson.Imaging 1999; 17: 1149-1161.

Weber OM, Verhagen A, Duc CO, Meier D, Leenders KL, Boesiger P. Effects of vigabatrin intake on brain GABA activity as monitored by spectrally edited magnetic resonance spectroscopy and positron emission tomography. Magn Reson Imaging 1999; 17: 417-425.

Welch KM, Windham J, Knight RA *et al.* A model to predict the histopathology of human stroke using diffusion and T2-weighted magnetic resonance imaging. Stroke 1995; 26: 1983-1989.

Wendel JD, Trenerry MR, Xu YC *et al.* The relationship between quantitative T2 relaxometry and memory in nonlesional temporal lobe epilepsy. Epilepsia 2001; 42: 863-868.

Werring DJ, Clark CA, Barker GJ *et al.* The structural and functional mechanisms of motor recovery: complementary use of diffusion tensor and functional magnetic resonance imaging in a traumatic injury of the internal capsule. J.Neurol.Neurosurg.Psychiatry 1998; 65: 863-869.

Werring DJ, Clark CA, Barker GJ, Thompson AJ, Miller DH. Diffusion tensor imaging of lesions and normal-appearing white matter in multiple sclerosis. Neurology 1999; 52: 1626-1632.

Wesbey GE, Moon K, Crooks L, Arakawa M, Brash R. Proton T2 reduction due to spin diffusion through pulsed-gradients in spin-echo NMR imaging. Imaging implications and applications. Magn Reson Med 1984; 273.

Westin CF, Maier SE, Mamata H, Nabavi A, Jolesz FA, Kikinis R. Processing and visualization for diffusion tensor MRI. Med Image Anal. 2002; 6: 93-108.

Wheeler-Kingshott CA, Hickman SJ, Parker GJ *et al.* Investigating cervical spinal cord structure using axial diffusion tensor imaging. Neuroimage 2002; 16: 93-102.

Whitley RJ. Viral encephalitis. N.Engl.J Med 1990; 323: 242-250.

Whitley RJ. Herpes simplex virus infections of the central nervous system. Encephalitis and neonatal herpes. Drugs 1991; 42: 406-427.

Whitley RJ, Alford CA, Hirsch MS *et al.* Vidarabine versus acyclovir therapy in herpes simplex encephalitis. N.Engl.J Med 1986; 314: 144-149.

Whitley RJ, Lakeman F. Herpes simplex virus infections of the central nervous system: therapeutic and diagnostic considerations. Clin.Infect.Dis. 1995; 20: 414-420.

Whittall KP, MacKay AL, Graeb DA, Nugent RA, Li DK, Paty DW. In vivo measurement of T2 distributions and water contents in normal human brain. Magn Reson Med 1997; 37: 34-43.

Whittall KP, MacKay AL, Li DK. Are mono-exponential fits to a few echoes sufficient to determine T2 relaxation for in vivo human brain? Magn Reson Med 1999; 41: 1255-1257.

Wick M, Nagatomo Y, Prielmeier F, Frahm J. Alteration of intracellular metabolite diffusion in rat brain in vivo during ischemia and reperfusion. Stroke 1995; 26: 1930-1933.

Wicks DA, Tofts PS, Miller DH *et al.* Volume measurement of multiple sclerosis lesions with magnetic resonance images. A preliminary study. Neuroradiology 1992; 34: 475-479.

Wieshmann UC. Clinical application of neuroimaging in epilepsy. J Neurol Neurosurg.Psychiatry 2003; 74: 466-470.

Wieshmann UC, Barker GJ, Symms MR, Bartlett PA, Stevens JM, Shorvon SD. Fast fluid-attenuated inversion-recovery imaging: first experience with a 3D version in epilepsy. Neuroradiology 1998a; 40: 483-489.

Wieshmann UC, Clark CA, Symms MR, Barker GJ, Birnie KD, Shorvon SD. Water diffusion in the human hippocampus in epilepsy. Magn Reson Imaging 1999a; 17: 29-36.

Wieshmann UC, Clark CA, Symms MR, Franconi F, Barker GJ, Shorvon SD. Anisotropy of water diffusion in corona radiata and cerebral peduncle in patients with hemiparesis. Neuroimage. 1999b; 10: 225-230.

Wieshmann UC, Clark CA, Symms MR, Franconi F, Barker GJ, Shorvon SD. Reduced anisotropy of water diffusion in structural cerebral abnormalities demonstrated with diffusion tensor imaging. Magn Reson Imaging 1999c; 17: 1269-1274.

Wieshmann UC, Franconi F, Symms MR, Clark CA, Barker GJ, Shorvon SD. The variability and accuracy of the apparent diffusion coefficient in diffusion-weighted EPI. Proceedings of the International Society for Magnetic Resonance in Medicine, fifth scientific meeting. 1997a; ISMRM, Berkeley, CA: 1748.

Wieshmann UC, Free SL, Everitt AD *et al.* Magnetic resonance imaging in epilepsy with a fast FLAIR sequence. J Neurol Neurosurg.Psychiatry 1996; 61: 357-361.

Wieshmann UC, Free SL, Stevens JM, Shorvon SD. Image contrast and hippocampal volumetric measurements. Magn Reson.Imaging 1998b; 16: 13-17.

Wieshmann UC, Lemieux L, Symms MR *et al.* Oversampling rejecting averaging correction algorithm for non-gated single shot diffusion-weighted EPI. Proceedings of the International Society for Magnetic Resonance in Medicine, sixth scientific meeting. 1998c; 1230.

Wieshmann UC, Symms MR, Clark CA *et al.* Wallerian degeneration in the optic radiation after temporal lobectomy demonstrated in vivo with diffusion tensor imaging. Epilepsia 1999d; 40: 1155-1158.

Wieshmann UC, Symms MR, Clark CA *et al.* Blunt-head trauma associated with widespread water-diffusion changes. Lancet 1999e; 353: 1242-1243.

Wieshmann UC, Symms MR, Parker GJ *et al.* Diffusion tensor imaging demonstrates deviation of fibres in normal appearing white matter adjacent to a brain tumour. J Neurol.Neurosurg.Psychiatry 2000; 68: 501-503.

Wieshmann UC, Symms MR, Shorvon SD. Diffusion changes in status epilepticus. Lancet 1997b; 493-494.

Wilkie H, Osei-Lah A, Chioza B *et al.* Association of mu-opioid receptor subunit gene and idiopathic generalized epilepsy. Neurology 2002; 59: 724-728.

Wilkinson ID, Chinn RJ, Hall-Craggs MA *et al.* Sub-cortical white-grey matter contrast on MRI as a quantitative marker of diffuse HIV-related parenchymal abnormality. Clin.Radiol. 1996; 51: 475-479.

Wilkinson ID, Lunn S, Miszkiel KA *et al.* Proton MRS and quantitative MRI assessment of the short term neurological response to antiretroviral therapy in AIDS. J Neurol.Neurosurg.Psychiatry 1997; 63: 477-482.

Williams CE, Gunn A, Gluckman PD. Time course of intracellular edema and epileptiform activity following prenatal cerebral ischemia in sheep. Stroke 1991; 22: 516-521.

Williams PL, Warwick R. Functional Neuroanatomy of Man. Philadelphia: Saunders, 1975.

Williamson PD, Thadani VM, Darcey TM, Spencer DD, Spencer SS, Mattson RH. Occipital lobe epilepsy: clinical characteristics, seizure spread patterns, and results of surgery. Ann.Neurol. 1992; 31: 3-13.

Willmore LJ. Post-traumatic epilepsy: cellular mechanisms and implications for treatment. Epilepsia 1990; 31 Suppl 3: S67-S73.

Willmore, L. J., Ballinger, W. E. Jr., Boggs, W., Sypert, G. W., and Rubin, J. J. Dendritic alterations in rat isocortex within an iron-induced chronic epileptic focus. Neurosurgery 7, 142-146. 1980.
Ref Type: Journal (Full)

Willmore LJ, Hiramatsu M, Kochi H, Mori A. Formation of superoxide radicals after FeCl3 injection into rat isocortex. Brain Res 1983; 277: 393-396.

Wilmes LJ, Hoehn-Berlage M, Els T *et al.* In vivo relaxometry of three brain tumors in the rat: effect of Mn-TPPS, a tumor-selective contrast agent. J Magn Reson Imaging 1993; 3: 5-12.

Wilson M, Tench CR, Morgan PS, Blumhardt LD. Pyramidal tract mapping by diffusion tensor magnetic resonance imaging in multiple sclerosis: improving correlations with disability. J Neurol Neurosurg.Psychiatry 2003; 74: 203-207.

Wimberger DM, Roberts TP, Barkovich AJ, Prayer LM, Moseley ME, Kucharczyk J. Identification of "premyelination" by diffusion-weighted MRI. J.Comput.Assist.Tomogr. 1995; 19: 28-33.

Witting LA. Vitamin E and lipid antioxidants in free-radical-initiated reactions. In: Pryor WA, editor. Free radicals in biology, Vol 4. New York: Academic Press, 1980: 295-319.

Woermann FG, Barker GJ, Birnie KD, Meencke HJ, Duncan JS. Regional changes in hippocampal T2 relaxation and volume: a quantitative magnetic resonance imaging study of hippocampal sclerosis. J Neurol.Neurosurg.Psychiatry 1998a; 65: 656-664.

Woermann FG, Free SL, Koepp MJ, Ashburner J, Duncan JS. Voxel-by-voxel comparison of automatically segmented cerebral gray matter--A rater-independent comparison of structural MRI in patients with epilepsy. Neuroimage 1999a; 10: 373-384.

Woermann FG, Free SL, Koepp MJ, Sisodiya SM, Duncan JS. Abnormal cerebral structure in juvenile myoclonic epilepsy (JME) demonstrated with voxel-based analysis of MRI. Brain 1999b; 2101-2107.

Woermann FG, Jokeit H, Luerding R *et al.* Language lateralization by Wada test and fMRI in 100 patients with epilepsy. Neurology 2003; 61: 699-701.

Woermann FG, McLean MA, Bartlett PA, Parker GJ, Barker GJ, Duncan JS. Short echo time single-voxel 1H magnetic resonance spectroscopy in magnetic resoance imaging-negative temporal lobe epilepsy: different biochemical profile compared with hippocampal sclerosis. Ann Neurol 1999c; 45: 369-376.

Woermann FG, Sisodiya SM, Free SL, Duncan JS. Quantitative MRI in patients with idiopathic generalized epilepsy. Evidence of widespread cerebral structural changes. Brain 1998b; 121: 1661-1667.

Woermann FG, Steiner H, Barker GJ *et al.* A fast FLAIR dual-echo technique for hippocampal T2 relaxometry: First experiences in patients with temporal lobe epilepsy. J Magn Reson Imaging 2001; 13: 547-552.

Woermann FG, van Elst LT, Koepp MJ *et al.* Reduction of frontal neocortical grey matter associated with affective aggression in patients with temporal lobe epilepsy: an objective voxel by voxel analysis of automatically segmented MRI. J Neurol Neurosurg.Psychiatry 2000; 68: 162-169.

Wohns RN, Wyler AR. Prophylactic phenytoin in severe head injuries. J Neurosurg. 1979; 51: 507-509.

Wolf HK, Muller MB, Spanle M, Zentner J, Schramm J, Wiestler OD. Ganglioglioma: a detailed histopathological and immunohistochemical analysis of 61 cases. Acta Neuropathol (Berl) 1994; 88: 166-173.

Wolff SD, Balaban RS. Magnetization transfer contrast (MTC) and tissue water proton relaxation in vivo. Magn Reson Med 1989; 10: 135-144.

Wolff SD, Balaban RS. Magnetization transfer imaging: practical aspects and clinical applications. Radiology 1994; 192: 593-599.

Wolff SD, Chesnick S, Frank JA, Lim KO, Balaban RS. Magnetization transfer contrast: MR imaging of the knee. Radiology 1991a; 179: 623-628.

Wolff SD, Eng J, Balaban RS. Magnetization transfer contrast: method for improving contrast in gradient-recalled-echo images. Radiology 1991b; 179: 133-137.

Wong JH, Awad IA, Kim JH. Ultrastructural pathological features of cerebrovascular malformations: a preliminary report. Neurosurgery 2000; 46: 1454-1459.

Wong MC, Suite ND, Labar DR. Seizures in human immunodeficiency virus infection. Arch.Neurol. 1990; 47: 640-642.

Woo TU, Finlay BL. Cortical target depletion and ingrowth of geniculocortical axons: implications for cortical specification. Cereb Cortex 1996; 6: 457-469.

Woo TU, Niederer JK, Finlay BL. Cortical target depletion and the developing lateral geniculate nucleus: implications for trophic dependence. Cereb Cortex 1996; 6: 446-456.

Wood AG, Saling MM, O'Shea MF, Berkovic SF, Jackson GD. Components of verbal learning and hippocampal damage assessed by T2 relaxometry. J Int.Neuropsychol.Soc. 2000; 6: 529-538.

Woods RP, Cherry SR, Mazziotta JC. Rapid automated algorithm for aligning and reslicing PET images. J Comput.Assist.Tomogr. 1992; 16: 620-633.

Worsley KJ. Instability of localisation of cerebral blood flow activation foci with parametric maps. J Cereb.Blood Flow Metab 1993; 13: 1041-1042.

Worsley KJ, Andermann M, Koulis T, MacDonald D, Evans AC. Detecting changes in nonisotropic images. Hum.Brain Mapp. 1999; 8: 98-101.

Worsley KJ, Marrett S, Neelin P, Friston KJ, Evans AC. A Unified Statistical Approach for Determining Significant Signals in Images of Cerebral Activation. San Diego: Academic Press, 1995.

Wright IC, Ellison ZR, Sharma T, Friston KJ, Murray RM, McGuire PK. Mapping of grey matter changes in schizophrenia. Schizophr.Res. 1999; 35: 1-14.

Wright IC, McGuire PK, Poline JB *et al.* A voxel-based method for the statistical analysis of gray and white matter density applied to schizophrenia. Neuroimage 1995; 2: 244-252.

Xing D, Papadakis NG, Huang CL, Lee VM, Carpenter TA, Hall LD. Optimised diffusion-weighting for measurement of apparent diffusion coefficient (ADC) in human brain. Magn Reson Imaging 1997; 15: 771-784.

Xue R, van Zijl PC, Crain BJ, Solaiyappan M, Mori S. In vivo three-dimensional reconstruction of rat brain axonal projections by diffusion tensor imaging. Magn Reson.Med. 1999; 42: 1123-1127.

Yakovlev PI, Lecours AR. The myelogenetic cycles of regional maturation of the brain. In: Minkrowski A, editor. Regional development of the brain in early life. Oxford: Blackwell, 1967: 3-70.

Yamanouchi H, Zhang W, Jay V, Becker LE. Enhanced expression of microtubule-associated protein 2 in large neurons of cortical dysplasia. Ann.Neurol. 1996; 39: 57-61.

Yanagawa Y, Tsushima Y, Tokumaru A *et al.* A quantitative analysis of head injury using T2*-weighted gradient-echo imaging. J Trauma 2000; 49: 272-277.

Ye FQ, Martin WR, Allen PS. Estimation of brain iron in vivo by means of the interecho time dependence of image contrast. Magn Reson Med 1996; 36: 153-158.

Yee AS, Simon JH, Anderson CA, Sze CI, Filley CM. Diffusion-weighted MRI of right-hemisphere dysfunction in Creutzfeldt-Jakob disease. Neurology 1999; 52: 1514-1515.

Yeh HS, Tew JM, Gartner M. Seizure control after surgery on cerebral arteriovenous malformations. J Neurosurg. 1993; 78: 12-18.

Yeung HN, Aisen AM. Magnetization transfer contrast with periodic pulsed saturation. Radiology 1992; 183: 209-214.

Ying Z, Babb TL, Comair YG, Bingaman W, Bushey M, Touhalisky K. Induced expression of NMDAR2 proteins and differential expression of NMDAR1 splice variants in dysplastic neurons of human epileptic neocortex. J Neuropathol.Exp.Neurol. 1998; 57: 47-62.

Ylikoski A, Erkinjuntti T, Raininko R, Sarna S, Sulkava R, Tilvis R. White matter hyperintensities on MRI in the neurologically nondiseased elderly. Analysis of cohorts of consecutive subjects aged 55 to 85 years living at home. Stroke 1995; 26: 1171-1177.

Yoneda Y, Tokui K, Hanihara T, Kitagaki H, Tabuchi M, Mori E. Diffusion-weighted magnetic resonance imaging: detection of ischemic injury 39 minutes after onset in a stroke patient. Ann.Neurol. 1999; 45: 794-797.

Yoon HH, Kwon HL, Mattson RH, Spencer DD, Spencer SS. Long-term seizure outcome in patients initially seizure-free after resective epilepsy surgery. Neurology 2003; 61: 445-450.

Yoshiura T, Higano S, Rubio A *et al.* Heschl and superior temporal gyri: low signal intensity of the cortex on T2-weighted MR images of the normal brain. Radiology 2000; 214: 217-221.

Yoshiura T, Mihara F, Ogomori K, Tanaka A, Kaneko K, Masuda K. Diffusion tensor in posterior cingulate gyrus: correlation with cognitive decline in Alzheimer's disease. Neuroreport 2002; 13: 2299-2302.

Young RS, Osbakken MD, Briggs RW, Yagel SK, Rice DW, Goldberg S. 31P NMR study of cerebral metabolism during prolonged seizures in the neonatal dog. Ann.Neurol. 1985; 18: 14-20.

Younkin D, Delvoria-Papadopoulos M, Maris J, Donlon E, Clancy R, Chance B. Cerebral metabolic effects of

neonatal seizures measured in vivo by ^{31}P NMR spectroscopy. Ann Neurol 1986; 513-519.

Yousem DM, Schnall MD, Dougherty L, Weinstein GS, Hayden RE. Magnetization transfer imaging of the head and neck: normative data. AJNR Am J Neuroradiol 1994; 15: 1117-1121.

Yousry TA, Seelos K, Mayer M *et al.* Characteristic MR lesion pattern and correlation of T1 and T2 lesion volume with neurologic and neuropsychological findings in cerebral autosomal dominant arteriopathy with subcortical infarcts and leukoencephalopathy (CADASIL). AJNR Am J Neuroradiol 1999; 20: 91-100.

Yuh WT, Crain MR, Loes DJ, Greene GM, Ryals TJ, Sato Y. MR imaging of cerebral ischemia: findings in the first 24 hours. AJNR Am J Neuroradiol 1991; 12: 621-629.

Zacharopoulos NG, Narayana PA. Selective measurement of white matter and gray matter diffusion trace values in normal human brain. Med Phys 1998; 25: 2237-2241.

Zentner J, Hufnagel A, Wolf HK *et al.* Surgical treatment of temporal lobe epilepsy: clinical, radiological, and histopathological findings in 178 patients. J Neurol Neurosurg Psychiatry 1995; 666-673.

Zentner J, Wolf HK, Ostertun B *et al.* Gangliogliomas: clinical, radiological, and histopathological findings in 51 patients. J Neurol Neurosurg Psychiatry 1994; 57: 1497-1502.

Zhong J, Petroff OA, Pleban LA, Gore JC, Prichard JW. Reversible, reproducible reduction of brain water apparent diffusion coefficient by cortical electroshocks. Magn Reson Med 1997; 37: 1-6.

Zhong J, Petroff OA, Prichard JW, Gore JC. Changes in water diffusion and relaxation properties of rat cerebrum during status epilepticus. Magn Reson Med 1993; 30: 241-246.

Zhong J, Petroff OA, Prichard JW, Gore JC. Barbiturate-reversible reduction of water diffusion coefficient in flurothyl-induced status epilepticus in rats. Magn Reson Med 1995; 33: 253-256.

Zhou J, Golay X, van Zijl PC *et al.* Inverse T (2) contrast at 1.5 Tesla between gray matter and white matter in the occipital lobe of normal adult human brain. Magn Reson Med 2001; 46: 401-406.

Zimmerman G, Lewis AI, Tew JM. Pure sylvian fissure arteriovenous malformations. J Neurosurg. 2000; 92: 39-44.

APPENDIX

Definition of statistical terms

"True positives" - the MRI-negative patients with a region of abnormality identified with advanced imaging techniques (used to calculate sensitivity for *"all abnormalities"*) and that concur with the best available localising information, usually ictal or interictal EEG recordings (used to calculate sensitivity for *"EEG concordant abnormalities"*).

"True negatives" - the control subject population without an abnormality on advanced imaging.

"False negatives " - the MRI-negative patients without a region of abnormality identified with advanced imaging techniques.

"False positives " - the control subjects with a region of abnormality identified with advanced imaging techniques (used to calculate specificity for *"all abnormalities"*) or MRI-negative patients with a discordant abnormality (used to calculate specificity for *"EEG concordant abnormalities"*.

Sensitivity -

$$\frac{TruePositives}{TruePositives + FalseNegatives}$$

Specificity -

$$\frac{TrueNegatives}{FalsePositives + TrueNegatives}$$